Linear response functions of Strongly Correlated Materials: LDA+DMFT approach

Von der Fakultät für Mathematik, Informatik und Naturwissenschaften der RWTH Aachen University zur Erlangung des akademischen Grades eines Doktors der Naturwissenschaften genehmigte Dissertation

vorgelegt von

Amin Kiani Sheikhabadi, M.Sc.
aus Isfahan, Iran

Berichter: Univ.-Prof. Eva Pavarini, Ph.D.
Univ.-Prof. Dr. Erik Koch

Tag der mündlichen Prüfung: 9 March 2015

Diese Dissertation ist auf den Internetseiten der Hochschulbibliothek online verfügbar.

Lineare Antwortfunktionen stark korrelierter Materialien: Ein Zugang mittels LDA+DMFT

Kurzfassung: Die außergewöhnlichen elektronischen und magnetischen Eigenschaften stark korrelierter Materialien bilden seit Jahrzehnten ein bedeutendes Forschungsgebiet der theoretischen Physik. Stark korreliert sind Materialien mit teilweise gefüllten lokalisierten d- oder f-, gelegentlich auch p-Schalen. Die Beschreibung ihrer Eigenschaften ist eine der zentralen Herausforderungen der theoretischen Festkörperphysik. Zu ihrer Untersuchung werden Modell Hamiltonoperatoren genutzt, die sich auf die niederenergetischen Anregungen beschränken. In den vergangenen Jahren wurden Methoden zur Bestimmung solcher Modelle entwickelnt, die auf ab-initio Dichtefunktional Methoden (DFT), zum Beispiel der lokalen-Dichte Näherung (LDA) beruhen. Die Berechnung der Eigenschaften dieser realistischen Modelle ist eine Herausforderung. Die Methode der Wahl ist die dynamische Molekularfeld-Theorie (DMFT). Im Rahmen der DMFT wird das Gitter-Modell auf ein selbstkonsistentes Störstellen-Modell abgebildet, welches mittels numerischer Techniken, beispielsweise der Quanten Monte-Carlo (QMC) Methode von Hirsch und Fye, behandelt werden kann. Dieser kombinierte Zugang wird LDA(DFT)+DMFT genannt und gibt uns einen praktikablen Zugang zur realistischen Beschreibung der elektronischen und magnetischen Eigenschaften stark korrelierter Materialien. Einen direkten Vergleich zwischen Theorie und Experiment ermöglichen jedoch erst die linearen Antwortfunktionen, deren Berechnung ein besonderes Problem darstellt.
Im Rahmen meiner Dissertation implementiere ich eine Methode zur Berechnung allgemeiner Antwortfunktionen (Gitter-Suszeptibilitäten) für realistische Modelle korrelierter Materialien. Das Programm zur numerischen Bestimmung dieser Antwortfunktionen basiert auf den folgenden beiden Schritten: i) Die *lokale* Suszeptibilität wirt mittels Hirsch-Fye QMC berechnet. Dabei erweist sich eine neuartige Methode zur Fouriertransformation der Greenschen Funktion innerhalb der QMC Rechnung als wichtiger Schritt. ii) Die Gitter-Suszeptibilität wird als Lösung der Bethe-Salpeter Gleichung bestimmt, wobei die Vertexfunktion durch den lokalen Vertex genähert wird. Als charakteristische Beispiele korrelierter Materialien untersuchen wir die Mott Isolatoren $VOMoO_4$ und Li_2VOSiO_4 mit besonderem Augenmerk auf ihren magnetischen Eigenschaften. Beide Materialien können durch ein J_1-J_2 Quanten-Heisenbergmodell beschrieben werden. Wir bestimmen die $\mathbf{q}$-abhängige Spinsuszeptibilität mit und ohne die Beiträge des lokalen Vertex. Es zeigt sich, dass die Vertex Korrekturen essentiell sind, um ein Curie-Weiss Verhalten zu erhalten. Beide Materialien sind im Grundzustand dreidimensional geordnet, mit ausgeprägter ebenenweiser Ordnung. Die Ordnung in den Ebenen ist kollineare antiferromagnetisch für Li_2VOSiO_4 und Neél antiferromagnetisch für $VOMoO_4$. Wir bestimmen die effektiven Austauschkopplungen aus dem Hochtemperaturverhalten der Suszeptibilität. Wir finden, dass die magnetische Ordnung in beiden Materialien schwach frustriert ist. Darüber hinaus zeigen wir, dass lokale Korrelationen für Li_2VOSiO_4 die Frustration deutlich erhöhen, während sie für $VOMoO_4$ nur einen eine leichte Änderung bewirken. Abschließend untersuchen wir die Bedeutung nicht-lokaler Effekte mittels Cluster DMFT (CDMFT) Rechnungen. Wir finden, dass sie für die magnetische Austauschkopplung nur von untergeordneter Bedeutung sind.

Stichworte: stark korrelierte Materialien, LDA+(Cluster)DMFT, Lineare Antwortfunktions, magnetische Suszeptibilität, lokale-Vertex Näherung, $VOMoO_4$, Li_2VOSiO_4, frustrierte Wechselwirkung, magnetische Austauschkopplung, J_1-J_2 quanten Heisenberg Modell, Curie-Weiss Gesetz.

Linear response functions of Strongly Correlated Materials: LDA+DMFT approach

Abstract: The exotic electronic and magnetic properties of strongly-correlated materials have attracted the attention of theoretical physicists since decades. Strongly correlated materials are a wide class of systems with localized and partially filled d- or f- and, sometimes, p-shells; the description of their properties is one of the central challenges of theoretical condensed-matter physics. To study them, low-energy quantum many-body model Hamiltonians are typically used; in recent years, it has been shown that the parameters of such models can be determined *ab-initio* by using density functional theory (DFT), e.g., in the local density approximation (LDA). Solving the realistic many-body model Hamiltonians built in this way is the major challenge. The state-of-the-art approach is dynamical mean field theory (DMFT). In DMFT, the lattice many-body problem is mapped onto a self-consistence impurity model, which is solved using numerical techniques such as the Hirsch-Fye quantum Monte-Carlo (QMC) method. This approach, known as LDA(DFT)+DMFT, allows us a realistic description of the electronic and magnetic properties of strongly correlated materials. To provide a connection between theory and experiments, however, linear response functions are crucial and they are particularly difficult to obtain. In the present thesis, I implement a method to calculate the general response functions (lattice susceptibility) for real materials. This general response function code is based on the following steps. i) The local susceptibility is calculated via the Hirsch-Fye QMC impurity solver. In order to extract the local susceptibility a new approach is used for computing the Fourier transform of the Green's function inside the QMC. ii) The lattice susceptibility is obtained by solving the Bethe-Salpeter equation using the local vertex approximation; in the latter, the momentum dependent vertex function is replaced by a local quantity. As representative examples, the Mott insulators $VOMoO_4$ and Li_2VOSiO_4 and their magnetic properties are studied. Both materials are considered realizations of the J_1-J_2 quantum Heisenberg model. The $\mathbf{q}$-dependent spin susceptibility is calculated with and without the local vertex contribution. It is shown that the vertex correction is essential to recover the Curie-Weiss law. It is found that, in the ground state, both materials are three dimensionally ordered with in-plane antiferromagnetic collinear order for Li_2VOSiO_4 and in-plane antiferromagnetic Neel order in plain for $VOMoO_4$. The effective exchange couplings are obtained from the high temperature susceptibility. It is shown that both materials are in weak frustration regime. Moreover, it is shown that local correlations push Li_2VOSiO_4 toward the frustration regime while they slightly changes the frustration degree in $VOMoO_4$. The non-local effects are also studied using cluster dynamical mean-field theory (cDMFT). It is found that they affect little the magnetic exchange couplings.

Keywords: Strongly correlated materials, LDA+(cluster)DMFT, Linear response function, Magnetic susceptibility, Local vertex approximation, $VOMoO_4$, Li_2VOSiO_4, Frustration, Magnetic exchange coupling, J_1-J_2 quantum Heisenberg model, Curie-Weiss law.

Contents

1 Introduction **1**

2 Combination of DFT and cluster DMFT **5**
2.1 Density functional theory . . . 5
2.1.1 The Hohenberg-Kohn theorem . . . 5
2.1.2 The Kohn-Sham equations . . . 6
2.1.3 Local density approximation . . . 8
2.2 Low-energy models and downfolding . . . 8
2.3 DMFT and DFT+DMFT . . . 10
2.3.1 DMFT approximation . . . 10
2.3.2 DMFT self-consistent loop . . . 12
2.3.3 Impurity solvers . . . 12
2.3.4 DFT+DMFT method . . . 13
2.3.5 The LDA+cluster DMFT method . . . 15

3 Impurity solver: Hirsch-Fye quantum Monte-Carlo **19**
3.1 Monte-Carlo method . . . 19
3.1.1 Basic concepts of the Monte-Carlo method . . . 20
3.2 Hirsch-Fye quantum Monte-Carlo . . . 23
3.2.1 Derivation of Hirsch-Fye QMC relations . . . 23
3.2.2 Hirsch-Fye QMC algorithm . . . 30
3.2.3 Minus sign problem . . . 31

4 Response function **33**
4.1 Modern experimental techniques . . . 33
4.1.1 Transport experiments . . . 34
4.1.2 Spectroscopic experiments . . . 34
4.2 Linear response theory . . . 36
4.3 General definition of the susceptibility in imaginary time and frequency space . . . 39
4.3.1 Bethe-Salpeter equation: A self-consistent equation for the susceptibility . . . 41
4.3.2 Lattice susceptibility and local vertex approximation within DMFT . . . 43
4.3.3 Legendre representation of the Bethe-Salpeter equation . . . 44
4.3.4 Spin susceptibility . . . 45
4.3.5 Density-density or charge susceptibility . . . 49
4.3.6 Spin-density susceptibility . . . 50
4.4 Properties of the susceptibility . . . 50
4.4.1 Properties of the susceptibility in τ space . . . 50
4.4.2 Properties of the susceptibility in Matsubara frequency space . . . 61
4.4.3 Behavior of the dynamical lattice susceptibility at large $\nu_n, \nu_{n'}$ . . . 66

5 Numerical details of calculating the lattice susceptibility within DMFT **75**
5.1 Algorithm . . . 76
5.2 One-particle Green's function and it's properties . . . 76
5.2.1 One-particle Green's function in τ or ν_n space . . . 76
5.2.2 Properties of one-particle Green's function . . . 77
5.3 Numerical methods for Fourier transform of Green's function . . . 83
5.3.1 1st method: Trapezoidal rule in one and two dimension . . . 83
5.3.2 2nd method: Direct Filon-trapezoidal rule in one and two dimension . . . 86
5.3.3 3rd method: Separating continuous and discontinuous part of the Green's function . . . 91
5.3.4 4th method: Transferring discontinuities of the Green's function to the border . . . 94
5.4 Computing *local* susceptibility using Hirsch-Fye QMC . . . 98
5.4.1 Two-particle correlation function *inside QMC block* . . . 98
5.4.2 Continuous part of the two-particle correlation function (after QMC) . . . 100
5.4.3 The local susceptibility (after QMC) . . . 101
5.4.4 The local (spin or charge) vertex function: A matrix algebra calculation . 105
5.4.5 Bare lattice (spin or charge) susceptibility (after QMC) . . . 108
5.4.6 The lattice (spin or charge) susceptibility . . . 108
5.4.7 Convergency of Matsubara sum: An extrapolation approach . . . 111
5.5 Tests and numerical details . . . 114

6 Nature of magnetism in Li_2VOSiO_4 and $VOMoO_4$ **119**
6.1 Frustrated antiferromagnets . . . 119
6.2 Vanadium oxide compounds: $VOMoO_4$ and Li_2VOSiO_4 . . . 122
6.2.1 Crystal structure . . . 122
6.2.2 Weakly frustrated two-dimensional J_1-J_2 Heisenberg model . . . 123
6.3 Method . . . 125
6.4 Results . . . 127
6.4.1 Electronic structure . . . 127
6.4.2 Static magnetic susceptibility: An LDA+DMFT calculation . . . 128
6.4.3 Static magnetic susceptibility: An LDA+Mean Field calculation . . . 131
6.4.4 Curie-Weiss temperature and magnetic moments . . . 137
6.4.5 Magnetic super-exchange coupling . . . 138
6.4.6 Non-local effects . . . 143

7 Summary **147**
7.1 Summary . . . 147

A Appendix **149**
A.1 Derivation of the general form of the susceptibility . . . 149
A.2 Derivation of the general form of the non-interacting susceptibility . . . 151
A.3 Derivation of the Bethe-Salpeter equation for paramagnetic systems . . . 151

B Appendix **155**
B.1 Derivation of the $\lim_{q\to 0}\chi^{0,zz}(q,\omega_0)$ for a one band system with two sites per unit cell . . . 155
B.1.1 Derivation of $\lim_{q\to 0}\chi^{0,zz}(q,\omega_0)$ using the magnetization . . . 155
B.1.2 Derivation of $\lim_{q\to 0}\chi^{0,zz}(q,\omega_0)$ using Matsubara summations . . . 158

C Appendix **161**
C.1 Matsubara summation . . . 161
C.2 Frequently used Matsubara summations . . . 165

D Appendix **167**
D.1 Legendre polynomial function $P_l(x)$ . . . 167
D.2 Digamma $\Psi(x)$ and Polygamma $\Psi^{(n)}(x)$ function . . . 169

E Appendix **173**
E.1 Single particle Green's function $\mathcal{G}$ in Legendre representation . . . 173
E.1.1 Matsubara Green's function in terms of Legendre coefficient $\mathcal{G}_l$ and high frequencies expansion . . . 177
E.2 Legendre representation of the susceptibility . . . 178
E.3 Legendre representation method in time discretized quantum Monte Carlo . . . 182

F Appendix **185**
F.1 2D trapezoidal Fourier transform of $\mathcal{G}(\tau,\tau')$ . . . 185
F.2 2D Filon-trapezoidal Fourier transform . . . 186
F.3 2D Filon-trapezoidal relations for Fourier transform of $\mathcal{G}(\tau',\tau'')$ . . . 186
F.4 Derivation: Two-particle correlation function inside the QMC . . . 188

G Appendix **193**
G.1 Least squares method . . . 193

Bibliography **195**

CHAPTER 1

Introduction

To calculate the properties of a material (or equivalently, a physical system) one has to solve the Schrödinger equation

$$\hat{H}|\Psi\rangle = E|\Psi\rangle, \tag{1.1}$$

where $|\Psi\rangle$ is the wave function which belongs to eigen energy E and H is the Hamiltonian of the system. Apart from the relativistic effects, the Hamiltonian is given by[1]

$$\hat{H} = \hat{T}_e + \hat{T}_n + \hat{V}_{en} + \hat{V}_{ee} + \hat{V}_{nn}, \tag{1.2}$$

where $\hat{T}_e$ and $\hat{T}_n$, respectively, denote the kinetic energy of electrons and nuclei

$$\hat{T}_e = -\frac{1}{2}\sum_i \nabla^2_{\mathbf{r}_i}, \tag{1.3}$$

$$\hat{T}_n = -\sum_\alpha \frac{1}{2M_\alpha}\nabla^2_{\mathbf{R}_\alpha}. \tag{1.4}$$

$\hat{V}_{ee}$, $\hat{V}_{en}$ and $\hat{V}_{nn}$ are the Coulomb interaction between two electrons, between electrons and nuclei and between two nuclei

$$\hat{V}_{ee} = \frac{1}{2}\sum_{i\neq i'} \frac{1}{|\mathbf{r}_i - \mathbf{r}_{i'}|}, \tag{1.5}$$

$$\hat{V}_{en} = -\sum_{\alpha,i} \frac{Z_\alpha}{|\mathbf{r}_i - \mathbf{R}_\alpha|}, \tag{1.6}$$

$$\hat{V}_{nn} = \frac{1}{2}\sum_{\alpha\neq\alpha'} \frac{Z_\alpha Z_{\alpha'}}{|\mathbf{R}_\alpha - \mathbf{R}_{\alpha'}|}. \tag{1.7}$$

In Eqs. (1.3-1.7), $\mathbf{r}_i$ and $\mathbf{R}_\alpha$ are electron and nucleus positions, respectively. Z_α is the atomic number and M_α the nuclear mass. Since the nucleus mass is much larger than the electron mass, one can use the Born-Oppenheimer approximation to separate dynamic of the electrons and nuclei by considering the product Ansatz $|\Psi\rangle = \Psi(\{\mathbf{r}_i\},\{\mathbf{R}_\alpha\}) = \psi(\{\mathbf{r}_i\};\{\mathbf{R}_\alpha\})\phi(\{\mathbf{R}_\alpha\})$. In this case, the Schrödinger equation for electrons becomes $\hat{H}_e\psi = \varepsilon\psi$ where

$$\hat{H}_e = -\frac{1}{2}\sum_i \nabla^2_{\mathbf{r}_i} + \frac{1}{2}\sum_{i\neq i'} \frac{1}{|\mathbf{r}_i - \mathbf{r}_{i'}|} - \sum_{\alpha,i} \frac{Z_\alpha}{|\mathbf{r}_i - \mathbf{R}_\alpha|} + \frac{1}{2}\sum_{\alpha\neq\alpha'} \frac{Z_\alpha Z_{\alpha'}}{|\mathbf{R}_\alpha - \mathbf{R}_{\alpha'}|}. \tag{1.8}$$

The exact solution of this equation is impossible to find due to its many-body nature. This complexity becomes more clear if one tries to solve the Schrödinger equation for a system with

[1] We choose *atomic units* to write the Hamiltonian wherein e, m_e and $1/4\pi\varepsilon_0$ have a value of 1.

N_e electrons. In this case, the wave function ψ, for a specific spin, depends on dimension d times N_e coordinates. Considering a grid with L points in each coordinate, one has to store L^{dN_e} values of the wave function. This becomes an unfeasible task even for moderated values of N_e, d and L.[2] For this reason approximative approaches are necessary to develop.

The most popular and successful approximate method, applied in condensed matter physics, chemistry and material science, is *density functional theory* (DFT) [1, 2]. DFT is a computational method to investigate the electronic structure of the many-body system. Within the DFT, the properties of the system are determined by using the functional of the ground state density. In this method, a fully interacting many-body system is mapped onto a fictitious non-interacting one with an effective external potential under the constraint that the ground state density of these two systems are identical. Since the functional is unknown, approximations such as local density approximation (LDA) are used. Though the DFT within the LDA works well for a vast class of materials, it often fails to investigate physical properties of strongly correlated materials [3, 4]. In this class of materials, the Coulomb interaction between electrons is comparable or larger than their kinetic energies and causes strong correlations between them. Transition-metal and rare-earth compounds with partially filled d- or f-shells belong to the category of the strongly correlated materials. To correct the weakness of DFT for investigating the rich phenomena of strongly correlated materials, alternative methods should be devised.

Most of the methods proposed for studying the strongly correlated systems are based on model Hamiltonians such as the Hubbard model [5, 6] and the Anderson impurity model [7]. Even though the effective Hamiltonians are simple, they are still a full many-body problem and, in general, there is no exact solution for them (apart from some special cases). Hence, numerical techniques like different kinds of quantum Monte-Carlo (QMC) methods (e.g., [8]), exact diagonalization (ED) (e.g., [9]), etc should be employed to study the model Hamiltonian. However, realistic model Hamiltonians which are implemented to study lattice systems and real materials, are in general intractable. For instance, the QMC often suffers from the infamous minus sign problem if the number of sites N_s in the model increases (e.g., [10]). In the exact diagonalization, the Hubbard model is described by a $4^{N_s} \times 4^{N_s}$ matrix. Exponential growth of the matrix size does not allow to study the model with large number of sites by using current computer facilities. Accordingly, alternative and approximative approaches are required to describe more general Hubbard models which can be used to explain real materials.

A very successful method which has been developed 25 years ago is the dynamical mean field theory (DMFT) [11, 12]. Within the DMFT approach, the lattice Hubbard model is mapped onto a self-consistent impurity problem which is still a many-body problem but exactly solvable by using numerical techniques. The DMFT approximation becomes exact in infinite dimension (or infinite coordination number). In finite dimension (or coordination number) it turned out to be, however, an excellent approximation. In the DMFT approximation, the most challenging part is the solution of the impurity model. One of the most flexible impurity solvers is Hirsch-Fye QMC [13]. Recently several classes of continuous time QMC have been devised which overcome some of the limitations of the Hirsch-Fye QMC [14].

To study the strongly correlated *real materials*, model Hamiltonian parameters (such as Coulomb interaction U and band width W) can be determined from the first principles using

[2] For instance, consider iron atom with $N_e = 26$, $d = 3$. Taking into account a grid with $L = 20$ points in x, y and z direction, $\sim 3 \times 10^{101}$ values of the wave function should be stored which exceed the total number of atoms in the universe ($\sim 10^{78}$-10^{82} atoms).

density functional theory. Then, the DMFT solution of the *ab-initio* model Hamiltonian provides the physical properties of the highly correlated real materials. This approach, known as DFT+DMFT method, is the state-of-the-art approach to study strongly correlated real materials [15].

It is always important how the current theoretical approaches are successful in describing the experimental data and/or in predicting physical features of the system or real materials. The quantity that provides a connection between experiment and theory is "*response function*". Within an experiment, the response function (e.g. magnetic response χ) is obtained by investigating the relation between a small external field F (e.g. static magnetic field $\mathbf{B}$) applied on the sample and the measured observable X (e.g. magnetization $\mathbf{M}$). Theoretically, the response function is just a correlation function of operator $\hat{X}$ (e.g. magnetization-magnetization or equivalently spin-spin correlation function). In the DFT+DMFT approach, evaluation of the general response function over all the Brillouin zone (lattice susceptibility) is a feasible but difficult task from numerical point of view. The difficulty is not only due to the many-body nature of the self-consistent impurity problem but also due to the complexity of one of the response function's ingredients, the vertex function. In DFT+DMFT, the lattice susceptibility is obtained by solving the Bethe-Salpeter equation, in which the momentum dependent vertex function is replaced by a local quantity [12].

In this thesis, we mainly focus on the computation of the lattice susceptibility for the strongly correlated real materials by using the LDA+DMFT approximation based on the Hirsch-Fye QMC impurity solver. We calculate the lattice magnetic susceptibility for two transition-metal oxides, $VOMoO_4$ and Li_2VOSiO_4, which are considered as a prototype of the two-dimensional J_1-J_2 Heisenberg model [16, 17, 18]. We employ the magnetic susceptibility to study the nature of magnetic interaction of these two Vanadium compounds.

This thesis is organized as follows:

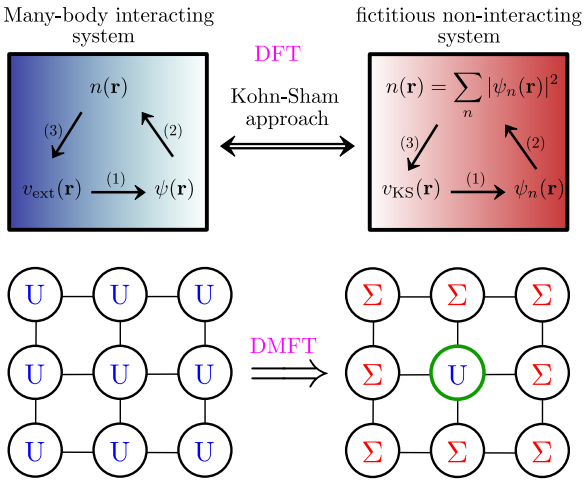

In the first part of the chapter 2, we overview the DFT by describing the Hohenberg-Kohn theorem and the Kohn-Sham equations. Then the LDA is introduced as a successful approximation to study electronic structure of weakly correlated materials. In the second part, the DMFT and its extension, cluster DMFT (cDMFT), are explained briefly. We finish the chapter 2 by a short description on combination of the DFT and the (c)DMFT.

Chapter 3 focuses on Monte-Carlo algorithm and the Hirsch-Fye QMC. Since the Hirsch-Fye QMC is our favorite impurity solver to solve the impurity problem and calculate the lattice susceptibility, we derive its equations in details.

Chapter 4 is allocated to the response function. Since our final goal is to compute the lattice susceptibility for strongly correlated materials, we discuss the response function of a

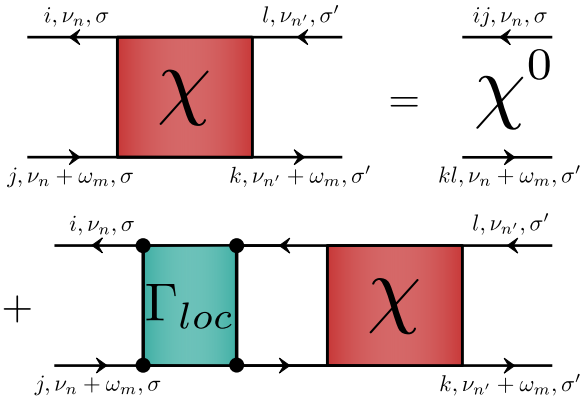

system in details. Furthermore, we derive the lattice susceptibility relation which is used within the LDA+(c)DMFT approach. Intrinsic properties of the susceptibility are crucial for programming the response function in the LDA+DMFT approach. For this reason, we analytically derive these properties for the lattice and local susceptibility.

In chapter 5, we explain the numerical algorithm that we employ to compute the lattice susceptibility. The bottleneck of the computation procedure is the determination of the local susceptibility with the Hirsch-Fye QMC. This can be very time consuming, although the calculation is performed only once at the end of the self-consistency loop. To obtain the local susceptibility, the Fourier transform of the *QMC Green's function* (not physical Green's function) is very important. We evaluate the Fourier transform of the QMC Green's function by shifting the discontinuities of the Green's function to border and using the two-dimensional Filon-Trapezoidal approximation, which turns out to be particularly efficient. Once the local susceptibility is derived, we are able to compute the local vertex function. Having the local vertex function and lattice Green's function from the LDA+(c)DMFT, we can use the Bethe-Salpeter equation to obtain the lattice susceptibility.

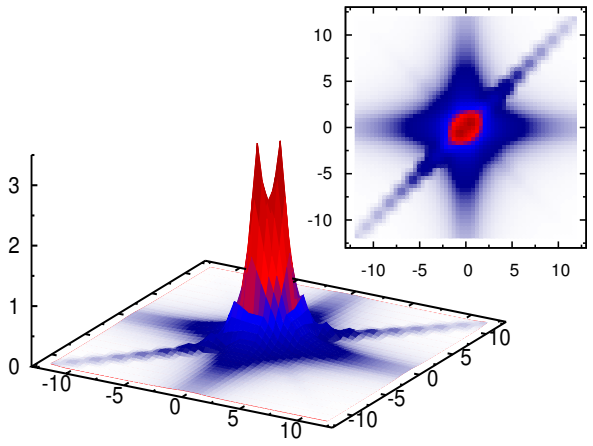

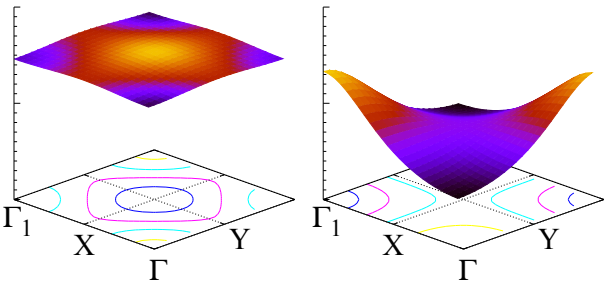

Chapter 6 presents our study on the nature of the magnetic interactions in two Vanadium compounds, $VOMoO_4$ and Li_2VOSiO_4. In this study, with the help of the static spin susceptibility, we discuss some physical features of $VOMoO_4$ and Li_2VOSiO_4 compounds such as magnetic ordering, effect of the local and non-local correlations on the frustration degree, importance of off-plane magnetic interactions and magnetic super-exchange couplings.

Chapter 7 summarizes the thesis.

CHAPTER 2

Combination of DFT and cluster DMFT

In this chapter, we describe briefly density functional theory (DFT) and its local density approximation (LDA) (for a general but short review see e.g. [19]). Although DFT is a very powerful approach to describe physical properties of a real material, it is not able to explain strongly correlated systems, i.e., systems in which Coulomb interaction is significant. To describe such interesting systems, we use the dynamical mean field theory (DMFT) approximation with the DFT (the so called DFT+DMFT approach). Here we discuss how the DFT+DMFT method can be implemented to study complicated real materials with partially filled d- or f-orbitals [20, 21, 22].

Contents

2.1 Density functional theory 5
2.1.1 The Hohenberg-Kohn theorem 5
2.1.2 The Kohn-Sham equations 6
2.1.3 Local density approximation 8
2.2 Low-energy models and downfolding 8
2.3 DMFT and DFT+DMFT 10
2.3.1 DMFT approximation 10
2.3.2 DMFT self-consistent loop 12
2.3.3 Impurity solvers 12
2.3.4 DFT+DMFT method 13
2.3.5 The LDA+cluster DMFT method 15

2.1 Density functional theory

2.1.1 The Hohenberg-Kohn theorem

In 1963, P. Hohenberg and W. Kohn proved that the knowledge of charge density $n(\mathbf{r})$ is sufficient to describe the ground state properties of a quantum mechanical system [23]. Using the density $n(\mathbf{r})$, the number of particles N and the external potential $v_{\text{ext}}(\mathbf{r})$

$$v_{\text{ext}}(\mathbf{r}) = -\sum_{i,\alpha} \frac{Z_\alpha}{|\mathbf{r}_i - \mathbf{R}_\alpha|} \tag{2.1}$$

of the interacting electrons system are determined uniquely (one-to-one correspondence between $n(\mathbf{r})$ and $v_{\text{ext}}(\mathbf{r})$). The Hamiltonian is then obtained by the calculated external potential $v_{\text{ext}}(\mathbf{r})$. Thus the ground state density $n(\mathbf{r})$ provides the Hamiltonian of the system and determines implicitly the relevant physical quantities such as the ground state wave function, ground

state energy, etc. As a result, the ground state energy is a functional of the electron density $n(\mathbf{r})$ and is minimized by the ground state density.

$$\begin{aligned} E[n(\mathbf{r})] &= \langle\psi|\hat{T}_e + \hat{V}_{ee}|\psi\rangle + \int d\mathbf{r}\; v_{\text{ext}}(\mathbf{r})n(\mathbf{r}) + \frac{1}{2}\sum_{\alpha\neq\alpha'}\frac{Z_\alpha Z_{\alpha'}}{|\mathbf{R}_\alpha - \mathbf{R}_{\alpha'}|} \\ &= F[n(\mathbf{r})] + \int d\mathbf{r}\; v_{\text{ext}}(\mathbf{r})n(\mathbf{r}) + E_{nn}. \end{aligned} \tag{2.2}$$

In this relation, $|\psi\rangle$ is the ground state of the system which is a functional of the density $n(\mathbf{r})$ and E_{nn} the energy shift due to nuclei-nuclei interaction. $F[n(\mathbf{r})] = T_e[n(\mathbf{r})] + V_{ee}[n(\mathbf{r})] = \langle\psi|\hat{T}_e + \hat{V}_{ee}|\psi\rangle$ is the sum of the kinetic $T_e[n(\mathbf{r})]$ and electron-electron interaction energy $V_{ee}[n(\mathbf{r})]$. The functional $F[n(\mathbf{r})]$ is universal and is identical for all the systems. However, it is an *unknown* functional.

Calculating the density $n(\mathbf{r})$ for the many-body Hamiltonian (1.8) remains impossible in the general case. However, in 1965, W. Kohn and L. Sham proposed to obtain the density $n(\mathbf{r})$ by solving an auxiliary non-interacting problem whose density $n_0(\mathbf{r})$ is the same as the one of the interacting system $n(\mathbf{r})$ [24]. This approach, schematically, is shown in Fig. 2.1 and discussed in the following.

2.1.2 The Kohn-Sham equations

Based on the Kohn-Sham approach [24], it is possible to obtain the ground state energy and density $n(\mathbf{r})$ of a many-body interacting system by solving the Schrödinger equation of a fictitious non-interacting one, providing that the external potential of the non-interacting system $v_{\text{R}}(\mathbf{r})$ is chosen in a way that the density of non-interacting system $n_0(\mathbf{r})$ equals to the density of the interacting one $n(\mathbf{r})$ (See Fig. 2.1).

$$n(\mathbf{r}) = n_0(\mathbf{r}) = \sum_{n}^{\text{occ}} |\psi_n(\mathbf{r})|^2 . \tag{2.3}$$

Considering the functionals $T_0[n(\mathbf{r})]$ as the kinetic energy of the non-interacting system, $V_H[n(\mathbf{r})] = \frac{1}{2}\int d\mathbf{r}\int d\mathbf{r}'\;\frac{n(\mathbf{r})n(\mathbf{r}')}{|\mathbf{r}-\mathbf{r}'|}$ the classical electrostatic Coulomb interaction (called Hartree term), and $E_{xc}[n(\mathbf{r})]$ the small exchange-correlation correction, the universal functional $F[n(\mathbf{r})]$ can be rewritten as follows

$$\begin{aligned} F[n(\mathbf{r})] &= T_e[n(\mathbf{r})] + V_{ee}[n(\mathbf{r})] \\ &= T_0[n(\mathbf{r})] + V_H[n(\mathbf{r})] + E_{xc}[n(\mathbf{r})] \\ &= T_0[n(\mathbf{r})] + \frac{1}{2}\int d\mathbf{r}\int d\mathbf{r}'\;\frac{n(\mathbf{r})n(\mathbf{r}')}{|\mathbf{r}-\mathbf{r}'|} + E_{xc}[n(\mathbf{r})], \end{aligned} \tag{2.4}$$

where the exchange-correlation energy functional is

$$E_{xc}[n(\mathbf{r})] = T_e[n(\mathbf{r})] - T_0[n(\mathbf{r})] + V_{ee}[n(\mathbf{r})] - V_H[n(\mathbf{r})]. \tag{2.5}$$

Using this functional, the total energy functional $E[n(\mathbf{r})]$ is

$$E[n(\mathbf{r})] = T_0[n(\mathbf{r})] + \int d\mathbf{r}\; v_{\text{ext}}(\mathbf{r})n(\mathbf{r}) + \frac{1}{2}\int d\mathbf{r}\int d\mathbf{r}'\;\frac{n(\mathbf{r})n(\mathbf{r}')}{|\mathbf{r}-\mathbf{r}'|} + E_{xc}[n(\mathbf{r})] + E_{nn}. \tag{2.6}$$

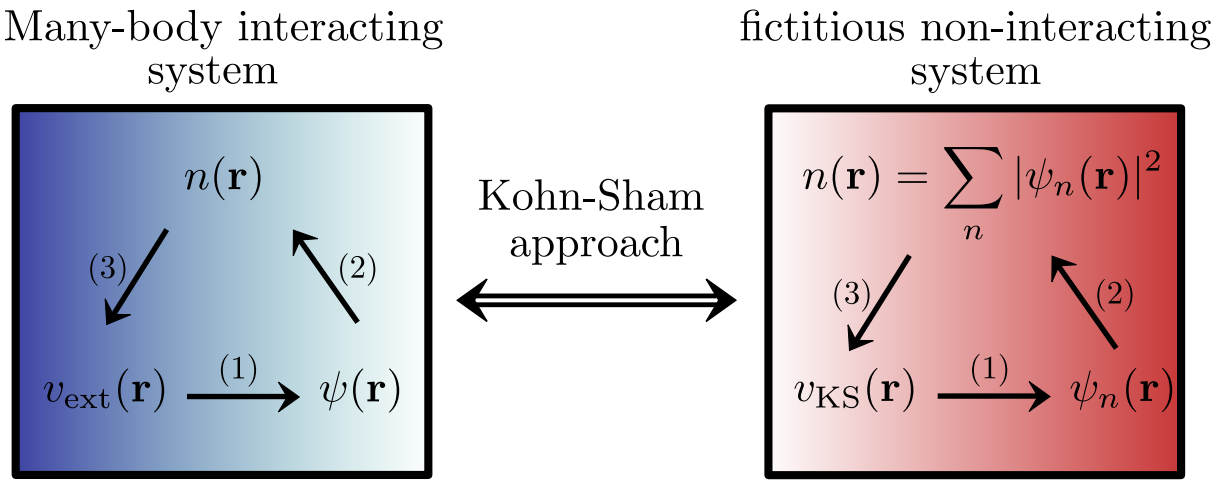

Figure 2.1: Schematic figure of how a fully interacting many-body system can be mapped onto a fictitious non-interacting one through the Kohn-Sham approach. v_{KS} is external potential of the non-interacting problem. (1): Using the (Kohn-Sham) potential v_{KS}, the ground state wave function is derived by solving the schrödinger equation. (2) Once the wave function is obtained, the ground state density is calculated. (3) Since the external potential is a functional of the ground state density, a new potential v is obtained. Theses steps are done until convergency is reached. According to Kohn-Sham approach, the ground state density of the fictitious non-interacting system is equal to the ground state density of a full interacting many-body system. Therefore, the computed $n(\mathbf{r})$ can be used to describe the ground state properties of the full interacting system.

By minimizing the total energy functional with the constraint $N = \int d\mathbf{r}\; n(\mathbf{r})$, where N is the total number of electrons, the Kohn-Sham equation is obtained as below

$$\left(-\frac{1}{2}\nabla^2 + v_{\text{R}}(\mathbf{r})\right)\psi_n(\mathbf{r}) = \varepsilon_n \psi_n(\mathbf{r}), \tag{2.7}$$

where the eigenvalues ε_n are the Lagrange multipliers used to minimize the energy functional considering the total number of particle N constraint. The reference potential v_{R} is

$$v_{\text{R}}(\mathbf{r}) = -\sum_{\alpha} \frac{Z_\alpha}{\mathbf{r} - \mathbf{R}_\alpha} + \int d\mathbf{r}'\; \frac{n(\mathbf{r}')}{|\mathbf{r} - \mathbf{r}'|} + v_{xc}(\mathbf{r}), \tag{2.8}$$

in which $v_{xc}(\mathbf{r})$ is called exchange and correlation potential, which depends on the density distribution and is obtained by

$$v_{xc}(\mathbf{r}) = \frac{\delta E_{xc}[n(\mathbf{r})]}{\delta n(\mathbf{r})}. \tag{2.9}$$

Equations (2.3), (2.7) and (2.9) are called Kohn-Sham equations and should be solved self-consistently. Starting form an initial guess for density $n_{\text{init}}(\mathbf{r})$, the Kohn-Sham equations are solved numerically to obtained the new density. This procedure continues until the converged density is derived.

2.1.3 Local density approximation

In order to study the ground state properties of a many-body system, the self-consistent Kohn-Sham equations should be exactly solved. For this purpose, it is necessary to know the exact exchange-correlation energy functional $E_{xc}[n(\mathbf{r})]$. However, $E_{xc}[n(\mathbf{r})]$ is an unknown functional and has to be approximated. Common approximations have a form as

$$E_{xc}[n(\mathbf{r})] = \int d\mathbf{r}\; e_{xc}\left(\mathbf{r}; [\tilde{n}(\mathbf{r})]\right) n(\mathbf{r}), \tag{2.10}$$

wherein $e_{xc}\left(r; [\tilde{n}(\mathbf{r})]\right)$ is the exchange-correlation functional energy per particle at $\mathbf{r}$ and $\tilde{n}(\mathbf{r})$ the density distribution around $\mathbf{r}$. The simplest form of approximation is the *local density approximation (LDA)* in which $e_{xc}\left(r; [\tilde{n}(\mathbf{r})]\right)$ is replaced by the exchange-correlation energy of uniform electron gas e_{ex}^{LDA} which is a *function* of density $n(\mathbf{r})$. Therefore, within the LDA, the exchange-correlation energy functional is approximated by

$$E_{xc}^{\mathrm{LDA}}[n(\mathbf{r})] = \int d\mathbf{r}\; e_{xc}^{\mathrm{LDA}}\left(n(\mathbf{r})\right) n(\mathbf{r}). \tag{2.11}$$

The exchange energy of the uniform electron gas can be calculated analytically [25]

$$e_{x}^{\mathrm{LDA}}\left(n(\mathbf{r})\right) = -\frac{3}{4}\left(\frac{3}{\pi}\right)^{1/3} \int d\mathbf{r}\; n(\mathbf{r})^{4/3}. \tag{2.12}$$

The correlation energy is, instead, computed numerically using quantum Monte-Carlo technique and fitting data for different values of $n(\mathbf{r})$ [26].

Although LDA works well to capture some properties of solids such as fermi surfaces and electronic band structures, it fails to describe essential features of strongly correlated materials, e.g., Mott-insulators, even in qualitative level. The main reason of this failure is the many-body effects between very localized electrons in d- or f-shells, which strongly interact through a large Coulomb interaction U. Electrons lose their individuality in such a system so that their dynamics highly depends on the ones which feel the Coulomb interaction U (i.e., particles are highly correlated). For instance, $KCuF_3$ is a well-known paramagnetic insulator with partially filled d- shell ($3d^9$) (see e.g. [27]). However, for such materials (nonmagnetic crystal with odd electrons per unit cell), the LDA predicts metallic regime due to spin degeneracy [22, 27]. To study physics of the strongly correlated systems, model Hamiltonians accompanied by a many-body method, for instance dynamical mean field theory (DMFT), are used (for a detailed review article, see e.g. [12]).

2.2 Low-energy models and downfolding

To capture low-energy physics of a system, in the model Hamiltonian, only the relevant bands (which are close to the Fermi level) and interactions (which are important for the case studied) are considered. High energy degrees of freedom are projected out (downfolded) in the sprit of Wilson renormalization group. Through the downfolding procedure, the effects of the high energy states are implicitly included to low energy ones.

The downfolding procedure is done as follows (see e.g. [28]): the Hamiltonian of the system is divided into the low-energy states and 'other' states which will be integrated out,

$$H = \begin{pmatrix} H_{00} & H_{01} \\ H_{10} & H_{11} \end{pmatrix}. \tag{2.13}$$

Here, H_{00} and H_{11} are block matrices (reduced Hilbert space) related to low- and high-energy states of the system, respectively. Furthermore, H_{01} and H_{10} describe transitions between low- and high-energy subspaces. The low-energy part of the resolvent $(\varepsilon - H)^{-1}_{00}$ is obtained easily by using inversion through partitioning of Eq. (2.13)

$$(\varepsilon - H)^{-1}_{00} = \left(\varepsilon - \left[H_{00} + H_{01}\left(\varepsilon - H_{11}\right)^{-1} H_{10}\right]\right)^{-1}, \tag{2.14}$$

where the energy dependent effective Hamiltonian (describes the physics of the full system) is

$$H_{\text{eff}}(\varepsilon) = H_{00} + H_{01}\left(\varepsilon - H_{11}\right)^{-1} H_{10}. \tag{2.15}$$

In most of the cases, one is interested to eigenenergies close to the ground state one. If the hopping matrix elements in H_{01} and H_{10} are small and the eigenenergies of H_{00} are well separated from those in the rest of the H, the energy dependent effective Hamiltonian $H_{\text{eff}}(\varepsilon)$ can be approximated by energy independent one $H_{\text{eff}}(\varepsilon_0)$

$$H_{\text{eff}}(\varepsilon_0) = H_{00} + H_{01}\left(\varepsilon_0 - H_{11}\right)^{-1} H_{10}, \tag{2.16}$$

where ε_0 is a typical energy for the states lying in the reduced Hilbert space. $H_{\text{eff}}(\varepsilon_0)$ is now the effective Hamiltonian which can be employed to extract low energy physics of a system.

In order to study a system with a narrow band at Fermi level, the most simple model that can be used is the Hubbard model

$$H = \sum_{ij}\sum_{\sigma} t_{ij} c^{\dagger}_{i\sigma} c_{j\sigma} + U \sum_{i} n_{i\uparrow} n_{i\downarrow} = \hat{H}_0 + \hat{U}, \tag{2.17}$$

where $c^{\dagger}_{i\sigma}$ ($c_{i\sigma}$) creates (annihilates) an electron at site i with spin $\sigma =\uparrow,\downarrow$ and $\hat{n}_{i\sigma} = c^{\dagger}_{i\sigma} c_{i\sigma}$ number of electron operator in state $i\sigma$. t_{ij} is the hopping matrix elements and U the on-site Coulomb repulsion. This simple model is able to cover the physics of a system from non-interacting limit ($U \ll t$) to a full interacting one ($U \gg t$). Although this model is extremely simple, it can be solved exactly only in some special cases (e.g. in one dimension [29]). Also in the case of a correlated system, where the Hubbard Coulomb interaction U is equal or greater than the band width W of the system ($U \geq W$), perturbation theory fails (for a very simple example see [30]). Thus, one should use a non-perturbative approach to study such interesting systems. As a non-perturbative method, the dynamical mean field theory (DMFT) and its extensions, is one of the successful methods which provided a huge progress in understanding the nature of metal-insulator transition even in real materials [20, 21, 22, 12].

In the following, we explain DMFT approximation and describe how *ab-initio* calculations can be done through DFT+DMFT method. Furthermore, we discuss cluster DMFT (cDMFT) and DFT+cDMFT in order to study non-local correlations in the highly correlated systems.

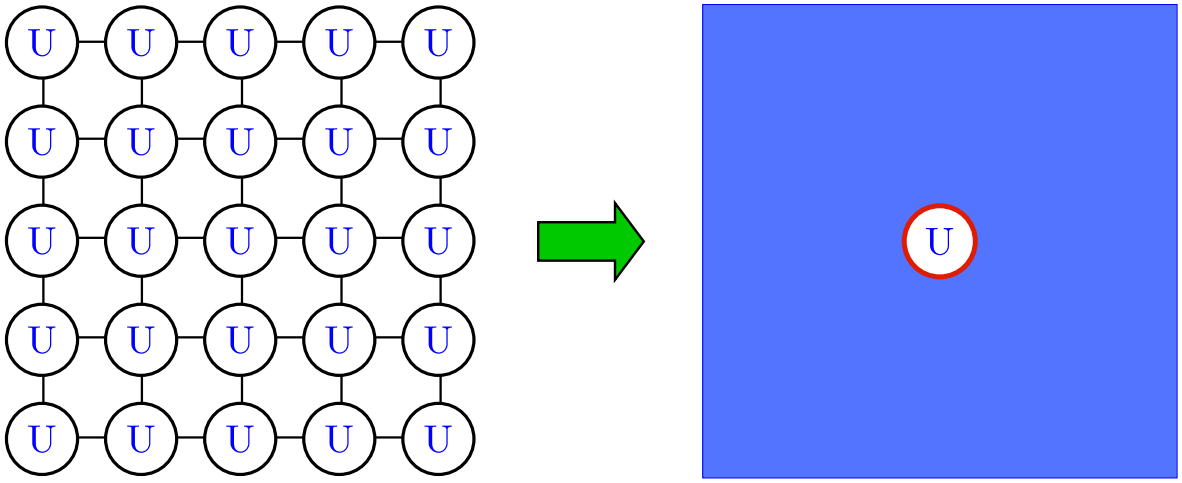

Figure 2.2: In the DMFT, a lattice model (left) is mapped onto an impurity one (right). In the lattice many-body model, the Coulomb interaction U exists for every site, while in the impurity model the interaction is described by the self-energy, except for the impurity site.

2.3 DMFT and DFT+DMFT

2.3.1 DMFT approximation

Dynamical mean field theory (DMFT) is based on the fact that the self-energy of a full interacting system $\Sigma(\mathbf{k}, i\nu_n)$ in large space dimension $d \to \infty$ or equivalently large coordination number $z \to \infty$ is momentum independent [31, 32, 33]

$$\Sigma(\mathbf{k}, i\nu_n) = \Sigma(i\nu_n).$$

It means that the self-energy matrix $\Sigma_{ij}(i\nu_n)$ in real space representation has non-zero elements only for $i = j$ (i.e., local elements)

$$\Sigma_{ij}(i\nu_n) = \Sigma_{ij}(i\nu_n)\delta_{ij}.$$

Therefore, in the limit of $d \to \infty$ or $z \to \infty$, the problem of the lattice Hubbard model in Eq. (2.13) can be reduced (or mapped) to the problem of Anderson impurity one with effective bath parameters

$$H_{\text{imp}} = \sum_{ij}\sum_{\sigma} t_{ij} c^{\dagger}_{i\sigma} c_{j\sigma} + \sum_{i}\sum_{\sigma}\left[V_i c^{\dagger}_{i\sigma} d_{\sigma} + h.c.\right] + \varepsilon_d \sum_{\sigma} d^{\dagger}_{\sigma} d_{\sigma} + U n_{\uparrow} n_{\downarrow}. \tag{2.18}$$

This model can be solved exactly through various numerical methods such as different flavors of the quantum Monte-Carlo. In the Anderson impurity model, Eq. (2.18), $d^{\dagger}_{\sigma}$ (d_{σ}) creates (annihilates) electron with spin σ on impurity site, while $c^{\dagger}_{\sigma}$ and c_{σ} are creator and annihilator operators of the non-interacting electrons. The operator $n_{\sigma} = d^{\dagger}_{\sigma} d_{\sigma}$ acts on the impurity site, described by impurity states $|0\rangle$, $|\uparrow\rangle$, $|\downarrow\rangle$ and $|\uparrow\downarrow\rangle$, and ε_d is the onsite energy of the impurity site. Each electron in the bath of non-interacting electrons may have a transition to the impurity site and vice versa with transition amplitude V. Furthermore, t_{ij} is the hopping matrix element of the non-interacting electrons. The effective parameters V and t in the Anderson impurity

Hamiltonian (2.18) should be determined in such a way that the impurity Green's function $\mathcal{G}_{\rm imp}$ coincides with the single site (local) Green's function of the lattice model

$$\underbrace{\mathcal{G}(i\nu_n) = \frac{1}{N_{\mathbf{k}}}\sum_{\mathbf{k}} \mathcal{G}(\mathbf{k}, i\nu_n)}_{\text{single site lattice Green's function}} \equiv \mathcal{G}_{\rm imp}(i\nu_n). \tag{2.19}$$

In this model, the impurity Green's function can be calculated by using the equation of motion [21].

$$\mathcal{G}_{\rm imp}(i\nu_n) = \left[i\nu_n - \varepsilon_d + \mu - \frac{1}{N_{\mathbf{k}}}\sum_{\mathbf{k}} \frac{|V(\mathbf{k})|^2}{i\nu_n - \varepsilon_{\mathbf{k}} + \mu} - \Sigma_{\rm imp}(i\nu_n) \right]^{-1}, \tag{2.20}$$

where $\nu_n = (2n+1)\pi/\beta$ is the fermionic Matsubara frequency, μ chemical potential, and $\varepsilon_{\mathbf{k}} = \sum_j t_{ij}\, e^{i\mathbf{k}.(\mathbf{R}_i - \mathbf{R}_j)}$.[1] The last term of Eq. (2.20), i.e., $\Sigma_{\rm imp}$, is related to Coulomb interaction on the impurity site. The other term, the so-called hybridization function,

$$\Delta(i\nu_n) = \frac{1}{N_{\mathbf{k}}}\sum_{\mathbf{k}} \frac{|V(\mathbf{k})|^2}{i\nu_n - \varepsilon_{\mathbf{k}} + \mu}, \tag{2.21}$$

comes from the hybridization of the impurity site with the bath of non-interacting electrons. In fact the effective parameters V and t appear only through the hybridization function. From Eq. (2.20), one can recognize that the bath (non-interacting) Green's function (wherein the Coulomb interaction U is switched off) is

$$G_0(i\nu_n) = \left[i\nu_n - \varepsilon_d + \mu - \frac{1}{N_{\mathbf{k}}}\sum_{\mathbf{k}} \frac{|V(\mathbf{k})|^2}{i\nu_n - \varepsilon_{\mathbf{k}} + \mu} \right]^{-1}, \tag{2.22}$$

and the impurity self-energy can be derived in terms of the impurity Green's function and the bath Green's function

$$\Sigma_{\rm imp}(i\nu_n) = G_0^{-1}(i\nu_n) - \mathcal{G}_{\rm imp}(i\nu_n). \tag{2.23}$$

Effective parameters in the hybridization function, i.e., V and t, are then determined from Eqs. (2.20, 2.22) and (2.23) self-consistently.

Up to now DMFT method maps the lattice Hubbard Hamiltonian onto an effective Anderson impurity model which is exact for $d \to \infty$ or $z \to \infty$ because physical quantities of the lattice model such as self-energy and Green's function are local in those limits. But, the DMFT approach can be used as an *approximation* for finite dimension d or coordination number z [32]. In the DMFT approximation, due to the mapping of the lattice model to an effective impurity one, spatial fluctuations are neglected, while dynamical onsite fluctuations are still considered. Therefore, the momentum dependence of the lattice self-energy $\Sigma(\mathbf{k}, i\nu_n)$ is ignored and approximated by self-energy of the impurity site (or local self-energy)

$$\Sigma(\mathbf{k}, i\nu_n) \approx \Sigma_{\rm imp}(i\nu_n). \tag{2.24}$$

[1] $\mathcal{G}(i\nu_n)$ is Fourier integral of the $\mathcal{G}(\tau)$ where τ is imaginary time. See Sec. 5.2.1 for detailed explanations about the Green's function and its properties.

Using this approximation, Eq. (2.19) can be rewritten as

$$\begin{aligned} \mathcal{G}(i\nu_n) &= \frac{1}{N_{\mathbf{k}}}\sum_{\mathbf{k}}\frac{1}{i\nu_n - \varepsilon_{\mathbf{k}} + \mu - \Sigma(\mathbf{k}, i\nu_n)} \\ &\approx \frac{1}{N_{\mathbf{k}}}\sum_{\mathbf{k}}\frac{1}{i\nu_n - \varepsilon_{\mathbf{k}} + \mu - \Sigma_{\mathrm{imp}}(i\nu_n)} \equiv \mathcal{G}_{\mathrm{imp}}(i\nu_n). \end{aligned} \tag{2.25}$$

Eqs. (2.23) and (2.25) are solved self-consistently to fix the effective impurity parameters and provide an approximate scheme of physics of the lattice Hubbard model. In the following, an iterative solution of these equations are explained.

2.3.2 DMFT self-consistent loop

Within the DMFT approach, the self-consistent DMFT equations (2.23) and (2.25) are solved iteratively based on the following steps.

1. The single site (or local) lattice Green's function is calculated by Eq. (2.25). The input for the self-energy in the first iteration could be, .e.g., zero (i.e., non-interacting system).

$$\mathcal{G}(i\nu_n) = \frac{1}{N_{\mathbf{k}}}\sum_{\mathbf{k}}\frac{1}{i\nu_n - \varepsilon_{\mathbf{k}} + \mu - \Sigma_{\mathrm{imp}}(i\nu_n)}.$$

2. The DMFT self-consistency condition, i.e., $\mathcal{G}(i\nu_n) = \mathcal{G}_{\mathrm{imp}}(i\nu_n)$ is applied first. Then by using the Dyson equation (2.23), the bath Green's function G_0 is calculated.

$$G_0^{-1}(i\nu_n) = \mathcal{G}_{\mathrm{imp}}^{-1}(i\nu_n) + \Sigma_{\mathrm{imp}}(i\nu_n).$$

3. The impurity Anderson model with this bath Green's function is solved by using an impurity solver. Then, the single impurity Green's function $\mathcal{G}_{\mathrm{imp}}(i\nu_n)$ is obtained.

4. The Dyson equation (2.23) is used again to compute a new approximation for the self-energy.

$$\Sigma_{\mathrm{imp}}(i\nu_n) = G_0^{-1}(i\nu_n) - \mathcal{G}_{\mathrm{imp}}(i\nu_n).$$

   This self-energy is used to obtain the new single site lattice Green's function in step 1. Iterations are going on till the self-energy used in step 1 as input becomes equal to the self-energy calculated in the step 4 with a given accuracy.

2.3.3 Impurity solvers

The most difficult step in iterative solution of the self-consistent DMFT equations is solving the impurity model to derive $\mathcal{G}_{\mathrm{imp}}$. Despite its simplicity, the impurity model is still a full many-body model. However, several numerically exact methods can be used to solve it.

- Different types of the quantum Monte-Carlo (QMC) method like Hirsch-Fye QMC [13], continuous time QMC (for a review see [14]) based on hybridization expansion (CT-HYB) [34, 35, 36] or interaction expansion (CT-INT) [37, 38].

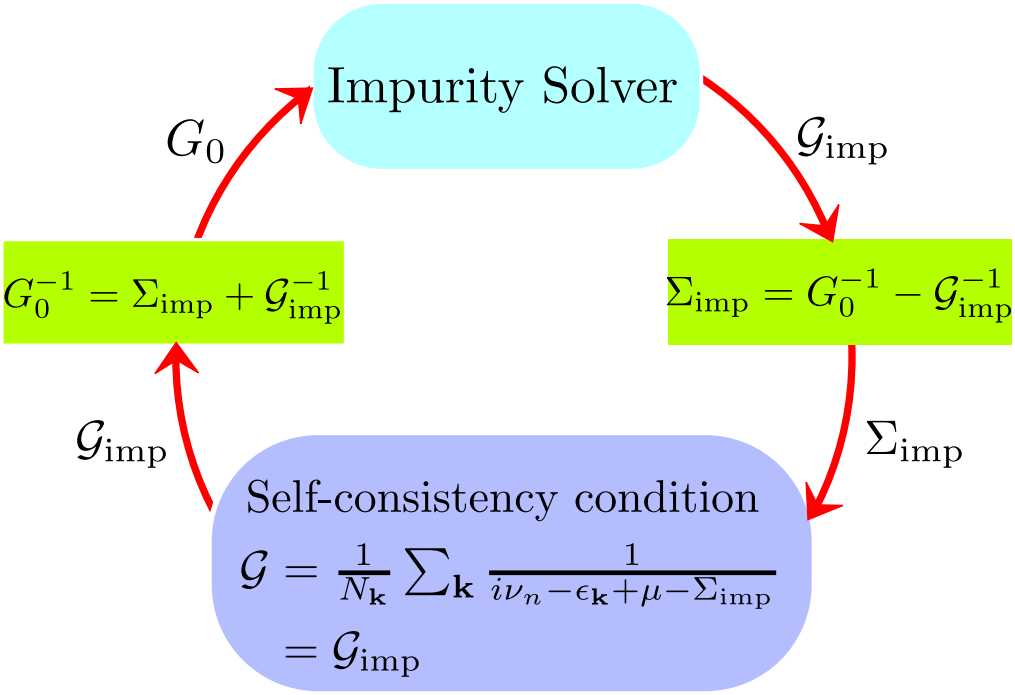

Figure 2.3: Iterative solution of the self-consistence DMFT equations.

- Exact diagonalization (ED) [39, 40, 22]
- Numerical renormalization group (NRG) [41]

and some approximate schemes like iterative perturbation theory (IPT) [32, 42].

In the current thesis, we use Hirsch-Fye QMC as an impurity solver. We will explain Hirsch-Fye algorithm in Sec. 3.2 in details.

2.3.4 DFT+DMFT method

Simple model Hamiltonians as described in Sec. 2.2 are very useful to understand the physics of strongly correlated systems such as Mott-insulators, metal-insulator transition, etc. However, these simple models are hardly sufficient to study physics of strongly correlated compounds of d- and f-elements. For such real materials, it is necessary to go beyond the simple model Hamiltonian and take into account a real crystal structure (with $d = 3$), in which more orbitals, crystal fields, lattice distortion, filled and excited states, etc are considered. DFT methods (and particularly the LDA) can be employed to construct a new Hamiltonian and to determine the Hamiltonian parameters (such as Coulomb interaction U, exchange interaction J) for strongly correlated real materials.

To construct a many-body Hamiltonian for real material, the Hilbert space is split into *'weakly correlated'* and *'strongly correlated'* subspaces. In the former one, kinetic energy is larger than the Coulomb interaction of the system. Therefore the LDA will be a good approximation to describe weakly correlated terms in the Hamiltonian. For the rest of the Hamiltonian, i.e., in the strongly correlated subspace, the Coulomb interaction term is larger or comparable with the kinetic term and it should be taken into account in the full form. Notice that in this subspace

the LDA fails to capture physical properties of the system, even qualitatively (see Sec. 2.1.3). In constructing the Hamiltonian through this approach, however, the Coulomb interaction is counted twice. Because on the one hand, the full form of the Coulomb interaction is added to the Hamiltonian. On the other hand it was already considered in the LDA calculation at a mean field level. Therefore, a double counting correction term should be added to the many-body Hamiltonian in order to cancel this extra electron-electron interaction.

The corresponding many-body Hamiltonian is then consisted of the LDA Hamiltonian term, i.e., $\hat{H}^{LDA}$, a Coulomb interaction $\hat{U}$, and a double-counting correction $\hat{H}_{DC}$

$$\hat{H} = \hat{H}^{LDA} + \hat{U} - \hat{H}_{DC}, \tag{2.26}$$

which is constructed in localized LDA Wannier function basis[2]

$$\psi_{im\sigma}(\mathbf{r}) = \frac{1}{\sqrt{N}} \sum_{\mathbf{k}} e^{-i\mathbf{R}_i\cdot\mathbf{k}}\, \psi_{m\mathbf{k}\sigma}(\mathbf{r}). \tag{2.27}$$

In Eq. (2.26), the LDA part of the Hamiltonian is

$$\hat{H}^{LDA} = -\sum_{\sigma\sigma'} \sum_{im,i'm'} t^{ii'}_{m\sigma m'\sigma'} c^{\dagger}_{im\sigma} c_{i'm'\sigma'}, \tag{2.28}$$

where $c^{\dagger}_{im\sigma}$ ($c_{im\sigma}$) creates (annihilates) an electron with spin σ in orbital m at site i, and

$$t^{ii'}_{m\sigma m'\sigma'} = -\int d\mathbf{r}\, \overline{\psi}_{im\sigma}(\mathbf{r}) \left[-\frac{1}{2}\nabla^2 + v_R(\mathbf{r})\right] \psi_{i'm'\sigma'}(\mathbf{r}). \tag{2.29}$$

$t^{ii'}_{m\sigma m'\sigma'}$ for $i \neq i'$ is hopping and $i = i'$ the crystal-field matrix elements. The Coulomb interaction $\hat{U}$ is given by

$$\hat{U} = \frac{1}{2} \sum_{ii'jj'} \sum_{\sigma\sigma'} \sum_{mm'\tilde{m}\tilde{m}'} U^{iji'j'}_{mm'\tilde{m}\tilde{m}'}\; c^{\dagger}_{im\sigma} c^{\dagger}_{jm'\sigma'} c_{j'\tilde{m}'\sigma'} c_{i'\tilde{m}\sigma}, \tag{2.30}$$

where

$$\begin{aligned} U^{iji'j'}_{mm'\tilde{m}\tilde{m}'} &= \langle im\sigma\; jm'\sigma' | \hat{U} | i'\tilde{m}\sigma'\; j'\tilde{m}'\sigma' \rangle \\ &= \int d\mathbf{r}_1 \int d\mathbf{r}_2\, \overline{\psi}_{im\sigma}(\mathbf{r}_1) \overline{\psi}_{jm'\sigma'}(\mathbf{r}_2) \frac{1}{|\mathbf{r}_1 - \mathbf{r}_2|} \psi_{j'\tilde{m}'\sigma'}(\mathbf{r}_2) \psi_{i'\tilde{m}\sigma}(\mathbf{r}_1). \end{aligned} \tag{2.31}$$

Such a full form of the Coulomb interaction is hard to deal with. For this reason, to the first approximation, one can assume that the Coulomb interaction $\hat{U}$ is local and the correlated electrons belong to a single shell

$$U^{l}_{mm'\tilde{m}\tilde{m}'} = U^{iiii}_{mm'\tilde{m}\tilde{m}'} \qquad\qquad m, m', \tilde{m}, \tilde{m}' \in nl \text{ shell}, \tag{2.32}$$

so that

$$\hat{H} = \hat{H}^{LDA} + \hat{U}^{l} - \hat{H}^{l}_{DC}. \tag{2.33}$$

[2] One of the successful methods to construct the localized Wannier functions is the *ab-initio* downfolding procedure based on Nth-order Muffin-Tin Orbital (NMTO) method [43]. In this thesis, the LDA part of the Hamiltonian is calculated based on this approach.

Considering this approximation, the double counting term $\hat{H}^l_{DC}$ is the mean-field value of $\hat{U}^l$ [22].[3] Determining the Coulomb interaction matrix elements is a difficult task. Approximate schemes, e.g., based on the DFT calculations with fixed values of orbital occupancies (the so-called constrained DFT [45]) can be used to find out approximate Coulomb matrix.

The full many-body Hamiltonian, described by Eqs. (2.28, 2.31) and (2.33) for realistic material, is still complicated enough so that we need to implement some approximations for real calculations. Hence, the DMFT method is applied to such many-body real material Hamiltonians, whose parameters are determined ab-initio through the DFT (or particularly the LDA). This approach, i.e., the combination of the DFT (LDA) with the DMFT, is the so called DFT(LDA)+DMFT method. In the LDA+DMFT approach, the Hamiltonian (2.33) is mapped onto a multi-orbital impurity model so that the Coulomb interaction considered in the impurity site is the same in the Eq. (2.33). Then the self-consistent DMFT equations should be solved iteratively to extract the physical properties of the real material.

- Using the LDA Hamiltonian, the single site (local) Green's function matrix of the lattice can be calculated by

$$\mathcal{G}_{m\sigma,m'\sigma}(i\nu_n) = \frac{1}{N_{\mathbf{k}}} \sum_{\mathbf{k}} \left(\frac{1}{i\nu_n \otimes \mathbb{1} - H^{LDA}(\mathbf{k}) + H_{DC} - \Sigma(i\nu_n)} \right)_{m\sigma,m'\sigma}, \tag{2.34}$$

  where $H^{LDA}(\mathbf{k})$ is the Fourier transform of the LDA hopping matrix and $\mathbb{1}$ is the unit matrix. In the *paramagnetic* case, spin $\uparrow$ and $\downarrow$ are equivalent and therefore one can omit the spin index in Eq. (2.34). In the first iteration, the self-energy matrix can be set to zero.

- Since in the DMFT approximation, a lattice Hubbard model is mapped onto an impurity model $\left[\mathcal{G}_{\rm imp}(i\nu_n)\right]_{m\sigma,m'\sigma'} = \left[\mathcal{G}(i\nu_n)\right]_{m\sigma,m'\sigma'}$, the bath Green's function is obtained by solving the Dyson equation

$$\left[G_0(i\nu_n)\right]^{-1}_{m\sigma,m'\sigma'} = \left[\Sigma_{\rm imp}(i\nu_n)\right]_{m\sigma,m'\sigma'} + \left[\mathcal{G}_{\rm imp}(i\nu_n)\right]^{-1}_{m\sigma,m'\sigma'}. \tag{2.35}$$

- Once the bath Green's function is determined, the impurity Anderson model is solved using an impurity solver (like QMC) and the new impurity Green's function is obtained.

- The Dyson equation is utilized again to derive new approximation for the self-energy of the system.

$$\left[\Sigma_{\rm imp}(i\nu_n)\right]_{m\sigma,m'\sigma'} = \left[G_0(i\nu_n)\right]^{-1}_{m\sigma,m'\sigma'} - \left[\mathcal{G}_{\rm imp}(i\nu_n)\right]^{-1}_{m\sigma,m'\sigma'}. \tag{2.36}$$

These steps are done iteratively till the convergency condition is achieved (See Sec. 2.3.1).

2.3.5 The LDA+cluster DMFT method

In the LDA+DMFT approach, since the real material Hamiltonian is associated to an impurity model, only local correlations are taken into account, i.e., non-local correlation effects appeared

[3] If the Coulomb interaction is the same for all considered correlated orbitals, the double counting term is just a constant, and can be considered as a shift in chemical potential [22, 44].

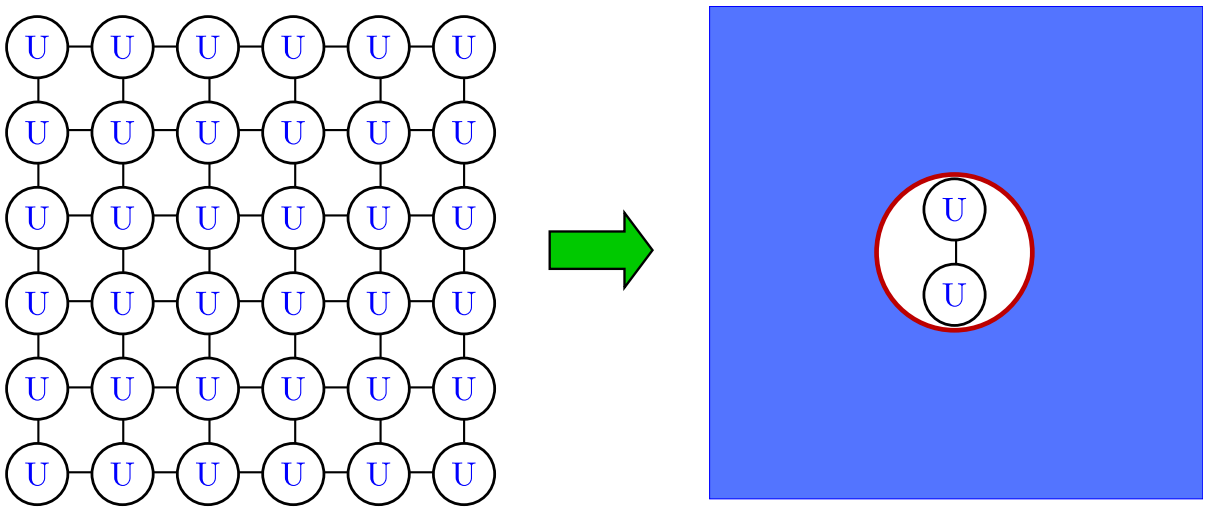

Figure 2.4: In the cDMFT, a lattice many-body problem is mapped onto a DMFT cluster. There are several interacting sites in the DMFT cluster (here two sites exist). Therefore, non-local interaction are considered through the cDMFT calculations.

between different atomic sites are neglected. It is however possible to consider such non-local correlations beyond the LDA+DMFT, the so called cluster LDA+DMFT approach. In this method, a cluster of sites (instead of a single DMFT site) is coupled to a non-interacting bath electrons. Inside the cluster, each atomic site may have several d- or f-orbitals and can have interaction with the rest of the atomic sites. Consequently, the self-energy is not anymore a local quantity, i.e., off diagonal terms of the self-energy matrix of the cluster are nonzero. A natural choice for the cluster is a super cell in real space [44, 22].

In this case, the local lattice Green's function matrix can be rewritten as (compare with Eq. (2.34))

$$\mathcal{G}_{\alpha m\sigma,\alpha' m'\sigma}(i\nu_n) = \frac{1}{N_{\mathbf{k}}}\sum_{\mathbf{k}}\left(\frac{1}{i\nu_n \otimes \mathbb{1} - H^{LDA}(\mathbf{k}) + H_{DC} - \Sigma(i\nu_n)}\right)_{\alpha m\sigma,\alpha' m'\sigma}, \tag{2.37}$$

where α is the correlated site in the unit cell.

Notice that the self-energy matrix $[\Sigma(i\nu_n)]_{\alpha m\sigma,\alpha' m'\sigma'}$, in the DMFT calculations is equal to $\left[\Sigma^{\mathrm{DMFT}}(i\nu_n)\right]_{\alpha m\sigma,\alpha' m'\sigma'} = \delta_{\alpha\alpha'}\left[\Sigma(i\nu_n)\right]_{\alpha m\sigma,\alpha' m'\sigma'}$, i.e., off-(block) diagonal terms is zero, whereas in cluster DMFT off-(block)diagonal elements are finite (See, e.g., Eqs. (2.39) and (2.40)).

Consider the paramagnetic $KCuF_3$ as an example. According to LDA band structure calculations [27], only $3d$ e_g bands, $|3z^2 - r^2\rangle$ and $|x^2 - y^2\rangle$, are close to the Fermi level. Therefore, the effective Hamiltonian can be constructed by downfolding other bands onto the e_g bands. Since the unit cell of the $KCuF_3$ contains two formula units (two atoms per unit cell $\alpha = 1, 2$), the LDA Hamiltonian will then be a 4×4 matrix for each $\mathbf{k}$ point and spin state. If we label $a \equiv |x^2 - y^2\rangle$ and $b \equiv |3z^2 - r^2\rangle$, the LDA Hamiltonian matrix is given by

$$H^{LDA}(\mathbf{k}) = \left(\begin{array}{cc|cc} H_{1a,1a} & H_{1a,1b} & H_{1a,2a} & H_{1a,2b} \\ H_{1b,1a} & H_{1b,1b} & H_{1b,2a} & H_{1b,2b} \\ \hline H_{2a,1a} & H_{2a,1b} & H_{2a,2a} & H_{2a,2b} \\ H_{2b,1a} & H_{2b,1b} & H_{2b,2a} & H_{2b,2b} \end{array}\right). \tag{2.38}$$

In DMFT calculations where only one impurity site interacts with the bath of non-interacting electrons, the self-energy matrix is

$$\Sigma^{\mathrm{DMFT}}(i\nu_n) = \left(\begin{array}{cc|cc} \Sigma_{1a,1a} & \Sigma_{1a,1b} & 0 & 0 \\ \Sigma_{1b,1a} & \Sigma_{1b,1b} & 0 & 0 \\ \hline 0 & 0 & \Sigma_{2a,2a} & \Sigma_{2a,2b} \\ 0 & 0 & \Sigma_{2b,2a} & \Sigma_{2b,2b} \end{array}\right), \tag{2.39}$$

whereas in the cDMFT, off-diagonal block matrices in $\Sigma^{\mathrm{DMFT}}(i\nu_n)$ matrix are not zero anymore

$$\Sigma^{\mathrm{cDMFT}}(i\nu_n) = \left(\begin{array}{cc|cc} \Sigma_{1a,1a} & \Sigma_{1a,1b} & \Sigma_{1a,2a} & \Sigma_{1a,2b} \\ \Sigma_{1b,1a} & \Sigma_{1b,1b} & \Sigma_{1b,2a} & \Sigma_{1b,2b} \\ \hline \Sigma_{2a,1a} & \Sigma_{2a,1b} & \Sigma_{2a,2a} & \Sigma_{2a,2b} \\ \Sigma_{2b,1a} & \Sigma_{2b,1b} & \Sigma_{2b,2a} & \Sigma_{2b,2b}, \end{array}\right). \tag{2.40}$$

Consequently, the Green's function matrix in DMFT and cDMFT are obtained as follows

$$G^{\mathrm{DMFT}}(\mathbf{k}, i\nu_n) = \left(\begin{array}{cc|cc} i\nu_n - H_{1a,1a} - \Sigma_{1a,1a} & -H_{1a,1b} - \Sigma_{1a,1b} & -H_{1a,2a} & -H_{1a,2b} \\ H_{1b,1a} - \Sigma_{1b,1a} & i\nu_n - H_{1b,1b} - \Sigma_{1b,1b} & -H_{1b,2a} & -H_{1b,2b} \\ \hline -H_{2a,1a} & -H_{2a,1b} & i\nu_n - H_{2a,2a} - \Sigma_{2a,2a} & -H_{2a,2b} - \Sigma_{2a,2b} \\ -H_{2b,1a} & -H_{2b,1b} & -H_{2b,2a} - \Sigma_{2b,2a} & i\nu_n - H_{2b,2b} - \Sigma_{2b,2b} \end{array}\right)^{-1}, \tag{2.41}$$

and

$$G^{\mathrm{cDMFT}}(\mathbf{k}, i\nu_n) = \left(\begin{array}{cc|cc} i\nu_n - H_{1a,1a} - \Sigma_{1a,1a} & -H_{1a,1b} - \Sigma_{1a,1b} & -H_{1a,2a} - \Sigma_{1a,2a} & -H_{1a,2b} - \Sigma_{1a,2b} \\ -H_{1b,1a} - \Sigma_{1b,1a} & i\nu_n - H_{1b,1b} - \Sigma_{1b,1b} & -H_{1b,2a} - \Sigma_{1b,2a} & -H_{1b,2b} - \Sigma_{1b,2b} \\ \hline -H_{2a,1a} - \Sigma_{2a,1a} & -H_{2a,1b} - \Sigma_{2a,1b} & i\nu_n - H_{2a,2a} - \Sigma_{2a,2a} & -H_{2a,2b} - \Sigma_{2a,2b} \\ -H_{2b,1a} - \Sigma_{2b,1a} & -H_{2b,1b} - \Sigma_{2b,1b} & -H_{2b,2a} - \Sigma_{2b,2a} & i\nu_n - H_{2b,2b} - \Sigma_{2b,2b}, \end{array}\right)^{-1}. \tag{2.42}$$

Notice that, due to the massive downfolding, we have only e_g correlated electrons, hence the double counting term is just a constant. Therefore, we consider the double counting term (and also the chemical potential) in the self-energy matrix. For further examples see Chap. 5.

CHAPTER 3

Impurity solver: Hirsch-Fye quantum Monte-Carlo

In this chapter, we will focus on the application of the Monte-Carlo technique to the fully interacting quantum impurity system based on the Hirsch-Fye algorithm. To do this, we first have an overview on the Monte-Carlo method to compute high dimensional integrals in an efficient way by using important sampling.

Contents

3.1 Monte-Carlo method 19
3.1.1 Basic concepts of the Monte-Carlo method 20
3.2 Hirsch-Fye quantum Monte-Carlo 23
3.2.1 Derivation of Hirsch-Fye QMC relations 23
3.2.2 Hirsch-Fye QMC algorithm 30
3.2.3 Minus sign problem 31

3.1 Monte-Carlo method

In physical systems typically there are a large number of degrees of freedom. Therefore, to calculate physical quantities of these systems, one has to compute a very large dimensional integral. Solving such a high dimensional integral by utilizing usual discretization approaches like trapezoidal or Simpson approximations is in principle impractical, because the computation time is prohibitively high. For instance, consider a d dimensional function and suppose that the integration grid is 100 points per dimension. Thus 100^d operations are needed to compute the integral which is computationally expensive.[1] To overcome this problem, the Monte-Carlo method provides an efficient way to compute high dimensional integrals. While in the standard grid based methods the integrand is calculated at a large number of points (within the grid), in the Monte-Carlo approach only sampling of the integrand is used to approximate the integral. This sampling procedure is very crucial in the Monte-Carlo method so that an appropriate sampling helps to approach the exact result *quickly*. In the following we describe how Monte-Carlo solves a complicated integral by using *important sampling* procedure.

[1] Furthermore, numerical errors of evaluating such d dimensional integrals grow when d increases. For example, trapezoidal method has an error of $\sim \frac{1}{M^{2/d}}$ where $M-1$ is the number of points in the grid [46]. For large dimensional integration, trapezoid has practically large error ~ 1.

3.1.1 Basic concepts of the Monte-Carlo method

To interpret the basic concept of the Monte-Carlo method, we start with the following d-dimensional integral.

$$\mathcal{I} = \int d\mathbf{x}\; g(\mathbf{x}), \tag{3.1}$$

where $\mathbf{x}$ is a set of variables $\{x_1, x_2, ..., x_d\}$ and $g(\mathbf{x})$ is an arbitrary function. Considering a function $p(\mathbf{x})$, which in principle can be any function of $\mathbf{x}$, we are able to rewrite the integral $\mathcal{I}$ as follows

$$\mathcal{I} = \int d\mathbf{x}\; p(\mathbf{x}) \underbrace{\left(\frac{g(\mathbf{x})}{p(\mathbf{x})}\right)}_{f(\mathbf{x})} = \int d\mathbf{x}\; p(\mathbf{x}) f(\mathbf{x}). \tag{3.2}$$

Here the function $p(\mathbf{x})$ is arbitrary; in the Monte-Carlo calculations, however, $p(\mathbf{x})$ is interpreted as *probability* distribution of variable $\mathbf{x}$ and should be chosen positive and normalized.[2] In this case, the integral (3.2) is just an average of the function $f(\mathbf{x})$ according to the weight (probability) $p(\mathbf{x})$.

$$\mathcal{I} \approx \frac{1}{N_c} \sum_{i=1}^{N_c} f(\mathbf{x}_i), \tag{3.3}$$

where N_c sets of variable $\mathbf{x}_i$ are generated *randomly* with the probability $p(\mathbf{x}_i)$.[3] In order to estimate deviation of $\mathcal{I}$ in Eq. (3.3) from its exact value, we can use the central limit theorem to calculate the variance of $\mathcal{I}$ in terms of $f(\mathbf{x})$ variance [47]

$$\sigma_{\mathcal{I}}^2 = \frac{1}{N_c} \sigma_f^2, \tag{3.4}$$

where

$$\sigma_f^2 = \frac{1}{N_c} \sum_{i=1}^{N_c} f(\mathbf{x}_i)^2 - \left(\frac{1}{N_c} \sum_{i=1}^{N_c} f(\mathbf{x}_i) \right)^2. \tag{3.5}$$

Thus the error of the Monte-Carlo computation of the integral (3.3) scales as $1/\sqrt{N_c}$.

[2] A prototype of such integrals is, e.g., the classical expectation value of an operator $\mathcal{O}$ which is obtained by

$$\langle \mathcal{O} \rangle = \frac{\int dq_1 dq_2 ... dq_{2N}\; e^{-\beta E(q_1, q_2, ..., q_{2N})} \mathcal{O}(q_1, q_2, ..., q_{2N})}{\int dq_1 dq_2 ... dq_{2N}\; e^{-\beta E(q_1, q_2, ..., q_{2N})}},$$

where β is the inverse temperature. We can rewrite this integral as follows.

$$\langle \mathcal{O} \rangle \quad = \int d\mathbf{q}\; p(\mathbf{q}) \mathcal{O}(\mathbf{q}),$$

where $\mathbf{q} = \{q_1, q_2, ..., q_{2N}\}$ and

$$p(\mathbf{q}) = \frac{e^{-\beta E(\mathbf{q})}}{\int d\mathbf{q}\; e^{-\beta E(\mathbf{q})}}; \qquad \int d\mathbf{q}\; p(\mathbf{q}) = 1; \qquad p(\mathbf{q}) \geq 0.$$

[3] Indeed, N_c is the number of Monte-Carlo samples or configurations.

In order to reduce the statistical error (3.4), we have two possibilities. First, we can consider a large number of Monte-Carlo samples generated randomly in order to do the average (3.3). However, due to the CPU time, there are limitations on the total number of Monte-Carlo sampling N_c. The other possibility is that we choose the probability distribution function $p(\mathbf{x})$ in a way that it approximately mimics drastic changes of the function $g(\mathbf{x})$. In this case, the function $f(\mathbf{x}) = g(\mathbf{x})/p(\mathbf{x})$ behaves almost smoothly and its variance σ_f reduces (consequently, $\sigma_{\mathcal{I}}$ decreases) [46]. The latter possibility is the efficient approach in the Monte-Carlo procedure.

The question arises here is that how can we actually generate a sets of $\mathbf{x}$ variables with probability distribution $p(\mathbf{x})$ efficiently? One common way to do this is using the Markov chains.

3.1.1.1 Markov chains

Markov chain is a stochastic or random process wherein one state (or set of variable $\mathbf{x}_i$) have a transition to the other state ($\mathbf{x}_j$) with a certain *transition probability* ($W_{i\to j}$) that depends only on the current state ($\mathbf{x}_i$).

The random process starts with an initial set of variables which we call it $\mathbf{x}_1$. Under the transition probability $W_{1\to 2}$, $\mathbf{x}_1$ moves to the other set of variables $\mathbf{x}_2$. $\mathbf{x}_3$ is achieved from $\mathbf{x}_2$ with $W_{2\to 3}$ probability and so on.

$$\mathbf{x}_1 \longrightarrow \mathbf{x}_2 \longrightarrow \mathbf{x}_3 \longrightarrow \dots .$$

The point about the Markov chain is that we generate a sequence of variables randomly which are not completely independent. The Markov chain is constructed in a way that

1. $\sum_{\mathbf{y}} W_{\mathbf{x}\to\mathbf{y}} = 1.$

2. *Ergodicity*: All states (or sets of variables $\mathbf{x}_i$) are accessible with non-zero transition probability W, i.e., there is always a way from $\mathbf{x}_i$ to go to $\mathbf{x}_j$.

3. *Balance condition:* Overall transition to e.g., $\mathbf{y}$ must be equal to overall transition away from $\mathbf{y}$.

$$\sum_{\mathbf{x}\neq\mathbf{y}} W_{\mathbf{x}\to\mathbf{y}}\; p(\mathbf{x}) = \sum_{\mathbf{y}\neq\mathbf{x}} W_{\mathbf{y}\to\mathbf{x}}\; p(\mathbf{y}). \tag{3.6}$$

   Notice that, $p(\mathbf{x})$ is stationary probability distribution.

4. *Detailed balance condition*: The special case of the balance condition is detailed balance wherein an *individual* transition from $\mathbf{x}$ to $\mathbf{y}$ is balanced with transition from $\mathbf{y}$ to $\mathbf{x}$.

$$W_{\mathbf{x}\to\mathbf{y}}\; p(\mathbf{x}) = W_{\mathbf{y}\to\mathbf{x}}\; p(\mathbf{y}) \tag{3.7}$$

   Once the detailed balance condition is satisfied, the balance condition is also satisfied. Therefore, the detailed balance condition is sufficient, however, it is not necessary.

The transition probability W should be chosen in a way that it satisfies above properties. Metropolis algorithm can be used to find W.

3.1.1.2 Metropolis algorithm

Metropolis algorithm is a way to find the transition probability W based on the so-called accept-reject scheme. The idea is to write the transition probability $W_{\mathbf{x}\to\mathbf{y}}$ as a product of two conditional probabilities

$$W_{\mathbf{x}\to\mathbf{y}} = T_{\mathbf{x}\to\mathbf{y}}\ A_{\mathbf{x}\to\mathbf{y}}. \tag{3.8}$$

Here, $T_{\mathbf{x}\to\mathbf{y}}$ is the probability of *proposing* a movement from $\mathbf{x}$ to $\mathbf{y}$ and $A_{\mathbf{x}\to\mathbf{y}}$ is the probability to *accept* the proposed movement from $\mathbf{x}$ to $\mathbf{y}$.

Basically, we are free to choose an arbitrary strategy to propose a movement from $\mathbf{x}$ to $\mathbf{y}$ ($T_{\mathbf{x}\to\mathbf{y}}$). Clever choice of $T_{\mathbf{x}\to\mathbf{y}}$ may lead to reduce computational costs. Ergodicity is implicitly encoded in $T_{\mathbf{x}\to\mathbf{y}}$. The acceptance probability $A_{\mathbf{x}\to\mathbf{y}}$ should be chosen in a way that satisfies the detailed balance condition

$$\begin{aligned} \frac{W_{\mathbf{x}\to\mathbf{y}}}{W_{\mathbf{y}\to\mathbf{x}}} &= \frac{T_{\mathbf{x}\to\mathbf{y}}A_{\mathbf{x}\to\mathbf{y}}}{T_{\mathbf{y}\to\mathbf{x}}A_{\mathbf{y}\to\mathbf{x}}} = \frac{p(\mathbf{y})}{p(\mathbf{x})} \\ \Rightarrow \frac{A_{\mathbf{x}\to\mathbf{y}}}{A_{\mathbf{y}\to\mathbf{x}}} &= \frac{T_{\mathbf{y}\to\mathbf{x}}\ p(\mathbf{y})}{T_{\mathbf{x}\to\mathbf{y}}\ p(\mathbf{x})} \end{aligned} \tag{3.9}$$

In the Metropolis method, $A_{\mathbf{y}\to\mathbf{x}} = 1$ and the transition from $\mathbf{x}$ to $\mathbf{y}$ is accepted if the ratio $\frac{T_{\mathbf{y}\to\mathbf{x}}\ p(\mathbf{y})}{T_{\mathbf{x}\to\mathbf{y}}\ p(\mathbf{x})} \geq 1$. Otherwise the transition is accepted with probability $\frac{T_{\mathbf{y}\to\mathbf{x}}\ p(\mathbf{y})}{T_{\mathbf{x}\to\mathbf{y}}\ p(\mathbf{x})}$. Therefore, the acceptance probability is given by

$$A_{\mathbf{x}\to\mathbf{y}} = \min\left\{1, \frac{T_{\mathbf{y}\to\mathbf{x}}\ p(\mathbf{y})}{T_{\mathbf{x}\to\mathbf{y}}\ p(\mathbf{x})}\right\}. \tag{3.10}$$

In many cases, the probability $T_{\mathbf{x}\to\mathbf{y}}$ is symmetric with respect to $\mathbf{x}$ and $\mathbf{y}$, i.e., $T_{\mathbf{x}\to\mathbf{y}} = T_{\mathbf{y}\to\mathbf{x}}$, so that $T_{\mathbf{x}\to\mathbf{y}}$ and $T_{\mathbf{y}\to\mathbf{x}}$ are cancelled in Eq. (3.10). Consequently, the Metropolis algorithm generates configurations based on probability distribution $p(\mathbf{x})$.

Finally, the Metropolis algorithm produces configurations as follows.

1. Start with an initial configuration $\mathbf{x}$ (or set of variables $\mathbf{x}$).
2. Randomly choose a new configuration $\mathbf{y}$ based on $T_{\mathbf{x}\to\mathbf{y}}$.
3. Accept the new configuration $\mathbf{y}$ according to $A_{\mathbf{x}\to\mathbf{y}}$. If $\mathbf{y}$ is not accepted as a new configuration, $\mathbf{y} = \mathbf{x}$ and nothing is updated.
4. Go to step 2 and generate N_c cofiguraions.

3.1.1.3 A classical example: 1D Ising model

To become more familiar with different type of probabilities, i.e., A, T and p, consider one-dimensional Ising model described by the Hamiltonian

$$H = J\sum_i \mathbf{S}_i \cdot \mathbf{S}_{i+1} - h\sum_i \mathbf{S}_i,$$

where J is anti-ferromagnet exchange coupling, h the magnetic field and $\mathbf{S}$ the spin. One of the measurable quantities is the magnetization of the system given by

$$\langle m \rangle = \frac{1}{\mathcal{Z}} \sum_{\mathbf{x}} e^{-\beta E(\mathbf{x})} m(\mathbf{x}).$$

In this relation $\mathbf{x}$ is a set of spins $\{s_1, s_2, s_3, ..., s_N\}$. In comparison with Eq. (3.2), $p(\mathbf{x}) = e^{-\beta E(\mathbf{x})}/\mathcal{Z}$. We start with initial configuration $\{\uparrow, \uparrow, ..., \uparrow\}$. We make some changes to generate a new configurations of spins. Notice that we are free to propose a new configuration. For example, we can choose a spin randomly and flip it to produce a new one. Therefore, $T_{\mathbf{x}\to\mathbf{y}} = 1/N$. Acceptance probability is then given by $A_{\mathbf{x}\to\mathbf{y}} = \min\{1, \exp[-\beta(E(\mathbf{y}) - E(\mathbf{x}))]\}$.

3.2 Hirsch-Fye quantum Monte-Carlo

Application of the Monte-Carlo technique on the quantum many-body systems is known as quantum Monte-Carlo (QMC) method. QMC is one of the most powerful approaches which has been implemented to study quantum many-body models. In dynamical mean field theory (DMFT), the crucial step in solving self-consistence DMFT equations is finding a solution to the Anderson impurity model. Hirsch-Fye QMC is one of the most successful impurity solvers used in DMFT approximation (see e.g., [20, 12]).

3.2.1 Derivation of Hirsch-Fye QMC relations

In the following, we basically follow Ref. [13] to describe Hirsch-Fye QMC algorithm thoroughly. We start with the Anderson impurity model in Eq. (2.18) and rephrase it as

$$H = H_0 + H_{\rm int}, \tag{3.11}$$

$$H_0 = \sum_p \sum_\sigma \left(\varepsilon_p + \frac{U}{2}\delta_{p,0}\right) c^\dagger_{p\sigma} c_{p\sigma} + \sum_{p>0}\sum_\sigma \left(V_{0p}\, c^\dagger_{0\sigma} c_{p\sigma} + V^*_{0p}\, c^\dagger_{p\sigma} c_{0\sigma}\right), \tag{3.12}$$

$$H_{\rm int} = U\left[n_{0\uparrow} n_{0\downarrow} - \frac{1}{2}(n_{0\uparrow} + n_{0\downarrow})\right], \tag{3.13}$$

where in this notation $p = 0$ is applied to the impurity while the rest of p, i.e., $p > 0$, are related to non-interacting bath electrons. This is a convenient notation to formulate the Hirsch-Fye QMC. To calculate a physical function, we need to know the partition function first.

$$\mathcal{Z} = \mathrm{Tr}\left\{e^{-\beta H}\right\}, \tag{3.14}$$

where β is the inverse temperature. To compute the partition function, we discretize imaginary time interval $[0, \beta]$ into L time slices of length $\Delta\tau$, so that $\beta = L\Delta\tau$. Consequently, the partition function is now obtained as

$$\begin{aligned} \mathcal{Z} &= \mathrm{Tr}\left\{e^{-\Delta\tau H} e^{-\Delta\tau H} ... \, e^{-\Delta\tau H}\right\} \\ &= \mathrm{Tr}\left\{\prod_{l=1}^{L} e^{-\Delta\tau(H_0 + H_{\rm int})}\right\}. \end{aligned} \tag{3.15}$$

Assuming that $\Delta\tau$ is small (or L is sufficiently big), we can use Trotter-Suzuki decomposition[4] (see, e.g., [48]) to approximate the partition function as

$$\mathcal{Z} \approx \mathrm{Tr}\left\{\prod_{l=1}^{L} e^{-\Delta\tau H_0} e^{-\Delta\tau H_{\mathrm{int}}}\right\} + \mathcal{O}(\Delta\tau^2 U). \tag{3.17}$$

This is the only approximation that is utilized in this approach. Eq. (3.17) can be rephrased more simple if we can get rid of the quartic term. This can be done by using the discretized Hubbard-Stratonovich method[5]

$$\begin{aligned} e^{-\Delta\tau U\left[n_{0\uparrow}n_{0\downarrow} - \frac{1}{2}(n_{0\uparrow}+n_{0\downarrow})\right]} &= e^{\Delta\tau U\left[\frac{1}{2}(n_{0\uparrow}-n_{0\downarrow})^2\right]} \\ &= \frac{1}{2}\sum_{s=\pm 1} e^{\lambda s(n_{0\uparrow}-n_{0\downarrow})}, \end{aligned} \tag{3.21}$$

wherein $s = \pm 1$ are Ising variables and $\cosh\lambda = e^{\Delta\tau U/2}$ (See footnote 5 for proof). Substituting Eq. (3.21) in Eq. (3.17) yields

$$\begin{aligned} \mathcal{Z} &= \mathrm{Tr}\left\{\prod_{l=1}^{L} e^{-\Delta\tau H_0}\frac{1}{2^L}\sum_{s_1,s_2,\ldots,s_L} e^{\lambda s_l(n_{0\uparrow}-n_{0\downarrow})}\right\} \\ &= \frac{1}{2^L}\sum_{s_1,s_2,\ldots,s_L}\mathrm{Tr}\left\{\prod_{l=1}^{L} e^{-\Delta\tau H_0+\lambda s_l(n_{0\uparrow}-n_{0\downarrow})}\right\} \\ &= \frac{1}{2^L}\sum_{s_1,s_2,\ldots,s_L}\mathcal{Z}_{s_1,s_2,\ldots,s_L}. \end{aligned} \tag{3.22}$$

[4] If $\mathcal{A}$ and $\mathcal{B}$ are two non-communicate operators, we have

$$\begin{aligned} e^{\Delta\tau(\mathcal{A}+\mathcal{B})} &= e^{\Delta\tau\mathcal{A}}e^{\Delta\tau\mathcal{B}}e^{-\frac{1}{2}(\Delta\tau)^2[\mathcal{A},\mathcal{B}]} \\ &\approx e^{\Delta\tau\mathcal{A}}e^{\Delta\tau\mathcal{B}} + \mathcal{O}(\Delta\tau)^2. \end{aligned} \tag{3.16}$$

[5] In the Hubbard-Stratonovich transformation, an exponential of the square of an operator, i.e., $\mathcal{A}^2$, can be expressed in terms of an exponential of the operator $\mathcal{A}$ which is coupled to an auxiliary field x according to the following relation:

$$e^{\frac{1}{2}\mathcal{A}^2} \equiv \sqrt{2\pi}\int_{-\infty}^{+\infty} dx\, e^{-\frac{1}{2}x^2 - x\mathcal{A}}. \tag{3.18}$$

Consequently, the discrete Hubbard-Stratonovich transformation in which the operator $\mathcal{A}$ couples to the auxiliary field like Ising field can be obtained by

$$e^{\frac{1}{2}\mathcal{A}^2} = \alpha\sum_{s=\pm 1} e^{\lambda s\mathcal{A}}, \tag{3.19}$$

where α and λ are coefficients that should be determined appropriately. For example, consider $\mathcal{A}^2 = \Delta\tau U\left[(n_{0\uparrow}-n_{0\downarrow})^2\right]$ where $n_0 = 0, 1$ is the number operator which acts on the impurity site so that $(n_{0\uparrow}-n_{0\downarrow}) = -1, 0, 1$. According to discrete Hubbard-Stratonovich transformation we have

$$e^{\frac{1}{2}\Delta\tau U\left[(n_{0\uparrow}-n_{0\downarrow})^2\right]} = \alpha\sum_{s=\pm 1} e^{\lambda s(n_{0\uparrow}-n_{0\downarrow})}. \tag{3.20}$$

For $(n_{0\uparrow}-n_{0\downarrow}) = 1, -1$ we have $e^{U\Delta\tau/2} = \alpha\left(e^{-\lambda}+e^{\lambda}\right)$. If $(n_{0\uparrow}-n_{0\downarrow}) = 0$, we get $1 = \alpha(1+1)$. Consequently, we obtain $\alpha = 1/2$ and $\lambda = \cosh^{-1}\left[e^{\Delta\tau U/2}\right]$.

With the Hubbard-Stratonovich formula, we could reduce the interacting problem to the non-interacting case where there are only quadratic terms. The price we paid is the extended Hilbert space with 2^L Ising spins. Due to the large phase space of Ising spins (2^L),[6] the summation over all spin configurations $\{s\} = \{s_1, s_2, ..., s_L\}$ in Eq. (3.22) is done by using the *Monte-Carlo* technique. The Metropolis or Heat-bath algorithm is implemented for importance sampling of Ising spin configurations $\{s\}$. All we should do now to compute the partition function in Eq. (3.22) is to rephrase $\mathcal{Z}_{s_1,s_2,...,s_L}$ relation (which is in a fixed Ising spin configuration) in an understandable form for the computer.

The non-interacting part of the Hamiltonian in Eq. (3.22) can be represented as a matrix form.

$$H_0 = \sum_{ij} \sum_{\sigma} c^{\dagger}_{i\sigma} h^0_{ij} c_{j\sigma}. \tag{3.23}$$

where h^0_{ij} is matrix representation of the H_0 operator. The partition function for a fixed Ising spin configuration, $\mathcal{Z}_{s_1,s_2,...,s_L}$, is then

$$\begin{aligned} \mathcal{Z}_{s_1,s_2,...,s_L} &= \mathrm{Tr}\left\{ \prod_{l=1}^{L} e^{-\Delta\tau \sum_{ij\sigma} c^{\dagger}_{i\sigma} h^0_{ij} c_{j\sigma} + \sum_{\sigma} c^{\dagger}_{0\sigma} \lambda\sigma s_l \delta_{ij} c_{0\sigma}} \right\} \\ &= \mathrm{Tr}\left\{ \prod_{l=1}^{L} e^{-\Delta\tau \sum_{ij\sigma} c^{\dagger}_{i\sigma} [h_{l\sigma}]_{ij} c_{j\sigma}} \right\}, \end{aligned} \tag{3.24}$$

wherein $[h_{l\sigma}]_{ij} = h^0_{ij} - \dfrac{\lambda}{\Delta\tau} s_l \sigma \delta_{i=j=0}$. The trace in this relation can be rewritten in a determinant form. This can be easily shown if we first write the matrix $[h_{l\sigma}]_{ij}$ in its diagonal form (for each time slice l and spin σ) using $h_{ij}\, \mathcal{U}_{j\alpha} = \mathcal{U}_{i\alpha}\, \varepsilon_{\alpha}$.

$$\begin{aligned} \mathcal{Z}_{s_1,s_2,...,s_L} &= \mathrm{Tr}\left\{ \prod_{l=1}^{L} e^{-\Delta\tau \sum_{ij\sigma} \sum_{\alpha} c^{\dagger}_{i\sigma}\, \mathcal{U}_{i\alpha}\, \mathcal{U}^{-1}_{\alpha i}\, [h_{l\sigma}]_{i,j}\, \mathcal{U}_{j\alpha}\, \mathcal{U}^{-1}_{\alpha j} c_{j\sigma}} \right\} \\ &= \mathrm{Tr}\left\{ \prod_{l=1}^{L} e^{-\Delta\tau \sum_{\sigma} \sum_{\alpha} c^{\dagger}_{\alpha\sigma}(\tau_l) \varepsilon^{\sigma}_{\alpha}(l) c_{\alpha\sigma}(\tau_l)} \right\}, \end{aligned} \tag{3.25}$$

where $c_{\alpha} = \sum_i \mathcal{U}^{-1}_{\alpha i}\, c_i$ and $\mathcal{U}^{-1}_{\alpha i}\, h_{ij}\, \mathcal{U}_{j\alpha} = \varepsilon_{\alpha}$. The trace is then can be done for each α state considering the fact that $n^{\sigma}_{\alpha}(l)$ is either 0 or 1 for fermions.

$$\begin{aligned} \mathcal{Z}_{s_1,s_2,...,s_L} &= \prod_{\sigma=\uparrow,\downarrow} \prod_{\alpha} \mathrm{Tr}_{\alpha} \left\{ \prod_{l=1}^{L} e^{-\Delta\tau \varepsilon^{\sigma}_{\alpha}(l) n_{\alpha\sigma}(\tau_l)} \right\} \\ &= \prod_{\sigma=\uparrow,\downarrow} \prod_{\alpha} \left(1 + \prod_{l=1}^{L} e^{-\Delta\tau \varepsilon^{\sigma}_{\alpha}(l)} \right) \\ &= \prod_{\sigma=\uparrow,\downarrow} \mathrm{Det} \left(1 + \prod_{l=1}^{L} e^{-\Delta\tau \varepsilon^{\sigma}_{\alpha}(l)} \right) \\ &\equiv \mathrm{Det}\left(1 + \widetilde{B}^{\uparrow}_{L} \widetilde{B}^{\uparrow}_{L-1} \, ... \, \widetilde{B}^{\uparrow}_{1} \right) \cdot \mathrm{Det}\left(1 + \widetilde{B}^{\downarrow}_{L} \widetilde{B}^{\downarrow}_{L-1} \, ... \, \widetilde{B}^{\downarrow}_{1} \right) \end{aligned} \tag{3.26}$$

[6] For instance, i) at low temperatures where β (and therefore L) is too big, ii) at large Coulomb interaction U where L should be big enough so that $\mathcal{O}(\Delta\tau^2 U)$ becomes small to use the Trotter-Suzuki decomposition (See Eq. (3.17)).

Here, $[\widetilde{B}_l^\sigma]_{\alpha\alpha} = e^{-\Delta\tau\varepsilon_\alpha^\sigma(l)}$ is a diagonal matrix. In terms of i,j indices, the matrix B_l^σ is obtained by $B_l^\sigma = \mathcal{U}\,\widetilde{B}_l^\sigma\,\mathcal{U}^{-1} = e^{-\Delta\tau h_{l\sigma}} = e^{-\Delta\tau h^0} e^{\lambda s_l \sigma \delta_{i=j=0}}$. Therefore, the partition function is given by the following relation.

$$\mathcal{Z} = \frac{1}{2^L} \sum_{s_1,s_2,...,s_L} \mathrm{Det}\left(1 + B_L^\uparrow B_{L-1}^\uparrow \ldots B_1^\uparrow\right) \cdot \mathrm{Det}\left(1 + B_L^\downarrow B_{L-1}^\downarrow \ldots B_1^\downarrow\right). \tag{3.27}$$

Using the partition function, we are able to calculate Green's function of the system[7]

$$\mathcal{G} \;=\; \frac{\sum_{s_1,s_2,...,s_L} \widetilde{G}_{s_1,s_2,...,s_L}\,\mathcal{Z}_{s_1,s_2,...,s_L}}{\sum_{s_1,s_2,...,s_L} \mathcal{Z}_{s_1,s_2,...,s_L}}. \tag{3.28}$$

Here, $\widetilde{G}$ is (quantum Monte-Carlo) Green's function for a single Ising spin configuration and it is given by

$$\left[\widetilde{G}_{ij}^\sigma(\tau_{l_1},\tau_{l_2})\right]_{s_1,s_2,...,s_L} = \frac{1}{\mathcal{Z}_{s_1,s_2,...,s_L}} \mathrm{Tr}\left\{\mathcal{T} c_{i\sigma}(\tau_{l_1}) c_{j\sigma}^\dagger(\tau_{l_2}) \prod_{l=1}^{L} e^{-\Delta\tau H_0 + \lambda s_l (n_{0\uparrow} - n_{0\downarrow})}\right\}, \tag{3.29}$$

in which $\mathcal{T}$ is time ordering operator. Similar to partition function derivation (Eq. (3.27)), we go to diagonal representation where the Hamiltonian and therefore the Green's function $\widetilde{G}$ are diagonal there.

$$\left[\widetilde{G}_{\alpha\alpha}^\sigma(\tau_{l_1},\tau_{l_2})\right]_{s_1,s_2,...,s_L} = \frac{1}{\mathcal{Z}_{s_1,s_2,...,s_L}} \mathrm{Tr}\left\{\mathcal{T} c_{\alpha\sigma}(\tau_{l_1}) c_{\alpha\sigma}^\dagger(\tau_{l_2}) \prod_{l=1}^{L} e^{-\Delta\tau \sum_\sigma \sum_\alpha c_{\alpha\sigma}^\dagger(\tau_l)\varepsilon_\alpha^\sigma(l) c_{\alpha\sigma}(\tau_l)}\right\}. \tag{3.30}$$

Due to the time ordering operator in the Green's function relation, we can rearrange time dependent terms in the above equation as

$$\begin{aligned}\left[\widetilde{G}_{\alpha\alpha}^\sigma(\tau_{l_1},\tau_{l_2})\right]_{s_1,s_2,...,s_L} &= \frac{1}{\mathcal{Z}_{s_1,s_2,...,s_L}} \mathrm{Tr}\left\{\mathcal{T} c_{\alpha\sigma}(\tau_{l_1}) c_{\alpha\sigma}^\dagger(\tau_{l_2}) U_1 \ldots U_{l_2} U_{l_2+2} \ldots U_{l_1} U_{l_1+1} \ldots U_L\right\} \\ &= \frac{1}{\mathcal{Z}_{s_1,s_2,...,s_L}} \mathrm{Tr}\left\{U_L \ldots U_{l_1} c_{\alpha\sigma}(\tau_{l_1}) U_{l_1-1} \ldots U_{l_2} c_{\alpha\sigma}^\dagger(\tau_{l_2}) U_{l_2-1} \ldots U_1\right\},\end{aligned} \tag{3.31}$$

where we supposed that $l_1 > l_2$ and $U_l \equiv e^{-\Delta\tau \sum_\sigma \sum_\alpha \varepsilon_\alpha^\sigma n_{\alpha\sigma}}$. We now use the cyclic permutation property of a trace to rewrite this relation as

$$\left[\widetilde{G}_{\alpha\alpha}^\sigma(\tau_{l_1},\tau_{l_2})\right]_{s_1,s_2,...,s_L} = \frac{1}{\mathcal{Z}_{s_1,s_2,...,s_L}} \mathrm{Tr}\left\{U_{l_2-1} \ldots U_1 U_L \ldots U_{l_1} c_{\alpha\sigma}(\tau_{l_1}) U_{l_1-1} \ldots U_{l_2} c_{\alpha\sigma}^\dagger(\tau_{l_2})\right\}. \tag{3.32}$$

The only non-zero term in the trace belongs to the empty state $|0\rangle$. Therefore, we have

$$\begin{aligned}\left[\widetilde{G}_{\alpha\alpha}^\sigma(\tau_{l_1},\tau_{l_2})\right]_{s_1,s_2,...,s_L} &= \frac{1}{\mathcal{Z}_{s_1,s_2,...,s_L}} \langle 0 | U_{l_2-1} \ldots U_1 U_L \ldots U_{l_1} c_{\alpha\sigma}(\tau_{l_1}) U_{l_1-1} \ldots U_{l_2} c_{\alpha\sigma}^\dagger(\tau_{l_2}) | 0\rangle \\ &= \frac{\left[\widetilde{B}_{l_1-1}^\sigma \widetilde{B}_{l_1-2}^\sigma \ldots \widetilde{B}_{l_2}^\sigma\right]}{\mathrm{Det}\left(1 + \widetilde{B}_L^\uparrow \widetilde{B}_{L-1}^\uparrow \ldots \widetilde{B}_1^\uparrow\right) \cdot \mathrm{Det}\left(1 + \widetilde{B}_L^\downarrow \widetilde{B}_{L-1}^\downarrow \ldots \widetilde{B}_1^\downarrow\right)}.\end{aligned} \tag{3.33}$$

[7] The Green's function in imaginary time is defined as $\mathcal{G}(\tau,\tau') = -\langle \mathcal{T} c(\tau) c^\dagger(\tau')\rangle$ (see Sec. 5.2.1 for more details). In the QMC method, the minus sign is dropped for simplicity. For this reason, in this chapter, we follow the QMC sign contract for the Green's functions.

To derive the above relation we used $U_l|0\rangle = |0\rangle$. Going back to the original (or non-diagonal) presentation of the Hamiltonian we have

$$\left[\widetilde{G}^{\sigma}_{ij}(\tau_{l_1},\tau_{l_2})\right]_{s_1,s_2,...,s_L} = \frac{B^{\sigma}_{l_1-1}B^{\sigma}_{l_1-2}\,...\,B^{\sigma}_{l_2}}{\mathrm{Det}\left(1+B^{\uparrow}_{L}B^{\uparrow}_{L-1}\,...\,B^{\uparrow}_{1}\right)\cdot\mathrm{Det}\left(1+B^{\downarrow}_{L}B^{\downarrow}_{L-1}\,...\,B^{\downarrow}_{1}\right)}, \qquad l_1 > l_2. \tag{3.34}$$

Similar relation for the Green's function $\left[\widetilde{G}^{\sigma}_{ij}(\tau_{l_1},\tau_{l_2})\right]_{s_1,s_2,...,s_L}$ when $l_1 < l_2$ can be obtained in the same way.

$$\left[\widetilde{G}^{\sigma}_{ij}(\tau_{l_1},\tau_{l_2})\right]_{s_1,s_2,...,s_L} = -\frac{B^{\sigma}_{l_1-1}B^{\sigma}_{l_1-2}\,...\,B^{\sigma}_{1}B^{\sigma}_{L}B^{\sigma}_{L-1}\,...\,B^{\sigma}_{l_2}}{\mathrm{Det}\left(1+B^{\uparrow}_{L}B^{\uparrow}_{L-1}\,...\,B^{\uparrow}_{1}\right)\cdot\mathrm{Det}\left(1+B^{\downarrow}_{L}B^{\downarrow}_{L-1}\,...\,B^{\downarrow}_{1}\right)}, \qquad l_1 < l_2. \tag{3.35}$$

In time variables τ_{l_1},τ_{l_2} and position-orbital i,j indices,[8] the $(LN)\times(LN)$ matrix $\left[\widetilde{G}^{\sigma}_{ij}(\tau_{l_1},\tau_{l_2})\right]_{s_1,s_2,...,s_L}$ can be written in a matrix form that covers Eqs. (3.34) and (3.35) simultaneously.[9]

$$\left[\widetilde{G}^{\sigma}_{s_1,s_2,...,s_L}\right]^{-1} = \begin{pmatrix} 1 & 0 & \cdots & 0 & B^{\sigma}_{L} \\ -B^{\sigma}_{1} & 1 & \cdots & \cdots & 0 \\ 0 & -B^{\sigma}_{2} & 1 & \cdots & 0 \\ \cdots & \cdots & \cdots & \cdots & \cdots \\ 0 & \cdots & \cdots & 1 & 0 \\ 0 & \cdots & \cdots & -B^{\sigma}_{L-1} & 1 \end{pmatrix}. \tag{3.36}$$

Based on Eqs. (3.26), (3.34), (3.35), and (3.36) we can conclude that

$$\mathcal{Z}_{s_1,s_2,...,s_L} = \mathrm{Det}\left[\widetilde{G}^{\uparrow}_{s_1,s_2,...,s_L}\right]^{-1}\cdot\mathrm{Det}\left[\widetilde{G}^{\downarrow}_{s_1,s_2,...,s_L}\right]^{-1}. \tag{3.37}$$

Inversion of the matrix $\left[\widetilde{G}^{\sigma}_{s_1,s_2,...,s_L}\right]^{-1}$ should be done for each set of Ising spin configurations $\{s_1,s_2,...,s_L\}$ which is computationally expensive. It is, however, possible to reduce the computational costs of the matrix inversion via effective procedure proposed by Hirsch and Fye in Ref. [13]. In this procedure two Green's function $\widetilde{G}$ and $\widetilde{G}'$, belonged to two different Ising spin configurations $\{s\} = \{s_1,s_2,...,s_L\}$ and $\{s'\} = \{s'_1,s'_2,...,s'_L\}$, are related to each other with a Dyson like equation (see Eq. (3.43)). Furthermore, if two sets of Ising spin configurations are different *only in one spin flip*, one can compute the Green's function $\widetilde{G}$ for a certain Ising spin configuration then use it to recalculate the green's function $\widetilde{G}'$ without matrix inversion (see Eq. (3.50)).

[8] Notice that N is the (number of orbitals) $\times$ (number of sites).

[9] To examine this matrix form, one can easily perform a simple matrix inversion for few lowest terms, i.e.,

$$\begin{pmatrix} 1 & 0 & B^{\sigma}_{3} \\ -B^{\sigma}_{1} & 1 & 0 \\ 0 & -B^{\sigma}_{2} & 1 \end{pmatrix}^{-1}.$$

to obtain Eqs. (3.34) and (3.35).

The relation between two Green's function $\widetilde{G}$ and $\widetilde{G}'$ corresponding to two Ising spin configurations $\{s\} = \{s_1, s_2, ..., s_L\}$ and $\{s'\} = \{s'_1, s'_2, ..., s'_L\}$ is one of the key equations in the Hirsch-Fye QMC that we derive in the following.

Consider the $N \times N$ matrix $B_l^\sigma = e^{-\Delta\tau h^0} e^{\lambda s_l \sigma \delta_{i=j=0}}$ which can be rewritten as

$$B_l^\sigma = e^{-\Delta\tau h^0} e^{V_l^\sigma}. \tag{3.38}$$

Here, $e^{V_l^\sigma} = \delta_{ij} + (e^{\lambda s_l \sigma} - 1)\delta_{i=j=0}$ is a $N \times N$ diagonal matrix presented by

$$e^{V_l^\sigma} = \begin{pmatrix} e^{\lambda s_l \sigma} & 0 & 0 & \cdots & 0 \\ 0 & 1 & 0 & \cdots & 0 \\ \cdots & \cdots & \cdots & \cdots & \cdots \\ 0 & 0 & 0 & \cdots & 1 \end{pmatrix}_{N\times N}. \tag{3.39}$$

Notice that in the base of time variables τ_l and orbital-position, $\left[e^{V^\sigma}\right]$ matrix is still a diagonal matrix expressed as

$$e^{V^\sigma} = \begin{pmatrix} e^{V_1^\sigma} & 0 & 0 & \cdots & 0 \\ 0 & e^{V_2^\sigma} & 0 & \cdots & 0 \\ \cdots & \cdots & \cdots & \cdots & \cdots \\ 0 & 0 & 0 & \cdots & e^{V_L^\sigma} \end{pmatrix}_{(LN)\times(LN)}, \tag{3.40}$$

where each $e^{V_l^\sigma}$ is a $N \times N$ matrix given by Eq. (3.39). For a certain Ising spin configuration $\{s_1, s_2, ..., s_L\}$, we calculate multiplication of two $(LN) \times (LN)$ matrices $\left[\widetilde{G}^\sigma\right]^{-1} e^{-V^\sigma}$.

$$\begin{aligned} \left(\widetilde{G}^\sigma\right)^{-1}\left(e^{-V^\sigma}\right) &= \begin{pmatrix} e^{-V_1^\sigma} & 0 & \cdots & 0 & B_L^\sigma e^{-V_L^\sigma} \\ -B_1^\sigma e^{-V_1^\sigma} & e^{-V_2^\sigma} & \cdots & \cdots & 0 \\ 0 & -B_2^\sigma e^{-V_2^\sigma} & e^{-V_2^\sigma} & \cdots & 0 \\ \cdots & \cdots & \cdots & \cdots & \cdots \\ 0 & \cdots & \cdots & e^{-V_{L-1}^\sigma} & 0 \\ 0 & \cdots & \cdots & -B_{L-1}^\sigma e^{-V_{L-1}^\sigma} & e^{-V_L^\sigma} \end{pmatrix} \\ &= \begin{pmatrix} e^{-V_1^\sigma} & 0 & \cdots & 0 & e^{-\Delta\tau h^0(L)} \\ -e^{-\Delta\tau h^0} & e^{-V_2^\sigma} & \cdots & \cdots & 0 \\ 0 & -e^{-\Delta\tau h^0} & e^{-V_2^\sigma} & \cdots & 0 \\ \cdots & \cdots & \cdots & \cdots & \cdots \\ 0 & \cdots & \cdots & e^{-V_{L-1}^\sigma} & 0 \\ 0 & \cdots & \cdots & -e^{-\Delta\tau h^0} & e^{-V_L^\sigma} \end{pmatrix}. \end{aligned} \tag{3.41}$$

Interestingly, *off-diagonal terms are independent of Ising spin configurations*. Consequently, if $\widetilde{G}'^\sigma$ and V' correspond to a new Ising spin configuration $\{s'\} = \{s'_1, s'_2, ..., s'_L\}$, we have

$$\left(\widetilde{G}^\sigma\right)^{-1}\left(e^{-V^\sigma}\right) - \left(\widetilde{G}'^\sigma\right)^{-1}\left(e^{-V'^\sigma}\right) = \left(e^{-V^\sigma}\right) - \left(e^{-V'^\sigma}\right). \tag{3.42}$$

After doing simple matrix algebra, we derive[10]

$$\widetilde{G}' - \widetilde{G} = (\widetilde{G} - 1)(e^{V'-V} - 1)\widetilde{G}'. \tag{3.43}$$

[10]For the sake of the simplicity in notation, we drop the spin index σ in the following equations.

The importance of this equation becomes evident in the numerical computation of summation over *all* sets of Ising configurations in (3.28) where *Monte-Carlo* sampling procedure is utilized. Based on Eq. (3.43), if we know $\widetilde{G}$ for a certain Ising spin configuration (related to V) and obtain new Ising spin configuration (concerning to V') by using *Markov chain* procedure, we can compute $\widetilde{G}'$. Furthermore, $(e^{V-V'}-1)$ matrix is nonzero only for the impurity site because e^V matrix is unity for each but the impurity site. This leads to a nonzero difference of $\widetilde{G}$ and $\widetilde{G}'$ on the impurity site. Consequently, the $(NL)\times(NL)$ matrix equation (3.43) reduces to a $L\times L$ matrix for the impurity site. Therefore,

$$\mathcal{A}\,\widetilde{G}' = \widetilde{G}\,; \qquad \mathcal{A} = 1 + (1-\widetilde{G})(e^{V'-V}-1) \tag{3.44}$$

is now for the impurity site and all the matrices $\widetilde{G}$, $\widetilde{G}'$, $\mathcal{A}$, and V are $L\times L$ matrices in time index. In Hirsch-Fye QMC, Eq. (3.44) is known as *clean update* relation.

If two Ising spin configurations $\{s\}$ and $\{s'\}$ are different in only one Ising spin (e.g., in s_p), the $(e^{V'-V}-1)$ matrix can be obtained as

$$(e^{V'-V}-1) = \begin{pmatrix} 0 & 0 & \cdots & 0 & 0 \\ \vdots & \ddots & \cdots & \vdots & \vdots \\ 0 & \cdots & e^{\lambda\sigma(s'_p-s_p)}-1 & \cdots & 0 \\ \vdots & \cdots & \cdots & \ddots & \vdots \\ 0 & 0 & \cdots & 0 & 0 \end{pmatrix}, \tag{3.45}$$

or equivalently, $(e^{V'-V}-1)_{ll'} = a\;\delta_{l=l'=p}$ where $a = e^{\lambda\sigma(s'_p-s_p)}-1$. Therefore, the matrix $\mathcal{A}$ is given by

$$\mathcal{A} = \begin{pmatrix} 1 & 0 & \cdots & \mathcal{A}_{1p} & \cdots & 0 & 0 \\ 0 & 1 & \cdots & \mathcal{A}_{2p} & \cdots & 0 & 0 \\ \vdots & \vdots & \ddots & \vdots & \cdots & \vdots & \vdots \\ 0 & 0 & \cdots & \mathcal{A}_{pp} & \cdots & \cdots & 0 \\ \vdots & \vdots & \cdots & \vdots & \ddots & \vdots & \vdots \\ 0 & 0 & \cdots & \mathcal{A}_{L-1p} & \cdots & 1 & 0 \\ 0 & 0 & \cdots & \mathcal{A}_{Lp} & \cdots & 0 & 1 \end{pmatrix}, \tag{3.46}$$

where

$$\mathcal{A}_{ll'} = \delta_{ll'} + \left(\delta_{ll'} - \widetilde{G}_{ll'}\right) a\;\delta_{l'p}. \tag{3.47}$$

The determinant of the matrix $\mathcal{A}$ is then

$$\mathrm{Det}(\mathcal{A}) = \mathcal{A}_{pp} = 1 + (1-\widetilde{G}_{pp})a, \tag{3.48}$$

and the matrix $\mathcal{A}^{-1}$ has the elements

$$(\mathcal{A}^{-1})_{ll'} = \delta_{ll'} + \frac{a}{1+a(1-\widetilde{G}_{pp})}(\widetilde{G}_{lp}-\delta_{lp})\delta_{l'p}. \tag{3.49}$$

To compute the Green's function $\widetilde{G}'$ for the new configuration, it is then sufficient to know $\widetilde{G}$ for the previous one.

$$\widetilde{G}'_{ll'} = \widetilde{G}_{ll'} + \frac{a}{1+a(1-\widetilde{G}_{pp})}(\widetilde{G}_{lp}-\delta_{lp})\widetilde{G}_{pl'}. \tag{3.50}$$

This equation, which is known as *fast update* relation, will be implemented to update the Green's function of the new Ising spin configuration. Based on Eq. (3.50), there is no need to calculate the inversion of the matrix $\mathcal{A}$ explicitly to evaluate the new Green's function $\widetilde{G}$.

Computation of the new Green's function from the fast update Eq. (3.50) and the clean update Eq. (3.44) needs L^2 and L^3 operations, respectively. Although using Eq. (3.50) is more reasonable and faster, in the Hirsch-Fye QMC, we must use both of them to produce new Green's function $\widetilde{G}$. The reason is that the computational round-off error is amplified if we use only Eq. (3.50) to generate the new Green's function.

3.2.2 Hirsch-Fye QMC algorithm

Through the Hirsch-Fye QMC, we are interested to obtain the Green's function

$$\mathcal{G}^{\sigma} = \frac{\sum_{\{s\}} \mathcal{Z}_{\{s\}}\ \widetilde{G}^{\sigma}_{\{s\}}}{\sum_{\{s\}} \mathcal{Z}_{\{s\}}}, \tag{3.51}$$

where $\mathcal{Z}_{\{s\}} = \mathrm{Det}[\widetilde{G}^{\uparrow}_{\{s\}}]^{-1} \cdot \mathrm{Det}[\widetilde{G}^{\downarrow}_{\{s\}}]^{-1}$ and $\{s\} = \{s_1, s_2, ..., s_L\}$. In this relation, the Green's function matrix is a $L \times L$ one.[11] In the practical QMC, number of time slices should be chosen big enough to reduce the systematic error due to the Trotter-Suzuki decomposition. As an applied example, we consider $L \sim 100$ to solve an impurity problem at temperature $\beta = 1/T \sim 1/30$ (eV)$^{-1}$. Such large number of time slices L is not problematic for matrix inversion but the total number of Ising spin configurations needed to obtain the Green's function $\mathcal{G}^{\sigma}$ (from Eq. (3.51)) is huge $2^L = 2^{100} \sim 10^{30}$. In this case, we use the Monte-Carlo and important sampling technique to evaluate the average (3.51).

To do that, we start with a random Ising spin configuration $\{s_1, s_2, ..., s_L\}$. With proposing (a movement) probability $T_{\mathbf{s}\to\mathbf{s}'} = 1/L$, we choose one Ising spin randomly and flip it ($s_p \to -s_p$). The new Ising spin configuration is then accepted with acceptance probability

$$\begin{aligned} A_{\mathbf{s}\to\mathbf{s}'} &= \min\left\{1, \frac{1/L\ p(\{s'\})}{1/L\ p(\{s\})}\right\} \\ &= \min\left\{1, \frac{\mathrm{Det}[\widetilde{G}^{\uparrow}_{\{s'\}}]^{-1} \cdot \mathrm{Det}[\widetilde{G}^{\downarrow}_{\{s'\}}]^{-1}}{\mathrm{Det}[\widetilde{G}^{\uparrow}_{\{s\}}]^{-1} \cdot \mathrm{Det}[\widetilde{G}^{\downarrow}_{\{s\}}]^{-1}}\right\} \\ &= \min\left\{1, \left[1 + (1 - \widetilde{G}^{\uparrow}_{pp})(e^{\lambda(s'_p - s_p)} - 1)\right]\left[1 + (1 - \widetilde{G}^{\downarrow}_{pp})(e^{-\lambda(s'_p - s_p)} - 1)\right]\right\}. \end{aligned} \tag{3.52}$$

where $p(\{s\}) = \mathrm{Det}[\widetilde{G}^{\uparrow}_{\{s\}}]^{-1} \cdot \mathrm{Det}[\widetilde{G}^{\downarrow}_{\{s\}}]^{-1}$ is the probability distribution (See Eq. (3.2)) and we used[12]

$$\frac{\mathrm{Det}[\widetilde{G}'^{\sigma}_{\{s\}}]^{-1}}{\mathrm{Det}[\widetilde{G}^{\sigma}_{\{s\}}]^{-1}} = 1 + (1 - \widetilde{G}^{\sigma}_{pp})(e^{\sigma\lambda(s'_p - s_p)} - 1). \tag{3.54}$$

[11] See Eq. (3.43) to understand why it is a $L \times L$ matrix.

[12] This relation can be easily obtained from Eq. (3.44) and considering the property of determinant where

$$\mathrm{Det}(AB) = \mathrm{Det}(A)\mathrm{Det}(B); \qquad A \text{ and } B \text{ are square matrices.} \tag{3.53}$$

We repeat this procedure to produce N_c configurations. For each accepted configuration,[13] we calculate the Green's function $\widetilde{G}_{\{s\}}$. Average over all "single configuration Green's function" returns the physical Green's function $\mathcal{G}$ in Eq. (3.51).

We can summarize the Hirsch-Fye algorithm as follows.

1. Start with non-interacting Green's function $\mathcal{G}^0(\tau,\tau')$. Write it in the matrix form $\mathcal{G}^0_{ll'}$ where $l,l'=1,2,...,L$.
2. Choose an initial Ising spin configuration randomly.
3. Calculate new Green's function $\widetilde{G}$ with *clean update* from
$$\widetilde{G}^\sigma = \mathcal{A}^\sigma \mathcal{G}^{0\sigma}, \tag{3.55}$$
where $\mathcal{A} = \delta_{ll'} e^{\lambda\sigma s_{l'}} + \widetilde{G}_{ll'}(e^{\lambda\sigma s_{l'}} - 1)$. Notice that $e^{\lambda\sigma s_l} = 1$ because we start with a non-interacting system.
4. Choose an Ising spin s_p $(1 \le p \le L)$ randomly and produce a new configuration with probability in Eq. (3.52).
5. Compute new Green's function $\widetilde{G}'^\sigma$ from $\widetilde{G}^\sigma$ by using the fast update equation (3.50).
6. During the fast update, numerical round-off errors may appear. In order to avoid them we must do clean update (see Eq. (3.44)) after a certain number of doing fast update.
7. Save the measurement ($\widetilde{G}^\sigma$) after warming up steps (when the distribution reaches equilibrium).
8. Go to step 4, and collect enough measurements.
9. Calculate the physical Green's function $\mathcal{G}(\tau)$ from $L\times L$ matrix $\mathcal{G}(\tau_l,\tau_{l'})$.

3.2.3 Minus sign problem

The infamous minus sign problem in QMC computations comes from the fact that the fermionic determinants in Eq. (3.27) are not always positive. This causes a problem in calculating the average in Eq. (3.51) by using the Monte-Carlo technique. Because in this case, the acceptance probability in Eq. (3.52) may have negative values which is not acceptable. To more this explicit, we rewrite the average (3.51) as follows.

$$\begin{aligned}
\mathcal{G}^\sigma &= \frac{\sum_{\{s\}} \mathcal{Z}_{\{s\}}\, \widetilde{G}^\sigma_{\{s\}}}{\sum_{\{s\}} \mathcal{Z}_{\{s\}}} \\
&= \frac{\sum_{\{s\}} \mathrm{sign}(\{s\}) |\mathcal{Z}_{\{s\}}|\, \widetilde{G}^\sigma_{\{s\}}}{\sum_{\{s\}} \mathrm{sign}(\{s\}) |\mathcal{Z}_{\{s\}}|} \\
&= \frac{\sum_{\{s\}} \mathrm{sign}(\{s\}) |\mathcal{Z}_{\{s\}}|\, \widetilde{G}^\sigma_{\{s\}} \,/\, \sum_{\{s\}} |\mathcal{Z}_{\{s\}}|}{\sum_{\{s\}} \mathrm{sign}(\{s\}) |\mathcal{Z}_{\{s\}}| \,/\, \sum_{\{s\}} |\mathcal{Z}_{\{s\}}|}.
\end{aligned} \tag{3.56}$$

[13] Notice that it takes time that the distribution probability reaches equilibrium. Some initial configurations should be thrown away, consequently.

Now we can consider $\left|\mathcal{Z}_{\{s\}}\right|$ as probability distribution $p(\{s\})$ in Eq. (3.52) to calculate

$$\begin{aligned}
\mathcal{G}^{\sigma} &= \frac{\sum_{\{s\}} \mathrm{sign}(\{s\}) p(\{s\})\ \widetilde{G}^{\sigma}_{\{s\}}\ /\ \sum_{\{s\}} p(\{s\})}{\sum_{\{s\}} \mathrm{sign}(\{s\}) p(\{s\})\ /\ \sum_{\{s\}} p(\{s\})} \\
&= \frac{\dfrac{1}{N_c}\displaystyle\sum_{\{s\}} \mathrm{sign}(\{s\})\ \widetilde{G}^{\sigma}_{\{s\}}}{\dfrac{1}{N_c}\displaystyle\sum_{\{s\}} \mathrm{sign}(\{s\})} \\
&\equiv \frac{\left\langle \mathrm{sign}\cdot \widetilde{G}^{\sigma} \right\rangle_{\mathrm{MC}}}{\left\langle \mathrm{sign} \right\rangle_{\mathrm{MC}}},
\end{aligned} \tag{3.57}$$

where N_c is the total number of (accepted) configurations and the index MC corresponds to Monte-Carlo average. In the DMFT, it is often possible to reduce the sign problem by simply running the simulation longer.

There are, however, some special cases that the fermionic determinant is always positive. For instance, in QMC computation of single band Impurity model [49] and Hubbard model at half-filling, where particle hole symmetry exists [50], no sign problem appears.

CHAPTER 4

Response function

In this chapter, first of all we will explain the concept of the response function χ by using the linear response theory and we will show how this physical quantity is related to experiments. Furthermore, we will present a general definition of the response function χ in imaginary time and frequency space. The Bethe-Salpeter equation will be introduced to calculate the response function of the system self-consistently. At the end of this chapter, we will describe in detail properties of the response function which are very useful for numerical calculation.

Contents

4.1 Modern experimental techniques . . . 33
4.1.1 Transport experiments . . . 34
4.1.2 Spectroscopic experiments . . . 34
4.2 Linear response theory . . . 36
4.3 General definition of the susceptibility in imaginary time and frequency space 39
4.3.1 Bethe-Salpeter equation: A self-consistent equation for the susceptibility . . . 41
4.3.2 Lattice susceptibility and local vertex approximation within DMFT . . . 43
4.3.3 Legendre representation of the Bethe-Salpeter equation . . . 44
4.3.4 Spin susceptibility . . . 45
4.3.5 Density-density or charge susceptibility . . . 49
4.3.6 Spin-density susceptibility . . . 50
4.4 Properties of the susceptibility . . . 50
4.4.1 Properties of the susceptibility in τ space . . . 50
4.4.2 Properties of the susceptibility in Matsubara frequency space . . . 61
4.4.3 Behavior of the dynamical lattice susceptibility at large $\nu_n, \nu_{n'}$ . . . 66

4.1 Modern experimental techniques

The ultimate goal of the theory is understanding and predicting the functional dependence of the measured value X_i on the forces F_j in the experiment. This functional dependency is linear for sufficiently weak forces,

$$X_i(\mathbf{r},t) = \int d\mathbf{r}' \int dt'\ \chi_{ij}(\mathbf{r},t;\mathbf{r}',t')F_j(\mathbf{r}',t') + \mathcal{O}(F^2). \tag{4.1}$$

In this relation, F_j is an experimental field, hence an adjustable quantity and X_i is the output of the experiment. The Kernel of this integral χ depends on intrinsic properties of the system.

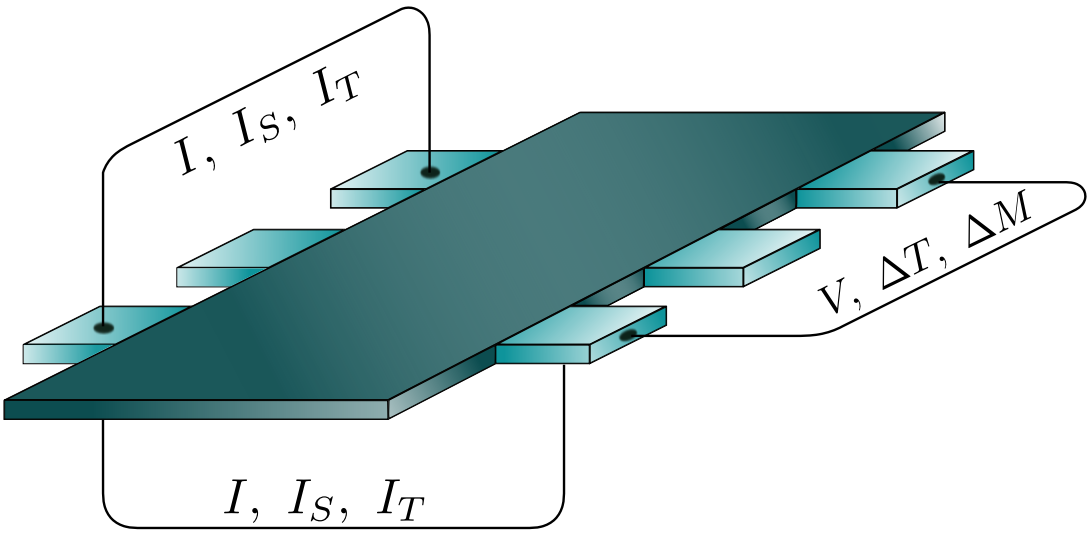

Figure 4.1: Schematic experimental set up for transport measurement [51].

χ describes how the system responds to the external perturbation (or spontaneous fluctuation) and this quantity is nothing but a correlation function in theoretical physics.

Experimentally, the response function is measured by relating the input F_j to the observed output X_i. Transport and spectroscopy are two major categories of experiments to study the dynamics and spatial fluctuation of the system [51].

4.1.1 Transport experiments

In these experiments, a general voltage U is applied to a sample. Thus a current I flows through the sample. The voltage U can be electrical V, temperature gradient ΔT, or magnetization gradient ΔM. The current flows due to different voltages are electrical current I carried by charge of mobile carriers, thermal current I_T carried by their energies and spin current I_s carried by their magnetic moment (see Fig. 4.1). The ratio of a current and a generalized voltage is the conductance which describes the transport behavior of a metal or thermal conductor properties of insulators.

4.1.2 Spectroscopic experiments

In spectroscopic experiments, a beam of either particles p (such as electrons, neutrons and etc) or a quanta of an electromagnetic radiation with momentum $\mathbf{k}_i$ and energy $\varepsilon_i(\mathbf{k}_i)$ is generated by a source. This beam is directed to the sample. After interaction with it, a secondary beam of particles p' with momentum $\mathbf{k}_f$ and energy $\varepsilon_f(\mathbf{k}_f)$ is scattered. A detector monitors the scattered beam in the laboratory (See Fig. 4.2). By using measurement of the momentum transfer $\Delta\mathbf{k} = \mathbf{k}_f - \mathbf{k}_i$, energy transfer $\Delta\varepsilon = \varepsilon_f - \varepsilon_i$ and the intensity of the scattered beam, one can infer the structural and dynamical properties of the system. In the following, some of the spectroscopic experiments are shortly reviewed [51].

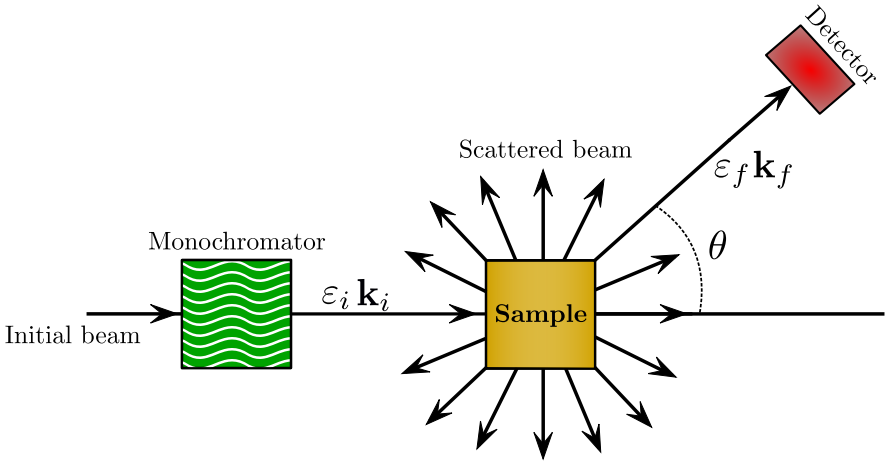

Figure 4.2: Schematic experimental set up for spectroscopy measurements [52].

4.1.2.1 X-ray spectroscopy

X-ray can easily penetrate in the sample and it is good to study the bulk properties. The electric field of the radiation interacts with electronic charge density of the crystal and scatters (see Fig. 4.3). From the elastic X-ray scattering ($\Delta\varepsilon = 0$), we can obtain useful information about the crystal structure, electronic charge distribution and charge-charge correlation[1]. Inelastic X-ray scattering gives information about the phonons throughout the Brillouin zone [52].

4.1.2.2 Electron spectroscopy

The electron beam directed to the sample interacts with the charged particles such as electrons and nuclei of the system. Within this process either electron or photon scatters. Due to Coulomb interaction between the incident beam and the charged particles in the sample, electrons can not penetrate deeply. Therefore, electron spectroscopy is a good tool to study the surface of the sample or thin films[2]. The inverse photoemission spectroscopy (IPES) in which the emitted electrons eject photons probes the spectral function above the Fermi energy [53].

4.1.2.3 Neutron spectroscopy

A beam of neutrons with energy ~ 80 meV hits the sample[3]. Since the neutrons are neutral, they interact with nucleons through nuclear forces. Therefore, they penetrate deeply to the

[1] In order to study the crystal structure and charge distribution we notice that the energy of the beam should be around 10-50 keV, because the wave length of the photons $\lambda = 2\pi\hbar c/\hbar\omega = 12398.5/\hbar\omega$ should be order of the Angstrom [52].

[2] It is easy to estimate the energy range of the incident electron beam. The energy of the free electron is $E = \hbar^2 k^2/2m_e$ in which $k = 2\pi/\lambda$ and $m_e c^2 \sim 0.5 \times 10^6$ eV. Since the lattice constant is order of Angstrom, the wave length of the incident beam should be around Angstrom ($\lambda \sim 1$Å). Thus the energy of the electron beam obtained from $\lambda = hc/\sqrt{2m_e c^2 E^{1/2}}$ is $E \sim 300$ eV. For this kind of spectroscopy the energy of incident beam is around $10 \leq E \leq 10^3$ eV [52].

[3] The energy of one neutron is calculated by $E = \hbar^2 k^2/2M_n$, where $k = 2\pi/\lambda$ and M_n is the neutron mass. It is obvious that the wave length of the neutrons is evaluated by $\lambda = 0.2862/\sqrt{E}$, where λ is in Angstrom and E in eV. Based on this relation, neutrons with wave length one Angstrom will have an energy around 80 meV which is in the same order of magnitude of $k_B T$ at room temperature, i.e., $k_B T \sim 23.538$ meV for $T \sim 273$ K [52].

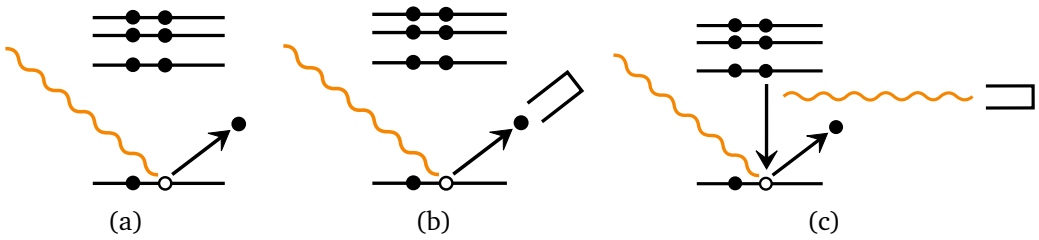

Figure 4.3: a) Due to ionization, the X-ray is absorbed. b) The emitted electrons are detected. c) A valence electron recombines with the core holes created by incident X-ray (X-ray fluorescence spectroscopy [51]).

sample and they are sensitive to the spatial distribution of the nuclei and their vibrations. Thus, like the X-ray scattering, elastic neutron scattering can be employed to obtain information about the crystal structure of the sample. Neutrons interact also with the magnetic moments in the sample. For this reason, inelastic and inelastic neutron scattering provide useful details about the magnetic properties of the system [52, 53].

4.1.2.4 Nuclear magnetic resonance (NMR) spectroscopy

The sample is placed in the static magnetic field $\mathbf{B} = B_0\hat{z}$. The magnetic field separates the spin states of the nuclei, i.e., $I_\uparrow = |\uparrow\rangle$ and $I_\downarrow = |\downarrow\rangle$ so that the energy difference between $m_I = +1/2$ and $m_I = -1/2$ is $\Delta E = g_I\mu_N B_0$, where μ_N is the nuclear magneton[4] and g_I is the g-factor of the nucleus[5]. In the NMR spectroscopy (see Fig. 4.4), an electromagnetic radiation with frequency ν is radiated to the sample[6]. The nuclear magnetic resonance occurs when the energy of the radiation $h\nu$ is exactly equal to ΔE. Therefore, a strong absorption happens as the spins make the transition from $|\uparrow\rangle$ to $|\downarrow\rangle$ [55]. Furthermore, each nucleus at site i interacts with the induced magnetic field by surrounding spins and orbitals (namely hyperfine interaction). This interaction produces a shift in the resonance absorption lines in NMR which is known as *Knight shift*. The Knight shift provides useful information about the magnetic properties conduction electrons and can be used as a method to detect the magnetic order [53].

4.2 Linear response theory

Linear response theory is the heart of physics. It provides a general framework to study the dynamical properties of a system close to thermal equilibrium. This theory states that the response of a system to a small external perturbation (or spontaneous fluctuation) is proportional to that external perturbation (or spontaneous perturbation). This proportionality tensor is actually the bridge of theoretical and experimental physics which is called response function. In the following, we derive the linear response theory formula.

[4] The nuclear magneton is $\mu_N = e\hbar/2m_p$, where m_p is the mass of the proton.

[5] The g-factors for proton and neutrons are $g_p \sim 5.586$ and $g_n \sim -3.826$, respectively.

[6] The electromagnetic radiation should be in radio frequency region ($\sim$ 3 Hz - 3 GHz) because e.g. for a magnetic field $\sim$ 1 T, the frequency is given by $\nu = \omega/2\pi = g_I\mu_N B_0/2\pi\hbar \sim 42.6$ MHz [54].

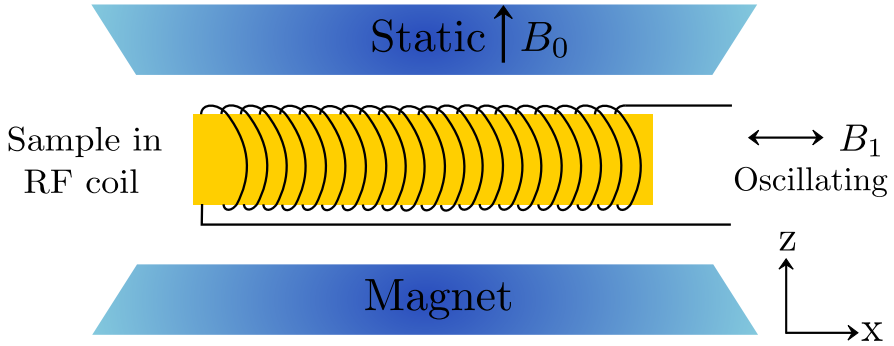

Figure 4.4: Schematic diagram for NMR spectroscopy. The static magnetic field is provided by a magnet. The sample resides in the radio frequency coil which generates the RF field [54].

If a physical system in equilibrium is explained by Hamiltonian H_0, then the expectation value of a physical quantity, $\langle A\rangle$, can be written by

$$\langle A\rangle = \frac{1}{\mathcal{Z}_0}\mathrm{Tr}\left[\rho_0 A\right] = \frac{1}{\mathcal{Z}_0}\sum_n e^{-\beta E_n}\langle n|A|n\rangle, \tag{4.2}$$

where $\rho_0 = \sum_n e^{-\beta E_n}|n\rangle\langle n|$ is density operator and $\mathcal{Z}_0 = \mathrm{Tr}\left[\rho_0\right]$ is partition function [56]. If this system in equilibrium is perturbed by a small external perturbation (or spontaneous fluctuation), H', at time $t = t_0$ so that

$$H(t) = H_0 + H'(t)\theta(t - t_0), \tag{4.3}$$

the system is not any more in equilibrium and the state $|n\rangle$ evolves into $|n(t)\rangle$. The expectation value of A, therefore, should be calculated for the evolved states

$$\langle A(t)\rangle = \frac{1}{\mathcal{Z}_0}\sum_n e^{-\beta E_n}\langle n(t)|A|n(t)\rangle. \tag{4.4}$$

Next, we use the interaction representation to rewrite $|n(t)\rangle$ as

$$|n(t)\rangle = e^{-iH_0 t}|n_I(t)\rangle = e^{-iH_0 t}\hat{U}(t,t_0)|n_I(t_0)\rangle, \tag{4.5}$$

where $|n_I(t_0)\rangle = e^{iH_0 t_0}|n(t_0)\rangle = |n\rangle$ and

$$\hat{U}(t,t_0) = \mathcal{T}\left(e^{-i\int_{t_0}^{t} dt' H'(t')}\right). \tag{4.6}$$

In the linear order of $\hat{U}$, we have $\hat{U}(t,t_0) \approx 1 - i\int_{t_0}^{t} dt' H'(t')$ and the expectation value of A is

$$\begin{aligned}
\langle A(t)\rangle &= \frac{1}{\mathcal{Z}_0}\sum_n e^{-\beta E_n}\langle n_I(t_0)|\left(1 + i\int_{t_0}^{t} H'(t')dt'\right)e^{iH_0 t}Ae^{-iH_0 t}\left(1 - i\int_{t_0}^{t} H'(t')dt'\right)|n_I(t_0)\rangle \\
&= \frac{1}{\mathcal{Z}_0}\sum_n e^{-\beta E_n}\langle n|A_I(t)|n\rangle \\
&\quad -i\int_{t_0}^{t} dt'\frac{1}{\mathcal{Z}_0}\sum_n e^{-\beta E_n}\langle n_I(t_0)|A_I(t)H'(t') - H'(t')A_I(t')|n_I(t_0)\rangle \\
&= \langle A\rangle_0 - i\int_{t_0}^{t} dt'\left\langle\left[A_I(t), H'(t')\right]\right\rangle_0,
\end{aligned} \tag{4.7}$$

where the $\langle ...\rangle_0$ means an average with respect to the H_0. The first term of Eq. (4.7) is independent of H', since it comes from an equilibrium ensemble average for A. From this equation it is clear that the physical quantity $\langle A(t)\rangle$ is expressed in terms of a retarded correlation function of the system in equilibrium.

In *imaginary time τ space*, it is possible to derive the linear response by using the partition function.

$$\begin{aligned}\mathcal{Z} &= \mathrm{Tr}\left\{e^{-\beta H}\right\} = \mathrm{Tr}\left\{e^{-\beta H_0}e^{\beta H_0}e^{-\beta H}\right\} \\ &= \mathrm{Tr}\left\{e^{-\beta H_0}\hat{U}(\beta,0)\right\} \\ &= \mathcal{Z}_0\,\mathcal{T}\left(e^{-\int_0^\beta d\tau' H'(\tau')}\right). \end{aligned} \tag{4.8}$$

The expectation value of A to the linear order of $\hat{U}$ is

$$\begin{aligned}\langle A(\tau)\rangle &= \frac{\mathrm{Tr}\left\{A(\tau)e^{-\beta H}\right\}}{\mathrm{Tr}\left\{e^{-\beta H}\right\}} = \frac{\left\langle \mathcal{T}A(\tau)e^{-\int_0^\beta d\tau' H'(\tau')}\right\rangle_0}{\left\langle \mathcal{T}e^{-\int_0^\beta d\tau' H'(\tau')}\right\rangle_0} \\ &\approx \left\langle \mathcal{T}A(\tau)\left(1-\int_0^\beta d\tau' H'(\tau')\right)\right\rangle_0 \left\langle\left(1+\int_0^\beta d\tau' H'(\tau')\right)\right\rangle_0 \\ &\approx \big\langle A(\tau)\big\rangle_0 - \int_0^\beta d\tau'\Big(\big\langle \mathcal{T}A(\tau)H'(\tau')\big\rangle_0 - \big\langle A(\tau)\big\rangle_0\big\langle H'(\tau')\big\rangle_0\Big). \end{aligned} \tag{4.9}$$

If the Hamiltonian of the system does not explicitly depend on time, the linear response depends on the difference of time coordinates only. In this case, it is easier to study the response function in the Fourier space. This is particularly useful when the external perturbation has the form

$$H'(t) = Bf(t), \tag{4.10}$$

where B is time independent operator and $f(t)$ is time dependent but not operator. The linear response relation in frequency domain can be written as

$$\delta\langle A\rangle \equiv \langle A(\omega)\rangle - \langle A(\omega)\rangle_0 = \chi(\omega)f(\omega), \tag{4.11}$$

in which χ is the response of the system to the small perturbation affected the system. An important point about relation (4.11) is that (in linear response regime) a perturbation acting at a certain frequency ω will cause a response of the same frequency. If the system responds at frequencies $\neq \omega$, we have a *nonlinear* response [51] and Eq. (4.11) has to be corrected. The correction is done by an expansion to nth order in e.g. Eq. (4.9). The expansion generates a response function which depends on n values of frequencies ω_i where $i = 1, 2, ..., n$ [57].

According to Eqs. (4.7, 4.9) and (4.10), the response of the system in real and imaginary time is

$$\chi(t,t') = -i\theta(t-t')\left\langle[A(t),B(t')]\right\rangle, \tag{4.12}$$

$$\chi(\tau,\tau') = \left\langle \mathcal{T}A(\tau)B(\tau')\right\rangle - \left\langle A(\tau)\right\rangle\left\langle B(\tau')\right\rangle, \tag{4.13}$$

where the expectation values are calculated in the equilibrium states.

The following table shows some different kinds of correlation functions that can be used to justify the related experimental measurements.

Experiment	Spectrum	Correlation function
ARPES	$I(\mathbf{k},\omega) \propto f(-\omega)A(\mathbf{k},-\omega)$	$\sim \langle c^{\dagger}_{\mathbf{k}}(0)c_{\mathbf{k}}(t)\rangle$
Inverse PES	$I(\omega) \propto \sum_{\mathbf{k}}(1-f(\omega))A(\mathbf{k},\omega)$	$\sim \langle c_{\mathbf{k}}(t)c^{\dagger}_{\mathbf{k}}(0)\rangle$
Neutron scattering	$S(\mathbf{q},\omega) \propto \Im m\left[\chi(\mathbf{q},\omega)\right]$	$\sim \langle \mathbf{S}_{\mathbf{q}}(t)\cdot\mathbf{S}_{-\mathbf{q}}(0)\rangle$
NMR	Knight shift and relaxation time $\propto \chi$	$\sim \langle \mathbf{S}_{\mathbf{q}=\mathbf{0}}(t)\cdot\mathbf{S}_{\mathbf{q}=\mathbf{0}}(0)\rangle$
Dielectric properties ε	$\varepsilon(\mathbf{q},\omega)$	$\sim \langle n_{\mathbf{q}}(t)n_{-\mathbf{q}}(0)\rangle$

4.3 General definition of the susceptibility in imaginary time and frequency space

Using Eq. (4.13), a general relation for the response function $\chi(\mathbf{q},\omega_m)$ in Fourier space and in terms of Matsubara frequencies can be obtained by

$$\begin{aligned}\chi(\mathbf{q},\omega_m) &= \int_0^{\beta} d\tau_1 \int_0^{\beta} d\tau_2\, e^{i\omega_m(\tau_1-\tau_2)} \sum_{\mathbf{ij}} e^{i\mathbf{q}.(\mathbf{R_j}-\mathbf{R_i})} \\ &\times\Big\{\Big\langle \mathcal{T}\hat{\mathcal{O}}_1(\mathbf{R_j},\tau_1)\hat{\mathcal{O}}_2(\mathbf{R_i},\tau_2)\Big\rangle - \Big\langle \hat{\mathcal{O}}_1(\mathbf{R_j},\tau_1)\Big\rangle\Big\langle \hat{\mathcal{O}}_2(\mathbf{R_i},\tau_2)\Big\rangle\Big\}. \end{aligned} \tag{4.14}$$

In this relation $\beta = 1/k_BT$ is the inverse temperature, $\omega_m = 2m\pi/\beta$ the bosonic Matsubara frequency, τ_1,τ_2 the imaginary times and $\mathcal{T}$ the time ordering operator. The operator $\hat{\mathcal{O}}$ is

$$\hat{\mathcal{O}}(\mathbf{R_j},\tau_1) = \sum_{\lambda\mu}\sum_{\kappa_\lambda\kappa_\mu}\sum_{\sigma} v^{\sigma}_{\mathbf{j};\mu\kappa_\mu,\lambda\kappa_\lambda}\; c^{\dagger}_{\mathbf{j},\lambda\kappa_\lambda\sigma}(\tau_1)c_{\mathbf{j},\mu\kappa_\mu\sigma}(\tau_1), \tag{4.15}$$

where $c_{\mu\kappa_\mu\sigma}$ ($c^{\dagger}_{\mu\kappa_\mu\sigma}$) operator annihilates (creates) an electron in orbital μ and site κ_μ with spin σ. Here v is *vertex factor* which varies for different type of the response functions such as magnetic susceptibility, density-density response function etc.

It is possible to make Eq. (4.14) simpler with substitution of operator $\hat{\mathcal{O}}(\mathbf{R},\tau)$ by its Fourier transformed version in $\mathbf{q}$-space (see Appendix A.1).

$$\hat{\mathcal{O}}(\mathbf{q},\tau_1) = \frac{1}{N_{\mathbf{k}}}\sum_{\mathbf{k}}\sum_{\lambda\mu}\sum_{\kappa_\lambda\kappa_\mu}\sum_{\sigma} v^{\sigma}_{\mathbf{k}\mathbf{k}+\mathbf{q};\lambda\alpha_\lambda,\mu\alpha_\mu}\; c^{\dagger}_{\mathbf{k},\lambda\kappa_\lambda\sigma}(\tau_1)c_{\mathbf{k}+\mathbf{q},\mu\kappa_\mu\sigma}(\tau_1), \tag{4.16}$$

in which $N_{\mathbf{k}}$ is number of $\mathbf{k}$-points. With the considering the Fourier integral of the creator and annihilator operators

$$c(\nu_n) = \int_0^{\beta} d\tau\; e^{i\nu_n\tau}c(\tau);\; c(\tau) = \frac{1}{\beta}\sum_{n=-\infty}^{+\infty} e^{-i\nu_n\tau}c(\nu_n)$$

$$c^{\dagger}(\nu_n) = \int_0^{\beta} d\tau\; e^{-i\nu_n\tau}c^{\dagger}(\tau);\; c^{\dagger}(\tau) = \frac{1}{\beta}\sum_{n=-\infty}^{+\infty} e^{i\nu_n\tau}c^{\dagger}(\nu_n),$$

and using Eq. (4.16), the lattice susceptibility is obtained by

$$\begin{aligned}\chi(\mathbf{q},\omega_m) &= \frac{1}{N_{\mathbf{k}}^2}\sum_{\mathbf{k}\mathbf{k}'}\sum_{\substack{\lambda\mu\\ \gamma\delta}}\sum_{\substack{\kappa_\lambda\kappa_\mu\\ \kappa_\gamma\kappa_\delta}}\sum_{\sigma\sigma'}\frac{1}{\beta^2}\sum_{n=-\infty}^{+\infty}\sum_{n'=-\infty}^{+\infty} v^{\sigma}_{\mathbf{k}\mathbf{k}+\mathbf{q};\lambda\kappa_\lambda,\mu\kappa_\mu} \\ &\times\; \chi^{\sigma\sigma'}_{\lambda\kappa_\lambda,\mu\kappa_\mu,\gamma\kappa_\gamma,\delta\kappa_\delta}(\mathbf{k},\nu_n,\mathbf{k}',\nu_{n'};\mathbf{q},\omega_m)\; v^{\sigma'}_{\mathbf{k}'+\mathbf{q}\mathbf{k}';\gamma\kappa_\gamma,\delta\kappa_\delta}, \end{aligned} \tag{4.17}$$

wherein

$$\begin{aligned}\chi^{\sigma\sigma'}_{\lambda\kappa_\lambda,\mu\kappa_\mu,\gamma\kappa_\gamma,\delta\kappa_\delta} &= \Big\langle c^\dagger_{\mathbf{k},\lambda\kappa_\lambda\sigma}(\nu_n)c_{\mathbf{k}+\mathbf{q},\mu\kappa_\mu\sigma}(\nu_n+\omega_m)c^\dagger_{\mathbf{k}'+\mathbf{q},\gamma\kappa_\gamma\sigma'}(\nu_{n'}+\omega_m)c_{\mathbf{k}',\delta\kappa_\delta\sigma'}(\nu_{n'})\Big\rangle \\ &\quad -\Big\langle c^\dagger_{\mathbf{k},\lambda\kappa_\lambda\sigma}(\nu_n)c_{\mathbf{k}+\mathbf{q},\mu\kappa_\mu\sigma}(\nu_n+\omega_m)\Big\rangle\Big\langle c^\dagger_{\mathbf{k}'+\mathbf{q},\gamma\kappa_\gamma\sigma'}(\nu_{n'}+\omega_m)c_{\mathbf{k}',\delta\kappa_\delta\sigma'}(\nu_{n'})\Big\rangle.\end{aligned} \tag{4.18}$$

Here, $\nu_n = (2n+1)\pi/\beta$ and $\nu_{n'} = (2n'+1)\pi/\beta$ are fermionic Matsubara frequencies, $\beta = 1/k_BT$ inverse temperature.

For non-interacting systems, we can use the Wick's theorem to obtain the lattice susceptibility in terms of the fully interacting Green's functions.

$$\begin{aligned}\chi^0(\mathbf{q},i\omega_m) &= \frac{1}{N^2_{\mathbf{k}}}\sum_{\mathbf{k}\mathbf{k}'}\sum_{\substack{\lambda\mu\\ \gamma\delta}}\sum_{\substack{\kappa_\lambda\kappa_\mu\\ \kappa_\gamma\kappa_\delta}}\sum_{\sigma\sigma'}\frac{1}{\beta^2}\sum_{n=-\infty}^{+\infty}\sum_{n'=-\infty}^{+\infty} v^\sigma_{\mathbf{k}\mathbf{k}+\mathbf{q};\lambda\kappa_\lambda,\mu\kappa_\mu} \\ &\quad\times\ \chi^{\mathbf{0},\sigma\sigma'}_{\lambda\kappa_\lambda,\mu\kappa_\mu,\gamma\kappa_\gamma,\delta\kappa_\delta}(\mathbf{k},\nu_n,\mathbf{k}',\nu_{n'};\mathbf{q},\omega_m)v^{\sigma'}_{\mathbf{k}'+\mathbf{q}\mathbf{k}';\gamma\kappa_\gamma,\delta\kappa_\delta},\end{aligned} \tag{4.19}$$

where

$$\begin{aligned}\chi^{\mathbf{0},\sigma\sigma'}_{\lambda\kappa_\lambda,\mu\kappa_\mu,\gamma\kappa_\gamma,\delta\kappa_\delta}(\mathbf{k},\nu_n,\mathbf{k}',\nu_{n'};\mathbf{q},\omega_m) &= -\beta^2\delta_{nn'}N^2_{\mathbf{k}}\ \delta_{\mathbf{k},\mathbf{k}'}\delta_{\sigma\sigma'} \\ &\quad\times\mathcal{G}^\sigma_{\mu\kappa_\mu,\gamma\kappa_\gamma}(\mathbf{k}+\mathbf{q},\nu_n+\omega_m)\mathcal{G}^{\sigma'}_{\delta\kappa_\delta,\lambda\kappa_\lambda}(\mathbf{k}',\nu_{n'}).\end{aligned} \tag{4.20}$$

The $\chi^0(\mathbf{q},\omega_m)$ is known as *bare lattice susceptibility*.

For the sake of simplicity in notation, we use a compact form of indices in which

$$\alpha_j \equiv j\kappa_j\sigma_j$$

are collective orbital (j), site (κ_j) and spin σ_j indices. In the considered cases here $\sigma_1 = \sigma_2 = \sigma$ and $\sigma_3 = \sigma_4 = \sigma'$. Also we use

$$\tilde{\mathbf{k}} \equiv (\mathbf{k}, i\nu_n),$$

which denotes that $\tilde{\mathbf{k}}$ consists of momenta $\mathbf{k}$ and Matsubara frequencies $i\nu_n$.

Consequently, the lattice susceptibility χ and it's mean field approximation $\chi^{\mathbf{0}}$ can be rephrased as

$$\begin{aligned}\chi_{\alpha_\lambda\alpha_\mu\alpha_\gamma\alpha_\delta}(\tilde{\mathbf{k}},\tilde{\mathbf{k}'};\tilde{\mathbf{q}}) &\equiv \chi^{\sigma\sigma'}_{\lambda\kappa_\lambda,\mu\kappa_\mu,\gamma\kappa_\gamma,\delta\kappa_\delta}(\mathbf{k},\nu_n,\mathbf{k}',\nu_{n'};\mathbf{q},\omega_m) \\ \chi^{\mathbf{0}}{}_{\alpha_\lambda\alpha_\mu\alpha_\gamma\alpha_\delta}(\tilde{\mathbf{k}},\tilde{\mathbf{k}'};\tilde{\mathbf{q}}) &\equiv -\beta^2\delta_{nn'}N^2_{\mathbf{k}}\ \delta_{\mathbf{k},\mathbf{k}'}\delta_{\sigma\sigma'}\mathcal{G}^\sigma_{\mu\kappa_\mu,\gamma\kappa_\gamma}(\mathbf{k}+\mathbf{q},\nu_n+\omega_m)\mathcal{G}^{\sigma'}_{\delta\kappa_\delta,\lambda\kappa_\lambda}(\mathbf{k}',\nu_{n'}).\end{aligned} \tag{4.21}$$

We can employ Eq. (4.18) to obtain the general form of the susceptibility in terms of the imaginary times $\boldsymbol{\tau} = (\tau_1,\tau_2,\tau_3,\tau_4)$. It is easy to show that

$$\begin{aligned}\chi_{\alpha_i\alpha_j\alpha_k\alpha_l}(\tilde{\mathbf{k}},\tilde{\mathbf{k}'};\tilde{\mathbf{q}}) &= \int_0^\beta d\tau_1\ldots\int_0^\beta d\tau_4\ e^{-i\nu_n\tau_1}e^{i(\nu_n+\omega_m)\tau_2} \\ &\quad\times e^{-i(\nu_{n'}+\omega_m)\tau_3}e^{i\nu_{n'}\tau_4}\ \chi_{\alpha_i\alpha_j\alpha_k\alpha_l}(\mathbf{k},\mathbf{k}',\mathbf{q};\boldsymbol{\tau}).\end{aligned} \tag{4.22}$$

wherein, the $\chi_{\alpha_i\alpha_j\alpha_k\alpha_l}(\mathbf{k},\mathbf{k}',\mathbf{q};\boldsymbol{\tau})$ is the general susceptibility in imaginary time space given by

$$\begin{aligned}\chi_{\alpha_i\alpha_j\alpha_k\alpha_l}(\mathbf{k},\mathbf{k}',\mathbf{q};\boldsymbol{\tau}) &= \left\langle \mathcal{T} c^{\dagger}_{\mathbf{k}\alpha_i}(\tau_1) c_{\mathbf{k}+\mathbf{q}\alpha_j}(\tau_2) c^{\dagger}_{\mathbf{k}'+\mathbf{q}\alpha_k}(\tau_3) c_{\mathbf{k}'\alpha_l}(\tau_4)\right\rangle \\ &\quad - \left\langle \mathcal{T} c^{\dagger}_{\mathbf{k}\alpha_i}(\tau_1) c_{\mathbf{k}+\mathbf{q}\alpha_j}(\tau_2)\right\rangle \left\langle \mathcal{T} c^{\dagger}_{\mathbf{k}'+\mathbf{q}\alpha_k}(\tau_3) c_{\mathbf{k}'\alpha_l}(\tau_4)\right\rangle . \quad (4.23)\end{aligned}$$

This relation is useful when we want to calculate the local susceptibility within impurity solver in dynamical mean field theory. Using this relation, it is easy to derive the bare lattice susceptibility in terms of the green's functions respect to $\boldsymbol{\tau}$.

$$\chi^{\mathbf{0}}_{\alpha_i\alpha_j\alpha_k\alpha_l}(\mathbf{k},\mathbf{k}',\mathbf{q};\boldsymbol{\tau}) = -\delta_{\sigma\sigma'} N_{\mathbf{k}}^2\, \delta_{\mathbf{k},\mathbf{k}'}\, \mathcal{G}_{\alpha_l\alpha_i}(\mathbf{k},\tau_4-\tau_1)\mathcal{G}_{\alpha_j\alpha_k}(\mathbf{k}+\mathbf{q},\tau_2-\tau_3). \quad (4.24)$$

In the following of this chapter, we will return to Eqs. (4.23) and (4.24) and discuss their properties.

4.3.1 Bethe-Salpeter equation: A self-consistent equation for the susceptibility

By using perturbation theory [56], we can evaluate the susceptibility with respect to the single particle green's function $\mathcal{G}$ and the irreducible two-particle *vertex function* $\mathbf{\Gamma}$. The irreducible two-particle vertex function describes interaction of two elementary excitations and consists of all interaction terms between two particles.[7] In Fig. 4.5, the lowest order expansion of the vertex function is shown.

The calculated $\chi^0(\mathbf{q},\omega_m)$ is the lowest order term in perturbation expansion of the lattice

[7] The concept of the vertex function can be understood as follows. Consider a two-particle correlation function in real space as $\mathcal{C}(1,2,3,4) = \langle c_1^{\dagger} c_2 c_3^{\dagger} c_4\rangle$, where $i = 1,..,4$ is a collective indices for imaginary time τ, positions, orbitals and spins. Using the mean field approximation, we can extract the fully interacting part as

$$\gamma(1,2,3,4) = \mathcal{C}(1,2,3,4) - \mathcal{C}_{\mathrm{MF}}(1,2,3,4),$$

where the noninteracting part is

$$\mathcal{C}_{\mathrm{MF}}(1,2,3,4) = \mathcal{G}(2,1)\mathcal{G}(4,3) - \mathcal{G}(2,3)\mathcal{G}(4,1).$$

Using the perturbation theory which couples the Green's functions by the interaction, we can easily see that

$$\gamma(1,2,3,4) = \int ... \int d1'...d4' \mathcal{G}(1,1')\mathcal{G}(2,2')\mathbf{\Gamma}(1',2',3',4')\mathcal{G}(3,3')\mathcal{G}(4,4'),$$

where $\mathbf{\Gamma}$ is the vertex function. In γ, at first the particles propagate from "x_1 and x_2" to "x_1' and x_2'". Then under interaction, they extend from "x_1' and x_2'" to "x_3' and x_4'" and finally propagate to positions "x_3 and x_4". The vertex function $\mathbf{\Gamma}(1,2,3,4)$ describes interactions of the two elementary excitations.

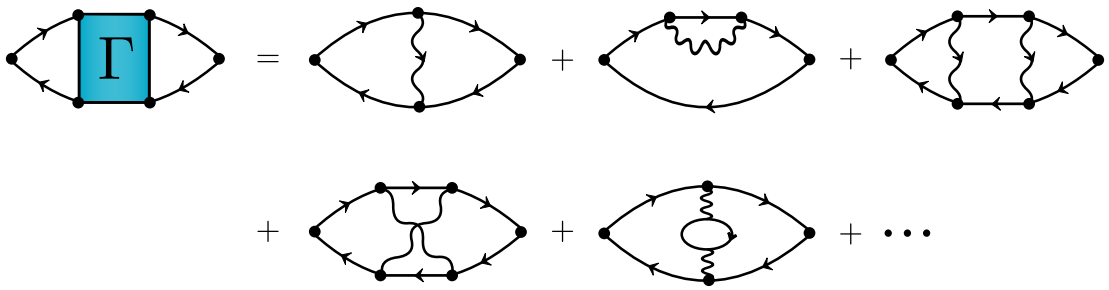

Figure 4.5: Irreducible Feynman diagrams which describe the interaction of two particles contributing to the lowest expansion of the vertex function $\mathbf{\Gamma}$ [56].

susceptibility. Higher order terms are obtained as follows.

$$\begin{aligned}
\chi(\mathbf{q},\omega_m) &= \left(\frac{1}{\beta N_{\mathbf{k}}}\right)^2 \sum_{\tilde{\mathbf{k}}\tilde{\mathbf{k}}'} \sum_{\alpha_i\alpha_j\alpha_k\alpha_l} v_{\mathbf{kk+q},\alpha_i\alpha_j} \chi^{\mathbf{0}}_{\alpha_i\alpha_j\alpha_k\alpha_l}(\tilde{\mathbf{k}},\tilde{\mathbf{k}}';\tilde{\mathbf{q}}) v_{\mathbf{k}'+\mathbf{qk}',\alpha_k\alpha_l} \\
&+ \left(\frac{1}{\beta N_{\mathbf{k}}}\right)^4 \sum_{\substack{\tilde{\mathbf{k}}\tilde{\mathbf{k}}'\\ \tilde{\mathbf{k}}_1\tilde{\mathbf{k}}_2}} \sum_{\substack{\alpha_i\alpha_j\alpha_k\alpha_l\\ \alpha_1\alpha_2\alpha_3\alpha_4}} v_{\mathbf{kk+q},\alpha_i\alpha_j} \chi^{\mathbf{0}}_{\alpha_i\alpha_j\alpha_1\alpha_2}(\tilde{\mathbf{k}},\tilde{\mathbf{k}}_1;\tilde{\mathbf{q}}) \\
&\quad \times \mathbf{\Gamma}_{\alpha_1\alpha_2\alpha_3\alpha_4}(\tilde{\mathbf{k}}_1,\tilde{\mathbf{k}}_2;\tilde{\mathbf{q}}) \chi^{\mathbf{0}}_{\alpha_3\alpha_4\alpha_k\alpha_l}(\tilde{\mathbf{k}}_2,\tilde{\mathbf{k}}';\tilde{\mathbf{q}}) v_{\mathbf{k}'+\mathbf{qk}',\alpha_k\alpha_l} \\
&+ \quad ... \\
&= \left(\frac{1}{\beta N_{\mathbf{k}}}\right)^2 \sum_{\tilde{\mathbf{k}}\tilde{\mathbf{k}}'} \sum_{\alpha_i\alpha_j\alpha_k\alpha_l} v^{\sigma}_{\mathbf{kk+q},\alpha_i\alpha_j} \chi^{\mathbf{0}}_{\alpha_i\alpha_j\alpha_k\alpha_l}(\tilde{\mathbf{k}},\tilde{\mathbf{k}}';\tilde{\mathbf{q}}) v_{\mathbf{k}'+\mathbf{qk}',\alpha_k\alpha_l} \\
&+ \left(\frac{1}{\beta N_{\mathbf{k}}}\right)^4 \sum_{\substack{\tilde{\mathbf{k}}\tilde{\mathbf{k}}'\\ \tilde{\mathbf{k}}_1\tilde{\mathbf{k}}_2}} \sum_{\substack{\alpha_i\alpha_j\alpha_k\alpha_l\\ \alpha_1\alpha_2\alpha_3\alpha_4}} v_{\mathbf{kk+q},\alpha_i\alpha_j} \chi^{\mathbf{0}}_{\alpha_i\alpha_j\alpha_1\alpha_2}(\tilde{\mathbf{k}},\tilde{\mathbf{k}}_1;\tilde{\mathbf{q}}) \\
&\quad \times \mathbf{\Gamma}_{\alpha_1\alpha_2\alpha_3\alpha_4}(\tilde{\mathbf{k}}_1,\tilde{\mathbf{k}}_2;\tilde{\mathbf{q}}) \chi_{\alpha_3\alpha_4\alpha_k\alpha_l}(\tilde{\mathbf{k}}_2,\tilde{\mathbf{k}}';\tilde{\mathbf{q}}) v_{\mathbf{k}'+\mathbf{qk}',\alpha_k\alpha_l}. \qquad (4.25)
\end{aligned}$$

Notice that the vertex function $\mathbf{\Gamma}_{\alpha_1\alpha_2\alpha_3\alpha_4}$ and also the (bare) lattice susceptibility $\chi_{\alpha_i\alpha_j\alpha_k\alpha_l}$ are tensor quantities. This equation is well known as Bethe-Salpeter equation [58] and can be easily understood by transforming it into the Feynman diagrams which is shown in Fig. 4.6. Regarding to Eqs. (4.17, 4.19) and (4.25), the full momentum and Matsubara frequency dependent of the susceptibility can be written by

$$\begin{aligned}
\chi_{\alpha_i\alpha_j\alpha_k\alpha_l}(\tilde{\mathbf{k}},\tilde{\mathbf{k}}';\tilde{\mathbf{q}}) &= \chi^{\mathbf{0}}_{\alpha_i\alpha_j\alpha_k\alpha_l}(\tilde{\mathbf{k}},\tilde{\mathbf{k}}';\tilde{\mathbf{q}}) + \left(\frac{1}{\beta N_{\mathbf{k}}}\right)^2 \sum_{\tilde{\mathbf{k}}_1\tilde{\mathbf{k}}_2} \sum_{\substack{\alpha_1\alpha_2\\ \alpha_3\alpha_4}} \chi^{\mathbf{0}}_{\alpha_i\alpha_j\alpha_1\alpha_3}(\tilde{\mathbf{k}},\tilde{\mathbf{k}}_1;\tilde{\mathbf{q}}) \\
&\quad \times \mathbf{\Gamma}_{\alpha_1\alpha_2\alpha_3\alpha_4}(\tilde{\mathbf{k}}_1,\tilde{\mathbf{k}}_2;\tilde{\mathbf{q}}) \chi_{\alpha_3\alpha_4\alpha_k\alpha_l}(\tilde{\mathbf{k}}_2,\tilde{\mathbf{k}}';\tilde{\mathbf{q}}), \qquad (4.26)
\end{aligned}$$

where in it's Feynman diagrams which is shown in Fig 4.7 there are no vertex factors. This *tensorial* equation can be written in terms of square matrices of dimension M so that each matrix depends on $\mathbf{q}$ and ω_m. In this case $\chi_{\alpha_i\alpha_j\alpha_k\alpha_l}(\tilde{\mathbf{k}},\tilde{\mathbf{k}}';\tilde{\mathbf{q}})$ can be represented by a $M \times M'$ square matrix $[\chi(\mathbf{q},\omega_m)]_{M,M'}$, where $M = \alpha_i n\mathbf{k}, \alpha_j n\mathbf{k}$ and $M' = \alpha_k n'\mathbf{k}', \alpha_l n'\mathbf{k}'$. Then the Bethe-Salpeter equation in the matrix form is obtained by

$$\Big[\chi(\mathbf{q},\omega_m)\Big] = \Big[\chi^{\mathbf{0}}(\mathbf{q},\omega_m)\Big] + \Big[\chi^{\mathbf{0}}(\mathbf{q},\omega_m)\Big]\Big[\mathbf{\Gamma}(\mathbf{q},\omega_m)\Big]\Big[\chi(\mathbf{q},\omega_m)\Big]. \qquad (4.27)$$

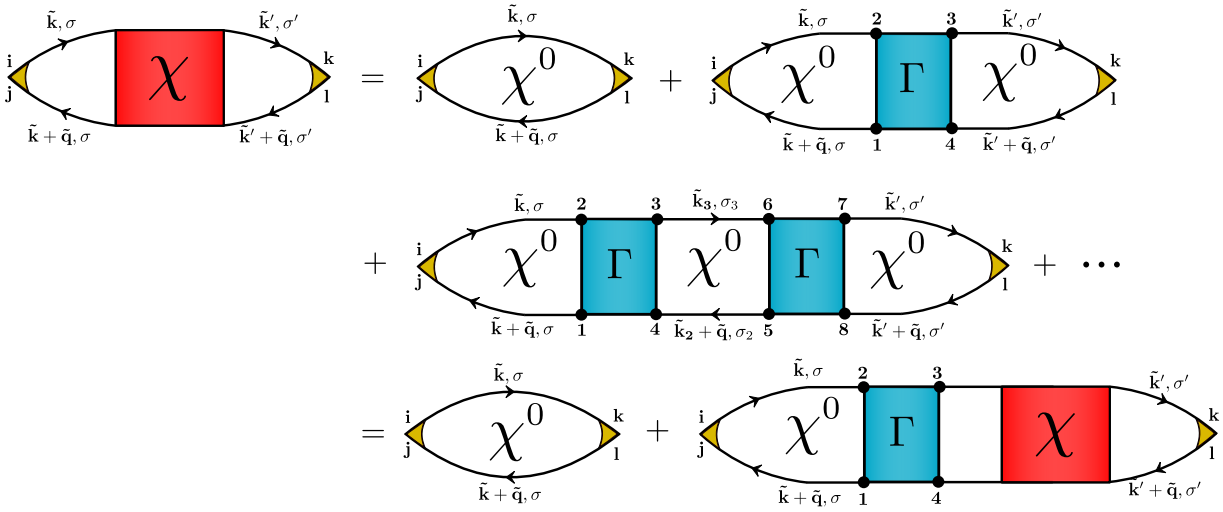

Figure 4.6: Feynman diagram representation of susceptibility $\chi(\mathbf{q}, i\omega_m)$.

With very simple algebra, the lattice susceptibility matrix is derived by

$$\Big[\chi(\mathbf{q},\omega_m)\Big]^{-1} = -\Big[\chi^{\mathbf{0}}(\mathbf{q},\omega_m)\Big]^{-1} + \Big[\mathbf{\Gamma}(\mathbf{q},\omega_m)\Big]. \tag{4.28}$$

Considering N_O as the number of orbitals, N_S the number of sites per unit cell, N_ν the number of fermionic Matsubara frequencies, $N_{\mathbf{k}}$ the number of $\mathbf{k}$-points, and $N_{\rm spin}$ the number of spins, each matrix in Eq. (4.27) has $(N_O^2 N_S^2 N_{\rm spin} N_\nu N_{\mathbf{k}}) \times (N_O^2 N_S^2 N_{\rm spin} N_\nu N_{\mathbf{k}})$ elements.

4.3.2 Lattice susceptibility and local vertex approximation within DMFT

In general, the exact solution of the Bethe-Salpeter equation is not known. Thus we need approximations to calculate the susceptibility from the Bethe-Salpeter equation. In the DMFT approach, the lattice Hamiltonian is modeled into a self consistent quantum impurity model described by a local Green's function $\mathcal{G}_{\mathbf{loc}}$. The same approximation is used to calculate response of the lattice model to external perturbation or fluctuation. Within the DMFT approximation, the full momentum dependent vertex function $\mathbf{\Gamma}(\tilde{\mathbf{k}}, \tilde{\mathbf{k}}'; \tilde{\mathbf{q}})$ is replaced by the local one,

$$\mathbf{\Gamma}_{\mathbf{loc}}(\nu_n, \nu_{n'}; \omega_m) = \frac{1}{N_{\mathbf{k}}^2} \sum_{\mathbf{k},\mathbf{k}'} \frac{1}{N_{\mathbf{q}}} \sum_{\mathbf{q}} \mathbf{\Gamma}(\tilde{\mathbf{k}}, \tilde{\mathbf{k}}'; \tilde{\mathbf{q}}). \tag{4.29}$$

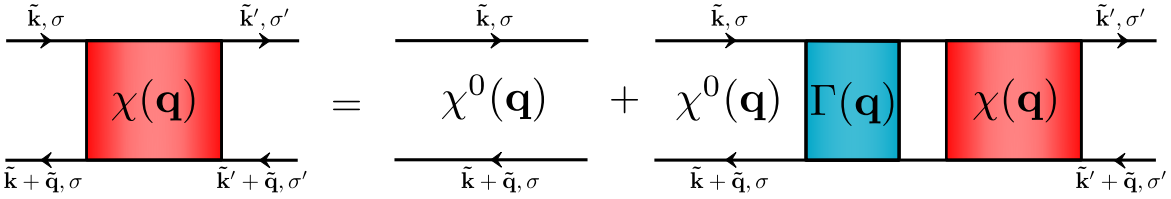

Figure 4.7: Bethe-Salpeter Feynman diagram of Eq. (4.26).

Hence, a crucial simplification appears in Eq. (4.26) where the $\mathbf{k}$-summations can be integrated out.

$$\begin{aligned}\chi_{\alpha_i\alpha_j\alpha_k\alpha_l}(\nu_n,\nu_{n'};\tilde{\mathbf{q}}) &= \chi^{\mathbf{0}}_{\alpha_i\alpha_j\alpha_k\alpha_l}(\nu_n,\nu_{n'};\tilde{\mathbf{q}}) + \frac{1}{\beta^2}\sum_{nn'}\sum_{\substack{\alpha_1\alpha_2\\ \alpha_3\alpha_4}}\chi^{\mathbf{0}}_{\alpha_i\alpha_j\alpha_1\alpha_3}(\nu_n,\nu_{n_1};\tilde{\mathbf{q}})\\ &\quad\times\mathbf{\Gamma}^{\alpha_1\alpha_2}_{\mathbf{loc},\alpha_3\alpha_4}(\nu_{n_1},\nu_{n_2};\omega_m)\chi_{\alpha_3\alpha_4\alpha_k\alpha_l}(\nu_{n_2},\nu_{n'};\tilde{\mathbf{q}}),\end{aligned} \tag{4.30}$$

in which

$$\chi_{\alpha_i\alpha_j\alpha_k\alpha_l}(\nu_n,\nu_{n'};\tilde{\mathbf{q}}) = \frac{1}{N^2_{\mathbf{k}}}\sum_{\mathbf{k},\mathbf{k}'}\chi_{\alpha_i\alpha_j\alpha_k\alpha_l}(\tilde{\mathbf{k}},\tilde{\mathbf{k}}';\tilde{\mathbf{q}}). \tag{4.31}$$

Here, $\chi(\nu_n,\nu_{n'};\tilde{\mathbf{q}})$ is known as *lattice susceptibility* due to its dependency to $\mathbf{q}$ vector.

If we consider $N=\alpha_i n,\alpha_j n$ and $N'=\alpha_k n',\alpha_l n'$, the matrix representation of the Bethe-Salpeter equation within the DMFT approximation is

$$\Big[\chi(\mathbf{q},\omega_m)\Big] = \Big[\chi^{\mathbf{0}}(\mathbf{q},\omega_m)\Big] + \Big[\chi^{\mathbf{0}}(\mathbf{q},\omega_m)\Big]\Big[\mathbf{\Gamma}_{\mathbf{loc}}(\omega_m)\Big]\Big[\chi(\mathbf{q},\omega_m)\Big]. \tag{4.32}$$

In the DMFT, the local vertex function $\mathbf{\Gamma}_{\mathbf{loc}}$ is computed by the knowledge of the local Green's function $\mathcal{G}_{\mathbf{loc}}$ and the local susceptibility $\chi_{\mathbf{loc}}$ given by

$$\mathcal{G}_{\mathbf{loc}}(\nu_n) = \frac{1}{N_{\mathbf{k}}}\sum_{\mathbf{k}}\mathcal{G}(\tilde{\mathbf{k}}), \tag{4.33}$$

$$\chi_{\mathbf{loc}}(\nu_n,\nu_{n'};\omega_m) = \frac{1}{N^2_{\mathbf{k}}}\sum_{\mathbf{k}}\frac{1}{N_{\mathbf{q}}}\sum_{\mathbf{q}}\chi(\tilde{\mathbf{k}},\tilde{\mathbf{k}}';\tilde{\mathbf{q}}). \tag{4.34}$$

Similar to Eq. (4.27), we can evaluate the local version of the Bethe-Salpeter equation to obtain the local vertex function as follows

$$\Big[\mathbf{\Gamma}_{\mathbf{loc}}(i\omega_m)\Big] = \Big[\chi^{\mathbf{0}}_{\mathbf{loc}}(i\omega_m)\Big]^{-1} - \Big[\chi_{\mathbf{loc}}(i\omega_m)\Big]^{-1}. \tag{4.35}$$

Hence, we can obtain the susceptibility of the system over all Brillouin zone, i.e., *the lattice susceptibility*, by substituting the local vertex function matrix in Eq. (4.32).

$$\boxed{\Big[\chi(\mathbf{q},\omega_m)\Big]^{-1} = \Big[\chi^{\mathbf{0}}_{\mathbf{loc}}(\omega_m)\Big]^{-1} - \Big[\chi^{\mathbf{0}}(\mathbf{q},\omega_m)\Big]^{-1} + \Big[\chi_{\mathbf{loc}}(\omega_m)\Big]^{-1}} \tag{4.36}$$

This procedure is shown in Fig. (4.8), wherein the local Bethe-Salpeter equation is employed to extract the local vertex function (the top diagram) and the calculated vertex function is used to obtain the lattice susceptibility (the lower diagram).

4.3.3 Legendre representation of the Bethe-Salpeter equation

It is possible to represent Eq. (4.32) in terms of the Legendre polynomials. In this method which is introduced recently by L. Boehnke and *et al.* [59], the Legendre coefficients of susceptibility $\chi_{ll'}(\omega_m)$ is calculated by using the susceptibility in the imaginary time space

$$\begin{aligned}\chi_{ll'}(\omega_m) &= \int_0^\beta d\tau_{12}\int_0^\beta d\tau_{34}\int_0^\beta d\tau_{14}\,\sqrt{2l+1}\sqrt{2l'+1}(-1)^{l'+1}\\ &\quad\times P_l\left[x(\tau_{12})\right]P_{l'}\left[x(\tau_{34})\right]e^{-i\omega_m\tau_{14}}\chi(\tau_{12},\tau_{34},\tau_{14}),\end{aligned} \tag{4.37}$$

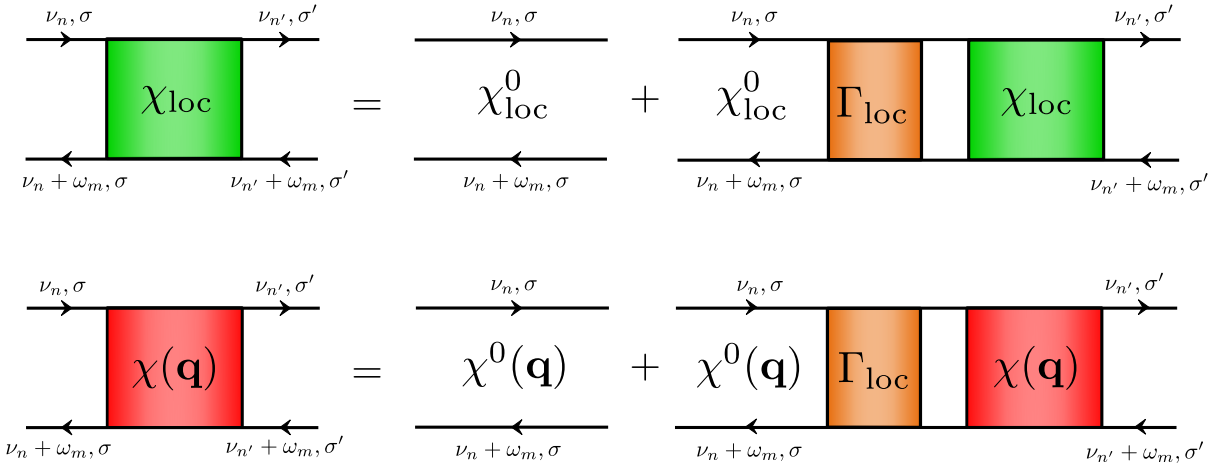

Figure 4.8: DMFT approach for calculating the lattice susceptibility by implementing the local vertex approximation in Feynman diagram language. First, the local vertex function is obtained from the local Bethe-Salpeter equation (top figure), then by utilizing the local vertex function, the $\mathbf{q}$-dependent Bethe-Salpeter equation is solved in order to calculate the lattice susceptibility (bottom figure).

where $P_l[x]$ is the Legendre polynomial function (see Appendix D.1) and $x(\tau) = 2\tau/\beta - 1$. $\chi_{ll'}(\omega_m)$ is connected to the Fourier transformed susceptibility $\chi(\nu_n, \nu_{n'}; \omega_m)$ by a unitary transformation.

$$\chi(\nu_n, \nu_{n'}; \omega_m) = \sum_{ll' \geq 0} T_{nl}\ \chi_{ll'}(\omega_m)\ T^*_{n'l'}, \tag{4.38}$$

in which the unitary transformation T_{nl} is

$$T_{nl} = (-1)^n i^{l+1} \sqrt{2l+1} j_l \left(\frac{(2n+1)\pi}{2} \right), \tag{4.39}$$

and $j_l(x)$ is the spherical Bessel functions. Furthermore, using this unitary transformation, one can obtain the Legendre-Fourier representation of the bare (lattice) susceptibilities. Thus in Eq. (4.32), each matrix has $L \times L'$ elements where $L = \alpha_i l, \alpha_j l$ and $L' = \alpha_k l', \alpha_l l'$. Notice that thorough this attractive method, the lattice susceptibility is given by

$$\chi(\mathbf{q}, \omega_m) = \frac{1}{\beta^2} \sum_{ll' \geq 0} (-1)^{l+l'} \sqrt{2l+1}\sqrt{2l'+1}\ \chi_{ll'}(\mathbf{q}, \omega_m). \tag{4.40}$$

For more details about this method, see Appendix (E.2).

4.3.4 Spin susceptibility

The magnetic susceptibility (normalized in a unit cell) for a single band system is given by [19]

$$\chi^{\alpha\beta}(\mathbf{R_i} - \mathbf{R_j}, \tau) = \frac{1}{\beta N_S V} \left\langle \hat{M}^\alpha_{\mathbf{i}}(\tau) \hat{M}^\beta_{\mathbf{j}}(0) \right\rangle - \frac{1}{\beta N_S V} \left\langle \hat{M}^\alpha_{\mathbf{i}}(\tau) \right\rangle \left\langle \hat{M}^\beta_{\mathbf{j}}(0) \right\rangle, \tag{4.41}$$

Where V is the volume of the supercell (which is equal to number of $\mathbf{k}$-points, $N_{\mathbf{k}}$), N_S the number of atomic sites per unit cell, $\hat{M}^{\alpha}_{\mathbf{i}} = -g\mu_B \hat{S}^{\alpha}_{\mathbf{i}}$ the magnetization operator at $\mathbf{R_i}$, and $\alpha, \beta = x, y, z, \pm$. μ_B is the Bohr magneton[8], $g \sim 2$ is the electron gyromagnetic ratio and S^{α}s are spin operators defined by

$$\begin{aligned} \hat{S}^{\alpha} &= \frac{1}{2}\sum_{\sigma\sigma'} c^{\dagger}_{\sigma}\sigma^{\alpha}c_{\sigma'}, \\ \hat{S}^{\pm} &= \hat{S}^{x} \pm i\hat{S}^{y}, \end{aligned} \tag{4.42}$$

in which σ^{α} are Pauli matrices

$$\sigma^{x} = \begin{pmatrix} 0 & 1 \\ 1 & 0 \end{pmatrix}, \quad \sigma^{y} = \begin{pmatrix} 0 & -i \\ i & 0 \end{pmatrix}, \quad \sigma^{z} = \begin{pmatrix} 1 & 0 \\ 0 & -1 \end{pmatrix}. \tag{4.43}$$

In comparison with Eq. (4.14), the operator $\hat{\mathcal{O}}$ replaces by the magnetization operator $\hat{M}$.

4.3.4.1 Longitudinal spin susceptibility

Longitudinal spin susceptibility is the response of z-component of the expectation value of magnetization operator to a small magnetic field in z-direction that couples linearly to the $\hat{M}$. The small magnetic field B_z enters the Hamiltonian by the following perturbation term [60]

$$\frac{1}{2}(g\mu_B)\int d\mathbf{r}'\hat{S}^{z}(\mathbf{r}')B_z(\mathbf{r}', t).$$

The longitudinal spin susceptibility χ^{zz} can be obtained by calculating the spin-spin correlation where $\hat{S}^{z} = 1/2\sum_{\sigma}\sigma c^{\dagger}_{\sigma}c_{\sigma}$.[9]

$$\begin{aligned} \chi^{zz}(\boldsymbol{\tau}) &= \frac{1}{\beta N_S V}\frac{1}{4}(g\mu_B)^2\sum_{\sigma\sigma'}\sigma\sigma'\Big[\Big\langle \mathcal{T}c^{\dagger}_{\sigma}(\tau_1)c_{\sigma}(\tau_2)c^{\dagger}_{\sigma'}(\tau_3)c_{\sigma'}(\tau_4)\Big\rangle \\ &\quad -\Big\langle \mathcal{T}c^{\dagger}_{\sigma}(\tau_1)c_{\sigma}(\tau_2)\Big\rangle\Big\langle \mathcal{T}c^{\dagger}_{\sigma'}(\tau_3)c_{\sigma'}(\tau_4)\Big\rangle\Big], \end{aligned} \tag{4.44}$$

where the value $\sigma = 1$ ($\sigma = -1$) is assigned to spin up (spin down). In comparison with Eq. (4.17), the vertex factor for the χ^{zz} is

$$v^{\sigma}_{\mathbf{k}\mathbf{k}+\mathbf{q};i\kappa_i,j\kappa_j} = \frac{1}{2}(g\mu_B)\sigma\delta_{ij}\delta_{\kappa_i\kappa_j}.$$

The Fourier integral of Eqs. (4.44) can be down easily by

$$\chi^{zz}(\nu_n, \nu_{n'}; \omega_m) = \int_0^{\beta} d\tau_1 \ldots \int_0^{\beta} d\tau_4 \; e^{-i\nu_n\tau_1}e^{i(\nu_n+\omega_m)\tau_2}e^{-i(\nu_{n'}+\omega_m)\tau_3}e^{i\nu_{n'}\tau_4}\chi^{zz}(\boldsymbol{\tau}), \tag{4.45}$$

and the non-interacting longitudinal spin susceptibility $\chi^{\mathbf{0},zz}$ is

$$\chi^{\mathbf{0},zz}(\nu_n, \nu_{n'}; \omega_m) = -\frac{1}{N_S}\beta\delta_{nn'}\frac{1}{4}(g\mu_B)^2\sum_{\sigma}\mathcal{G}^{\sigma}(\nu_n)\mathcal{G}^{\sigma}(\nu_n + \omega_m). \tag{4.46}$$

[8] In atomic units the Bohr magneton is $\mu_B = 1/2$.

[9] Since the momenta, orbital and atomic site dependencies are identical with Eq. (4.18), for the sake of simplicity, here and in the following, we do not write the momenta dependency of the susceptibility.

Notice to pre-factors which is appeared in $\chi^{\mathbf{0},zz}$ due to the definition of the spin susceptibility in comparison with the general definition of the non-interacting susceptibility in Eq. (4.20).

In order to compute the magnetic susceptibility within the DMFT, we need to solve the Bethe-Salpeter equation (Eq. (4.36)) using the matrix algebra. In *paramagnetic* systems, we can use even simpler Bethe-Salpeter equation, wherein the trace over spins is done already. If we define

$$\mathbf{\Gamma}^{zz} = \frac{1}{4}\sum_{\sigma\sigma'}\sigma\sigma'\mathbf{\Gamma}^{\sigma\sigma'} \quad ; \quad \chi^{\mathbf{0},zz} = \frac{1}{4}\sum_{\sigma\sigma'}\sigma\sigma'\chi^{\mathbf{0},\sigma\sigma'},$$

we can easily obtain (See Appendix (A.3))

$$\left[\chi^{zz}(\mathbf{q},\omega_m)\right]^{-1} = \left[\chi^{\mathbf{0},zz}(\mathbf{q},\omega_m)\right]^{-1} - \left[\chi^{\mathbf{0},zz}_{\mathbf{loc}}(\omega_m)\right]^{-1} + \left[\chi^{zz}_{\mathbf{loc}}(\omega_m)\right]^{-1}. \tag{4.47}$$

In this relation, considering N_O as the number of orbitals, N_S the number of sites and N_ν the number of Matsubara frequencies, each matrix has $N \times N$ elements where $N = N_O^2 N_S^2 N_\nu$. Comparing to Eq. (4.36), here, each matrix size is reduced[10] by a factor of N^2_{spin}.

4.3.4.2 Transverse spin susceptibility

Transverse spin susceptibility is the linear response of a system to a small magnetic field which is perpendicular to the spin quantization axis, denoted by z-direction. The perturbation term which is added to the Hamiltonian is [60]

$$\frac{1}{4}(g\mu_B)\int d\mathbf{r}'\left[\hat{S}^+(\mathbf{r}')B^-(\mathbf{r}',t) + \hat{S}^-(\mathbf{r}')B^+(\mathbf{r}',t)\right],$$

where $B^\pm = B_x \pm iB_y$. Considering $\hat{S}^x = 1/2\sum_\sigma c^\dagger_\sigma c_{-\sigma}$, $\hat{S}^y = -i/2\sum_\sigma \sigma c^\dagger_\sigma c_{-\sigma}$, we can derive the transverse χ as follows

$$\chi^{xx}(\boldsymbol{\tau}) = \frac{1}{\beta N_S V}\frac{1}{4}(g\mu_B)^2\sum_{\sigma\sigma'}\left\langle \mathcal{T}c^\dagger_\sigma(\tau_1)c_{-\sigma}(\tau_2)c^\dagger_{\sigma'}(\tau_3)c_{-\sigma'}(\tau_4)\right\rangle, \tag{4.48}$$

$$\chi^{xy}(\boldsymbol{\tau}) = \frac{1}{\beta N_S V}\frac{-i}{4}(g\mu_B)^2\sum_{\sigma\sigma'}\sigma'\left\langle \mathcal{T}c^\dagger_\sigma(\tau_1)c_{-\sigma}(\tau_2)c^\dagger_{\sigma'}(\tau_3)c_{-\sigma'}(\tau_4)\right\rangle, \tag{4.49}$$

$$\chi^{yx}(\boldsymbol{\tau}) = \frac{1}{\beta N_S V}\frac{-i}{4}(g\mu_B)^2\sum_{\sigma\sigma'}\sigma\left\langle \mathcal{T}c^\dagger_\sigma(\tau_1)c_{-\sigma}(\tau_2)c^\dagger_{\sigma'}(\tau_3)c_{-\sigma'}(\tau_4)\right\rangle, \tag{4.50}$$

$$\chi^{yy}(\boldsymbol{\tau}) = \frac{1}{\beta N_S V}\frac{1}{4}(g\mu_B)^2\sum_{\sigma\sigma'}\sigma\sigma'\left\langle \mathcal{T}c^\dagger_\sigma(\tau_1)c_{-\sigma}(\tau_2)c^\dagger_{\sigma'}(\tau_3)c_{-\sigma'}(\tau_4)\right\rangle. \tag{4.51}$$

Based on Eqs. (4.48-4.51) and Eq. (4.17) we can conclude that the vertex factor $v^\sigma_{\mathbf{kk+q};i\kappa_i,j\kappa_j}$ for the χ^{xx} and χ^{yy} are $1/2(g\mu_B)\delta_{ij}\delta_{\kappa_i\kappa_j}$ and $1/2(g\mu_B)\sigma\delta_{ij}\delta_{\kappa_i\kappa_j}$, respectively. For χ^{xy}, the vertex factors are $v^\sigma_{\mathbf{kk+q};i\kappa_i,j\kappa_j} = i^{3/2}/2(g\mu_B)\delta_{ij}\delta_{\kappa_i\kappa_j}$ and $v^{\sigma'}_{\mathbf{k+qk};i\kappa_k,j\kappa_l} = i^{3/2}/2(g\mu_B)\sigma'\delta_{kl}\delta_{\kappa_k\kappa_l}$. Vertex factors for χ^{yx} can be obtained similarly. In addition, the response functions χ^{+-} and χ^{-+} can

[10] This would be very helpful when the response function matrix is to be computed "*numerically*".

be easily calculated by utilizing the response functions $\chi^{xx}, \chi^{xy}, \chi^{yx}$ and χ^{yy}.

$$\begin{aligned}\chi^{+-} &= \chi^{xx} - i\chi^{xy} + i\chi^{yx} + \chi^{yy} \\ &= \frac{1}{\beta N_S V}(g\mu_B)^2 \left\langle \mathcal{T} c_\uparrow^\dagger(\tau_1) c_\downarrow(\tau_2) c_\downarrow^\dagger(\tau_3) c_\uparrow(\tau_4) \right\rangle, \qquad (4.52) \\ \chi^{-+} &= \chi^{xx} + i\chi^{xy} - i\chi^{yx} + \chi^{yy} \\ &= \frac{1}{\beta N_S V}(g\mu_B)^2 \left\langle \mathcal{T} c_\downarrow^\dagger(\tau_1) c_\uparrow(\tau_2) c_\uparrow^\dagger(\tau_3) c_\downarrow(\tau_4) \right\rangle. \qquad (4.53)\end{aligned}$$

Using the Wick's theorem, we can obtain the transverse spin susceptibilities for the non-interacting cases. In Matsubara space the non-interacting transverse spin susceptibilities are

$$\begin{aligned}\chi^{\mathbf{0},xx} &= -\frac{1}{N_S}\beta\delta_{nn'}\frac{1}{4}(g\mu_B)^2 \sum_\sigma \mathcal{G}^\sigma(\nu_n)\mathcal{G}^{-\sigma}(\nu_n+\omega_m), \qquad (4.54) \\ \chi^{\mathbf{0},xy} &= -\frac{1}{N_S}\beta\delta_{nn'}\frac{i}{4}(g\mu_B)^2 \sum_\sigma \sigma\, \mathcal{G}^\sigma(\nu_n)\mathcal{G}^{-\sigma}(\nu_n+\omega_m), \qquad (4.55) \\ \chi^{\mathbf{0},yx} &= \frac{1}{N_S}\beta\delta_{nn'}\frac{i}{4}(g\mu_B)^2 \sum_\sigma \sigma\, \mathcal{G}^\sigma(\nu_n)\mathcal{G}^{-\sigma}(\nu_n+\omega_m), \qquad (4.56) \\ \chi^{\mathbf{0},yy} &= \frac{1}{N_S}\beta\delta_{nn'}\frac{1}{4}(g\mu_B)^2 \sum_\sigma \mathcal{G}^\sigma(\nu_n)\mathcal{G}^{-\sigma}(\nu_n+\omega_m), \qquad (4.57)\end{aligned}$$

and finally

$$\begin{aligned}\chi^{\mathbf{0},+-} &= -\frac{1}{N_S}\beta\delta_{nn'}(g\mu_B)^2 \mathcal{G}^\uparrow(\nu_n)\mathcal{G}^\downarrow(\nu_n+\omega_m), \qquad (4.58) \\ \chi^{\mathbf{0},-+} &= -\frac{1}{N_S}\beta\delta_{nn'}(g\mu_B)^2 \mathcal{G}^\downarrow(\nu_n)\mathcal{G}^\uparrow(\nu_n+\omega_m). \qquad (4.59)\end{aligned}$$

For a system with *axial rotational symmetry*, the transverse spin susceptibility is completely decoupled from the longitudinal spin susceptibility [60], because the correlation function of the $\hat{S}^z$ and $\hat{S}^\pm$ is zero due to the rotational symmetry.[11]

In order to compute the lattice transverse spin susceptibility, χ^{+-}(and similarly χ^{-+}), for a general case by using the DMFT approach we need to solve the following matrix equation

$$\left[\chi^{+-}(\mathbf{q},\omega_m)\right]^{-1} = \left[\chi^{\mathbf{0},+-}(\mathbf{q},\omega_m)\right]^{-1} - \left[\chi^{\mathbf{0},+-}_{\mathbf{loc}}(\omega_m)\right]^{-1} + \left[\chi^{+-}_{\mathbf{loc}}(\omega_m)\right]^{-1}. \qquad (4.60)$$

[11] In a system with axial rotational symmetry, the spin operator in z-direction and the Hamiltonian commute $[\hat{S}^z, H] = 0$. So $|\alpha\rangle$ is the common eigenstate of the $\hat{S}^z$ and the Hamiltonian. Using the Lehman representation, the correlation function $\langle \hat{S}^z \hat{S}^\pm \rangle$ can be written as

$$\begin{aligned}\langle \hat{S}^z \hat{S}^\pm \rangle &= \frac{1}{\mathcal{Z}} \sum_{\alpha\alpha'} e^{-\beta E_\alpha} \langle \alpha | \hat{S}^z | \alpha' \rangle \langle \alpha' | \hat{S}^\pm | \alpha \rangle \\ &= \frac{1}{\mathcal{Z}} \sum_{\alpha\alpha'} e^{-\beta E_\alpha} s_\alpha \delta_{\alpha\alpha'} \langle \alpha' | \hat{S}^\pm | \alpha \rangle = 0.\end{aligned}$$

4.3.5 Density-density or charge susceptibility

The charge susceptibility (normalized in a unit cell) of a single band system can be obtained by

$$\chi^{ch}(\mathbf{R_i}-\mathbf{R_j},\tau)=\frac{1}{\beta N_S V}\Big\langle \hat{n}_{\mathbf{i}}(\tau)\hat{n}_{\mathbf{j}}(0)\Big\rangle-\frac{1}{\beta N_S V}\Big\langle \hat{n}_{\mathbf{i}}(\tau)\Big\rangle\Big\langle \hat{n}_{\mathbf{j}}(0)\Big\rangle, \tag{4.61}$$

where $\hat{n}$ is the density operator defined by

$$\hat{n}=\frac{1}{2}\sum_{\sigma}c^{\dagger}_{\sigma}c_{\sigma}. \tag{4.62}$$

In fact, the charge susceptibility explains the response of the $\langle\hat{n}\rangle$ to a scaler external potential V_{ext} that couples linearly to the $\hat{n}$.

In comparison with the general definition of the susceptibility in (4.17), the vertex factor of the charge susceptibility is

$$v^{\sigma}_{\mathbf{k}\mathbf{k}+\mathbf{q};i\kappa_i,j\kappa_j}=\frac{1}{2}\,\delta_{ij}\delta_{\kappa_i\kappa_j}.$$

The operator $\hat{\mathcal{O}}$ in Eq. (4.14) replaces by the density operator $\hat{n}$ so that the charge susceptibility in terms of the creator and annihilator operators can be obtained by[12]

$$\begin{aligned}\chi^{ch}(\boldsymbol{\tau}) &= \frac{1}{\beta N_S V}\frac{1}{4}\sum_{\sigma\sigma'}\chi^{\sigma\sigma'}(\boldsymbol{\tau})\\ &= \frac{1}{\beta N_S V}\frac{1}{4}\sum_{\sigma\sigma'}\Big[\Big\langle \mathcal{T}c^{\dagger}_{\sigma}(\tau_1)c_{\sigma}(\tau_2)c^{\dagger}_{\sigma'}(\tau_3)c_{\sigma'}(\tau_4)\Big\rangle\\ &\quad -\Big\langle \mathcal{T}c^{\dagger}_{\sigma}(\tau_1)c_{\sigma}(\tau_2)\Big\rangle\Big\langle \mathcal{T}c^{\dagger}_{\sigma'}(\tau_3)c_{\sigma'}(\tau_4)\Big\rangle\Big].\end{aligned} \tag{4.63}$$

The non-interacting part of the charge susceptibility in Matsubara space can be easily obtained by

$$\chi^{\mathbf{0},ch}=-\frac{1}{N_S}\beta\delta_{nn'}\frac{1}{4}\sum_{\sigma}\mathcal{G}^{\sigma}(\nu_n)\mathcal{G}^{\sigma}(\nu_n+\omega_m). \tag{4.64}$$

Notice that in atomic units wherein $\mu_B=1/2$, the non-interacting spin and charge susceptibility are equal (see Eq. (4.46)).

Within DMFT method, the $\mathbf{q}$-dependent charge susceptibility can be obtained by the following Bethe-Salpeter equation (See Appendix (A.3)).

$$\Big[\chi^{ch}(\mathbf{q},\omega_m)\Big]^{-1}=\Big[\chi^{\mathbf{0},ch}(\mathbf{q},\omega_m)\Big]^{-1}-\Big[\chi^{\mathbf{0},ch}_{\mathbf{loc}}(\omega_m)\Big]^{-1}+\Big[\chi^{ch}_{\mathbf{loc}}(\omega_m)\Big]^{-1}, \tag{4.65}$$

where,

$$\mathbf{\Gamma}^{ch}=\frac{1}{4}\sum_{\sigma\sigma'}\mathbf{\Gamma}^{\sigma\sigma'}\quad;\quad\chi^{\mathbf{0},ch}=\frac{1}{4}\sum_{\sigma\sigma'}\chi^{\mathbf{0},\sigma\sigma'}.$$

[12] Here, the momenta, orbital and atomic sites dependency of the susceptibility are the same as the ones in Eq. (4.18). Thus we don't write the momenta dependency of the charge susceptibility for the sake of simplicity.

4.3.6 Spin-density susceptibility

Spin-density susceptibility (normalized in a unit cell) is the response of the density to a longitudinal small magnetic field which is given by

$$\chi_{SD}(\mathbf{R_i}-\mathbf{R_j},\tau)=\frac{1}{\beta N_S V}\Big\langle \hat{M}^z_{\mathbf{i}}(\tau)\hat{n}_{\mathbf{j}}(0)\Big\rangle-\frac{1}{\beta N_S V}\Big\langle \hat{M}^z_{\mathbf{i}}(\tau)\Big\rangle\Big\langle \hat{n}_{\mathbf{j}}(0)\Big\rangle. \tag{4.66}$$

In second quantization,

$$\begin{aligned}\chi_{SD}(\boldsymbol{\tau}) &= \frac{1}{\beta N_S V}\frac{1}{4}(g\mu_B)\sum_{\sigma\sigma'}\sigma\Big[\Big\langle \mathcal{T}c^\dagger_\sigma(\tau_1)c_\sigma(\tau_2)c^\dagger_{\sigma'}(\tau_3)c_{\sigma'}(\tau_4)\Big\rangle\\ &\quad-\Big\langle \mathcal{T}c^\dagger_\sigma(\tau_1)c_\sigma(\tau_2)\Big\rangle\Big\langle \mathcal{T}c^\dagger_{\sigma'}(\tau_3)c_{\sigma'}(\tau_4)\Big\rangle\Big],\end{aligned} \tag{4.67}$$

which implies that the vertex factors in Eq. (4.17) are $v^{\sigma}_{\mathbf{kk+q};i\kappa_i,j\kappa_j}=1/2(g\mu_B)\sigma\delta_{ij}\delta_{\kappa_i\kappa_j}$ and $v^{\sigma'}_{\mathbf{k'+qk'};k\kappa_k,l\kappa_l}=1/2\ \delta_{kl}\delta_{\kappa_k\kappa_l}$. Also, one of the $\hat{\mathcal{O}}$ operators in Eq. (4.14) replaces with the magnetization one and the other with the density operator.

The non-interacting spin-density response function in Matsubara space is

$$\chi^{\mathbf{0}}_{SD}=-\frac{1}{N_S}\beta\delta_{nn'}\frac{1}{4}(g\mu_B)\sum_{\sigma}\sigma\mathcal{G}^\sigma(\nu_n)\mathcal{G}^\sigma(\nu_n+\omega_m). \tag{4.68}$$

In *paramagnetic* systems, where $\chi^{\uparrow\uparrow}=\chi^{\downarrow\downarrow}$ and $\chi^{\uparrow\downarrow}=\chi^{\downarrow\uparrow}$, the spin-density susceptibility is zero. Therefore, the spin and charge (density) responses are decoupled [60].

4.4 Properties of the susceptibility

In the following, we explain the properties of the susceptibility in details with their proofs in three categories. First, we demonstrate how the the susceptibility behaves in imaginary time. We show some mathematical characteristics of the two-particle correlation function which depends on four imaginary times $\boldsymbol{\tau}=(\tau_1,\tau_2,\tau_3,\tau_4)$. Second, we illustrate some important symmetries of the general susceptibility in Matsubara space which are very crucial to consider them in numerical computations. Then in the last part, we study the high frequency part of the susceptibility and calculate an analytical relation for the large frequencies by using *digamma* and *trigamma* functions.

4.4.1 Properties of the susceptibility in $\boldsymbol{\tau}$ space

From Eq. (4.23) one can easily conclude that the all properties of second term in this equation, i.e.,

$$\Big\langle \mathcal{T}c^\dagger_{\mathbf{k}\alpha_i}(\tau_1)c_{\mathbf{k+q}\alpha_j}(\tau_2)\Big\rangle\Big\langle \mathcal{T}c^\dagger_{\mathbf{k'+q}\alpha_k}(\tau_3)c_{\mathbf{k'}\alpha_l}(\tau_4)\Big\rangle,$$

are implicitly in the first term, i.e.,

$$\Big\langle \mathcal{T}c^\dagger_{\mathbf{k}\alpha_i}(\tau_1)c_{\mathbf{k+q}\alpha_j}(\tau_2)c^\dagger_{\mathbf{k'+q}\alpha_k}(\tau_3)c_{\mathbf{k'}\alpha_l}(\tau_4)\Big\rangle.$$

For this reason, at first we introduce and prove the properties of the *two-particle correlation function* or *two-particle Green's function* which is defined by

$$\mathcal{C}_{\alpha_i\alpha_j\alpha_k\alpha_l}(\mathbf{p},\boldsymbol{\tau}) = \left\langle \mathcal{T} c^{\dagger}_{\mathbf{k}\alpha_i}(\tau_1) c_{\mathbf{k}+\mathbf{q}\alpha_j}(\tau_2) c^{\dagger}_{\mathbf{k}'+\mathbf{q}\alpha_k}(\tau_3) c_{\mathbf{k}'\alpha_l}(\tau_4) \right\rangle, \tag{4.69}$$

where $\mathbf{p} = (\mathbf{k},\mathbf{k}',\mathbf{q}) \equiv (\mathbf{k},\mathbf{k}+\mathbf{q},\mathbf{k}'+\mathbf{q},\mathbf{k}')$ and $\boldsymbol{\tau} = (\tau_1,\tau_2,\tau_3,\tau_4)$. Every property that is obtained for the two-particle Green's function can be extended to the general susceptibility either.[13]

Before proceeding to extract the $\mathcal{C}$'s features, let us discuss the physical meaning of Eq. (4.69). The physics of the two-particle Green's function depends on time ordering of the creation and annihilation operators in $\langle ... \rangle$ [61].

$\tau_1,\tau_2 > \tau_3,\tau_4$: The $\mathcal{C}$ is a propagation of a particle-hole pair which gives some informations about excited states of N particle system.

$\tau_2,\tau_4 < \tau_1,\tau_3$: Here, $\mathcal{C}$ gives some informations about a system with $N+2$ holes or $N-2$ particles.

$\tau_2,\tau_4 > \tau_1,\tau_3$: In this case, $\mathcal{C}$ describes the propagation of a pair additional particle and gives some informations about energy states of a system with $N+2$ particles.

Practically, in the case of $\tau_2,\tau_4 < \tau_1,\tau_3$ or $\tau_2,\tau_4 > \tau_1,\tau_3$, the two-particle Green's function is useful to study superconductivity. In case of the response functions such as spin, charge and current susceptibilities, the two-particle Green's function is in particle-hole channel as we derived in details before.[14]

During the introduction of the properties of the two-particle Green's function, wherever the orbitals or sites or momenta are irrelevant on those specific properties (or have not any effect on those properties), we drop them in $\mathcal{C}$ relation for the sake of simplicity.

1. The $\mathcal{C}(\tau_1,\tau_2,\tau_3,\tau_4)$ is β-antiperiodic in each $\tau_i < 0$ where $i = 1,...,4$.

$$\begin{aligned}\mathcal{C}(\tau_1,\tau_2,\tau_3,\tau_4) &= -\mathcal{C}(\tau_1+\beta,\tau_2,\tau_3,\tau_4) = -\mathcal{C}(\tau_1,\tau_2+\beta,\tau_3,\tau_4)\\ &= -\mathcal{C}(\tau_1,\tau_2,\tau_3+\beta,\tau_4) = -\mathcal{C}(\tau_1,\tau_2,\tau_3,\tau_4+\beta).\end{aligned} \tag{4.70}$$

This property can be easily proved as follows.

$$\begin{aligned}\mathcal{C}(\tau_1+\beta,\tau_2,\tau_3,\tau_4) &= \frac{1}{\mathcal{Z}}\,\mathrm{Tr}\Big\{e^{-\beta H}e^{(\tau_1+\beta)H}c^{\dagger}e^{(\tau_2-\tau_1-\beta)H}c\,e^{(\tau_3-\tau_2)H}c^{\dagger}e^{-(\tau_3-\tau_4)H}c\,e^{-\tau_4 H}\Big\}\\ &= \frac{1}{\mathcal{Z}}\,\mathrm{Tr}\Big\{e^{-\beta H}e^{\tau_2 H}c\,e^{-\tau_2 H}e^{\tau_3 H}c^{\dagger}e^{-\tau_3 H}e^{\tau_4 H}c\,e^{-\tau_4 H}e^{\tau_1 H}c^{\dagger}e^{-\tau_1 H}\Big\}\\ &= -\frac{1}{\mathcal{Z}}\,\mathrm{Tr}\Big\{e^{-\beta H}\mathcal{T}\left[c^{\dagger}(\tau_1)c(\tau_2)c^{\dagger}(\tau_3)c(\tau_4)\right]\Big\}\\ &= -\mathcal{C}(\tau_1,\tau_2,\tau_3,\tau_4).\end{aligned}$$

[13] In some special cases, the second term in Eq. (4.23) has a role in the properties such as continuity and discontinuity of the susceptibility. In these special cases, we explicitly use the susceptibility instead of the two-particle Green's function.

[14] In particle-hole channel one can write the two-particle Green's function in terms of complete set of the eigenstates $|\phi_s\rangle$ of the real system i.e. $\mathcal{C} = \sum_s \langle\phi_0|\mathcal{T}c_{\mathbf{k}+\mathbf{q}\alpha_j}(\tau_2)c^{\dagger}_{\mathbf{k}\alpha_i}(\tau_1)|\phi_s\rangle\langle\phi_s|\mathcal{T}c_{\mathbf{k}'\alpha_l}(\tau_4)c^{\dagger}_{\mathbf{k}'+\mathbf{q}\alpha_k}(\tau_3)|\phi_0\rangle$, where $\langle\phi_s|...|\phi_0\rangle$ is the wave function of the particle and hole in the excited state $|\phi_s\rangle$ [61].

Here $\mathcal{Z}$ is the partition function and H the Hamiltonian. From this proof, we can infer that if the β is added to odd (even) number of the time arguments in the $\mathcal{C}(\tau_1,\tau_2,\tau_3,\tau_4)$, the two-particle Green's function remains unchanged (changes by a (-1) factor). For instance

$$\begin{aligned}\mathcal{C}(\tau_1,\tau_2,\tau_3,\tau_4) &= \mathcal{C}(\tau_1+\beta,\tau_2+\beta,\tau_3,\tau_4)=\mathcal{C}(\tau_1+\beta,\tau_2+\beta,\tau_3+\beta,\tau_4+\beta)\\ &= -\mathcal{C}(\tau_1+\beta,\tau_2,\tau_3,\tau_4)=-\mathcal{C}(\tau_1+\beta,\tau_2+\beta,\tau_3+\beta,\tau_4).\end{aligned}$$

2. The noninteracting two-particle Green's function $\mathcal{C}^0(\tau_1,\tau_2,\tau_3,\tau_4)$ is *discontinuous* function[15] at $\tau_1=\tau_2$, $\tau_3=\tau_4$, $\tau_1=\tau_4$ and $\tau_2=\tau_3$.

   The noninteracting part of the two-particle Green's function can be calculated using the Wick's theorem as follows.

$$\mathcal{C}^0(\tau_1,\tau_2,\tau_3,\tau_4) = -\mathcal{G}(\tau_4,\tau_1)\mathcal{G}(\tau_2,\tau_3)+\mathcal{G}(\tau_2,\tau_1)\mathcal{G}(\tau_4,\tau_3). \tag{4.71}$$

   In this relation each one-particle Green's function $\mathcal{G}(\tau_i,\tau_j)$ is discontinuous at $\tau_i=\tau_j$ because

$$\begin{aligned}\Delta\mathcal{G}(\tau_i,\tau_j)\Big|_{\tau_i=\tau_j} &= \mathcal{G}(\tau_j^-,\tau_j)-\mathcal{G}(\tau_j^+,\tau_j)\\ &= -\Big\langle \mathcal{T}c(\tau_j^-)c^\dagger(\tau_j)\Big\rangle+\Big\langle \mathcal{T}c(\tau_j^+)c^\dagger(\tau_j)\Big\rangle\\ &= 1.\end{aligned}$$

3. $\mathcal{C}(\tau_1,\tau_2,\tau_3,\tau_4)$ is a *discontinuous* function at $\tau_1=\tau_2$, $\tau_3=\tau_4$, $\tau_1=\tau_4$ and $\tau_2=\tau_3$.

   To prove this feature we use definition of the discontinuous function. We show that the values of the $\mathcal{C}(\tau_1,\tau_2,\tau_3,\tau_4)$ e.g., at $\tau_1\to\tau_2^+$ and $\tau_1\to\tau_2^-$ are not equal. Therefore, $\mathcal{C}$ is discontinuous at $\tau_1=\tau_2$.

$$\begin{aligned}\Delta\mathcal{C}(\tau_1,\tau_2,\tau_3,\tau_4)\Big|_{\tau_1=\tau_2} &= \mathcal{C}(\tau_1^+,\tau_1^-,\tau_3,\tau_4)-\mathcal{C}(\tau_1^-,\tau_1^+,\tau_3,\tau_4)\\ &= \Big\langle \mathcal{T}c^\dagger(\tau_1^+)c(\tau_1^-)c^\dagger(\tau_3)c_{i_4\sigma_4}(\tau_4)\Big\rangle-\Big\langle \mathcal{T}c^\dagger(\tau_1^-)c(\tau_1^+)c^\dagger(\tau_3)c(\tau_4)\Big\rangle\\ &= \Big\langle \mathcal{T}c^\dagger(\tau_3)c(\tau_4)\Big\rangle\\ &= -\mathcal{G}(\tau_4,\tau_3).\end{aligned}$$

   In general, $\Delta\mathcal{C}_{\alpha_i\alpha_j\alpha_k\alpha_l}(\mathbf{p};\tau_1,\tau_2,\tau_3,\tau_4)\Big|_{\tau_1=\tau_2} = -N_{\mathbf{k}}^2\,\delta(\mathbf{q})\,\delta_{\alpha_i\alpha_j}\delta_{\sigma\sigma'}\mathcal{G}_{\alpha_k\alpha_l}(\mathbf{k}'+\mathbf{q},\mathbf{k}';\tau_4,\tau_3)$.

4. The fully interacting part of the two-particle Green's function that is defined by

$$\widetilde{\gamma}(\boldsymbol{\tau}) = \mathcal{C}(\boldsymbol{\tau})-\mathcal{C}^0(\boldsymbol{\tau}), \tag{4.72}$$

   is a *continuous* function but has *kinks* at $\tau_1=\tau_2$, $\tau_3=\tau_4$, $\tau_1=\tau_4$, and $\tau_2=\tau_3$. To show how $\widetilde{\gamma}(\tau_1,\tau_2,\tau_3,\tau_4)$ is continuous e.g. at $\tau_1=\tau_2$, we proceed as follows.

$$\begin{aligned}\Delta\widetilde{\gamma}(\tau_1,\tau_2,\tau_3,\tau_4)\Big|_{\tau_1=\tau_2} &= \widetilde{\gamma}(\tau_1^+,\tau_1,\tau_3,\tau_4)-\widetilde{\gamma}(\tau_1^-,\tau_1,\tau_3,\tau_4)\\ &= \big[\mathcal{C}(\tau_1^+,\tau_1^-,\tau_3,\tau_4)-\mathcal{C}(\tau_1^-,\tau_1^+,\tau_3,\tau_4)\big]\\ &\quad -\big[\mathcal{C}^0(\tau_1^+,\tau_1^-,\tau_3,\tau_4)-\mathcal{C}^0(\tau_1^-,\tau_1^+,\tau_3,\tau_4)\big]\\ &= -\mathcal{G}(\tau_4,\tau_3)+\big[\mathcal{G}(\tau_1^-,\tau_1)-\mathcal{G}(\tau_1^+,\tau_1)\big]\,\mathcal{G}(\tau_3,\tau_4)=0.\end{aligned}$$

[15] The function $f(x)$ is discontinuous at $x=a$ if $\lim_{x\to a^-}f(x)\neq\lim_{x\to a^+}f(x)$.

To show that the the first derivative of the $\widetilde{\gamma}(\tau_1,\tau_2,\tau_3,\tau_4)$ is discontinuous, we can use the Lehman representation and using the fact that $dc(\tau)/d\tau = [H, c(\tau)]$, where H is the Hamiltonian.

5. Due to the time invariance, the $\mathcal{C}(\tau_1,\tau_2,\tau_3,\tau_4)$ has three independent time arguments.

$$\mathcal{C}(\tau_1,\tau_2,\tau_3,\tau_4) = \mathcal{C}(\tau_{14},\tau_{24},\tau_{34},0), \tag{4.73}$$

where $\tau_{ij} = \tau_i - \tau_j$. This feature can be easily seen by

$$\begin{aligned}
\mathcal{C}(\tau_1,\tau_2,\tau_3,\tau_4) &= \left\langle \mathcal{T} c^\dagger(\tau_1)c(\tau_2)c^\dagger(\tau_3)c(\tau_4)\right\rangle \\
&= \frac{1}{\mathcal{Z}}\,\mathrm{Tr}\Big\{ e^{-\beta H}e^{\tau_1 H}c^\dagger e^{-(\tau_1-\tau_2)H}c\, e^{-(\tau_2-\tau_3)H}c^\dagger e^{-(\tau_3-\tau_4)H}c\, e^{-\tau_4 H}\Big\} \\
&= \frac{1}{\mathcal{Z}}\,\mathrm{Tr}\Big\{ e^{-\beta H}e^{(\tau_1-\tau_4)H}c^\dagger e^{-(\tau_1-\tau_4)H}e^{(\tau_2-\tau_4)H} \\
&\quad \times c\, e^{-(\tau_2-\tau_4)H}e^{(\tau_3-\tau_4)H}c^\dagger e^{-(\tau_3-\tau_4)H}\Big\} \\
&= \frac{1}{\mathcal{Z}}\,\mathrm{Tr}\Big\{ e^{-\beta H}\mathcal{T}\left[c^\dagger(\tau_1-\tau_4)c(\tau_2-\tau_4)c^\dagger(\tau_3-\tau_4)c(0)\right]\Big\} \\
&= \mathcal{C}(\tau_{14},\tau_{24},\tau_{34},0).
\end{aligned}$$

6. On the basis of the mentioned properties of the two-particle Green's function, it is easy to see that the general susceptibility defined in Eq. (4.23) in $\boldsymbol{\tau}$-space is *discontinuous* at "$\tau_1 = \tau_4$ and $\tau_2 = \tau_3$" and has *kinks* at "$\tau_1 = \tau_2$ and $\tau_3 = \tau_4$". Figs. 4.9, 4.10a, and 4.10b show these properties of the susceptibility.

7. Boundary condition of the susceptibility $\chi(\tau_1,\tau_2,\tau_3) \equiv \chi(\tau_{14},\tau_{24},\tau_{34},0)$ at $\tau_{ij} = \beta^-$.

   We can use the introduced properties to calculate the susceptibility at the boundaries. Using these boundary conditions, we are able to compute the susceptibility at $\tau_{ij} = \beta^-$. This would save time and computational memory in the numerical computations.

   - $\chi(\tau_1,\tau_2,\beta)$ for ($\tau_1 \neq 0,\beta$ and $\tau_2 \neq 0,\beta$) :

$$\chi(\tau_1,\tau_2,\beta) = -\chi(\tau_1,\tau_2,0^+). \tag{4.74}$$

   Since $\chi(\tau_1,\tau_2,\tau_3)$ is β-antiperiodic in τ, it is clear that $\chi(\tau_1,\tau_2,\beta) = -\chi(\tau_1,\tau_2,0^-)$. Our favor is to obtain the relation between $\chi(\tau_1,\tau_2,\tau_3=\beta)$ and $\chi(\tau_1,\tau_2,\tau_3=0^+)$. To find this relation we do as follows.

$$\begin{aligned}
\Delta\chi_{\alpha_i\alpha_j\alpha_k\alpha_l} &= \chi_{\alpha_i\alpha_j\alpha_k\alpha_l}(\tau_1,\tau_2,0^+) - \chi_{\alpha_i\alpha_j\alpha_k\alpha_l}(\tau_1,\tau_2,0^-) \\
&= \left\langle \mathcal{T} c^\dagger_{\alpha_i}(\tau_1)c_{\alpha_j}(\tau_2)\left\{c^\dagger_{\alpha_k},c_{\alpha_l}\right\}\right\rangle \\
&\quad -\left\langle \mathcal{T} c^\dagger_{\alpha_i}(\tau_1)c_{\alpha_j}(\tau_2)\right\rangle\left(\mathcal{G}_{\alpha_l\alpha_k}(0^+) - \mathcal{G}_{\alpha_l\alpha_k}(0^-)\right) \\
&= -\mathcal{G}_{\alpha_j\alpha_i}(\tau_2,\tau_1)\delta_{\alpha_k\alpha_l} + \mathcal{G}_{\alpha_j\alpha_i}(\tau_2,\tau_1)\left(\mathcal{G}_{\alpha_l\alpha_k}(0^+) - (\mathcal{G}_{\alpha_l\alpha_k}(0^+) + \delta_{\alpha_l\alpha_k})\right) \\
&= 0.
\end{aligned}$$

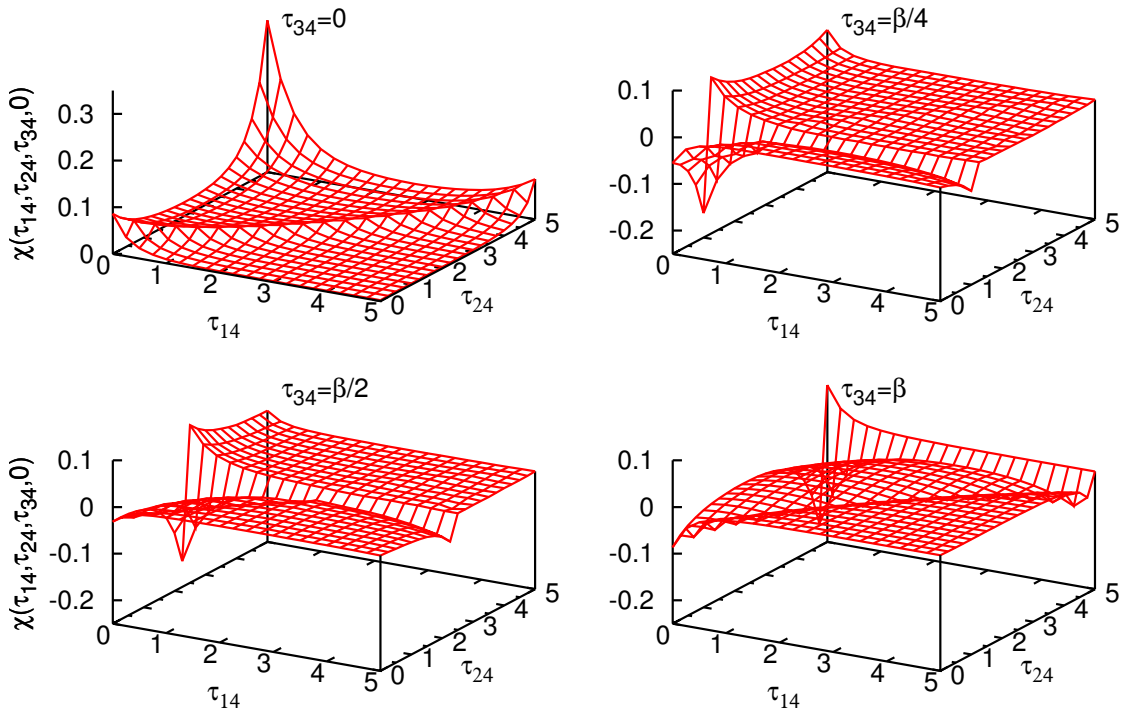

Figure 4.9: Behavior of the susceptibility in $\boldsymbol{\tau}$-space. The kink at $\tau_1 = \tau_2$ and the discontinuity at $\tau_2 = \tau_3$ are clear in this plot. This is the "*paramagnetic local spin susceptibility*" of the $KCuF_3$ material in which we considered $U = 3$, $J = 0.3$, $\beta = 5$, and $i = j = k = l = 1$.

Therefore, $\chi_{\alpha_i\alpha_j\alpha_k\alpha_l}(\tau_1, \tau_2, 0^+) = \chi_{\alpha_i\alpha_j\alpha_k\alpha_l}(\tau_1, \tau_2, 0^-)$. This proof implies that the susceptibility is continuous at $\tau_2 = 0$.

- $\chi(\tau_1, \beta, \tau_3)$ for ($\tau_1 \neq 0, \beta$ and $\tau_3 \neq 0, \beta$) :

$$\chi(\tau_1, \beta, \tau_3) = -\chi(\tau_1, 0^+, \tau_3). \tag{4.75}$$

Since there is no discontinuity in $\chi(\tau_1, \tau_2, \tau_3)$ at $\tau_2 = 0$, we can conclude that $\chi(\tau_1, 0^+, \tau_3) = \chi(\tau_1, 0^-, \tau_3)$. Then according to anti-periodicity property of susceptibility at $\tau_2 < 0$, i.e., $\chi(\tau_1, \tau_2 + \beta, \tau_3) = -\chi(\tau_1, \tau_2, \tau_3)$, we can see that $\chi(\tau_1, \beta, \tau_3) = -\chi(\tau_1, 0^-, \tau_2) = -\chi(\tau_1, 0^+, \tau_2)$.

- $\chi_{\alpha_i\alpha_j\alpha_k\alpha_l}(\beta, \tau_2, \tau_3)$ for ($\tau_2 \neq \tau_3$, $\tau_2 \neq 0, \beta$ and $\tau_3 \neq 0, \beta$) :

$$\chi_{\alpha_i\alpha_j\alpha_k\alpha_l}(\beta, \tau_2, \tau_3) = -\chi_{\alpha_i\alpha_j\alpha_k\alpha_l}(0^+, \tau_2, \tau_3) - \mathcal{G}_{\alpha_j\alpha_k}(\tau_2, \tau_3)\delta_{\alpha_i\alpha_l}. \tag{4.76}$$

In this case, the susceptibility clearly is discontinuous at $\tau_1 = 0$ (i.e., $\tau_{14} = 0$). We can measure the difference of the susceptibility at $\tau_1 = 0^-$ and $\tau_1 = 0^+$ when "$\tau_2 \neq \tau_3$,

$\tau_2 \neq 0, \beta$ and $\tau_3 \neq 0, \beta$".

$$\begin{aligned}
\Delta\chi_{\alpha_i\alpha_j\alpha_k\alpha_l} &= \chi_{\alpha_i\alpha_j\alpha_k\alpha_l}(0^+,\tau_2,\tau_3) - \chi_{\alpha_i\alpha_j\alpha_k\alpha_l}(0^-,\tau_2,\tau_3) \\
&= \Big\langle \mathcal{T} c^\dagger_{\alpha_i}(0^+) c_{\alpha_j}(\tau_2) c^\dagger_{\alpha_k}(\tau_3) c_{\alpha_l}(0) \Big\rangle \\
&\quad - \Big\langle \mathcal{T} c^\dagger_{\alpha_i}(0^-) c_{\alpha_j}(\tau_2) c^\dagger_{\alpha_k}(\tau_3) c_{\alpha_l}(0) \Big\rangle \\
&\quad - \Big\langle \mathcal{T} c^\dagger_{\alpha_i}(0^+) c_{\alpha_j}(\tau_2) \Big\rangle \Big\langle c^\dagger_{\alpha_k}(\tau_3) c_{\alpha_l}(0) \Big\rangle \\
&\quad + \Big\langle \mathcal{T} c^\dagger_{\alpha_i}(0^-) c_{\alpha_j}(\tau_2) \Big\rangle \Big\langle c^\dagger_{\alpha_k}(\tau_3) c_{\alpha_l}(0) \Big\rangle \\
&= \Big\langle c_{\alpha_j}(\tau_2) c^\dagger_{\alpha_k}(\tau_3) \Big\{ c^\dagger_{\alpha_i}, c_{\alpha_l} \Big\} \Big\rangle \\
&= -\mathcal{G}_{\alpha_j\alpha_k}(\tau_2,\tau_3)\delta_{\alpha_i\alpha_l}.
\end{aligned}$$

- $\chi(0^+,\beta,\tau_3)$ for $(\tau_3 \neq 0,\beta)$:

$$\chi(0^+,\beta,\tau_3) = -\chi(0^+,0^+,\tau_3). \tag{4.77}$$

Since there is no discontinuity in $\chi(\tau_1,\tau_2,\tau_3)$ at $\tau_1 = \tau_2$, we can set $\tau_1 = 0$ in Eq. (4.75). Then we can easily obtain $\chi(0^+,\beta,\tau_3) = -\chi(0^+,0^+,\tau_3)$.

- $\chi_{\alpha_i\alpha_j\alpha_k\alpha_l}(\beta,\tau_2,0^+)$ for $(\tau_2 \neq 0,\beta)$:

$$\chi_{\alpha_i\alpha_j\alpha_k\alpha_l}(\beta,\tau_2,0^+) = -\chi_{\alpha_i\alpha_j\alpha_k\alpha_l}(0^+,\tau_2,0^+) - \mathcal{G}_{\alpha_j\alpha_k}(\tau_2,0)\delta_{\alpha_i\alpha_l}. \tag{4.78}$$

According to the continuous behavior of the susceptibility at $\tau_3 = 0$, we can put $\tau_3 = 0^+$ in Eq. (4.76) to get appropriate boundary condition.

- $\chi(\tau_1,0^+,\beta)$ for $(\tau_1 \neq 0,\beta)$:

$$\chi(\tau_1,0^+,\beta) = -\chi(\tau_1,0^+,0^+). \tag{4.79}$$

To examine the validity of this boundary condition,

$$\begin{aligned}
\Delta\chi_{\alpha_i\alpha_j\alpha_k\alpha_l} &= \chi_{\alpha_i\alpha_j\alpha_k\alpha_l}(\tau_1,0^+,0^-) - \chi_{\alpha_i\alpha_j\alpha_k\alpha_l}(\tau_1,0^+,0^+) \\
&= \Big\langle \mathcal{T} c^\dagger_{\alpha_i}(\tau_1) c_{\alpha_j}(0^+) c^\dagger_{\alpha_k}(0^-) c_{\alpha_l}(0) \Big\rangle \\
&\quad - \Big\langle \mathcal{T} c^\dagger_{\alpha_i}(\tau_1) c_{\alpha_j}(0^+) \Big\rangle \Big\langle \mathcal{T} c^\dagger_{\alpha_k}(0^-) c_{\alpha_l}(0) \Big\rangle \\
&\quad - \Big\langle \mathcal{T} c^\dagger_{\alpha_i}(\tau_1) c_{\alpha_j}(0^+) c^\dagger_{\alpha_k}(0^+) c_{\alpha_l}(0) \Big\rangle \\
&\quad + \Big\langle \mathcal{T} c^\dagger_{\alpha_i}(\tau_1) c_{\alpha_j}(0^+) \Big\rangle \Big\langle \mathcal{T} c^\dagger_{\alpha_k}(0^+) c_{\alpha_l}(0) \Big\rangle \\
&= \Big\langle \mathcal{T} c^\dagger_{\alpha_i}(\tau_1) c_{\alpha_j}(0^+) \Big\{ c^\dagger_{\alpha_k}, c_{\alpha_l} \Big\} \Big\rangle - \Big\langle \mathcal{T} c^\dagger_{\alpha_i}(\tau_1) c_{\alpha_j}(0^+) \Big\rangle \Big\{ c^\dagger_{\alpha_k}, c_{\alpha_l} \Big\} \\
&= 0.
\end{aligned}$$

This boundary can be infered from this point that the $\chi(\tau_1,\tau_2,\tau_3)$ is continuous function at $\tau_3 = 0$ (i.e., $\tau_{34} = 0$).

- $\chi(0^+,\tau_2,\beta)$ for $(\tau_2 \neq 0,\beta)$:

$$\chi(0^+,\tau_2,\beta) = -\chi(0^+,\tau_2,0^+). \tag{4.80}$$

Since the susceptibility is continuous $\tau_3 = 0$ (i.e., $\tau_{34} = 0$), we can substitute $\tau_1 = 0^+$ in Eq. (4.74).

- $\chi_{\alpha_i\alpha_j\alpha_k\alpha_l}(\tau_1,\beta,0^+)$ for $(\tau_1 \neq 0,\beta)$:

$$\begin{aligned}\chi_{\alpha_i\alpha_j\alpha_k\alpha_l}(\tau_1,\beta,0^+) &= -\chi_{\alpha_i\alpha_j\alpha_k\alpha_l}(\tau_1,0^+,0^+) - \mathcal{G}_{\alpha_l\alpha_i}(\beta-\tau_1,0)\delta_{\alpha_j\alpha_k} \\ &\quad +\mathcal{G}_{\alpha_j\alpha_i}(\beta-\tau_1,0)\ \delta_{\alpha_k\alpha_l}. \end{aligned} \tag{4.81}$$

Because $\tau_3 = 0^+$, and for $\tau_2 = \tau_3$ there is a discontinuity in the susceptibility, we can obain the difference of $\chi_{ijrs}(\tau_1,0^+,0^-)$ and $\chi_{ijrs}(\tau_1,0^-,0^+)$ by

$$\begin{aligned}\Delta\chi_{\alpha_i\alpha_j\alpha_k\alpha_l} &= \chi_{\alpha_i\alpha_j\alpha_k\alpha_l}(\tau_1,0^+,0^-) - \chi_{\alpha_i\alpha_j\alpha_k\alpha_l}(\tau_1,0^-,0^+) \\ &= \left\langle \mathcal{T} c^\dagger_{\alpha_i}(\tau_1) c_{\alpha_j}(0^+) c^\dagger_{\alpha_k}(0^-) c_{\alpha_l}(0)\right\rangle \\ &\quad -\left\langle \mathcal{T} c^\dagger_{\alpha_i}(\tau_1) c_{\alpha_j}(0^+)\right\rangle \left\langle \mathcal{T} c^\dagger_{\alpha_k}(0^-) c_{\alpha_l}(0)\right\rangle \\ &\quad -\left\langle \mathcal{T} c^\dagger_{\alpha_i}(\tau_1) c_{\alpha_j}(0^-) c^\dagger_{\alpha_k}(0^+) c_{\alpha_l}(0)\right\rangle \\ &\quad +\left\langle \mathcal{T} c^\dagger_{\alpha_i}(\tau_1) c_{\alpha_j}(0^-)\right\rangle \left\langle \mathcal{T} c^\dagger_{\alpha_k}(0^+) c_{\alpha_l}(0)\right\rangle \\ &= \left\langle \mathcal{T} c^\dagger_{\alpha_i}(\tau_1) \left\{ c_{\alpha_j}, c^\dagger_{\alpha_k}\right\} c_{\alpha_l}\right\rangle - \left\langle \mathcal{T} c^\dagger_{\alpha_i}(\tau_1) c_{\alpha_j}(0)\right\rangle \left\{ c^\dagger_{\alpha_k}, c_{\alpha_l}\right\} \\ &= \mathcal{G}_{\alpha_l\alpha_i}(\beta-\tau_1,0)\ \delta_{\alpha_j\alpha_k} - \mathcal{G}_{\alpha_j\alpha_i}(\beta-\tau_1,0)\ \delta_{\alpha_k\alpha_l}. \end{aligned}$$

By using Eq. (4.79) and the anti-periodicity property of susceptibility, i.e., $\chi(\tau_1,0^+,0^-) = -\chi(\tau_1,0^+,\beta)$, and $\chi(\tau_1,0^-,0^+) = -\chi(\tau_1,\beta,0^+)$, we can obtain Eq. (4.81).

- $\chi_{\alpha_i\alpha_j\alpha_k\alpha_l}(\beta,\beta,\tau_3)$ for $(\tau_3 \neq 0,\beta)$:

$$\chi_{\alpha_i\alpha_j\alpha_k\alpha_l}(\beta,\beta,\tau_3) = \chi_{\alpha_i\alpha_j\alpha_k\alpha_l}(0^+,0^+,\tau_3) - \mathcal{G}_{\alpha_j\alpha_k}(\beta,\tau_3)\ \delta_{\alpha_i\alpha_l}. \tag{4.82}$$

Considering this point that there is no discontinuity in susceptibility at $\tau_1 = \tau_2$, we can substitute $\tau_2 = \beta$ in Eq. (4.76). Then we use Eq. (4.77) to obtain Eq. (4.82). Notice that the origin of the second term in Eq. (4.82) comes from discontinuity of the susceptibility at $\tau_1 = 0$ (i.e., $\tau_{14} = 0$).

- $\chi_{\alpha_i\alpha_j\alpha_k\alpha_l}(\beta,\tau_2,\beta)$ for $(\tau_2 \neq 0,\beta)$:

$$\chi_{\alpha_i\alpha_j\alpha_k\alpha_l}(\beta,\tau_2,\beta) = \chi_{\alpha_i\alpha_j\alpha_k\alpha_l}(0^+,\tau_2,0^+) + \mathcal{G}_{\alpha_j\alpha_k}(\tau_2,0)\ \delta_{\alpha_i\alpha_l}. \tag{4.83}$$

Due to the continuous behavior of the susceptibility at $\tau_3 = 0$ (while "$\tau_2 \neq 0,\beta$"), it is clear that $\chi(\beta,\tau_2,0^+) = \chi(\beta,\tau_2,0^-)$. With the knowledge that $\chi(\beta,\tau_2,0^-) = -\chi(\beta,\tau_2,\beta)$, we can use Eq. (4.78) to derive Eq. (4.83).

- $\chi(\tau_1,\beta,\beta)$ for $(\tau_1 \neq 0,\beta)$:

$$\chi(\tau_1,\beta,\beta) = \chi(\tau_1,0^+,0^+). \tag{4.84}$$

To prove this boundary condition, we proceed as follows

$$\begin{aligned}
\Delta\chi_{\alpha_i\alpha_j\alpha_k\alpha_l} &= \chi_{\alpha_i\alpha_j\alpha_k\alpha_l}(\tau_1,0^+,0^+)-\chi_{\alpha_i\alpha_j\alpha_k\alpha_l}(\tau_1,0^-,0^-)\\
&= \Big\langle \mathcal{T}c^\dagger_{\alpha_i}(\tau_1)c_{\alpha_j}(0^+)c^\dagger_{\alpha_k}(0^+)c_{\alpha_l}(0)\Big\rangle\\
&\quad -\Big\langle \mathcal{T}c^\dagger_{\alpha_i}(\tau_1)c_{\alpha_j}(0^-)c^\dagger_{\alpha_k}(0^-)c_{\alpha_l}(0)\Big\rangle\\
&\quad -\Big\langle \mathcal{T}c^\dagger_{\alpha_i}(\tau_1)c_{\alpha_j}(0^+)\Big\rangle\Big\langle \mathcal{T}c^\dagger_{\alpha_k}(0^+)c_{\alpha_l}(0)\Big\rangle\\
&\quad +\Big\langle \mathcal{T}c^\dagger_{\alpha_i}(\tau_1)c_{\alpha_j}(0^-)\Big\rangle\Big\langle \mathcal{T}c^\dagger_{\alpha_k}(0^-)c_{\alpha_l}(0)\Big\rangle\\
&= \Big\langle \mathcal{T}c^\dagger_{\alpha_i}(\tau_1)c_{\alpha_j}(0^+)\Big\{c^\dagger_{\alpha_k},c_{\alpha_l}\Big\}\Big\rangle-\Big\langle \mathcal{T}c^\dagger_{\alpha_i}(\tau_1)c_{\alpha_j}(0)\Big\rangle\Big\{c^\dagger_{\alpha_k},c_{\alpha_l}\Big\}\\
&= 0,
\end{aligned}$$

where $\chi(\tau_1,0^-,0^-)=\chi(\tau_1,\beta,\beta)$.

- $\chi(0^+,\beta,\beta)$:

$$\chi(0^+,\beta,\beta)=\chi(0^+,0^+,0^+). \tag{4.85}$$

We can utilize Eq. (4.84) and put $\tau_1=0^+$ to obtain $\chi(0^+,\beta,\beta)=\chi(0^+,0^+,0^+)$.

- $\chi_{\alpha_i\alpha_j\alpha_k\alpha_l}(\beta,0^+,\beta)$:

$$\chi_{\alpha_i\alpha_j\alpha_k\alpha_l}(\beta,0^+,\beta)=\chi_{\alpha_i\alpha_j\alpha_k\alpha_l}(0^+,0^+,0^+)+\mathcal{G}_{\alpha_j\alpha_k}(0^+,0)\,\delta_{\alpha_i\alpha_l}. \tag{4.86}$$

This relation can be easily derived by implementing Eq. (4.79) and Eq. (4.89). In Eq. (4.79) we can put $\tau_1=\beta^-$ to obtain $\chi_{ijrs}(\beta,0^+,\beta)=-\chi_{ijrs}(\beta,0^+,0^+)$. Then Eq. (4.89) will help us to get Eq. (4.86).

- $\chi_{\alpha_i\alpha_j\alpha_k\alpha_l}(\beta,\beta,0^+)$:

$$\begin{aligned}
\chi_{\alpha_i\alpha_j\alpha_k\alpha_l}(\beta,\beta,0^+) &= \chi_{\alpha_i\alpha_j\alpha_k\alpha_l}(0^+,0^+,0^+)+\mathcal{G}_{\alpha_l\alpha_i}(0^+,0)\,\delta_{\alpha_j\alpha_k}\\
&\quad -\mathcal{G}_{\alpha_l\alpha_i}(0^+,0)\,\delta_{\alpha_j\alpha_k}+\mathcal{G}_{\alpha_j\alpha_k}(0^+,0)\,\delta_{\alpha_i\alpha_l}.
\end{aligned} \tag{4.87}$$

To prove this relation, it is sufficient to put $\tau_1=\beta$ in Eq. (4.81).

$$\chi_{\alpha_i\alpha_j\alpha_k\alpha_l}(\beta,\beta,0^+)=-\chi_{\alpha_i\alpha_j\alpha_k\alpha_l}(\beta,0^+,0^+)-\mathcal{G}_{\alpha_l\alpha_i}(0^+,0)\delta_{\alpha_j\alpha_k}+\mathcal{G}_{\alpha_j\alpha_i}(0^+,0)\,\delta_{\alpha_k\alpha_l}.$$

Then we use Eq. (4.89) in which $\chi_{\alpha_i\alpha_j\alpha_k\alpha_l}(\beta,0^+,0^+)$ is calculated.

$$\begin{aligned}
\chi_{\alpha_i\alpha_j\alpha_k\alpha_l}(\beta,\beta,0^+) &= -\Big(-\chi_{\alpha_i\alpha_j\alpha_k\alpha_l}(0^+,0^+,0^+)-\mathcal{G}_{\alpha_j\alpha_k}(0^+,0)\,\delta_{\alpha_i,\alpha_l}\Big)\\
&\quad -\mathcal{G}_{\alpha_l\alpha_i}(0^+,0)\delta_{\alpha_j\alpha_k}+\mathcal{G}_{\alpha_j\alpha_i}(0^+,0)\,\delta_{\alpha_k\alpha_l}\\
&= \chi_{\alpha_i\alpha_j\alpha_k\alpha_l}(0^+,0^+,0^+)+\mathcal{G}_{\alpha_j\alpha_k}(0^+,0)\,\delta_{\alpha_i\alpha_l}\\
&\quad -\mathcal{G}_{\alpha_l\alpha_i}(0^+,0)\,\delta_{\alpha_j\alpha_k}+\mathcal{G}_{\alpha_j\alpha_i}(0^+,0)\,\delta_{\alpha_k\alpha_l}.
\end{aligned}$$

- $\chi(0^+,0^+,\beta)$:

$$\chi(0^+,0^+,\beta)=-\chi(0^+,0^+,0^+). \tag{4.88}$$

Since the behavior of the susceptibility at τ_1 is independent of it's behavior at the chosen values of τ_2 and τ_3, we can put $\tau_1=0^+$ in Eq. (4.79). We should notice that the susceptiblity is not well-defined at $\tau_2=\tau_3$. For this reason the behavior of the susceptibility highly depends on chosen values for τ_2 and/or τ_3 but not on τ_1.

- $\chi_{\alpha_i\alpha_j\alpha_k\alpha_l}(\beta, 0^+, 0^+)$:

$$\chi_{\alpha_i\alpha_j\alpha_k\alpha_l}(\beta, 0^+, 0^+) = -\chi_{\alpha_i\alpha_j\alpha_k\alpha_l}(0^+, 0^+, 0^+) - \mathcal{G}_{\alpha_j\alpha_k}(0^+, 0)\ \delta_{\alpha_i\alpha_l}. \tag{4.89}$$

We can derive this relation as follows.

$$\begin{aligned}
\Delta\chi_{\alpha_i\alpha_j\alpha_k\alpha_l} &= \chi_{\alpha_i\alpha_j\alpha_k\alpha_l}(0^+, 0^+, 0^+) - \chi_{\alpha_i\alpha_j\alpha_k\alpha_l}(0^-, 0^+, 0^+) \\
&= \left\langle \mathcal{T} c^\dagger_{\alpha_i}(0^+) c_{\alpha_j}(0^+) c^\dagger_{\alpha_k}(0^+) c_{\alpha_l}(0) \right\rangle \\
&\quad - \left\langle \mathcal{T} c^\dagger_{\alpha_i}(0^-) c_{\alpha_j}(0^+) c^\dagger_{\alpha_k}(0^+) c_{\alpha_l}(0) \right\rangle \\
&= -\mathcal{G}_{\alpha_j\alpha_k}(0^+, 0)\ \delta_{\alpha_i\alpha_l}.
\end{aligned}$$

- $\chi_{\alpha_i\alpha_j\alpha_k\alpha_l}(0^+, \beta, 0^+)$:

$$\begin{aligned}
\chi_{\alpha_i\alpha_j\alpha_k\alpha_l}(0^+, \beta, 0^+) &= -\chi_{\alpha_i\alpha_j\alpha_k\alpha_l}(0^+, 0^+, 0^+) + \delta_{\alpha_l\alpha_i}\delta_{\alpha_j\alpha_k} - \delta_{\alpha_j\alpha_i}\delta_{\alpha_k\alpha_l} \\
&\quad + \mathcal{G}_{\alpha_l\alpha_i}(0^+, 0)\ \delta_{\alpha_j\alpha_k} - \mathcal{G}_{\alpha_j\alpha_i}(0^+, 0)\ \delta_{\alpha_k\alpha_l}.
\end{aligned} \tag{4.90}$$

If we substitute τ_1 with $\tau_1 = 0^+$ in Eq. (4.81), we obtain

$$\begin{aligned}
\chi_{\alpha_i\alpha_j\alpha_k\alpha_l}(0^+, \beta, 0^+) &= -\chi_{\alpha_i\alpha_j\alpha_k\alpha_l}(0^+, 0^+, 0^+) - \mathcal{G}_{\alpha_l\alpha_i}(\beta, 0)\ \delta_{\alpha_j\alpha_k} \\
&\quad + \mathcal{G}_{\alpha_j\alpha_i}(\beta, 0)\ \delta_{\alpha_k\alpha_l} \\
&= -\chi_{\alpha_i\alpha_j\alpha_k\alpha_l}(0^+, 0^+, 0^+) - \left[-\delta_{\alpha_l\alpha_i} - \mathcal{G}_{\alpha_l\alpha_i}(0^+, 0)\right] \delta_{\alpha_j\alpha_k} \\
&\quad + \left[-\delta_{\alpha_j\alpha_i} - \mathcal{G}_{\alpha_j\alpha_i}(0^+, 0)\right] \delta_{\alpha_k\alpha_l} \\
&= -\chi_{\alpha_i\alpha_j\alpha_k\alpha_l}(0^+, 0^+, 0^+) + \delta_{\alpha_l\alpha_i}\delta_{\alpha_j\alpha_k} - \delta_{\alpha_j\alpha_i}\delta_{\alpha_k\alpha_l} \\
&\quad + \mathcal{G}_{\alpha_l\alpha_i}(0^+, 0)\ \delta_{\alpha_j\alpha_k} - \mathcal{G}_{\alpha_j\alpha_i}(0^+, 0)\ \delta_{\alpha_k\alpha_l},
\end{aligned} \tag{4.91}$$

where we used $\mathcal{G}_{\alpha_i\alpha_j}(\beta) = -\mathcal{G}_{\alpha_i\alpha_j}(0^-) = -\delta_{\alpha_i\alpha_j} - \mathcal{G}_{\alpha_i\alpha_j}(0^+)$.

- $\chi_{\alpha_i\alpha_j\alpha_k\alpha_l}(\beta, \beta, \beta)$:

$$\chi_{\alpha_i\alpha_j\alpha_k\alpha_l}(\beta, \beta, \beta) = -\chi_{\alpha_i\alpha_j\alpha_k\alpha_l}(0^+, 0^+, 0^+) - \mathcal{G}_{\alpha_j\alpha_k}(0^+, 0)\ \delta_{\alpha_i\alpha_l} \tag{4.92}$$

In the vicinity of $\tau_1 = 0$, we proceed as we did in deriving Eq. (4.76).

$$\begin{aligned}
\Delta\chi_{\alpha_i\alpha_j\alpha_k\alpha_l} &= \chi_{\alpha_i\alpha_j\alpha_k\alpha_l}(0^+, \beta, \beta) - \chi_{\alpha_i\alpha_j\alpha_k\alpha_l}(0^-, \beta, \beta) \\
&= \left\langle \mathcal{T} c^\dagger_{\alpha_i}(0^+) c_{\alpha_j}(\beta) c^\dagger_{\alpha_k}(\beta) c_{\alpha_l}(0) \right\rangle \\
&\quad - \left\langle \mathcal{T} c^\dagger_{\alpha_i}(0^-) c_{\alpha_j}(\beta) c^\dagger_{\alpha_k}(\beta) c_{\alpha_l}(0) \right\rangle \\
&\quad - \left\langle \mathcal{T} c^\dagger_{\alpha_i}(0^+) c_{\alpha_j}(\beta) \right\rangle \left\langle \mathcal{T} c^\dagger_{\alpha_k}(\beta) c_{\alpha_l}(0) \right\rangle \\
&\quad + \left\langle \mathcal{T} c^\dagger_{\alpha_i}(0^-) c_{\alpha_j}(\beta) \right\rangle \left\langle \mathcal{T} c^\dagger_{\alpha_k}(\beta) c_{\alpha_l}(0) \right\rangle \\
&= \left\langle c_{\alpha_j}(\beta) c^\dagger_{\alpha_k}(\beta) \left\{ c^\dagger_{\alpha_i}, c_{\alpha_l} \right\} \right\rangle \\
&= -\mathcal{G}_{\alpha_j\alpha_k}(0^+)\ \delta_{\alpha_i\alpha_l}.
\end{aligned}$$

Considering Eq. (4.85) where we have $\chi_{ijrs}(0^+, \beta, \beta) = \chi_{ijrs}(0^+, 0^+, 0^+)$, we can easily obtain Eq. (4.92).

- $\chi_{\alpha_i\alpha_j\alpha_k\alpha_l}(\tau_1,\tau_2,\tau_2)$:

$$\chi_{\alpha_i\alpha_j\alpha_k\alpha_l}(\tau_1,\tau_2^+,\tau_2^-)-\chi_{\alpha_i\alpha_j\alpha_k\alpha_l}(\tau_1,\tau_2^-,\tau_2^+)=-\mathcal{G}_{\alpha_l\alpha_i}(\beta-\tau_1,0)\,\delta_{\alpha_j\alpha_k}. \quad (4.93)$$

$$\begin{aligned}\Delta\chi_{\alpha_i\alpha_j\alpha_k\alpha_l} &= \chi_{\alpha_i\alpha_j\alpha_k\alpha_l}(\tau_1,\tau_2^+,\tau_2^-)-\chi_{\alpha_i\alpha_j\alpha_k\alpha_l}(\tau_1,\tau_2^-,\tau_2^+)\\ &= \left\langle \mathcal{T}c^\dagger_{\alpha_i}(\tau_1)c_{\alpha_l}(0)\left\{c_{\alpha_j},c^\dagger_{\alpha_k}\right\}\right\rangle\\ &= \mathcal{G}_{\alpha_l\alpha_i}(0,\tau_1)\,\delta_{\alpha_j\alpha_k}=-\mathcal{G}_{\alpha_l\alpha_i}(\beta-\tau_1)\,\delta_{\alpha_j\alpha_k}.\end{aligned}$$

  In Figs. 4.9, 4.10a and 4.10b the calculated *spin susceptibility* for different values of τ_{14}, τ_{24} and τ_{34} is illustrated.

8. By using time invariant property of the two-particle Green's function, we can obtain a new two-particle Green's function which depends on new imaginary times τ_{12},τ_{34} and τ_{14}.

$$\mathcal{C}(\tau_{12},\tau_{34},\tau_{14})=\frac{1}{\beta}\int_0^\beta d\tau'\,\mathcal{C}(\tau_{14}+\tau',\tau_{14}-\tau_{12}+\tau',\tau_{34}+\tau',\tau'). \quad (4.94)$$

- $\mathcal{C}(\tau_{12},\tau_{34},\tau_{14})$ is β-periodic in τ_{14} and β-antiperiodic in τ_{12} and τ_{34}.

$$\mathcal{C}(\tau_{12},\tau_{34},\tau_{14})=\begin{cases}\mathcal{C}(\tau_{12},\tau_{34},\tau_{14}+\beta)\\ -\mathcal{C}(\tau_{12},\tau_{34}+\beta,\tau_{14})\\ -\mathcal{C}(\tau_{12}+\beta,\tau_{34},\tau_{14}).\end{cases} \quad (4.95)$$

  This property can be easily shown using Eq. (4.94). For instance,

$$\begin{aligned}\mathcal{C}(\tau_{12},\tau_{34},\tau_{14}+\beta) &= \frac{1}{\beta}\int_0^\beta d\tau'\,\mathcal{C}(\tau_{14}+\beta+\tau',\tau_{14}+\beta-\tau_{12}+\tau',\tau_{34}+\tau',\tau')\\ &= \frac{1}{\beta}\int_0^\beta d\tau'\,\mathcal{C}(\tau_{14}+\tau',\tau_{14}-\tau_{12}+\tau',\tau_{34}+\tau',\tau')\\ &= \mathcal{C}(\tau_{12},\tau_{34},\tau_{14}).\end{aligned}$$

- $\mathcal{C}(\tau_{12},\tau_{34},\tau_{14})$ is discontinuous at $\tau_{14}=\tau_{12}+\tau_{34}$ and $\tau_{14}=0$.
  For example, in the latter one we can calculate the discontinuity value as follows

$$\begin{aligned}\Delta\mathcal{C}_{\alpha_i\alpha_j\alpha_k\alpha_l}(\tau_{12},\tau_{34},\tau_{14}) &= \left\langle \mathcal{T}c_{\alpha_j}(\tau_{24})c^\dagger_{\alpha_k}(\tau_{34})\left\{c^\dagger_{\alpha_i},c_{\alpha_l}\right\}\right\rangle\\ &= -\mathcal{G}_{\alpha_j\alpha_k}(\tau_2,\tau_3)\,\delta_{\alpha_i\alpha_l}.\end{aligned}$$

  This should be noticed that the $\mathcal{C}(\tau_{12},\tau_{34},\tau_{14})$ is continuous at $\tau_{12}=0$ but its first derivative is discontinuous.

The most important advantage of calculation of the $\mathcal{C}(\tau_{12},\tau_{34},\tau_{14})$ is that we can expand it in terms of the Legendre polynomials (for τ_{12} and τ_{34}) and Fourier modes (for τ_{14}) in the following form

$$\begin{aligned}\mathcal{C}(\tau_{12},\tau_{34},\tau_{14}) &= \sum_{l,l'\geq 0}\sum_{m\in Z}\frac{\sqrt{2l+1}\sqrt{2l'+1}}{\beta^3}(-1)^{l+l'}\\ &\quad\times P_l[x(\tau_{12})]P_{l'}[x(\tau_{34})]e^{i\omega_m\tau_{14}}\mathcal{C}_{ll'}(\omega_m),\end{aligned} \quad (4.96)$$

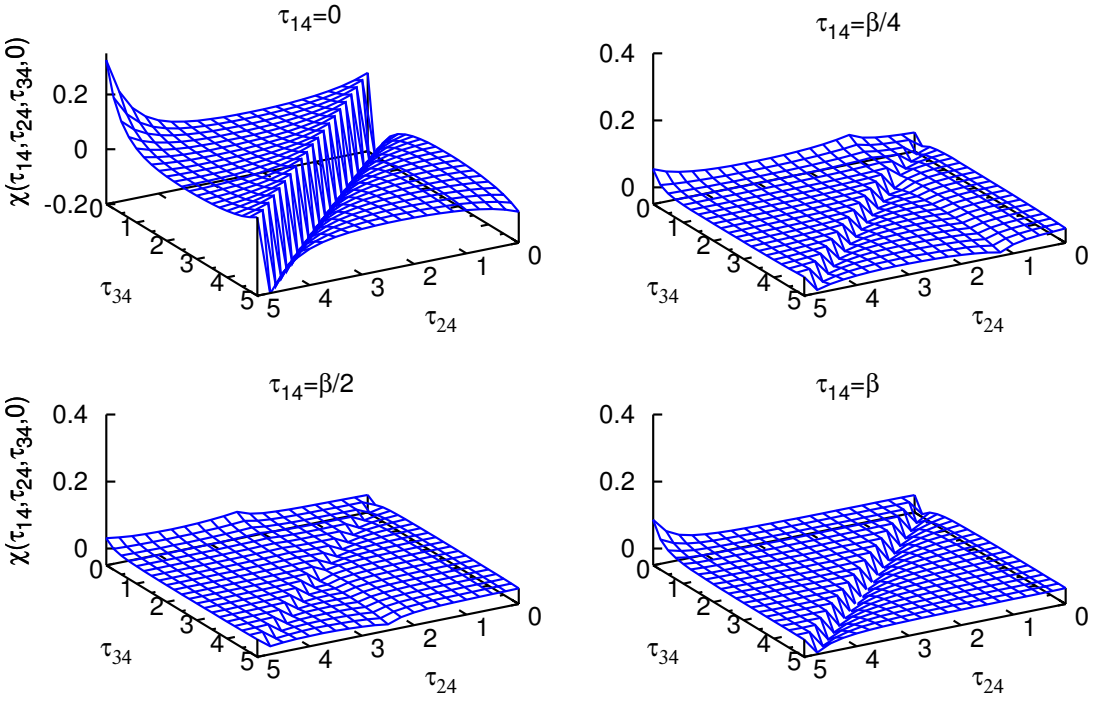

(a)

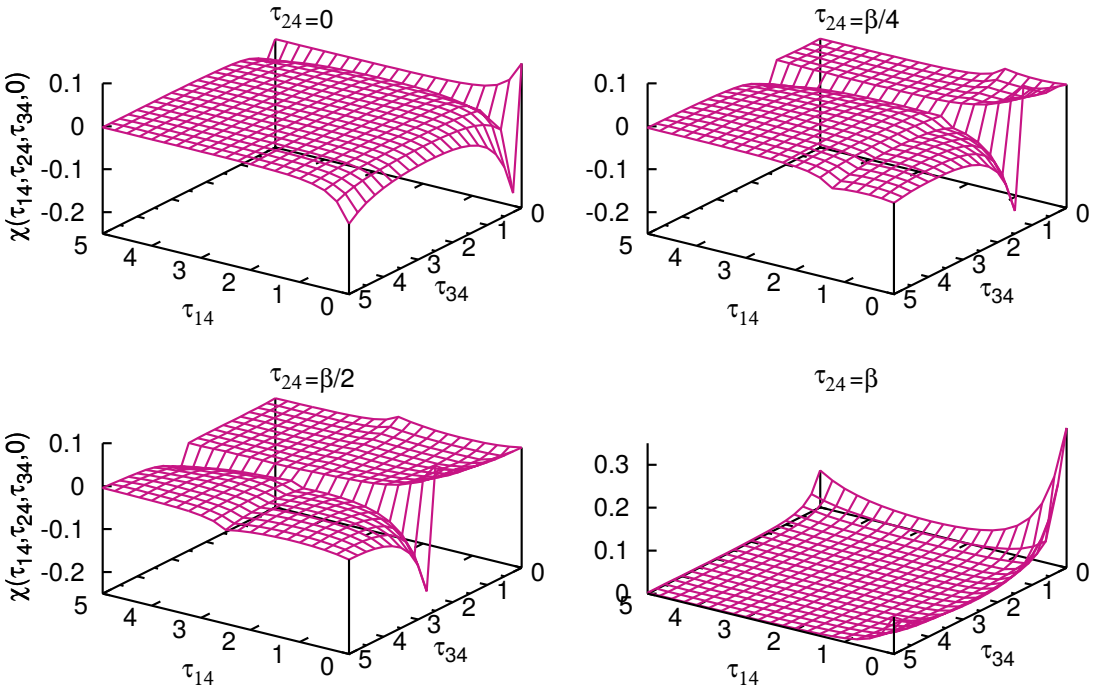

(b)

Figure 4.10: Kinks and discontinuities of the local spin susceptibility in $\boldsymbol{\tau}$-space. The *paramagnetic local spin susceptibility* of $KCuF_3$ is calculated for $U = 3$, $J = 0.3$, $\beta = 5$ and $i = j = k = l = 1$. In subfigure (a) and (b), the *local spin susceptibility* $\chi(\tau_{14}, \tau_{24}, \tau_{34})$ is computed at $\tau_{14} = 0, \beta/4, \beta/2, \beta$ and $\tau_{24} = 0, \beta/4, \beta/2, \beta$, respectively.

where $x(\tau) = 2\tau/\beta - 1$ and $\mathcal{C}_{ll'}(\omega_m)$ is Legendre coefficients. The reason of this particular choice of time arguments is that many equations that involve the susceptibility such as Bethe-Salpeter equation are diagonal in ω_m. Furthermore, the Bethe-Saltpeter equation can be solved directly in the Legendre representation. The coefficient decays faster and the error which appears due to truncation of matrices in Bethe-Salpeter equation decreases [59]. In Appendix E, we describe the Legendre-Fourier presentation of the susceptibility in details.

9. The complex conjugate of the two-particle Green's function $\mathcal{C}_{\alpha_i\alpha_j\alpha_k\alpha_l}(\mathbf{p},\boldsymbol{\tau})$ tensor is given by

$$\left[\mathcal{C}_{\alpha_i\alpha_j\alpha_k\alpha_l}(\mathbf{p},\boldsymbol{\tau})\right]^* = \mathcal{C}_{\alpha_l\alpha_k\alpha_j\alpha_i}(\bar{\mathbf{p}},-\bar{\boldsymbol{\tau}}), \tag{4.97}$$

where $\mathbf{p} = (\mathbf{k},\mathbf{k}',\mathbf{q})$, $\bar{\mathbf{p}} = (\mathbf{k}',\mathbf{k},\mathbf{q})$, $\boldsymbol{\tau} = (\tau_1,\tau_2,\tau_3,\tau_4)$, and $\bar{\boldsymbol{\tau}} = (\tau_4,\tau_3,\tau_2,\tau_1)$.

This property can be derived by

$$\begin{aligned}
\left[\mathcal{C}_{\alpha_i\alpha_j\alpha_k\alpha_l}(\mathbf{p},\boldsymbol{\tau})\right]^* &= \frac{1}{\mathcal{Z}}\mathrm{Tr}\Big\{e^{-\beta H}e^{\tau_1 H}c^\dagger_{\mathbf{k}\alpha_i}e^{-(\tau_1-\tau_2)H}c_{\mathbf{k}+\mathbf{q}\alpha_j}e^{-(\tau_2-\tau_3)H} \\
&\quad\times c^\dagger_{\mathbf{k}'+\mathbf{q}\alpha_k}e^{-(\tau_3-\tau_4)H}c_{\mathbf{k}'\alpha_l}e^{-\tau_4 H}\Big\}^* \\
&= \frac{1}{\mathcal{Z}}\mathrm{Tr}\Big\{e^{-\tau_4 H}c^\dagger_{\mathbf{k}'\alpha_l}e^{-(\tau_3-\tau_4)H}c_{\mathbf{k}'+\mathbf{q}\alpha_k}e^{-(\tau_2-\tau_3)H}c^\dagger_{\mathbf{k}+\mathbf{q}\alpha_j} \\
&\quad\times e^{-(\tau_1-\tau_2)H}c_{\mathbf{k}\alpha_i}e^{\tau_1 H}e^{-\beta H}\Big\} \\
&= \frac{1}{\mathcal{Z}}\mathrm{Tr}\Big\{e^{-\beta H}c^\dagger_{\mathbf{k}'\alpha_l}(-\tau_4)c_{\mathbf{k}'+\mathbf{q}\alpha_k}(-\tau_3)c^\dagger_{\mathbf{k}+\mathbf{q}\alpha_j}(-\tau_2)c_{\mathbf{k}\alpha_i}(-\tau_1)\Big\} \\
&= \mathcal{C}_{\alpha_l\alpha_k\alpha_j\alpha_i}(\bar{\mathbf{p}},-\bar{\boldsymbol{\tau}}).
\end{aligned}$$

Notice that $c_{\mathbf{k}} = \sum_j e^{i\mathbf{k}.\mathbf{R_j}}c_j$ and $c^\dagger_{\mathbf{k}} = \sum_j e^{-i\mathbf{k}.\mathbf{R_j}}c^\dagger_j$.

10. The $(\mathbf{q})$-dependent and $(-\mathbf{q})$-dependent two-particle correlation functions are connected by

$$\mathcal{C}_{\alpha_i\alpha_j\alpha_k\alpha_l}(\tau_1,\tau_2,\tau_3,\tau_4;\mathbf{p}) = \mathcal{C}_{\alpha_k\alpha_l\alpha_i\alpha_j}(\tau_3,\tau_4,\tau_1,\tau_2;\mathbf{p'}), \tag{4.98}$$

where $\mathbf{p'} = (\mathbf{k}'+\mathbf{q},\mathbf{k}+\mathbf{q},-\mathbf{q})$ and $\mathbf{p} = (\mathbf{k},\mathbf{k}',\mathbf{q})$ (see Eq. (4.69)).

This property can be easily proved by using the time ordering property.

$$\begin{aligned}
\mathcal{C}_{\alpha_i\alpha_j\alpha_k\alpha_l}(\tau_1,\tau_2,\tau_3,\tau_4;\mathbf{p}) &= \left\langle \mathcal{T}c^\dagger_{\mathbf{k},\alpha_i}(\tau_1)c_{\mathbf{k}+\mathbf{q},\alpha_j}(\tau_2)c^\dagger_{\mathbf{k}'+\mathbf{q},\alpha_k}(\tau_3)c_{\mathbf{k}',\alpha_l}(\tau_4)\right\rangle \\
&= \left\langle \mathcal{T}c^\dagger_{\mathbf{k}'+\mathbf{q},\alpha_k}(\tau_3)c_{\mathbf{k}',\alpha_l}(\tau_4)c^\dagger_{\mathbf{k},\alpha_i}(\tau_1)c_{\mathbf{k}+\mathbf{q},\alpha_j}(\tau_2)\right\rangle \\
&= \mathcal{C}_{\alpha_k\alpha_l\alpha_i\alpha_j}(\tau_3,\tau_4,\tau_1,\tau_2;\mathbf{p'}).
\end{aligned}$$

4.4.2 Properties of the susceptibility in Matsubara frequency space

The Fourier integral of the $\mathbf{q}$-dependent two-particle Green's function is

$$\begin{aligned}
\mathcal{C}_{\alpha_i\alpha_j\alpha_k\alpha_l}(\mathbf{p},\boldsymbol{\nu}) &= \int_0^\beta d\tau_1 \ldots \int_0^\beta d\tau_4\, e^{-i\nu_n\tau_1}e^{i(\nu_n+\omega_m)\tau_2}e^{-i(\nu_{n'}+\omega_m)\tau_3}e^{i\nu_{n'}\tau_4} \\
&\quad\times\left\langle \mathcal{T}c^\dagger_{\mathbf{k},\alpha_i}(\tau_1)c_{\mathbf{k}+\mathbf{q},\alpha_j}(\tau_2)c^\dagger_{\mathbf{k}'+\mathbf{q},\alpha_k}(\tau_3)c_{\mathbf{k}',\alpha_l}(\tau_4)\right\rangle \\
&= \left\langle c^\dagger_{\mathbf{k},\alpha_i}(\nu_n)c_{\mathbf{k}+\mathbf{q},\alpha_j}(\nu_n+\omega_m)c^\dagger_{\mathbf{k}'+\mathbf{q},\alpha_k}(\nu_{n'}+\omega_m)c_{\mathbf{k}',\alpha_l}(\nu_{n'})\right\rangle,
\end{aligned} \tag{4.99}$$

where $\boldsymbol{\nu} = (\nu_n, \nu_{n'}; \omega_m)$. Using this definition and the properties of the two-particle Green's function in $\boldsymbol{\tau}$-space, we can obtain following properties.

1. One of the useful property of the two-particle Green's function is its complex conjugate relation.

$$\Big[\mathcal{C}_{\alpha_i\alpha_j\alpha_k\alpha_l}(\mathbf{p}, \boldsymbol{\nu})\Big]^* = \mathcal{C}_{\alpha_i\alpha_j\alpha_k\alpha_l}(\mathbf{p}, -\boldsymbol{\nu}). \tag{4.100}$$

we can calculate the complex conjugate of the two-particle Green's function by using the definition (4.99).

$$\begin{aligned}
\Big[\mathcal{C}_{\alpha_i\alpha_j\alpha_k\alpha_l}(\mathbf{p}, \boldsymbol{\nu})\Big]^* &= \int_0^\beta d\tau_1 \ldots \int_0^\beta d\tau_4 \; e^{i\nu_n\tau_1} e^{-i(\nu_n+\omega_m)\tau_2} e^{i(\nu_{n'}+\omega_m)\tau_3} e^{-i\nu_{n'}\tau_4} \\
&\quad \times \Big\langle \mathcal{T} c^\dagger_{\mathbf{k}',\alpha_l}(-\tau_4) c_{\mathbf{k}'+\mathbf{q},\alpha_k}(-\tau_3) c^\dagger_{\mathbf{k}+\mathbf{q},\alpha_j}(-\tau_2) c_{\mathbf{k},\alpha_i}(-\tau_1) \Big\rangle \\
&= \int_0^\beta d\tau_1 \ldots \int_0^\beta d\tau_4 \; e^{i(-\nu_n)(-\tau_1)} e^{-i(-\nu_n-\omega_m)(-\tau_2)} e^{i(-\nu_{n'}-\omega_m)(-\tau_3)} \\
&\quad \times e^{-i(-\nu_{n'})(-\tau_4)} \Big\langle \mathcal{T} c_{\mathbf{k},\alpha_i}(-\tau_1) c^\dagger_{\mathbf{k}+\mathbf{q},\alpha_j}(-\tau_2) c_{\mathbf{k}'+\mathbf{q},\alpha_k}(-\tau_3) c^\dagger_{\mathbf{k}',\alpha_l}(-\tau_4) \Big\rangle \\
&= \mathcal{C}_{\alpha_i\alpha_j\alpha_k\alpha_l}(\mathbf{p}, -\boldsymbol{\nu}).
\end{aligned}$$

From this property we can easily conclude that for a fixed momenta $\mathbf{P} = (\mathbf{k}, \mathbf{k}', \mathbf{q})$, we have

- $\Re e\left[\chi_{\alpha_i\alpha_j\alpha_k\alpha_l}(\nu_n, \nu_{n'}; \omega_m)\right] = \Re e\left[\chi_{\alpha_i\alpha_j\alpha_k\alpha_l}(-\nu_n, -\nu_{n'}; -\omega_m)\right]$. This means that for the static case ($\omega = 0$), the real part of the susceptibility is an even function of ν_n and ν'_n (See Fig. 4.11b).
- $\Im m\left[\chi_{\alpha_i\alpha_j\alpha_k\alpha_l}(\nu_n, \nu_{n'}; \omega_m)\right] = -\Im m\left[\chi_{\alpha_i\alpha_j\alpha_k\alpha_l}(-\nu_n, -\nu_{n'}; -\omega_m)\right]$. At $\omega = 0$, where we are in static regime, the imaginary part of the susceptibility is an odd function of fermionic Matsubara frequencies ν_n and $\nu_{n'}$ and therefore it is anti-symmetric in ν_n-$\nu_{n'}$ plane (See Fig. 4.11d).
- For $\chi(\omega_m)$ which is obtained by tracing over ν_n and $\nu_{n'}$ by $1/\beta^2 \sum_{nn'} \chi(\nu_n, \nu_{n'}; \omega_m)$, $\Re e\left[\chi_{\alpha_i\alpha_j\alpha_k\alpha_l}(\omega_m)\right]$ and $\Im m\left[\chi_{\alpha_i\alpha_j\alpha_k\alpha_l}(\omega_m)\right]$ are an even and odd function of the bosonic Matsubara frequency ω_m, respectively.

2. Considering the time ordering operator in the two-particle correlation function, we can extract the following feature.

$$\mathcal{C}_{\alpha_i\alpha_j\alpha_k\alpha_l}(\mathbf{p}, \boldsymbol{\nu}) = \mathcal{C}_{\alpha_l\alpha_k\alpha_j\alpha_i}(\bar{\mathbf{p}}, \bar{\boldsymbol{\nu}}), \tag{4.101}$$

where $\bar{\mathbf{p}} = (\mathbf{k}', \mathbf{k}, \mathbf{q})$ and $\bar{\boldsymbol{\nu}} = (\nu_{n'}, \nu_n; \omega_m)$ provided that the local Hamiltonian is real.[16]

By exchanging the indices 1 and 4, 2 and 3 in the integrand in Eq. (4.99), we find [19]

$$\begin{aligned}
\mathcal{C}_{\alpha_i\alpha_j\alpha_k\alpha_l}(\mathbf{p}, \boldsymbol{\nu}) &= \int_0^\beta d\tau_1 \ldots \int_0^\beta d\tau_4 \; e^{-i\nu_n\tau_4} e^{i(\nu_n+\omega_m)\tau_3} e^{-i(\nu_{n'}+\omega_m)\tau_2} e^{i\nu_{n'}\tau_1} \\
&\quad \times \Big\langle \mathcal{T} c_{\mathbf{k}',\alpha_l}(\tau_1) c^\dagger_{\mathbf{k}'+\mathbf{q},\alpha_k}(\tau_2) c_{\mathbf{k}+\mathbf{q},\alpha_j}(\tau_3) c^\dagger_{\mathbf{k},\alpha_i}(\tau_4) \Big\rangle, \\
&= \Big\langle c_{\mathbf{k}',\alpha_l}(\nu_{n'}) c^\dagger_{\mathbf{k}'+\mathbf{q},\alpha_k}(\nu_{n'}+\omega_m) c_{\mathbf{k}+\mathbf{q},\alpha_j}(\nu_n+\omega_m) c^\dagger_{\mathbf{k},\alpha_i}(\nu_n) \Big\rangle \\
&= \mathcal{C}_{\alpha_l\alpha_k\alpha_j\alpha_i}(\bar{\mathbf{p}}, \bar{\boldsymbol{\nu}}).
\end{aligned}$$

[16] The local Hamiltonian may not be real if it contains e.g. spin-orbit coupling term.

As we show in Fig. 4.11, if $\alpha_i = \alpha_j = \alpha_k = \alpha_l$, then $\nu_n = \nu_{n'}$ is a reflection axis of the absolute value of (4.99).

3. The property of the two-particle Green's function that connects different Matsubara frequencies ν_n and $\nu_{n'}$ in the same ω_m sector is

$$\left[\mathcal{C}_{\alpha_i\alpha_j\alpha_k\alpha_l}(\mathbf{p},\boldsymbol{\nu})\right]^* = \mathcal{C}_{\alpha_k\alpha_l\alpha_i\alpha_j}(\mathbf{p'};\nu_{n'}+\omega_m,\nu_n+\omega_m,\omega_m), \tag{4.102}$$

where $\mathbf{p'} = (\mathbf{k'}+\mathbf{q},\mathbf{k}+\mathbf{q},-\mathbf{q})$.

This feature can be proved by exchanging indices 1 and 2 with 3 and 4, respectively.

$$\begin{aligned}
\mathcal{C}_{\alpha_i\alpha_j\alpha_k\alpha_l}(\mathbf{p},\boldsymbol{\nu}) &= \int_0^\beta d\tau_1 \ldots \int_0^\beta d\tau_4\; e^{-i\nu_n\tau_1} e^{i(\nu_n+\omega_m)\tau_2} e^{-i(\nu_{n'}+\omega_m)\tau_3} e^{i\nu_{n'}\tau_4} \\
&\quad \times \left\langle \mathcal{T}\, c^\dagger_{\mathbf{k},\alpha_i}(\tau_1) c_{\mathbf{k}+\mathbf{q},\alpha_j}(\tau_2) c^\dagger_{\mathbf{k'}+\mathbf{q},\alpha_k}(\tau_3) c_{\mathbf{k'},\alpha_l}(\tau_4) \right\rangle. \\
&= \int_0^\beta d\tau_1 \ldots \int_0^\beta d\tau_4\; e^{-i\nu_n\tau_3} e^{i(\nu_n+\omega_m)\tau_4} e^{-i(\nu_{n'}+\omega_m)\tau_1} e^{i\nu_{n'}\tau_2} \\
&\quad \times \left\langle \mathcal{T}\, c^\dagger_{\mathbf{k'}+\mathbf{q},\alpha_k}(\tau_1) c_{\mathbf{k'},\alpha_l}(\tau_2) c^\dagger_{\mathbf{k},\alpha_i}(\tau_3) c_{\mathbf{k}+\mathbf{q},\alpha_j}(\tau_4) \right\rangle. \\
&= \mathcal{C}_{\alpha_k\alpha_l\alpha_i\alpha_j}(\mathbf{k'}+\mathbf{q},\mathbf{k}+\mathbf{q},-\mathbf{q},\nu_{n'}+\omega_m,\nu_n+\omega_m;-\omega_m) \\
&= \mathcal{C}_{\alpha_k\alpha_l\alpha_i\alpha_j}(\mathbf{p'};\nu_{n'}+\omega_m,\nu_n+\omega_m,-\omega_m).
\end{aligned}$$

Using Eq. (4.100), we can derive Eq. (4.102).

For the local two-particle Green's function where the momentums $\mathbf{p}$ *are integrated out, we have*

$$\left[\mathcal{C}_{\alpha_i\alpha_j\alpha_k\alpha_l}(\nu_n,\nu_{n'};\omega_m)\right]^* = \mathcal{C}_{\alpha_k\alpha_l\alpha_i\alpha_j}(-\nu_{n'}-\omega_m,-\nu_n-\omega_m;\omega_m). \tag{4.103}$$

This property implies that the $\nu_n = -\nu_{n'} - \omega_m$ is a mirror line if $\alpha_i = \alpha_k$ and $\alpha_j = \alpha_l$ [19].

4. The non-interacting part of the two-particle Green's function in imaginary frequency space is given by

$$\begin{aligned}
\mathcal{C}^0_{\alpha_i\alpha_j\alpha_k\alpha_l}(\mathbf{p},\boldsymbol{\nu}) &= -\beta^2\delta_{nn'}\, N_{\mathbf{k}}^2\, \delta_{\mathbf{k}\mathbf{k'}}\, \mathcal{G}_{\alpha_l\alpha_i}(\mathbf{k},\nu_n)\, \mathcal{G}_{\alpha_j\alpha_k}(\mathbf{k}+\mathbf{q},\nu_n+\omega_m) \\
&\quad +\beta^2\delta_{m,0}\, N_{\mathbf{k}}^2\, \delta_{\mathbf{q},\mathbf{0}}\, \mathcal{G}_{\alpha_j\alpha_i}(\mathbf{k},\nu_n)\, \mathcal{G}_{\alpha_l\alpha_i}(\mathbf{k'},\nu_{n'}).
\end{aligned} \tag{4.104}$$

5. A very useful property of the non-interacting two-particle Green's function is derived by

$$\left[\mathcal{C}^0_{\alpha_i\alpha_j\alpha_k\alpha_l}(\nu_n,\nu_{n'};\mathbf{q},\omega_m)\right]^* = \mathcal{C}^0_{\alpha_k\alpha_l\alpha_i\alpha_j}(-\nu_{n'}-\omega_m,-\nu_n-\omega_m;\mathbf{q},\omega_m). \tag{4.105}$$

Since the Hamiltonian is Hermitian, we have $[\mathcal{G}_{ij}(\mathbf{k},\nu_n)]^* = \mathcal{G}_{ji}(\mathbf{k},-\nu_n)$.

6. The fully interacting part of the two-particle Green's function (and also the susceptibility) which is continuous in $\boldsymbol{\tau}$-space is given by

$$\begin{aligned}
\widetilde{\gamma}(\boldsymbol{\nu}) &= \mathcal{C}(\boldsymbol{\nu}) - \mathcal{C}^0(\boldsymbol{\nu}) \\
&= \chi(\boldsymbol{\nu}) - \chi^0(\boldsymbol{\nu}).
\end{aligned} \tag{4.106}$$

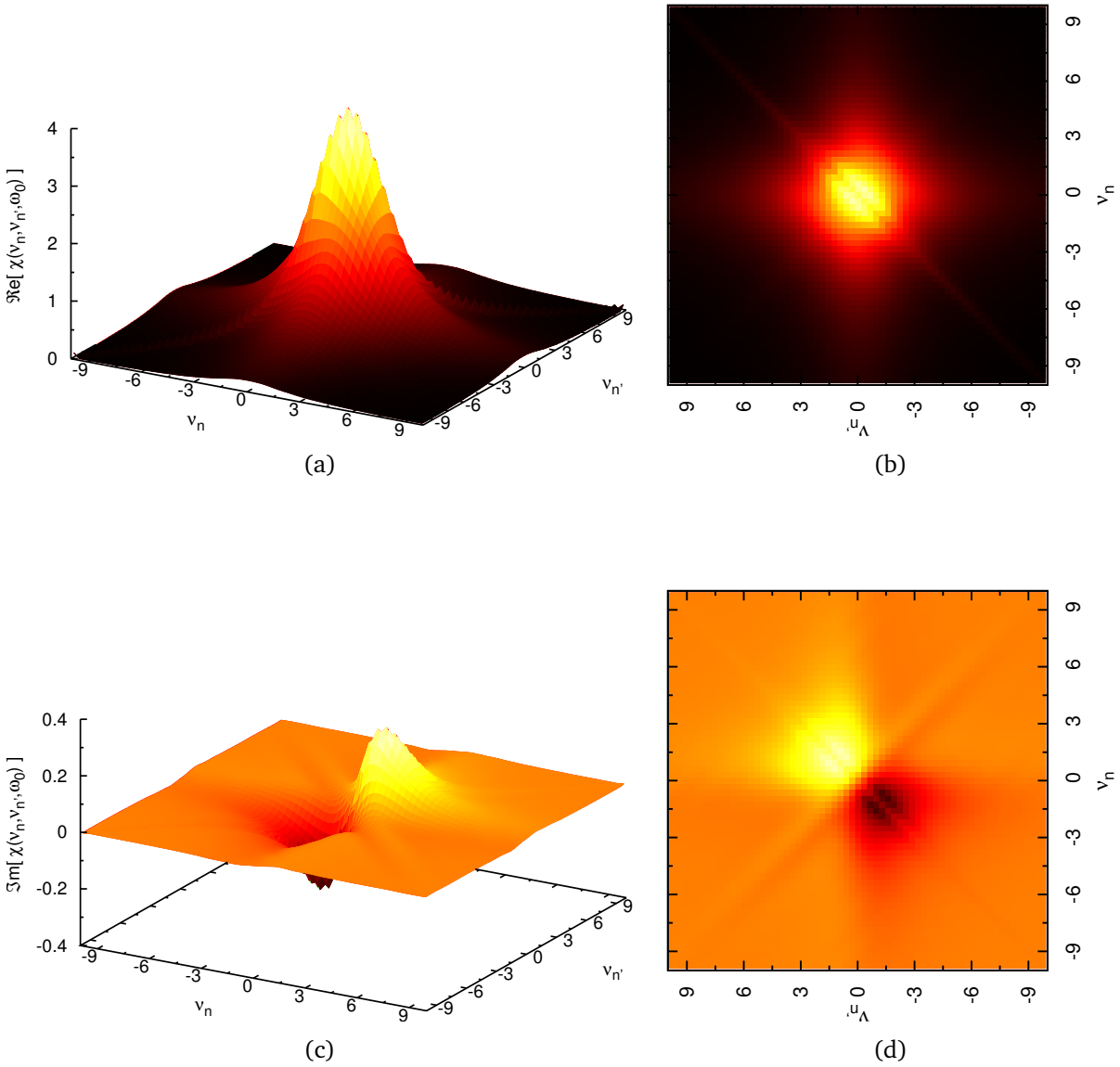

Figure 4.11: The local spin susceptibility of a single band insulator (Li_2VOSiO_4) is shown. In this case the $U = 5$ and $\beta = 20$. a) The real part of the local spin susceptibility in 3D. b) The real part of the spin susceptibility that is mapped on a plane. The symmetries are clear from this plot. c) The imaginary part of the local spin susceptibility. As it is clear, imaginary part of the local *spin* susceptibility is anti-symmetry. d) The imaginary part of the local spin susceptibility is shown in a plane.

7. In *paramagnetic systems*, there are some additional symmetries which are related to the spin directions in the two-particle Green's function (or susceptibility). For this reason, we consider specifically the spin direction of the two-particle Green's function (and susceptibility) in the following formulas to show their properties in *paramagnetic system*. Considering

$$\mathcal{C}^{\sigma\sigma'}(\boldsymbol{\tau}) = \Big\langle \mathcal{T} c^{\dagger}_{\sigma}(\tau_1) c_{\sigma}(\tau_2) c^{\dagger}_{\sigma'}(\tau_3) c_{\sigma'}(\tau_4) \Big\rangle,$$

we can find

- $\mathcal{C}^{\uparrow\uparrow}(\boldsymbol{\tau}) = \mathcal{C}^{\downarrow\downarrow}(\boldsymbol{\tau}) \Rightarrow \chi^{\uparrow\uparrow}(\boldsymbol{\tau}) = \chi^{\downarrow\downarrow}(\boldsymbol{\tau})$.
- $\mathcal{C}^{\uparrow\downarrow}(\boldsymbol{\tau}) = \mathcal{C}^{\downarrow\uparrow}(\boldsymbol{\tau}) \Rightarrow \chi^{\uparrow\downarrow}(\boldsymbol{\tau}) = \chi^{\downarrow\uparrow}(\boldsymbol{\tau})$.
- The longitudinal spin and charge susceptibility are given by

$$\chi^{zz}(\boldsymbol{\tau}) = \frac{1}{2}\Big(\chi^{\uparrow\uparrow}(\boldsymbol{\tau}) - \chi^{\uparrow\downarrow}(\boldsymbol{\tau})\Big), \tag{4.107}$$

$$\chi^{ch}(\boldsymbol{\tau}) = \frac{1}{2}\Big(\chi^{\uparrow\uparrow}(\boldsymbol{\tau}) + \chi^{\uparrow\downarrow}(\boldsymbol{\tau})\Big). \tag{4.108}$$

8. Since the vertex function $\boldsymbol{\Gamma}$ inherits from the two-particle correlation function, it obeys symmetry properties of the two-particle Green's function.

9. The static $\omega \to 0$ and uniform $\mathbf{q} \to \mathbf{0}$ non-interacting (bare-) spin and charge susceptibility are related to density of states at Fermi level.

$$\chi^{\mathbf{0},zz}(\mathbf{0},0) = -\frac{1}{N_{\mathbf{k}} N_S}\sum_{\mathbf{k}}\frac{1}{2}(g\mu_B)^2\sum_{\sigma}\frac{\partial n_F(\varepsilon^{\sigma}_{\mathbf{k}}-\mu)}{\partial\varepsilon_{\mathbf{k}}}, \tag{4.109}$$

$$\chi^{\mathbf{0},ch}(\mathbf{0},0) = -\frac{1}{N_{\mathbf{k}} N_S}\sum_{\mathbf{k}}\frac{1}{2}\sum_{\sigma}\frac{\partial n_F(\varepsilon^{\sigma}_{\mathbf{k}}-\mu)}{\partial\varepsilon_{\mathbf{k}}}, \tag{4.110}$$

where $\varepsilon_{\mathbf{k}}$ is single particle energy and μ is the chemical potential. To show how the uniform and static susceptibility in non-interacting systems (or metals) is proportional to the density of state, we start with the non-interacting spin susceptibility.[17] For simplicity, we consider a system with one site per unit cell ($N_S = 1$) and one band. In Appendix B.1 we extend, the following proof for a multi-sites and multi-orbital cases.

$$\begin{aligned}\chi^{\mathbf{0},zz}(\mathbf{q},\omega_m) &= -\frac{1}{N_{\mathbf{k}}}\sum_{\mathbf{k}}\frac{1}{4}(g\mu_B)^2\sum_{\sigma}\frac{1}{\beta}\sum_{n}\mathcal{G}^{\sigma}(\mathbf{k},\nu_n)\mathcal{G}^{\sigma}(\mathbf{k}+\mathbf{q},\nu_n+\omega_m)\\ &= -\frac{1}{N_{\mathbf{k}}}\sum_{\mathbf{k}}\frac{1}{4}(g\mu_B)^2\sum_{\sigma}\frac{1}{\beta}\sum_{n}\frac{1}{i\nu_n-\varepsilon^{\sigma}_{\mathbf{k}}+\mu}\times\frac{1}{i(\nu_n+\omega_m)-\varepsilon^{\sigma}_{\mathbf{k}+\mathbf{q}}+\mu}.\end{aligned}$$

In this relation, $\mathcal{G}^{\sigma} = 1/(i\nu_n - \varepsilon^{\sigma}_{\mathbf{k}} + \mu)$ is the Green's function of the non-interacting systems. Using the Matsubara sums in Appendix (C), we have

$$\begin{aligned}\chi^{\mathbf{0},zz}(\mathbf{q},\omega_m) &= \frac{1}{N_{\mathbf{k}}}\sum_{\mathbf{k}}\frac{1}{4}(g\mu_B)^2\sum_{\sigma}\left\{\frac{n_F(\varepsilon^{\sigma}_{\mathbf{k}}-\mu)}{i\omega_m+\varepsilon^{\sigma}_{\mathbf{k}}-\varepsilon^{\sigma}_{\mathbf{k}+\mathbf{q}}}+\frac{n_F(-i\omega_m+\varepsilon^{\sigma}_{\mathbf{k}+\mathbf{q}}-\mu)}{-i\omega_m+\varepsilon^{\sigma}_{\mathbf{k}}-\varepsilon^{\sigma}_{\mathbf{k}+\mathbf{q}}}\right\}\\ &= \frac{1}{N_{\mathbf{k}}}\sum_{\mathbf{k}}\frac{1}{4}(g\mu_B)^2\sum_{\sigma}\frac{n_F(\varepsilon^{\sigma}_{\mathbf{k}}-\mu)-n_F(\varepsilon^{\sigma}_{\mathbf{k}+\mathbf{q}}-\mu)}{i\omega_m+\varepsilon^{\sigma}_{\mathbf{k}}-\varepsilon^{\sigma}_{\mathbf{k}+\mathbf{q}}},\end{aligned}$$

[17] The same proof can be easily done for the charge susceptibility.

where $n_F(\varepsilon^\sigma_{\mathbf{k}} \pm i\omega_m) = n_F(\varepsilon^\sigma_{\mathbf{k}})$. In the limit of $\mathbf{q} \to \mathbf{0}$ and at $i\omega_m = 0$, we have

$$\begin{aligned}\chi^{\mathbf{0},zz}(\mathbf{0},0) &= \frac{1}{N_{\mathbf{k}}}\sum_{\mathbf{k}}\frac{1}{4}(g\mu_B)^2\sum_\sigma \frac{n_F(\varepsilon^\sigma_{\mathbf{k}}-\mu) - \left[n_F(\varepsilon^\sigma_{\mathbf{k}}-\mu) + \mathbf{q}\frac{\partial\varepsilon^\sigma_{\mathbf{k}}}{\partial\mathbf{k}}\frac{\partial n_F(\varepsilon^\sigma_{\mathbf{k}}-\mu)}{\partial\varepsilon^\sigma_{\mathbf{k}}}\right]}{\varepsilon^\sigma_{\mathbf{k}} - \left[\varepsilon^\sigma_{\mathbf{k}} + \mathbf{q}\frac{\partial\varepsilon^\sigma_{\mathbf{k}}}{\partial\mathbf{k}}\right]} \\ &= \frac{1}{N_{\mathbf{k}}}\sum_{\mathbf{k}}\frac{1}{4}(g\mu_B)^2\sum_\sigma \frac{\partial n_F(\varepsilon^\sigma_{\mathbf{k}}-\mu)}{\partial\varepsilon^\sigma_{\mathbf{k}}}.\end{aligned}$$

4.4.3 Behavior of the dynamical lattice susceptibility at large $\nu_n, \nu_{n'}$

Using the Fourier integral of the local susceptibility, we study the susceptibility at high frequencies $\nu_n \to \pm\infty$ and $\nu_{n'} \to \pm\infty$, i.e., $\chi(\nu_n \to \pm\infty, \nu_{n'} \to \pm\infty) \equiv \chi^{\mathbf{HH}}$,[18] and derive an analytical relation for the Matsubara sum in this regime. We will show that at high frequency $\chi^{\mathbf{HH}}$ is non-zero only for $\nu_n = \nu_{n'}$.

The extension to the lattice susceptibility can be done similarly.

4.4.3.1 Derivation of high frequency part of the susceptibility ($\chi^{\mathbf{HH}}$)

The Fourier transform of $\chi_{\alpha_i\alpha_j\alpha_k\alpha_l}$ is given by

$$\begin{aligned}\chi_{\alpha_i\alpha_j\alpha_k\alpha_l}(\nu_n,\nu_{n'};\omega_m) &= \int_0^\beta d\tau_1\, e^{-i\nu_n\tau_1}\int_0^\beta d\tau_2\, e^{i(\nu_n+\omega_m)\tau_2}\int_0^\beta d\tau_3\, e^{-i(\nu_{n'}+\omega_m)\tau_3} \\ &\quad\times\int_0^\beta d\tau_4\, e^{i\nu_{n'}\tau_4}\,\chi_{\alpha_i\alpha_j\alpha_k\alpha_l}(\tau_1,\tau_2,\tau_3,\tau_4) \\ &= \beta\int_0^\beta d\tau_{14}\, e^{-i\nu_n\tau_{14}}\int_0^\beta d\tau_{24}\, e^{i(\nu_n+\omega_m)\tau_{24}} \\ &\quad\times\int_0^\beta d\tau_{34}\, e^{-i(\nu_{n'}+\omega_m)\tau_{34}}\,\chi_{\alpha_i\alpha_j\alpha_k\alpha_l}(\tau_{14},\tau_{24},\tau_{34}). \qquad (4.111)\end{aligned}$$

According to the properties of the imaginary time local susceptibility, $\chi_{\alpha_i\alpha_j\alpha_k\alpha_l}(\tau_{14},\tau_{24},\tau_{34})$ is discontinuous only at $\tau_{24} = \tau_{34}$ and $\tau_{14} = 0$ and has kinks at $\tau_{14} = \tau_{24}$ and $\tau_{34} = 0$. Therefore, we can use integration by part[19] to calculate high frequency behavior of the local susceptibility,

[18] If we rephrase the susceptibility $\chi(\nu_n,\nu_{n'})$ in a matrix form in Matsubara frequencies bases, we have

$$\chi = \begin{pmatrix} \chi^{\mathbf{HH}}\,(\nu_n\to-\infty,\nu_{n'}\to-\infty) & \chi^{\mathbf{HL}}\,(\nu_n\to-\infty,\nu_{n'}) & \chi^{\mathbf{HH}}\,(\nu_n\to-\infty,\nu_{n'}\to+\infty) \\ \chi^{\mathbf{LH}}\,(\nu_n,\nu_{n'}\to-\infty) & \chi^{\mathbf{LL}}\,(\nu_n,\nu_{n'}) & \chi^{\mathbf{LH}}\,(\nu_n,\nu_{n'}\to+\infty) \\ \chi^{\mathbf{HH}}\,(\nu_n\to+\infty,\nu_{n'}\to-\infty) & \chi^{\mathbf{HL}}\,(\nu_n\to+\infty,\nu_{n'}) & \chi^{\mathbf{HH}}\,(\nu_n\to+\infty,\nu_{n'}\to+\infty) \end{pmatrix},$$

where **L** and **H** denote low and high frequencies regions. In this relation each $\chi^{\mathbf{LL}}$, $\chi^{\mathbf{LH}}$, $\chi^{\mathbf{LH}}$ and $\chi^{\mathbf{HH}}$ are block matrices. For instance, $\chi^{\mathbf{LH}}$ is the block matrix of susceptibility in which ν_n is finite (**L**ow frequency) and $\nu_{n'} \to \pm\infty$ (**H**igh frequency).

[19] **The integration by parts theorem:** if f and g are *differentiable* functions on an interval $[a,b]$ and if the functions f' and g' are *integrable* on $[a,b]$, then $\int_a^b f(x)g'(x)dx = f(b)g(b) - f(a)g(a) - \int_a^b f'(x)g(x)dx$.

i.e., $\chi^{\mathbf{HH}}$, by considering the concept of the improper integrals[20].

$$\begin{aligned}
\chi_{\alpha_i\alpha_j\alpha_k\alpha_l}(\nu_n,\nu_{n'};\omega_m) \overset{|\nu_n|\to\infty}{\approx} & \beta\int_0^\beta d\tau_{24}\left[\int_0^{\tau_{24}^-} d\tau_{34}+\int_{\tau_{24}^+}^\beta d\tau_{34}\right] e^{i(\nu_n+\omega_m)\tau_{24}}e^{i(\nu_{n'}+\omega_m)\tau_{34}} \\
& \times\Bigg\{\left(\frac{-1}{i\nu_n}\right)e^{-i\nu_n\tau_{14}}\chi_{\alpha_i\alpha_j\alpha_k\alpha_l}(\tau_{14},\tau_{24},\tau_{34})\Big|_{\tau_{14}=0}^{\tau_{14}=\beta} \\
& +\left(\frac{1}{\nu_n}\right)^2 e^{-i\nu_n\tau_{14}}\,\frac{\partial}{\partial\tau_{14}}\chi_{\alpha_i\alpha_j\alpha_k\alpha_l}(\tau_{14},\tau_{24},\tau_{34})\Big|_{\tau_{14}=0}^{\tau_{14}=\beta} \\
& +\mathcal{O}\left(\frac{1}{i\nu_n}\right)^3\Bigg\} \\
= & \beta\left(\frac{-1}{i\nu_n}\right)\mathcal{I}_1(\nu_n,\nu_{n'};\omega_m)+\beta\left(\frac{1}{\nu_n}\right)^2 e^{-i\nu_n\tau_{14}}\frac{\partial\mathcal{I}_2}{\partial\tau_{14}}\Big|_0^\beta+\mathcal{O}\left(\frac{1}{i\nu_n}\right)^3.
\end{aligned}$$

Considering the jump that occurs in boundary values (See Eq. (4.76)), the first integral, $\mathcal{I}_1$, at high frequencies is obtained by

$$\begin{aligned}
\mathcal{I}_1(\nu_n,\nu_{n'};\omega_m) &= \delta_{\alpha_l\alpha_i}\int_0^\beta d\tau_{24}\left[\int_0^{\tau_{24}^-} d\tau_{34}+\int_{\tau_{24}^+}^\beta d\tau_{34}\right]\mathcal{G}_{\alpha_j\alpha_k}(\tau_{24}-\tau_{34}) \\
&= \beta\,\delta_{\alpha_l\alpha_i}\,\delta_{nn'}\,\mathcal{G}_{\alpha_j\alpha_k}(\nu_n+\omega_m) \\
&\overset{|\nu_n|\to\infty}{\approx} \beta\,\delta_{\alpha_l\alpha_i}\,\delta_{nn'}\left(\frac{\delta_{\alpha_j\alpha_k}}{i(\nu_n+\omega_m)}+\frac{b}{(\nu_n+\omega_m)^2}\right), \qquad (4.112)
\end{aligned}$$

where b is the coefficient of $-1/\nu_n^2$ in Eq. (5.32).[21] The second integral can be calculated approximately for $|\nu_{n'}|\to\infty$ by using the definition of *improper integrals*.

$$\begin{aligned}
\mathcal{I}_2 &= \int_0^\beta d\tau_{24}\,e^{i(\nu_n+\omega_m)\tau_{24}}\left[\int_0^{\tau_{24}^-} d\tau_{34}+\int_{\tau_{24}^+}^\beta d\tau_{34}\right]e^{-i(\nu_{n'}+\omega_m)\tau_{34}}\chi_{\alpha_i\alpha_j\alpha_k\alpha_l}(\tau_{14},\tau_{24},\tau_{34}) \\
&\overset{|\nu_{n'}|\to\infty}{\approx} \int_0^\beta d\tau_{24}\,e^{i(\nu_n+\omega_m)\tau_{24}}\Bigg\{\frac{-1}{i(\nu_{n'}+\omega_m)}\Big(-\chi_{\alpha_i\alpha_j\alpha_k\alpha_l}(\tau_{14},\tau_{24},0)-\chi_{\alpha_i\alpha_j\alpha_k\alpha_l}(\tau_{14},\tau_{24},\beta) \\
&\quad +e^{-i(\nu_{n'}+\omega_m)\tau_{24}}\left[\chi_{\alpha_i\alpha_j\alpha_k\alpha_l}(\tau_{14},\tau_{24},\tau_{24}^-)-\chi_{\alpha_i\alpha_j\alpha_k\alpha_l}(\tau_{14},\tau_{24},\tau_{24}^+)\right]\Big)+\mathcal{O}\left(\frac{1}{\nu_{n'}}\right)^2\Bigg\} \\
&\approx \frac{-1}{i(\nu_{n'}+\omega_m)}\,\mathcal{G}'^{\sigma}_{\alpha_l\alpha_i}(\beta-\tau_{14})\int_0^\beta d\tau_{24}\,e^{i(\nu_n-\nu_{n'})\tau_{24}}\,\delta_{\alpha_j\alpha_k} \\
&\approx -\beta\,\delta_{\alpha_j\alpha_k}\delta_{nn'}\left[\frac{1}{i(\nu_{n'}+\omega_m)}\right]\mathcal{G}'^{\sigma}_{\alpha_l\alpha_i}(\beta-\tau_{14}).
\end{aligned}$$

[20] **Improper integral definition:** if f is continuous on the interval $[a,b]$ except for an infinite discontinuity at a point c in (a,b), then the improper integral of f over interval $[a,b]$ is defined as $\int_a^b f(x)dx=\int_a^c f(x)dx+\int_c^b f(x)dx$. The improper integral is said to converge if both terms converge and diverge if either term diverges.

[21] This parameter can be obtained by fitting data to the tail of the Green's function.

To derive $\mathcal{I}_2$, we used Eq. (4.93) and (4.74). Finally, the high frequency behavior of the local susceptibility $\chi^{\mathbf{HH}}$ can be obtained by

$$\begin{aligned}\chi^{\mathbf{HH}}_{\alpha_i\alpha_j\alpha_k\alpha_l}(\nu_n,\nu_{n'};\omega_m) &\approx -\beta^2\,\delta_{\alpha_l\alpha_i}\,\delta_{nn'}\left(\frac{1}{i\nu_n}\right)\left(\frac{\delta_{\alpha_j\alpha_k}}{i(\nu_n+\omega_m)}+\frac{b}{(\nu_n+\omega_m)^2}\right)\\ &- \beta^2\delta_{\alpha_j\alpha_k}\delta_{nn'}\left(\frac{1}{\nu_n}\right)^2\frac{1}{i(\nu_{n'}+\omega_m)}\left[\frac{\partial}{\partial\tau_{14}}\mathcal{G}_{\alpha_l\alpha_i}(\beta)+\frac{\partial}{\partial\tau_{14}}\mathcal{G}_{\alpha_l\alpha_i}(0)\right]\\ &\approx \beta^2\delta_{nn'}\left(\frac{\delta_{\alpha_l\alpha_i}\delta_{\alpha_j\alpha_k}}{\nu_n(\nu_n+\omega_m)}+i\frac{b}{\nu_n(\nu_n+\omega_m)}\left[\frac{\delta_{\alpha_l\alpha_i}}{\nu_n+\omega_m}+\frac{\delta_{\alpha_j\alpha_k}}{\nu_n}\right]\right),\end{aligned} \tag{4.113}$$

where $b=\left[\frac{\partial}{\partial\tau_{14}}\mathcal{G}_{\alpha_l\alpha_i}(\beta)+\frac{\partial}{\partial\tau_{14}}\mathcal{G}_{\alpha_l\alpha_i}(0)\right]$ (See Eq. (5.32)). Based on this relation, the $\chi^{\mathbf{HH}}$ has non-zero effect if $\nu_n=\nu_{n'}$.

4.4.3.2 Matsubara sum of the high frequency part of the susceptibility $\chi^{\mathbf{HF}}$

In order to obtain the dynamical susceptibility we should perform the Matsubara sums over fermionic frequencies ν_n and $\nu_{n'}$.

$$\chi(\omega_m)=\frac{1}{\beta^2}\sum_{n=-\infty}^{+\infty}\sum_{n'=-\infty}^{+\infty}\chi(\nu_n,\nu_{n'};\omega_m).$$

In numerical calculations, it is impossible to consider infinite number of Matsubara frequencies to evaluate $\chi(\omega_m)$. For this reason one may truncate the Matsubara summations, i.e.,

$$\begin{aligned}\sum_{n=-\infty}^{+\infty} &= \sum_{n=-\infty}^{-N-2}+\sum_{n=-N-1}^{N}+\sum_{n=N+1}^{+\infty}\\ &\approx \sum_{n=-N-1}^{N}.\end{aligned}$$

where N is the truncated value and should be large enough. Therefore, some numerical errors due to the truncation are created in the calculation of the susceptibility. In the following we show how we can calculate the $\sum_{n=-\infty}^{-N-2}$ and $\sum_{n=N+1}^{+\infty}$ analytically, by utilizing the high frequency susceptibility. We start with

$$\begin{aligned}\chi^{\mathbf{HF}}_{\alpha_i\alpha_j\alpha_k\alpha_l} &\approx \frac{1}{\beta^2}\delta_{\alpha_l\alpha_i}\delta_{\alpha_j\alpha_k}\sum_{nn'}\delta_{nn'}\frac{\beta^2}{\nu_{n'}(\nu_n+\omega_m)}\\ &\approx A\left(\sum_{n=-N-1}^{-n_c-1}+\sum_{n=n_c}^{N}\right)f(n,m),\end{aligned}$$

where $A=\delta_{\alpha_l\alpha_i}\delta_{\alpha_j\alpha_k}\beta^2/\pi^2$ and $f(n,m)=[(2n+1)(2n+2m+1)]^{-1}$. In this relation we supposed that for all ν_n outside $-\nu_{n_c}<\nu_n<\nu_{n_c}$, the susceptibility is obtained from Eq. (4.113).

Considering the properties of the susceptibility, we can rewrite the $\chi^{\mathbf{HF}}$ as follows.

$$\begin{aligned}\chi^{\mathbf{HF}}_{\alpha_i\alpha_j\alpha_k\alpha_l} &= A\left(\sum_{n=-N-1}^{-n_c-1} f(n,m)+\sum_{n=n_c}^{N} f(n,m)\right)\\ &= A\left(\sum_{n=-N-1}^{-n_c-1} f(-n-1,-m)+\sum_{n=n_c}^{N} f(n,m)\right)\\ &= A\sum_{n=n_c}^{N}\left(f(n,-m)+f(n,m)\right).\end{aligned}$$

Now, we can solve the above summation for high frequency lattice susceptibility exactly by using the digamma function (See Appendix D.2 for more detail).

$$\begin{aligned}\chi^{\mathbf{HF}}_{\alpha_i\alpha_j\alpha_k\alpha_l} &= A\sum_{n=0}^{N}\left(f(n,-m)+f(n,m)\right)-A\sum_{n=0}^{n_c-1}\left(f(n,-m)+f(n,m)\right)\\ &= \frac{A}{2m}\left(\sum_{n=0}^{N}-\sum_{n=0}^{n_c-1}\right)\left(\frac{-1}{(2n+1)}+\frac{1}{(2n-2m+1)}+\frac{1}{(2n+1)}-\frac{1}{(2n+2m+1)}\right)\\ &= \frac{A}{4m}\left(\sum_{n=0}^{N}-\sum_{n=0}^{n_c-1}\right)\left(\frac{1}{(n-m+\frac{1}{2})}-\frac{1}{(n+m+\frac{1}{2})}\right),\end{aligned}$$

and finally we have

$$\begin{aligned}\chi^{\mathbf{HF}}_{\alpha_i\alpha_j\alpha_k\alpha_l} &= -\frac{A}{4m}\Bigg\{\Psi\left(N+\frac{3}{2}+m\right)-\Psi\left(N+\frac{3}{2}-m\right)\\ &\quad -\Psi\left(n_c+\frac{1}{2}+m\right)+\Psi\left(n_c+\frac{1}{2}-m\right)\Bigg\}.\end{aligned}\tag{4.114}$$

Since m, n_c and N are integer values, the Ψ-function is well-defined for all values of these parameters due to the fractional arguments in digamma functions (Eq. (4.114)).

In the following, we study the Eq. (4.114) in some special limits $m \to 0$, $N \to \infty$ and $n_c \to \infty$.

- Convergence of Eq. (4.114) if $m \to 0$:

  With the Taylor series expansion of $\Psi(n+x)$ around $x = 0$

  $$\Psi(n+x) = \Psi(n) + \Psi'(n)\,x + \frac{1}{2!}\Psi''(n)\,x^2 + \frac{1}{3!}\Psi^{(3)}(n)\,x^3 + \mathcal{O}\left(x^4\right),$$

  we can calculate Eq. (4.114) at $m = 0$.

$$\begin{aligned}\lim_{m\to 0}\chi^{\mathbf{HF}}_{\alpha_i\alpha_j\alpha_k\alpha_l}(\omega_m) &= -\frac{A}{4}\left\{2\Psi'\left(N+\frac{3}{2}\right)-2\Psi'\left(n_c+\frac{1}{2}\right)\right\}\\ &= \frac{2A}{(2N+1)^2}-\frac{A}{2}\left\{\Psi'\left(N+\frac{1}{2}\right)-\Psi'\left(n_c+\frac{1}{2}\right)\right\}.\end{aligned}\tag{4.115}$$

- Asymptotic values for Eq. (4.114) if $m \to 0$ and $N \to \infty$:

$$\chi^{\mathbf{HF}}_{\alpha_i\alpha_j\alpha_k\alpha_l}(\omega_0) = \delta_{\alpha_l\alpha_i}\delta_{\alpha_j\alpha_k}\frac{\beta^2}{2\pi^2}\,\Psi'\left(n_c+\frac{1}{2}\right). \tag{4.116}$$

  According to this relation, one can easily see that in the limit of $n_c \to \infty$, $\chi^{\mathbf{HF}}_{\alpha_i\alpha_j\alpha_k\alpha_l}(\omega_0)$ goes to zero as it is expected.

- Estimating the cut-off n_c:

  From Eq. (4.114), we can conclude that the cut-off n_c (at least) should be larger than m in Bosonic frequency ω_m, because the last term in this equation, i.e., $\Psi\left(n_c+\frac{1}{2}-m\right)$, should have a positive argument to be a well-defined function (see Fig. 4.12).

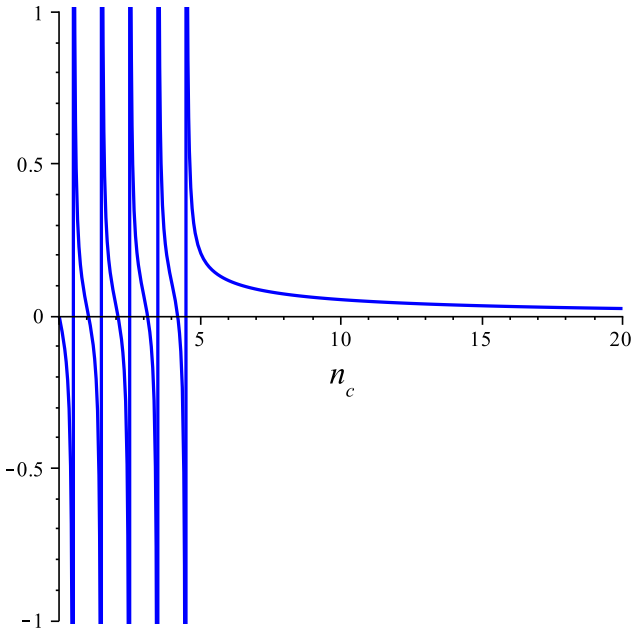

Figure 4.12: In this plot we considered $m = 5$, $N \to \infty$ and $A = 1$. The vertical axis is dynamical lattice susceptibility. According to this plot, one can easily see that for $n_c \leq m$ the function is undefined.

In the same way, we can calculate the higher order terms in the $\chi^{\mathbf{HF}}$ by taking into account higher order approximation in Eq. (4.113).

$$\begin{aligned}
\chi^{\mathbf{HF}}_{\alpha_i\alpha_j\alpha_k\alpha_l}(\omega_m) &\approx C\left[\sum_{n=-N-1}^{-nc-1}+\sum_{n=n_c}^{N}\right]\left(\frac{1}{i\nu_n}+\frac{a}{\nu_n^2}\right)\left(\frac{1}{i(\nu_n+\omega_m)}+\frac{b}{(\nu_n+\omega)^2}\right)\\
&\approx C\left[\sum_{n=-N-1}^{-nc-1}+\sum_{n=n_c}^{N}\right]\left\{\left(\frac{b}{i\nu_n(\nu_n+\omega_m)^2}+\frac{a}{i\nu_n^2(\nu_n+\omega_m)}\right)\right.\\
&\quad\left.+\left(\frac{-1}{\nu_n(\nu_n+\omega_m)}+\frac{ab}{\nu_n^2(\nu_n+\omega_m)^2}\right)\right\}\\
&\equiv \Re e\left[\chi^{\mathbf{HF}}_{\alpha_i\alpha_j\alpha_k\alpha_l}(\omega_m)\right]+i\,\Im m\left[\chi^{\mathbf{HF}}_{\alpha_i\alpha_j\alpha_k\alpha_l}(\omega_m)\right],
\end{aligned}$$

where a and b are constant values which can be determined numerically by fitting the tail of the Green's function and $C = \delta_{\alpha_l\alpha_i}\delta_{\alpha_j\alpha_k}$.

The imaginary part of $\chi^{\mathbf{HF}}_{\mathbf{latt}}(\mathbf{q},\omega_m)$ is then calculated by

$$\begin{aligned}
\Im m\left[\chi^{\mathbf{HF}}_{\alpha_i\alpha_j\alpha_k\alpha_l}(\omega_m)\right] &= C\left[\sum_{n=-N-1}^{-nc-1}+\sum_{n=n_c}^{N}\right]\left(\frac{b}{\nu_n(\nu_n+\omega_m)^2}+\frac{a}{\nu_n^2(\nu_n+\omega_m)}\right)\\
&= C\sum_{n=n_c}^{N}\left(\frac{-b}{\nu_n(\nu_n-\omega_m)^2}+\frac{-a}{\nu_n^2(\nu_n-\omega_m)}+\frac{b}{\nu_n(\nu_n+\omega_m)^2}+\frac{a}{\nu_n^2(\nu_n+\omega_m)}\right)\\
&= \frac{C\beta^3}{\pi^3}\sum_{n=n_c}^{N}\left\{\frac{1}{4}\frac{-b+a}{(2n+2m+1)\,m^2}+\frac{1}{4}\frac{b-a}{(2n+1)\,m^2}-\frac{1}{2}\frac{b}{m\,(2n+2m+1)^2}\right.\\
&\quad+\frac{1}{2}\frac{a}{m\,(2n+1)^2}+\frac{1}{4}\frac{b-a}{(2n-2m+1)\,m^2}+\frac{1}{4}\frac{-b+a}{(2n+1)\,m^2}\\
&\quad\left.-\frac{1}{2}\frac{b}{m\,(2n-2m+1)^2}+\frac{1}{2}\frac{a}{m\,(2n+1)^2}\right\}.
\end{aligned}$$

Now we use Ψ-function definition to get the $\Im m\left[\chi^{\mathbf{HF}}_{\mathbf{latt}}(\mathbf{q},\omega_m)\right]$,

$$\begin{aligned}
\Im m\left[\chi^{\mathbf{HF}}_{\alpha_i\alpha_j\alpha_k\alpha_l}(\omega_m)\right] &= \delta_{\alpha_l\alpha_i}\delta_{\alpha_j\alpha_k}\frac{\beta^3}{8m^2\pi^3}\left\{(a-b)\left[\Psi\left(N+\frac{3}{2}+m\right)-\Psi\left(n_c+m+\frac{1}{2}\right)\right]\right.\\
&\quad+b\,m\left[\Psi'\left(N+\frac{3}{2}+m\right)-\Psi'\left(n_c+m+\frac{1}{2}\right)\right]\\
&\quad-2\,a\,m\left[\Psi'\left(N+\frac{3}{2}\right)-\Psi'\left(n_c+\frac{1}{2}\right)\right]\\
&\quad-(a-b)\left[\Psi\left(N+\frac{3}{2}-m\right)-\Psi\left(n_c-m+\frac{1}{2}\right)\right]\\
&\quad\left.+b\,m\left[\Psi'\left(N+\frac{3}{2}-m\right)-\Psi'\left(n_c-m+\frac{1}{2}\right)\right]\right\}. \qquad (4.117)
\end{aligned}$$

The real part of the dynamical susceptibility at large frequencies with some mathematics

can be easily obtained.

$$\begin{aligned}
\Re e\left[\chi^{\mathbf{HF}}_{\alpha_i\alpha_j\alpha_k\alpha_l}(\omega_m)\right] &= \delta_{\alpha_l\alpha_i}\delta_{\alpha_j\alpha_k}\frac{\beta^2}{4m\pi^2}\left[-1+\frac{\beta^2}{\pi^2}\frac{ab}{2m^2}\right] \\
&\times\Bigg\{\Psi\left(N+\frac{3}{2}+m\right)-\Psi\left(N+\frac{3}{2}-m\right) \\
&-\Psi\left(n_c+\frac{3}{2}+m\right)+\Psi\left(n_c+\frac{3}{2}-m\right)\Bigg\} \\
&+\delta_{\alpha_l\alpha_i}\delta_{\alpha_j\alpha_k}\frac{ab\beta^4}{16m^2\pi^4}\Bigg\{-\Psi'\left(N+\frac{3}{2}+m\right)+\Psi'\left(n_c+\frac{1}{2}+m\right) \\
&-\Psi'\left(N+\frac{3}{2}-m\right)+\Psi'\left(n_c+\frac{1}{2}-m\right) \\
&-2\Psi'\left(N+\frac{3}{2}\right)+2\Psi'\left(n_c+\frac{1}{2}\right)\Bigg\}. \qquad (4.118)
\end{aligned}$$

At the special limits, $m\to 0$ and $N\to\infty$, we find that

$$\begin{aligned}
\lim_{N\to\infty}\lim_{m\to 0}\Im m\left[\chi^{\mathbf{HF}}_{\alpha_i\alpha_j\alpha_k\alpha_l}(\omega_m)\right] &= 0, \qquad (4.119)\\
\lim_{N\to\infty}\lim_{m\to 0}\Re e\left[\chi^{\mathbf{HF}}_{\alpha_i\alpha_j\alpha_k\alpha_l}(\omega_m)\right] &= \frac{\beta^2}{2\pi^2}\delta_{\alpha_l\alpha_i}\delta_{\alpha_j\alpha_k}\Psi'\left(n_c+\frac{1}{2}\right) \\
&+\frac{ab\beta^4}{48\pi^4}\delta_{\alpha_l\alpha_i}\delta_{\alpha_j\alpha_k}\Psi^{(3)}\left(n_c+\frac{1}{2}\right), \qquad (4.120)
\end{aligned}$$

where we used the *Hopital's* rule to derive these relations. Notice that for $m\to 0$, $a=b$. In the limit of $n_c\to 0$, we use the Polygamma function properties, $\Psi^{(3)}(1/2)=\pi^4$ and $\Psi'(1/2)=\pi^2/2$, to obtain

$$\lim_{n_c\to 0}\lim_{N\to\infty}\lim_{m\to 0}\Re e\left[\chi^{\mathbf{HF}}_{\alpha_i\alpha_j\alpha_k\alpha_l}(\omega_m)\right] = \left(\frac{\beta^2}{4}+\frac{\beta^4}{48}ab\right)\delta_{\alpha_l\alpha_i}\delta_{\alpha_j\alpha_k}. \qquad (4.121)$$

Equation (4.121) which is calculated using the special functions $\Psi(x)$ in the special limits $n_c\to 0, m\to 0$, and $N\to\infty$ can be obtained by using the Matsubara sums (See Appendix C) and considering Eq. (4.113) as follows.

$$\begin{aligned}
\Im m\left[\chi^{\mathbf{HF}}_{\alpha_i\alpha_j\alpha_k\alpha_l}(\omega_0)\right] &= \frac{1}{\beta^2}\sum_{nn'}\Im m\left[\chi^{\mathbf{HF}}_{\alpha_i\alpha_j\alpha_k\alpha_l}(\nu_n,\nu_{n'};\omega_0)\right] \\
&= -\beta\lim_{(\tau_{14}-\tau_{23})\to 0}\left(\frac{1}{\beta}\sum_{n=-\infty}^{\infty}e^{i\nu_n(\tau_{14}-\tau_{23})}\frac{a+b}{i\nu_n^3}\,\delta_{\alpha_l\alpha_i}\delta_{\alpha_j\alpha_k}\right) \\
&= -(a+b)\beta\delta_{\alpha_l\alpha_i}\delta_{\alpha_j\alpha_k}\lim_{\tau\to 0}\left(\frac{1}{\beta}\sum_{n=-\infty}^{\infty}\frac{e^{-i\nu_n\tau}}{(i\nu_n)^3}\right), \qquad (4.122)
\end{aligned}$$

where the pre-factors a and b are equal in this special limits. To calculate this summation, we need to use some mathematical techniques. Considering the well-known Matsubara sum rules,

the Fourier transformation of the non-interacting Green's function is given by [56]

$$\frac{1}{\beta}\sum_{n=-\infty}^{n=\infty}\frac{e^{-i\nu_n\tau}}{i\nu_n-E}=\begin{cases}\left(\frac{1}{1+e^{\beta E}}\right)e^{-E\tau} & \tau<0\\ -\left(1-\frac{1}{e^{\beta E}+1}\right)e^{-E\tau} & \tau>0\end{cases}. \tag{4.123}$$

The second derivative of the above relation at $E\to 0$ gives us

$$\frac{2}{\beta}\sum_{n=-\infty}^{n=\infty}\frac{e^{-i\nu_n\tau}}{(i\nu_n)^3}=\begin{cases}\tau(\tau+\beta)/2 & \tau<0\\ \tau(-\tau+\beta)/2 & \tau>0\end{cases}. \tag{4.124}$$

From this relation, we can easily see that

$$\begin{aligned}\Im m\left[\chi^{\mathbf{HF}}_{\alpha_i\alpha_j\alpha_k\alpha_l}(\omega_0)\right] &= -(a+b)\beta\delta_{\alpha_l\alpha_i}\delta_{\alpha_j\alpha_k}\lim_{\tau\to 0}\left(\frac{1}{\beta}\sum_{n=-\infty}^{\infty}\frac{e^{-i\nu_n\tau}}{(i\nu_n)^3}\right)\\ &= -(a+b)\beta\delta_{\alpha_l\alpha_i}\delta_{\alpha_j\alpha_k}\times\lim_{\tau\to 0}\begin{cases}-\tau(\tau+\beta)/2 & \tau<0\\ -\tau(-\tau+\beta)/2 & \tau>0\end{cases}\\ &= 0.\end{aligned} \tag{4.125}$$

Notice that the higher order *even* derivative of Eq. (4.123) at $E\to 0$ and $\tau\to 0^{\pm}$ is equal to zero. For example the forth derivative gives us

$$\frac{4!}{\beta}\sum_{n=-\infty}^{n=\infty}\frac{e^{-i\nu_n\tau}}{(i\nu_n)^5}=\begin{cases}\tau(-\beta^3+2\tau^2\beta+\tau^3)/2 & \tau<0\\ \tau(-\beta^3+2\tau^2\beta-\tau^3)/2 & \tau>0\end{cases}, \tag{4.126}$$

which is zero for $\tau\to 0$.

For the real part of the lattice susceptibility, we calculate the first and the third derivative of Eq. (4.123).

$$\frac{1}{\beta}\sum_{n=-\infty}^{n=\infty}\frac{e^{-i\nu_n\tau}}{(i\nu_n)^2}=\begin{cases}-(\beta+2\tau)/4 & \tau<0\\ -(\beta-2\tau)/4 & \tau>0\end{cases}, \tag{4.127}$$

$$\frac{3!}{\beta}\sum_{n=-\infty}^{n=\infty}\frac{e^{-i\nu_n\tau}}{(i\nu_n)^4}=\begin{cases}(\beta^3-6\beta\tau^2-4\tau^3)/8 & \tau<0\\ (\beta^3-6\beta\tau^2+4\tau^3)/8 & \tau>0\end{cases}. \tag{4.128}$$

Therefore the $\Re e\left[\chi^{\mathbf{HF}}_{\alpha_i\alpha_j\alpha_k\alpha_l}(\omega_0)\right]$ in Eq. (4.121) can be re-derived by

$$\begin{aligned}\Re e\left[\chi^{\mathbf{HF}}_{\alpha_i\alpha_j\alpha_k\alpha_l}(\omega_0)\right] &= \beta\,\delta_{\alpha_l\alpha_i}\delta_{\alpha_j\alpha_k}\lim_{\tau\to 0}\left(\frac{1}{\beta}\sum_{n=-\infty}^{\infty}-\frac{e^{-i\nu_n\tau}}{(i\nu_n)^2}+ab\,\frac{e^{-i\nu_n\tau}}{(i\nu_n)^4}\right)\\ &= \left(\frac{\beta^2}{4}+ab\,\frac{\beta^4}{48}\right)\delta_{\alpha_l\alpha_i}\delta_{\alpha_j\alpha_k}.\end{aligned} \tag{4.129}$$

Eqs. (4.117) and (4.118) will be useful in numerical computation of the susceptibility. We can use them to find an appropriate polynomial function to extrapolate summations over infinite fermionic Matsubara frequencies. Detailed explanations are provided in section 5.4.7 where we investigate convergency of the Matsubara sum.

CHAPTER 5

Numerical details of calculating the lattice susceptibility within DMFT

In this chapter, we will explain how the lattice susceptibility $\chi(q, \omega)$ can be computed numerically by using the dynamical mean field theory and the local vertex approximation. We will start with a brief description about the Green's function and it's properties. We will introduce a new numerical method to calculate the Fourier integral of the Green's function inside the quantum Monte Carlo which is used to compute the two-particle correlation function. Then we will explain how we solve the tensorial Bethe-Salpeter equation by employing the matrices to extract the local vertex function and the lattice susceptibility.

Contents

5.1 Algorithm 76

5.2 One-particle Green's function and it's properties 76

5.2.1 One-particle Green's function in τ or ν_n space 76

5.2.2 Properties of one-particle Green's function 77

5.3 Numerical methods for Fourier transform of Green's function 83

5.3.1 1st method: Trapezoidal rule in one and two dimension 83

5.3.2 2nd method: Direct Filon-trapezoidal rule in one and two dimension 86

5.3.3 3rd method: Separating continuous and discontinuous part of the Green's function 91

5.3.4 4th method: Transferring discontinuities of the Green's function to the border 94

5.4 Computing *local* susceptibility using Hirsch-Fye QMC 98

5.4.1 Two-particle correlation function *inside QMC block* 98

5.4.2 Continuous part of the two-particle correlation function (after QMC) 100

5.4.3 The local susceptibility (after QMC) 101

5.4.4 The local (spin or charge) vertex function: A matrix algebra calculation . . 105

5.4.5 Bare lattice (spin or charge) susceptibility (after QMC) 108

5.4.6 The lattice (spin or charge) susceptibility 108

5.4.7 Convergency of Matsubara sum: An extrapolation approach 111

5.5 Tests and numerical details 114

5.1 Algorithm

In order to calculate the lattice susceptibility by using the *local vertex approximation*, we will proceed as follows.

1. In the last iteration of solving self-consistence DMFT equations, *in the QMC block*, we calculate
   (a) Fourier transform of the local QMC Green's function (for only one QMC configuration) $\widetilde{G}(\nu_n, \nu_{n'})$
   (b) *Local* two particle correlation function (for only one QMC configuration) $\widetilde{C}(\nu_n, \nu_{n'}; \omega_m)$
2. After QMC, we compute
   (a) Continuous part of the local susceptibility $\gamma(\nu_n, \nu_{n'}; \omega_m)$.
   (b) Bare-local susceptibility $\chi^{\mathbf{0}}(\nu_n, \nu_{n'}; \omega_m)$ by using the Fourier transform of the *physical* Green's function $\mathcal{G}(\tau - \tau')$ with spline (which is considered as a very accurate method).
   (c) The local susceptibility by $\chi(\nu_n, \nu_{n'}; \omega_m) = \gamma(\nu_n, \nu_{n'}; \omega_m) + \chi^{\mathbf{0}}(\nu_n, \nu_{n'}; \omega_m)$.
   (d) The local vertex function $\mathbf{\Gamma_{loc}}(\nu_n, \nu_{n'}; \omega_m)$.
   (e) The bare-lattice susceptibility $\chi^{\mathbf{0}}(\nu_n, \nu_{n'}; \mathbf{q}, \omega_m)$ by using local self-energy $\Sigma(\nu_n)$ and the LDA Hamiltonian $H^{\mathrm{LDA}}(\mathbf{k})$.
   (f) The lattice susceptibility $\chi(\mathbf{q}, \omega_m)$ within the local vertex approximation approach.

In the following of the current chapter, we explain each step in details.

5.2 One-particle Green's function and it's properties

5.2.1 One-particle Green's function in τ or ν_n space

The imaginary-time Green's function is defined as

$$\begin{aligned} \mathcal{G}_{i\kappa_i\sigma, j\kappa_j\sigma}(\tau, \tau') &= -\left\langle \mathcal{T}\, c_{i\kappa_i\sigma}(\tau) c^{\dagger}_{j\kappa_j\sigma}(\tau') \right\rangle \\ &= -\left\{ \Theta(\tau - \tau') c_{i\kappa_i\sigma}(\tau) c^{\dagger}_{j\kappa_j\sigma}(\tau') + \Theta(\tau' - \tau) c^{\dagger}_{j\kappa_j\sigma}(\tau') c_{i\kappa_i\sigma}(\tau) \right\}, \quad (5.1) \end{aligned}$$

where $\mathcal{T}$ is the time ordering operator and $c_{i\kappa_i\sigma}$ ($c^{\dagger}_{j\kappa_j\sigma}$) annihilates (creates) a particle in orbital i (j) and site κ_i (κ_j) with spin σ. For the sake of simplicity in notation, we consider a collective representation of indices $\alpha_i = i\kappa_i\sigma$ and $\alpha_j = j\kappa_j\sigma'$, where $\sigma = \sigma'$.

The Green's function $\mathcal{G}_{\alpha_i\alpha_j}(\tau, \tau')$ is β-antiperiodic in each τ and is a function of time difference, $\tau - \tau'$.

$$\mathcal{G}_{\alpha_i\alpha_j}(\tau, \tau') = \mathcal{G}_{\alpha_i\alpha_j}(\tau - \tau'), \quad (5.2)$$

$$\mathcal{G}_{\alpha_i\alpha_j}(\tau - \tau') = -\mathcal{G}_{\alpha_i\alpha_j}(\tau - \tau' + \beta) \qquad \text{for } -\beta < \tau - \tau' < 0. \quad (5.3)$$

(See the properties of the Green's function in Sec. 5.2.2 of the current chapter).

The Fourier transform on the Matsubara axis is given by

$$\mathcal{G}_{\alpha_i\alpha_j}(\nu_n) = \frac{1}{2}\int_{-\beta}^{\beta} d\tau\ e^{i\nu_n\tau}\mathcal{G}_{\alpha_i\alpha_j}(\tau) = \int_{0}^{\beta} d\tau\ e^{i\nu_n\tau}\mathcal{G}_{\alpha_i\alpha_j}(\tau), \tag{5.4}$$

where $\nu_n = (2n+1)\pi/\beta$ is the fermionic Matsubara frequency. The inverse Fourier transform is obtained by

$$\mathcal{G}_{\alpha_i\alpha_j}(\tau) = \frac{1}{\beta}\sum_{n=-\infty}^{+\infty} e^{-i\nu_n\tau}\mathcal{G}_{\alpha_i\alpha_j}(\nu_n). \tag{5.5}$$

The convergence of this Green's function is guaranteed only if $-\beta < \tau < \beta$.

- **Remark:**
  In the QMC, for each configuration, the Green's function $\widetilde{G}$ is defined by

$$\widetilde{G}_{\alpha_i\alpha_j}(\tau,\tau') = \left\langle \mathcal{T} c_{\alpha_i}(\tau) c^{\dagger}_{\alpha_j}(\tau') \right\rangle_{\mathbf{s}}, \tag{5.6}$$

  where 's' in $\langle ... \rangle_{\mathbf{s}}$ refers to a single Monte Carlo configuration. The $\widetilde{G}_{\alpha_i\alpha_j}(\tau,\tau')$ is calculated for all possible configurations during the Monte Carlo sampling and for $\tau,\tau' \in [0,\beta)$. After averaging over all possible Monte Carlo configurations, we can obtain the physical Green's function $\mathcal{G}_{\alpha_i\alpha_j}(\tau,\tau')$ by

$$\mathcal{G}_{\alpha_i\alpha_j}(\tau,\tau') \quad = \quad -\frac{1}{N_c}\sum_{\{\mathbf{s}\}}\left[\widetilde{G}_{\alpha_i\alpha_j}(\tau,\tau')\right]_{\{\mathbf{s}\}}, \tag{5.7}$$

  where N_c is the number of all accepted Monte Carlo configurations. At equal times, i.e., $\tau = \tau'$, the QMC calculates $\widetilde{G}_{\alpha_i\alpha_j}(\tau^+,\tau^-)$. In some cases, e.g., in computation of the two-particle correlation function inside QMC, we need $\widetilde{G}_{\alpha_i\alpha_j}(\tau^-,\tau^+)$ where it can be obtained by

$$\widetilde{G}_{\alpha_i\alpha_j}(\tau^-,\tau^+) = \widetilde{G}_{\alpha_i\alpha_j}(\tau^+,\tau^-) - \delta_{\alpha_i,\alpha_j}. \tag{5.8}$$

  The computed Green's function $\widetilde{G}_{\alpha_i\alpha_j}(\tau,\tau')$ which belongs to *one configuration* does not depend on time difference (unlike the physical Green's function wherein $\mathcal{G}(\tau,\tau') = \mathcal{G}(\tau-\tau')$), so that

$$\widetilde{G}_{\alpha_i\alpha_j}(\tau,\tau') \neq \widetilde{G}_{\alpha_i\alpha_j}(\tau-\tau'). \tag{5.9}$$

5.2.2 Properties of one-particle Green's function

In the following, we describe the main properties of the Green's function in imaginary time and Matsubara fermionic frequencies which are frequently used in numerical calculation. The high frequency part of the Green's function (large $i\nu_n$) is also studied. This property would be useful in numerical computation of the Fourier transform of the Green's function.

5.2.2.1 Properties of the Green's function in imaginary time τ-space

1. The Green's function $\mathcal{G}(\tau,\tau')$ is a function of time difference $\tau-\tau'$.

$$\mathcal{G}_{\alpha_i\alpha_j}(\tau,\tau') = \mathcal{G}_{\alpha_i\alpha_j}(\tau-\tau'). \tag{5.10}$$

This can be shown by using the invariance of the trace of the product of the operators under cyclic permutation.

$$\begin{aligned}
\mathcal{G}_{\alpha_i\alpha_j}(\tau,\tau') &= -\frac{1}{\mathcal{Z}}\mathrm{Tr}\left\{e^{-\beta H}e^{\tau H}c_{\alpha_i}e^{-\tau H}e^{\tau' H}c^\dagger_{\alpha_j}e^{\tau' H}\right\}\\
&= -\frac{1}{\mathcal{Z}}\mathrm{Tr}\left\{e^{-\beta H}e^{(\tau-\tau')H}c_{\alpha_i}e^{-(\tau-\tau')H}c^\dagger_{\alpha_j}\right\}\\
&= \mathcal{G}_{\alpha_i\alpha_j}(\tau-\tau').
\end{aligned}$$

2. The Green's function $\mathcal{G}(\tau,\tau')$ is β-antiperiodic in each τ argument (Fig. 5.1).

$$\mathcal{G}_{\alpha_i\alpha_j}(\tau,\tau') = \begin{cases} -\mathcal{G}_{\alpha_i\alpha_j}(\tau+\beta,\tau') & \text{if } \tau<0\\ -\mathcal{G}_{\alpha_i\alpha_j}(\tau,\tau'+\beta) & \text{if } \tau'<0\\ \mathcal{G}_{\alpha_i\alpha_j}(\tau+\beta,\tau'+\beta) & \text{if } \tau<0,\tau'<0 \end{cases}. \tag{5.11}$$

For instance,

$$\begin{aligned}
\mathcal{G}_{\alpha_i\alpha_j}(\tau+\beta,\tau') &= -\frac{1}{\mathcal{Z}}\mathrm{Tr}\left\{e^{-\beta H}e^{(\tau+\beta)H}c_{\alpha_i}e^{-(\tau+\beta)H}e^{\tau' H}c^\dagger_{\alpha_j}e^{-\tau' H}\right\}\\
&= -\frac{1}{\mathcal{Z}}\mathrm{Tr}\left\{e^{\tau H}c_{\alpha_i}e^{-\tau H}\left(e^{-\beta H}e^{\tau' H}c^\dagger_{\alpha_j}e^{\tau H}\right)\right\}\\
&= -\frac{1}{\mathcal{Z}}\mathrm{Tr}\left\{e^{-\beta H}\mathcal{T}\left(c^\dagger_{\alpha_j}(\tau')c_{\alpha_i}(\tau)\right)\right\}\\
&= \frac{1}{\mathcal{Z}}\mathrm{Tr}\left\{e^{-\beta H}\mathcal{T}\left(c_{\alpha_i}(\tau)c^\dagger_{\alpha_j}(\tau')\right)\right\}\\
&= -\mathcal{G}_{\alpha_i\alpha_j}(\tau,\tau'). \qquad \text{for } \tau<0
\end{aligned}$$

3. Convergence of $\mathcal{G}(\tau,\tau')$ is guaranteed only if $-\beta<\tau-\tau'<\beta$.

The convergency condition can be shown by using the Lehman representation of the Green's function.

$$\begin{aligned}
\mathcal{G}_{\alpha_i\alpha_j}(\tau,\tau') &= \mathcal{G}_{\alpha_i\alpha_j}(\tau-\tau')\\
&= -\frac{1}{\mathcal{Z}}\sum_n \left\langle n\middle| e^{-\beta H}e^{(\tau-\tau')H}c_{\alpha_i}e^{-(\tau-\tau')H}c^\dagger_{\alpha_j}\middle|n\right\rangle\\
&= -\frac{1}{\mathcal{Z}}\sum_n e^{-[\beta-\tau+\tau']E_n}\left\langle n\middle| c_{\alpha_i}e^{-(\tau-\tau')H}c^\dagger_{\alpha_j}\middle|n\right\rangle.
\end{aligned}$$

For convergency, the factor $\exp(-[\beta-\tau+\tau']E_n)$ should be finite for large values of E_n. For this reason $(\beta-\tau+\tau')$ should be positive ($\beta>\tau-\tau'$). Similarly, for $\tau<\tau'$, we have $-\beta<\tau-\tau'$.

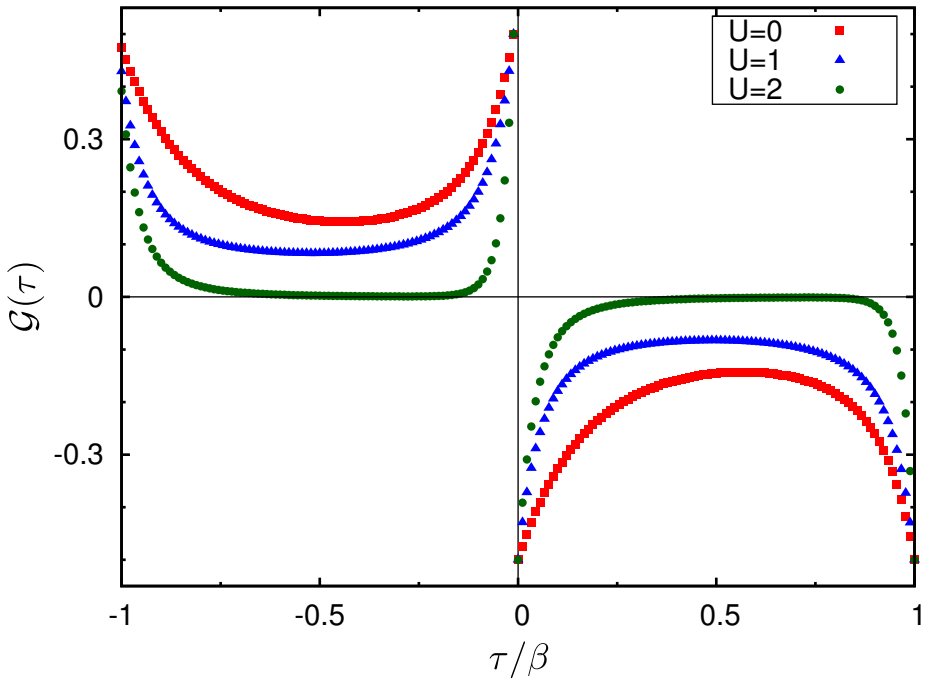

Figure 5.1: β-antiperiodicity of the Green's function $\mathcal{G}(\tau)$ for a single band system, $VOMoO_4$ at half-filling and $\beta = 30$. For a one-dimensional Green's function, a discontinuity at $\tau = 0$ appears.

4. The complex conjugate of the Green's function is given by

$$\left[\mathcal{G}_{\alpha_i\alpha_j}(\tau,\tau')\right]^* = \mathcal{G}_{\alpha_j\alpha_i}(-\tau',-\tau). \tag{5.12}$$

This relation can be proved by using the properties of the trace of operators and considering time ordering.

$$\begin{aligned}\left[\mathcal{G}_{\alpha_i\alpha_j}(\tau,\tau')\right]^* &= \left(-\frac{1}{\mathcal{Z}}\mathrm{Tr}\left\{e^{-\beta H}e^{\tau H}c_{\alpha_i}e^{-\tau H}e^{\tau' H}c^\dagger_{\alpha_j}e^{\tau' H}\right\}\right)^* \\ &= -\frac{1}{\mathcal{Z}}\mathrm{Tr}\left\{e^{-\tau' H}c_{\alpha_j}e^{\tau' H}e^{-\tau H}c^\dagger_{\alpha_i}e^{\tau H}e^{-\beta H}\right\} \\ &= \frac{1}{\mathcal{Z}}\mathrm{Tr}\left\{e^{-\beta H}\mathcal{T}\left(c_{\alpha_j}(-\tau')c^\dagger_{\alpha_i}(-\tau)\right)\right\} \\ &= \mathcal{G}_{\alpha_j\alpha_i}(-\tau',-\tau).\end{aligned}$$

Based on Eq. (5.10), we can obtain

$$\left[\mathcal{G}_{\alpha_i\alpha_j}(\tau)\right]^* = \mathcal{G}_{\alpha_j\alpha_i}(\tau). \tag{5.13}$$

5. *If the local Hamiltonian of the system is real,* the Green's function $\mathcal{G}_{\alpha_i\alpha_j}(\tau,\tau')$ is real too. Therefore, its complex conjugate equals to $\mathcal{G}_{\alpha_i\alpha_j}(\tau,\tau')$.[1]

$$\begin{aligned}\left[\mathcal{G}_{\alpha_i\alpha_j}(\tau,\tau')\right]^* &= \mathcal{G}_{\alpha_j\alpha_i}(-\tau',-\tau) \\ &= \mathcal{G}_{\alpha_i\alpha_j}(\tau,\tau').\end{aligned} \tag{5.14}$$

[1] if we consider the local Green's function for a system with inversion symmetry, this property still holds.

From this relation, we can also find that

$$\Big[\mathcal{G}_{\alpha_i\alpha_j}(\tau)\Big]^* = \mathcal{G}_{\alpha_j\alpha_i}(\tau) = \mathcal{G}_{\alpha_i\alpha_j}(\tau). \tag{5.15}$$

6. The Green's function $\mathcal{G}_{\alpha_i\alpha_j}(\tau)$ at boundaries $\tau = 0^{\pm}$ and $\tau = \beta^{\pm}$ is given by

$$\begin{aligned}
\mathcal{G}_{\alpha_i\alpha_j}(0^+) &= n_{\alpha_i\alpha_j} - \delta_{\alpha_i,\alpha_j}, && (5.16)\\
\mathcal{G}_{\alpha_i\alpha_j}(0^-) &= \mathcal{G}_{\alpha_i\alpha_j}(0^+) + \delta_{\alpha_i,\alpha_j} = n_{\alpha_i\alpha_j}, && (5.17)\\
\mathcal{G}_{\alpha_i\alpha_j}(\beta^-) &= -\mathcal{G}_{\alpha_i\alpha_j}(0^+) - \delta_{\alpha_i,\alpha_j} = -n_{\alpha_i\alpha_j}, && (5.18)\\
\mathcal{G}_{\alpha_i\alpha_j}(\beta^+) &= -\mathcal{G}_{\alpha_i\alpha_j}(0^+) = -n_{\alpha_i\alpha_j} + \delta_{\alpha_i,\alpha_j}, && (5.19)
\end{aligned}$$

where $n_{\alpha_i\alpha_j} = \langle c^\dagger_{\alpha_i} c_{\alpha_j}\rangle$.

For the QMC Green's function which is obtained for single configuration, we have

$$\begin{aligned}
\widetilde{G}_{\alpha_i\alpha_j}(\tau = \beta, \tau') &= -\widetilde{G}_{\alpha_i\alpha_j}(0^+, \tau') + \delta_{\alpha_i,\alpha_j}\delta_{0,\tau'}, && (5.20)\\
\widetilde{G}_{\alpha_i\alpha_j}(\tau, \tau' = \beta) &= -\widetilde{G}_{\alpha_i\alpha_j}(\tau, 0), && (5.21)\\
\widetilde{G}_{\alpha_i\alpha_j}(\tau = \beta, \tau' = \beta) &= \begin{cases} \widetilde{G}_{\alpha_i\alpha_j}(0^+, 0) & \text{if } \tau > \tau' \\ \widetilde{G}_{\alpha_i\alpha_j}(0^+, 0) - \delta_{\alpha_i,\alpha_j} & \text{if } \tau < \tau' \end{cases}, && (5.22)
\end{aligned}$$

which are implemented directly inside the QMC.

7. The Green's function $\mathcal{G}_{\alpha_i\alpha_j}(\tau, \tau')$ is a discontinuous function at $\tau = \tau'$ (See Fig. 5.2).

$$\begin{aligned}
\Delta\mathcal{G}_{\alpha_i\alpha_j}(\tau, \tau') &= \mathcal{G}_{\alpha_i\alpha_j}(\tau^+, \tau) - \mathcal{G}_{\alpha_i\alpha_j}(\tau, \tau^+)\\
&= \Big\langle \mathcal{T} c_{\alpha_i}(\tau^+) c^\dagger_{\alpha_j}(\tau)\Big\rangle - \Big\langle \mathcal{T} c_{\alpha_i}(\tau) c^\dagger_{\alpha_j}(\tau^+)\Big\rangle\\
&= \Big\langle \mathcal{T} c_{\alpha_i}(\tau^+) c^\dagger_{\alpha_j}(\tau)\Big\rangle + \Big\langle \mathcal{T} c^\dagger_{\alpha_j}(\tau^+) c_{\alpha_i}(\tau)\Big\rangle\\
&= \Big\langle \Big\{ c^\dagger_{\alpha_j}(\tau), c_{\alpha_i}(\tau)\Big\}\Big\rangle = \delta_{\alpha_i,\alpha_j}. && (5.23)
\end{aligned}$$

Similarly, we can show that the Green's function $\mathcal{G}_{\alpha_i\alpha_j}(\tau)$ is discontinuos at $\tau = 0, \beta$ (See Fig. 5.1).

The presence of the discontinuities at $\tau = \tau'$ in $\mathcal{G}_{\alpha_i\alpha_j}(\tau, \tau')$ causes noticable numerical error in computing its Fourier integral. However, the Fourier transform of the $\mathcal{G}_{\alpha_i\alpha_j}(\tau)$ has less numerical problems, because the discontinuities are in the border and the $\mathcal{G}_{\alpha_i\alpha_j}(\tau)$ is a smooth function[2] for all $\tau \neq 0, \beta$. We will return to this point in the following of this chapter where we explain several numerical methods to calculate the Fourier integral of the Green's function.

[2] A smooth function is a function that has continuous derivatives up to some desired orders over some domains. A function can therefore be said to be smooth over a restricted interval such as (a,b) or [a,b]. The number of continuous derivatives necessary for a function to be considered smooth depends on the problem at hand, and may vary from two to infinity. A function for which all orders of derivatives are continuous is called a C-infty-function. (http://mathworld.wolfram.com/SmoothFunction.html)

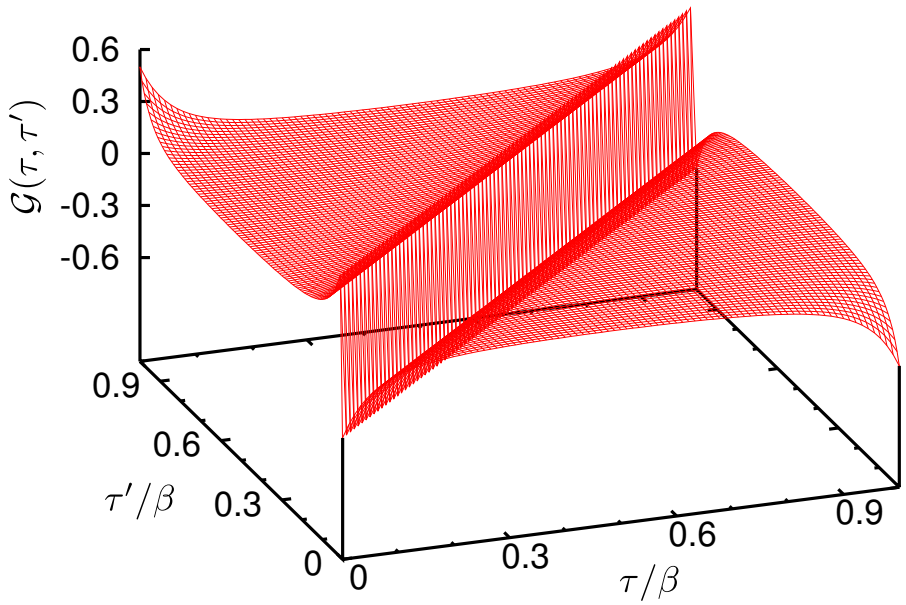

Figure 5.2: Discontinuity of the Green's function $\mathcal{G}(\tau,\tau')$ along $\tau=\tau'$ plane.

5.2.2.2 Properties of the Green's function in imaginary frequency $i\nu_n$ space

1. The complex conjugate of the Matsubara Green's function $\mathcal{G}_{\alpha_i\alpha_j}(\nu_n)$ is given by

$$\Big[\mathcal{G}_{\alpha_i\alpha_j}(\nu_n,\nu_{n'})\Big]^* = \mathcal{G}_{\alpha_j\alpha_i}(-\nu_{n'},-\nu_n), \tag{5.24}$$

$$\Big[\mathcal{G}_{\alpha_i\alpha_j}(\nu_n)\Big]^* = \mathcal{G}_{\alpha_j\alpha_i}(-\nu_n). \tag{5.25}$$

This property can be proved by utilizing the Eqs. (5.12-5.13) and the definition of the Fourier integral in Eq. (5.4) as follows

$$\begin{aligned}\Big[\mathcal{G}_{\alpha_i\alpha_j}(\nu_n,\nu_{n'})\Big]^* &= \int_0^\beta d\tau\int_0^\beta d\tau'\; e^{-i[\nu_n\tau-\nu_{n'}\tau']}\Big[\mathcal{G}_{\alpha_i\alpha_j}(\tau,\tau')\Big]^*\\ &= \int_0^\beta d\tau\int_0^\beta d\tau'\; e^{-i[\nu_n\tau-\nu_{n'}\tau']}\;\mathcal{G}_{\alpha_j\alpha_i}(-\tau',-\tau)\\ &= \int_0^\beta d\tau\int_0^\beta d\tau'\; e^{-i[\nu_n\tau-\nu_{n'}\tau']}\;\mathcal{G}_{\alpha_j\alpha_i}(\beta-\tau',\beta-\tau)\\ &= \mathcal{G}_{\alpha_j\alpha_i}(-\nu_{n'},-\nu_n).\end{aligned} \tag{5.26}$$

For real Hamiltonian since $\mathcal{G}_{\alpha_i\alpha_j}(\tau)=\mathcal{G}_{\alpha_j\alpha_i}(\tau)$ *and* $\mathcal{G}_{\alpha_i\alpha_j}(\tau,\tau')=\mathcal{G}_{\alpha_j\alpha_i}(-\tau',-\tau)$ *we have*

$$\Big[\mathcal{G}_{\alpha_i\alpha_j}(\nu_n)\Big]^* = \mathcal{G}_{\alpha_j\alpha_i}(-\nu_n)=\mathcal{G}_{\alpha_i\alpha_j}(-\nu_n), \tag{5.27}$$

$$\Big[\mathcal{G}_{\alpha_i\alpha_j}(\nu_n,\nu_{n'})\Big]^* = \mathcal{G}_{\alpha_j\alpha_i}(-\nu_{n'},-\nu_n)=\mathcal{G}_{\alpha_i\alpha_j}(-\nu_n,-\nu_{n'}). \tag{5.28}$$

2. The Matsubara Green's function $\mathcal{G}_{\alpha_i\alpha_j}(\nu_n,\nu_{n'})$ can be expressed in terms of the $\mathcal{G}_{\alpha_i\alpha_j}(\nu_n)$ by

$$\mathcal{G}_{\alpha_i\alpha_j}(\nu_n,\nu_{n'})=\beta\;\delta_{nn'}\;\mathcal{G}_{\alpha_i\alpha_j}(\nu_n). \tag{5.29}$$

This relation is obtained as follows

$$\begin{aligned}
\mathcal{G}_{\alpha_i\alpha_j}(\nu_n,\nu_{n'}) &= \int_0^\beta d\tau \int_0^\beta d\tau'\; e^{i[\nu_n\tau-\nu_{n'}\tau']}\; \mathcal{G}_{\alpha_i\alpha_j}(\tau,\tau') \\
&= \int_0^\beta d\tau \int_0^\beta d\tau'\; e^{i[\nu_n\tau-\nu_{n'}\tau']}\; \mathcal{G}_{\alpha_i\alpha_j}(\tau-\tau') \\
&= \frac{1}{\beta}\sum_{m=-\infty}^{+\infty} \mathcal{G}_{\alpha_i\alpha_j}(\nu_n,\nu_{n'})\; e^{-i\nu_m(\tau-\tau')} \int_0^\beta d\tau \int_0^\beta d\tau'\; e^{i[\nu_n\tau-\nu_{n'}\tau']} \\
&= \frac{1}{\beta}\sum_{m} \mathcal{G}_{\alpha_i\alpha_j}(\nu_n,\nu_{n'})(\beta\delta_{nm})(\beta\delta_{nn'}) \\
&= \beta\;\delta_{nn'}\;\mathcal{G}_{\alpha_i\alpha_j}(\nu_n). \qquad (5.30)
\end{aligned}$$

Eqs. (5.16-5.30) will be implemented in the QMC code to reduce CPU time for computing the local susceptibility.

5.2.2.3 High frequency behavior of the Green's function

High frequency part of the $\mathcal{G}_{\alpha_i\alpha_j}(\nu_n)$ is derived by integrating by part of the Fourier integral (5.4) as follows

$$\begin{aligned}
\mathcal{G}_{\alpha_i\alpha_j}(\nu_n) &= \int_0^\beta d\tau\; e^{i\nu_n\tau}\; \mathcal{G}_{\alpha_i\alpha_j}(\tau) \\
&\approx \left(\frac{1}{i\nu_n}\right) e^{i\nu_n\tau}\; \mathcal{G}_{\alpha_i\alpha_j}(\tau)\Big|_{\tau=0}^{\tau=\beta} - \left(\frac{1}{i\nu_n}\right)^2 e^{i\nu_n\tau}\frac{\partial}{\partial\tau}\mathcal{G}_{\alpha_i\alpha_j}(\tau)\Big|_{\tau=0}^{\tau=\beta} + \mathcal{O}\left(\frac{1}{i\nu_n}\right)^3 \\
&\approx \left(\frac{-1}{i\nu_n}\right)\left(\mathcal{G}_{\alpha_i\alpha_j}(\beta^-) + \mathcal{G}_{\alpha_i\alpha_j}(0^+)\right) + \left(\frac{1}{i\nu_n}\right)^2\left(\partial_\tau\mathcal{G}_{\alpha_i\alpha_j}(\beta^-) + \partial_\tau\mathcal{G}_{\alpha_i\alpha_j}(0^+)\right) \\
&\quad + \mathcal{O}\left(\frac{1}{i\nu_n}\right)^3.
\end{aligned}$$

The lowest order approximation in high frequency limit is

$$\mathcal{G}_{\alpha_i\alpha_j}(\nu_n) \approx \delta_{\alpha_i\alpha_j}\left(\frac{1}{i\nu_n}\right) + b\left(\frac{1}{i\nu_n}\right)^2 + \mathcal{O}\left(\frac{1}{i\nu_n}\right)^3, \qquad (5.31)$$

wherein the coefficient b is obtained by

$$\begin{aligned}
b &= \left(\partial_\tau\mathcal{G}_{\alpha_i\alpha_j}(\beta^-) + \partial_\tau\mathcal{G}_{\alpha_i\alpha_j}(0^+)\right) \\
&= \left(-\partial_\tau\mathcal{G}_{\alpha_i\alpha_j}(0^-) + \partial_\tau\mathcal{G}_{\alpha_i\alpha_j}(0^+)\right) \\
&= \left\langle c^\dagger_{\alpha_j}\;[H,c_{\alpha_i}]\right\rangle + \left\langle [H,c_{\alpha_i}]\;c^\dagger_{\alpha_j}\right\rangle. \qquad (5.32)
\end{aligned}$$

Here, we used the equation of motion of the annihilator operator c_{α_i} which is defined as

$$\frac{dc_{\alpha_i}}{d\tau} = [H, c_{\alpha_i}]. \qquad (5.33)$$

Depending on the Hamiltonian, we can calculate analytically the commutator $[H, c_i]$. Numerically, we obtain the coefficient b by fitting data to the tail of the Green's fucntion.

5.3 Numerical methods for Fourier transform of Green's function

5.3.1 1st method: Trapezoidal rule in one and two dimension

In the trapezoidal method, we approximate a given function $f(x)$ as a piecewise linear function [62]. The mesh of the points are equally spaced,

$$h = \frac{b-a}{N},$$

where a and b are end points of the interval $[a, b]$ and N is number of slices. Therefore, in every subinterval $[x_j, x_{j+1}]$, $x_j = a + (j-1)h$ and $\int_{x_j}^{x_j+1} f(x)dx \approx h(f_j + f_{j+1})/2$. The trapezoidal approximation to the integral over the entire interval is given by

$$\begin{aligned}
\int_a^b f(x)\,dx &\approx \sum_{l=0}^{N} w_l f(x_l) \\
&\approx h\sum_{l=0}^{N-1}\int_{x_l}^{x_{l+1}} f(x)dx \\
&\approx \frac{h}{2}\sum_{l=0}^{N-1}(f(x_l)+f(x_{l+1})) \\
&\approx \frac{h}{2}\left\{\sum_{l=1}^{N-1} f(x_l) + f(x_0) + \sum_{l=1}^{N-1} f(x_l) + f(x_N)\right\} \\
&\approx h\sum_{l=1}^{N-1} f(x_l) + \frac{h}{2}(f(x_0)+f(x_N)),
\end{aligned} \tag{5.34}$$

where

$$w_l = h \times \begin{cases} 1 & \text{if } l \neq 0 \text{ and } l \neq N \\ 1/2 & \text{otherwise} \end{cases}.$$

In case of two dimensional function, $f(x, y)$, we can evaluate the function f at corners $[x_i, y_j]$ (the lower left corner), $[x_i, y_{j+1}]$ (the upper left corner), $[x_{i+1}, y_j]$ (the lower right corner) and $[x_{i+1}, y_{j+1}]$ (the upper right corner) then we calculate the average of them. Therefore, the integral of $f(x, y)$ is approximated by the corresponding sum

$$\begin{aligned}
\int_a^b dx \int_c^d dy f(x,y) &\approx h^2 \sum_{i=0}^{N-1}\sum_{j=0}^{N-1} \frac{1}{4}\left[f(x_i,y_j)+f(x_i,y_{j+1})+f(x_{i+1},y_j)+f(x_{i+1},y_{j+1})\right] \\
&\approx \sum_{i=0}^{N}\sum_{j=0}^{N} w_{ij} f(x_i, x_j),
\end{aligned} \tag{5.35}$$

where w_{ij} is the ijth element of weight matrix w,

$$w = \frac{h^2}{4}\begin{pmatrix} 1 & 2 & 2 & \dots & 2 & 2 & 1 \\ 2 & 4 & 4 & \dots & 4 & 4 & 2 \\ \vdots & \vdots & \vdots & \ddots & \vdots & \vdots & \vdots \\ 2 & 4 & 4 & \dots & 4 & 4 & 2 \\ 1 & 2 & 2 & \dots & 2 & 2 & 1 \end{pmatrix}. \tag{5.36}$$

To prove this relation it is sufficient to apply the trapezoidal rule in each direction[3].

Accordingly, the 1D Fourier integral of the Green's Function is

$$\begin{aligned}
\mathcal{G}_{\alpha_i\alpha_j}(\nu_n) &= \int_0^\beta d\tau\ e^{i\nu_n\tau}\mathcal{G}_{\alpha_i\alpha_j}(\tau) \\
&\approx \sum_{l=1}^{L+1} w_l\ \mathcal{G}_{\alpha_i\alpha_j}(\tau_l)\ e^{i\nu_n\tau_l} \\
&\approx \frac{\beta}{L}\sum_{l=2}^{L}\mathcal{G}_{\alpha_i\alpha_j}(\tau_l)e^{i\nu_n\tau_l} + \frac{\beta}{2L}\left(-\mathcal{G}_{\alpha_i\alpha_j}(\beta^-) + \mathcal{G}_{\alpha_i\alpha_j}(0^+)\right) \\
&\approx \frac{\beta}{L}\sum_{l=2}^{L}\mathcal{G}_{\alpha_i\alpha_j}(\tau_l)e^{i\nu_n\tau_l} + \frac{\beta}{L}\left(\mathcal{G}_{\alpha_i\alpha_j}(0^+) + \frac{1}{2}\delta_{\alpha_i\alpha_j}\right), \qquad (5.37)
\end{aligned}$$

where $\Delta\tau = \beta/L$ and $\tau_l = (l-1)\Delta\tau$. Using the antiperiodicity property of the Green's function, we can obtain the Fourier transformed Green's function without any requirement to $\mathcal{G}(\tau)$ at $\tau = \beta$. For this reason, in the QMC, the Green's function $\widetilde{G}_{\alpha_i,\alpha_j}(\tau,\tau')$ is calculated for $\tau,\tau' \in [0,\beta)$. The Fourier transform of the Green's function $\mathcal{G}_{\alpha_i\alpha_j}(\tau,\tau')$ in trapezoidal approach can be computed by (See Appendix F.1 for more details)

$$\begin{aligned}
\mathcal{G}_{\alpha_i\alpha_j}(\nu_n,\nu_{n'}) &= \int_0^\beta d\tau\int_0^\beta d\tau' e^{i[\nu_n\tau-\nu_{n'}\tau']}\mathcal{G}_{\alpha_i\alpha_j}(\tau,\tau') \\
&\approx \left(\frac{\beta}{L}\right)^2\sum_{l=2}^{L}\Big\{\mathcal{G}_{\alpha_i\alpha_j}(\tau_l,0)e^{i\nu_n\tau_l} + \mathcal{G}_{\alpha_i\alpha_j}(0,\tau_l)e^{-i\nu_{n'}\tau_l} \\
&\quad + \sum_{l'=2}^{L} e^{i\nu_n\tau_l}e^{-i\nu_{n'}\tau_{l'}}\mathcal{G}_{\alpha_i\alpha_j}(\tau_l,\tau'_{l'})\Big\} \\
&\quad + \left(\frac{\beta}{L}\right)^2\left[\mathcal{G}_{\alpha_i\alpha_j}(0,0) + \frac{1}{4}\delta_{\alpha_i,\alpha_j}\right]. \qquad (5.38)
\end{aligned}$$

Similar relation can be found for the QMC Green's function as follows.

$$\begin{aligned}
\widetilde{G}_{\alpha_i\alpha_j}(\nu_n,\nu_{n'}) &\approx \left(\frac{\beta}{L}\right)^2\sum_{l=2}^{L}\Big\{\widetilde{G}_{\alpha_i\alpha_j}(\tau_l,0)e^{i\nu_n\tau_l} + \widetilde{G}_{\alpha_i\alpha_j}(0,\tau_l)e^{-i\nu_{n'}\tau_l} \\
&\quad + \sum_{l'=2}^{L} e^{i\nu_n\tau_l}e^{-i\nu_{n'}\tau'_{l'}}\widetilde{G}_{\alpha_i\alpha_j}(\tau_l,\tau'_{l'})\Big\} \\
&\quad + \left(\frac{\beta}{L}\right)^2\left[\widetilde{G}_{\alpha_i\alpha_j}(0,0) - \frac{1}{4}\delta_{\alpha_i,\alpha_j}\right]. \qquad (5.39)
\end{aligned}$$

5.3.1.1 Results and discussion

Trapezoidal method for the Fourier integral of the Green's function $\mathcal{G}_{\alpha_i\alpha_j}(\tau)$, as it is shown in Fig. 5.3, gives periodic results with period $\nu_n \sim 2\pi L/\beta$ for $\mathcal{G}_{\alpha_i\alpha_j}(\nu_n)$ and does not capture the high frequency behavior of the Green's function in Eq. (5.31). Furthermore, the results for

[3] "*double trapezoid*" rule

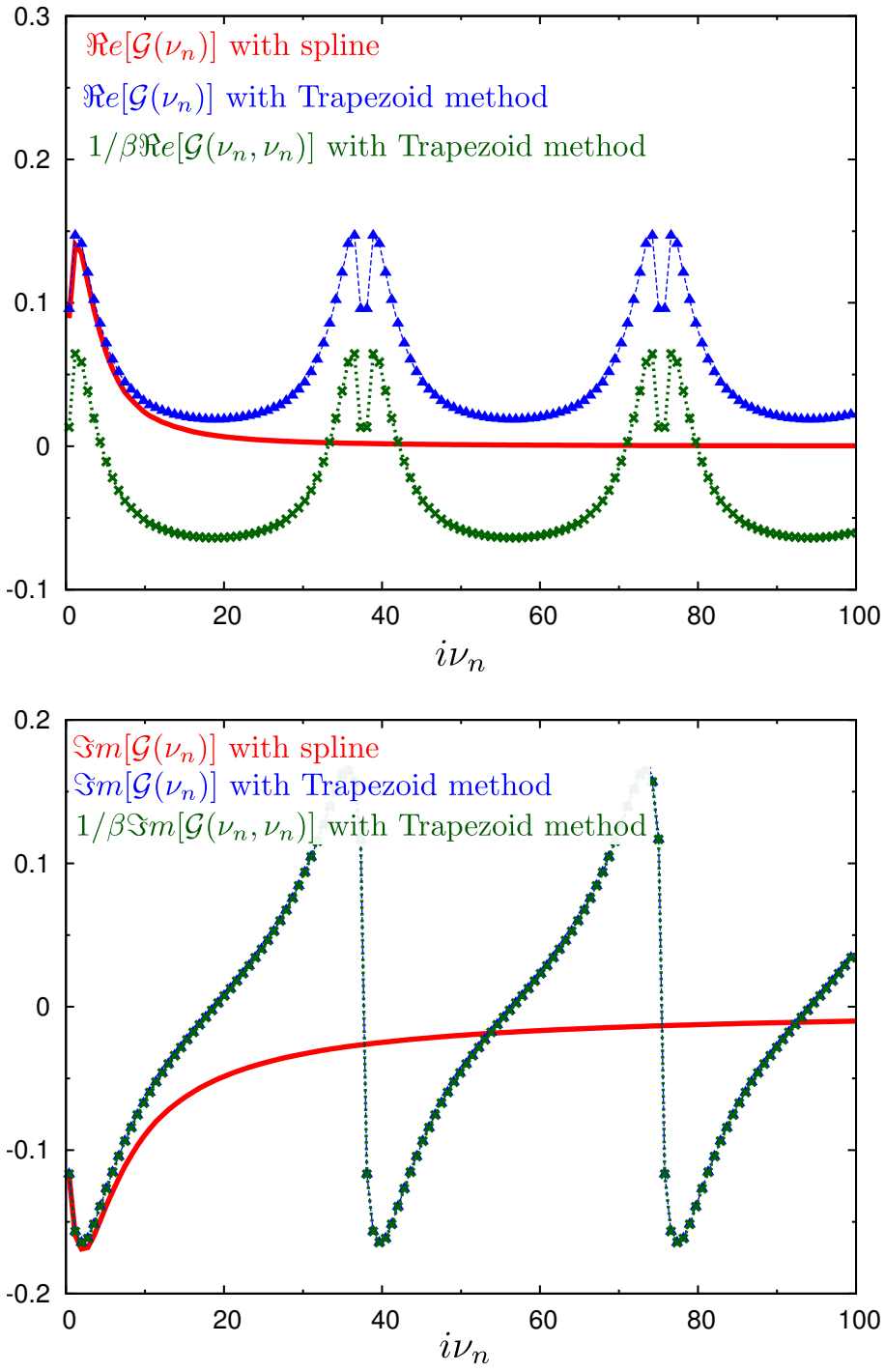

Figure 5.3: The Fourier integral of the Green's function $\mathcal{G}$ with spline (red curve) and trapezoidal rule (blue and green curves) of one e_g orbital of $KCuF_3$. This plot shows that the calculated $\mathcal{G}(\nu_n)$ and $\frac{1}{\beta}\mathcal{G}(\nu_n, \nu_{n'})$ by trapezoidal approximation are periodic. Since the Green's function $\mathcal{G}(\tau)$ has discontinuities at borders, it's Fourier transform is more accurate than the Fourier transform of $\mathcal{G}(\tau, \tau')$ which has discontinuities at $\tau = \tau'$. In this figure, $L = 48$, $\beta = 8$ eV^{-1}, $U = 5.0$ eV, $J = 0.4$ eV.

the $\mathcal{G}_{\alpha_i\alpha_j}(\nu_n, \nu_{n'})$ are even worse, because the Green's function $\mathcal{G}_{\alpha_i\alpha_j}(\tau, \tau')$ has discontinuities at $\tau = \tau'$ (which are not at borders like $\mathcal{G}_{\alpha_i\alpha_j}(\tau)$) and this causes large numerical errors in trapezoidal approach (See Fig. 5.3). For this reason this method can not be used unless $\nu_n \Delta\tau \ll 1$, because the validity of the trapezoidal approximation is based on the assumption that the whole integrand varies linearly over an interval of $\Delta\tau = \beta/L$.

5.3.2 2nd method: Direct Filon-trapezoidal rule in one and two dimension

Filon's quadrature is a formula for approximation of Fourier integrals such as

$$I[f] = \int_a^b f(x) e^{i\omega g(x)}\, dx, \tag{5.40}$$

which retains uniform accuracy even for large ω, where many oscillations of the integrand can occur within a given small δx of the range of integration [62, 63].

By considering the case of a Fourier integral, where $g(x) = x$ in Eq. (5.40), the trapezoidal rule gives

$$I[f] \approx h \sum_{j=1}^{N-1} f_j e^{i\omega x_j} + \frac{1}{2} h (f_0 e^{i\omega a} + f_N e^{i\omega b}),$$

where $f_j \equiv f(x_j)$ and $h = \frac{b-a}{N}$. This approximation can not be used unless $\omega h \ll 1$.

A better approximation, i.e., Filon-trapezoidal method is obtained by approximating $f(x)$ by a piecewise linear function,

$$p_j(x) = f_j + \frac{x - x_j}{h}(f_{j+1} - f_j), \quad x \in [x_j, x_{j+1}], \quad j = 0 \ldots N. \tag{5.41}$$

Taking into account $x - x_j = th$ and $\theta = h\omega$, the integral over $[x_j, x_{j+1}]$ can then be approximated by

$$\begin{aligned} \int_{x_j}^{x_{j+1}} p_j(x) e^{i\omega x}\, dx &= h e^{i\omega x_j} \left\{ f_j \int_0^1 e^{i\omega t}\, dt + (f_{j+1} - f_j) \int_0^1 t e^{i\omega t h}\, dt \right\} \\ &= h e^{i\omega x_j} \left[(\alpha - \eta) f_j + \eta f_{j+1} \right], \end{aligned}$$

where

$$\begin{aligned} \alpha &= \int_0^1 dx\, e^{i\theta x} = \frac{1}{i\theta}(\exp(i\theta) - 1), \\ \eta &= \int_0^1 dx\, x\, e^{i\theta x} = \frac{\exp(i\theta)}{i\theta} + \frac{1}{\theta^2}(\exp(i\theta) - 1). \end{aligned}$$

Therefore, $I[f]$ can be approximated by

$$I[f] = \sum_{j=0}^{N-1} \tilde{w}_j(\theta) e^{i\omega x_j} f_j, \tag{5.42}$$

wherein

$$\begin{aligned}
\tilde{w}_0(\theta) &= \frac{h}{\theta^2}(1+i\theta-e^{-i\theta}),\\
\tilde{w}_j(\theta) &\equiv \tilde{w}(\theta)=h\left(\frac{\sin(\frac{\theta}{2})}{\frac{\theta}{2}}\right)^2, = \tilde{w}_0(\theta)+\tilde{w}_N(\theta) \quad j\neq 0,N,\\
\tilde{w}_N(\theta) &= \frac{h}{\theta^2}(1-i\theta-e^{-i\theta}),
\end{aligned} \tag{5.43}$$

We can extract the boundary values of the function $f(x)$ and obtain the following relation for the Fourier transform.

$$\begin{aligned}
I[f] &= \sum_{j=0}^{N-1}\int_{x_j}^{x_{j+1}} p_j(x)e^{i\omega x}\,dx\\
&\approx h(\alpha-\eta)\sum_{j=0}^{N-1} f_j e^{i\omega x_j}+h\eta\sum_{j=1}^{N} f_j e^{i\omega(x_j-h)}\\
&= \left[(\alpha-\eta)h+h\eta e^{-i\theta}\right]\sum_{j=0}^{N-1} f_j e^{i\omega x_j}+h\eta e^{-i\theta}\left[f_N e^{i\omega x_N}-f_0 e^{i\omega x_0}\right]\\
&= \tilde{w}(\theta)\sum_{j=0}^{N-1} f_j e^{i\omega x_j}+\tilde{w}_N(\theta)\,\left(f_N e^{i\omega x_N}-f_0 e^{i\omega x_0}\right).
\end{aligned} \tag{5.44}$$

This relation would be more simple if the function f is (anti)periodic, i.e., $f_N=f_0$ ($f_N=-f_0$). For instance, the Green's function, $\mathcal{G}(\tau)$, is an antiperiodic function in τ and we can find the following approximate relation for its Fourier transform.

$$\begin{aligned}
\mathcal{G}_{\alpha_i\alpha_j}(\nu_n) &= \int_0^\beta \mathcal{G}_{\alpha_i\alpha_j}(\tau)e^{i\nu_n\tau}\,d\tau\\
&\approx \tilde{w}(\theta)\sum_{l=1}^{L}\mathcal{G}_{\alpha_i\alpha_j}(\tau_l)e^{i\nu_n\tau_l}+\tilde{w}_{L+1}(\theta)\left(\mathcal{G}_{\alpha_i\alpha_j}(\beta)e^{i\nu_n\beta}-\mathcal{G}_{\alpha_i\alpha_j}(0)e^{i\nu_n 0}\right)\\
&\approx \tilde{w}(\theta)\sum_{l=1}^{L}\mathcal{G}_{\alpha_i\alpha_j}(\tau_l)e^{i\nu_n\tau_l}+\tilde{w}_{L+1}(\theta)\,\delta_{\alpha_i\alpha_j}.
\end{aligned} \tag{5.45}$$

Here, L is time slices, $\Delta\tau=\beta/L$, $\tau_l=(l-1)\Delta\tau$ and $\theta=\nu_n\Delta\tau$. In order to derive this relation, we used properties of the Green's function in Eqs. (5.16) and (5.18).

Notice that the Filon-trapezoidal method gives the correct tail for the imaginary part at large frequencies ν_n. But for the real part, the tail has a periodic but small error which decays with increasing frequencies[4] (Fig. 5.4). This behavior can be easily derived

$$\tilde{w}\left(\frac{\beta}{L}\nu_n\right) = \frac{\beta}{L}\left(\frac{\sin(\frac{\beta}{2L}\nu_n)}{\frac{\beta}{2L}\nu_n}\right)^2\Bigg|_{\nu_n\gg 1}\longrightarrow 0, \tag{5.46}$$

$$\tilde{w}_{L+1}\left(\frac{\beta}{L}\nu_n\right) = \frac{\beta}{L}\frac{1-i\frac{\beta}{L}\nu_n-e^{i\frac{\beta}{L}\nu_n}}{\left(\frac{\beta}{L}\nu_n\right)^2}\Bigg|_{\nu_n\gg 1}\approx\begin{cases}\dfrac{1}{i\nu_n} & \text{for } \Im m[\tilde{w}_{L+1}]\\ \dfrac{L}{\beta}\dfrac{1-\cos(\frac{\beta}{L}\nu_n)}{{\nu_n}^2} & \text{for } \Re e[\tilde{w}_{L+1}]\end{cases}. \tag{5.47}$$

[4]This is an error of the Filon-trapezoidal method only and it does not depend on behavior of the function.

This systematic error goes to zero if $\Delta\tau = \beta/L \to 0$ (see Fig 5.5).

For 2D Filon-trapezoidal approximation, we can do similar approach to derive its formulas.

$$\begin{aligned} I[f] &= \int_a^b \int_a^b f(x,y) e^{i\omega x} e^{i\nu y}\, dx\, dy \\ &\approx \sum_{i=0}^{N-1} \sum_{j=0}^{N-1} \int_{x_i}^{x_{i+1}} \int_{y_j}^{y_{j+1}} p_{ij}(x,y) e^{i\omega x} e^{i\nu y}\, dx\, dy, \end{aligned} \tag{5.48}$$

in which

$$\begin{aligned} p_{ij}(x,y) &= f_{ij} + \frac{x-x_i}{h}(f_{i+1,j} - f_{ij}) + \frac{y-y_j}{h}(f_{i,j+1} - f_{ij}) \\ &\quad + \frac{(x-x_i)(y-y_j)}{h^2}(f_{i+1,j+1} - f_{i+1,j} - f_{i,j+1} + f_{ij}), \end{aligned} \tag{5.49}$$

and $f_{ij} \equiv f(x_i, y_j)$, $h = (b-a)/N$. The double integrals in Eq. (5.48) can be obtained analytically by

$$\begin{aligned} \int_{x_i}^{x_{i+1}} \int_{y_j}^{y_{j+1}} p_{ij}(x,y) e^{i\omega x} e^{i\nu y}\, dx\, dy &= h^2\, e^{i\omega x_i} e^{i\nu y_j} \Big\{ (\alpha_x - \eta_x)(\alpha_y - \eta_y) f_{ij} + \eta_x (\alpha_y - \eta_y) f_{i+1,j} \\ &\quad + \eta_y (\alpha_x - \eta_x) f_{i,j+1} + \eta_x \eta_y f_{i+1,j+1} \Big\}. \end{aligned}$$

Therefore, the approximate relation for $I[f]$ is given by (See Appendix F.2 for details)

$$\begin{aligned} I[f] \approx\ & \tilde{w}(\theta_x)\tilde{w}(\theta_y) \sum_{i=0}^{N-1} \sum_{j=0}^{N-1} e^{i\omega x_i} e^{i\nu y_j} f_{ij} \\ & + \tilde{w}_N(\theta_x)\tilde{w}(\theta_y) \sum_{i=0}^{N-1} e^{i\nu y_j} \left(e^{i\omega x_N} f_{Ni} - e^{i\omega x_0} f_{oi} \right) \\ & + \tilde{w}(\theta_x)\tilde{w}_N(\theta_y) \sum_{i=0}^{N-1} e^{i\omega x_i} \left(e^{i\nu y_i} f_{iN} - e^{i\nu y_0} f_{i0} \right) \\ & + \tilde{w}_N(\theta_x)\tilde{w}_N(\theta_y) \Big\{ e^{i\omega x_N} \left(e^{i\nu y_i} f_{NN} - e^{i\nu y_0} f_{N0} \right) - e^{i\omega x_0} \left(e^{i\nu y_N} f_{0N} - e^{i\nu y_0} f_{00} \right) \Big\}, \end{aligned} \tag{5.50}$$

in which $\theta_x = \omega h$ and $\theta_y = \nu h$. This result can be written in a more simple form for the Fourier integral of $\mathcal{G}_{\alpha_i\alpha_j}(\tau,\tau')$ by virtue of substantial simplification following the fact that $\mathcal{G}_{\alpha_i\alpha_j}(\tau,\tau')$

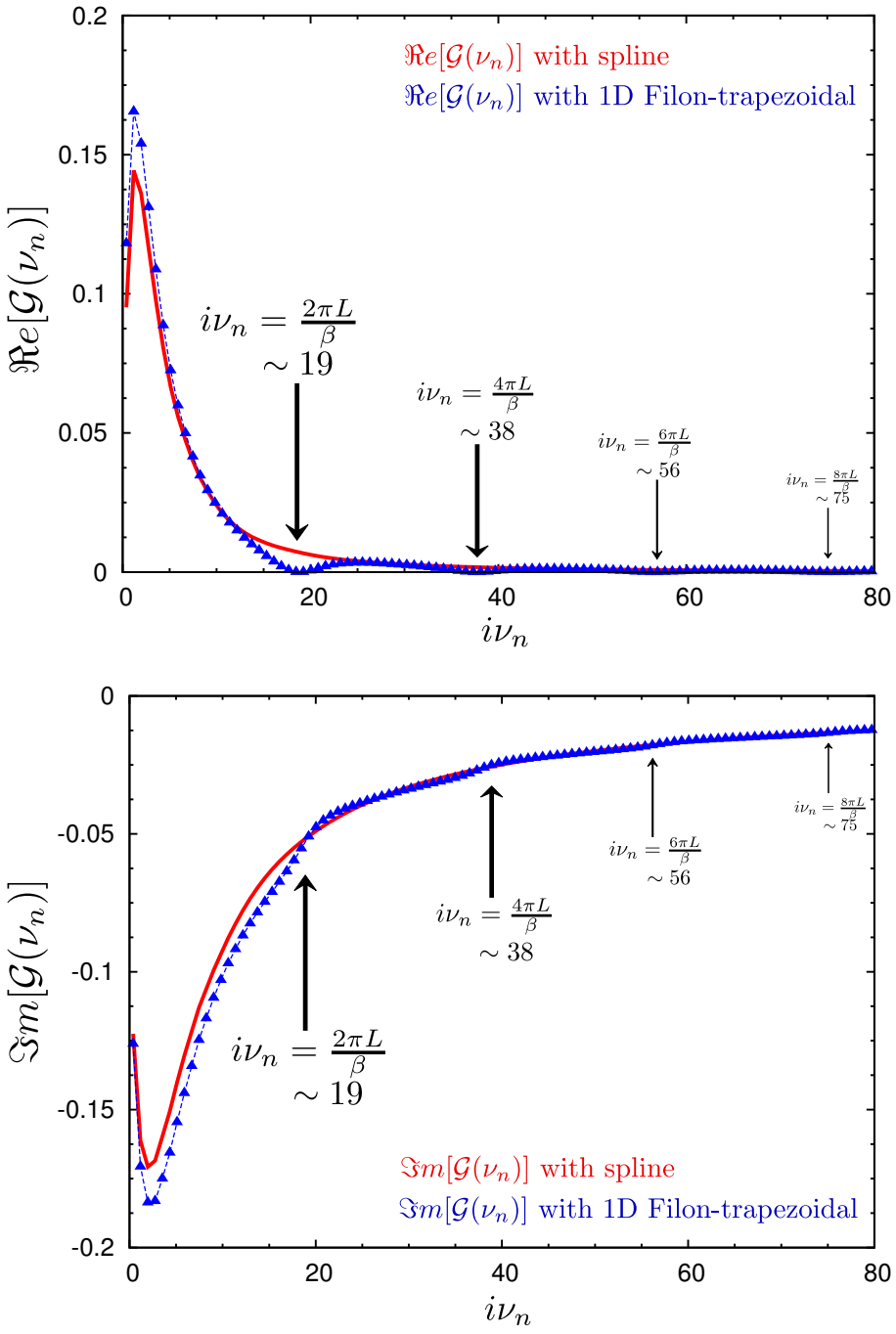

Figure 5.4: Asymptotic behavior of real and imaginary part of the Green's function, $\mathcal{G}(\nu_n)$. There is a periodic but small error which decays in large frequencies. In this figure, $L = 24$, $\beta = 8$ and therefore $\Delta\tau \sim 0.33$. Systematic errors appear at $\nu_n = \frac{2\pi L}{\beta}$, $2 \times \frac{2\pi L}{\beta}, \cdots, M \times \frac{2\pi L}{\beta}$ in which $\sin(\frac{\beta}{2L}\nu_n) \sim 0$.

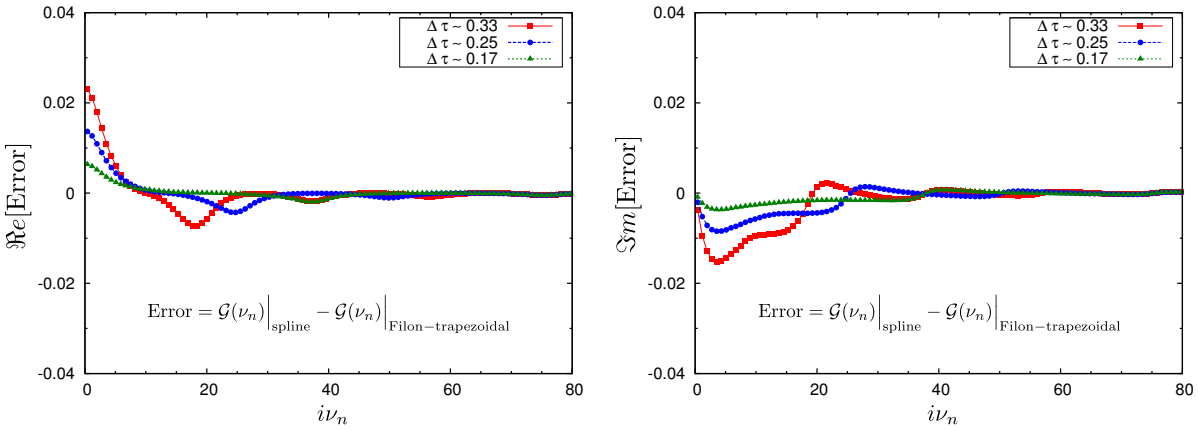

Figure 5.5: Systematic error of the direct 1D Filon-trapezoidal method for different $\Delta\tau$.

is antiperiodic.

$$
\begin{aligned}
\mathcal{G}_{\alpha_i\alpha_j}(\nu_n,\nu_{n'}) &= \int_0^\beta\int_0^\beta e^{i\nu_n\tau}e^{-i\nu_{n'}\tau'}\mathcal{G}_{\alpha_i\alpha_j}(\tau,\tau')\,d\tau d\tau' \\
&\approx \tilde{w}(\frac{\beta}{L}\nu_n)\tilde{w}(-\frac{\beta}{L}\nu_{n'})\sum_{l=1}^{L}\sum_{l'=1}^{L}e^{i\nu_n\tau_l}e^{-i\nu_{n'}\tau'_{l'}}\,\mathcal{G}_{\alpha_i\alpha_j}(\tau,\tau') \\
&\quad+\tilde{w}_{L+1}(\frac{\beta}{L}\nu_n)\tilde{w}(-\frac{\beta}{L}\nu_{n'})\sum_{l'=1}^{L}e^{-i\nu_{n'}\tau'_{l'}}\left\{e^{i\nu_n\beta}\,\mathcal{G}_{\alpha_i\alpha_j}(\beta,\tau'_{l'})-\mathcal{G}_{\alpha_i\alpha_j}(0,\tau'_{l'})\right\} \\
&\quad+\tilde{w}(\frac{\beta}{L}\nu_n)\tilde{w}_{L+1}(-\frac{\beta}{L}\nu_{n'})\sum_{l=1}^{L}e^{i\nu_n\tau_l}\left\{e^{-i\nu_{n'}\beta}\,\mathcal{G}_{\alpha_i\alpha_j}(\tau_l,\beta)-\mathcal{G}_{\alpha_i\alpha_j}(\tau_l,0)\right\} \\
&\quad+\tilde{w}_{L+1}(\frac{\beta}{L}\nu_n)\tilde{w}_{L+1}(-\frac{\beta}{L}\nu_{n'})\left\{e^{i\nu_n\beta}\left(e^{-i\nu_{n'}\beta}\,\mathcal{G}_{\alpha_i\alpha_j}(\beta,\beta)-\mathcal{G}_{\alpha_i\alpha_j}(\beta,0)\right)\right\} \\
&\quad-\tilde{w}_{L+1}(\frac{\beta}{L}\nu_n)\tilde{w}_{L+1}(-\frac{\beta}{L}\nu_{n'})\left\{e^{-i\nu_{n'}\beta}\,\mathcal{G}_{\alpha_i\alpha_j}(0,\beta)-\mathcal{G}_{\alpha_i\alpha_j}(0,0)\right\}.
\end{aligned}
$$

Using properties of the Green's function at boundaries, we can find the following relation for the 2D Fourier transforming of the Green's function $\mathcal{G}_{\alpha_i\alpha_j}(\tau,\tau')$.

$$
\begin{aligned}
\mathcal{G}_{\alpha_i\alpha_j}(\nu_n,\nu_{n'}) &\approx \tilde{w}(\frac{\beta}{L}\nu_n)\tilde{w}(\frac{\beta}{L}\nu_{n'})\sum_{l=1}^{L}\sum_{l'=1}^{L}e^{i\nu_n\tau_l}e^{-i\nu_{n'}\tau_{l'}}\,\mathcal{G}_{\alpha_i\alpha_j}(\tau_l,\tau_{l'}) \\
&\quad+\left[\tilde{w}(\frac{\beta}{L}\nu_{n'})-\tilde{w}^*_{L+1}(\frac{\beta}{L}\nu_{n'})\right]\tilde{w}_{L+1}(\frac{\beta}{L}\nu_n)\,\delta_{\alpha_i\alpha_j}. \qquad (5.51)
\end{aligned}
$$

In this relation, $\tilde{w}(-\frac{\beta}{L}\nu_{n'})=\tilde{w}(\frac{\beta}{L}\nu_{n'})$, $\tilde{w}_{L+1}(-\frac{\beta}{L}\nu_{n'})=\tilde{w}^*_{L+1}(\frac{\beta}{L}\nu_{n'})$ and at equal times $\tau=\tau'$, $\mathcal{G}_{\alpha_i\alpha_j}(\tau^+,\tau)$ is considered.

Inside the QMC block, the Fourier transform of the Green's function is computed by

$$\begin{aligned}\widetilde{G}_{\alpha_i\alpha_j}(\nu_n,\nu_{n'}) \;\approx\; & \tilde{w}(\frac{\beta}{L}\nu_n)\tilde{w}(\frac{\beta}{L}\nu_{n'})\sum_{l=1}^{L}\sum_{l'=1}^{L} e^{i\nu_n\tau_l}e^{-i\nu_{n'}\tau_{l'}}\;\widetilde{G}_{\alpha_i\alpha_j}(\tau_l,\tau_{l'}) \\ & -\left[\tilde{w}(\frac{\beta}{L}\nu_{n'})-\tilde{w}^*_{L+1}(\frac{\beta}{L}\nu_{n'})\right]\tilde{w}_{L+1}(\frac{\beta}{L}\nu_n)\;\delta_{\alpha_i\alpha_j}. \end{aligned} \tag{5.52}$$

Asymptotic behavior of the $\mathcal{G}_{\alpha_i\alpha_j}(\nu_n,\nu_{n'})$ shows incorrect results for imaginary and real part of the Green's function at large frequencies. For instants at $\nu_n=\nu_{n'}$ (diagonal part) we can derive the following relations for asymptotic behavior of the Green's function.

$$\tilde{w}\left(\frac{\beta}{L}\nu_n\right)\tilde{w}\left(\frac{\beta}{L}\nu_n\right)\Big|_{\nu_n\gg 1} \;\longrightarrow\; 0, \tag{5.53}$$

$$T=\left[\tilde{w}\left(\frac{\beta}{L}\nu_{n'}\right)-\tilde{w}^*_{L+1}\left(\frac{\beta}{L}\nu_{n'}\right)\right]\tilde{w}_{L+1}\left(\frac{\beta}{L}\nu_n\right)\Big|_{\nu_n\gg 1} \;\approx\; \begin{cases}0 & \text{for } \Im m[T]\\ -\dfrac{1}{\nu_n^2} & \text{for } \Re e[T]\end{cases} \tag{5.54}$$

In Fig 5.9, this asymptotic behavior is shown.

5.3.2.1 Direct Filon-trapezoidal method's results

We implemented this method to calculate the Fourier transform of the Green's functions $\mathcal{G}_{\alpha_i\alpha_j}(\tau)$ and $\mathcal{G}_{\alpha_i\alpha_j}(\tau,\tau')$. Analytically we know that $\mathcal{G}_{\alpha_i\alpha_j}(\nu_n,\nu_{n'})=\beta\mathcal{G}_{\alpha_i\alpha_j}(\nu_n)$ but as it is shown in Fig. (5.9), the direct Filon-trapezoidal method gives different results for $\beta\mathcal{G}_{\alpha_i\alpha_j}(\nu_n)$ and $\mathcal{G}_{\alpha_i\alpha_j}(\nu_n,\nu_{n'})$. According to Fig. (5.9), we conclude that

(I) the Filon-trapezoidal method is accurate enough if we use it to calculate the Fourier integral of $\mathcal{G}_{\alpha_i\alpha_j}(\tau)$ (1D direct Filon-trapezoidal). Especially this method gives us the correct tail of the Green's function at large frequencies. Smoothness and presence of discontinuities in the border of the $\mathcal{G}_{\alpha_i\alpha_j}(\tau)$ are reasons for obtaining accurate $\mathcal{G}_{\alpha_i\alpha_j}(\nu_n)$.

(II) Fourier transform of the $\mathcal{G}_{\alpha_i\alpha_j}(\tau,\tau')$ with the 2D direct Filon-trapezoidal method is not accurate enough. This is related to discontinuities of $\mathcal{G}(\tau,\tau')$ which are placed along the $\tau=\tau'$ (unlike the one dimensional Green's function $\mathcal{G}(\tau)$ with discontinuity at boundaries). The 2D Filon-trapezoidal rule does not even produce the correct tail of $\mathcal{G}_{\alpha_i\alpha_j}(\nu_n,\nu_{n'})$ (for large frequencies $\nu_n\gg 1$, $\Im m[\mathcal{G}(\nu_n,\nu_n)]\to 0$ and $\Re e[\mathcal{G}(\nu_n,\nu_n)]\to -1/\nu_n^2$. See Eq. (5.54))

Later, we use a trick to utilize the 2D Filon-trapezoidal approximation to calculate the Fourier transform of $\mathcal{G}(\tau,\tau')$ with the same accuracy of 1D Filon-trapezoidal Fourier integral for $\mathcal{G}(\tau)$.

5.3.3 3rd method: Separating continuous and discontinuous part of the Green's function

Accuracy of numerical Fourier transform of a function highly depends on it's behavior. If the function has discontinuities or kinks, it's Fourier transform has large numerical errors. In the case of periodic or antiperiodic functions like the Green's function in imaginary time space, if the discontinuities or kinks are appeared in the border of function, numerical errors are decreased.

This is shown e.g., in Fig. 5.4 and 5.9 in which the Fourier transform of the Green's function is calculated by using the direct Filon-trapezoidal approximation.

In order to decrease numerical problem of Fourier transform of the 2D Green's function, we proceed as follows [64]. First, we split off a one dimension part of the Green's function $\mathcal{G}(\tau,\tau')$ (or $\widetilde{G}(\tau,\tau')$), containing the discontinuities at borders $g(\tau-\tau')$ (or $\widetilde{g}(\tau-\tau')$) and the remaining two dimensional part $\delta g(\tau,\tau')$ (or $\widetilde{\delta g}(\tau,\tau')$) which is free of discontinuities. In the case of the *physical Green's function*

$$\mathcal{G}_{\alpha_i\alpha_j}(\tau,\tau') = g_{\alpha_i\alpha_j}(\tau-\tau') + \delta g_{\alpha_i\alpha_j}(\tau,\tau'). \tag{5.55}$$

According to Eq. (5.29), $g_{\alpha_i\alpha_j}(\tau-\tau') = \mathcal{G}_{\alpha_i\alpha_j}(\tau-\tau')$ and therefore, $\delta g_{\alpha_i\alpha_j}(\tau,\tau') = 0$. For the

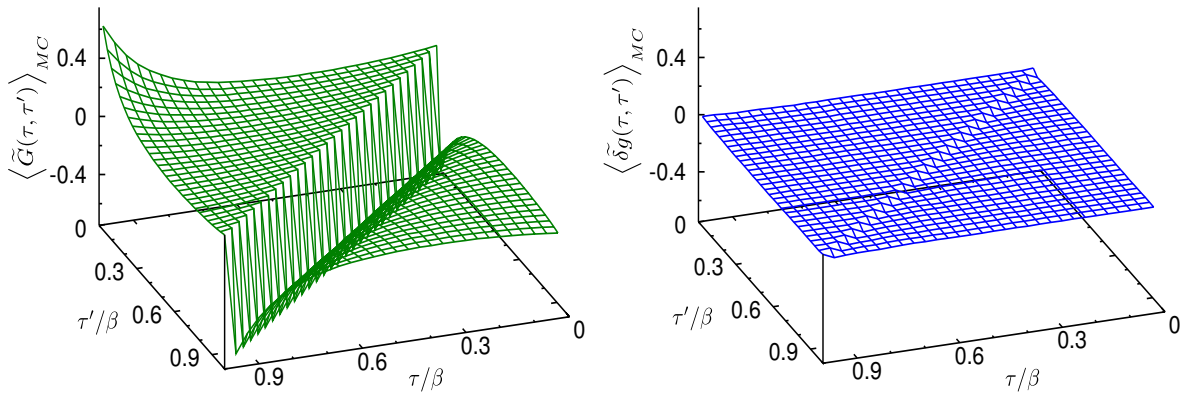

Figure 5.6: Behavior of the $\widetilde{G}$ and $\widetilde{\delta g}$ after averaging over all Monte-Carlo configurations.

QMC Green's function where,

$$\widetilde{G}_{\alpha_i\alpha_j}(\tau,\tau') = \widetilde{g}_{\alpha_i\alpha_j}(\tau-\tau') + \widetilde{\delta g}_{\alpha_i\alpha_j}(\tau,\tau'), \tag{5.56}$$

since $\widetilde{G}_{\alpha_i\alpha_j}(\tau,\tau') \neq \widetilde{G}_{\alpha_i\alpha_j}(\tau-\tau')$, the 2D continuous part is not zero $\widetilde{\delta g}_{\alpha_i\alpha_j}(\tau,\tau') \neq 0$ and the 1D discontinuous part is obtained by

$$\widetilde{g}_{\alpha_i\alpha_j}(\tau-\tau') = \frac{1}{L}\sum_{l=1}^{L} \widetilde{G}_{\alpha_i\alpha_j}(\tau-\tau'+\tau_l,\tau_l). \tag{5.57}$$

In this relation,

$$\widetilde{G}_{\alpha_i\alpha_j}(\tau-\tau'+\tau_l,\tau_l) = \begin{cases} -\widetilde{G}_{\alpha_i\alpha_j}(\tau-\tau'+\tau_l-\beta,\tau_l) & \text{if } \tau-\tau'+\tau_l > \beta \\ -\widetilde{G}_{\alpha_i\alpha_j}(\tau-\tau'+\tau_l+\beta,\tau_l) & \text{if } \tau-\tau'+\tau_l < 0 \end{cases}, \tag{5.58}$$

where $\Delta\tau = \beta/L$ and $\tau_l = (l-1)\Delta\tau$. Based on Eqs. (5.20-5.22), we have

$$\begin{aligned} \widetilde{G}_{\alpha_i\alpha_j}(\beta,\tau') &= -\widetilde{G}_{\alpha_i\alpha_j}(0^+,\tau') + \delta_{\alpha_i\alpha_j}\delta_{0,\tau'} \\ &= -\left\{\widetilde{g}_{\alpha_i\alpha_j}(0^+-\tau') + \widetilde{\delta g}_{\alpha_i\alpha_j}(0^+,\tau')\right\} + \delta_{ij}\delta_{0,\tau'} \\ &= \left\{\widetilde{g}_{\alpha_i\alpha_j}(0^+-\tau') + \delta_{\alpha_i\alpha_j}\delta_{0,\tau'}\right\} - \widetilde{\delta g}_{\alpha_i\alpha_j}(0^+,\tau'), \end{aligned}$$

and

$$\begin{aligned}\widetilde{G}_{\alpha_i\alpha_j}(\tau,\beta) &= -\widetilde{G}_{\alpha_i\alpha_j}(\tau,0)\\ &= -\widetilde{g}_{\alpha_i\alpha_j}(\tau-0)-\widetilde{\delta g}_{\alpha_i\alpha_j}(\tau,0),\end{aligned}$$

which imply boundary conditions as follows

$$\widetilde{g}_{\alpha_i\alpha_j}(\beta-\tau') = -\widetilde{g}_{\alpha_i\alpha_j}(0^- -\tau') = -\widetilde{g}_{\alpha_i\alpha_j}(0^+ -\tau') + \delta_{\alpha_i\alpha_j}\delta_{0,\tau'}, \tag{5.59}$$

$$\widetilde{g}_{\alpha_i\alpha_j}(\tau-\beta) = -\widetilde{g}_{\alpha_i\alpha_j}(\tau),$$

$$\widetilde{\delta g}_{\alpha_i\alpha_j}(\beta,\tau') = -\widetilde{\delta g}_{\alpha_i\alpha_j}(0,\tau'), \tag{5.60}$$

$$\widetilde{\delta g}_{\alpha_i\alpha_j}(\tau,\beta) = -\widetilde{\delta g}_{\alpha_i\alpha_j}(\tau,0). \tag{5.61}$$

Therefore, the Fourier integral of the time translationally invariant part of $\widetilde{G}_{\alpha_i\alpha_j}(\tau,\tau')$, i.e., $\widetilde{g}(\tau-\tau')$ can be done by using 1D Filon-trapezoidal method (Eq. (5.45)) or spline. Moreover, two-dimensional and continuous part $\widetilde{\delta g}_{\alpha_i\alpha_j}(\tau,\tau')$ is Fourier transformed by 2D Filon-trapezoidal approximation.

$$\widetilde{G}_{\alpha_i\alpha_j}(\nu_n,\nu_{n'}) = \beta\delta_{nn'}\widetilde{g}_{\alpha_i\alpha_j}(\nu_n) + \widetilde{\delta g}_{\alpha_i\alpha_j}(\nu_n,\nu_{n'}), \tag{5.62}$$

where

$$\widetilde{\delta g}_{\alpha_i\alpha_j}(\nu_n,\nu_{n'}) \approx \tilde{w}(\frac{\beta}{L}\nu_n)\tilde{w}(\frac{\beta}{L}\nu_{n'})\sum_{l=1}^{L}\sum_{l'=1}^{L} e^{i\nu_n\tau_l}e^{-i\nu_{n'}\tau'_{l'}}\widetilde{\delta g}_{\alpha_i\alpha_j}(\tau_l,\tau'_{l'}), \tag{5.63}$$

$$\widetilde{g}_{\alpha_i\alpha_j}(\nu_n) \approx \tilde{w}(\frac{\beta}{L}\nu_n)\sum_{l=1}^{L} e^{i\nu_n\tau_l}\widetilde{g}_{\alpha_i\alpha_j}(\tau_l) - \tilde{w}_{L+1}(\frac{\beta}{L}\nu_n)\delta_{\alpha_i\alpha_j}. \tag{5.64}$$

It should be noticed that after averaging over all Monte Carlo configurations we have

$$\left\langle\widetilde{\delta g}_{\alpha_i\alpha_j}(\nu_n,\nu_{n'})\right\rangle_{\rm MC} \longrightarrow 0, \tag{5.65}$$

$$\left\langle\widetilde{g}_{\alpha_i\alpha_j}(\nu_n)\right\rangle_{\rm MC} \longrightarrow \mathcal{G}_{\alpha_i\alpha_j}(\nu_n). \tag{5.66}$$

Although the second term in Eq. (5.62) after Monte Carlo average goes to zero, it has non-zero contribution in each configuration and it is very crucial to consider it for computing the two-particle correlation function.

5.3.3.1 Discussion and results

Splitting the Green's function $\widetilde{G}_{\alpha_i\alpha_j}(\tau,\tau')$ into continuous, $\widetilde{g}_{\alpha_i\alpha_j}$, and discontinuous, $\widetilde{\delta g}_{\alpha_i\alpha_j}$, not only increases accuracy of the numerical Fourier transformation comparing to the trapezoidal rule and the 2D Filon-trapezoidal method, but also increases the CPU time. Considering N_O as number of orbitals, N_S number of sites, N_τ number of time slices and N_ν (N_ω) number of fermionic (bosonic) frequencies; the Fourier transform of the Green's function requires $2N_O^2N_S^2N_\tau^2$ operations to split the continuous and discontinuous part of the Green's function and $2(N_\nu+N_\omega)N_O^2N_S^2N_\tau + 2(N_\nu+N_\omega)^2N_O^2N_S^2N_\tau^2$ operations to compute the Fourier transform of $\widetilde{g}_{\alpha_i\alpha_j}(\tau-\tau')$ and $\widetilde{\delta g}_{\alpha_i\alpha_k}(\tau,\tau')$. This method, however, can be used to compute the two-particle correlation function in Matsubara frequency space.

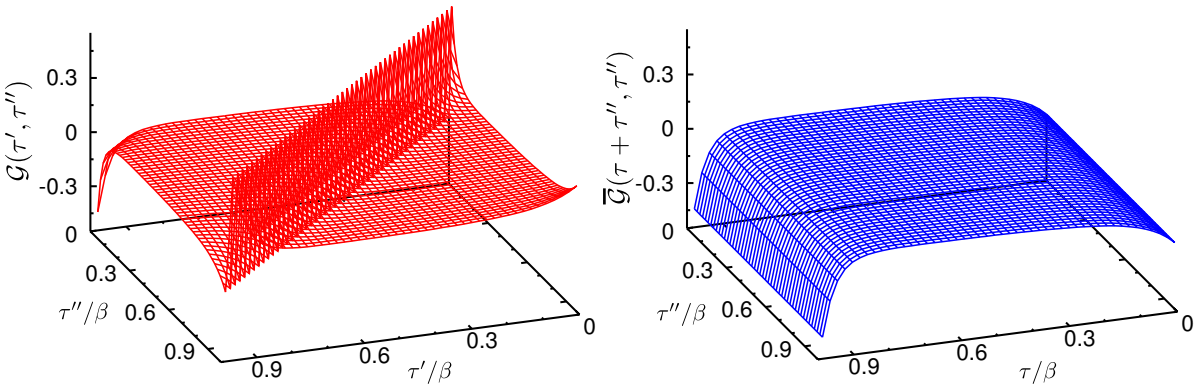

Figure 5.7: Position of the discontinuities in $\mathcal{G}(\tau', \tau'')$ and $\overline{\mathcal{G}}(\tau+\tau'', \tau'')$.

5.3.4 4th method: Transferring discontinuities of the Green's function to the border

In this method, to perform the Fourier transform of $\mathcal{G}(\tau', \tau'')$ (or for the QMC Green's function $\widetilde{G}(\tau', \tau'')$) we construct a new Green's function $\overline{\mathcal{G}}(\tau+\tau'', \tau'')$ (or inside the QMC block, $\overline{G}(\tau+\tau'', \tau'')$) whose discontinuities are shifted to the boundaries, i.e., at $\tau = 0$ and $\tau = \beta$ (See Fig. 5.7).

$$\overline{\mathcal{G}}_{\alpha_i\alpha_j}(\tau+\tau'', \tau'') = \begin{cases} \mathcal{G}_{\alpha_i\alpha_j}(\tau+\tau'', \tau'') & \text{for } \tau+\tau'' < \beta \\ -\mathcal{G}_{\alpha_i\alpha_j}(\tau+\tau''-\beta, \tau'') & \text{for } \tau+\tau'' \geq \beta \end{cases}, \tag{5.67}$$

where $\overline{\mathcal{G}}(\tau+\tau'', \tau'')$ is β-periodic in τ'' and β-antiperiodic in τ.

The Fourier transform of $\mathcal{G}$ can be expressed as a function of $\overline{\mathcal{G}}$ as follows (See Fig. 5.8)

$$\begin{aligned} \mathcal{G}_{\alpha_i\alpha_j}(\nu_n, \nu_{n'}) &= \int_0^\beta d\tau' \int_0^\beta d\tau''\, e^{i\nu_n\tau'} e^{-i\nu_{n'}\tau''} \mathcal{G}_{\alpha_i\alpha_j}(\tau+\tau'', \tau'') \\ &= \int_0^\beta d\tau'' e^{i(\nu_n-\nu_{n'})\tau''} \int_{-\tau''}^{\beta-\tau''} d\tau\, e^{i\nu_n\tau}\, \mathcal{G}_{\alpha_i\alpha_j}(\tau+\tau'', \tau'') \\ &= \int_0^\beta d\tau \int_0^\beta d\tau''\, e^{i\nu_n\tau} e^{i(\nu_n-\nu_{n'})\tau''}\, \overline{\mathcal{G}}_{\alpha_i\alpha_j}(\tau+\tau'', \tau''). \end{aligned} \tag{5.68}$$

To calculate this integral, we use two dimensional Filon-trapezoidal approximation. We split the interval $[0, \beta]$ in L time slices $\tau_l = l\Delta\tau$ with $l = 1, ..., L+1$, $\Delta\tau = \beta/L$ and approximate $\overline{\mathcal{G}}(\tau+\tau'', \tau'')$ by a piecewise polynomial function in the interval $\tau \in [\tau_l, \tau_l + \Delta\tau]$

$$\begin{aligned} \overline{\mathcal{G}}(\tau+\tau'', \tau'') \sim\ & \overline{\mathcal{G}}_{l_1,l_2} + \frac{(\tau-\tau_l)}{\Delta\tau}\left(\overline{\mathcal{G}}_{l_1+1,l_2} - \overline{\mathcal{G}}_{l_1,l_2}\right) + \frac{(\tau''-\tau_{l_2})}{\Delta\tau}\left(\overline{\mathcal{G}}_{l_1,l_2+1} - \overline{\mathcal{G}}_{l_1,l_2}\right) \\ & + \frac{(\tau-\tau_{l_1})(\tau''-\tau_{l_2})}{\Delta\tau^2}\left(\overline{\mathcal{G}}_{l_1+1,l_2+1} - \overline{\mathcal{G}}_{l_1+1,l_2} - \overline{\mathcal{G}}_{l_1,l_2+1} + \overline{\mathcal{G}}_{l_1,l_2}\right) + ..., \end{aligned} \tag{5.69}$$

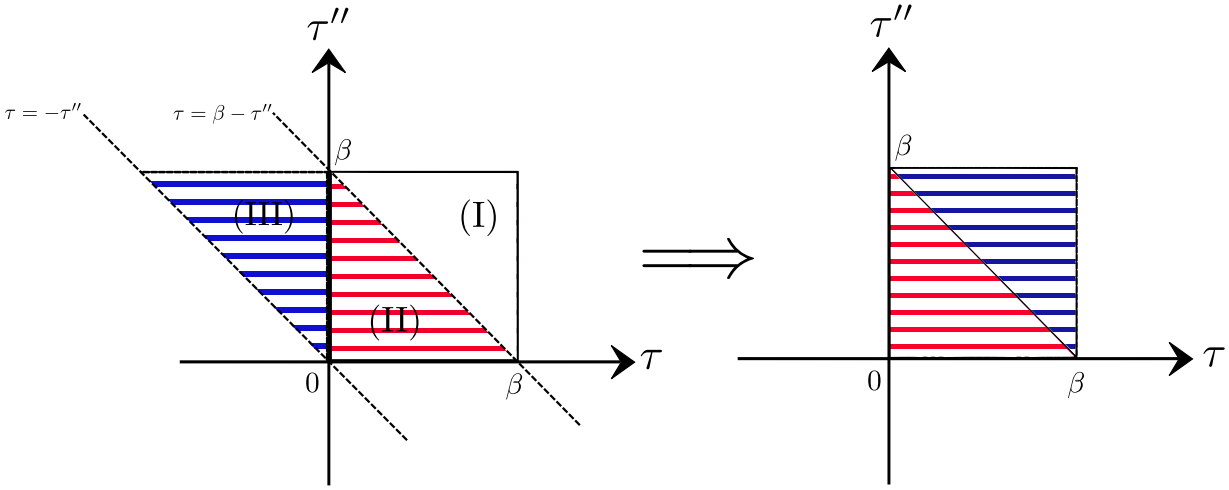

Figure 5.8: Integration area of the Fourier transform of the Green's function. The Green's function in the area (I) is $-\mathcal{G}(-\beta+\tau+\tau'',\tau'')$ and in the (II) and (III) area $\mathcal{G}(\tau+\tau'',\tau'')$ (left figure). Therefore, by using definition (5.67) we can use the integration area $\tau,\tau''\in[0,\beta]$ (right figure).

where $\overline{\mathcal{G}}_{l_1,l_2}=\overline{\mathcal{G}}(\tau_{l_1}+\tau_{l_2},\tau_{l_2})$. Through this approximation, we find

$$\begin{aligned}\mathcal{G}_{\alpha_i\alpha_j}(\nu_n,\nu_{n'}) &\approx \sum_{l_1=1}^{L}\sum_{l_2=1}^{L}\int_{\tau_{l_1}}^{\tau_{l_2}} d\tau \int_{\tau''_{l_2}}^{\tau''_{l_2}+1} d\tau'' e^{i\nu_n\tau} e^{i(\nu_n-\nu_{n'})\tau''}\ \overline{\mathcal{G}}_{\alpha_i\alpha_j}(\tau+\tau'',\tau'')\\ &\approx \sum_{l_1=1}^{L+1}\sum_{l_2=1}^{L+1} w_{l_1}(\theta_1)w_{l_2}(\theta_2)e^{i\nu_n\tau_{l_1}}e^{i(\nu_n-\nu_{n'})\tau_{l_2}}\ \overline{\mathcal{G}}_{\alpha_i\alpha_j}(\tau_{l_1}+\tau_{l_2},\tau_{l_2}),\end{aligned} \tag{5.70}$$

where $\theta_1=\Delta\tau\nu_n$, $\theta_2=\Delta\tau(\nu_n-\nu_{n'})$ and

$$w_l(\theta)=\begin{cases} w_0(\theta)=\Delta\tau\left[\dfrac{1+i\theta-e^{i\theta}}{\theta^2}\right] & l=0\\ w_{L+1}(\theta)=w_0(-\theta) & l=L+1\\ w(\theta)\equiv w_0(\theta)+w_{L+1}(\theta) & l\neq 1,L+1\end{cases}, \tag{5.71}$$

Using properties of the Green's function at boundaries, we can simplify Eq. (5.70) as follows (See Appendix F.3 for more details)

$$\begin{aligned}\mathcal{G}_{\alpha_i\alpha_j}(\nu_n,\nu_{n'}) &\approx w(\theta_1)w(\theta_2)\sum_{l_1=1}^{L}\sum_{l_2=1}^{L} e^{i\nu_n\tau_{l_1}}e^{i(\nu_n-\nu_{n'})\tau_{l_2}}\ \overline{\mathcal{G}}_{\alpha_i\alpha_j}(\tau_{l_1}+\tau_{l_2},\tau_{l_2})\\ &\quad +w_{L+1}(\theta_1)\beta\delta_{nn'}\delta_{\alpha_i,\alpha_j}.\end{aligned} \tag{5.72}$$

To derive this equation, we used an analytic relation for the delta function $\delta_{nn'}$.

$$\beta\delta_{nn'}=\int_0^\beta d\tau\ e^{i(\nu_n-\nu_{n'})\tau}w(\theta_2)\approx\sum_{l=1}^{L}e^{i(\nu_n-\nu_{n'})\tau_l}. \tag{5.73}$$

In Eq. (5.71), we can show that the coefficient $w(\theta)$ is real and is given by

$$w(\theta) = w_0(\theta) + w_{L+1}(\theta) = \Delta\tau \left(\frac{\sin(\theta/2)}{\theta/2}\right)^2. \tag{5.74}$$

For $\theta_2 = \Delta\tau(\nu_n - \nu_{n'})$, due to numerical reasons, we consider

$$w(\theta_2) = \Delta\tau \times \begin{cases} 1 - \dfrac{\theta_2^2}{12} + \dfrac{\theta_2^4}{360} - \dfrac{\theta_2^6}{20160} + \ldots & \text{for } \theta_2 \to 0 \\ \left(\dfrac{\sin(\theta_2/2)}{\theta_2/2}\right)^2 & \text{otherwise} \end{cases}. \tag{5.75}$$

Similar relation can be obtained for the QMC Green's function $\widetilde{G}$ inside the QMC block.

$$\begin{aligned} \widetilde{G}_{\alpha_i\alpha_j}(\nu_n, \nu_{n'}) \;\approx\; & w(\theta_1)w(\theta_2) \sum_{l_1=1}^{L}\sum_{l_2=1}^{L} e^{i\nu_n\tau_{l_1}} e^{i(\nu_n-\nu_{n'})\tau_{l_2}}\, \overline{G}_{\alpha_i\alpha_j}(\tau_{l_1}+\tau_{l_2}, \tau_{l_2}) \\ & -w_{L+1}(\theta_1)\beta\delta_{nn'}\delta_{\alpha_i,\alpha_j}. \end{aligned} \tag{5.76}$$

Thanks to the shift of the singularities to the border because we can automatically recover the proper limit at equal times[5]

$$\overline{\mathcal{G}}_{\alpha_i\alpha_j}(\tau+\tau'', \tau'') \longrightarrow \overline{\mathcal{G}}_{\alpha_i\alpha_j}(0^+, 0),$$

as well as the correct $1/i\nu_n$ decay of the Green's function. This is shown in Fig. 5.9 for a test case. The last point about this method is that we can construct the new Green's function $\overline{\mathcal{G}}(\tau', \tau+\tau')$ by

$$\overline{\mathcal{G}}_{\alpha_i\alpha_j}(\tau', \tau+\tau') = \begin{cases} \mathcal{G}_{\alpha_i\alpha_j}(\tau', \tau+\tau') & \text{for } \tau+\tau' < \beta \\ -\mathcal{G}_{\alpha_i\alpha_j}(\tau', \tau+\tau'-\beta) & \text{for } \tau+\tau' \geq \beta \end{cases},$$

where at equal times

$$\overline{\mathcal{G}}_{\alpha_i\alpha_j}(\tau', \tau+\tau') \longrightarrow \overline{\mathcal{G}}_{\alpha_i\alpha_j}(0, 0^+).$$

Using this choice of the new Green's function, we obtain the same results for the Fourier transform of the Green's function $\mathcal{G}(\nu_n, \nu_{n'})$ if we use

$$\begin{aligned} \mathcal{G}_{\alpha_i\alpha_j}(\nu_n, \nu_{n'}) \;\approx\; & \sum_{l_1=1}^{L+1}\sum_{l_2=1}^{L+1} w_{l_1}(\theta_1)w_{l_2}(\theta_2) e^{-i\nu_{n'}\tau_{l_1}} e^{-i(\nu_{n'}-\nu_n)\tau_{l_2}}\, \overline{\mathcal{G}}_{\alpha_i\alpha_j}(\tau_{l_2}, \tau_{l_1}+\tau_{l_2}) \\ \approx\; & w(\theta_1)w(\theta_2) \sum_{l_1=1}^{L}\sum_{l_2=1}^{L} e^{-i\nu_{n'}\tau_{l_1}} e^{-i(\nu_{n'}-\nu_n)\tau_{l_2}}\, \overline{\mathcal{G}}_{\alpha_i\alpha_j}(\tau_{l_2}, \tau_{l_1}+\tau_{l_2}) \\ & +w_{L+1}(-\theta_1)\beta\delta_{nn'}\delta_{\alpha_i,\alpha_j}. \end{aligned} \tag{5.77}$$

Comparing with Eq. (5.72), ν_n and $\nu_{n'}$ are changed to $-\nu_{n'}$ and $-\nu_n$, respectively.

[5] The behavior of the Green's function at equal time is crucial in calculating the two-particle correlation function due to the time ordering operator in the correlation function. Using this method, we do not obsess with time ordering of the Green's function at $\tau = \tau'$.

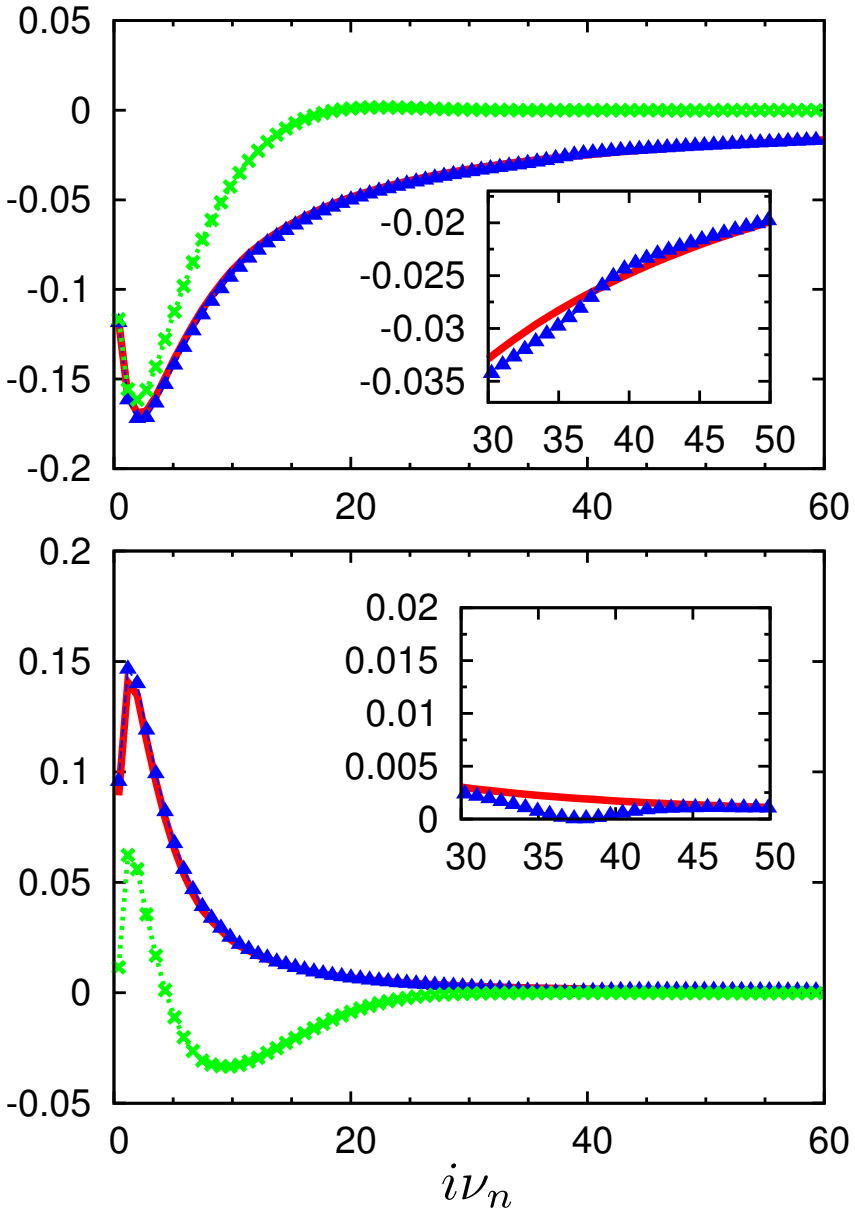

Figure 5.9: Fourier transform of a typical Green's function. Top: Imaginary part. Bottom: Real part. Solid line: $\mathcal{G}(\nu_n)$ calculated via a spline at the end of the QMC run; this is the numerically exact result. Crosses: $\frac{1}{\beta}\mathcal{G}(\nu_n, \nu_n)$ calculated via direct Fourier transform of $\mathcal{G}(\tau', \tau'')$ without shifting the singularities to the border, leading to an incorrect high-frequency behavior. Triangles: Fourier transform of $\overline{\mathcal{G}}(\tau + \tau'', \tau'')$ in which the singularities have been moved to the border via the Filon-trapezoidal method. The results shown are for $\beta = 8\ \mathrm{eV}^{-1}$ and $L = 48$, $\Delta\tau \sim 0.17$. The error remains small (at most 5%) even for $\Delta\tau$ as large as ~ 0.33. The insets show the small deviations between the Filon-trapezoidal calculation and the exact result. The systematic numerical error of Fourier transform of $\mathcal{G}(\tau)$ by using the Filon-trapezoidal method is the same as the Fourier transform of the $\mathcal{G}(\tau, \tau')$ while we transfer its discontinuities to the border.

5.3.4.1 Discussion and results

The Fourier transform based on the Filon-trapezoidal deviates from the exact result at $\nu_n = 2\pi M\Delta\tau$ and $\nu_{n'} + 2\pi M\Delta\tau$ where $M = 1, 2, 3, ...$ However, for a typical values of $\Delta\tau = \beta/L$, because of the pre-factor $w(\theta_1)w(\theta_2)$, the Green's function $\mathcal{G}(i\nu_n, i\nu_n)$ is already small at these frequencies; this is shown in the insets of Fig. 5.9. Furthermore, we found that this method gives us enough accurate results for the Fourier integral of the 2D Green's function, $\mathcal{G}_{\alpha_i\alpha_j}(\tau, \tau')$, in order to calculate the *local susceptibility* using QMC. The error of the calculated $\mathcal{G}_{\alpha_i\alpha_j}(\nu_n, \nu_{n'})$ with this method is almost equal to those errors which come from computing the Fourier transform of $\mathcal{G}_{\alpha_i\alpha_j}(\tau)$ via the direct Filon-trapezoidal method. Moreover, to obtain $\mathcal{G}_{\alpha_i\alpha_j}(\nu_n, \nu_{n'})$, we need to do $2(N_\nu + N_\omega)^2 N_O^2 N_S^2 N_\tau^2$ operations. In comparison with the 3rd method [64], method number 4 is preferable to calculate the local susceptibility because it is faster at low temperature and (or) large Coulomb interaction (where we need to consider more Monte Carlo sweeps to calculate the Green's function and therefore the local susceptibility) and (or) multi-orbitals and -sites systems. Therefore, *we adopt method 4 to calculate the local susceptibility*.

5.4 Computing *local* susceptibility using Hirsch-Fye QMC

Our strategy for calculating the local susceptibility is as follows. First, we compute two-particle correlation function in Matsubara frequency space inside the QMC block. Then, we extract the continuous part of the two-particle Green's function $\gamma(\nu_n, \nu_{n'}; \omega_m)$ by subtracting the non-interacting two-particle correlation function $\mathcal{C}^0(\nu_n, \nu_{n'}; \omega_m)$ from fully interacting one $\mathcal{C}(\nu_n, \nu_{n'}; \omega_m)$ as it is described in Eq. (4.72). This is a very crucial step. The numerical errors appeared in the Fourier transformed of the $\mathcal{C}(\nu_n, \nu_{n'}; \omega_m)$ due to discontinuities in $\langle c^\dagger(\tau_1)c(\tau_2)c^\dagger(\tau_3)c(\tau_4)\rangle$ are canceled. In the last step, after QMC, we compute the $\mathcal{C}^0(\nu_n, \nu_{n'}; \omega_m) \sim \mathcal{G}(\nu_n)\mathcal{G}(\nu_n + \omega_m)$ to obtain the local susceptibility where it can be done using very precise numerical method named spline[6] [65].

5.4.1 Two-particle correlation function *inside QMC block*

In the Hirsch-Fye QMC impurity solver, the auxiliary Ising fields $\{\mathbf{s}\} = s_1 s_2 ... s_L$ are used to decouple the interaction term in the Hamiltonian. Therefore, fermions in the two-particle correlation function $\left\langle \mathcal{T} c^\dagger_{i\sigma}(\tau_1)c_{j\sigma}(\tau_2)c^\dagger_{k\sigma'}(\tau_3)c_{l\sigma'}(\tau_4)\right\rangle$ interact only with the auxiliary fields so that the Wick's theorem is hold for a fixed QMC configuration. For this reason, we can rewrite the *local* two-particle correlation function with respect to the product of two single particle correla-

[6] Since after QMC block we have the physical Green's function $\mathcal{G}(\tau, \tau')$ which is equal to $\mathcal{G}(\tau - \tau')$, we can use a very precise method called spline to calculate the Fourier transform of the 1D Green's function. We are not worried about the CPU time to do it, because the time consuming part, i.e., computation of the local susceptibility, is already done.

tion function [10, 12].

$$\begin{aligned}
\mathcal{C}^{\sigma\sigma'}_{ijkl} &= \left\langle \mathcal{T} c^{\dagger}_{i\sigma}(\tau_1) c_{j\sigma}(\tau_2) c^{\dagger}_{k\sigma'}(\tau_3) c_{l\sigma'}(\tau_4) \right\rangle \\
&= \frac{1}{N_c} \sum_{\{\mathbf{s}\}} \left\langle \mathcal{T} c^{\dagger}_{i\sigma}(\tau_1) c_{j\sigma}(\tau_2) c^{\dagger}_{k\sigma'}(\tau_3) c_{l\sigma'}(\tau_4) \right\rangle_{\{\mathbf{s}\}} \\
&= \frac{1}{N_c} \sum_{\{\mathbf{s}\}} \Bigg\{ \left\langle \mathcal{T} c^{\dagger}_{i\sigma}(\tau_1) c_{j\sigma}(\tau_2) \right\rangle \left\langle \mathcal{T} c^{\dagger}_{k\sigma'}(\tau_3) c_{l\sigma'}(\tau_4) \right\rangle \\
&\quad - \delta_{\sigma\sigma'} \left\langle \mathcal{T} c_{l\sigma'}(\tau_4) c^{\dagger}_{i\sigma}(\tau_1) \right\rangle \left\langle \mathcal{T} c_{j\sigma}(\tau_2) c^{\dagger}_{k\sigma'}(\tau_3) \right\rangle \Bigg\}_{\{\mathbf{s}\}} \\
&= \frac{1}{N_c} \sum_{\{\mathbf{s}\}} \left\{ \widetilde{G}^{\sigma}_{ji}(\tau_2, \tau_1) \widetilde{G}^{\sigma'}_{lk}(\tau_4, \tau_3) - \delta_{\sigma\sigma'}\, \widetilde{G}^{\sigma'}_{li}(\tau_4, \tau_1) \widetilde{G}^{\sigma}_{jk}(\tau_2, \tau_3) \right\}_{\{\mathbf{s}\}} \\
&= \frac{1}{N_c} \sum_{\{\mathbf{s}\}} \left\{ \widetilde{\mathcal{C}}^{\sigma\sigma'}_{ijkl}(\tau_1, \tau_2, \tau_3, \tau_4) \right\}_{\{\mathbf{s}\}}, \qquad (5.78)
\end{aligned}$$

where $\mathcal{C}$ is the physical *local* two-particle correlation function, $\widetilde{\mathcal{C}}$ the *local* two-particle correlation function for *only* one QMC configuration, i, j, k, l orbitals, σ, σ' spins, N_c number of all accepted QMC configurations and $\{\mathbf{s}\}$ are Ising auxiliary fields. In this relation, the atomic sites κ and momenta $\mathbf{k}, \mathbf{k}'$ are ignored because we are interested in calculating a local quantity (the local susceptibility) within LDA+DMFT. We notice that the QMC Green's function $\widetilde{G}(\tau, \tau')$ is not time translational invariant.

$$\widetilde{G}(\tau, \tau') \neq \widetilde{G}(\tau - \tau').$$

Due to numerical problems,[7] it is preferable to calculate the Fourier transform of the two-particle correlation function *inside* the QMC block [64].

$$\boxed{\begin{aligned}
\widetilde{\mathcal{C}}^{\sigma\sigma'}_{ijkl}(\nu_n, \nu_{n'}; \omega_m) &= \widetilde{G}^{\sigma}_{ji}(\nu_n + \omega_m, \nu_n) \widetilde{G}^{\sigma'}_{lk}(\nu_{n'}, \nu_{n'} + \omega_m) \\
&\quad - \delta_{\sigma\sigma'}\, \widetilde{G}^{\sigma'}_{li}(\nu_{n'}, \nu_n) \widetilde{G}^{\sigma}_{jk}(\nu_n + \omega_m, \nu_{n'} + \omega_m),
\end{aligned}} \qquad (5.79)$$

where the Fourier transform of each QMC Green's function is performed by shifting it's discontinuities to borders (Eq. (5.76)) followed by these relations.

$$\begin{aligned}
\widetilde{G}^{\sigma'}_{li}(\nu_{n'}, \nu_n) &= \int_0^\beta \int_0^\beta d\tau_1\, d\tau'_4\, e^{-i(\nu_n - \nu_{n'})\tau_1} e^{i\nu_n \tau'_4}\, \widetilde{G}^{\sigma'}_{li}(\tau'_4 + \tau_1, \tau_1), \\
\widetilde{G}^{\sigma}_{jk}(\nu_n + \omega_m, \nu_{n'} + \omega_m) &= \int_0^\beta \int_0^\beta d\tau'_2\, d\tau_3\, e^{i(\nu_n - \nu_{n'})\tau_3} e^{i(\nu_n + \omega_m)\tau'_2}\, \widetilde{G}^{\sigma}_{jk}(\tau'_2 + \tau_3, \tau_3), \\
\widetilde{G}^{\sigma}_{ji}(\nu_n + \omega_m, \nu_n) &= \int_0^\beta \int_0^\beta d\tau_1\, d\tau'_2\, e^{i\omega_m \tau_1} e^{i(\nu_n + \omega_m)\tau'_2}\, \widetilde{G}^{\sigma}_{ji}(\tau_1 + \tau'_2, \tau_1), \\
\widetilde{G}^{\sigma'}_{lk}(\nu_{n'}, \nu_{n'} + \omega_m) &= \int_0^\beta \int_0^\beta d\tau_3\, d\tau'_4\, e^{-i(\nu_{n'} + \omega_m)\tau_3} e^{-i\omega_m \tau'_4}\, \widetilde{G}^{\sigma'}_{lk}(\tau_3 + \tau'_4, \tau_3).
\end{aligned}$$

[7] The first numerical problem is related to computational random access memory to store the huge array of two particle correlation function. The second problem is that the Fourier integral of the two-particle correlation function $\mathcal{C}$ has large numerical errors due to its discontinuities and non-analytic points. However, if we proceed to do Fourier integral inside the QMC, we are dealing with Fourier integral of the QMC Green's function $\widetilde{G}(\tau, \tau')$ with discontinuities at $\tau = \tau'$ which can be transferred in boundaries in order to decrease numerical errors of Fourier transform.

Inside the QMC block, *if the local Hamiltonian is real*, we can prove that the two-particle correlation function *for a fixed configuration* can be obtained by (see appendix F.4)

$$\widetilde{\chi}^{\sigma\sigma'}_{ijkl}(\nu_n,\nu_{n'};\omega_m) \equiv \frac{1}{2}\left(\widetilde{\mathcal{C}}^{\sigma\sigma'}_{ijkl}(\nu_n,\nu_{n'};\omega_m) + \widetilde{\mathcal{C}}^{\sigma'\sigma}_{lkji}(\nu_{n'},\nu_n;\omega_m)\right). \tag{5.80}$$

This relation guarantees that the property of the *physical* (local) two-particle correlation function in Eq. (4.101) holds. Therefore, for a system with *real local Hamiltonian*, we can use the following relation to compute the *local* two-particle correlation function.

$$\begin{aligned}\widetilde{\chi}^{\sigma\sigma'}_{ijkl}(\nu_n,\nu_{n'};\omega_m) &= -\frac{1}{2}\delta_{\sigma\sigma'}\Big\{\widetilde{G}^{\sigma'}_{li}(\nu_{n'},\nu_n)\widetilde{G}^{\sigma}_{jk}(\nu_n+\omega_m,\nu_{n'}+\omega_m)\\ &\quad +\widetilde{G}^{\sigma}_{il}(\nu_n,\nu_{n'})\widetilde{G}^{\sigma'}_{kj}(\nu_{n'}+\omega_m,\nu_n+\omega_m)\Big\}\\ &+ \frac{1}{2}\Big\{\widetilde{G}^{\sigma}_{ji}(\nu_n+\omega_m,\nu_n)\widetilde{G}^{\sigma'}_{lk}(\nu_{n'},\nu_{n'}+\omega_m)\Big\}\\ &\quad +\widetilde{G}^{\sigma'}_{kl}(\nu_{n'}+\omega_m,\nu_{n'})\widetilde{G}^{\sigma}_{ij}(\nu_n,\nu_n+\omega_m)\Big\}.\end{aligned} \tag{5.81}$$

In order to decrease CPU time of computing the *local* two-particle correlation function, we can use the following properties.

$$\widetilde{\chi}^{\sigma\sigma'}_{ijkl}(-\nu_n,-\nu_{n'};-\omega_m) = \left[\widetilde{\chi}^{\sigma\sigma'}_{ijkl}(\nu_n,\nu_{n'};\omega_m)\right]^*, \tag{5.82}$$

$$\widetilde{\chi}^{\sigma\sigma'}_{ijkl}(\nu_n,\nu_{n'};\omega_m) = \widetilde{\chi}^{\sigma'\sigma}_{lkji}(\nu_{n'},\nu_n;\omega_m), \qquad \text{for real local Hamiltonian} \tag{5.83}$$

Using these properties, we can compute $\widetilde{\chi}^{\sigma\sigma'}_{ijkl}(\nu_n,\nu_{n'};\omega_m)$ for $-N_\nu-1\le n\le N_\nu$, $n\le n'\le N_\nu$ and $m\ge 0$, i.e., for half of the all values of Matsubara frequencies (see Fig. 5.10).

5.4.2 Continuous part of the two-particle correlation function (after QMC)

After QMC block, the physical two-particle correlation function in Matsubara space is obtained by an average over all QMC configurations.

$$\begin{aligned}\mathcal{C}^{\sigma\sigma'}_{ijkl}(\nu_n,\nu_{n'};\omega_m) &= \left\langle\widetilde{\mathcal{C}}^{\sigma\sigma'}_{ijkl}(\nu_n,\nu_{n'};\omega_m)\right\rangle_{\rm MC},\\ &= \left\langle\widetilde{\chi}^{\sigma\sigma'}_{ijkl}(\nu_n,\nu_{n'};\omega_m)\right\rangle_{\rm MC} \qquad \text{For real local Hamiltonian.}\end{aligned} \tag{5.84}$$

Since the *local* two-particle correlation function has discontinuities which are present implicitly in its non-interacting part, numerical errors may appear in the Fourier transform of the *local* two-particle correlation function $\mathcal{C}^{\sigma\sigma'}_{ijkl}(\nu_n,\nu_{n'};\omega_m)$. In order to decrease the numerical errors, the trick is that we subtract the non-interacting *local* two-particle correlation function from the fully interacting one to extract the continuous part as follows.

$$\boxed{\begin{aligned}\gamma^{\sigma\sigma'}_{ijkl}(\nu_n,\nu_{n'};\omega_m) &= \left\langle\widetilde{\mathcal{C}}^{\sigma\sigma'}_{ijkl}(\nu_n,\nu_{n'};\omega_m)\right\rangle_{\rm MC}\\ &\quad -\left\langle\widetilde{G}^{\sigma}_{ji}(\nu_n+\omega_m,\nu_n)\right\rangle_{\rm MC}\left\langle\widetilde{G}^{\sigma'}_{lk}(\nu_{n'},\nu_{n'}+\omega_m)\right\rangle_{\rm MC}\\ &\quad +\delta_{\sigma\sigma'}\left\langle\widetilde{G}^{\sigma'}_{li}(\nu_{n'},\nu_n)\right\rangle_{\rm MC}\left\langle\widetilde{G}^{\sigma}_{jk}(\nu_n+\omega_m,\nu_{n'}+\omega_m)\right\rangle_{\rm MC}.\end{aligned}} \tag{5.85}$$

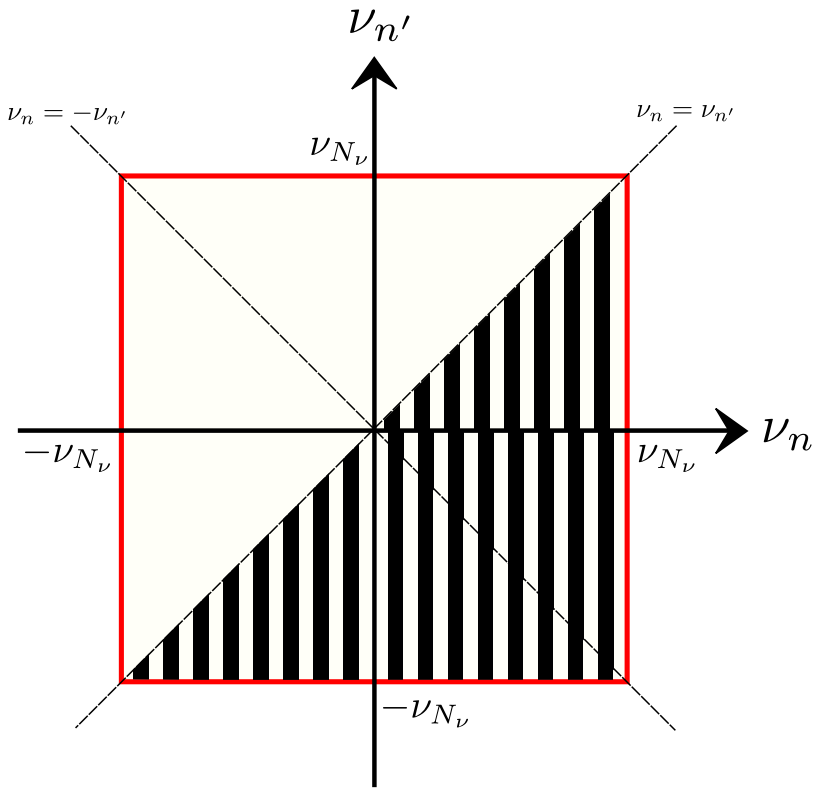

Figure 5.10: For numerical calculation, we can save CPU time by computing χ for half of the frequencies (shaded area) and $m \geq 0$. The rest is obtained by using the properties of the two-particle correlation function.

In this way, some numerical errors arising from discontinuities in one- and two-particle correlation function are canceled specially along the $\nu_n = \nu_{n'}$. In this equation, we emphasize that the $\widetilde{G}(\nu_n, \nu_{n'})$ is computed inside the QMC by the Filon-trapezoid method when the two-particle correlation function is simultaneously computed.

5.4.3 The local susceptibility (after QMC)

Using the Hirsch-Fye QMC, we can also calculate the local Green's function $\mathcal{G}^{\sigma}_{ij}(\tau)$ in imaginary time space. The Fourier integral of the $\mathcal{G}^{\sigma}_{ij}(\tau)$ can be evaluated by *spline* accurately. For this reason, the non-interacting part of the *local* two-particle correlation function (Eq. (4.104)) can be calculated precisely.

$$\begin{aligned} \mathcal{C}^{0,\sigma\sigma'}_{ijkl}(\nu_n, \nu_{n'}; \omega_m) &= -\beta^2 \delta_{nn'} \delta_{\sigma\sigma'} \mathcal{G}^{\sigma'}_{li}(\nu_n) \mathcal{G}^{\sigma}_{jk}(\nu_n + \omega_m) \\ &\quad + \beta^2 \delta_{m,0}\, \mathcal{G}^{\sigma}_{ji}(\nu_n + \omega_m) \mathcal{G}^{\sigma'}_{lk}(\nu_{n'}). \end{aligned} \tag{5.86}$$

Also, according to Eq. (4.106), the fully interacting part (or continuous part) of the susceptibility is equal to the difference of $\mathcal{C}$ and $\mathcal{C}^0$. Therefore,

$$\boxed{\begin{aligned} \chi^{\sigma\sigma'}_{ijkl}(\nu_n, \nu_{n'}; \omega_m) &= \gamma^{\sigma\sigma'}_{ijkl}(\nu_n, \nu_{n'}; \omega_m) + \chi^{\mathbf{0},\sigma\sigma'}_{ijkl}(\nu_n, \nu_{n'}; \omega_m) \\ &= \gamma^{\sigma\sigma'}_{ijkl}(\nu_n, \nu_{n'}; \omega_m) - \beta^2 \delta_{nn'} \delta_{\sigma\sigma'} \mathcal{G}^{\sigma'}_{li}(\nu_n) \mathcal{G}^{\sigma}_{jk}(\nu_n + \omega_m). \end{aligned}} \tag{5.87}$$

From this relation, we are able to obtain the *local* spin and charge susceptibility by considering the *vertex factors* in Eq. (4.44) and (4.63).

$$\chi^{zz}(\omega_m) = \frac{1}{\beta}\frac{1}{4}(g\mu_B)^2 \sum_{\sigma\sigma'} \sigma\sigma' \sum_{ijkl} \delta_{ij}\delta_{kl} \frac{1}{\beta^2} \sum_{nn'} \chi^{\sigma\sigma'}_{ijkl}(\nu_n, \nu_{n'}; \omega_m), \tag{5.88}$$

$$\chi^{ch}(\omega_m) = \frac{1}{\beta}\frac{1}{4} \sum_{\sigma\sigma'} \sum_{ijkl} \delta_{ij}\delta_{kl} \frac{1}{\beta^2} \sum_{nn'} \chi^{\sigma\sigma'}_{ijkl}(\nu_n, \nu_{n'}; \omega_m). \tag{5.89}$$

In *paramagnetic systems*, for calculating the $\mathbf{q}$-dependent spin and charge susceptibility $\chi(\mathbf{q}, \omega_m)$ by using the local vertex approximation, we need the following quantities to obtain the local vertex function from Eqs. (4.47) and (4.65).[8]

$$\begin{cases} \chi^{s}_{ijkl}(\nu_n, \nu_{n'}; \omega_m) = \frac{1}{\beta}\frac{1}{4}(g\mu_B)^2 \sum_{\sigma\sigma'} \sigma\sigma' \ \chi^{\sigma\sigma'}_{ijkl}(\nu_n, \nu_{n'}; \omega_m) \\ \chi^{\mathbf{0},s}_{ijkl}(\nu_n, \nu_{n'}; \omega_m) = -\beta\delta_{nn'}\frac{1}{4}(g\mu_B)^2 \sum_{\sigma} \mathcal{G}^{\sigma}_{li}(\nu_n)\mathcal{G}^{\sigma}_{jk}(\nu_n + \omega_m) \end{cases}, \tag{5.90}$$

and for the charge susceptibility,

$$\begin{cases} \chi^{c}_{ijkl}(\nu_n, \nu_{n'}; \omega_m) = \frac{1}{\beta}\frac{1}{4} \sum_{\sigma\sigma'} \sigma\sigma' \ \chi^{\sigma\sigma'}_{ijkl}(\nu_n, \nu_{n'}; \omega_m) \\ \chi^{\mathbf{0},c}_{ijkl}(\nu_n, \nu_{n'}; \omega_m) = -\beta\delta_{nn'}\frac{1}{4} \sum_{\sigma} \mathcal{G}^{\sigma}_{li}(\nu_n)\mathcal{G}^{\sigma}_{jk}(\nu_n + \omega_m) \end{cases}. \tag{5.91}$$

5.4.3.1 QMC results of local magnetic response function

As a case study, we consider a single band model at half-filling. we calculate the local spin susceptibility $\chi^s(\nu_n, \nu_{n'}; \omega_m)$ and it's fully interacting part, i.e., $\gamma^s(\nu_n, \nu_{n'}; \omega_m)$ at zero bosonic frequency ($\omega_m = 0$). In Fig. 5.11, we present $\Re e[\chi^s]$ and $\Re e[\gamma^s] = \Re e[\chi^s - \chi^{\mathbf{0},s}]$. At $\nu_n = \nu_{n'}$, the non-interacting spin susceptibility $\chi^{\mathbf{0},s}$ mainly contributes to the χ^s plot. For this reason, in γ^s plot, diagonal term is almost zero. The other point about χ plot is that $\Re e[\chi^s]$ decays fast unless along $\nu_n = \nu_{n'}$, $\nu_n = 0$ ($\forall\nu_{n'}$) and $\nu_{n'} = 0$ ($\forall\nu_n$). This is also true for $\Im m[\chi^s]$ and $\Im m[\gamma^s]$ shown in Fig. 5.12. But the imaginary part of the spin susceptibility decays faster than the real part one. This can be inferred from high frequency behavior of χ in Eq. (4.113). Along $\nu_n = \nu_{n'}$, asymptotic behavior of the $\Re e[\chi^s]$ and $\Im m[\chi^s]$ are $\sim 1/\nu_n^2$ and $\sim 1/\nu_n^3$ respectively.

Slow decays in the susceptibility $\chi^s(\nu_n, \nu_{n'}; \omega_0)$ plots are consequences of discontinuities and non-analytic points (kinks) in the $\chi^s(\tau_1, \tau_2, \tau_3, \tau_4)$ (see Figs. 4.9, 4.10a, 4.10b). So discontinuities along $\tau_2 = \tau_3$ and $\tau_1 = \tau_4$ result slow decays at $\nu_n = \nu_{n'}$ (typically $\sim 1/\nu_n^2$) and kinks at $\tau_1 = \tau_2$ and $\tau_3 = \tau_4$ yield decays along $\nu_n = 0$ ($\forall\nu_{n'}$) and $\nu_{n'} = 0$ ($\forall\nu_n$), respectively.

[8] The coefficient $1/N_S = 1$ because χ^s and $\chi^{\mathbf{0},s}$ in Eq. (5.90) are local quantities and for local quantities $N_S = 1$.

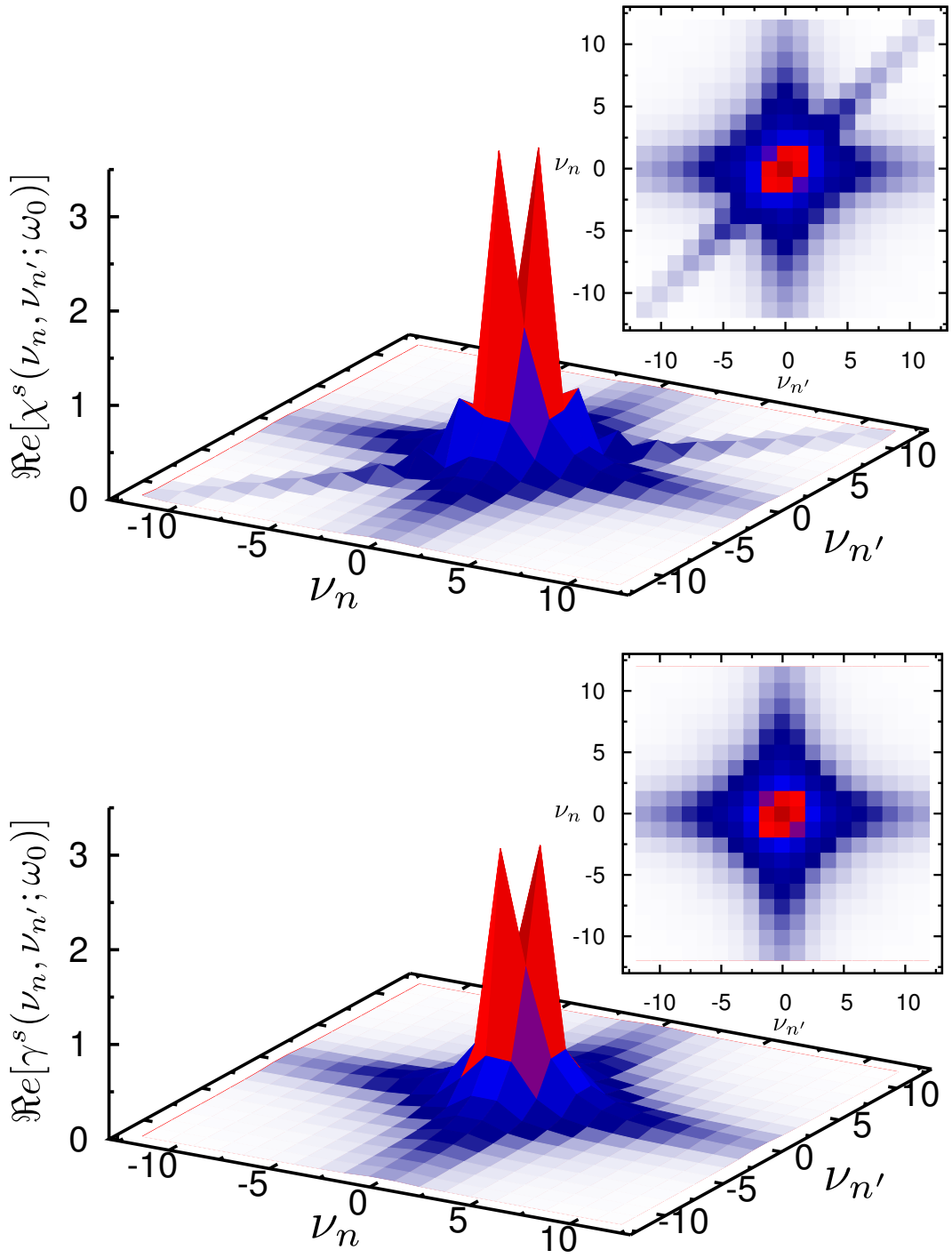

Figure 5.11: Real part of the spin local susceptibility (top) and continuous part (or fully interacting part) of the spin susceptibility (bottom) for a single band system $VOMoO_4$ at $U = 2$ eV, $\beta = 5$ eV^{-1} and $\Delta\tau \sim 0.33$. Slow decay along $\nu_n = \nu_{n'}$ comes from the non-interacting part of the spin susceptibility contribution, i.e., bare local spin susceptibility ($\chi^{\mathbf{0},s}$) which is zero in the fully interacting part (bottom plot).

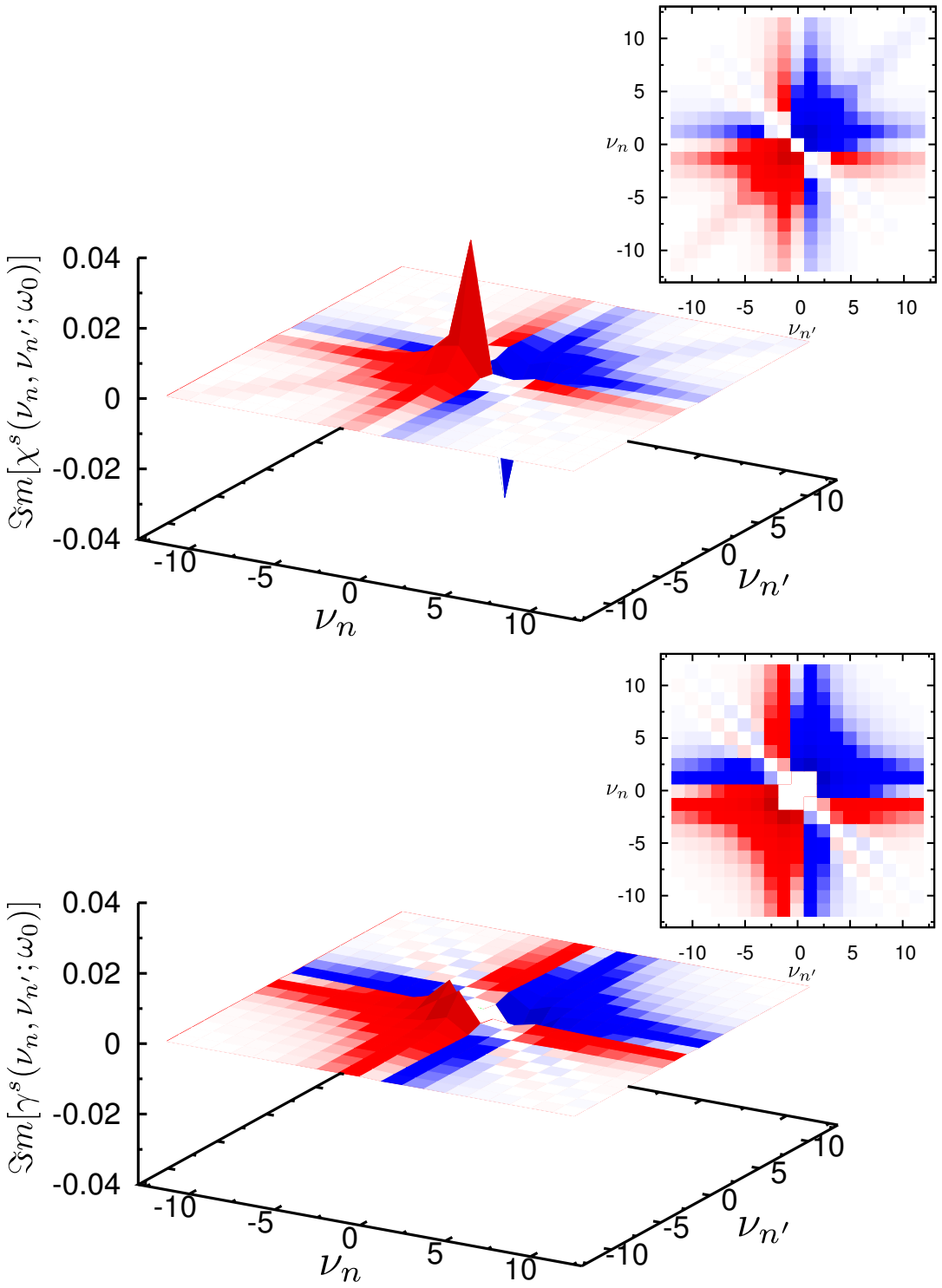

Figure 5.12: Imaginary part of the spin susceptibility (top) and its fully interacting part (bottom) for $VOMoO_4$ at $U = 2$ eV, $\beta = 5$ eV^{-1} and $\Delta\tau \sim 0.33$. Contribution of the non-interacting part of the spin susceptibly along diagonal part $\nu_n = \nu_{n'}$ is the main difference of the top and bottom plots. In addition, the imaginary part of the static susceptibility is anti-symmetric in Fermionic Matsubara frequencies. For this reason, summation over ν_n and $\nu_{n'}$ of $\Im m[\chi^s(\nu_n, \nu_{n'}; \omega_0)]$ is zero. Therefore, the local magnetic susceptibility $\frac{1}{\beta^2}\sum_n\sum_{n'}\chi^s(\nu_n, \nu_{n'}; \omega_0)$ is purely real.

5.4.4 The local (spin or charge) vertex function: A matrix algebra calculation

The *local* vertex function $\mathbf{\Gamma}(\omega_m)$ is derived from the tensorial *local* Bethe-Salpeter equation. In order to compute the $\mathbf{\Gamma}(\omega_m)$, we rewrite the local Bethe-Salpeter equation in matrix form so that each matrix is indexed by the fermionic Matsubara frequencies and orbital indices. For instance, in the case of paramagnetic solution, the *local spin* (or charge) vertex function is derived

$$\Big[\mathbf{\Gamma}^s(i\omega_m)\Big] = \Big[\chi^{\mathbf{0},s}(i\omega_m)\Big]^{-1} - \Big[\chi^s(i\omega_m)\Big]^{-1}. \tag{5.92}$$

which is rewritten in matrix form.

To solve Eq. (5.92), we use the following arrangement of the *local* matrix $\big[\chi^s(\omega_m)\big]$ (and identically $\big[\chi^{\mathbf{0},s}(\omega_m)\big]$ and $\big[\mathbf{\Gamma}^s(\omega_m)\big]$).

$$\begin{aligned}\big[\chi^s(\omega_m)\big] &= \begin{array}{c} \\ n=-N_\nu-1 \\ \vdots \\ N_\nu \end{array}\!\!\begin{array}{c} \overset{n'=-N_\nu-1}{} \quad \cdots \quad \overset{N_\nu}{} \\ \begin{pmatrix} \underline{\chi}^s(-N_\nu-1,-N_\nu-1;\omega_m) & \dots & \underline{\chi}^s(-N_\nu-1,N_\nu;\omega_m) \\ \vdots & \ddots & \vdots \\ \underline{\chi}^s(N_\nu,-N_\nu-1;\omega_m) & \cdots & \underline{\chi}^s(N_\nu,N_\nu;\omega_m) \end{pmatrix}_{(2N_\nu+2)\times(2N_\nu+2)} \end{array} \\ &=: \big\langle n\big|\underline{\chi}^s(\nu_n,\nu_{n'};\omega_m)\big|n'\big\rangle, \end{aligned} \tag{5.93}$$

where N_ν is the number of fermionic Matsubara frequencies. In analytic relations, e.g., in Matsubara sums, $N_\nu \to \infty$, but for numerical calculation we should consider a finite (cut-off) value for it. At the end of this chapter, we describe how we are able to consider $N_\nu \to \infty$ in our calculations via an appropriate extrapolation. In matrix (5.93), each element, $\underline{\chi}^s$, is itself a matrix in paris of orbital indices as follows.

$$\begin{aligned}\underline{\chi}^s &= \begin{array}{c} \\ i=1\ \left\{\begin{array}{c} j=1 \\ \vdots \\ j=N_O \end{array}\right. \\ \vdots \\ i=N_O\ \left\{\begin{array}{c} j=1 \\ \vdots \\ j=N_O \end{array}\right. \end{array}\!\!\begin{array}{c} \overbrace{}^{k=1} \quad \cdots \quad \overbrace{}^{k=N_O} \\ \begin{pmatrix} \overbrace{l=1 \quad \cdots \quad l=N_O}^{} & \cdots & \overbrace{l=1 \quad \cdots \quad l=N_O}^{} \\ \chi^s_{1111} \quad \cdots \quad \chi^s_{111N_O} & & \chi^s_{11N_O1} \quad \cdots \quad \chi^s_{11N_ON_O} \\ \vdots \quad \ddots \quad \vdots & \cdots & \vdots \quad \ddots \quad \vdots \\ \chi^s_{1N_O11} \quad \cdots \quad \chi^s_{1N_O1N_O} & & \chi^s_{1N_ON_O1} \quad \cdots \quad \chi^s_{1N_ON_ON_O} \\ \vdots \quad\quad \vdots & \ddots & \vdots \\ \chi_{N_O111} \quad \cdots \quad \chi^s_{N_O11N_O} & & \chi^s_{N_O1N_O1} \quad \cdots \quad \chi^s_{N_O1N_ON_O} \\ \vdots \quad \ddots \quad \vdots & \cdots & \vdots \quad \ddots \quad \vdots \\ \chi^s_{N_ON_O11} \quad \cdots \quad \chi^s_{N_ON_O1N_O} & & \chi^s_{N_ON_ON_O1} \quad \cdots \quad \chi^s_{N_ON_ON_ON_O} \end{pmatrix}_{N_O^2\times N_O^2} \end{array} \\ &=: \big\langle i,j\big|\chi^s_{ijkl}\big|k,l\big\rangle \end{aligned} \tag{5.94}$$

where i,j,k,l are orbital indices in Eq. (5.90) and N_O number of the orbitals. Based on Eq. (5.94), we pair the orbital i with orbital j and orbital k with orbital l so that each row and column of this matrix is organized by $i+(j-1)N_O$ and $k+(l-1)N_O$, respectively.[9] Furthermore,

[9] This means that we are dealing with e.g. matrix $\boldsymbol{A}$ wherein, each row and column is written as follows.

$$\boldsymbol{A} = \begin{array}{c} \\ 1 \\ \vdots \\ i+(j-1)N_O \end{array}\!\!\begin{array}{c} \overset{1}{} \quad \cdots \quad \overset{k+(l-1)N_O}{} \\ \begin{pmatrix} \boldsymbol{a}_{1,1} & \cdots & \boldsymbol{a}_{1,k+(l-1)N_O} \\ \vdots & \ddots & \vdots \\ \boldsymbol{a}_{i+(j-1)N_O,1} & \cdots & \boldsymbol{a}_{i+(j-1)N_O,k+(l-1)N_O} \end{pmatrix}_{N_O^2\times N_O^2} \end{array}. \tag{5.95}$$

In comparison with Eq. (5.94), here e.g., $\boldsymbol{a}_{i+(j-1)N_O,1} \equiv \chi_{N_ON_O11}$, $\boldsymbol{a}_{i+(j-1)N_O,k+(l-1)N_O} = \chi_{N_ON_ON_ON_O}$ etc.

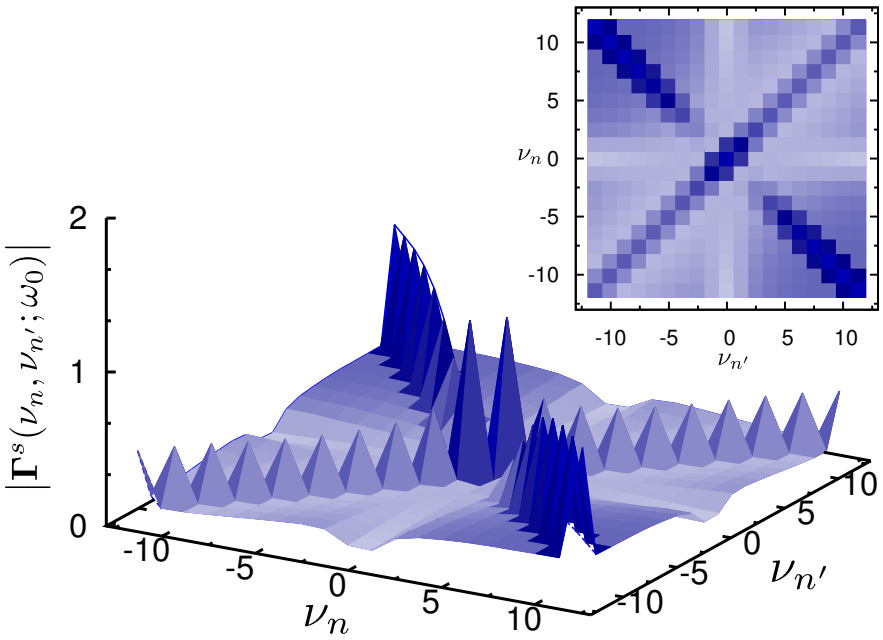

Figure 5.13: Absolute value of the vertex function $|\mathbf{\Gamma}^s|$ for $VOMoO_4$ material. Here $U = 2$ eV and $\beta = 5\ \mathrm{eV}^{-1}$.

by considering the size of the matrices in Eqs. (5.93) and (5.94), we can easily see that each matrix in the *local* Bethe-Salpeter equation has $(2N_\nu+2)N_O^2 \times (2N_\nu+2)N_O^2$ elements. According to this notation, e.g., the *local* (spin) susceptibility matrix is represented by

$$\big[\chi^s(\omega_m)\big] := \big\langle n\big| \otimes \underbrace{\big\langle i,j\big|\chi^s_{ijkl}(\nu_n,\nu_{n'};\omega_m)\big|k,l\big\rangle}_{\underline{\chi}^s(\nu_n,\nu_{n'};\omega_m)} \otimes \big|n'\big\rangle. \tag{5.96}$$

5.4.4.1 QMC results of local (spin) vertex function

In the following of our calculation of the local susceptibilities of a half-filled single band system (Figs. 5.11 and 5.12), we compute the local vertex function by solving Eq. (5.92). In Fig. 5.13, we show the absolute value of the local vertex function $|\mathbf{\Gamma}^s| = \sqrt{(\Re e[\mathbf{\Gamma}^s])^2 + (\Im m[\mathbf{\Gamma}^s])^2}$ computed for $VOMoO_4$ material and $U = 2$ eV. Since the local (spin) vertex function derived from the local (and bare local) spin susceptibility, it obeys symmetry properties of the local susceptibility.

In non-interacting limit, the local susceptibility is equal to bare local susceptibility ($\chi = \chi^{\mathbf{0}}$).[10] Therefore, the local vertex function has no contribution in non-correlated systems (See Fig. 5.14). For highly correlated system, where the Hubbard interaction U is large (insulators), the vertex function has an important role in describing the response of the function overall the Brillouin zone. Fig. 5.13 shows how the vertex function changes for different Us. Interestingly, in insulating regime, the vertex function increases if energy gap becomes bigger. This is shown in the last two plots in Fig. 5.14.

[10] Because in non-interacting system (metals), the two-particle correlation function turns into two one-particle correlation function by using Wick's theorem (See e.g., Eqs. (4.19) and (4.20)).

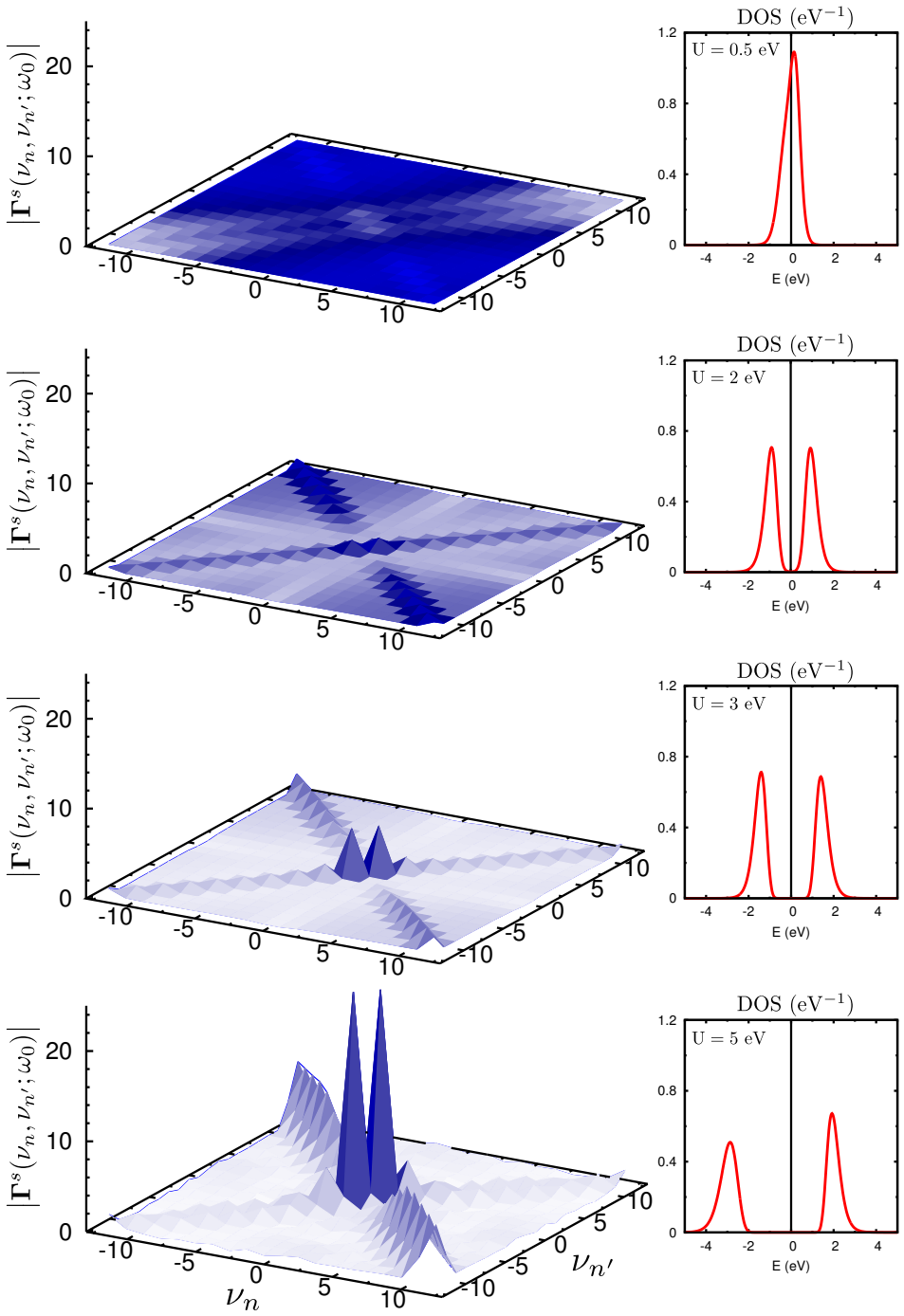

Figure 5.14: Left: Absolute value of the vertex function $|\mathbf{\Gamma}^s|$ for $VOMoO_4$ at $\beta = 5\ \mathrm{eV}^{-1}$ and $U = 0.5\ \mathrm{eV},\ 2\ \mathrm{eV},\ 3\ \mathrm{eV},\ 5\ \mathrm{eV}$ (from top to bottom). Right: Density of states of $VOMoO_4$ for the related vertex function. In metallic regime ($U = 0.5\ \mathrm{eV}$) the vertex function is almost zero. But in insulators $U \gtrsim 3\ \mathrm{eV}$, where two-particle interaction is considerable, vertex function has the main role in response function.

5.4.5 Bare lattice (spin or charge) susceptibility (after QMC)

In order to calculate the bare lattice susceptibility, first we evaluate the fully interacting Green's function for a supper-cell by using the local self-energy and the LDA Hamiltonian.

$$\mathcal{G}_{\alpha_i\alpha_j}(\mathbf{k},\nu_n)=\left(\frac{1}{i\nu_n+\mu-H^{LDA}(\mathbf{k})-\Sigma(\nu_n)}\right)_{\alpha_i\alpha_j}, \tag{5.97}$$

where $\alpha_p=p\kappa_p\sigma_p$ is a collective indices and $p=i,j$ is the orbital, κ_p the atomic site; σ_p the spin. Here, $\sigma_i=\sigma_j\equiv\sigma$. Based on Eqs. (4.19), (4.20) and (4.41), the bare lattice spin susceptibility is[11]

$$\chi^{\mathbf{0},s}_{\alpha_i\alpha_j\alpha_k\alpha_l}(\nu_n,\nu_{n'};\mathbf{q},\omega_m)=-\beta\delta_{nn'}\frac{1}{4}(g\mu_B)^2\sum_{\sigma}\frac{1}{N_{\mathbf{k}}}\sum_{\mathbf{k}}\mathcal{G}_{\alpha_l\alpha_i}(\mathbf{k},\nu_n)\mathcal{G}_{\alpha_j\alpha_k}(\nu_n+\omega_m;\mathbf{k}+\mathbf{q}). \tag{5.98}$$

Considering the definition of the charge susceptibility (Eq. (4.61)), Similar relation can be derived for the bare lattice charge susceptibility.

5.4.6 The lattice (spin or charge) susceptibility

To solve the spin (or similarly the charge) Bethe-Salpeter equation (4.47), we first construct new matrices for the (bare) spin lattice susceptibility in which atomic sites (per unit cell) are also considered. For instance, the lattice spin susceptibility matrix is arranged as follow

$$\chi^s = \begin{array}{c} \\ \boldsymbol{\kappa_i}=1 \\ \vdots \\ \boldsymbol{\kappa_i}=N_S \end{array}\!\!\begin{array}{c} \overbrace{\phantom{\underline{\chi}^s_{1111}\cdots\underline{\chi}^s_{111N_S}}}^{\boldsymbol{\kappa_k}=1} \\ \begin{array}{c}\boldsymbol{\kappa_j}=1\\ \vdots\\ \boldsymbol{\kappa_j}=N_S\end{array}\left\{\begin{array}{ccc} \boldsymbol{\kappa_l}=1 & \cdots & \boldsymbol{\kappa_l}=N_S \\ \underline{\underline{\chi}}^s_{\boldsymbol{1111}} & \cdots & \underline{\underline{\chi}}^s_{\boldsymbol{111N_S}} \\ \vdots & \ddots & \vdots \\ \underline{\underline{\chi}}^s_{\boldsymbol{1N_S11}} & \cdots & \underline{\underline{\chi}}^s_{\boldsymbol{1N_S1N_S}} \\ \vdots & \ddots & \vdots \\ \underline{\underline{\chi}}^s_{\boldsymbol{N_S111}} & \cdots & \underline{\underline{\chi}}^s_{\boldsymbol{N_S11N_S}} \\ \vdots & \ddots & \vdots \\ \underline{\underline{\chi}}^s_{\boldsymbol{N_SN_S11}} & \cdots & \underline{\underline{\chi}}^s_{\boldsymbol{N_SN_S1N_S}} \end{array}\right. \end{array}\!\!\begin{array}{c} \\ \cdots \\ \\ \cdots \\ \\ \cdots \\ \\ \cdots \end{array}\!\!\begin{array}{c} \overbrace{\phantom{\underline{\chi}^s_{11N_S1}\cdots\underline{\chi}^s_{11N_SN_S}}}^{\boldsymbol{\kappa_k}=N_S} \\ \begin{array}{ccc} \boldsymbol{\kappa_l}=1 & \cdots & \boldsymbol{\kappa_l}=N_S \\ \underline{\underline{\chi}}^s_{\boldsymbol{11N_S1}} & \cdots & \underline{\underline{\chi}}^s_{\boldsymbol{11N_SN_S}} \\ \vdots & \ddots & \vdots \\ \underline{\underline{\chi}}^s_{\boldsymbol{1N_SN_S1}} & \cdots & \underline{\underline{\chi}}^s_{\boldsymbol{1N_SN_SN_S}} \\ \vdots & \ddots & \vdots \\ \underline{\underline{\chi}}^s_{\boldsymbol{N_S1N_S1}} & \cdots & \underline{\underline{\chi}}^s_{\boldsymbol{N_S1N_SN_S}} \\ \vdots & \ddots & \vdots \\ \underline{\underline{\chi}}^s_{\boldsymbol{N_SN_SN_S1}} & \cdots & \underline{\underline{\chi}}^s_{\boldsymbol{N_SN_SN_SN_S}} \end{array} \end{array}\!\!\Bigg)_{N_S^2\times N_S^2}$$

$$=:\ \big\langle \boldsymbol{\kappa_i},\boldsymbol{\kappa_j}\big|\chi^s_{\boldsymbol{\kappa_i\kappa_j\kappa_k\kappa_l}}\big|\boldsymbol{\kappa_k},\boldsymbol{\kappa_l}\big\rangle, \tag{5.99}$$

where $\kappa_i,\kappa_j,\kappa_k$ and κ_l are the atomic sites and N_S number of atomic site in a unit cell. In this matrix, each element, $\underline{\underline{\chi}}^s$, is itself a matrix in Matsubara frequencies, ν_n and $\nu_{n'}$, and in pairs of orbital indices given by Eqs. (5.93) and (5.94), respectively. Based on our notation for matrices (see Eq. (5.96)), the $\mathbf{q}$-dependent lattice susceptibility matrix is

$$\Big[\chi^s(\mathbf{q},\omega_m)\Big]:=\big\langle\kappa_i\kappa_j\big|\otimes\overbrace{\big\langle n\big|\otimes\underbrace{\big\langle i,j\big|\underline{\underline{\chi}}^s_{i\boldsymbol{\kappa_i},j\boldsymbol{\kappa_j},k\boldsymbol{\kappa_k},l\boldsymbol{\kappa_l}}(\nu_n,\nu_{n'};\mathbf{q},\omega_m)\big|k,l\big\rangle}_{\underline{\underline{\chi}}^s_{\boldsymbol{\kappa_i\kappa_j\kappa_k\kappa_l}}(\nu_n,\nu_{n'};\mathbf{q},\omega_m)}\otimes\big|n'\big\rangle}^{\underline{\underline{\chi}}^s_{\boldsymbol{\kappa_i\kappa_j\kappa_k\kappa_l}}(\mathbf{q},\omega_m)}\otimes\big|\kappa_k,\kappa_l\big\rangle. \tag{5.100}$$

Each row and column of the matrix (5.100) can be coded as follows.

[11] See footnote 8.

```
!NO: Number of orbitals; NS: Number of sites;
!2*Nnu+2: Number of Fermionic Matsubara frequencies
do i=1,NO; do j=1,NO; do k=1,NO; do l=1,NO
  do kappa_i=1,NS; do kappa_j=1,NS;do kappa_k=1,NS;do kappa_l=1,NS

! Row of the matrix  chi_mat(row,column)
  row = j+(i-1)*NO+(n-1)*(NO**2)+(kappa_j-1)*(2*Nnu+2)*(NO**2)&
  &+(kappa_i-1)*(2*Nnu+2)*(NO**2)*NS
! Column of the matrix  chi_mat(row,column)
  column = l+(k-1)*NO+(np-1)*(NO**2)+(kappa_l-1)*(2*Nnu+2)*(NO**2)&
  &+(kappa_k-1)*(2*Nnu+2)*(NO**2)*NS
! Saving the susceptibility tensor in a matrix form.
  chi_mat(row,column)=chi_tensor(orbital_ijkl,site_ijkl,nu_n,nu_np)

  enddo; enddo; enddo; enddo
enddo; enddo;enddo; enddo
```

It should be noticed that, in the new bases, the local vertex function matrix $\left[\mathbf{\Gamma}^s\right]$ has non-zero elements *only* at $\boldsymbol{\kappa_i} = \boldsymbol{\kappa_j} = \boldsymbol{\kappa_k} = \boldsymbol{\kappa_l}$.

$$\mathbf{\Gamma}^s = \begin{array}{c} \\ \boldsymbol{\kappa_i}=1 \left\{\begin{array}{c}\boldsymbol{\kappa_j}=1\\ \vdots \\ \boldsymbol{\kappa_j}=N_S\end{array}\right. \\ \vdots \\ \boldsymbol{\kappa_i}=N_S \left\{\begin{array}{c}\boldsymbol{\kappa_j}=1\\ \vdots \\ \boldsymbol{\kappa_j}=N_S\end{array}\right. \end{array} \begin{array}{c} \overbrace{\boldsymbol{\kappa_k}=1}^{} \quad\quad\quad\quad\quad\quad \overbrace{\boldsymbol{\kappa_k}=N_S}^{} \\ \overbrace{\boldsymbol{\kappa_l}=1\cdots\boldsymbol{\kappa_l}=N_S}^{} \quad \cdots \quad \overbrace{\boldsymbol{\kappa_l}=1 \quad \cdots \quad \boldsymbol{\kappa_l}=N_S}^{} \\ \begin{pmatrix} \underline{\underline{\mathbf{\Gamma}}}^s_{\mathbf{1111}} & \cdots & 0 & & 0 & \cdots & 0 \\ \vdots & \ddots & \vdots & \cdots & \vdots & \ddots & \vdots \\ 0 & \cdots & 0 & & 0 & \cdots & 0 \\ & \vdots & & \ddots & & \vdots & \\ 0 & \cdots & 0 & & 0 & \cdots & 0 \\ \vdots & \ddots & \vdots & \cdots & \vdots & \ddots & \vdots \\ 0 & \cdots & 0 & & 0 & \cdots & \underline{\underline{\mathbf{\Gamma}}}^s_{\boldsymbol{N_S N_S N_S N_S}} \end{pmatrix} \end{array}, \quad (5.101)$$

wherein each $\underline{\underline{\mathbf{\Gamma}}}^s$ is itself a matrix in Matsubara frequencies and orbital indices (See Eqs. (5.93) and (5.94)).

5.4.6.1 QMC results of the q-dependent spin susceptibility in Matsubara space

In order to investigate the $\mathbf{q}$-dependent susceptibility, we calculate the $\chi^s_{\kappa_i\kappa_j\kappa_k\kappa_l}(\nu_n, \nu_{n'}; \mathbf{q}, \omega_m)$ for the considered model, a one-band system with two atomic sites per unit cell ($VOMoO_4$) [12] at $\mathbf{q} = (0, 0, 0)$.

Results are shown in Fig. 5.15 in which the general behavior of the $\mathbf{q}$-dependent spin susceptibility for different sites is the same as the local spin susceptibility. χ^s_{1111} and χ^s_{2222} have slow decays along $\nu_n = 0;\ \forall\nu_{n'}$, $\nu_{n'} = 0;\ \forall\nu_n$ and $\nu_n = \nu_{n'}$. In comparison with χ^s_{1111} and χ^s_{2222}, χ^s_{1122} and χ^s_{2211} also decay slowly along $\nu_n = 0;\ \forall\nu_{n'}$ and $\nu_{n'} = 0;\ \forall\nu_n$ but fast at $\nu_n = \nu_{n'}$ which is due to the delta functions which appear in high-frequency behavior of the susceptibility (See Eq. (4.113)). For $\mathbf{q} = \mathbf{0}$, although the general treatment of

[12] Since the system has only one orbital, for the sake of simplicity, we drop the orbital indices in $\chi^s_{i\kappa_i,j\kappa_j,k\kappa_k,l\kappa_l}(\nu_n, \nu_{n'}; \mathbf{q}, \omega_m) \to \chi^s_{\kappa_i\kappa_j\kappa_k\kappa_l}(\nu_n, \nu_{n'}; \mathbf{q}, \omega_m)$.

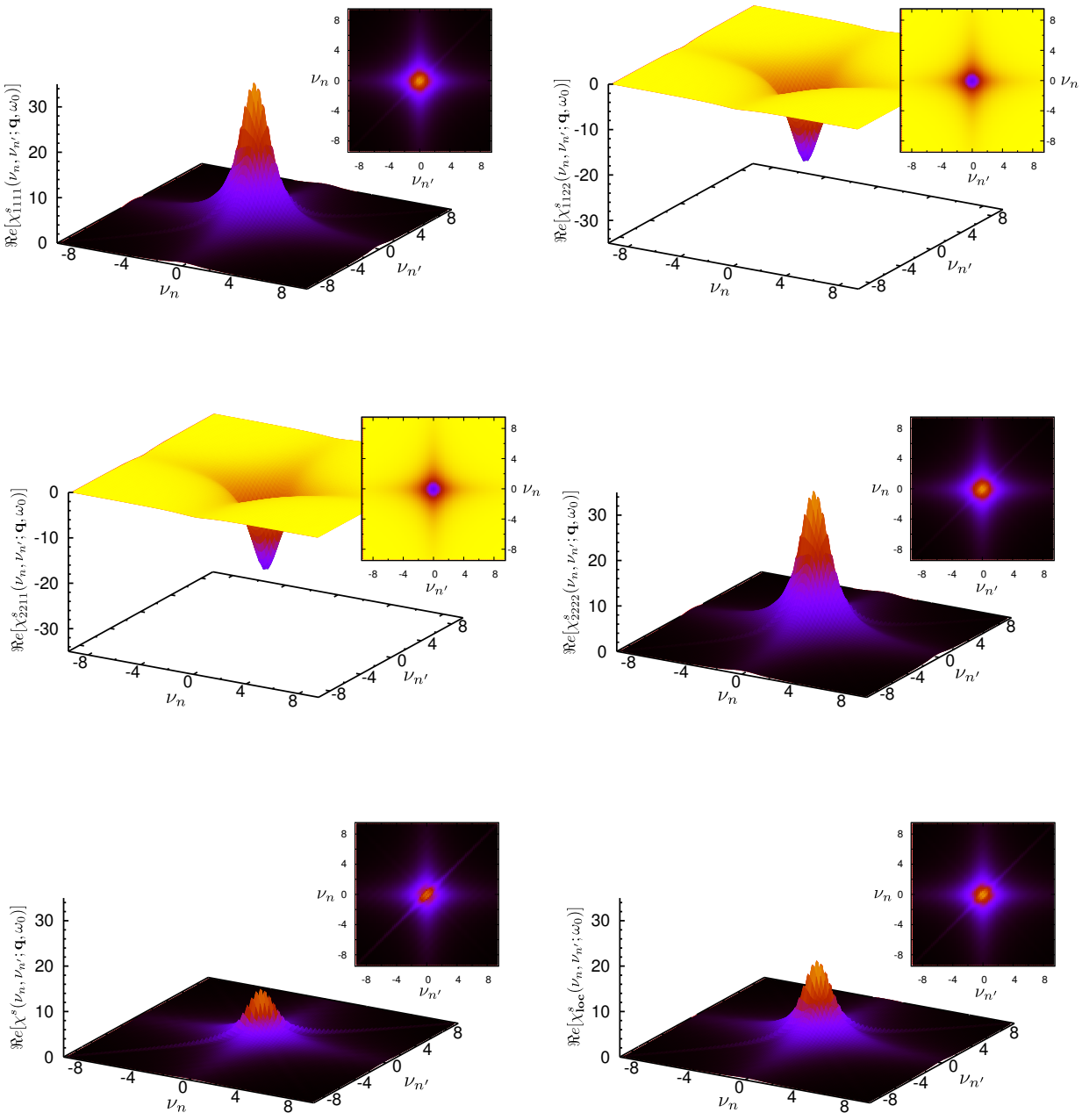

Figure 5.15: The first 4 figures are the lattice magnetic response $\chi^s_{\kappa_i\kappa_j\kappa_k\kappa_l}(\nu_n,\nu_{n'};\mathbf{q},\omega_m)$ at $\mathbf{q}=(0,0,0)$ for different sites κ. The last two plots are the $\mathbf{q}$-dependent magnetic response $\chi^s(\nu_n,\nu_{n'};\mathbf{0},\omega_m)=\frac{1}{N_S}\sum_{\kappa_i\kappa_j\kappa_k\kappa_l}\delta_{\kappa_i,\kappa_j}\delta_{\kappa_k,\kappa_l}\chi^s_{\kappa_i\kappa_j\kappa_k\kappa_l}(\nu_n,\nu_{n'};\mathbf{0},\omega_m)$ and the local spin susceptibility $\chi^s(\nu_n,\nu_{n'};\omega_m)=\frac{1}{N_\mathbf{q}}\sum_\mathbf{q}\chi^s(\nu_n,\nu_{n'};\mathbf{q},\omega_m)$. Here, $U=3$ eV, $\beta=30$ eV^{-1} and the considered material is $VOMoO_4$.

$\chi^s(\nu_n,\nu_{n'};\mathbf{0},\omega_m)=\frac{1}{N_S}\sum_{\kappa_i\kappa_j\kappa_k\kappa_l}\delta_{\kappa_i,\kappa_j}\delta_{\kappa_k,\kappa_l}\chi^s_{\kappa_i\kappa_j\kappa_k\kappa_l}(\nu_n,\nu_{n'};\mathbf{0},\omega_m)$ is quite similar to the local one, but their order of magnitude is sizably different.

5.4.7 Convergency of Matsubara sum: An extrapolation approach

Once we derived the $\mathbf{q}$-dependent susceptibility matrix $\left[\chi^s(\mathbf{q},\omega_m)\right]$, we need to sum over all Fermionic Matsubara frequencies in order to get the spin (charge) lattice susceptibility.

$$\chi^{zz}(\mathbf{q},\omega_m) \;=\; \frac{1}{\beta^2}\sum_{n=-\infty}^{+\infty}\sum_{n'=-\infty}^{+\infty}\chi^s(\nu_n,\nu_{n'};\mathbf{q},\omega_m). \tag{5.102}$$

In order to compute the Matsubara sum in Eq. (5.102) for infinite value of n and n' numerically, we need to consider an upper N_ν and a lower $-N_\nu-1$ limit in Matsubara sums as follows.

$$\chi^{zz}(\mathbf{q},\omega_m) \;=\; \frac{1}{\beta^2}\lim_{N_\nu\to\infty}\left(\sum_{n=-N_\nu-1}^{N_\nu}\sum_{n'=-N_\nu-1}^{N_\nu}\right)\chi^s(\nu_n,\nu_{n'};\mathbf{q},\omega_m). \tag{5.103}$$

Since at large frequencies $\nu_n,\nu_{n'}\gg 1$ the lattice susceptibility like the local one decays as $\sim(1/\nu_n^2)$ and $\sim(1/\nu_n^3)$ for real and imaginary part, respectively (see Eq. (4.113)), it's Matsubara sums for a big enough cut-off value $n_c<N_\nu$ is proportional to $\sim(1/\nu_{n_c}^2)$ (Eqs. (4.115), (4.117) and (4.118)). Therefore, the convergency of the Matsubara frequencies sum in Eq. (5.102) can be obtained by using extrapolation. To do this, we proceed as follows. First, we determine an approximate value for the cut-off number $n_c<N_\nu$ which satisfies the following condition

$$\Re\mathrm{e}\left[\chi^s(\nu_{n_c},\nu_{n_c};\omega_m)\right]+\frac{\beta}{\nu_{n_c}(\nu_{n_c}+\omega_m)}\leq\xi;\quad \xi\ll 1. \tag{5.104}$$

Notice that n_c depends on the system, temperature and interaction. Once we calculate the local susceptibility, we are able to estimate n_c (See Fig. 5.16). Second, we compute the $\mathbf{q}$-dependent susceptibility as a function of $1/N_p$ where $n_c\leq N_p\leq N_\nu$.

$$\chi^{zz}(\mathbf{q},\omega_m;N_p^{-1})=\frac{1}{\beta^2}\sum_{n=-N_p-1}^{N_p}\sum_{n'=-N_p-1}^{N_p}\chi^s(\nu_n,\nu_{n'};\mathbf{q},\omega_m). \tag{5.105}$$

Finally, we extrapolate the $\chi^{zz}(\mathbf{q},\omega_m;N_p^{-1})$ for $n\geq n_c$ by using a quadratic and cubic equation for the real and imaginary part of the susceptibility, respectively.

In the case of static susceptibility $\chi^{zz}(\mathbf{q},\omega_0;N_p^{-1})$, the imaginary part

$$\Im\mathrm{m}\left[\chi^{zz}(\mathbf{q},\omega_0;N_p^{-1})\right]=\frac{1}{\beta^2}\sum_{n=-N_p-1}^{N_p}\sum_{n'=-N_p-1}^{N_p}\Im\mathrm{m}\left[\chi^s(\nu_n,\nu_{n'};\mathbf{q},\omega_0)\right]=0, \tag{5.106}$$

because in paramagnetic systems, $\Im m\left[\chi^s(\nu_n,\nu_{n'};\mathbf{q},\omega_m)\right]$ is anti-symmetric (See Fig. 4.11c and 4.11d). For the real part of the static spin susceptibility $\Re e\left[\chi^{zz}(\mathbf{q},\omega_m;N_p^{-1})\right]$, appropriate fitting polynomial equation is $Y=a(1/(N_p+1/2))^2-2a(1/(N_P+1/2))+b$ in which a and b are constant. This can be shown by using Eqs. (4.115) and (D.25) as follows.

$$\begin{aligned}\chi^{zz}(\mathbf{q},\omega_0;N_p^{-1})\Big|_{\text{High frequency}} &= \frac{2a}{(N_p+1/2)^2}-2a\,\Psi\left(N_p+\frac{1}{2}\right)+b\\ &\approx \frac{2a}{(N_p+1/2)^2}-2a\left(\frac{1}{N_p+1/2}+\frac{1}{2(N_p+1/2)^2}\right)+b\\ &\approx a\left(\frac{1}{N_p+1/2}\right)^2-2a\left(\frac{1}{N_p+1/2}\right)+b.\end{aligned} \tag{5.107}$$

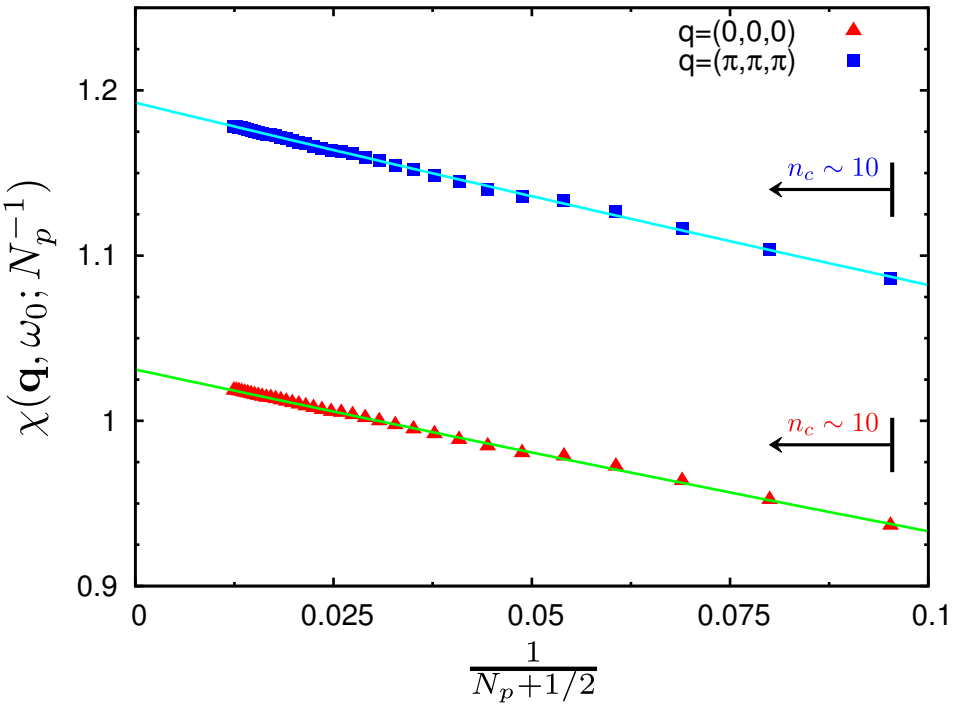

Figure 5.16: In order to calculate Matsubara sum for infinite number of fermionic Matsubara frequencies $\frac{1}{\beta^2}\sum_{n=-\infty}^{+\infty}\sum_{-\infty}^{+\infty}(\cdots)$, we use extrapolation. The polynomial line is a least square fit using Eq. (5.107). Here, the spin susceptibility is calculated at $\mathbf{q}=(0,0,0)$ and $\mathbf{q}=(\pi,\pi,\pi)$ for $VOMoO_4$, $U = 2$ eV and $\beta = 5$ eV^{-1}. In this case, the spin susceptibility is in its high frequency regime if $n_c \geq 10$. Therefore, the polynomial line can be fitted for $N_p \geq 10$.

The intersect with the Y axis is the static magnetic response function $\chi^{zz}(\mathbf{q}, \omega_m = 0)$ obtained from Eq. (5.102). For fitting a polynomial equation to the susceptibility, we use least square method which is described in appendix G.1.

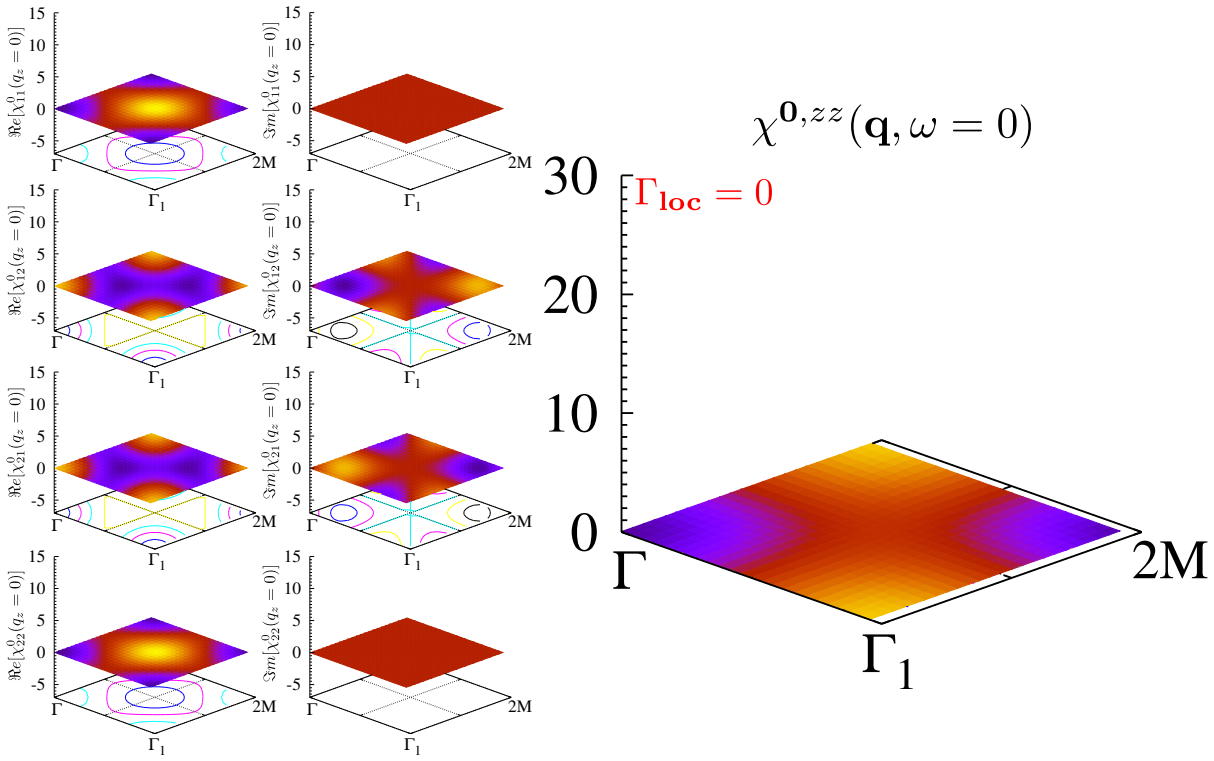

Figure 5.17: The $\mathbf{q}$-dependent magnetic susceptibility *without* the local vertex contribution, $\chi^{\mathbf{0},zz}(\mathbf{q},\omega_0)$ for $VOMoO_4$. The Coulomb interaction is $U=3$ eV and the inverse temperature $\beta=30$ eV^{-1}. Here, $\Gamma=(0,0,q_z)$, $\Gamma_1=(2\pi,0,q_z)$, and $2\mathrm{M}=(2\pi,2\pi,q_z)$. Real and Imaginary part of $\chi^{\mathbf{0},zz}_{\kappa_i\kappa_j}(\mathbf{q},\omega_0)$ are shown in the left of the Figure. On the right, the $\chi^{\mathbf{0},zz}(\mathbf{q},\omega_0)$ is plotted which is obtained from Eq. (5.108). In this figure, we considered $q_z=0$.

5.4.7.1 QMC results of the static q-dependent spin susceptibility by using extrapolation

We used the described extrapolation method to calculate the Matsubara sum for infinite number of Matsubara fermionic frequencies. Accordingly, we calculate the static lattice susceptibility $\chi^{zz}(\mathbf{q},\omega_0)$ and the static bare lattice susceptibility $\chi^{\mathbf{0},zz}(\mathbf{q},\omega_0)$ for $VOMoO_4$ (a single band model with two atoms per unit cell) overall the first Brillouin zone. Notice that the susceptibility of this system can be obtained from a two-site supercell by

$$\chi^{zz}(\mathbf{q},\omega_m)=\frac{1}{N_S}\sum_{\boldsymbol{\kappa_i},\boldsymbol{\kappa_j}=1}^{N_S}\frac{1}{\beta^2}\sum_{n=-\infty}^{+\infty}\sum_{n'=-\infty}^{+\infty}e^{-i\mathbf{q}.(\mathbf{T}_{\kappa_i}-\mathbf{T}_{\kappa_j})}\,\chi^{s}_{\boldsymbol{\kappa_i\kappa_j}}(\nu_n,\nu_{n'};\mathbf{q},\omega_m), \tag{5.108}$$

where $\mathbf{T}$ is the lattice vector of the supercell and $\chi^s_{\kappa_i\kappa_j}$ is the abbreviation of $\chi^s_{\kappa_i\kappa_i\kappa_j\kappa_j}$. Since $VOMoO_4$ is described effectively by a single orbital Hamiltonian, we dropped the orbital indices for the sake of the simplicity. Furthermore, the phase term $\phi_{\kappa_i\kappa_j}=\mathbf{q}.(\mathbf{T}_{\kappa_i}-\mathbf{T}_{\kappa_j})$ for the $VOMoO_4$ is given by $\phi_{11}=\phi_{22}=0$ and $\phi_{12}=-\phi_{21}=(q_x+q_y)/2-q_z$ (See Chap. 6 for more details). The results are shown in Figs. 5.17 and 5.18 for $U=3$ eV and $\beta=30$ eV^{-1}.

Thanks to $\chi^{\mathbf{0},zz}(\mathbf{q},\omega_m)$ since the lattice susceptibility $\chi^{zz}(\mathbf{q},\omega_0)$ owes it's $\mathbf{q}$-dependency to it (See Figs. 5.17 and 5.18). Besides, thanks to the local vertex approximation that causes sizable correction in the lattice susceptibility. This is clear from Fig. 5.17, where the vertex correction

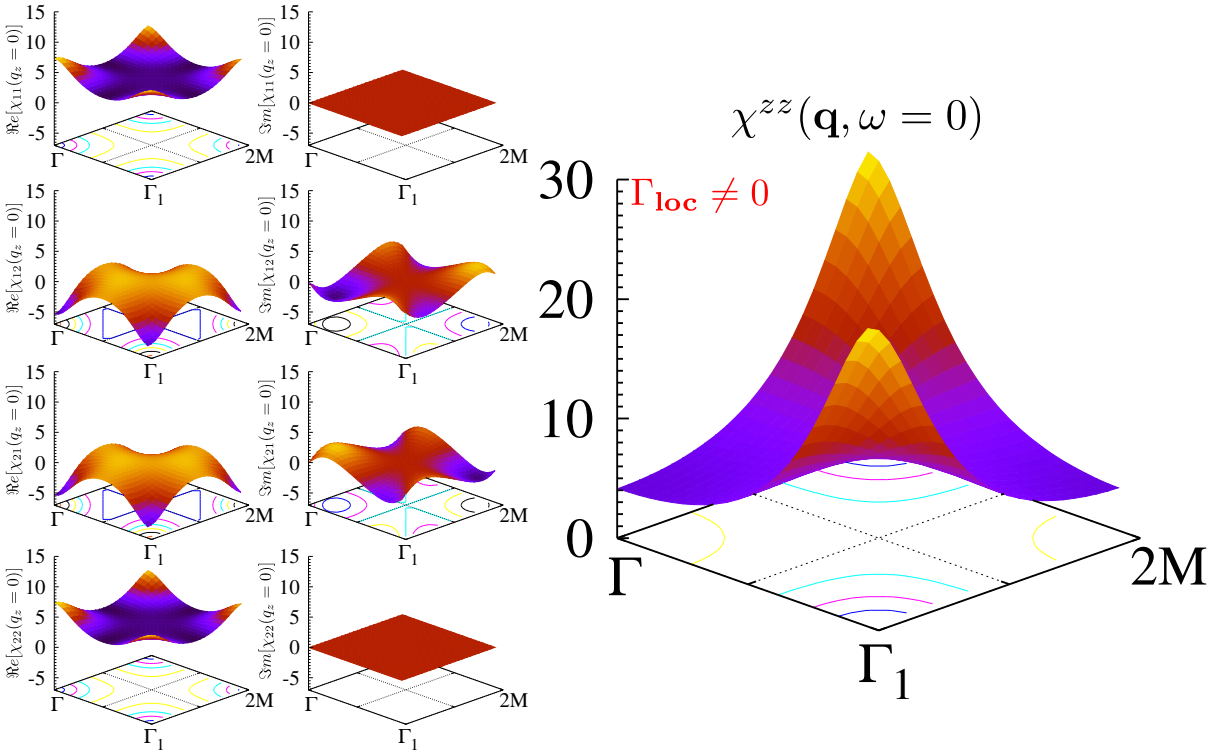

Figure 5.18: The $\mathbf{q}$-dependent magnetic susceptibility *with* the local vertex correction $\chi^{zz}(\mathbf{q}, \omega_0)$ for $VOMoO_4$. The Coulomb interaction is $U = 3$ eV and the inverse temperature $\beta = 30$ eV^{-1}. Here, $\Gamma = (0, 0, q_z)$, $\Gamma_1 = (2\pi, 0, q_z)$, and $2\mathrm{M} = (2\pi, 2\pi, q_z)$, where $q_z = 0$. At $\mathbf{q} = \Gamma_1$ point, the $VOMoO_4$ is anti-ferromagnetically ordered. The first and second columns of figures are real and imaginary part of the inter-site susceptibility $\chi^{zz}_{\kappa_i\kappa_j}(\mathbf{q}, \omega_0)$. The big plot, on the right, is the magnetic susceptibly $\chi^{\mathbf{0},zz}(\mathbf{q}, \omega_0)$ calculated from Eq. (5.108). In comparison with Fig. 5.17, the local vertex approximation enhances the magnetic response.

is zero to obtain $\chi^{\mathbf{0},zz}(\mathbf{q}, \omega_m)$ and Fig. 5.18 in which the vertex correction is non-zero to obtain $\chi^{zz}(\mathbf{q}, \omega_m)$.

5.5 Tests and numerical details

To check the implementation of the spin susceptibility, we calculate the static uniform spin susceptibility by using the LDA+DMFT in two different ways [12] and comparing them.

In the first approach, first we calculate the local spin susceptibility and it's mean field term (bare local spin susceptibility) by employing the Hirsch-Fye QMC as described in Eqs. (5.87) and (5.90) in the last iteration of solving DMFT self-consistent equations. Then we do a matrix inversion to obtain the local vertex matrix (Eq. (5.92)). By the knowledge of the self-energy, we obtain the bare lattice susceptibility matrix $\left[\chi^{\mathbf{0},s}(\mathbf{q}, \omega_m)\right]$. A second matrix inversion yields the lattice susceptibility $\left[\chi^{s}(\mathbf{q}, \omega_m)\right]$ matrix. At the end, we sum over orbitals, atomic sites and Matsubara frequencies $\nu_n, \nu_{n'}$ to derive the spin susceptibility overall the Brillouin zone as explained in Eq. (5.102).

In the second approach, we apply a small uniform external magnetic field h in system so that

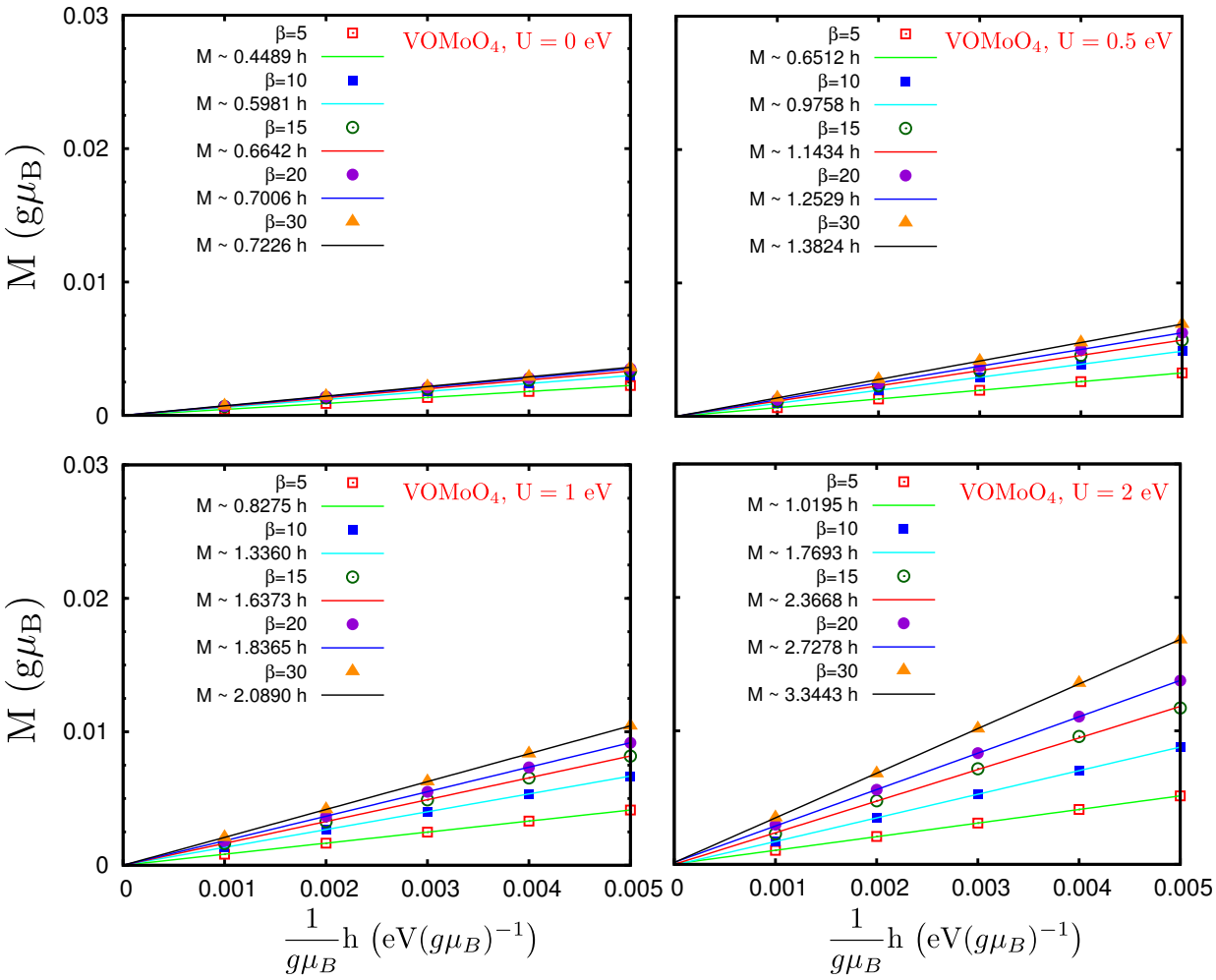

Figure 5.19: Magnetization $M(h)$ of $VOMoO_4$ versus h. For each β the linear line is lease square fit of $M(h) = \chi^{zz}h$.

the system remains in linear response regime. We solve the self-consistent DMFT equations to derive magnetization of the system by using total occupation number for spin up $n_\uparrow = -\mathcal{G}^\uparrow(\tau = \beta)$ and spin down $n_\downarrow = -\mathcal{G}^\downarrow(\tau = \beta)$ based on Eq. (B.4). The static uniform spin susceptibility is then obtained by $\chi^{zz}(\mathbf{0}, 0) \sim M/h$ (See Eq. (B.6)). In order to decrease numerical errors due to the Monte Carlo procedure, we calculate $M(h)$ for different values of h for each temperature (β^{-1}). The slope of the linear line fitted on $M(h)$ versus h, is the static uniform magnetic susceptibility. Although this method is simpler than the firs one, we can use it to compute the static uniform response function only. This is a method used e.g. in [66, 67]

5.5.0.2 A one band system with two atoms per unit cell: $VOMoO_4$

We consider a half-filled single band model whose unit cell has two atoms. This is a typical model used to explain such a material like $VOMoO_4$.[13] In order to calculate the static uniform magnetic response in different Coulomb interactions $U = 0$ eV, 0.5 eV, 1 eV, and $U = 2$ eV,

[13] In the next chapter, we explain the structure of $VOMoO_4$ in details.

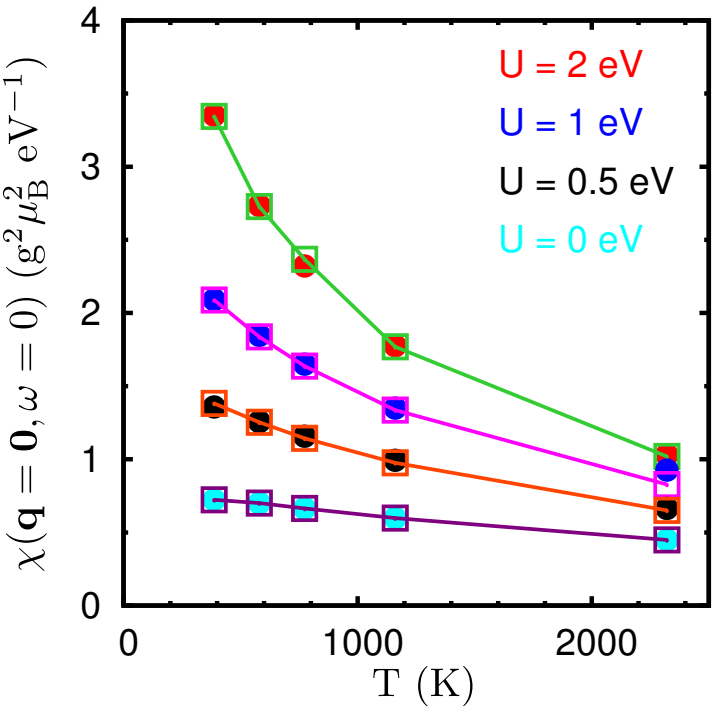

Figure 5.20: The static uniform magnetic susceptibility $\chi^{zz}(\mathbf{0},0)$ of $VOMoO_4$ is calculated at high temperature $387\ \mathrm{K} \lesssim T \lesssim 2320\ \mathrm{K}$ for different Coulomb interactions $U = 2\ \mathrm{eV},\ 1\ \mathrm{eV},\ 0.5\ \mathrm{eV},\ 0\ \mathrm{eV}$ from top to bottom, respectively. Circles: The static uniform spin susceptibility obtained from the Bethe-Salpeter equation (4.47) by using the local vertex approximation. Squares: The static uniform spin susceptibility calculated from $\chi^{zz}(\mathbf{0},0) = \left(\frac{\partial M}{\partial h}\right)_{h\to 0}$, wherein the magnetization M is obtained from solving self-consistent DMFT equations.

we apply a small magnetic field of the order of 10^{-3} eV so that the magnetization of the system changes linearly with respect to the magnetic field (See Fig. 5.19). We compute $\chi^{zz}(\mathbf{0},0)$ for different temperatures from ~ 390 K till ~ 2300 K. Since in the absence of the magnetic field the system has no magnetic order, $\lim_{h\to 0} M(h) \to 0$ (See Fig. (5.19)). The slope of the linear line fitted on $M(h)$ versus h data is the static uniform magnetic susceptibility $\chi^{zz}(\mathbf{q}=\mathbf{0},\omega_m=0)$.

In comparison to the static uniform magnetic susceptibility computed by solving the Bethe-Salpeter equation (4.47) within the local vertex approximation framework, we find it is almost identical to the one obtained from magnetization, $\chi^{zz} \sim M/h$ (See Fig. 5.20). This shows that the Filon-trapezoidal approximation[14] we utilized to calculate the local susceptibility and therefore the local vertex function is accurate enough to evaluate the $\mathbf{q}$-dependent susceptibility.

We will return to $VOMoO_4$ material to study the nature of magnetism of this material in the next chapter.

[14]Notice that the main source of the numerical error in this approach is related to the Filon-trapezoidal approximation for calculating the Fourier integral of the local susceptibility.

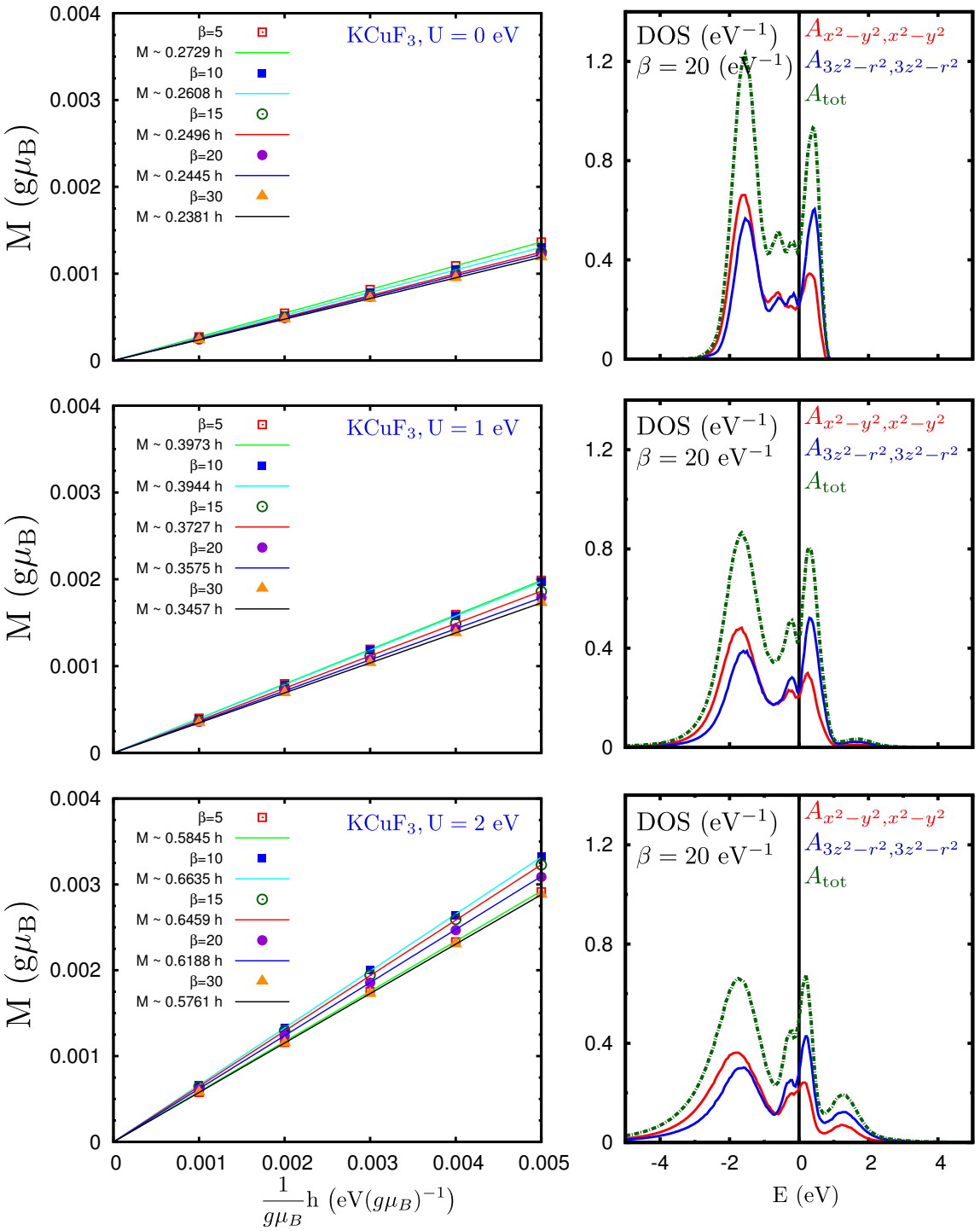

Figure 5.21: Left: Magnetization $M(h)$ of $KCuF_3$ versus h. For each β the linear line is least square fit of $M(h) = \chi^{zz}h$. Right: Spectral function of $KCuF_3$ at $\beta = 20$ eV^{-1} and $U = 0$ eV, 1 eV, and 2 eV from top to bottom, respectively.

5.5.0.3 A two band system with two atoms per unit cell: $KCuF_3$

As a multi-orbitals and multi-sites example, we consider a system with two atoms per unit cell where each atom has two orbitals. A typical model which is employed to describe materials like $KCuF_3$ [68]. We calculate the static uniform magnetic susceptibility at high temperature $390\ \mathrm{K} \lesssim T \lesssim 2300\ \mathrm{K}$ for different Coulomb interactions $U = 0\ \mathrm{eV},\ 1\ \mathrm{eV},\ 2\ \mathrm{eV}$, and exchange coupling $J = 0\ \mathrm{eV}$. For the considered interactions, the system shows metallic properties as shown in Fig. 5.21. We consider small magnetic field $h \sim 10^{-3}$ eV so that the system responds linearly. The magnetization of each orbital versus the external applied magnetic field are computed separately. Total magnetization is then $M = M_{11} + M_{22}$.[15]. In the case of $KCuF_3$, two e_g orbitals contribute to the total magnetization $M = M_{x^2-y^2,x^2-y^2} + M_{3z^2-r^2,3z^2-r^2}$. Using the linear square method, we fit a linear line on $M(h)$ data (Fig. 5.21). The slope of the line is the static uniform magnetic susceptibility (See Fig. 5.22). We also evaluate the χ^{zz} by solving the self-consistent Bethe-Salpeter equation in the local vertex approximation framework in order to compare it with $\chi^{zz} = \left(\frac{\partial M}{\partial h}\right)_{h\to 0}$. The juxtaposition is shown in Fig. 5.22.

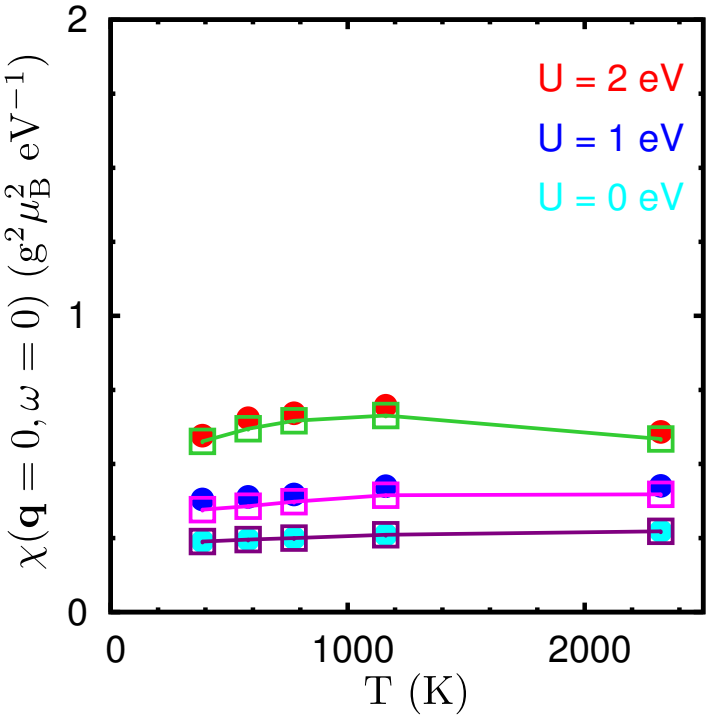

Figure 5.22: The static uniform magnetic susceptibility $\chi^{zz}(\mathbf{0}, 0)$ of $KCuF_3$. Filled circles: $\chi^{zz}(\mathbf{0}, 0)$ obtained from Eq. (4.47). Squares: $\chi^{zz}(\mathbf{0}, 0) = \left(\frac{\partial M}{\partial h}\right)_{h\to 0}$. The exchange coupling $J = 0$ eV and $U = 2\ \mathrm{eV},\ 1\ \mathrm{eV},\ 0\ \mathrm{eV}$ from top to bottom.

[15] Since two atomic sites are equivalent in the DMFT, we calculate the magnetization (and therefore the static uniform spin susceptibility) for only one site. In the cluster DMFT, interaction between two atoms are considered. In this case, the magnetization is obtained by Eq. (B.4)

CHAPTER 6

Nature of magnetism in Li_2VOSiO_4 and $VOMoO_4$

Li_2VOSiO_4 and $VOMoO_4$ are often considered as prototypes of the two-dimensional J_1-J_2 Heisenberg model. In this chapter, we will use the LDA+(c)DMFT method to study magnetic properties of both materials. We investigate magnetic ordering, $\mathbf{q}$-dependent magnetic critical temperature and effects of the local correlations on degrees of frustration and three-dimensionality.

At first, we will overview the physics of the frustrated antiferromagnets. Then, we will explain the crystal structure of Li_2VOSiO_4 and $VOMoO_4$, and review experiments and theoretical works which have been done up to now. Next, we will describe our approach to study the nature of magnetic interactions in Li_2VOSiO_4 and $VOMoO_4$ and present our results.

Contents

6.1 Frustrated antiferromagnets . . . 119
6.2 Vanadium oxide compounds: $VOMoO_4$ and Li_2VOSiO_4 . . . 122
6.2.1 Crystal structure . . . 122
6.2.2 Weakly frustrated two-dimensional J_1-J_2 Heisenberg model . . . 123
6.3 Method . . . 125
6.4 Results . . . 127
6.4.1 Electronic structure . . . 127
6.4.2 Static magnetic susceptibility: An LDA+DMFT calculation . . . 128
6.4.3 Static magnetic susceptibility: An LDA+Mean Field calculation . . . 131
6.4.4 Curie-Weiss temperature and magnetic moments . . . 137
6.4.5 Magnetic super-exchange coupling . . . 138
6.4.6 Non-local effects . . . 143

6.1 Frustrated antiferromagnets

Frustration occurs in a system wherein the energy for bonds between pair of spins can not be minimized simultaneously. Frustration leads to a large degeneracy of the ground state of the system [69, 70]. The origin of the frustration can be the geometry of a system [71, 72] and/or the kind of interactions in the Hamiltonian [69, 73].

As an example, let us consider a two-dimensional square lattice spin system (see Fig. 6.1) with an antiferromagnetic interaction between nearest neighbor spins (J_1).

$$H = -\frac{1}{2}J_1 \sum_{\langle i,j \rangle} S_i^z S_j^z; \qquad J_1 < 0\text{: antiferromagnetic exchange coupling,} \tag{6.1}$$

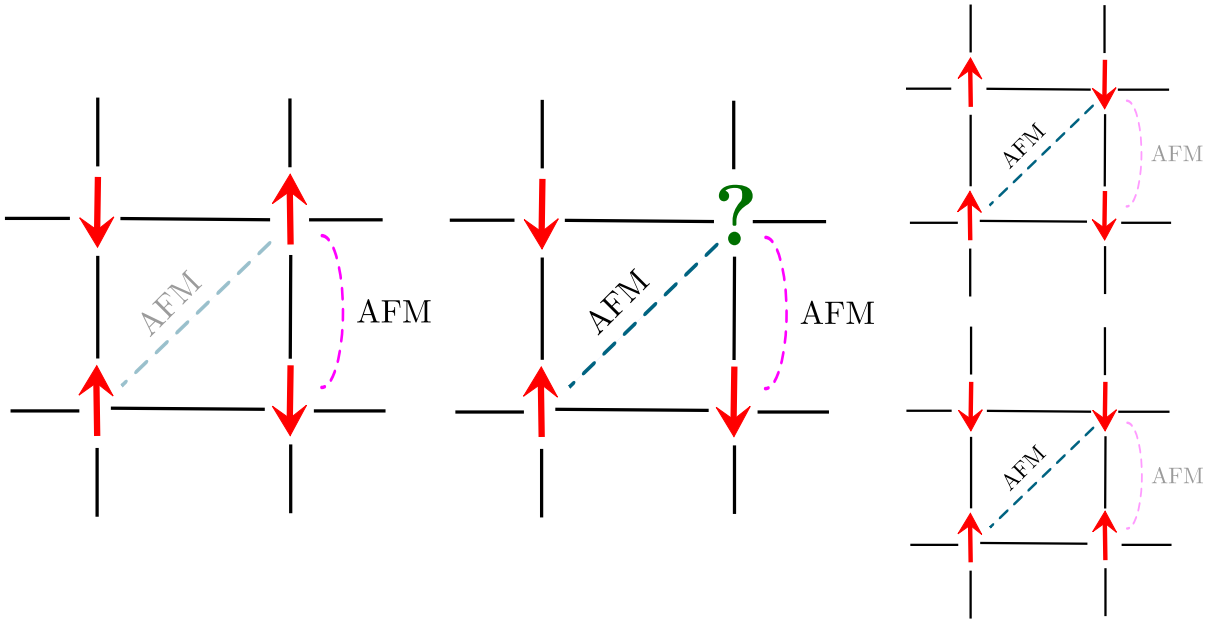

Figure 6.1: Two-dimensional J_1-J_2 square lattice model. *Left:* The nearest neighbor antiferromagnetic interaction J_1 is stronger than the antiferromagnetic next nearest interaction J_2. Hence, all neighboring spins choose an anti-parallel configuration to minimize the energy. *Middle:* For $J_2 \sim J_1/2$, all four spins in the corner of the square can not be anti-parallel at the same time. This is an example of frustration. *Right:* If $J_2 \gg J_1$, antiferromagnetic collinear order appear in the system. In this case, all the spins in a row are parallel but anti-parallel along a column or vice versa. Hence, the ground state is degenerate.

where i runs over all lattice sites and j runs over nearest neighbors to i. In this case, in the antiferromagnetic state, each pair of spins individually minimizes its energy so that nearest neighbor spins choose antiparallel configuration (Fig. 6.1). The situation becomes complicated if the antiferromagnetic interaction between next nearest neighbor spins (J_2) is taken into account

$$H = -\frac{1}{2}J_1 \sum_{\langle i,j \rangle} S_i^z S_j^z - \frac{1}{2}J_2 \sum_{\langle\langle i,j \rangle\rangle} S_i^z S_j^z, \tag{6.2}$$

where $\sum_{\langle\langle i,j \rangle\rangle}$ denotes to summation over next nearest neighbor spins. In this case, when $|J_2| \sim |J_1|/2$ energy of the 4th spin (the question mark in the middle panel of Fig. 6.1) is the same if the spin points upward or downward. Therefore, the energy of each bond can not be simultaneously minimized and frustration occurs. The ground state of this model depends on the (J_2/J_1) ratio. For $|J_2| < |J_1|/2$, nearest neighbor spins in the ground state are antiparallel. Once the value of J_2 approaches $\sim 1/2\ |J_1|$, spin fluctuations increase and frustration becomes important. This gives rise to a transition from antiferromagnetic Neel order to a disordered state. Increasing $|J_2|$ to values larger than $1/2\ |J_1|$ leads to collinear order in the system. In the collinear ordered state, spins are aligned ferromagnetically along the x-axis and antiferromagnetically along the y-axis or vice versa. Therefore, system has two degenerate ground states.

One of the relevant quantities to identify frustrated materials is the temperature (T) dependent magnetic susceptibility χ. The presence of divergency or peak in χ signals a transition

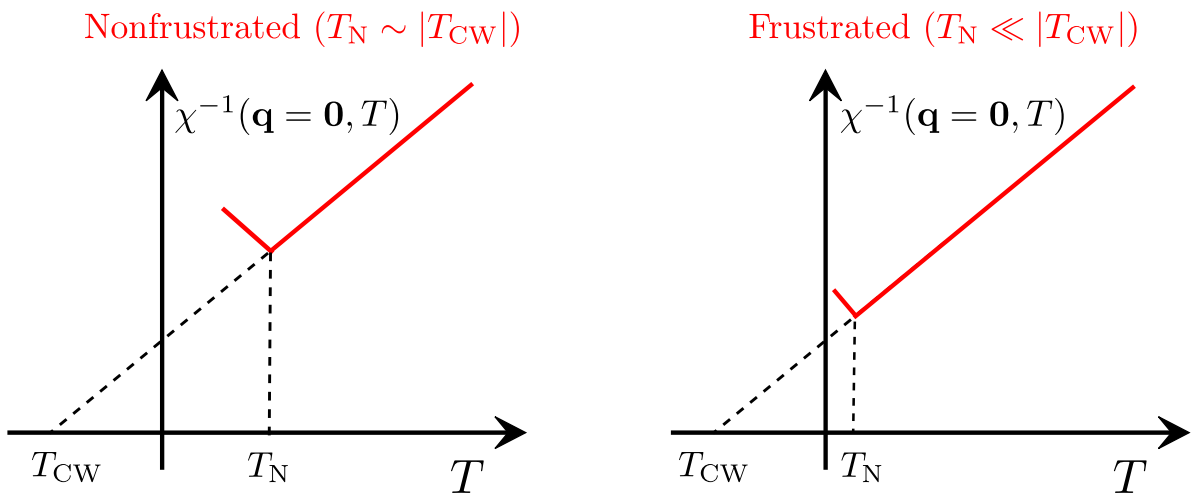

Figure 6.2: *Left:* Typical behavior of the inverse susceptibility $\chi^{-1}(\mathbf{q}=\mathbf{0},T)$ of non-frustrated antiferromagnetic systems where the ratio $F = T_{CW}/T_N \sim 1$. *Right:* $\chi^{-1}(\mathbf{q}=\mathbf{0},T)$ behavior with respect to the temperature T where the ordering temperature T_N is much smaller than the Curie-Weiss temperature. Therefore, for frustrated systems $F = T_{CW}/T_N > 1$.

from paramagnetic state to magnetic ordering. Furthermore, at high temperatures, the inverse of the static uniform magnetic susceptibility $\chi^{-1}(\mathbf{q}=\mathbf{0},T)$ behaves linearly with respect to the temperature T (the so-called Curie-Weiss law)

$$\chi^{-1}(\mathbf{q}=\mathbf{0},T) \sim T - T_{CW}, \tag{6.3}$$

for T greater than the transition temperature. In this relation, T_{CW} is Curie-Weiss temperature and can be used to determine the type of the magnetic ordering in a material. For instance, for the J_1-J_2 square lattice model described in Eq. (6.2), if $T_{CW} = 0$, the material is paramagnetic. $T_{CW} > 0$ indicates that the material is ferromagnetic and the susceptibility diverges at $T_c = T_{CW}$. For the same model, negative Curie-Weiss temperature $T_{CW} < 0$ points to antiferromagnetic ordering of a material. In the latter case, the material undergoes a magnetic transition to the ordered state at Neel temperature T_N.

In the following we mainly focus on the class of materials which goes through the magnetic transition to antiferromagnetic order and can be explained by the Heisenberg Hamiltonian

$$H = -\frac{1}{2}\sum_{ij} J_{ij}\ \mathbf{S}_i \cdot \mathbf{S}_j. \tag{6.4}$$

In order to investigate the difference between general behavior of the high temperatures magnetic susceptibilities in frustrated and non-frustrated materials, we employ mean field approach. Through the mean filed approximation, the high temperature magnetic susceptibility is given by

$$\chi(\mathbf{q},T) = \frac{C}{T - T_{\mathbf{q}}^{MF}}, \tag{6.5}$$

where

$$T_{\mathbf{q}}^{MF} = \frac{1}{3}J(\mathbf{q})\ S(S+1), \qquad C = \frac{1}{3}(g\mu_B)^2 S(S+1). \tag{6.6}$$

Here, $J(\mathbf{q})$ is the Fourier integral of the $J_{ij} = J(\mathbf{R}_i - \mathbf{R}_j)$ and a function of nearest neighbor (J_1), next nearest neighbor (J_2) etc coupling constants.
In the case of the J_1-J_2 spin half ($S = 1/2$) Heisenberg model (see Eq. (6.2)), $J(\mathbf{q})$ is given by $\sim 2J_1(\cos q_x + \cos q_y) + 4J_2 \cos q_x \cos q_y$. For this model, at $\mathbf{q} = \mathbf{0}$ the Curie-Weiss temperature is $T_{\mathrm{CW}} = T_{\mathbf{q}=\mathbf{0}} \sim 4J_1 + 4J_2$ and the transition temperature T_{N} can be approximately obtained through the mean field via $T_{\mathrm{N}} \sim 4J_2 - 4J_1$ [74]. In this model, for *non-frustrated* cases where $|J_1| \gg |J_2|$ or $|J_1| \ll |J_2|$, the Curie and Neel temperature are almost identical $T_{\mathrm{N}} \sim |T_{\mathrm{CW}}|$, while for the *frustrated* case $|J_2| \sim |J_1|/2$, the ordering temperature T_{N} is much lower than the Curie-Weiss temperature $T_{\mathrm{N}} \ll |T_{\mathrm{CW}}|$. This leads to a conclusion that the ratio

$$F = \left|\frac{T_{\mathrm{CW}}}{T_{\mathrm{N}}}\right| \approx \left|\frac{J_1 + J_2}{J_2 - J_1}\right|, \tag{6.7}$$

provides quality of the frustration, so that for non-frustrated regime $F \sim 1$ while for the frustrated case $F > 1$ [72]. Furthermore, for both frustrated and non-frustrated systems, the inverse magnetic susceptibility $\chi^{-1}(\mathbf{q} = \mathbf{0}, T)$ remains linear in temperature for $T > T_{\mathrm{N}}$, as it is shown schematically in Fig. 6.2. Deviation from the linearity behavior with respect to T can arise from increasing the correlation length. Therefore, in the frustrated regime where large fluctuations are present and correlation length is small in comparison with the non-frustrated case, $\chi^{-1}(\mathbf{q} = \mathbf{0}, T)$ extends the temperature region in which the Curie-Weiss law holds (Compare the left and right panels of Fig. 6.2).
In general, if the frustration occurs due to the competition of antiferromagnetic exchange couplings among neighbors (see, e.g., Eq. (6.2)), the high temperature magnetic susceptibility may provide informations regarding the exchange couplings and consequently about the degree of frustration $f = J_2/J_1$ in the system.

Experimentally, several compounds have been identified as possible frustrated materials: $NaTiO_2$ (triangular magnetic lattice), FeF_3 (pyrochlore structure), Li_2VOSiO_4 and $VOMoO_4$ (quasi two-dimensional square lattice) [69, 72, 75]. In this thesis, we mainly focus on the prototype of two-dimensional lattice systems Li_2VOSiO_4 and $VOMoO_4$ materials which experimentally have been studied thorough NMR and neutron powder- and high resolution X-ray diffraction [16, 17, 76] and theoretically by LDA (+ perturbation theory) band structure calculations [18, 77, 78]. Our aim is to study these systems with the state-of-the-art approach for correlated materials, the LDA+(c)DMFT method.

6.2 Vanadium oxide compounds: $VOMoO_4$ and Li_2VOSiO_4

6.2.1 Crystal structure

The crystal structure of $VOMoO_4$ consists of VO_5 pyramids and MoO_4 tetrahedra. VO_5 pyramids form layers as shown in Fig. 6.3; each pyramid is connected to four MoO_4 tetrahedra by corner sharing [79]. In $VOMoO_4$, Vanadium ion V^{+4} has one electron in d-orbital (t_{2g}) and forms a spin half ($S = 1/2$). The unit cell of $VOMoO_4$ contains two atoms. Within a single layer, the VO_5 pyramids are rotated and they alternatively point upward and downward. This compound can be effectively described by a single band model Hamiltonian [18] because there is only one band at Fermi level.

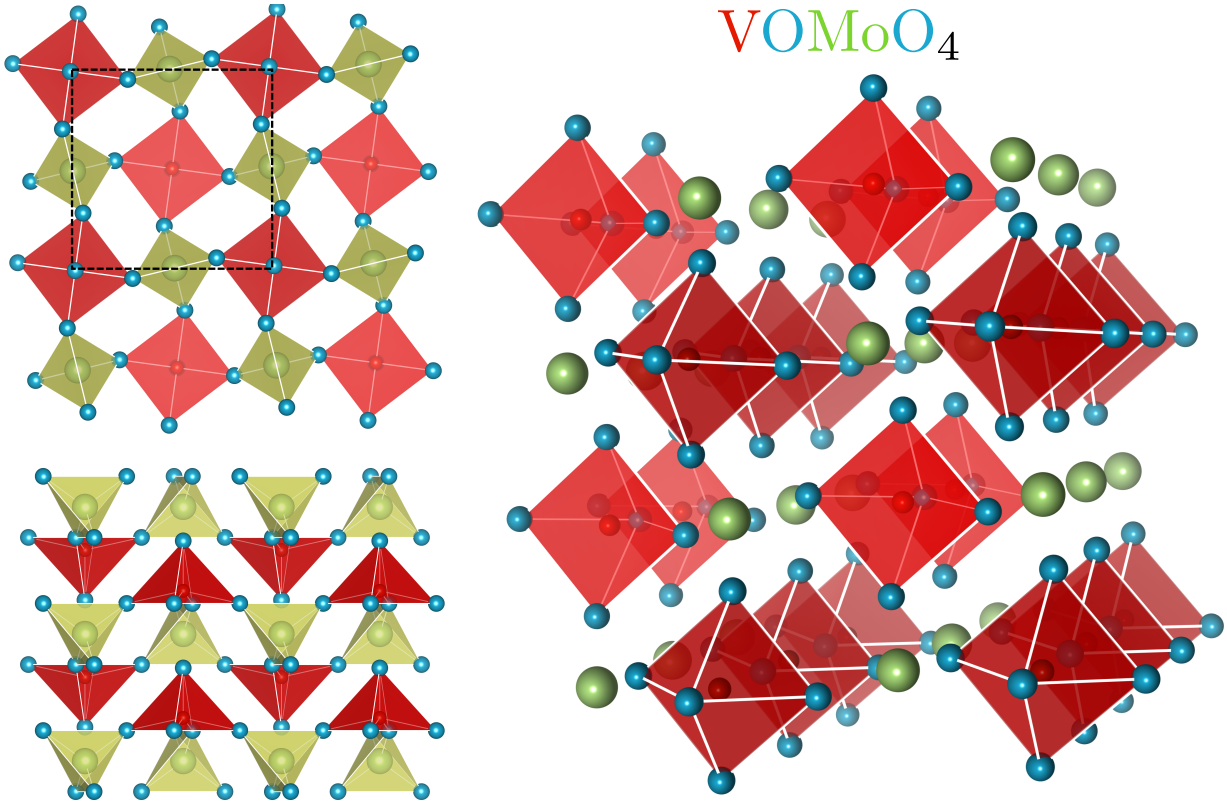

Figure 6.3: $VOMoO_4$ crystal structure. *Right:* A perspective view of VO_5 pyramids which are connected to MoO_4 tetrahedra (not shown here). *Upper left panel:* the crystal structure of $VOMoO_4$ seen from the **c** direction, showing a small rotation of VO_5 pyramids and MoO_4 tetrahedra. The unit cell is highlighted with a square dash line. *Lower Left panel:* two layers of $VOMoO_4$ are shown. Alternatively, VO_5 pyramids in a single layer is pointing upward and downward.

Crystal structure of Li_2VOSiO_4 is made by VO_5 square pyramids and SiO_4 tetrahedra [80]. In each layer, the VO_5 pyramids are sharing corners with the SiO_4 tetrahedra. Lithium cations are then inserted between layers in the crystal (See Fig. 6.4). Similar to $VOMoO_4$ crystal, inside a layer of $VOSiO_4$, VO_5 square pyramids are pointing in opposite direction alternately. Furthermore, Vanadium cations (V^{+4}) have one electron with $S = 1/2$ in t_{2g} orbital. Within a single layer, pyramids form a pseudo-square lattice with neighboring V^{+4} ions. The unit cell of Li_2VOSiO_4 contains two formula units. Different from $VOMoO_4$, square pyramids are not rotated. Again an effective single band model Hamiltonian can be utilized to investigate the low energy physics of Li_2VOSiO_4.

6.2.2 Weakly frustrated two-dimensional J_1-J_2 Heisenberg model

Within a single layer of $VOMoO_4$ and Li_2VOSiO_4, neighboring Vanadium ions form a pseudo-square lattice. The antiferromagnetic exchange interactions J_1 and J_2 are between V ions in this pseudo square lattice. J_1 and J_2 are associated to the exchange interactions along the side and along diagonal of the square, respectively (see Fig. 6.5).

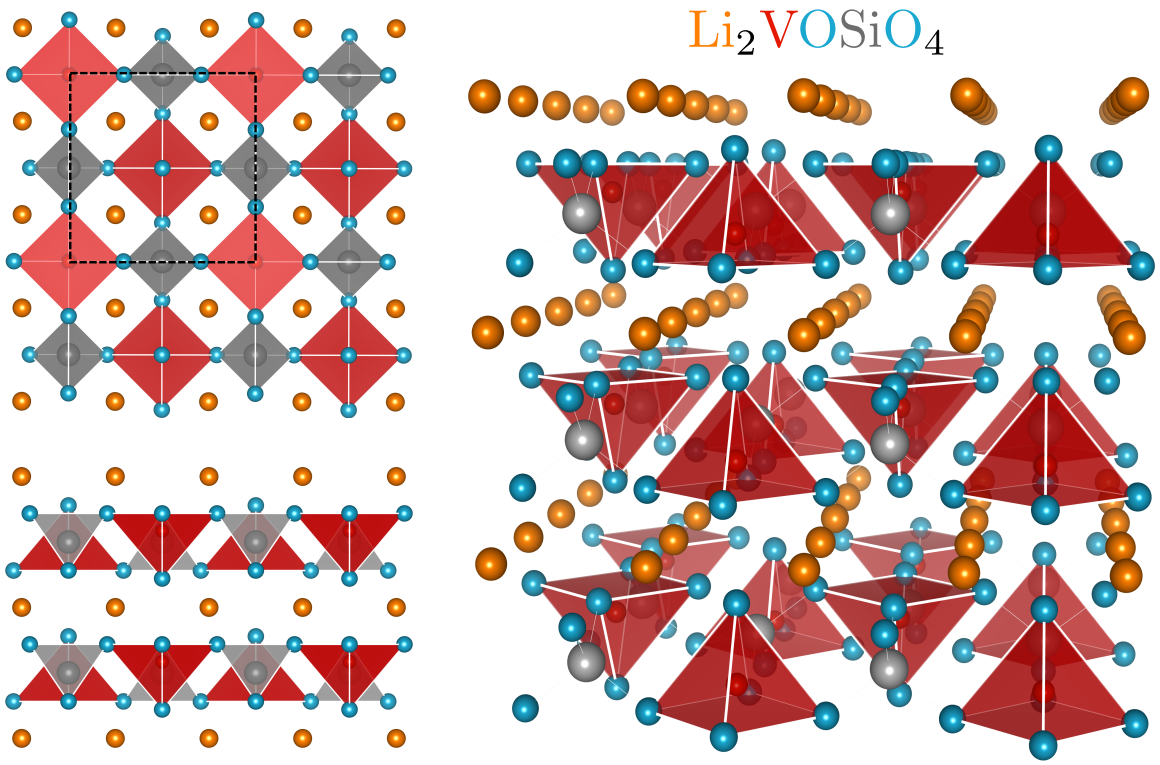

Figure 6.4: Li_2VOSiO_4 crystal structure. *Right:* A perspective view of Li_2VOSiO_4 crystal. VO_5 square pyramids are placed in each layer (SiO_4 tetrahedra are not shown here). *Upper left panel:* the crystal structure of Li_2VOSiO_4 (view from **c** axis). In comparison with Fig. 6.3, pyramids and tetrahedra are not rotated. *Lower left panel:* two layers of Li_2VOSiO_4 are displayed. Similar to $VOMoO_4$, VO_5 pyramids are pointing in opposite directions within a layer. The shaded square is the unit cell of Li_2VOSiO_4.

Several experiments such as NMR, muon-spin rotation, magnetization and specific measurements, neutron and high resolution X-ray diffraction have been done to study magnetic properties of Li_2VOSiO_4 and $VOMoO_4$ [16, 17, 18, 76, 77]. All these experiments suggest that both materials can be considered as prototypes of the two-dimensional J_1-J_2 quantum antiferromagnetic Heisenberg model.

For Li_2VOSiO_4, R. Melzi *et al.* [16] performed NMR and muon-spin rotation measurements; they reported an antiferromagnetic collinear order at 2.8 K. Later on, the same group estimated $J_1 + J_2 \sim 8.5$ K and $J_2/J_1 \sim 1.1$ via thermodynamic measurements [17]. Similar observations (with sizably larger $J_1 + J_2 \sim 155$ K) were reached for $VOMoO_4$ within the NMR experiments by P. Carretta *et al.* [18]. They also found that the magnetic susceptibility of $VOMoO_4$ and Li_2VOSiO_4 show similar behavior with respect to $T/T_{\rm CW}$ ratio.

In addition to NMR, muon-spin rotation and thermodynamic measurements, theoretical studies based on *ab-initio* calculations have been done for Li_2VOSiO_4 and $VOMoO_4$. In the case of Li_2VOSiO_4, H. Rosner *et al.* [78, 81] obtained $J_2/J_1 \sim 12 \gg 1/2$ which places this material well inside the collinear regime. In contrast to NMR and thermodynamic measurements, the LDA calculations show weakly frustration picture of Li_2VOSiO_4. In the case of $VOMoO_4$, P. Carretta *et al.* [18] obtained $J_2/J_1 \sim 0.2$ that indicates this material is antiferromagnetically

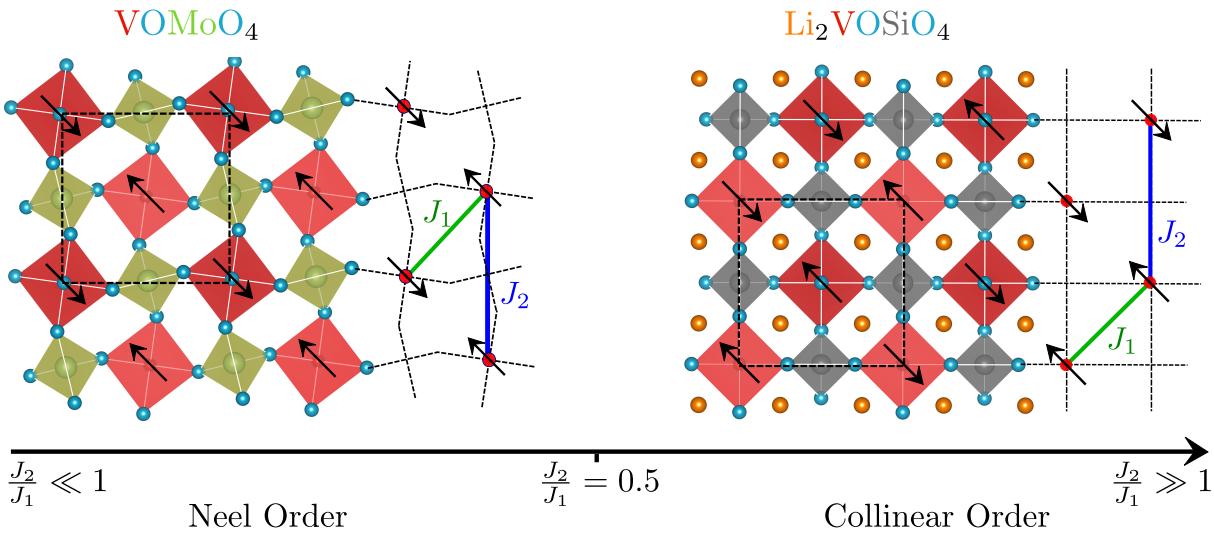

Figure 6.5: Nearest and next nearest antiferromagnetic coupling (J_1 and J_2) are shown between Vanadium ions in Li_2VOSiO_4 and $VOMoO_4$. *Left:* Neel order of $VOMoO_4$ is established below $T_N \sim 42$ K [18]. *Right:* Below $T_N \sim 2.8$ K, collinear order appears in Li_2VOSiO_4 [17].

Neel ordered, i.e., in the opposite side of the Li_2VOSiO_4 on the frustration axis (see Fig. 6.5).

Neutron diffraction and high resolution x-ray scattering experiments on Li_2VOSiO_4 and $VOMoO_4$ report three-dimensional magnetic ordering for both materials with in-plane antiferromagnetic collinear order for Li_2VOSiO_4 [77] and in-plane antiferromagnetic Neel order for $VOMoO_4$ [76] which are consistent with the LDA calculations.

To understand the role of the purely electronic mechanism and consequently, the local electronic correlation and non-local effects in the frustration, we go beyond the LDA+perturbation theory (LDA+PT). We use the LDA+(c)DMFT method and calculate the magnetic response function. Through analysis of the magnetic susceptibility, we are able to provide informations on the degree of frustration, magnetic ordering and strength of magnetic exchange coupling constants.

6.3 Method

Using the LDA+(c)DMFT approach, we investigate the magnetic properties of Li_2VOSiO_4 and $VOMoO_4$. In the first step, we construct a generalized Hubbard Hamiltonian for the Vanadium d bands as follows

$$\begin{aligned} H &= -\sum_{ii'}\sum_{\alpha\alpha'}\sum_{mm'}\sum_{\sigma\sigma'} t^{i\alpha,i'\alpha'}_{m\sigma,m'\sigma'} c^{\dagger}_{i\alpha m\sigma} c_{i'\alpha' m'\sigma'} + \sum_{i}\sum_{m} U_{mm} n_{i\alpha m\uparrow} n_{i\alpha m\downarrow} \\ &\quad + \frac{1}{2}\sum_{i}\sum_{\alpha}\sum_{m(\neq m)}\sum_{\sigma\sigma'} (U_{mm'} - J\delta_{\sigma\sigma'}) n_{i\alpha m\sigma} n_{i\alpha m'\sigma'}. \end{aligned} \tag{6.8}$$

In this Hamiltonian, $c^{\dagger}_{i\alpha m\sigma}$ ($c_{i\alpha m\sigma}$) creates (annihilates) an electron with spin σ in orbital $m = t_{2g}$ on lattice site i and atomic site in the unit cell α; $n_{i\alpha m\sigma} = c^{\dagger}_{i\alpha m\sigma} c_{i\alpha m\sigma}$ is the number operator. $t^{i\alpha,i'\alpha'}_{m\sigma,m'\sigma'}$ is the matrix elements of hopping ($i \neq i'$) and crystal field ($i = i'$ and

$\alpha = \alpha'$) integral (see Eq. (2.29)). We compute it *ab-initio* by downfolding the high-energy bands to the Vanadium $3d$ orbital (based on the Nth-order Muffin-Tin Orbital (NMTO) [43]) and constructing a localized Wannier function basis. The parameters $U_{mm'} = U - 2J(1 - \delta_{mm'})$ and J are direct and exchange Coulomb interaction, respectively. In the case of Li_2VOSiO_4 and $VOMoO_4$, there is only one partially filled band, $m = xy$-like band *per atom in a unit cell* which is well separated from the xz- and yz-like bands due to crystal field splitting. Hence we perform further downfolding to xy band. Consequently, the third term in the Hamiltonian (6.8) does not contribute. In the second step, we solve this Hamiltonian with DMFT and cluster DMFT. We use the Hirsch-Fye quantum Monte-Carlo method as impurity solver. In the last (c)DMFT iteration, we calculate the local two-particle correlation function (see Eq. 5.84). Using that, the local spin susceptibility $[\chi^s]$ and the (spin) local vertex function $[\mathbf{\Gamma}^s]$ are computed by Eqs. (5.87, 5.90) and (5.92). Next, we use the local vertex approximation in which the $\mathbf{q}$-dependent vertex function $\Gamma^s(\mathbf{q}, \omega_m)$ is approximated by the local one $\mathbf{\Gamma}^s(\omega_m) = \frac{1}{N_\mathbf{q}} \sum_\mathbf{q} \mathbf{\Gamma}^s(\mathbf{q}, \omega_m)$, to compute the $\mathbf{q}$-dependent susceptibility tensor by the following matrix equation

$$\chi^s(\mathbf{q}, \omega_m) = \left[\left[\chi^{\mathbf{0},s}(\mathbf{q}, \omega_m)\right]^{-1} - \left[\mathbf{\Gamma^s}(\omega_m)\right]^{-1} \right]^{-1}, \tag{6.9}$$

where $\chi^{\mathbf{0},s}$ is the spin susceptibility without vertex contribution ($\mathbf{\Gamma}^s = 0$) obtained by Eq. (5.98). In the case of Li_2VOSiO_4 and $VOMoO_4$, where there are two atomic sites per unit cell, the supercell magnetic susceptibility is calculated by[1]

$$\begin{aligned} \chi(\mathbf{q}, \omega_m) &= \frac{1}{\beta^2} \sum_{nn'} \frac{1}{N_S} \sum_{\kappa_i \kappa_j} e^{-i\mathbf{q}.(\mathbf{T}_{\kappa_i} - \mathbf{T}_{\kappa_j})} \chi^s_{\kappa_i \kappa_j}(\nu_n, \nu_{n'}; \mathbf{q}, \omega_m) \\ &= \frac{1}{\beta^2} \sum_{nn'} \frac{1}{N_S} \sum_{\kappa_i \kappa_j} e^{-i\phi_{\kappa_i \kappa_j}} \chi^s_{\kappa_i \kappa_j}(\nu_n, \nu_{n'}; \mathbf{q}, \omega_m), \end{aligned} \tag{6.10}$$

where we consider $\chi^s_{\kappa_i \kappa_j} \equiv \chi^s_{\kappa_i \kappa_i \kappa_j \kappa_j}$ for the sake of simplicity; $\mathbf{T}$ is the lattice vector and the phase term $\phi_{\kappa_i \kappa_j}$ is given by

$$\begin{cases} \phi_{11} = \phi_{22} = 0 \\ \phi_{12} = -\phi_{21} = \dfrac{q_x + q_y}{2} - q_z \end{cases}. \tag{6.11}$$

It is, however, convenient to consider

$$\phi_{12} \to \phi_{12} + \pi = \frac{[q_x + \pi] + [q_y + \pi]}{2} - q_z, \tag{6.12}$$

so that in the plot the origin is $\Gamma_1 = (2\pi, 0)$ point, hence $\mathrm{M} = (\pi, \pi)$ point of the *small* Brillouin zone (a point where the AFM order will be identified), as it is shown in the *right panel* of Fig. 6.6. Notice that if we do not consider the phase term (i.e., $\phi_{\kappa_i \kappa_j} = 0$), then $\chi(\mathbf{q}, \omega_m)$ will be the response function to a magnetic field which is on phase (or identical) on sites 1 and 2. In Eq. (6.10), the summation should be done over infinite number of frequencies. Numerically, we perform sum over N_p number of Matsubara frequencies and then we use an extrapolation to recover infinite N_p limit (see Sec. 5.4.7 for more details).

[1] From now on, we consider the magnetic susceptibility χ^{zz} as χ for the sake of simplicity.

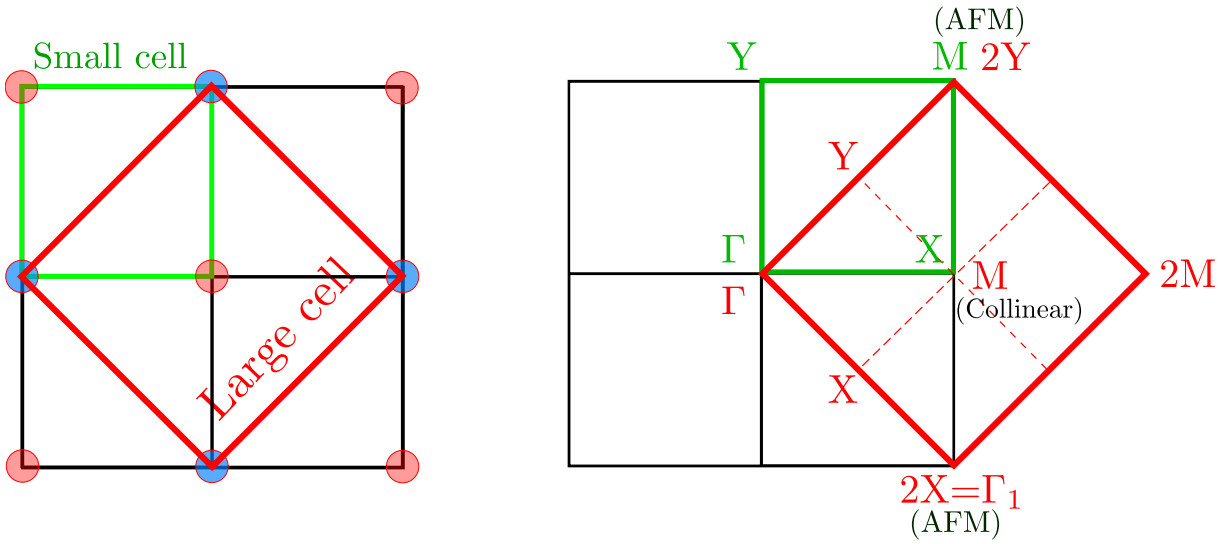

Figure 6.6: *Left panel*: Doubling of the unit cell. The small and large (or unit) cells are distinguishable with green and red colors. *Right panel*: The Brillouin zones related to small and large cells are distinguishable with their colors; green and red squares are the Brillouin zone of the small and large cells, respectivley. In this panel, $\Gamma = (0,0)$, $\mathrm{X} = (\pi,0)$, $\mathrm{M} = (\pi,\pi)$, $\mathrm{Y} = (0,\pi)$, and $\Gamma_1 = (2\pi,0)$. The lattice susceptibility is calculated for the red and rotated square. In this square, the antiferromagnetic (AFM) order is realized at $\Gamma_1 = 2\mathrm{X} = (2\pi,0)$, $2\mathrm{Y} = (0,2\pi)$, and collinear order at $\mathrm{M} = (\pi,\pi)$ (or $\mathrm{X} = (\pi,0)$). Considering a π shift in the phase term, i.e. $\phi_{12} \to \phi_{12} + \pi$, the origin corresponds to Γ_1 point.

6.4 Results

6.4.1 Electronic structure

Both $VOMoO_4$ and Li_2VOSiO_4 are characterized by two bands at Fermi level (since there are two V in a unit cell) which are narrow and well separated from the other valence bands below the Fermi level; in case of $VOMoO_4$, the band width is $W \sim 1.1$ eV while for Li_2VOSiO_4 the band width is sizably smaller $W \sim 0.4$ eV (See Fig. 6.7).

Within a single layer, hopping parameters between nearest neighbors (t_1) and next nearest neighbors (t_2) are quite different. Nearest neighbor hopping in $VOMoO_4$ is $t_1 \sim 0.1367$ eV, while it is one order of magnitude smaller $t_1 \sim 0.0107$ eV for Li_2VOSiO_4. The next nearest neighbor hopping parameter for both materials is comparable: $t_2 \sim 0.0332$ eV for $VOMoO_4$ and $t_2 \sim -0.0376$ eV for Li_2VOSiO_4. Along the z-direction, there are two different hopping parameters; i) a hopping between Vanadium ions in neighboring layers (on the top of each other) in pyramids pointing in the same direction t_z, ii) a hopping between Vanadium ions in neighboring layers in the pyramids pointing in opposite direction t_1'. From the LDA calculations, the hopping t_z is also comparable for the two materials, so that we obtain $t_z \sim 0.0121$ eV for $VOMoO_4$ and $t_z \sim -0.0148$ eV for Li_2VOSiO_4. However, the hopping t_1' is quite different in two materials. The hopping t_1' in $VOMoO_4$ is around $t_1' \sim 0.0115$ eV, while it is almost negligible for Li_2VOSiO_4.

The two narrow bands at Fermi level originate from t_{2g} orbitals ($3d^1$ electronic configura-

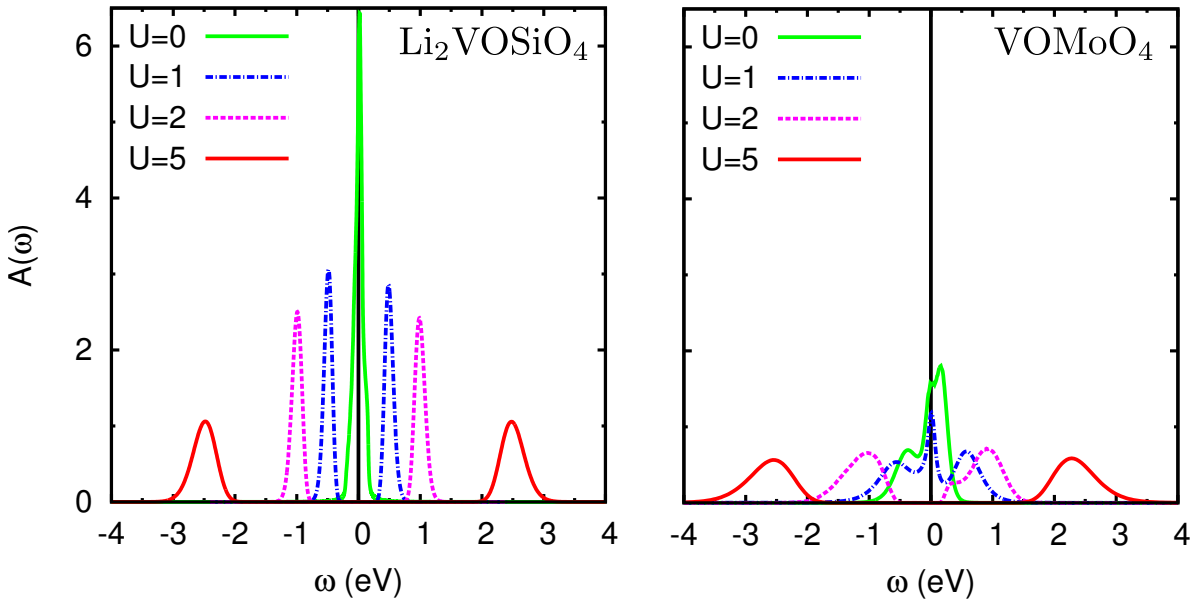

Figure 6.7: Density of states $A(\omega)(\mathrm{eV}^{-1})$ for Li_2VOSiO_4 and $VOMoO_4$ for $T \sim 387$ K and different values of U obtained from LDA+DMFT calculations.

tion), and are half filled. Experimentally, both materials are Mott insulators and therefore strong correlation effects are crucial. Since, to the best of our knowledge, there is no experimental value of the energy gap, we calculate the correlated bands and the magnetic response function for several values of the direct screened Coulomb repulsion U(=1-5) eV by the LDA+DMFT approach. The largest value, $U = 5$ eV, is a typical value for vanadate oxides [82, 83]. Our calculations show that a metal-insulator transition occurs for U between 1.5 eV and 2 eV in $VOMoO_4$, and U slightly smaller than 1 eV for Li_2VOSiO_4 (see Fig. 6.7). After extracting the self energy on the real axis $\Sigma(\omega)$ we are able to compute the correlated bands (Hubbard bands) over the Brillouin zone by

$$A(\mathbf{k},\omega) = -\frac{1}{\pi}\Im m\left[\mathcal{G}(\mathbf{k},\omega)\right] = -\frac{1}{\pi}\Im m\left[\frac{1}{\omega+\mu-H^{\mathrm{LDA}}(\mathbf{k})-\Sigma(\omega)}\right]. \tag{6.13}$$

Results for a realistic $U = 5$ eV are shown in Fig. 6.8. Dispersion of the Hubbard bands for both materials are almost identical to dispersion of the LDA bands (see Fig. **??**). Energy gap is similar for both materials; $\Delta \sim 3.8$ eV for $VOMoO_4$ and $\Delta \sim 4$ eV for Li_2VOSiO_4. The energy gap increases linearly with U.

6.4.2 Static magnetic susceptibility: An LDA+DMFT calculation

Using the LDA+DMFT method, we calculate the static magnetic lattice susceptibility $\chi(\mathbf{q},\omega=0)$ for the realistic value of the Coulomb interaction $U = 5$ eV. To understand the role of the vertex function in magnetic properties of $VOMoO_4$ and Li_2VOSiO_4, we perform these calculations in presence and absence of the local vertex function. We use Eq. (6.10) and consider the phase term described in Eq. (6.12). Our results have been shown in Fig. 6.9 for $VOMoO_4$ and Fig. 6.10 for Li_2VOSiO_4.

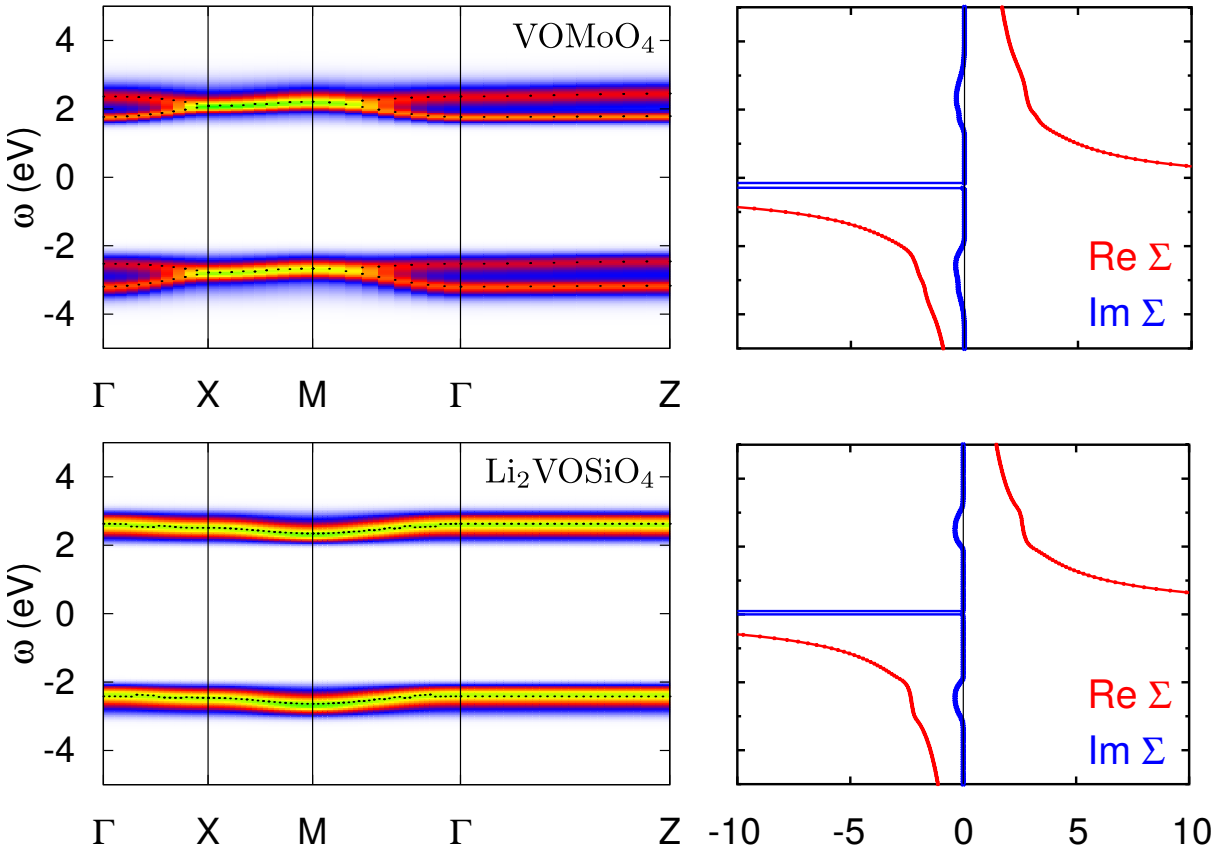

Figure 6.8: Hubbard bands for $VOMoO_4$ (upper left panel) and Li_2VOSiO_4 (lower left panel) for realistic $U = 5$ eV. Here, $\Gamma = (0,0,0)$, $X = (\pi,0,0)$, $M = (\pi,\pi,0)$, and $Z = (0,0,\pi)$. Small dots are the poles of the Green's function which return the energy dispersion of the system. *Right panel:* Real and imaginary part of the self energy on the real axis.

Without the vertex corrections, the spin susceptibility is weakly temperature dependent, and is very far from the the Curie-Weiss law. Furthermore, we find that the absence of the vertex function leads to strong decrease of the magnetic susceptibility when U increases. As it is shown in Fig. 6.9, the $\mathbf{q}$-dependent magnetic response of $VOMoO_4$ is strongly enhanced by the vertex function, so that $\chi^{-1}(\mathbf{q},\omega = 0)$ behaves linearly with T at high temperatures, in line with Curie-Weiss law. The magnetic susceptibility changes slightly with q_z. This shows that the coupling constant along the z-direction is weak.[2] Moreover, a peak appears in the $\chi(\mathbf{q},\omega = 0)$ at $\mathbf{q}_C = (2\pi, 0, q_z)$. Remarkably, we find that $\chi(\mathbf{q}_C)$ has its maximum value at $q_z = 0$ (or $q_z = 2\pi$). Hence, if super-exchange dominates, two Vanadium ions on the top of each other are ferromagnetically ordered (see Fig. 6.11). This suggests that the magnetic order is three dimensional in $VOMoO_4$, in line with neutron powder- and high resolution X-ray diffraction [76], although the coupling between Vanadium sites in neighboring layers is small.

For Li_2VOSiO_4, similar to $VOMoO_4$, we find that the vertex correction has a dominant role in the $\mathbf{q}$-dependent magnetic susceptibility (see the difference between upper and lower panels in Fig. 6.10); $\chi(\mathbf{q},\omega = 0)$ is maximum at $M = (\pi,\pi,q_z)$ which is related to in-plane antiferromag-

[2] In the Sec. 6.4.5, we calculate the value of this coupling constant.

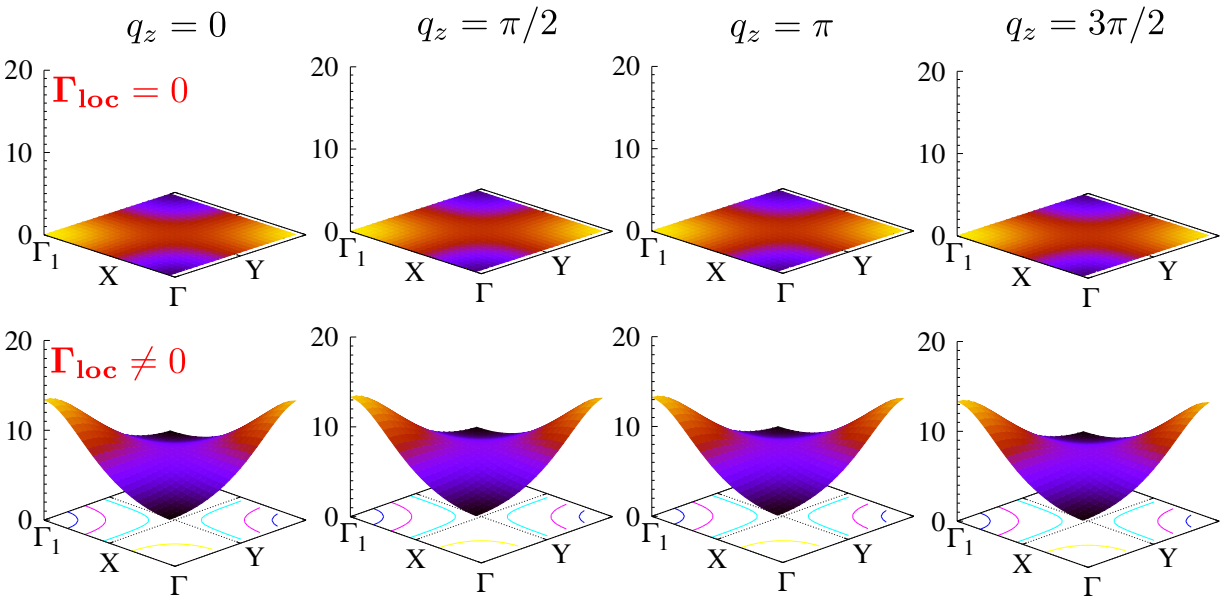

Figure 6.9: Static $\mathbf{q}$-dependent spin susceptibility $\chi(\mathbf{q}, \omega = 0)$ of $VOMoO_4$ in the q_x, q_y plane for different values of q_z, for $U = 5$ eV and $T = 387$ K. *Top:* $\chi(\mathbf{q}, \omega = 0)$ without vertex correction. *Bottom:* $\chi(\mathbf{q}, \omega = 0)$ with the vertex correction. The susceptibility is maximum at the $\Gamma_1 = (2\pi, 0, q_z)$ point; it is related to antiferromagnetic Neel order in plane.

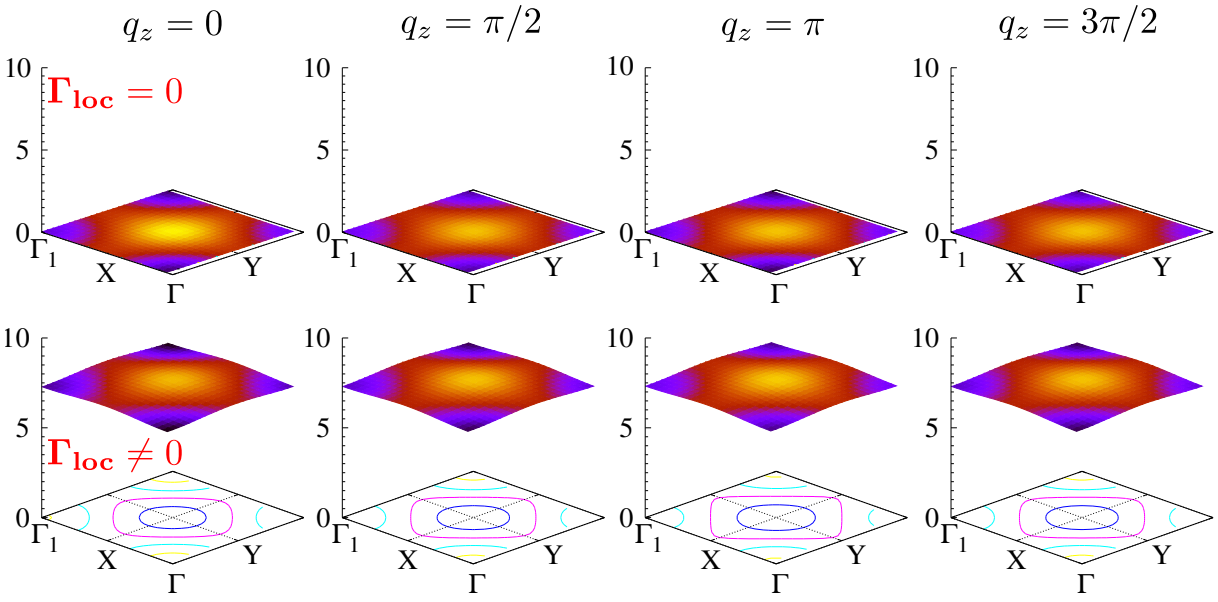

Figure 6.10: Static $\mathbf{q}$-dependent spin susceptibility $\chi(\mathbf{q}, \omega = 0)$ of Li_2VOSiO_4 in the q_x, q_y plane for different values of q_z, for $U = 5$ eV and $T \sim 387$ K. *Top:* The magnetic susceptibility in the absence of the vertex funciton. *Bottom:* The magnetic susceptibility in the presence of the vertex function. The susceptibility is maximum at $\mathrm{M} = (\pi, \pi, q_z)$; it is related to antiferromagnetic collinear order in plane.

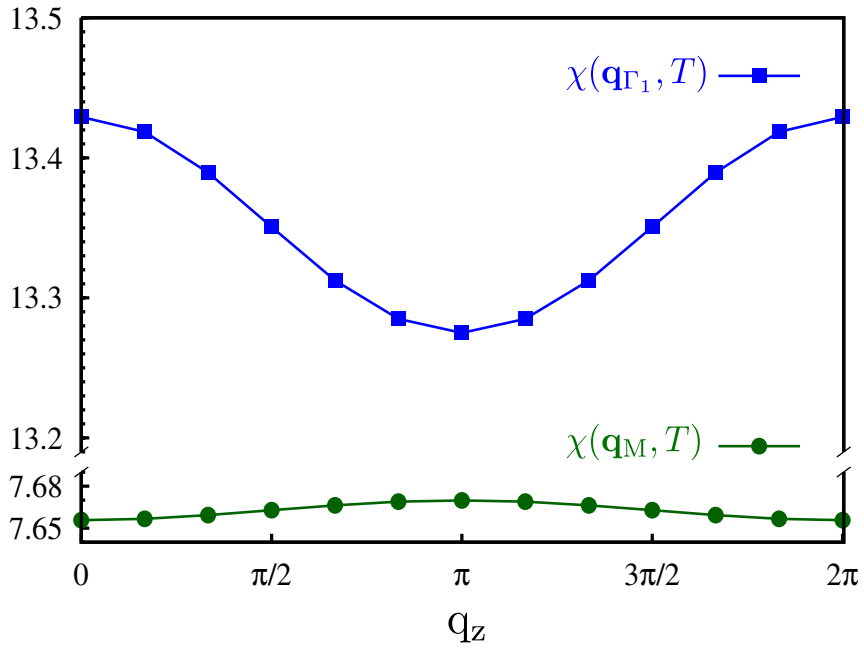

Figure 6.11: $\chi(\mathbf{q}_{\Gamma_1}, T = 387\ \mathrm{K})$ and $\chi(\mathbf{q}_{\mathbf{M}}, T = 387\ \mathrm{K})$ are shown for $VOMoO_4$ and Li_2VOSiO_4, respectively. $\chi(\mathbf{q}_{\Gamma_1}, T)$ has its maximum at $q_z = 0, 2\pi$ which indicates that $VOMoO_4$ is ordered ferromagnetically along z-direction. While $\chi(\mathbf{q}_{\mathrm{M}}, T)$ at $q_z = \pi$ is slightly bigger than the other q_z showing Li_2VOSiO_4 has antiferromagnetic order along the z-direction.

netic collinear order. The variation of the $\chi(\mathbf{q}_{\mathrm{M}}, \omega = 0)$ with respect to q_z is much smaller than in $VOMoO_4$ (see Fig. 6.11), however, the favored ordering along z-direction is anti-ferromagnetic. This inter-layer magnetic was reported to be ferromagnetic in neutron powder-diffraction experiment [77]. A possible reason is that inter-site Coulomb exchange (ferromagnetic) dominates over super-exchange thus it is changing the inter-layer magnetic ordering in Li_2VOSiO_4.

Our results for the in-plane magnetic ordering, i.e., antiferromagnetic Neel order for $VOMoO_4$ and collinear order for Li_2VOSiO_4, are in agreement with the neutron and high resolution X-ray scattering experiments [76, 77].

Interestingly, for both material, we find that the static magnetic susceptibility $\chi(\mathbf{q}, \omega = 0)$ for $\mathbf{q}_{\mathrm{X}} = (\pi, 0, \pi/2)$ and $\mathbf{q}_{\mathrm{Y}} = (0, \pi, \pi/2)$ is $\sim \beta(g\mu_B)^2 S_{\mathrm{eff}}^2$ which indicates that the critical magnetic temperature $T_{\mathbf{q}}$ is zero for $\mathbf{q} = \mathbf{q}_{\mathrm{X}}$ and $\mathbf{q} = \mathbf{q}_{\mathrm{Y}}$ points.

6.4.3 Static magnetic susceptibility: An LDA+Mean Field calculation

Using the LDA+second order perturbation theory results for the hopping parameters t_1, t_2, t_1' and t_z, we are able to calculate the static uniform spin susceptibility through mean-field (MF) theory. In the large limit U/t, the doubly occupied states are downfolded, and the effective spin Hamiltonian is (see e.g., [19])

$$H = -\frac{1}{2}\sum_{ij}\sum_{\alpha\beta} J^{\alpha\beta}(\mathbf{R}_i - \mathbf{R}_j)\ \mathbf{S}^{\alpha}(\mathbf{R}_i)\cdot\mathbf{S}^{\beta}(\mathbf{R}_j), \tag{6.14}$$

where $J^{\alpha\beta}(\mathbf{R}_i - \mathbf{R}_j) = -4[t^{\alpha\beta}(\mathbf{R}_i - \mathbf{R}_j)]^2/U$ is the coupling constant ($t^{i\alpha,j\beta} \equiv t^{\alpha\beta}(\mathbf{R}_i - \mathbf{R}_j)$); i, j are the lattice sites and α, β are atomic sites in the cell. Since for our system the Hamiltonian is single band, we drop the orbital indices m, m' here.[3] The spin operator can be rewritten as follows

$$\mathbf{S}_i^\alpha = \langle \mathbf{S}_i^\alpha \rangle + (\mathbf{S}_i^\alpha - \langle \mathbf{S}_i^\alpha \rangle), \tag{6.15}$$

where we use the notation $\mathbf{S}_i^\alpha \equiv \mathbf{S}^\alpha(\mathbf{R}_i)$ for the sake of simplicity. The first term is average of the spin and the second term describes fluctuation of the spin with respect to its average. If the fluctuation term is small enough so that $\mathcal{O}\left(\mathbf{S}_i^\alpha - \langle \mathbf{S}_i^\alpha \rangle\right)^2 \sim 0$, we can derive the following mean-field Hamiltonian

$$H_{\mathbf{MF}} \approx \frac{1}{2}\sum_{ij}\sum_{\alpha\beta} J^{\alpha\beta}(\mathbf{R}_i - \mathbf{R}_j)\, \langle \mathbf{S}_i^\alpha \rangle \cdot \langle \mathbf{S}_j^\beta \rangle - \sum_{ij}\sum_{\alpha\beta} J^{\alpha\beta}(\mathbf{R}_i - \mathbf{R}_j)\, \mathbf{S}_i^\alpha \cdot \langle \mathbf{S}_j^\beta \rangle. \tag{6.16}$$

The first term in $H_{\mathbf{MF}}$ is constant, and causes a shift in energy. Therefore we ignore it in the following. In the MF calculations, we replace the exchange interaction in the Hamiltonian (6.14) by the Zeeman term in Eq. (6.16), so that the spins are now coupled to an effective field

$$\mathrm{h}_i^\alpha = \sum_j \sum_\beta J^{\alpha\beta}(\mathbf{R}_i - \mathbf{R}_j)\langle \mathbf{S}_j^\beta \rangle. \tag{6.17}$$

Using the Fourier transform of the spin operators

$$\mathbf{S}_i^\alpha = \frac{1}{\sqrt{N}}\sum_{\mathbf{k}} e^{i\mathbf{k}.\mathbf{R}_i}\, \mathbf{S}_{\mathbf{k}}^\alpha; \qquad \mathbf{S}_{\mathbf{k}}^\alpha = \frac{1}{\sqrt{N}}\sum_i e^{-i\mathbf{k}.\mathbf{R}_i}\, \mathbf{S}_i^\alpha, \tag{6.18}$$

we can rewrite the effective field as follows

$$\begin{aligned}
\mathrm{h}_i^\alpha &= \sum_j\sum_\beta J^{\alpha\beta}\left(\mathbf{R}_i - \mathbf{R}_j\right)\langle \mathbf{S}_j^\beta \rangle = \sum_j\sum_\beta \frac{1}{\sqrt{N}}\sum_{\mathbf{k}} J^{\alpha\beta}\left(\mathbf{R}_i - \mathbf{R}_j\right)\, e^{i\mathbf{k}.\mathbf{R}_j}\langle \mathbf{S}_{\mathbf{k}}^\beta \rangle \\
&= \sum_j\sum_\beta \frac{1}{\sqrt{N}}\sum_{\mathbf{k}} J^{\alpha\beta}\left(\mathbf{R}_j - \mathbf{R}_i\right) e^{i\mathbf{k}.(\mathbf{R}_j - \mathbf{R}_i)} e^{i\mathbf{k}.\mathbf{R}_i}\langle \mathbf{S}_{\mathbf{k}}^\beta \rangle \\
&= \frac{1}{\sqrt{N}}\sum_{\mathbf{k}}\sum_\beta J^{\alpha\beta}(\mathbf{k})\, e^{i\mathbf{k}.\mathbf{R}_i}\langle \mathbf{S}_{\mathbf{k}}^\beta \rangle \\
&= \frac{1}{\sqrt{N}}\sum_{\mathbf{k}}\sum_\beta \left(-\frac{J^{\alpha\beta}(\mathbf{k})}{g\mu_B}\right)\, e^{i\mathbf{k}.\mathbf{R}_i}\langle \mathrm{M}_{\mathbf{k}}^\beta \rangle,
\end{aligned} \tag{6.19}$$

where $J^{\alpha\beta}(\mathbf{R}_i - \mathbf{R}_j) = J^{\alpha\beta}(\mathbf{R}_j - \mathbf{R}_i)$ and $\mathrm{M}_{\mathbf{k}}^\beta = -g\mu_B \mathbf{S}_{\mathbf{k}}^\beta$ is the magnetization operator.

In order to calculate the static uniform magnetic susceptibility, we use the linear response theory; we apply an small external magnetic field

$$\widetilde{\mathrm{B}}_i = \frac{1}{\sqrt{N}}\sum_{\mathbf{k}} \widetilde{\mathrm{B}}_{\mathbf{k}}\, e^{i\mathbf{k}.\mathbf{R}_i}, \tag{6.20}$$

[3] Note that a constant term is appeared in the Hamiltonian (6.14) which causes a shift in the energy. We absorb this term in the H.

which couples to each spin, and the spin system linearly responds to it. Considering the effective field which comes from the MF approximation (Eq. (6.19)), we can write the linear response relation as below

$$\begin{aligned}\langle \mathrm{M}_i^{\alpha}\rangle &= \sum_j \sum_{\beta} \frac{1}{T}\langle \mathrm{M}_i^{\alpha}\cdot \mathrm{M}_j^{\beta}\rangle \left[\left(\frac{-1}{g\mu_B}\right)\widetilde{\mathrm{B}}_j^{\beta}+\left(\frac{-1}{g\mu_B}\right)\mathrm{h}_j^{\beta}\right] \\ &= \sum_j \sum_{\beta} \underset{\sim}{\chi}^{\alpha\beta}\left(\mathbf{R}_i-\mathbf{R}_j\right)\left[\mathrm{B}_j^{\beta}+\Big(\frac{-1}{g\mu_B}\Big)\mathrm{h}_j^{\beta}\right], \end{aligned} \tag{6.21}$$

where $\underset{\sim}{\chi}^{\alpha\beta}=\langle \mathrm{M}^{\alpha}\cdot \mathrm{M}^{\beta}\rangle/T$ and $\mathrm{B}_j^{\beta}=\big(\frac{-1}{g\mu_B}\big)\widetilde{\mathrm{B}}_j^{\beta}$. The static magnetic susceptibility at vector $\mathbf{q}$ is then calculated as $\chi_{\mathrm{MF}}\propto \partial \mathrm{M}/\partial \mathrm{B}$. Let us assume that the system has an instability at vector $\mathbf{q}$. Since we are interested in the response to a field of the same vector of the instability, the magnetic response to those fields is obtained as follows.

$$\begin{aligned}\frac{1}{\sqrt{N}}\sum_i e^{-i\mathbf{q}.\mathbf{R}_i}\langle \mathrm{M}_i^{\alpha}\rangle &= \frac{1}{\sqrt{N}}\sum_i e^{-i\mathbf{q}.\mathbf{R}_i}\sum_j\sum_{\beta}\underset{\sim}{\chi}^{\alpha\beta}\left(\mathbf{R}_i-\mathbf{R}_j\right) \\ &\quad\times\left[\frac{1}{\sqrt{N}}\sum_{\mathbf{k}}\mathrm{B}_{\mathbf{k}}^{\beta}\,e^{i\mathbf{k}.\mathbf{R}_j}+\frac{1}{\sqrt{N}}\sum_{\mathbf{k}}\sum_{\alpha'}\frac{J^{\beta\alpha'}(\mathbf{k})}{(g\mu_B)^2}\,e^{i\mathbf{k}.\mathbf{R}_j}\,\langle \mathrm{M}_{\mathbf{k}}^{\alpha'}\rangle\right] \\ &= \sum_{ij}\sum_{\beta}\underset{\sim}{\chi}^{\alpha\beta}\left(\mathbf{R}_i-\mathbf{R}_j\right)e^{-i\mathbf{q}.(\mathbf{R}_i-\mathbf{R}_j)}\left[\frac{1}{N}\sum_{\mathbf{k}}\mathrm{B}_{\mathbf{k}}^{\beta}\,e^{i(\mathbf{k}-\mathbf{q}).\mathbf{R}_j}\right] \\ &\quad+\sum_{ij}\sum_{\beta}\underset{\sim}{\chi}^{\alpha\beta}\left(\mathbf{R}_i-\mathbf{R}_j\right)e^{-i\mathbf{q}.(\mathbf{R}_i-\mathbf{R}_j)} \\ &\quad\times\left[\frac{1}{N}\sum_{\mathbf{k}}\sum_{\alpha'}\frac{J^{\beta\alpha'}(\mathbf{k})}{(g\mu_B)^2}\,e^{i(\mathbf{k}-\mathbf{q}).\mathbf{R}_j}\langle \mathrm{M}_{\mathbf{k}}^{\alpha'}\rangle\right] \\ \Rightarrow \langle \mathrm{M}_{\mathbf{q}}^{\alpha}\rangle &= \sum_{\beta}\underset{\sim}{\chi}^{\alpha\beta}(\mathbf{q})\left[\mathrm{B}_{\mathbf{q}}^{\beta}+\sum_{\alpha'}\frac{J^{\beta\alpha'}(\mathbf{q})}{(g\mu_B)^2}\,\langle \mathrm{M}_{\mathbf{q}}^{\alpha'}\rangle\right]. \end{aligned} \tag{6.22}$$

For $VOMoO_4$ and Li_2VOSiO_4, there are two atoms per unit cell. Therefore, J and $\underset{\sim}{\chi}$ are 2×2 matrices, and M and B are vectors.

$$\begin{pmatrix}\langle \mathrm{M}_{\mathbf{q}}^{1}\rangle\\ \langle \mathrm{M}_{\mathbf{q}}^{2}\rangle\end{pmatrix}=\begin{pmatrix}\underset{\sim}{\chi}^{11}(\mathbf{q}) & \underset{\sim}{\chi}^{12}(\mathbf{q})\\ \underset{\sim}{\chi}^{21}(\mathbf{q}) & \underset{\sim}{\chi}^{22}(\mathbf{q})\end{pmatrix}\left[\begin{pmatrix}\mathrm{B}_{\mathbf{q}}^{1}\\ \mathrm{B}_{\mathbf{q}}^{2}\end{pmatrix}+\frac{1}{(g\mu_B)^2}\begin{pmatrix}J^{11}(\mathbf{q}) & J^{12}(\mathbf{q})\\ J^{21}(\mathbf{q}) & J^{22}(\mathbf{q})\end{pmatrix}\begin{pmatrix}\langle \mathrm{M}_{\mathbf{q}}^{1}\rangle\\ \langle \mathrm{M}_{\mathbf{q}}^{2}\rangle\end{pmatrix}\right], \tag{6.23}$$

Within the mean-field calculation, we can approximate $\underset{\sim}{\chi}$ as below

$$\begin{aligned}\underset{\sim}{\chi}^{\alpha\beta} &= \frac{1}{T}\,\langle \mathrm{M}^{\alpha}\cdot \mathrm{M}^{\beta}\rangle \\ &\approx \frac{1}{T}\,\langle \mathrm{M}^{\alpha}\rangle\cdot\langle \mathrm{M}^{\beta}\rangle\,(1-\delta_{\alpha\beta})+\frac{1}{T}\,\delta_{\alpha\beta}\,\langle \mathrm{M}^{\alpha}\cdot \mathrm{M}^{\beta}\rangle \\ &\approx \frac{1}{T}\,\langle \mathrm{M}^{\alpha}\cdot \mathrm{M}^{\beta}\rangle\,\delta_{\alpha\beta} \\ &\approx (g\mu_B)^2\,\frac{S(S+1)}{3T}\,\delta_{\alpha\beta}. \end{aligned} \tag{6.24}$$

where $\langle \mathrm{M} \rangle = 0$, because we are studying a paramagnetic phase.[4] Consequently, for $S = 1/2$ system, $\underset{\sim}{\chi}$ is given by the following matrix

$$\underset{\sim}{\chi} \approx \frac{\beta}{4}(g\mu_B)^2 \begin{pmatrix} 1 & 0 \\ 0 & 1 \end{pmatrix}. \tag{6.25}$$

we solve the matrix equation (6.23) to obtain the susceptibility matrix

$$\begin{pmatrix} \langle \mathrm{M}^1_{\mathbf{q}} \rangle \\ \langle \mathrm{M}^2_{\mathbf{q}} \rangle \end{pmatrix} = \begin{pmatrix} \chi^{11}_{\mathrm{MF}}(\mathbf{q},T) & \chi^{12}_{\mathrm{MF}}(\mathbf{q},T) \\ \chi^{21}_{\mathrm{MF}}(\mathbf{q},T) & \chi^{22}_{\mathrm{MF}}(\mathbf{q},T) \end{pmatrix} \begin{pmatrix} \mathrm{B}^1_{\mathbf{q}} \\ \mathrm{B}^2_{\mathbf{q}} \end{pmatrix}, \tag{6.26}$$

wherein

$$\chi^{11}_{\mathrm{MF}}(\mathbf{q},T) = \frac{1}{\mathcal{D}}\frac{\beta}{4}(g\mu_B)^2 \left[1 - \frac{\beta}{4}J^{11}(\mathbf{q})\right] = \chi^{22}_{\mathrm{MF}}(\mathbf{q},T), \tag{6.27}$$

$$\chi^{12}_{\mathrm{MF}}(\mathbf{q},T) = \frac{1}{\mathcal{D}}\frac{\beta}{4}(g\mu_B)^2 \left[\frac{\beta}{4}J^{12}(\mathbf{q})\right] = \left[\chi^{21}_{\mathrm{MF}}(\mathbf{q},T)\right]^*, \tag{6.28}$$

and $\mathcal{D}$ is given by

$$\mathcal{D} = \left(1 - \frac{\beta}{4}J^{11}(\mathbf{q})\right)^2 - \left|\frac{\beta}{4}J^{12}(\mathbf{q})\right|^2. \tag{6.29}$$

To derive the MF susceptibility, we used $J^{11} = J^{22}$ and $J^{12} = \left(J^{21}\right)^*$. Notice that J^{11} is the antiferromagnetic exchange coupling between atom 1 in a unit cell and atom 1 in the other unit cells. Similarly, J^{12} is the antiferromagnetic exchange coupling between atom 1 in a unit cell and atom 2 in either the current unit cell or the other ones. J^{11}, J^{12}, J^{21}, and J^{22} can be calculated in terms of the nearest and next nearest neighbor (either intra- or inter-layer) exchange couplings. Let us define

$$\begin{aligned} J_1 &\equiv \text{nearest neighbor intra-layer (in plane) exchange coupling,} \\ J_2 &\equiv \text{next nearest neighbor intra-layer (in plane) exchange coupling,} \\ J_z &\equiv \text{nearest neighbor inter-layer exchange coupling,} \\ J'_1 &\equiv \text{next nearest neighbor inter-layer exchange coupling,} \end{aligned}$$

as it is shown in Fig. (6.12); from the LDA calculations, one obtains $J_1 = -4t_1^2/U$, $J_2 = -4t_2^2/U$, $J'_1 = -4{t'_1}^2/U$ and $J_z = -4t_z^2/U$. Based on the Fourier transform of the $J^{\alpha\beta}(\mathbf{q})$ coupling

$$J^{\alpha\beta}(\mathbf{q}) = \sum_{\Delta\mathbf{R}} e^{i\mathbf{q}.(\mathbf{R}_i - \mathbf{R}_j)} J^{\alpha\beta}(\mathbf{R}_i - \mathbf{R}_j), \tag{6.30}$$

each element of the $[J(\mathbf{q})]$ matrix can be easily obtained. Let us label atoms in the unit cell as 'atom a' and 'atom b'. Atoms with the same labels have interaction with each others in the

[4] Notice that

$$\langle S_z^2 \rangle = \langle S_y^2 \rangle = \langle S_x^2 \rangle = \frac{1}{3}\langle S_x^2 + S_y^2 + S_z^2 \rangle = \frac{1}{3}\langle \mathbf{S}^2 \rangle.$$

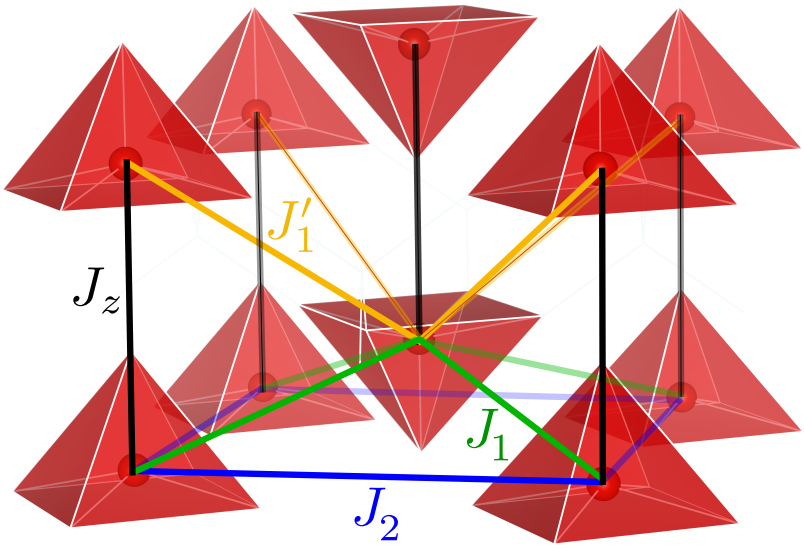

Figure 6.12: J_1, J_2, J_z and J_1' magnetic exchange coupling constants are shown for $VOMoO_4$.

surrounded unit cells through J_2 and J_z exchange couplings (see Fig. 6.12). Thus $J^{11}(\mathbf{q})$ and $J^{22}(\mathbf{q})$ can be obtained by

$$\begin{aligned} J^{11}(\mathbf{q}) &= \sum_{\Delta\mathbf{R}} e^{i\mathbf{q}.(\mathbf{R}_i-\mathbf{R}_j)} J_2 + \sum_{\Delta\mathbf{R}'} e^{i\mathbf{q}.(\mathbf{R}_i'-\mathbf{R}_j')} J_z \\ &= J_2\left(e^{iq_x} + e^{iq_y} + e^{-iq_x} + e^{-iq_y}\right) + J_z\left(e^{iq_z} + e^{-iq_z}\right) \\ &= 2J_2\left(\cos q_x + \cos q_y\right) + 2J_z \cos q_z \\ &= J^{22}(\mathbf{q}). \end{aligned} \tag{6.31}$$

J_1 and J_1' exchange coupling constants appear in the interaction of atoms with different labels placed in the neighborhood unit cells. $J^{12}(\mathbf{q})$ and $J^{21}(\mathbf{q})$ matrix elements of $J(\mathbf{q})$ is then obtained as

$$\begin{aligned} J^{12}(\mathbf{q}) &= \sum_{\Delta\mathbf{R}} e^{i\mathbf{q}.(\mathbf{R}_i-\mathbf{R}_j)} J_1 + \sum_{\Delta\mathbf{R}'} e^{i\mathbf{q}.(\mathbf{R}_i'-\mathbf{R}_j')} J_1' \\ &= J_1\Big\{1 + e^{iq_x} + e^{i(q_x+q_y)} + e^{iq_y}\Big\}\, e^{-iq_z} \\ &\quad + J_1'\Big\{1 + e^{iq_x} + e^{i(q_x+q_y)} + e^{iq_y}\Big\} \\ &= \left(1 + e^{iq_x}\right)\left(1 + e^{iq_y}\right)\Big\{J_1 e^{-iq_z} + J_1'\Big\} \\ &= 4J_1 \cos\frac{q_x}{2} \cos\frac{q_y}{2}\Big\{1 + e^{iq_z}\left(\frac{J_1'}{J_1}\right)\Big\}\, e^{i\phi_{12}} \\ &= \left(J^{21}(\mathbf{q})\right)^*, \end{aligned} \tag{6.32}$$

where $\phi_{12} = (q_x + q_y)/2 - q_z$ is the phase term (see Eqs. (6.10), (6.11), and (6.12)). Notice that $J(\mathbf{q})$ is Hermitian $J^{\alpha\beta}(\mathbf{q}) = \left(J^{\beta\alpha}(\mathbf{q})\right)^*$. Diagonalizing $[J(\mathbf{q})]$ matrix returns the following

eigenvalues

$$\begin{aligned}\widetilde{J}_{\pm}(\mathbf{q}) &= J^{11}(\mathbf{q}) \pm \left|J^{12}(\mathbf{q})\right| \\ &= 2J_2\left(\cos q_x + \cos q_y\right) + 2J_z \cos q_z \\ &\quad \pm 4J_1 \cos\frac{q_x}{2}\cos\frac{q_y}{2}\left[1 + 2\left(\frac{J_1'}{J_1}\right)\cos q_z + \left(\frac{J_1'}{J_1}\right)^2\right]^{1/2}. \end{aligned} \tag{6.33}$$

In order to calculate the MF susceptibility, we set for simplicity $J_1' = 0$ in Eq. (6.32) and substitute Eq. (6.31) and Eq. (6.32) into Eqs. (6.27) and (6.28). The static $\mathbf{q}$-dependent spin susceptibility in the MF approximation approach is then obtained as follows

$$\chi^{11}_{\mathrm{MF}}(\mathbf{q},T) = \frac{1}{\mathcal{D}}\frac{\beta}{4}(g\mu_B)^2\left[1 - \frac{\beta}{2}\left(J_2\left(\cos q_x + \cos q_y\right) + J_z\cos q_z\right)\right], \tag{6.34}$$

$$\chi^{12}_{\mathrm{MF}}(\mathbf{q},T) = \frac{1}{\mathcal{D}}\frac{\beta}{4}(g\mu_B)^2\beta\ J_1\cos\frac{q_x}{2}\cos\frac{q_y}{2}\ e^{i\phi_{12}}, \tag{6.35}$$

$$\chi^{21}_{\mathrm{MF}}(\mathbf{q},T) = \left[\chi^{12}_{\mathrm{MF}}(\mathbf{q},T)\right]^*, \tag{6.36}$$

$$\chi^{22}_{\mathrm{MF}}(\mathbf{q},T) = \chi^{11}_{\mathrm{MF}}(\mathbf{q},T), \tag{6.37}$$

where

$$\mathcal{D} = \left(1 - \frac{\beta}{2}\left[J_2\left(\cos q_x + \cos q_y\right) + J_z\cos q_z\right]\right)^2 - \beta^2 J_1^2\cos^2\frac{q_x}{2}\cos^2\frac{q_y}{2}. \tag{6.38}$$

Finally, the total static spin susceptibility is calculated by

$$\begin{aligned}\chi_{\mathrm{MF}}(\mathbf{q},T) &= \frac{1}{N_S}\sum_{\alpha\beta} e^{-i\phi_{\alpha\beta}}\ \chi^{\alpha\beta}_{\mathrm{MF}}(\mathbf{q},T) \\ &= \frac{\dfrac{\beta}{4}(g\mu_B)^2}{1 - \dfrac{\beta}{2}\left[J_2\left(\cos q_x + \cos q_y\right) + J_z\cos q_z\right] - \beta J_1\cos\dfrac{q_x}{2}\cos\dfrac{q_y}{2}} \\ &= \frac{\dfrac{1}{4}(g\mu_B)^2}{T - T^{\mathrm{MF}}(\mathbf{q})}, \end{aligned} \tag{6.39}$$

where $N_S = 2$ is the number of atomic sites and $T^{\mathrm{MF}}(\mathbf{q})$ is the mean-field magnetic critical temperature given by

$$\begin{aligned}T^{\mathrm{MF}}(\mathbf{q}) &= \frac{1}{4}\widetilde{J}_+(\mathbf{q})\Big|_{J_1'=0} \\ &= \frac{1}{2}\left\{J_2\left(\cos q_x + \cos q_y\right) + J_z\cos q_z\right\} + J_1\cos\frac{q_x}{2}\cos\frac{q_y}{2}. \end{aligned} \tag{6.40}$$

Results for static magnetic susceptibility of $VOMoO_4$ and Li_2VOSiO_4 show that the LDA+MF calculations return correct magnetic ordering for $VOMoO_4$ and Li_2VOSiO_4 materials, i.e., $\chi_{\mathrm{MF}}(\mathbf{q})$ is maximum at $\mathbf{q}_{\Gamma_1} = (2\pi, 0, q_z)$ and $\mathbf{q}_{\mathrm{M}}(\pi,\pi,q_z)$ points for $VOMoO_4$ and Li_2VOSiO_4, respectively. Moreover, the mean-filed critical temperature $T^{\mathrm{MF}}(\mathbf{q})$ is zero at $\mathbf{q}_{\mathrm{X}} = (\pi, 0, \pi/2)$ and

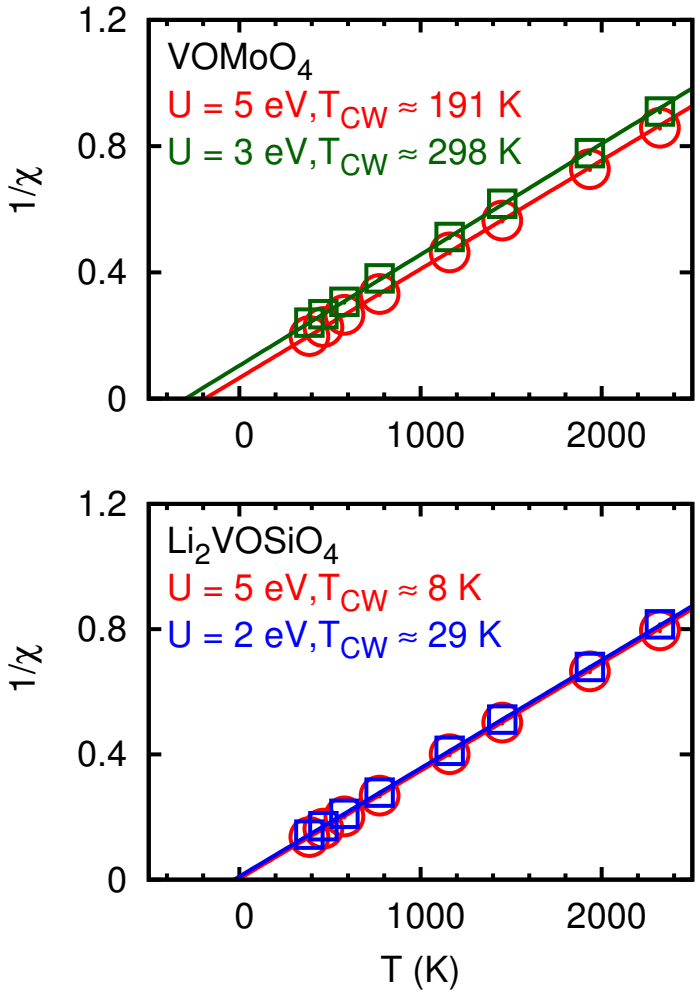

Figure 6.13: Inverse uniform static spin susceptibility $[\chi(\mathbf{q}=\mathbf{0},\omega=0)]^{-1}$ for $VOMoO_4$ and Li_2VOSiO_4. The linear lines are least square fit of the inverse susceptibility data. The Curie-Weiss temperature for realistic $U=5$ eV for both materials is in very good agreement with NMR observations.

$\mathbf{q}_Y=(0,\pi,\pi/2)$ for both materials. Our results for mean-field magnetic susceptibility and critical temperature has similar behavior to those obtained from LDA+DMFT but quantitatively they are different. This analogy between LDA+DMFT and LDA+MF will help us to study magnetic properties of both materials while the local correlations are taken into account (see Sec. 6.4.5).

In the following sections, we employ the static magnetic susceptibility to study magnetic critical temperature $T_{\mathbf{q}}$, super-exchange couplings and frustration degree (Sec. 6.4.5) by using the LDA+DMFT method.

6.4.4 Curie-Weiss temperature and magnetic moments

In order to calculate the Curie-Weiss temperature from Eq. (6.3), we plot inverse of the uniform static magnetic susceptibility $\chi^{-1}(\mathbf{q}=\mathbf{0},\omega=0)$ in terms of the temperature T. As it is shown in Fig. 6.13, $\chi^{-1}(\mathbf{q}=\mathbf{0},\omega=0)$ linearly changes for a wide range of temperature. To obtain

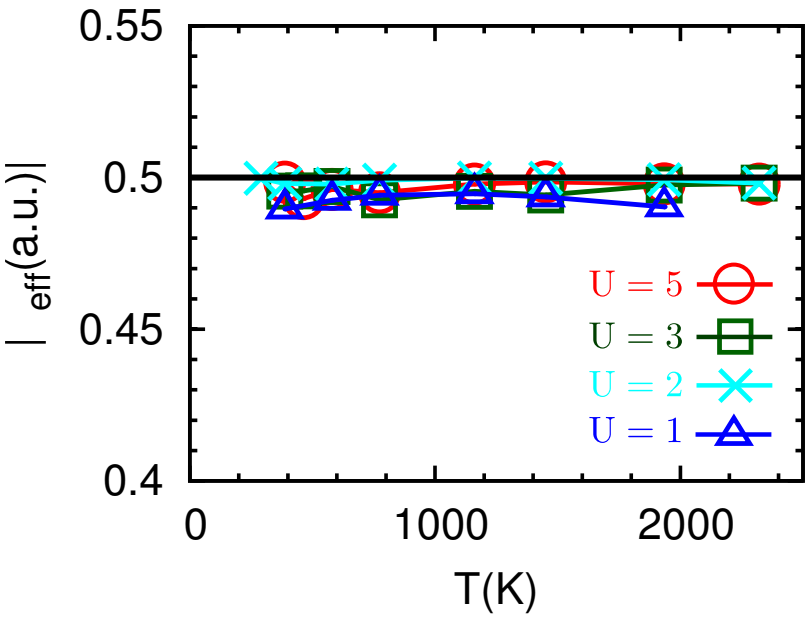

Figure 6.14: Effective magnetic moment for $VOMoO_4$ for different values of U.

the Curie-Weiss temperature, we fit the function $\chi^{-1}(\mathbf{q} = \mathbf{0}, \omega = 0)$ with a line $aT + b$ by using the least square method (see Appendix G.1). The intersection with the temperature axis yields the Curie-Weiss temperature. We obtain $T_{\rm CW}$ for different values of Coulomb interaction $U = 1, ..., 5$ eV. We find that the Curie-Weiss temperature decreases with increasing U (see Fig. 6.13); for realistic $U = 5$ eV, we obtain $T_{\rm CW} \sim 191$ K for $VOMoO_4$ and $T_{\rm CW} \sim 8$ K for Li_2VOSiO_4 which are in very good agreement with the NMR estimates.

Moreover, we compute the effective magnetic moment from the static uniform magnetic susceptibility at high temperatures by

$$\mu_{\rm eff} = g\mu_B S_{\rm eff} = \sqrt{(T - T_{\rm CW})\chi(T)}. \tag{6.41}$$

for both materials, we find that for $U = 5$ eV, the effective local magnetic moment $\mu_{\rm eff}$ is close to $0.5\ \mu_B$. This indicates that the charge fluctuations in these two materials are small for a realistic $U = 5$ eV. Consequently, the small magnetic moment ($\mu_z \sim 0.41\ \mu_B$) measured in the neutron diffraction experiment [76] can not be related to the charge fluctuations unless the Coulomb interaction is much smaller than 5 eV. Interestingly, we find sizable effective magnetic moment not only in insulating regime but also in the metallic one. For instance, for $VOMoO_4$ as it is shown in Fig. 6.14, we obtain $\mu_{\rm eff} \sim 0.498\ \mu_B$ for $U = 5$ eV (insulating regime) to be compared with $\mu_{\rm eff} \sim 0.449\ \mu_B$ for $U = 1$ eV (metallic regime).

6.4.5 Magnetic super-exchange coupling

Since the high temperature spin susceptibility calculated by the LDA+DMFT method shows Curie-Weiss behavior, and the local moments are well defined, we can define the critical magnetic temperature at a given vector $\mathbf{q}$ by

$$T_{\mathbf{q}} \sim T - \mu_{\rm eff}^2\ \chi^{-1}(\mathbf{q}, T) \tag{6.42}$$

in analogy with the static mean-filed expression. The critical temperature at vector $\mathbf{q}$ is proportional to the exchange coupling constant J at those $\mathbf{q}$

$$\begin{aligned} T_{\mathbf{q}} &\propto \widetilde{J}_{+}(\mathbf{q}) \\ &\propto 4J_1 \cos\frac{q_x}{2}\cos\frac{q_y}{2}\left[1+2\left(\frac{J_1'}{J_1}\right)\cos q_z+\left(\frac{J_1'}{J_1}\right)^2\right]^{1/2}+2J_2\left(\cos q_x+\cos q_y\right)+2J_z\cos q_z. \end{aligned}$$

Therefore, we can use the static magnetic susceptibility to study $T_{\mathbf{q}}$, the effective magnetic couplings J_1, J_2, J_1' and J_z, degree of frustration $f = J_2/J_1$, and three-dimensionality $f_3 = (J_1' + J_z)/(J_1 + J_2)$ within the LDA+DMFT approach. The effect of the dynamical correlation can be understood if we compare these results with the mean field outcomes.

We calculate the critical temperature $T_{\mathbf{q}}$ within LDA+DMFT for different values of the Coulomb interaction $U = 2 - 5$ eV; for $VOMoO_4$ and Li_2VOSiO_4, we find that i) $\mathbf{q}$-dependency of the magnetic critical temperature are similar for different values of U. ii) $T_{\mathbf{q}}$ is zero for $\mathbf{q} = \mathbf{q}_{\mathrm{X}} = (\pi, 0, \pi/2)$ and $\mathbf{q} = \mathbf{q}_{\mathrm{Y}} = (0, \pi, \pi/2)$. iii) Critical temperature $T_{\mathbf{q}}$ is maximum at $\mathbf{q} = \mathbf{q}_{\Gamma_1} = (2\pi, 0, q_z)$ and $\mathbf{q} = \mathbf{q}_{\mathrm{M}} = (\pi, \pi, q_z)$ for $VOMoO_4$ and Li_2VOSiO_4, respectively. Absolute value of the critical temperature decreases non-uniformly when the Coulomb interaction increases (see Fig. 6.15).

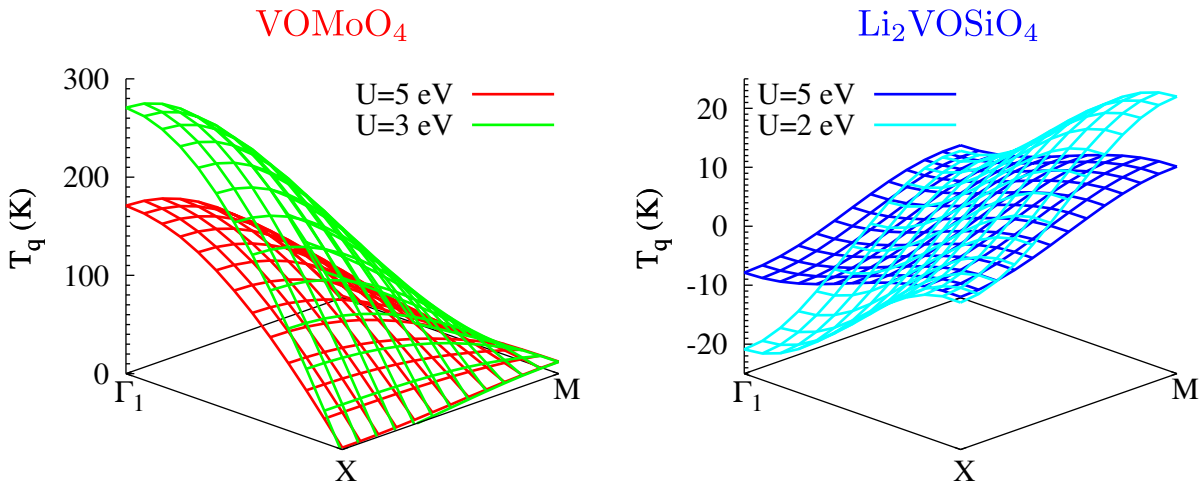

Figure 6.15: LDA+DMFT calculation of static $\mathbf{q}$-dependent magnetic critical temperature for different values of Coulomb interaction U, $\beta = 30$ eV^{-1}, and $q_z = \pi/2$; *left panel* for $VOMoO_4$ and *right panel* for Li_2VOSiO_4.

6.4.5.1 Effect of the dynamical correlation on the magnetic couplings

In order to study the effect of the dynamical correlation on the magnetic couplings, we first analyze the momentum dependency of the $J(\mathbf{q})$. From Eq. (6.33), it is clear that

$$J(\mathbf{q}) \sim \begin{cases} 0 & \text{for } \mathbf{q}_{\mathrm{X}} = (0, \pi, \pi/2) \\ -4J_2 & \text{for } \mathbf{q}_{\mathrm{M}} = (\pi, \pi, \pi/2) \\ 2J_z & \text{for } \mathbf{q}'_{\mathrm{X}} = (0, \pi, 0) \\ 2J_1 + 2J'_1 + 2J_z & \text{for } \mathbf{q}_1 = (\pi/2, \pi/2, 0) \\ 2J_1 - 2J'_1 - 2J_z & \text{for } \mathbf{q}_2 = (\pi/2, \pi/2, \pi) \end{cases} . \tag{6.43}$$

Using these relations, we can obtain the degree of frustration by[5]

$$f = \frac{J_2}{J_1} \sim \frac{\chi^{-1}(\mathbf{q}_{\mathrm{M}}, T) - \chi^{-1}(\mathbf{q}_{\mathrm{X}}, T)}{\chi^{-1}(\mathbf{q}_1, T) + \chi^{-1}(\mathbf{q}_2, T) - 2\chi^{-1}(\mathbf{q}_{\mathrm{X}}, T)}. \tag{6.44}$$

Surprisingly, in the full range of $U = 2 - 5$ eV, $f = J_2/J_1$ is weakly temperature dependent and slightly changes with U. In the case of $VOMoO_4$ for $U = 5$ eV, we obtain $f \sim 0.058$, which is close but slightly larger than the one computed through LDA+second order perturbation theory (LDA+PT). In the case of Li_2VOSiO_4 for $U = 5$ eV, we find $f \sim 5.45$, while in the LDA+PT $f \sim 12.35$ is obtained. Consequently, for Li_2VOSiO_4, the degree of frustration is increased due to dynamical correlations. In conclusion, our calculations on the frustration parameter show that although the local correlation does not sizably affect the frustration of $VOMoO_4$, it pushes Li_2VOSiO_4 into the frustrated area, i.e., the local correlation increases frustration in Li_2VOSiO_4.

We can also employ the static magnetic susceptibility to extract the ratio $f_3 = (J'_1 + J_z)/(J_1 + J_2)$ which determines the degree of three-dimensionality.[6]

$$f_3 = \frac{J'_1 + J_z}{J_1 + J_2} \sim \frac{\chi^{-1}(\mathbf{q}_2, T) - \chi^{-1}(\mathbf{q}_1, T)}{\chi^{-1}(\mathbf{q}_{\mathrm{M}}, T) - \chi^{-1}(\mathbf{q}_{\mathrm{X}}, T)} \times \frac{1}{1 + f^{-1}}. \tag{6.45}$$

Remarkably, this ratio is also weakly temperature dependent and changes slightly with the Coulomb interaction U. In the case of $VOMoO_4$ for $U = 5$ eV, $f_3 \sim 0.018$ which is slightly bigger than $f_3 \sim 0.014$ estimated within LDA+PT. For Li_2VOSiO_2 for $U = 5$ eV, we find that $f_3 \sim 0.122$ in LDA+DMFT which is slightly smaller than $f_3 \sim 0.144$ computed within the LDA+PT. Hence, our LDA+DMFT results show that the magnetic couplings between layers of Li_2VOSiO_4 are smaller than the LDA+PT prediction, and this material can indeed be described by a quasi two-dimensional system.

[5] In the LDA+second order perturbation theory (LDA+PT), the frustration parameter is obtained by

$$f = \frac{J_2}{J_1} = \frac{-4t_2^2}{U} \times \frac{1}{\frac{-4t_1^2}{U}} = \left(\frac{t_2}{t_1}\right)^2.$$

[6] In the LDA+PT, the three-dimensionality parameter can be obtained in terms of the hopping parameters as

$$f_3 = \frac{J'_1 + J_z}{J_1 + J_2} = \frac{t'^2_1 + t_z^2}{t_1^2 + t_2^2}.$$

$VOMoO_4$	J_2/J_1	$(J_z+J_1')/(J_1+J_2)$	$J_z/(J_1+J_2)$	$J_1'/(J_1+J_2)$
LDA+DMFT	~ 0.058	~ 0.018	~ 0.007	~ 0.0113
LDA+PT	~ 0.059	~ 0.014	~ 0.007	~ 0.007

Li_2VOSiO_4	J_2/J_1	$(J_z+J_1')/(J_1+J_2)$	$J_z/(J_1+J_2)$	$J_1'/(J_1+J_2)$
LDA+DMFT	~ 5.45	~ 0.122	~ 0.117	~ 0.005
LDA+PT	~ 12.35	~ 0.144	~ 0.143	< 0.001

Table 6.1: Magnetic exchange coupling constant ratios for $VOMoO_4$ and Li_2VOSiO_4 for $U = 5$ eV. For the LDA results, $J_i = -4t_i^2/U$. Therefore, $J_2/J_1 = t_2^2/t_1^2$, $(J_z + J_1')/(J_1 + J_2) = (t_z^2 + t_1'^2)/(t_1^2 + t_2^2)$, ect.

Moreover, we can study the role of the magnetic exchange couplings J_z and J_1' in both materials by calculating the ratio $f_z = J_z/(J_1 + J_2)$ by

$$f_z = \frac{J_z}{J_1+J_2} \sim \frac{\chi^{-1}(\mathbf{q}_{\mathrm{X}},T) - \chi^{-1}(\mathbf{q}'_{\mathrm{X}},T)}{\chi^{-1}(\mathbf{q}_{\mathrm{M}},T) - \chi^{-1}(\mathbf{q}_{\mathrm{X}},T)} \times \frac{2}{1+f^{-1}}. \tag{6.46}$$

For $VOMoO_4$ at $U = 5$ eV, we find that $f_z \sim 0.007$, and consequently $J_1'/(J_1+J_2) \sim 0.0113$. This indicates that in this material, q_z-dependence is dominated by the term which is proportional to J_1'. However, for Li_2VOSiO_4 we find that the opposite is true. For this material for $U = 5$ eV, we obtain $f_z \sim 0.117$ and hereby $J_1'/(J_1+J_2) \sim 0.005$; this shows that q_z-dependency is mainly due to the J_z exchange coupling between Vanadium ions in neighboring layers. Based on the values of J_z and J_1' for both materials, we can conclude that, if super-exchange dominates, in the ground state of $VOMoO_4$ the Vanadium ions with parallel spins should belong to the pyramids on the top of each other (hence ferromagnetic order along z-direction), while in the ground state of Li_2VOSiO_4 parallel spins belong to pyramids which should point in opposite direction (hence two V ions placing in pyramids in top of each other have antiferromagnetic order along z-direction.).

Using the LDA+DMFT, not only we are able to estimate the f, f_3 and f_z ratios but also we are able to calculate roughly the values of J_1, J_2, J_z and J_1' in order to compare with experiments. To do so, we first calculate the ratio $\mathrm{R}_{\mathrm{DMFT}}$ defined by

$$\mathrm{R}_{\mathrm{DMFT}}(\mathbf{q},T) = \frac{\chi_{12}(\mathbf{q},T)+\chi_{21}(\mathbf{q},T)}{\chi_{11}(\mathbf{q},T)+\chi_{22}(\mathbf{q},T)}. \tag{6.47}$$

In order to obtain the ratio $\mathrm{R}_{\mathrm{DMFT}}$, we employ the static Bethe-Salpeter equation $[\chi(\mathbf{q},T)]^{-1} = [\chi^{\mathbf{0}}(\mathbf{q},T)]^{-1} - [\mathbf{\Gamma_{loc}}(T)]$, so that

$$\begin{pmatrix} \chi_{11}(\mathbf{q},T) & \chi_{12}(\mathbf{q},T) \\ \chi_{21}(\mathbf{q},T) & \chi_{22}(\mathbf{q},T) \end{pmatrix} = \frac{\frac{-1}{\mathbf{\Gamma_{loc}}(T)}}{\left(1-\frac{\bar{\chi}^{\mathbf{0}}_{11}(\mathbf{q},T)}{\mathbf{\Gamma_{loc}}(T)}\right)^2 - \left|\frac{\bar{\chi}^{\mathbf{0}}_{12}(\mathbf{q},T)}{\mathbf{\Gamma_{loc}}(T)}\right|^2} \times \begin{pmatrix} 1-\frac{\bar{\chi}^{\mathbf{0}}_{11}(\mathbf{q},T)}{\mathbf{\Gamma_{loc}}(T)} & -\frac{\bar{\chi}^{\mathbf{0}}_{12}(\mathbf{q},T)}{\mathbf{\Gamma_{loc}}(T)} \\ -\frac{\bar{\chi}^{\mathbf{0}}_{21}(\mathbf{q},T)}{\mathbf{\Gamma_{loc}}(T)} & 1-\frac{\bar{\chi}^{\mathbf{0}}_{22}(\mathbf{q},T)}{\mathbf{\Gamma_{loc}}(T)} \end{pmatrix}, \tag{6.48}$$

$VOMoO_4$	$\lvert J_1\rvert$	$\lvert J_2\rvert$	$\lvert J_z\rvert$	$\lvert J_1'\rvert$
LDA+DMFT	$\sim 179\ (\pm 5)$ K	~ 10.3 K	~ 1.36 K	~ 2.1 K
LDA+PT	~ 173 K	~ 10.2 K	~ 1.35 K	~ 1.2 K

Li_2VOSiO_4	$\lvert J_1\rvert$	$\lvert J_2\rvert$	$\lvert J_z\rvert$	$\lvert J_1'\rvert$
LDA+DMFT	$\sim 1.3\ (\pm 1)$ K	~ 7.1 K	~ 1 K	~ 0.09 K
LDA+PT	~ 1 K	~ 13 K	~ 2 K	~ 0.0045 K

Table 6.2: Magnetic exchange coupling constants J_1, J_2, J_z and J_1' for $VOMoO_4$ and Li_2VOSiO_4 for $U = 5$ eV. For the LDA results, $J_i = -4t_i^2/U$.

where

$$\begin{aligned} \bar{\chi}^{\mathbf{0}}_{\alpha\beta} &= \frac{1}{\mathrm{Det}}\,\chi^{\mathbf{0}}_{\alpha\beta} \\ \mathrm{Det} &= \chi^{\mathbf{0}}_{11}\chi^{\mathbf{0}}_{22} - \chi^{\mathbf{0}}_{12}\chi^{\mathbf{0}}_{21}. \end{aligned} \tag{6.49}$$

Finally, we derive the following relation for the ratio $\mathrm{R}_{\mathrm{DMFT}}(\mathbf{q}, T)$

$$\mathrm{R}_{\mathrm{DMFT}}(\mathbf{q}, T) = \frac{\Re e\left[-\dfrac{\bar{\chi}^{\mathbf{0}}_{12}(\mathbf{q}, T)}{\mathbf{\Gamma_{loc}}(T)}\right]}{1 - \dfrac{\bar{\chi}^{\mathbf{0}}_{11}(\mathbf{q}, T)}{\mathbf{\Gamma_{loc}}(T)}}. \tag{6.50}$$

Since the static magnetic susceptibility obtained from LDA+MF and LDA+DMFT show Curie-Weiss behavior at high temperatures, and since they obey similar $J(\mathbf{q})$ dependency, we can rewrite $\mathrm{R}_{\mathrm{DMFT}}(\mathbf{q}, T)$ in terms of $J(\mathbf{q})$. By comparing Eq. (6.48) and Eq. (6.27), the ratio $\mathrm{R}_{\mathrm{DMFT}}(\mathbf{q}, T)$ can be derived as

$$\begin{aligned} \mathrm{R}_{\mathrm{DMFT}}(\mathbf{q}, T) &= \frac{\chi_{12}(\mathbf{q}, T) + \chi_{21}(\mathbf{q}, T)}{\chi_{11}(\mathbf{q}, T) + \chi_{22}(\mathbf{q}, T)} \\ &\sim \frac{\dfrac{\beta}{4}\,\Re e\left[J^{12}(\mathbf{q})\right]}{1 - \dfrac{\beta}{4}J^{11}(\mathbf{q})} \\ &\sim \frac{\beta\,\cos\dfrac{q_x}{2}\cos\dfrac{q_y}{2}\left\{J_1\cos(\dfrac{q_x+q_y}{2} - q_z) + J_1'\cos(\dfrac{q_x+q_y}{2})\right\}}{1 - \dfrac{\beta}{2}\left(J_2\left(\cos q_x + \cos q_y\right) + J_z\cos q_z\right)}. \end{aligned} \tag{6.51}$$

From LDA+DMFT calculations, we know the static magnetic susceptibility, and hence, the ratio $\mathrm{R}_{\mathrm{DMFT}}(\mathbf{q}, T)$. We also already calculated the ratios $f = J_2/J_1$, $f_3 = (J_1' + J_z)/(J_1 + J_2)$ and $f_z = J_z/(J_1 + J_2)$. Consequently, we can use them to obtain the values of couplings J_1, J_2, J_z and J_1'.

In the case of $VOMoO_4$, we find that $|J_1| \sim 179\ (\pm 5)$ K, $|J_2| \sim 10.3$ K, $|J_z| \sim 1.36$ K and $|J_1'| \sim 2.1$ K (see Tab. 6.2). Comparing the LDA calculations where $|J_1| \sim 173$ K, $|J_2| \sim 10.2$ K, $|J_z| \sim 1.35$ K and $|J_1'| \sim 1.2$ K, all the coupling constants are almost identical and the local

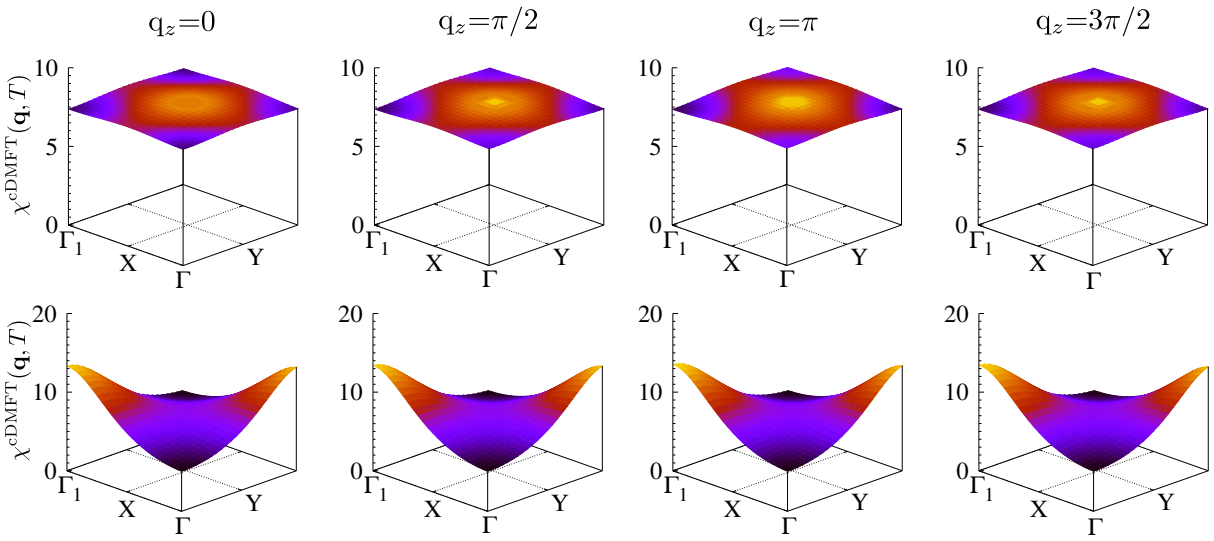

Figure 6.16: Static lattice spin susceptibility obtained from cluster calculations for $U = 5$ eV for Li_2VOSiO_4 (*upper panle*) and $VOMoO_4$ (*lower panel*).

correlation does not have strong effect on them. However, our calculations for $|J_1| + |J_2| \sim 189\ (\pm 10)$ K are in a good agreement with the NMR estimates $|J_1| + |J_2| \sim 155$ K [18].

For Li_2VOSiO_4, we obtain $|J_1| \sim 1.3\ (\pm 1)$ K, $|J_2| \sim 7.1$ K, $|J_z| \sim 1.0$ K, and $|J_1'| \sim 0.09$ K to be compared with the LDA results, $|J_1| \sim 1$ K, $|J_2| \sim 13$ K, $|J_z| \sim 2$ K and $|J_1'| < 10^{-2}$ K (see Tab. 6.2). Although the correlation effects enhance the J_2 coupling, the other magnetic coupling constants are almost similar to the LDA outcomes. Moreover, our LDA+DMFT result for $|J_1| + |J_2| \sim 8.4$ K is very close to NMR observations $|J_1| + |J_2| \sim 8.2$ K [77].

6.4.6 Non-local effects

To study the non-local effects on the frustration and three-dimensionality degree, we perform 2-site cluster DMFT calculations. In this case, the vertex function and Green's function matrices have non-zero off-diagonal matrix elements which can in principle change the $\mathbf{q}$-dependent magnetic susceptibility.

We perform cluster calculations in the full temperature range between 380 K and 2500 K and for $U \gtrsim 2$ eV and calculate supper-cell lattice spin susceptibility. For both $VOMoO_4$ and Li_2VOSiO_4, we find that difference between $\mathbf{q}$-dependent magnetic susceptibility obtained from DMFT and cDMFT are small (see Fig.6.16). Magnetic critical temperature $T_{\mathbf{q}}$ decreases in the presence of the non-local effects; with fitting high-temperature uniform susceptibility data, we obtain $T_{\rm CW} \sim 185(\pm 1)$ K for $VOMoO_4$ and $T_{\rm CW} \sim 7$ K (for $U = 5$ eV) which slightly enhance. Furthermore, we find that the frustration and three-dimensionality degrees are almost similar to the LDA+DMFT outcomes. Hence, non-local effects are small and do not affect the magnetic properties of these two materials such as the ratios J_2/J_1 and $(J_z + J_1')/(J_1 + J_2)$ sizably.

In order to compute the value of magnetic exchange coupling constants, similar to what we did for DMFT calculations, we compute the ratio

$$\mathrm{R}_{\rm cDMFT}(\mathbf{q}, T) = \frac{\chi_{12}(\mathbf{q}, T) + \chi_{21}(\mathbf{q}, T)}{\chi_{11}(\mathbf{q}, T) + \chi_{22}(\mathbf{q}, T)}, \tag{6.52}$$

where $\chi_{\alpha\beta}$ are site selective static spin susceptibility computed through the LDA+cDMFT. To obtain the effective magnetic exchange couplings J_1, J_2, J_1' and J_z through the LDA+cDMFT calculations, we rewrite the ratio $\mathrm{R_{cDMFT}}(\mathbf{q},T)$ in terms of the exchange magnetic coupling constants with considering the non-local effects. To do this, we first derive the susceptibility matrix by solving the Bethe-Salpeter equation, wherein the vertex function matrix has non-zero off-diagonal elements due to non-local effects.

$$\begin{pmatrix} \chi_{11}(\mathbf{q},T) & \chi_{12}(\mathbf{q},T) \\ \\ \chi_{21}(\mathbf{q},T) & \chi_{22}(\mathbf{q},T) \end{pmatrix} \approx \frac{\dfrac{-1}{\mathbf{\Gamma}_{11}(T)}}{\left(1-\dfrac{\bar{\chi}^{\mathbf{0}}_{11}(\mathbf{q},T)}{\mathbf{\Gamma}_{11}(T)}\right)^2 - \left|\dfrac{\bar{\chi}^{\mathbf{0}}_{12}(\mathbf{q},T)+\mathbf{\Gamma}_{12}(T)}{\mathbf{\Gamma}_{11}(T)}\right|^2} \times \begin{pmatrix} 1-\dfrac{\bar{\chi}^{\mathbf{0}}_{11}(\mathbf{q},T)}{\mathbf{\Gamma}_{11}(T)} & -\dfrac{\bar{\chi}^{\mathbf{0}}_{12}(\mathbf{q},T)}{\mathbf{\Gamma}_{11}(T)} - \dfrac{\mathbf{\Gamma}_{12}(T)}{\mathbf{\Gamma}_{11}(T)} \\ \\ -\dfrac{\bar{\chi}^{\mathbf{0}}_{21}(\mathbf{q},T)}{\mathbf{\Gamma}_{11}(T)} - \dfrac{\mathbf{\Gamma}_{21}(T)}{\mathbf{\Gamma}_{11}(T)} & 1-\dfrac{\bar{\chi}^{\mathbf{0}}_{22}(\mathbf{q},T)}{\mathbf{\Gamma}_{11}(T)} \end{pmatrix}, \tag{6.53}$$

where $\bar{\chi}^{\mathbf{0}}_{\alpha\beta} = \chi^{\mathbf{0}}_{\alpha\beta}/\mathrm{Det}[\chi^{\mathbf{0}}]$. Hence, $\mathrm{R_{cDMFT}}(\mathbf{q},T)$ is given by

$$\mathrm{R_{cDMFT}}(\mathbf{q},T) = \frac{\Re\mathrm{e}\left[-\dfrac{\bar{\chi}^{\mathbf{0}}_{12}(\mathbf{q},T)}{\mathbf{\Gamma}_{11}(T)} - \dfrac{\mathbf{\Gamma}_{12}(T)}{\mathbf{\Gamma}_{11}(T)}\right]}{1-\dfrac{\bar{\chi}^{\mathbf{0}}_{11}(\mathbf{q},T)}{\mathbf{\Gamma}_{11}(T)}}. \tag{6.54}$$

By comparing the static mean field where the $\chi_{12}(\mathbf{q},T)$ term, i.e., $-\dfrac{\bar{\chi}^{\mathbf{0}}_{12}(\mathbf{q},T)}{\mathbf{\Gamma}_{11}(T)} - \dfrac{\mathbf{\Gamma}_{12}(T)}{\mathbf{\Gamma}_{11}(T)}$, corresponds to $\beta/4\ J^{21}_{\mathrm{cDMFT}}(\mathbf{q})$ and $\chi_{12}(\mathbf{q},T)$ term, i.e., $-\dfrac{\bar{\chi}^{\mathbf{0}}_{11}(\mathbf{q},T)}{\mathbf{\Gamma}_{11}(T)}+1$, corresponds to $1-\beta/4\ J^{11}_{\mathrm{cDMFT}}(\mathbf{q})$, we can rewrite the ratio $\mathrm{R_{cDMFT}}(T)$ in terms of the $J(\mathbf{q})$ couplings as follows

$$\mathrm{R_{cDMFT}}(\mathbf{q},T) \sim \frac{\dfrac{\beta}{4}\,\Re e\left[J^{12}_{\mathrm{cDMFT}}(\mathbf{q})\right]}{1-\dfrac{\beta}{4}J^{11}_{\mathrm{cDMFT}}(\mathbf{q})}. \tag{6.55}$$

Since the non-local effects mainly affect the off-diagonal terms of $J(\mathbf{q})$ matrix, we can consider that $J^{11}_{\mathrm{cDMFT}}(\mathbf{q}) \approx 2J_2\left(\cos q_x + \cos q_y\right) + 2J_z \cos q_z$. Furthermore, we can express $J^{12}_{\mathrm{cDMFT}}(\mathbf{q}) \approx J^{12}(\mathbf{q}) + \Delta J$, where the non-local effects are considered in ΔJ which corresponds to $-\mathbf{\Gamma}_{12}/\mathbf{\Gamma}_{11}$ in Eq. (6.54) and $J^{12}(\mathbf{q})$ is given by Eq. (6.32). Finally, we can rewrite the ratio $\mathrm{R_{cDMFT}}(\mathbf{q},T)$ in terms of effective magnetic J couplings and ΔJ as below

$$\begin{aligned} \mathrm{R_{cDMFT}}(\mathbf{q},T) \approx & \frac{\beta\ J_1 \cos\frac{q_x}{2}\cos\frac{q_y}{2}\left\{\cos(\frac{q_x+q_y}{2}-q_z) + \dfrac{J_1'}{J_1}\cos(\frac{q_x+q_y}{2})\right\}}{1-\dfrac{\beta}{2}\left(J_2\left(\cos q_x+\cos q_y\right)+J_z\cos q_z\right)} \\ & + \frac{\dfrac{\beta}{4}\,\Delta J}{1-\dfrac{\beta}{2}\left(J_2\left(\cos q_x+\cos q_y\right)+J_z\cos q_z\right)}. \end{aligned} \tag{6.56}$$

From the LDA+cDMFT, we know the values of ratios $\mathrm{R}_{\mathrm{cDMFT}}(\mathbf{q},T)$ for each $\mathbf{q}$-point. Hence, there are $N_{\mathbf{q}}$ known values for $\mathrm{R}_{\mathrm{cDMFT}}(\mathbf{q},T)$ but 5 unknown variables (J_1, J_2, J_z, J_1' and ΔJ). We obtain them by fitting our data for $\mathrm{R}_{\mathrm{cDMFT}}(\mathbf{q},T)$ with Eq. (6.56).

At $\mathbf{q}_{\mathrm{X}}=(0,\pi,\pi/2)$, we have

$$\Delta J \sim \frac{4}{\beta}\,\mathrm{R}_{\mathrm{cDMFT}}(\mathbf{q}_{\mathrm{X}},T). \tag{6.57}$$

For $VOMoO_4$, for $U=5$ eV and $\beta=30$ eV^{-1}, we find $\mathrm{R}_{\mathrm{cDMFT}}\sim 0.007444$, and thus $\Delta J\approx 0.000992$ eV ~ 11.5 K. From point $\mathbf{q}_3=(\pi/2,\pi/2,\pi/2)$, we obtain the value of J_1

$$J_1=\frac{2}{\beta}\,\mathrm{R}_{\mathrm{cDMFT}}(\mathbf{q}_3,T)-\frac{1}{2}\Delta J, \tag{6.58}$$

where $\mathrm{R}_{\mathrm{cDMFT}}(\mathbf{q}_3,T=1/30)\sim -0.22382$ from the LDA+cDMFT. Finally, the magnetic coupling $|J_1|\sim 0.0154$ eV ~ 178.7 K. Other magnetic couplings are obtained similarly; $|J_2|\sim 10.6$ K, $|J_z|\sim 1$ K and $|J_1'|\sim 0.4$ K. Effective exchange couplings J_1, J_2, J_z and J_1' slightly change as well as the degree of frustration $J_2/J_1\sim 0.059$ and three-dimensionality parameter $J_3/(J_1+J_2)\sim 0.007$. However, due to ΔJ which is appeared due to non-local effects, the Curie-Weiss temperature slightly enhances[7].

We follow a similar procedure for Li_2VOSiO_4 for $U=5$ eV. We obtain $\Delta J\sim 0.000355$ eV ~ 4.1 K, $|J_1|\sim 1.16$ K, $|J_2|\sim 6.38$ K, $|J_z|\sim 0.90$ K and $|J_1'|\sim 0.01$ K. This indicates that the frustration and three-dimensionality parameters as well as Curie-Weiss temperature are slightly changed due to non-local effects.

[7] Here, the Curie-Weiss temperature is obtained by

$$T_{\mathrm{CW}}\sim |J_1+J_2+J_1'+\frac{1}{2}J_z+\frac{1}{4}\Delta J|=|-178.7-10.6-0.4-0.5+2.9|\sim 187\ \mathrm{K},$$

which is consistent with the Curie-Weiss temperature ($T_{\mathrm{CW}}\sim 185(\pm 1)$ K) obtained from our least square fitting data on high-temperature lattice spin susceptibility $\chi^{\mathrm{cDMFT}}(\mathbf{q},T)$ at $\mathbf{q}=\mathbf{0}$.

CHAPTER 7

Summary

7.1 Summary

In this thesis, we study the nature of the magnetism in strongly correlated real materials. To this end, we calculate the lattice magnetic susceptibility using the LDA+DMFT and LDA+cDMFT approaches. We employ the Hirsch-Fye quantum Monte-Carlo method as an impurity solver. Within the LDA+(c)DMFT approach, we compute the lattice susceptibility using the local-vertex approximation; in the first part of the thesis, we extend our general LDA+(c)DMFT code to compute the local (cluster) susceptibility. In oder to extract the local (cluster) susceptibility from the Hirsch-Fye QMC block, we introduce a new approach to calculate the Fourier transform of the Green's function inside the QMC. To speed up the code, we use the symmetry properties of the local susceptibility and Green's function. In the second part of the thesis, we implement our algorithm to compute the super-cell susceptibility. The implementation is general and can be used for multi-bands and multi-sites systems. To speed up our code, we parallelize it and successfully run it on the Jülich super computers (Blue Gene) and on the RWTH Aachen cluster.

As represenative application, we investigate the nature of magnetic interactions in two Vanadium oxides, $VOMoO_4$ and Li_2VOSiO_4. These systems are Mott insulators and are considered as a realization of the square lattice quantum Heisenberg model. In the absence of experimental values for the gap, we scan the Coulomb interaction U from 1 to 5 eV. The largest value $U \sim 5$ eV is a typical value for Vanadium oxides. We find that the vertex contribution is crucial to describe the magnetic properties of $VOMoO_4$ and Li_2VOSiO_4. Hereby, for $U = 5$ eV, we obtain a Curie-Weiss temperature in agreement with the NMR experiments. For this value of the Coulomb interaction, we find very well defined local magnetic moments and tiny charge fluctuations in both materials. Within a single layer, we find that $VOMoO_4$ has antiferromagnetic and Li_2VOSiO_4 has collinear order. This is in line with neutron diffraction experiments. Moreover, we observe that both materials should be three dimensionally ordered; along the z-direction, $VOMoO_4$ should be ferromagnetically and Li_2VOSiO_4 antiferromagnetically ordered. We find that, however, the coupling between neighboring layers is very small in Li_2VOSiO_4, which can be indeed considered as a prototype of a square lattice AFM quantum Heisenberg system. We also extract the effective magnetic exchange coupling constants from the magnetic susceptibility by both LDA+DMFT and LDA+mean field approaches. Our results prove that i) both $VOMoO_4$ and Li_2VOSiO_4 are in the weak frustration regime, in agreement with neutron diffraction experiments, ii) local correlation pushes Li_2VOSiO_4 towards the frustration regime while it slightly changes the frustration degree in $VOMoO_4$. Furthermore, we find that non-local effects affect little the super-exchange magnetic couplings. Hence the weak frustration picture is still valid for both materials.

APPENDIX A

Appendix

A.1 Derivation of the general form of the susceptibility

To derive Eqs. (4.17) and (4.18), first we need to calculate Fourier transform of the operator $\hat{\mathcal{O}}(\mathbf{R_i}, \tau_1)$ in Eq. (4.15).

$$\begin{aligned}
\hat{\mathcal{O}}(\mathbf{q}, \tau_1) &= \sum_{\lambda\mu} \sum_{\kappa_\lambda \kappa_\mu} \sum_{\sigma} \sum_{\mathbf{j}} v^{\sigma}_{\mathbf{j};\lambda\kappa_\lambda,\mu\kappa_\mu} e^{i\mathbf{q}.\mathbf{R_j}} \frac{1}{N_{\mathbf{k}}} \sum_{\mathbf{k}} e^{i\mathbf{k}.\mathbf{R_j}} c^{\dagger}_{\mathbf{k},\lambda\kappa_\lambda\sigma}(\tau_1) \frac{1}{N_{\mathbf{k}}} \sum_{\mathbf{k}} e^{-i\mathbf{k}.\mathbf{R_j}} c_{\mathbf{k},\mu\kappa_\mu\sigma}(\tau_1) \\
&= \frac{1}{N^2_{\mathbf{k}}} \sum_{\mathbf{k}\mathbf{k}'} \sum_{\lambda\mu} \sum_{\kappa_\lambda\kappa_\mu} \sum_{\sigma} \sum_{\mathbf{j}} v^{\sigma}_{\mathbf{j};\lambda\kappa_\lambda,\mu\kappa_\mu} e^{i(\mathbf{k}+\mathbf{q}).\mathbf{R_j}} e^{-i\mathbf{k}'.\mathbf{R_j}} \; c^{\dagger}_{\mathbf{k},\lambda\kappa_\lambda\sigma}(\tau_1) c_{\mathbf{k}',\mu\kappa_\mu\sigma}(\tau_1) \\
&= \frac{1}{N_{\mathbf{k}}} \sum_{\mathbf{k}} \sum_{\lambda\mu} \sum_{\kappa_\lambda\kappa_\mu} \sum_{\sigma} v^{\sigma}_{\mathbf{k}\mathbf{k}+\mathbf{q};\lambda\kappa_\lambda,\mu\kappa_\mu} \; c^{\dagger}_{\mathbf{k},\lambda\kappa_\lambda\sigma}(\tau_1) c_{\mathbf{k}+\mathbf{q},\mu\kappa_\mu\sigma}(\tau_1), \qquad \text{(A.1)}
\end{aligned}$$

where we used

$$c_{\mathbf{i}} = \frac{1}{N_{\mathbf{k}}} \sum_{k} e^{i\mathbf{k}.\mathbf{R_i}} c_{\mathbf{k}}; \; c^{\dagger}_{\mathbf{i}} = \frac{1}{N_{\mathbf{k}}} \sum_{k} e^{-i\mathbf{k}.\mathbf{R_i}} c^{\dagger}_{\mathbf{k}}. \qquad \text{(A.2)}$$

The transformation of the creator and annihilator operators from imaginary time to Matsubara space is also needed which is given by

$$\begin{aligned}
c(\nu_n) &= \int_0^{\beta} d\tau \; e^{i\nu_n\tau} c(\tau); \; c(\tau) = \frac{1}{\beta} \sum_{n=-\infty}^{+\infty} e^{-i\nu_n\tau} c(\nu_n), \\
c^{\dagger}(\nu_n) &= \int_0^{\beta} d\tau \; e^{-i\nu_n\tau} c^{\dagger}(\tau); \; c^{\dagger}(\tau) = \frac{1}{\beta} \sum_{n=-\infty}^{+\infty} e^{i\nu_n\tau} c^{\dagger}(\nu_n).
\end{aligned}$$

Now we substitute $\hat{\mathcal{O}}(\mathbf{q}, \tau_1)$ in the general definition of the susceptibility in Eq. (4.14) and we use $c(\nu_n)$ and $c^{\dagger}(\nu_n)$ to obtain Eqs. (4.17) and (4.18) as follows.

$$\begin{aligned}
\chi(\mathbf{q}, \omega_m) &= \frac{1}{N^2_{\mathbf{k}}} \sum_{\mathbf{k}\mathbf{k}'} \sum_{\substack{\lambda\mu \\ \gamma\delta}} \sum_{\substack{\kappa_\lambda\kappa_\mu \\ \kappa_\gamma\kappa_\delta}} \sum_{\sigma\sigma'} v^{\sigma}_{\mathbf{k}\mathbf{k}+\mathbf{q};\lambda\kappa_\lambda,\mu\kappa_\mu} v^{\sigma'}_{\mathbf{k}'+\mathbf{q}\mathbf{k}';\gamma\kappa_\gamma,\delta\kappa_\delta} \int_0^{\beta} d\tau_1 \int_0^{\beta} d\tau_2 \; e^{i\omega_m(\tau_1-\tau_2)} \\
&\times \Big\{ \Big\langle \mathcal{T} c^{\dagger}_{\mathbf{k},\lambda\kappa_\lambda\sigma}(\tau_1) c_{\mathbf{k}+\mathbf{q},\mu\kappa_\mu\sigma}(\tau_1) c^{\dagger}_{\mathbf{k}'+\mathbf{q},\gamma\kappa_\gamma\sigma'}(\tau_2) c_{\mathbf{k}',\delta\kappa_\delta\sigma'}(\tau_2) \Big\rangle \\
&- \Big\langle c^{\dagger}_{\mathbf{k},\lambda\kappa_\lambda\sigma}(\tau_1) c_{\mathbf{k}+\mathbf{q},\mu\kappa_\mu\sigma}(\tau_1) \Big\rangle \Big\langle c^{\dagger}_{\mathbf{k}'+\mathbf{q},\gamma\kappa_\gamma\sigma'}(\tau_2) c_{\mathbf{k}',\delta\kappa_\delta\sigma'}(\tau_2) \Big\rangle \Big\}. \qquad \text{(A.3)}
\end{aligned}$$

Since mathematical calculation for the first and second term is identical, for the sake of simplicity, we skip the second term in the following proof.

$$\begin{aligned}
\chi(\mathbf{q},\omega_m) &= \frac{1}{N_{\mathbf{k}}^2}\sum_{\mathbf{k}\mathbf{k}'}\sum_{\substack{\lambda\mu\\ \gamma\delta}}\sum_{\substack{\kappa_\lambda\kappa_\mu\\ \kappa_\gamma\kappa_\delta}}\sum_{\sigma\sigma'} v^{\sigma}_{\mathbf{k}\mathbf{k}+\mathbf{q};\lambda\kappa_\lambda,\mu\kappa_\mu} v^{\sigma'}_{\mathbf{k}'+\mathbf{q}\mathbf{k}';\gamma\kappa_\gamma,\delta\kappa_\delta}\int_0^\beta d\tau_1\int_0^\beta d\tau_2\, e^{i\omega_m(\tau_1-\tau_2)} \\
&\times\Bigg\{\Big\langle\frac{1}{\beta}\sum_{n_1=-\infty}^{+\infty} e^{i\nu_n\tau_1} c^\dagger_{\mathbf{k},\lambda\kappa_\lambda\sigma}(\nu_{n_1})\frac{1}{\beta}\sum_{n_1'=-\infty}^{+\infty} e^{-i\nu_{n_1'}\tau_1} c_{\mathbf{k}+\mathbf{q},\mu\kappa_\mu\sigma}(\nu_{n_1'}) \\
&\quad \frac{1}{\beta}\sum_{n_2=-\infty}^{+\infty} e^{i\nu_{n_2}\tau_2} c^\dagger_{\mathbf{k}'+\mathbf{q},\gamma\kappa_\gamma\sigma'}(\nu_{n_2})\frac{1}{\beta}\sum_{n_2'=-\infty}^{+\infty} e^{-i\nu_{n_2'}\tau_2} c_{\mathbf{k}',\delta\kappa_\delta\sigma'}(\nu_{n_2'})\Big\rangle - \text{2nd term.}\Bigg\} \\
&= \frac{1}{N_{\mathbf{k}}^2}\sum_{\mathbf{k}\mathbf{k}'}\sum_{\substack{\lambda\mu\\ \gamma\delta}}\sum_{\substack{\kappa_\lambda\kappa_\mu\\ \kappa_\gamma\kappa_\delta}}\sum_{\sigma\sigma'} v^{\sigma}_{\mathbf{k}\mathbf{k}+\mathbf{q};\lambda\kappa_\lambda,\mu\kappa_\mu} v^{\sigma'}_{\mathbf{k}'+\mathbf{q}\mathbf{k}';\gamma\kappa_\gamma,\delta\kappa_\delta}\frac{1}{\beta^4}\int_0^\beta d\tau_1\int_0^\beta d\tau_2 \\
&\times\sum_{n_1 n_1'} e^{i(\omega_m+\nu_{n_1}-\nu_{n_1'})\tau_1}\sum_{n_2 n_2'} e^{i(-\omega_m-\nu_{n_2}+\nu_{n_2'})\tau_2} \\
&\times\Bigg\{\Big\langle c^\dagger_{\mathbf{k},\lambda\kappa_\lambda\sigma}(\nu_{n_1}) c_{\mathbf{k}+\mathbf{q},\mu\kappa_\mu\sigma}(\nu_{n_1'}) c^\dagger_{\mathbf{k}'+\mathbf{q},\gamma\kappa_\gamma\sigma'}(\nu_{n_2}) c_{\mathbf{k}',\delta\kappa_\delta\sigma'}(\nu_{n_2'})\Big\rangle - \text{2nd term.}\Bigg\},
\end{aligned}$$

in which

$$\int_0^\beta d\tau\, e^{i(\omega_m+\nu_n-\nu_{n'})\tau} = \beta\,\delta_{\nu_{n'},\nu_n+\omega_m}; \qquad \text{for } \omega_m+\nu_n-\nu_{n'} \text{ which is bosonic.}$$

Thus we have

$$\begin{aligned}
\chi(\mathbf{q},\omega_m) &= \frac{1}{N_{\mathbf{k}}^2}\sum_{\mathbf{k}\mathbf{k}'}\sum_{\substack{\lambda\mu\\ \gamma\delta}}\sum_{\substack{\kappa_\lambda\kappa_\mu\\ \kappa_\gamma\kappa_\delta}}\sum_{\sigma\sigma'} v^{\sigma}_{\mathbf{k}\mathbf{k}+\mathbf{q};\lambda\kappa_\lambda,\mu\kappa_\mu} v^{\sigma'}_{\mathbf{k}'+\mathbf{q}\mathbf{k}';\gamma\kappa_\gamma,\delta\kappa_\delta}\frac{1}{\beta^2}\sum_{n_1 n_2} \\
&\times\Big\{\Big\langle c^\dagger_{\mathbf{k},\lambda\kappa_\lambda\sigma}(\nu_{n_1}) c_{\mathbf{k}+\mathbf{q},\mu\kappa_\mu\sigma}(\nu_{n_1}+\omega_m) c^\dagger_{\mathbf{k}'+\mathbf{q},\gamma\kappa_\gamma\sigma'}(\nu_{n_2}+\omega_m) c_{\mathbf{k}',\delta\kappa_\delta\sigma'}(\nu_{n_2})\Big\rangle \\
&-\Big\langle c^\dagger_{\mathbf{k},\lambda\kappa_\lambda\sigma}(\nu_{n_1}) c_{\mathbf{k}+\mathbf{q},\mu\kappa_\mu\sigma}(\nu_{n_1}+\omega_m)\Big\rangle\Big\langle c^\dagger_{\mathbf{k}'+\mathbf{q},\gamma\kappa_\gamma\sigma'}(\nu_{n_2}+\omega_m) c_{\mathbf{k}',\delta\kappa_\delta\sigma'}(\nu_{n_2})\Big\rangle\Big\}.
\end{aligned} \tag{A.4}$$

Notice that the one-particle correlation function in Eq. (4.18) is actually the one-particle Green's function which is given by

$$\begin{aligned}
\mathcal{G}^\sigma_{ij}(\mathbf{k},\nu_n;\mathbf{k}',\nu_{n'}) &= -\int_0^\beta d\tau\, e^{i\nu_n\tau}\int_0^\beta d\tau'\, e^{-i\nu_{n'}\tau'}\Big\langle\mathcal{T}\, c_{\mathbf{k},i\sigma}(\tau) c^\dagger_{\mathbf{k}',j\sigma}(\tau')\Big\rangle \\
&= -\Big\langle c_{\mathbf{k},i\sigma}(\nu_n) c^\dagger_{\mathbf{k}',j\sigma}(\nu_{n'})\Big\rangle.
\end{aligned} \tag{A.5}$$

A.2 Derivation of the general form of the non-interacting susceptibility

For non-interacting case, we can use Wick's theorem to decouple the two-particle correlation function $\mathcal{C}$ in Eq. (A.3).

$$\begin{aligned}\mathcal{C} &= \Big\langle c^{\dagger}_{\mathbf{k},\lambda\kappa_\lambda\sigma}(\nu_{n_1})c_{\mathbf{k}+\mathbf{q},\mu\kappa_\mu\sigma}(\nu_{n_1}+\omega_m)c^{\dagger}_{\mathbf{k}'+\mathbf{q},\gamma\kappa_\gamma\sigma'}(\nu_{n_2}+\omega_m)c_{\mathbf{k}',\delta\kappa_\delta\sigma'}(\nu_{n_2})\Big\rangle \\ &\quad -\Big\langle c^{\dagger}_{\mathbf{k},\lambda\kappa_\lambda\sigma}(\nu_{n_1})c_{\mathbf{k}+\mathbf{q},\mu\kappa_\mu\sigma}(\nu_{n_1}+\omega_m)\Big\rangle\Big\langle c^{\dagger}_{\mathbf{k}'+\mathbf{q},\gamma\kappa_\gamma\sigma'}(\nu_{n_2}+\omega_m)c_{\mathbf{k}',\delta\kappa_\delta\sigma'}(\nu_{n_2})\Big\rangle \\ &\approx -\Big\langle c_{\mathbf{k}',\delta\kappa_\delta\sigma'}(\nu_{n_2})c^{\dagger}_{\mathbf{k},\lambda\kappa_\lambda\sigma}(\nu_{n_1})\Big\rangle\Big\langle c_{\mathbf{k}+\mathbf{q},\mu\kappa_\mu\sigma}(\nu_{n_1}+\omega_m)c^{\dagger}_{\mathbf{k}'+\mathbf{q},\gamma\kappa_\gamma\sigma'}(\nu_{n_2}+\omega_m)\Big\rangle. \quad \text{(A.6)}\end{aligned}$$

Since for a system with time and translational invariance $\mathcal{G}^{\sigma}(\mathbf{R_i},\mathbf{R_j},\tau,\tau') = \mathcal{G}^{\sigma}(\mathbf{R_i}-\mathbf{R_j},\tau-\tau')$ we have

$$\begin{aligned}\mathcal{G}^{\sigma}_{ij}(\mathbf{k},\nu_n;\mathbf{k}',\nu_{n'}) &= -\Big\langle c_{\mathbf{k},i\sigma}(\nu_n)c^{\dagger}_{\mathbf{k}',j\sigma}(\nu_{n'})\Big\rangle \\ &= \int_0^{\beta}d\tau\; e^{i\nu_n\tau}\int_0^{\beta}d\tau'\; e^{-i\nu_{n'}\tau'}\sum_{\mathbf{ij}}e^{i(\mathbf{k}.\mathbf{R_i}-\mathbf{k}'.\mathbf{R_j})}\mathcal{G}^{\sigma}(\mathbf{R_i},\mathbf{R_j},\tau,\tau') \\ &= \int_0^{\beta}d\tau\; e^{i\nu_n\tau}\int_0^{\beta}d\tau'\; e^{-i\nu_{n'}\tau'}\sum_{\mathbf{ij}}e^{i(\mathbf{k}.\mathbf{R_i}-\mathbf{k}'.\mathbf{R_j})}\mathcal{G}^{\sigma}(\mathbf{R_i}-\mathbf{R_j},\tau-\tau') \\ &= \int_0^{\beta}d\tau\; e^{i\nu_n\tau}\int_0^{\beta}d\tau'\; e^{-i\nu_{n'}\tau'}\sum_{\mathbf{ij}}e^{i(\mathbf{k}.\mathbf{R_i}-\mathbf{k}'.\mathbf{R_j})} \\ &\quad \times\Big\{\frac{1}{N_{\mathbf{k}}}\sum_k e^{-i\mathbf{p}.(\mathbf{R_i}-\mathbf{R_j})}\frac{1}{\beta}\sum_p e^{-i\nu_p(\tau-\tau')}\mathcal{G}^{\sigma}_{ij}(\mathbf{p},\nu_p)\Big\} \\ &= N_{\mathbf{k}}\delta_{\mathbf{k}\mathbf{k}'}\beta\delta_{nn'}\;\mathcal{G}^{\sigma}_{ij}(\mathbf{k},\nu_n), \quad \text{(A.7)}\end{aligned}$$

for the non-interacting susceptibility we can obtain

$$\begin{aligned}\chi^{\mathbf{0}}(\mathbf{q},\omega_m) &= -\frac{1}{N^2_{\mathbf{k}}}\sum_{\mathbf{k}\mathbf{k}'}\sum_{\substack{\lambda\mu\\ \gamma\delta}}\sum_{\substack{\kappa_\lambda\kappa_\mu\\ \kappa_\gamma\kappa_\delta}}\sum_{\sigma\sigma'}v^{\sigma}_{\mathbf{k}\mathbf{k}+\mathbf{q};\lambda\kappa_\lambda,\mu\kappa_\mu}v^{\sigma'}_{\mathbf{k}'+\mathbf{q}\mathbf{k}';\gamma\kappa_\gamma,\delta\kappa_\delta}\frac{1}{\beta^2}\sum_{n_1n_2} \\ &\quad\times\Big\langle c_{\mathbf{k}',\delta\kappa_\delta\sigma'}(\nu_{n_2}+\omega_m)c^{\dagger}_{\mathbf{k},\lambda\kappa_\lambda\sigma}(\nu_{n_1})\Big\rangle\Big\langle c_{\mathbf{k}+\mathbf{q},\mu\kappa_\mu\sigma}(\nu_{n_1}+\omega_m)c^{\dagger}_{\mathbf{k}'+\mathbf{q},\gamma\kappa_\gamma\sigma'}(\nu_{n_2})\Big\rangle \\ &= -\frac{1}{N^2_{\mathbf{k}}}\sum_{\mathbf{k}\mathbf{k}'}\sum_{\substack{\lambda\mu\\ \gamma\delta}}\sum_{\substack{\kappa_\lambda\kappa_\mu\\ \kappa_\gamma\kappa_\delta}}\sum_{\sigma\sigma'}\frac{1}{\beta^2}\sum_{nn'}v^{\sigma}_{\mathbf{k}\mathbf{k}+\mathbf{q};\lambda\kappa_\lambda,\mu\kappa_\mu}v^{\sigma'}_{\mathbf{k}'+\mathbf{q}\mathbf{k}';\gamma\kappa_\gamma,\delta\kappa_\delta} \\ &\quad\times\beta^2N^2_{\mathbf{k}}\;\delta_{\sigma\sigma'}\delta_{nn'}\delta_{\mathbf{k}\mathbf{k}'}\;\mathcal{G}^{\sigma'}_{\delta\kappa_\delta,\lambda\kappa_\lambda}(\mathbf{k},\nu_n)\mathcal{G}^{\sigma}_{\mu\kappa_\mu,\gamma\kappa_\gamma}(\mathbf{k}+\mathbf{q},\nu_n+\omega_m). \quad \text{(A.8)}\end{aligned}$$

A.3 Derivation of the Bethe-Salpeter equation for paramagnetic systems

Each matrix in the general form of the Bethe-Salpeter equation introduced in Eq. (4.27) depends on momentums $\mathbf{k}$ and $\mathbf{k}'$, Matsubara frequencies ν_n and $\nu_{n'}$, orbitals i,j,k and l, sites

$\kappa_i, \kappa_j, \kappa_k$, and κ_l and spins σ and σ'. Therefore, every matrix in Eq. (4.27) has $N_{\mathbf{k}}^2 N_\nu^2 N_O^4 N_S^4 N_{spin}^2$ elements[1].

In case of the *paramagnetic systems*, it is possible to trace over spins in Eq. (4.27) in order to decrease the matrix size (4 times smaller) and computational running time.

In the following, we show how we can derive the Bethe-Salpeter equation for the spin susceptibility (Eq. 4.47) which is used in LDA+DMFT method so that the trace over spins were already done. For a fixed orbitals i, j, k, l, sites $\kappa_i, \kappa_j, \kappa_k, \kappa_l$, Matsubara frequencies $\nu_n, \nu_{n'}$, ω_m and momentum $\mathbf{q}$, we can rewrite the Bethe-Salpeter equation as follows.

$$[\chi] = [\chi^{\mathbf{0}}] + [\chi^{\mathbf{0}}][\mathbf{\Gamma}][\chi], \tag{A.9}$$

where

$$[\chi] = \begin{pmatrix} \chi^{\uparrow\uparrow} & \chi^{\uparrow\downarrow} \\ \chi^{\downarrow\uparrow} & \chi^{\downarrow\downarrow} \end{pmatrix}, \qquad [\chi^{\mathbf{0}}] = \begin{pmatrix} \chi^{\mathbf{0},\uparrow\uparrow} & 0 \\ 0 & \chi^{\mathbf{0},\downarrow\downarrow} \end{pmatrix}, \qquad [\Gamma] = \begin{pmatrix} \Gamma^{\uparrow\uparrow} & \Gamma^{\uparrow\downarrow} \\ \Gamma^{\downarrow\uparrow} & \Gamma^{\downarrow\downarrow} \end{pmatrix}. \tag{A.10}$$

From this relation we can easily obtain

$$\chi^{\uparrow\uparrow} = \chi^{\mathbf{0},\uparrow\uparrow}\Big(1 + \mathbf{\Gamma}^{\uparrow\uparrow}\chi^{\uparrow\uparrow} + \mathbf{\Gamma}^{\uparrow\downarrow}\chi^{\downarrow\uparrow}\Big), \tag{A.11}$$

$$\chi^{\uparrow\downarrow} = \chi^{\mathbf{0},\uparrow\uparrow}\Big(0 + \mathbf{\Gamma}^{\uparrow\uparrow}\chi^{\uparrow\downarrow} + \mathbf{\Gamma}^{\uparrow\downarrow}\chi^{\downarrow\downarrow}\Big), \tag{A.12}$$

$$\chi^{\downarrow\uparrow} = \chi^{\mathbf{0},\downarrow\downarrow}\Big(0 + \mathbf{\Gamma}^{\downarrow\uparrow}\chi^{\uparrow\uparrow} + \mathbf{\Gamma}^{\downarrow\downarrow}\chi^{\downarrow\uparrow}\Big), \tag{A.13}$$

$$\chi^{\downarrow\downarrow} = \chi^{\mathbf{0},\downarrow\downarrow}\Big(1 + \mathbf{\Gamma}^{\downarrow\downarrow}\chi^{\downarrow\downarrow} + \mathbf{\Gamma}^{\downarrow\uparrow}\chi^{\uparrow\downarrow}\Big). \tag{A.14}$$

Due to properties of the *paramagnetic systems* wherein

$$\chi^{\uparrow\uparrow} = \chi^{\downarrow\downarrow}, \qquad \chi^{\uparrow\downarrow} = \chi^{\downarrow\uparrow}, \tag{A.15}$$

$$\mathbf{\Gamma}^{\uparrow\uparrow} = \mathbf{\Gamma}^{\downarrow\downarrow}, \qquad \mathbf{\Gamma}^{\uparrow\downarrow} = \mathbf{\Gamma}^{\downarrow\uparrow}, \tag{A.16}$$

we can derive the spin susceptibility by

$$\begin{aligned}
\chi^{zz} &= \frac{1}{4}\sum_{\sigma\sigma'}\sigma\sigma'\chi^{\sigma\sigma'} = \frac{1}{4}\Big(\chi^{\uparrow\uparrow} - \chi^{\uparrow\downarrow} - \chi^{\downarrow\uparrow} + \chi^{\downarrow\downarrow}\Big) \\
&= \frac{1}{2}\Big(\chi^{\uparrow\uparrow} - \chi^{\uparrow\downarrow}\Big) \\
&= \frac{1}{2}\Big(\chi^{\mathbf{0},\uparrow\uparrow}\Big\{1 + \mathbf{\Gamma}^{\uparrow\uparrow}\Big[\chi^{\uparrow\uparrow} - \chi^{\uparrow\downarrow}\Big] + \mathbf{\Gamma}^{\uparrow\downarrow}\Big[\chi^{\downarrow\uparrow} - \chi^{\downarrow\downarrow}\Big]\Big\}\Big) \\
&= \frac{1}{2}\chi^{\mathbf{0},\uparrow\uparrow} + \frac{1}{2}\chi^{\mathbf{0},\uparrow\uparrow}\Big(\mathbf{\Gamma}^{\uparrow\uparrow} - \mathbf{\Gamma}^{\uparrow\downarrow}\Big)\Big(\chi^{\uparrow\uparrow} - \chi^{\uparrow\downarrow}\Big) \\
&= \chi^{\mathbf{0},zz} + 4\,\chi^{\mathbf{0},zz}\,\mathbf{\Gamma}^{zz}\,\chi^{zz}.
\end{aligned} \tag{A.17}$$

In LDA+DMFT approach, the lattice and local vertex function are obtained by

$$\mathbf{\Gamma}^{zz}(\mathbf{q},\omega_m) = \frac{1}{4}\Big[\chi^{\mathbf{0},zz}(\mathbf{q},\omega_m)\Big]^{-1} - \frac{1}{4}\Big[\chi^{zz}(\mathbf{q},\omega_m)\Big]^{-1}, \tag{A.18}$$

$$\mathbf{\Gamma}^{zz}_{\mathbf{loc}}(\omega_m) = \frac{1}{4}\Big[\chi^{\mathbf{0},zz}_{\mathbf{loc}}(\omega_m)\Big]^{-1} - \frac{1}{4}\Big[\chi^{zz}_{\mathbf{loc}}(\omega_m)\Big]^{-1}, \tag{A.19}$$

[1] In LDA+DMFT approach for a simple system with two orbitals, two atomic sites at high temperature $\beta \sim 30$, we consider $N_\nu \sim 140$. Thus, we are dealing with huge matrices with $\sim 10^7$ elements.

Within the local vertex approximation $\mathbf{\Gamma}^{zz}(\mathbf{q},\omega_m) \approx \mathbf{\Gamma}^{zz}_{\mathbf{loc}}(\omega_m)$ and considering Eq. (A.18) and Eq. (A.19), we can obtain

$$\begin{aligned}
&\frac{1}{4}\Big[\chi^{\mathbf{0},zz}(\mathbf{q},\omega_m)\Big]^{-1} - \frac{1}{4}\Big[\chi^{zz}(\mathbf{q},\omega_m)\Big]^{-1} = \frac{1}{4}\Big[\chi^{\mathbf{0},zz}_{\mathbf{loc}}(\omega_m)\Big]^{-1} - \frac{1}{4}\Big[\chi^{zz}_{\mathbf{loc}}(\omega_m)\Big]^{-1} \\
&\quad \Rightarrow \Big[\chi^{zz}(\mathbf{q},\omega_m)\Big]^{-1} = \Big[\chi^{\mathbf{0},zz}(\mathbf{q},\omega_m)\Big]^{-1} - \Big[\chi^{\mathbf{0},zz}_{\mathbf{loc}}(\omega_m)\Big]^{-1} + \Big[\chi^{zz}_{\mathbf{loc}}(\omega_m)\Big]^{-1}. \qquad \text{(A.20)}
\end{aligned}$$

Similar argument can be done to derive the Bethe-Salpeter equation (4.65) for the $\mathbf{q}$-dependent charge susceptibility in *paramagnetic* systems.

APPENDIX B

Appendix

B.1 Derivation of the $\lim_{q\to 0}\chi^{0,zz}(q,\omega_0)$ for a one band system with two sites per unit cell

An effective Hamiltonian with one orbital and two atomic sites per unit cell can be used to describe some real materials like Vanadate compounds $VOMoO_4$ and Li_2VOSiO_4. In this appendix, we derive the static $\omega = 0$, uniform $\mathbf{q} = \mathbf{0}$ non-interacting spin susceptibility $\chi^{0,zz}(\mathbf{0},\omega_0)$ in terms of the Fermi-Dirac distribution function n_F. We use two different approaches to derive it. In the first approach, we calculate the static uniform magnetic susceptibility using the magnetization of the system created by small uniform external magnetic field. In the second approach, we use directly the non-interacting relation for the $\chi^{0,zz}(\mathbf{q},\omega_m)$ and calculate it in the limit of $\mathbf{q}\to\mathbf{0}$ and $\omega_m = 0$.

B.1.1 Derivation of $\lim_{q\to 0}\chi^{0,zz}(q,\omega_0)$ using the magnetization

In presence of small magnetic field $\mathbf{h} = h\hat{z}$, system is magnetized along the z-direction so that the magnetization is obtained by

$$M = \sum_{\alpha_i,\alpha_j} \delta_{\alpha_i,\alpha_j} M_{\alpha_i\alpha_j}, \tag{B.1}$$

where,

$$M_{\alpha_i,\alpha_j} = \langle \hat{M}_{\alpha_i\alpha_j}\rangle = -g\mu_B\langle \hat{S}_{\alpha_i\alpha_j}\rangle, \tag{B.2}$$

$\alpha_i = i\kappa_i\sigma$ ($\alpha_j = j\kappa_j\sigma$) is collective indices of orbital i (j), atomic site κ_i (κ_j) and spin σ_i (σ_j) so that $\sigma_i = \sigma_j \equiv \sigma$. In this relation, the spin operator in z-direction is defined as

$$\hat{S}_{\alpha_i\alpha_j} = \frac{1}{2}\sum_{\sigma} \sigma c^{\dagger}_{\alpha_i} c_{\alpha_j}. \tag{B.3}$$

Using the definition of one particle Green's function, we can rewrite the magnetization relation in terms of the Green's function as follows.

$$\begin{aligned} M_{\alpha_i\alpha_j} &= -\frac{1}{2}(g\mu_B)\sum_{\sigma}\sigma \left\langle \mathcal{T} c^{\dagger}_{\alpha_i}(\tau = 0^+) c_{\alpha_j}\right\rangle \\ &= \frac{1}{2}(g\mu_B)\sum_{\sigma}\sigma\, \mathcal{G}_{\alpha_j\alpha_i}(\tau = 0^-) \\ &= \frac{1}{2}(g\mu_B)\frac{1}{\beta}\sum_{n=-\infty}^{+\infty} e^{i\nu_n 0^+}\frac{1}{N_{\mathbf{k}}}\sum_{k}\sum_{\sigma}\sigma\, \mathcal{G}_{\alpha_j\alpha_i}(\mathbf{k},\nu_n). \end{aligned} \tag{B.4}$$

In this relation, the Green's function is given by

$$\mathcal{G}_{\alpha_i\alpha_j}(\mathbf{k},\nu_n)=\left(\frac{1}{[i\nu_n+1/2(g\mu_B)h\sigma]\otimes\mathbb{1}-H(\mathbf{k})-\Sigma(\mathbf{k},\nu_n)}\right)_{\alpha_i\alpha_j}, \tag{B.5}$$

where $\mathbb{1}$ is the identity matrix. Considering this relation, we are able to calculate the static uniform susceptibility *per site* by

$$\chi^{\mathbf{0}}(\mathbf{0},0)=\frac{1}{N_S}\sum_{\alpha_i,\alpha_j}\delta_{\alpha_i,\alpha_j}\frac{\partial M_{\alpha_i\alpha_j}}{\partial h}\bigg|_{h\to 0}. \tag{B.6}$$

For a system with two atomic sites, $\kappa_i=1,2$, and one band $i=1$, in the absence of the Coulomb interaction $U=0$, the magnetization is a 2×2 matrix that can be obtained as follows.

$$\begin{aligned} M &= \frac{1}{2}(g\mu_B)\frac{1}{\beta}\sum_{n=-\infty}^{\infty}e^{i\nu_n 0^+}\frac{1}{N_{\mathbf{k}}}\sum_{\mathbf{k}}\sum_{\sigma}\sigma \\ &\quad\times\begin{pmatrix} i\nu_n-H_{11}(\mathbf{k})+1/2(g\mu_B)h\sigma & -H_{12}(\mathbf{k}) \\ -H_{21}(\mathbf{k}) & i\nu_n-H_{22}(\mathbf{k})+1/2(g\mu_B)h\sigma\end{pmatrix}^{-1}. \end{aligned} \tag{B.7}$$

Since the Hamiltonian is Hermitian, $H_{12}(\mathbf{k})=H_{21}^{*}(\mathbf{k})$. Furthermore, we consider that two atomic sites in the unit cell are equivalent so that $H_{11}(\mathbf{k})=H_{22}(\mathbf{k})$. Using this relation, we are able to derive the onsite magnetization by

$$M_{11}=\frac{1}{2}(g\mu_B)\frac{1}{\beta}\sum_{n=-\infty}^{\infty}e^{i\nu_n 0^+}\frac{1}{N_{\mathbf{k}}}\sum_{\mathbf{k}}\sum_{\sigma}\sigma\frac{i\nu_n-H_{11}(\mathbf{k})+1/(g\mu_B)h\sigma}{(i\nu_n-H_{11}(\mathbf{k})+1/2(g\mu_B)h\sigma)^2-|H_{12}(\mathbf{k})|^2}. \tag{B.8}$$

To continue the calculation, we must notice that $|H_{12}(\mathbf{k})|^2$ is a real value. For this reason with using complex algebra, we can rewrite this term by

$$|H_{12}(\mathbf{k})|^2={H'_{12}}^2+{H''_{12}}^2\equiv R^2(\mathbf{k}), \tag{B.9}$$

where $H'_{12}(\mathbf{k})\equiv\Re e[H_{12}(\mathbf{k})]$ and $H''_{12}(\mathbf{k})\equiv\Im m[H_{12}(\mathbf{k})]$. In the following, for the sake of simplicity, we define $\varepsilon^{+}_{\mathbf{k}}\equiv H_{11}(\mathbf{k})+R(\mathbf{k})$ and $\varepsilon^{-}_{\mathbf{k}}\equiv H_{11}(\mathbf{k})-R(\mathbf{k})$.

$$\begin{aligned} M_{11} &= \frac{1}{2}(g\mu_B)\frac{1}{\beta}\sum_{n=-\infty}^{\infty}e^{i\nu_n 0^+}\frac{1}{N_{\mathbf{k}}}\sum_{\mathbf{k}}\sum_{\sigma}\sigma\frac{i\nu_n-H_{11}(\mathbf{k})+1/2(g\mu_B)h\sigma}{(i\nu_n-H_{11}(\mathbf{k})+1/2(g\mu_B)h\sigma)^2-R^2(\mathbf{k})} \\ &= \frac{1}{2}(g\mu_B)\frac{1}{\beta}\sum_{n=-\infty}^{\infty}e^{i\nu_n 0^+}\frac{1}{N_{\mathbf{k}}}\sum_{\mathbf{k}}\sum_{\sigma}\sigma\frac{1}{2} \\ &\quad\times\left\{\frac{1}{i\nu_n-\varepsilon^{+}_{\mathbf{k}}+1/2(g\mu_B)h\sigma}+\frac{1}{i\nu_n-\varepsilon^{-}_{\mathbf{k}}+1/2(g\mu_B)h\sigma}\right\} \\ &= \frac{1}{2}(g\mu_B)\frac{1}{N_{\mathbf{k}}}\sum_{\mathbf{k}}\sum_{\sigma}\sigma\frac{1}{2}\left\{n_F(\varepsilon^{+}_{\mathbf{k}}-1/2(g\mu_B)h\sigma)+n_F(\varepsilon^{-}_{\mathbf{k}}-1/2(g\mu_B)h\sigma)\right\} \\ &= \frac{1}{2}(g\mu_B)\frac{1}{N_{\mathbf{k}}}\sum_{\mathbf{k}}\sum_{\sigma}\sigma\frac{1}{2}\left\{n_F(\varepsilon^{+}_{\mathbf{k}})+n_F(\varepsilon^{-}_{\mathbf{k}})-1/2(g\mu_B)h\sigma\left(\frac{\partial n_F(\varepsilon^{+}_{\mathbf{k}})}{\partial\varepsilon^{+}_{\mathbf{k}}}+\frac{\partial n_F(\varepsilon^{-}_{\mathbf{k}})}{\partial\varepsilon^{-}_{\mathbf{k}}}\right)\right\} \\ &= -\frac{1}{N_{\mathbf{k}}}\sum_{\mathbf{k}}\frac{1}{4}(g\mu_B)^2h\left(\frac{\partial n_F(\varepsilon^{+}_{\mathbf{k}})}{\partial\varepsilon^{+}_{\mathbf{k}}}+\frac{\partial n_F(\varepsilon^{-}_{\mathbf{k}})}{\partial\varepsilon^{-}_{\mathbf{k}}}\right), \end{aligned} \tag{B.10}$$

wherein n_F is the Fermi-Dirac distribution function and we used $\sum_\sigma \sigma^2 = 2$ and $\sum_\sigma \sigma = 0$.

Similar calculation can be done for M_{12} if $H_{12}(\mathbf{k}) \neq 0$ (otherwise $M_{12} = 0$).

$$\begin{aligned}
M_{12} &= \frac{1}{2}(g\mu_B)\frac{1}{\beta}\sum_{n=-\infty}^{\infty} e^{i\nu_n 0^+}\frac{1}{N_\mathbf{k}}\sum_{\mathbf{k}}\sum_{\sigma}\sigma\frac{H_{12}(\mathbf{k})}{(i\nu_n - H_{11}(\mathbf{k}) + 1/2(g\mu_B)h\sigma)^2 - R^2(\mathbf{k})} \\
&= \frac{1}{2}(g\mu_B)\frac{1}{\beta}\sum_{n=-\infty}^{\infty} e^{i\nu_n 0^+}\frac{1}{N_\mathbf{k}}\sum_{\mathbf{k}}\sum_{\sigma}\sigma\frac{R(\mathbf{k})\exp\left(i\frac{H''_{12}}{H'_{12}}\right)}{(i\nu_n - H_{11}(\mathbf{k}) + 1/2(g\mu_B)h\sigma)^2 - R^2(\mathbf{k})} \\
&= \frac{1}{2}(g\mu_B)\frac{1}{\beta}\sum_{n=-\infty}^{\infty} e^{i\nu_n 0^+}\frac{1}{N_\mathbf{k}}\sum_{\mathbf{k}}\sum_{\sigma}\frac{\sigma}{2}\exp\left(i\frac{H''_{12}}{H'_{12}}\right) \\
&\quad\times\left\{\frac{1}{i\nu_n - \varepsilon^+_\mathbf{k} + 1/2(g\mu_B)h\sigma} - \frac{1}{i\nu_n - \varepsilon^-_\mathbf{k} + 1/2(g\mu_B)h\sigma}\right\} \\
&= \frac{1}{2}(g\mu_B)\frac{1}{\beta}\sum_{n=-\infty}^{\infty} e^{i\nu_n 0^+}\frac{1}{N_\mathbf{k}}\sum_{\mathbf{k}}\sum_{\sigma}\frac{\sigma}{2}\exp\left(i\frac{H''_{12}}{H'_{12}}\right) \\
&\quad\times\left\{n_F(\varepsilon^+_\mathbf{k} - 1/2(g\mu_B)h\sigma) - n_F(\varepsilon^-_\mathbf{k} - 1/2(g\mu_B)h\sigma)\right\} \\
&= -\frac{1}{N_\mathbf{k}}\sum_{\mathbf{k}}\frac{1}{4}(g\mu_B)^2 h\exp\left(i\frac{H''_{12}}{H'_{12}}\right)\left(\frac{\partial n_F(\varepsilon^+_\mathbf{k})}{\partial\varepsilon^+_\mathbf{k}} - \frac{\partial n_F(\varepsilon^-_\mathbf{k})}{\partial\varepsilon^-_\mathbf{k}}\right). \qquad \text{(B.11)}
\end{aligned}$$

Therefore, the magnetization matrix is

$$\begin{aligned}
M &= -\frac{1}{N_\mathbf{k}}\sum_{\mathbf{k}}\frac{1}{4}(g\mu_B)^2 h \\
&\quad\times\begin{pmatrix} \frac{\partial n_F(\varepsilon^+_\mathbf{k})}{\partial\varepsilon^+_\mathbf{k}} + \frac{\partial n_F(\varepsilon^-_\mathbf{k})}{\partial\varepsilon^-_\mathbf{k}} & \exp\left(i\frac{H''_{12}}{H'_{12}}\right)\left(\frac{\partial n_F(\varepsilon^+_\mathbf{k})}{\partial\varepsilon^+_\mathbf{k}} - \frac{\partial n_F(\varepsilon^-_\mathbf{k})}{\partial\varepsilon^-_\mathbf{k}}\right) \\ \exp\left(i\frac{H''_{21}}{H'_{21}}\right)\left(\frac{\partial n_F(\varepsilon^+_\mathbf{k})}{\partial\varepsilon^+_\mathbf{k}} - \frac{\partial n_F(\varepsilon^-_\mathbf{k})}{\partial\varepsilon^-_\mathbf{k}}\right) & \frac{\partial n_F(\varepsilon^+_\mathbf{k})}{\partial\varepsilon^+_\mathbf{k}} + \frac{\partial n_F(\varepsilon^-_\mathbf{k})}{\partial\varepsilon^-_\mathbf{k}} \end{pmatrix}. \qquad \text{(B.12)}
\end{aligned}$$

According to Eq. (B.6), the static uniform magnetic response for non-interacting system is given by

$$\begin{aligned}
\chi(\mathbf{0},0) &= -\frac{1}{N_S}\frac{1}{4}(g\mu_B)^2\frac{1}{N_\mathbf{k}}\sum_{\mathbf{k}}2\left(\frac{\partial n_F(\varepsilon^+_\mathbf{k})}{\partial\varepsilon^+_\mathbf{k}} + \frac{\partial n_F(\varepsilon^-_\mathbf{k})}{\partial\varepsilon^-_\mathbf{k}}\right) \\
&= -\frac{1}{4}(g\mu_B)^2\frac{1}{N_\mathbf{k}}\sum_{\mathbf{k}}\left(\frac{\partial n_F(\varepsilon^+_\mathbf{k})}{\partial\varepsilon^+_\mathbf{k}} + \frac{\partial n_F(\varepsilon^-_\mathbf{k})}{\partial\varepsilon^-_\mathbf{k}}\right). \qquad \text{(B.13)}
\end{aligned}$$

B.1.2 Derivation of $\lim_{q\to 0}\chi^{0,zz}(q,\omega_0)$ using Matsubara summations

Based on Eqs. (4.19) and (4.46), the bare lattice spin susceptibility in non-interacting systems is given by

$$\begin{aligned}\chi^{\mathbf{0},zz}(\mathbf{q},\omega_m) &= \frac{1}{N_S}\frac{1}{\beta}\sum_{n=-\infty}^{\infty}\frac{1}{N_{\mathbf{k}}}\sum_{\mathbf{k}}\sum_{\alpha_i\alpha_j}\frac{1}{2}(g\mu_B)\delta_{\alpha_i,\alpha_j}\sum_{\alpha_k\alpha_k}\frac{1}{2}(g\mu_B)\delta_{\alpha_k,\alpha_l}\\ &\quad\times\left[-\delta_{\sigma\sigma'}\mathcal{G}_{\alpha_l\alpha_i}(\mathbf{k},\nu_n)\mathcal{G}_{\alpha_j\alpha_k}(\mathbf{k}+\mathbf{q},\nu_n+\omega_m)\right]\\ &= -\frac{1}{4}(g\mu_B)^2\frac{1}{N_S}\frac{1}{\beta}\sum_{n=-\infty}^{\infty}\frac{1}{N_{\mathbf{k}}}\sum_{\mathbf{k}}\sum_{\alpha_i\alpha_j}\sum_{\alpha_k\alpha_k}\delta_{\alpha_i,\alpha_j}\delta_{\alpha_k,\alpha_l}\delta_{\sigma\sigma'}\\ &\quad\times\mathcal{G}_{\alpha_l\alpha_i}(\mathbf{k},\nu_n)\mathcal{G}_{\alpha_j\alpha_k}(\mathbf{k}+\mathbf{q},\nu_n+\omega_m),\end{aligned}\tag{B.14}$$

where, α_i is the collective indices of orbital i, atomic sites κ_i, spins σ so that we take into account $\sigma_1=\sigma_2\equiv\sigma$ and $\sigma_3=\sigma_4\equiv\sigma'$. Since the considered system has two atomic sites per unit cell $N_S=2$ and each atom has one oribtal $N_O=1$, the Green's function $\mathcal{G}_{\alpha_i\alpha_j}$ is a 2×2 matrix for a given spin σ, Matsubara frequency $i\nu_n$ and momentum $\mathbf{k}$.

$$\Big[\mathcal{G}(\mathbf{k},\nu_n)\Big]=\begin{pmatrix}i\nu_n-H_{11}(\mathbf{k}) & -H_{12}(\mathbf{k})\\ -H_{21}(\mathbf{k}) & i\nu_n-H_{22}(\mathbf{k})\end{pmatrix}^{-1},\tag{B.15}$$

Notice that in paramagnetic systems, $\mathcal{G}^{\uparrow}=\mathcal{G}^{\downarrow}$, we drop the spin indices in this relation. Therefore, the non-interacting spin susceptibility is the trace of a 2×2 matrix given by

$$\begin{aligned}\chi^{\mathbf{0},zz}(\mathbf{q},\omega_m) &= -\frac{1}{4}(g\mu_B)^2\frac{1}{N_S}\frac{1}{\beta}\sum_{n=-\infty}^{\infty}\frac{1}{N_{\mathbf{k}}}\sum_{\mathbf{k}}2\Big(\mathcal{L}_{11}+\mathcal{L}_{22}\Big),\\ &= -\frac{1}{4}(g\mu_B)^2\frac{1}{\beta}\sum_{n=-\infty}^{\infty}\frac{1}{N_{\mathbf{k}}}\sum_{\mathbf{k}}\Big(\mathcal{L}_{11}+\mathcal{L}_{22}\Big),\end{aligned}\tag{B.16}$$

where the pre-factor 2 comes from $\sum_\sigma$ and

$$\begin{aligned}\mathcal{L}_{11} &= \frac{\big(i\nu_n-H_{11}(\mathbf{k})\big)\big(i\nu_n+i\omega_m-H_{11}(\mathbf{k}+\mathbf{q})\big)+H_{12}(\mathbf{k})H_{21}(\mathbf{k}+\mathbf{q})}{\big((i\nu_n-H_{11}(\mathbf{k}))^2-R(\mathbf{k})^2\big)\big((i\nu_n+i\omega_m-H_{11}(\mathbf{k}+\mathbf{q}))^2-R(\mathbf{k}+\mathbf{q})^2\big)},\\ \mathcal{L}_{22} &= \frac{\big(i\nu_n-H_{11}(\mathbf{k})\big)\big(i\nu_n+i\omega_m-H_{11}(\mathbf{k}+\mathbf{q})\big)+H_{21}(\mathbf{k})H_{12}(\mathbf{k}+\mathbf{q})}{\big((i\nu_n-H_{11}(\mathbf{k}))^2-R(\mathbf{k})^2\big)\big((i\nu_n+i\omega_m-H_{11}(\mathbf{k}+\mathbf{q}))^2-R(\mathbf{k}+\mathbf{q})^2\big)}.\end{aligned}$$

In oder to obtain $\mathcal{L}_1$ and $\mathcal{L}_2$, we supposed that the two atomic sites in the unit cell are equivalent, thus $H_{11}=H_{22}$.

In the limit of $\mathbf{q}\to\mathbf{0}$, we can easily obtain that

$$\begin{aligned}\lim_{\mathbf{q}\to\mathbf{0}}\mathcal{L}_{11} &= \lim_{\mathbf{q}\to\mathbf{0}}\mathcal{L}_{22},\\ \lim_{\mathbf{q}\to\mathbf{0}}\Big(H_{12}(\mathbf{k})H_{21}(\mathbf{k}+\mathbf{q})\Big) &\approx |H_{12}(\mathbf{k})|^2=R(\mathbf{k})^2,\\ \lim_{\mathbf{q}\to\mathbf{0}}\Big(R(\mathbf{k})R(\mathbf{k}+\mathbf{q})\Big) &\approx R(\mathbf{k})^2,\\ \lim_{\mathbf{q}\to\mathbf{0}}\Big(H_{12}(\mathbf{k})H_{21}(\mathbf{k}+\mathbf{q})\Big) &\approx \lim_{\mathbf{q}\to\mathbf{0}}\Big(R(\mathbf{k})R(\mathbf{k}+\mathbf{q})\Big).\end{aligned}\tag{B.17}$$

Therefore, with considering

$$\varepsilon^{\pm}_{\mathbf{k}} = H_{11}(\mathbf{k}) \pm R(\mathbf{k}), \tag{B.18}$$

the static uniform non-interacting spin susceptibility can be calculated as follows.

$$\begin{aligned}
\chi^{\mathbf{0},zz}(\mathbf{0},0) &= -\frac{1}{4}(g\mu_B)^2\frac{1}{N_{\mathbf{k}}}\sum_{\mathbf{k}}\frac{1}{\beta}\sum_{n=-\infty}^{\infty}\lim_{\mathbf{q}\to\mathbf{0}}\lim_{i\omega_m\to 0} \\
&\quad\times\left\{\frac{1}{\left(i\nu_n-\varepsilon^{+}_{\mathbf{k}}\right)\left(i\nu_n+i\omega_m-\varepsilon^{+}_{\mathbf{k+q}}\right)}+\frac{1}{\left(i\nu_n-\varepsilon^{-}_{\mathbf{k}}\right)\left(i\nu_n+i\omega_m-\varepsilon^{-}_{\mathbf{k+q}}\right)}\right\} \\
&= -\frac{1}{4}(g\mu_B)^2\frac{1}{N_{\mathbf{k}}}\sum_{\mathbf{k}}\lim_{\mathbf{q}\to\mathbf{0}}\lim_{i\omega_m\to 0} \\
&\quad\times\left\{\frac{n_F(\varepsilon^{+}_{\mathbf{k}})-n_F(\varepsilon^{+}_{\mathbf{k+q}}-i\omega_m)}{i\omega_m+\varepsilon^{+}_{\mathbf{k}}-\varepsilon^{+}_{\mathbf{k+q}}}+\frac{n_F(\varepsilon^{-}_{\mathbf{k}})-n_F(\varepsilon^{-}_{\mathbf{k+q}}-i\omega_m)}{i\omega_m+\varepsilon^{-}_{\mathbf{k}}-\varepsilon^{-}_{\mathbf{k+q}}}\right\} \\
&= -\frac{1}{4}(g\mu_B)^2\frac{1}{N_{\mathbf{k}}}\sum_{\mathbf{k}}\left\{\frac{\partial n_F(\varepsilon^{+}_{\mathbf{k}})}{\partial\varepsilon^{+}_{\mathbf{k}}}+\frac{\partial n_F(\varepsilon^{-}_{\mathbf{k}})}{\partial\varepsilon^{-}_{\mathbf{k}}}\right\},
\end{aligned} \tag{B.19}$$

which is the same as Eq. (B.13) obtained by the other approach.

APPENDIX C

Appendix

C.1 Matsubara summation

Summations over Matsubara frequencies often occur in condensed matter physics. For instance, the summation over fermionic frequencies of the Green's function

$$\mathcal{G} = \frac{1}{\beta}\sum_n \mathcal{G}(\nu_n), \qquad \nu_n = (2n+1)\pi/\beta,$$

or bare-susceptibility

$$\chi^{\mathbf{0}}(\omega_m) = -\frac{1}{\beta}\sum_n \mathcal{G}(\nu_n)\mathcal{G}(\nu_n+\omega_m), \qquad \omega_m = 2m\pi/\beta,$$

or even more

$$\mathcal{G}(\tau) = \frac{1}{\beta}\sum_n e^{-i\nu_n\tau}\mathcal{G}(i\nu_n), \tag{C.1}$$

which can be used to obtain the Green's function in imaginary time space and

$$S(\tau\to 0^+) = \frac{1}{\beta}\sum_n e^{i\nu_n\tau}\mathcal{G}(i\nu_n)\Big|_{\tau\to 0^+}, \tag{C.2}$$

where it appears in (loop) Feynman diagrams.

In more general case we often deal with summations like

$$S = \frac{1}{\beta}\sum_n G(ip_n); \qquad p_n = \begin{cases}\nu_n = (2n+1)\pi/\beta & \text{Fermionic}\\ \omega_n = 2n\pi/\beta & \text{Bosonic}\end{cases}, \tag{C.3}$$

where $G(z)$ is a complex function that may have poles at $z = z_j$. To calculate Eq. (C.3), the trick is to rewrite this summation in terms of the integral over the complex variables to use the residue theory. For this purpose, we consider a complex auxiliary pole-generating function $f(z)$ where $f(z)$ has poles on the imaginary axis at $z = ip_n$. In principle, any complex function with poles $z = ip_n$ can be used. Therefore, the contour integral in which $G(z)$ dose not have any singularities and encloses *only one of* $z = ip_n$ *points* is

$$\oint dz\; f(z)G(z) \;=\; 2\pi i\; \mathcal{R}es\Big[f(z)G(ip_n)\Big]_{z=ip_n} \tag{C.4}$$

Now, if we consider contour C, so that it surrounds *all the points* $z = ip_n$ on the imaginary axis while the $G(z)$ is analytic (See Fig. C.1), we have

$$\frac{1}{2\pi i}\int_C f(z)G(z) = \sum_n \mathcal{R}es\Big[f(z)G(z)\Big]_{z=ip_n}. \tag{C.5}$$

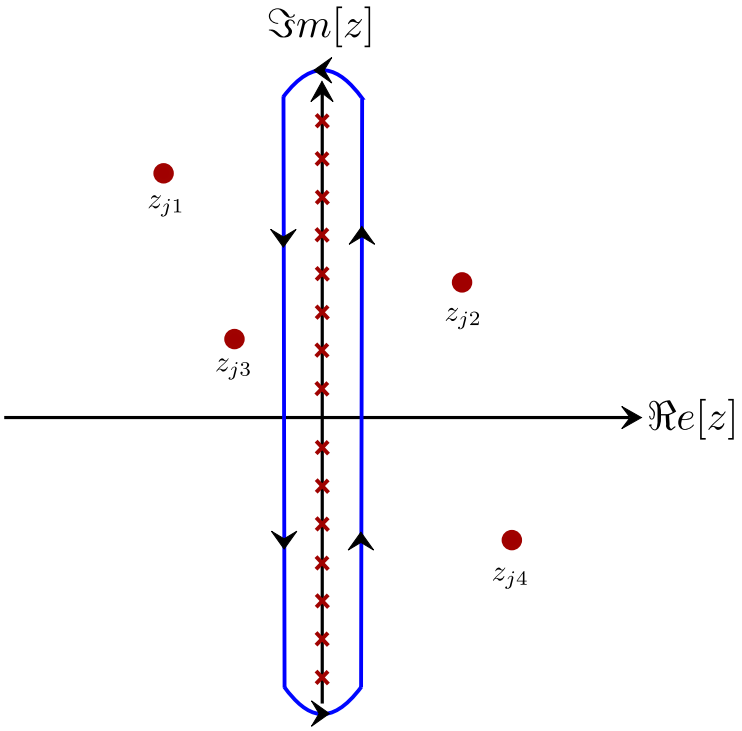

Figure C.1: The integration contour for calculating the Matsubara summation if $G(z)$ does not have poles on the imaginary axis.

If the integrand $|f(z)G(z)|$ decays faster than $1/z$ when $z \to \infty$, we can consider an infinite circle contour, C_∞, that covers the entire complex plane so that the poles of the $G(z)$ at $z = z_j$ are excluded as shown in Fig. C.2. Such a contour gives us the contribution from poles of $f(z)$ at $z = ip_n$ and $G(z)$ at $z = z_j$. Furthermore, due to the fast decays of the integrand, the contour integral itself is zero and we have

$$\begin{aligned} \frac{1}{2\pi i}\int_{C_\infty} dz f(z)G(z) &= \sum_n \mathcal{R}es\Big[f(z)G(z)\Big]_{z=ip_n} + \sum_j \mathcal{R}es\Big[G(z)\Big]_{z=z_j} f(z_j) \\ &= 0. \end{aligned}$$

Thus we have

$$\sum_n \mathcal{R}es\Big[f(z)G(z)\Big]_{z=ip_n} = -\sum_j \mathcal{R}es\Big[G(z)\Big]_{z=z_j} f(z_j). \tag{C.6}$$

To find an appropriate $f(z)$ which produces poles on Fermionic frequencies $i\nu_n$, we have to consider that the integrand $|f(z)G(z)|$ must decay faster than $1/z$. For the cases

$$G(z) = h(z)e^{+\tau z}; \qquad \tau > 0, \tag{C.7}$$

and

$$G(z) = h(z)e^{-\tau z}; \qquad \tau > 0 \tag{C.8}$$

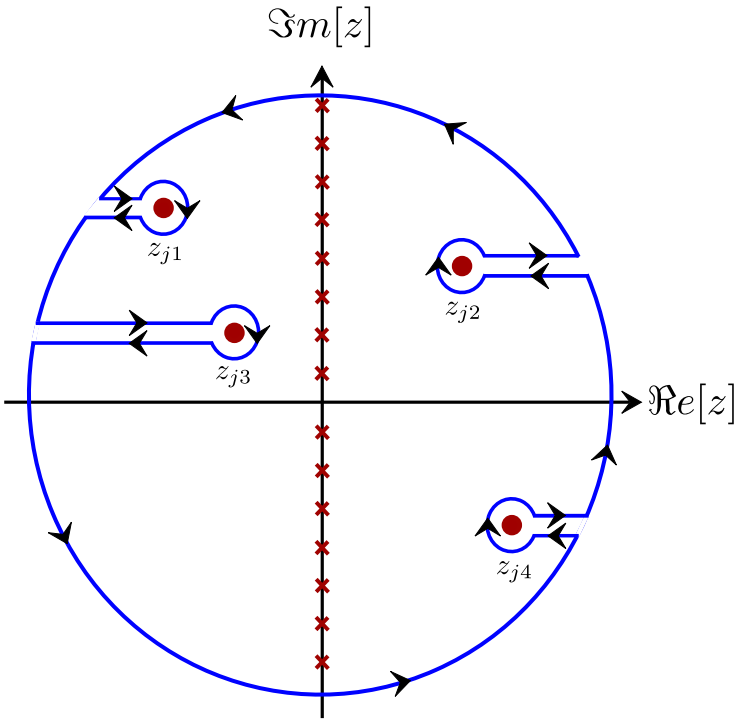

Figure C.2: The integration contour in which the poles of the $G(z)$ at $z = z_j$ are excluded.

where $h(z)$ can be e.g. a green's function $\mathcal{G}(z) = 1/(z - E)$, we can choose

$$f(z) = \frac{1}{1 + e^{\beta z}} = n_F(z) \tag{C.9}$$

and

$$f(z) = -\frac{1}{1 + e^{-\beta z}} = -n_F(-z) = (n_F(z) - 1), \tag{C.10}$$

respectively. Because in one hand the $f(z)$ has poles at $z = i\nu_n$

$$\mathcal{R}es\Big[n_F(z)\Big]_{z=i\nu_n} = \left[\frac{z - i\nu_n}{e^{\beta z} + 1}\right]_{z=i\nu_n} = \left[\frac{1}{\beta e^{\beta z}}\right]_{z=i\nu_n} = -\frac{1}{\beta}, \tag{C.11}$$

$$\mathcal{R}es\Big[(n_F(z) - 1)\Big]_{z=i\nu_n} = -\left[\frac{z - i\nu_n}{e^{-\beta z} + 1}\right]_{z=i\nu_n} = -\left[\frac{1}{\beta e^{-\beta z}}\right]_{z=i\nu_n} = \frac{1}{\beta} \tag{C.12}$$

and on the other hand the integrand decays faster that $1/z$

$$e^{\tau z} n_F(z) = \frac{e^{\tau z}}{1 + e^{\beta z}} \propto \begin{cases} e^{(\tau - \beta)\Re e[z]} \to 0 & \text{for } \Re e[z] > 0 \\ e^{\tau \Re e[z]} \to 0 & \text{for } \Re e[z] < 0 \end{cases}, \tag{C.13}$$

and

$$e^{-\tau z} n_F(-z) = \frac{e^{-\tau z}}{1 + e^{-\beta z}} \propto \begin{cases} e^{-\tau \Re e[z]} \to 0 & \text{for } \Re e[z] > 0 \\ e^{(\beta - \tau)\Re e[z]} \to 0 & \text{for } \Re e[z] < 0 \end{cases}. \tag{C.14}$$

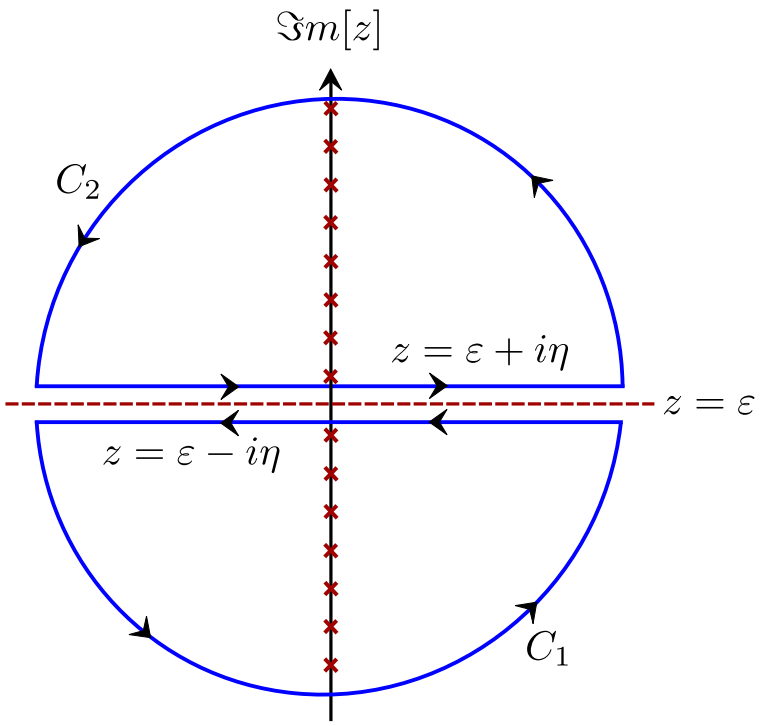

Figure C.3: For a function with known branch cuts, the contour $C = C_1 + C_2$ is considered to perform Matsubara sum. Such a function is analytic in the whole plane except on the branch cut $z = \varepsilon$. At $|z| \to \infty$, the contribution of the circular path is zero and only the path along the branch cut remains.

Therefore, for the Matsubara summation we have

$$\frac{1}{\beta}\sum_n G(i\nu_n) = \frac{1}{\beta}\sum_n h(i\nu_n)e^{i\nu_n\tau} = \sum_j \mathcal{R}es\Big[h(z)\Big]_{z=z_j} n_F(z_j)e^{\tau z_j}, \tag{C.15}$$

$$\frac{1}{\beta}\sum_n G(i\nu_n) = \frac{1}{\beta}\sum_n h(i\nu_n)e^{-i\nu_n\tau} = \sum_j \mathcal{R}es\Big[h(z)\Big]_{z=z_j} (n_F(z_j)-1)e^{-\tau z_j}, \tag{C.16}$$

where z_j are poles of the complex function $h(z)$ and $\tau > 0$. Similarly, for the bosonic Matsubara summation, we can obtain

$$\frac{1}{\beta}\sum_n G(i\omega_n) = \frac{1}{\beta}\sum_n h(i\omega_n)e^{i\omega_n\tau} = -\sum_j \mathcal{R}es\Big[h(z)\Big]_{z=z_j} n_B(z_j)e^{\tau z_j}, \tag{C.17}$$

$$\frac{1}{\beta}\sum_n G(i\omega_n) = \frac{1}{\beta}\sum_n h(i\omega_n)e^{-i\omega_n\tau} = -\sum_j \mathcal{R}es\Big[h(z)\Big]_{z=z_j} (n_B(z_j)+1)e^{-\tau z_j}. \tag{C.18}$$

In some cases where the function $G(z)$ in Eq. (C.3) has branch cuts, we should deform the contour to avoid the branch cuts as shown in Fig. (C.3). This contour includes all $z = ip_n$ points and no singularities of the G. This situation happens e.g. for the Green's function in presence of interaction, where we do not know the poles of the Green's function. But we obviously know that the Green's function is an analytic function for z not on the real axis [56]. Therefore, we

can calculate the summation (C.3) by using Eqs. (C.15) and (C.17) as follows.

$$\begin{aligned}\frac{1}{\beta}\sum_n G(i\nu_n) &= -\frac{1}{2\pi i}\int_{C_1+C_2} dz\; n_F(z)G(z) \\ &= -\frac{1}{2\pi i}\int_{-\infty}^{+\infty} d\varepsilon\; n_F(\varepsilon)\big[G(\varepsilon+i\eta)-G(\varepsilon-i\eta)\big],\end{aligned} \tag{C.19}$$

and similarly

$$\frac{1}{\beta}\sum_n G(i\omega_n) = \frac{1}{2\pi i}\int_{-\infty}^{+\infty} d\varepsilon\; n_B(\varepsilon)\big[G(\varepsilon+i\eta)-G(\varepsilon-i\eta)\big]. \tag{C.20}$$

C.2 Frequently used Matsubara summations

In the following Matsubara summation we assign that

$$n_\xi(E) = \begin{cases} n_F(E) & \text{if } \xi = +1 \\ n_B(E) & \text{if } \xi = -1 \end{cases} .$$

1. $G(z) = (z-E)^{-1}$

$$\frac{1}{\beta}\sum_n G(ip_n)e^{-ip_n\tau} = -e^{E(\beta-\tau)}n_\xi(E) \qquad \tau > 0, \tag{C.21}$$

$$\frac{1}{\beta}\sum_n G(ip_n)e^{ip_n\tau} = \xi e^{\tau E}n_\xi(E) \qquad \tau > 0. \tag{C.22}$$

From this relation, we immediately conclude that

- Green's function at $\tau \to 0^-$

$$\mathcal{G}(\tau = 0^-) = \frac{1}{\beta}\sum_{ip_n}\frac{e^{ip_n 0^+}}{ip_n - E} = \begin{cases} n_F(E) & \text{for Fermions} \\ -n_B(E) & \text{for Bosons} \end{cases} , \tag{C.23}$$

- Green's function at $\tau \to 0^+$

$$\mathcal{G}(\tau = 0^+) = \frac{1}{\beta}\sum_{ip_n}\frac{e^{ip_n 0^-}}{ip_n - E} = \begin{cases} -(1-n_F(E)) & \text{for Fermions} \\ -(1+n_B(E)) & \text{for Bosons} \end{cases} , \tag{C.24}$$

2. $G(z) = (z-E)^{-2}$

$$\frac{1}{\beta}\sum_n G(ip_n)e^{-ip_n\tau} = e^{E(\beta-\tau)}n_\xi(E)(\tau + \xi\beta n_\xi(E)) \qquad \tau > 0, \tag{C.25}$$

$$\frac{1}{\beta}\sum_n G(ip_n)e^{ip_n\tau} = e^{\tau E}n_\xi(E)(\xi\tau - \beta e^{\beta E}n_\xi(E)) \qquad \tau > 0. \tag{C.26}$$

3. $G(z) = (z - E_1)^{-1}(z - E_2)^{-1}$

$$\frac{1}{\beta}\sum_n G(ip_n)e^{-ip_n\tau} = \frac{-1}{E_1 - E_2}\left[e^{E_1(\beta-\tau)}n_\xi(E_1) - e^{E_2(\beta-\tau)}n_\xi(E_2)\right] \qquad \tau > 0, \tag{C.27}$$

$$\frac{1}{\beta}\sum_n G(ip_n)e^{ip_n\tau} = \frac{\xi}{E_1 - E_2}\left[e^{\tau E_1}n_\xi(E_1) - e^{\tau E_2}n_\xi(E_2)\right] \qquad \tau > 0. \tag{C.28}$$

APPENDIX D

Appendix

D.1 Legendre polynomial function $P_l(x)$

The Legendre polynomials $P_l(x)$ $(l = 0, 1, 2, ..)$ can be defined by the formula of Rodrigues [84]:

$$P_0(x) = 1,\ P_l(x) = \frac{1}{2^l l!}\frac{d^l}{dx^l}(x^2 - 1)^l \quad (l = 1, 2, 3, ...) \tag{D.1}$$

Thus

$$\begin{aligned} P_1(x) &= x, \\ P_2(x) &= \frac{3}{2}x^2 - \frac{1}{2}, \\ P_3(x) &= \frac{5}{2}x^3 - \frac{3}{2}x,\ \ldots . \end{aligned} \tag{D.2}$$

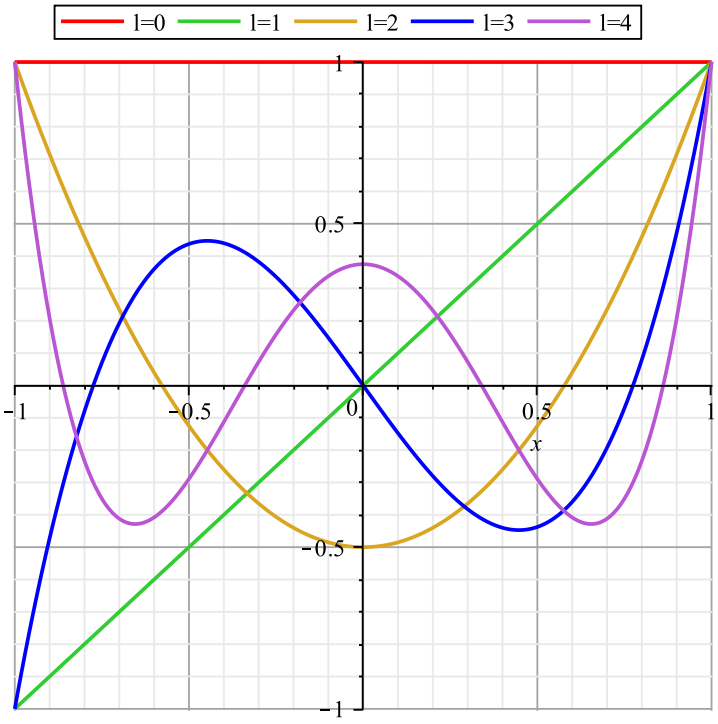

Figure D.1: $P_l(x)$ for different values of $l = 0, ..., 4$.

1. Explicit expression for $P_l(x)$:

$$P_l(x) = \frac{1}{2^l} \sum_{k=0}^{\lfloor l/2 \rfloor} \frac{(-1)^k (2l-2k)!}{k!(l-k)!(l-2k)!} x^{l-2k}, \tag{D.3}$$

   in which $\lfloor l/2 \rfloor$ is integer part of $l/2$.

2. From the definition of Legendre function, it can be inferred that $P_l(x)$ is an odd or even function according to whether l is odd or even. Therefore, we have the following relations for $P_l(x)$ $(l = 1, 2, 3, ..)$.

$$P_l(x) = xP_{l-1}(x) + \frac{x^2-1}{l} P'_{l-1}(x), \tag{D.4}$$

$$P'_l(x) = xP'_{l-1}(x) + lP_{l-1}(x). \tag{D.5}$$

3. The Legendre polynomial $P_l(x)$ satisfies these relations:

   - $P'_{l+1}(x) - P'_{l-1}(x) = (2l+1)P_l(x) \;\; (l \geq 1)$,
   - $\frac{d}{dx}[(1-x^2)P'_l(x)] + l(l+1)P_l(x) = 0$,
   - $P_{l+1}(x) = \frac{(2l+1)xP_l(x) - lP_{l-1}(x)}{l+1} \;\; (l \geq 1)$,
   - $P_l(1) = 1, \;\; P_l(-1) = (-1)^l, \;\; P_l(-x) = (-1)^l P_l(x)$,
   - $\frac{1-x^2}{l^2} P'^2_l(x) + P^2_l(x) = \frac{1-x^2}{l^2} P'^2_{l-1}(x) + P^2_{l-1}(x)$,
   - $\frac{1-x^2}{l^2} P'^2_l(x) + P^2_l(x) \leq 1 \;\; (n \geq 1, |x| \leq 1)$,
   - $|P_l(x)| \leq 1 \;\; (|x| \leq 1)$,
   - x^n can be expressed as a linear combination of $P_0(x), ..., P_l(x)$.

$$\begin{aligned} 1 &= P_0(x), \\ x &= P_1(x), \\ x^2 &= \frac{1}{3}(2P_2(x) + P_0(x)), \\ x^3 &= \frac{1}{5}(2P_3(x) + 3P_1(x)), \;\; \ldots . \end{aligned} \tag{D.6}$$

4. Legendre polynomial function $P_l(x) \;\; (l = 0, 1, 2, ...)$ is orthogonal.

$$\int_{-1}^{1} dx P_l(x) P_{l'}(x) = \frac{2\delta_{ll'}}{2l+1} \tag{D.7}$$

   Accordingly, we can expand an arbitrary function $f(x)$ which is continuous for $-1 \leq x \leq 1$ with respect to Legendre polynomial funciton $P_l(x)$.

$$f(x) = \sum_{l=0}^{\infty} c_l P_l(x). \tag{D.8}$$

   Here c_l can be obtained by using orthogonality condition.

$$c_l = \frac{2l+1}{2} \int_{-1}^{1} f(x) P_l(x) dx. \tag{D.9}$$

5. If $f(x)$ is very smooth for $x \in [-1,1]$, then the Legendre series of $f(x)$ converges uniformly to $f(x)$ for $x \in [-1,1]$.

$$|c_l P_l(x)| \leq const.\ (2l-3)^{-\frac{3}{2}} \quad (l \geq 2) \tag{D.10}$$

6. The Fourier Transform of Legendre polynomial can be written in terms of spherical Bessel functions $j_l(x)$:

$$\begin{aligned} \int_{-1}^{1} e^{i\alpha x} P_l(x) dx &= i^l \sqrt{\frac{2\pi}{\alpha}} J_{l+\frac{1}{2}}(\alpha) \\ &= 2 i^l j_l(\alpha) \end{aligned} \tag{D.11}$$

Here, J is Bessel function and $j_l(\alpha) = \sqrt{\frac{2\pi}{\alpha}} J_{l+\frac{1}{2}}(\alpha)$ denotes the spherical Bessel functions which is explicitly expressed by the following relation:

$$\begin{aligned} j_l(x) &= x^{-1} \Bigg\{ \sin\left(x - \frac{\pi l}{2}\right) \sum_{k=0}^{\lfloor \frac{l}{2} \rfloor} (-1)^k \frac{(l+2k)!(2x)^{-2k}}{(2k)!(l-2k)!} \\ &\quad + \cos\left(x - \frac{\pi l}{2}\right) \sum_{k=0}^{\lfloor \frac{l-1}{2} \rfloor} (-1)^k \frac{(l+2k+1)!(2x)^{-2k-1}}{(2k+1)!(l-2k-1)!} \Bigg\}. \end{aligned} \tag{D.12}$$

These properties of Legendre functions would be enough to reexpress single and two-particle Green's functions in Legendre representation.

D.2 Digamma $\Psi(x)$ and Polygamma $\Psi^{(n)}(x)$ function

The Ψ-function or *digamma* function [84] is defined as

$$\Psi(x) = \frac{d}{dx}\left[\ln \Gamma(z)\right] = \frac{\Gamma'(x)}{\Gamma(x)}, \tag{D.13}$$

in which the Gamma-function is given by

$$\Gamma(x) = \int_0^1 \left[\ln\left(\frac{1}{t}\right)\right]^{x-1} dt. \tag{D.14}$$

The Ψ-function has infinite values for $x = -n$ where $n \in N$, diverges if $x \to \infty$ and it is an undefined function for $x =\to -\infty$ (Fig. D.2).

- integral representation of the Ψ-function:

$$\begin{aligned} \Psi(x) &= \int_0^\infty \left(\frac{e^{-t}}{t} - \frac{e^{-xt}}{1-e^{-t}}\right) dt \\ \Psi(x) &= \int_0^\infty \left\{e^{-t} - \frac{1}{(1+t)^x}\right\} \frac{dt}{t}. \end{aligned} \tag{D.15}$$

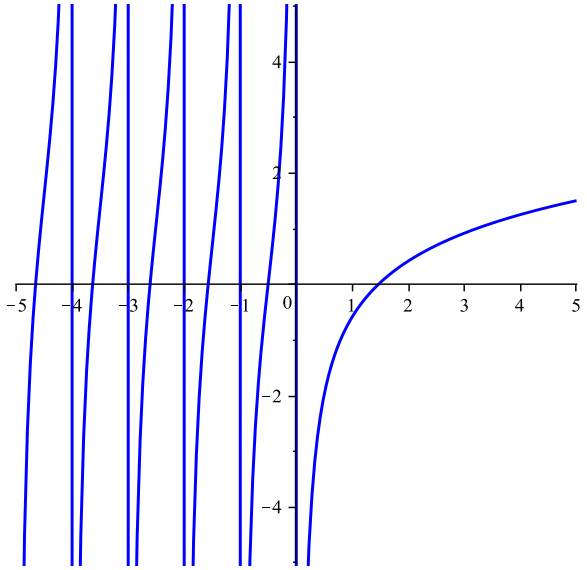

Figure D.2: Ψ-function behavior for different values of x.

- Series representation of the Ψ-function:

$$\begin{aligned}
\Psi(x) &= \Psi(1) - \sum_{k=0}^{\infty}\left(\frac{1}{x+k} - \frac{1}{k+1}\right) \\
\Psi(x+1) &= \Psi(1) + \sum_{k=2}^{\infty}(-1)^k \zeta(k) x^{k-1} \\
\Psi(x) - \Psi(y) &= \sum_{k=0}^{\infty}\left(\frac{1}{y+k} - \frac{1}{x+k}\right).
\end{aligned} \tag{D.16}$$

  In this relation, $\zeta(x)$ is well-known zeta-function which is equal to $\sum_{n=1}^{\infty}\frac{1}{n^x}$.

- Recurrence formulas:

$$\begin{aligned}
\Psi(x+1) &= \Psi(x) + \frac{1}{x} \\
\Psi(x+n) &= \frac{1}{(n-1)+x} + \frac{1}{(n-2)+x} + \ldots + \frac{1}{2+x} + \frac{1}{1+x} + \Psi(1+x)
\end{aligned} \tag{D.17}$$

- Reflection formula

$$\Psi(1-x) = \Psi(x) + \pi\cot(\pi x) \tag{D.18}$$

- Duplication formula

$$\Psi(2x) = \frac{1}{2}\Psi(x) + \frac{1}{2}\Psi(x+\frac{1}{2}) + \ln 2 \tag{D.19}$$

- Asymptotic formula ($x \to \infty$):

$$\begin{aligned}\Psi(x) &\approx \ln x - \frac{1}{2x} - \sum_{n=1}^{\infty} \frac{B_{2n}}{2n} \frac{1}{x^{2n}} \\ &= \ln x - \frac{1}{2x} - \frac{1}{12x^2} + \frac{1}{120x^4} - \frac{1}{252x^6} + \dots .\end{aligned} \tag{D.20}$$

In this relation, B_n is the Bernoulli function that is defined by

$$\frac{t\, e^{tx}}{e^t - 1} = \sum_{n=0}^{\infty} B_n(x) \frac{t^n}{n!}. \tag{D.21}$$

The first few Bernoulli polynomials are

$$\begin{aligned}B_0(x) &= 1, \\ B_1(x) &= x - \frac{1}{2}, \\ B_2(x) &= x^2 - x + \frac{1}{6}, \\ B_3(x) &= x^3 - \frac{3}{2}x^2 + \frac{1}{2}x, \\ B_4(x) &= x^4 - 2x^3 + x^2 - \frac{1}{30}, \\ B_5(x) &= x^5 - \frac{5}{2}x^4 + \frac{5}{3}x^3 - \frac{1}{6}x, \\ B_6(x) &= x^6 - 3x^5 + \frac{5}{2}x^4 - \frac{1}{2}x^2 + \frac{1}{42}.\end{aligned} \tag{D.22}$$

In Eq. (D.20), $B_{2n} = B_{2n}(x = 0)$.

- Polygamma function:

$$\Psi^{(n)}(x) = \frac{d^n}{dx^n}\Psi(x) = \frac{d^{n+1}}{dx^{n+1}} \ln \Gamma(x). \qquad (n = 1, 2, 3, ...) \tag{D.23}$$

For instance we plot the first derivative of the Ψ-function in Fig. D.3.

- Recurrence formula of the Polygamma function:

$$\Psi^{(n)}(x+1) = \Psi^{(n)}(x) + (-1)^n\, n!\, x^{-n-1} \tag{D.24}$$

- Asymptotic formula of the Polygamma function:

$$\begin{aligned}\Psi^{(n)}(x) &\approx (-1)^{n-1} \left[\frac{(n-1)!}{x^n} + \frac{n!}{2x^{n+1}} + \sum_{k=1}^{\infty} B_{2k} \frac{(2k+n-1)!}{(2k)!} \frac{1}{x^{2k+n}} \right], \\ \Psi'(x) &\approx \frac{1}{x} + \frac{1}{2x^2} + \frac{1}{6x^3} - \frac{1}{30x^5} + \frac{1}{42x^7} - \dots .\end{aligned} \tag{D.25}$$

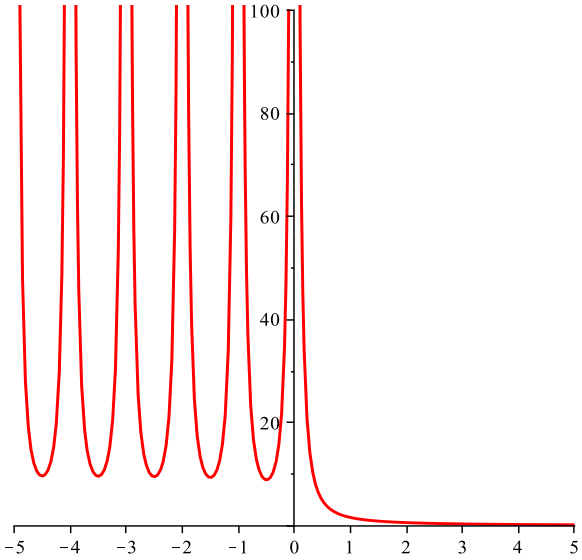

Figure D.3: Polygamma function, $\Psi'(x)$ behavior for different values of x.

- integer / fraction values:

$$\begin{aligned}
\Psi(1) &= -0.5772156649, \\
\Psi(\frac{1}{2}) &= \Psi(1) - 2\ln 2 = -1.963510026 \\
\Psi(n) &= -\Psi(1) + \sum_{k=1}^{n-1} \frac{1}{k}, \qquad (n \geq 2) \\
\Psi(n+\frac{1}{2}) &= \Psi(1) - 2\ln 2 + \sum_{k=0}^{n-1} \frac{1}{k+\frac{1}{2}}.
\end{aligned} \tag{D.26}$$

$$\begin{aligned}
\Psi'(1) &= \frac{1}{6}\pi^2, \\
\Psi'(\frac{1}{2}) &= \frac{1}{2}\pi^2, \\
\Psi^{(n)}(1) &= (-1)^{n+1} n! \zeta(n+1), \\
\Psi^{(n)}(\frac{1}{2}) &= (-1)^{n+1} n! (2^{n+1}-1)\zeta(n+1), \qquad (n \geq 1) \\
\Psi'(n+\frac{1}{2}) &= \Psi'(\frac{1}{2}) - \sum_{k=1}^{n} \frac{1}{(k-\frac{1}{2})^2}.
\end{aligned} \tag{D.27}$$

APPENDIX E

Appendix

E.1 Single particle Green's function $\mathcal{G}$ in Legendre representation

Imaginary time single particle Green's function $\mathcal{G}(\tau)$, which is defined in $\tau \in [0, \beta]$, is expanded in terms of Legendre function $P_l(x(\tau))$ defined for $x \in [-1, 1]$ by the following relation:

$$\mathcal{G}(\tau) = \sum_{l \geq 0} \frac{\sqrt{2l+1}}{\beta} P_l(x(\tau))\ \mathcal{G}_l. \tag{E.1}$$

where $x(\tau) = 2\tau/\beta - 1$. To obtain an appropriate equation for $\mathcal{G}_l$, first we use the orthogonality of $P_l(x)$:

$$\begin{aligned} \int_{-1}^{1} dx\ P_l(x(\tau))\mathcal{G}(\tau) &= \int_{-1}^{1} dx \sum_{l \geq 0} \frac{\sqrt{2l+1}}{\beta} P_l(x(\tau))P_{l'}(x(\tau))\ \mathcal{G}_l \\ &= \sum_{l \geq 0} \frac{\sqrt{2l+1}}{\beta} \frac{2\delta_{ll'}}{2l+1}\ \mathcal{G}_l \\ &= \frac{2}{\beta} \frac{1}{\sqrt{2l+1}}\ \mathcal{G}_l \end{aligned} \tag{E.2}$$

Now, by changing the variables in the integral ($dx = 2/\beta\ d\tau$), we have

$$\begin{aligned} \mathcal{G}_l &= \frac{\beta}{2}\sqrt{2l+1} \int_{-1}^{1} dx\ \mathcal{G}(\tau)P_l(x(\tau)) \\ &= \sqrt{2l+1} \int_{0}^{\beta} d\tau\ P_l(x(\tau))\ \mathcal{G}(\tau). \end{aligned} \tag{E.3}$$

Here, $\mathcal{G}_l$ denotes to coefficient of $\mathcal{G}(\tau)$ in Legendre basis. Also, we can expand $\mathcal{G}(-\tau)$ in terms of the $P_l(x(\tau))$ which we will use it later.

$$\begin{aligned} \mathcal{G}(-\tau) &= -\mathcal{G}(-\tau + \beta) \\ &= -\sum_{l \geq 0} \frac{\sqrt{2l+1}}{\beta} P_l(x(-\tau+\beta))\ \mathcal{G}_l \\ &= -\sum_{l \geq 0} \frac{\sqrt{2l+1}}{\beta} P_l(-x(\tau))\ \mathcal{G}_l \\ &= \sum_{l \geq 0} \frac{\sqrt{2l+1}}{\beta} (-1)^{l+1} P_l(x(\tau))\ \mathcal{G}_l, \end{aligned} \tag{E.4}$$

and as a result,

$$\mathcal{G}_l = (-1)^{l+1}\sqrt{2l+1}\int_0^\beta d\tau\ P_l(x(\tau))\mathcal{G}(-\tau), \tag{E.5}$$

where we used $x(-\tau+\beta) = -x(\tau)$ and anti-periodicity property of Green's function $\mathcal{G}$.

In principle, we can use every polynomial functions such as Chebyshev polynomials, but the advantage of using Legendre functions for the expansion of the $\mathcal{G}(\tau)$ is that the transformation between Legendre representations and Matsubara representation can be written in terms of the unitary matrix T_{nl}. To show this, we write the Fourier transformation of $\mathcal{G}(\tau)$ with respect to Legendre polynomials:

$$\begin{aligned}\mathcal{G}(\nu_n) &= \sum_{l\geq 0}\mathcal{G}_l\ \frac{\sqrt{2l+1}}{\beta}\int_0^\beta d\tau\ e^{i\nu_n\tau}P_l(x(\tau)) \\ &= \sum_{l\geq 1}T_{nl}\ \mathcal{G}_l.\end{aligned} \tag{E.6}$$

For checking whether T_{nl} is unitary or not, it is sufficient to calculate $\sum_n T_{nl}\ T^*_{nl'}$.

$$\begin{aligned}\sum_n T_{nl}\ T^*_{nl'} &= \frac{\sqrt{2l+1}\sqrt{2l'+1}}{\beta}\int_0^\beta\int_0^\beta d\tau d\tau' P_l(x(\tau))P_{l'}(x(\tau'))\frac{1}{\beta}\sum_n e^{-i\nu_n(\tau-\tau')} \\ &= \frac{\sqrt{2l+1}\sqrt{2l'+1}}{\beta}\int_0^\beta\int_0^\beta d\tau d\tau' P_l(x(\tau))P_{l'}(x(\tau'))\delta(\tau-\tau') \\ &= \frac{\sqrt{2l+1}\sqrt{2l'+1}}{\beta}\int_0^\beta \frac{\beta}{2}\,dx P_l(x(\tau))P_{l'}(x(\tau)) \\ &= \delta_{ll'}.\end{aligned} \tag{E.7}$$

It is also possible to calculate the matrix elements of T_{nl} which is independent of β. According to (Eq. D.11), T_{nl} can be written in terms of spherical Bessel function

$$\begin{aligned}T_{nl} &= \frac{\sqrt{2l+1}}{\beta}\int_{-1}^1 \frac{\beta}{2}\,dx\ e^{i\nu_n\frac{\beta}{2}}e^{i\nu_n\frac{\beta}{2}x}P_l(x(\tau)) \\ &= \frac{\sqrt{2l+1}}{2}e^{i(2n+1)\frac{\pi}{2}}\int_{-1}^1 dx\ e^{i\nu_n\frac{\beta}{2}x}P_l(x(\tau)) \\ &= (-1)^n i^{l+1}\sqrt{2l+1}j_l(\frac{\beta\nu_n}{2}) \\ &= (-1)^n i^{l+1}\sqrt{2l+1}j_l(\frac{\bar{\nu}_n}{2}) \\ &= (-1)^n i^{l+1}\sqrt{2l+1}j_l\left(\frac{(2n+1)\pi}{2}\right),\end{aligned} \tag{E.8}$$

or in the form of series expansion by using (Eq. D.12).

$$\begin{aligned} T_{nl} &= (-1)^n i^{l+1}\sqrt{2l+1}(\frac{2}{\beta\nu_n})\Bigg\{ \sin(\frac{\bar{\nu}_n}{2}-\frac{\pi l}{2})\sum_{k=0}^{\lfloor\frac{l}{2}\rfloor}(-1)^k\frac{(l+2k)!(\bar{\nu}_n)^{-2k}}{(2k)!(l-2k)!} + \\ &\quad + \cos(\frac{\bar{\nu}_n}{2}-\frac{\pi l}{2})\sum_{k=0}^{\lfloor\frac{l-1}{2}\rfloor}(-1)^k\frac{(l+2k+1)!(\bar{\nu}_n)^{-2k-1}}{(2k+1)!(l-2k-1)!}\Bigg\} \\ &= -2i^l\sqrt{2l+1}\Bigg\{\cos(\frac{\pi l}{2})\sum_{k=0}^{\lfloor\frac{l}{2}\rfloor}\frac{(l+2k)!}{(2k)!(l-2k)!}\frac{1}{(i\bar{\nu}_n)^{2k+1}} \\ &\quad + i\sin(\frac{\pi l}{2})\sum_{k=0}^{\lfloor\frac{l-1}{2}\rfloor}\frac{(l+2k+1)!}{(2k+1)!(l-2k-1)!}\frac{1}{(i\bar{\nu}_n)^{2k+2}}\Bigg\}, \end{aligned} \tag{E.9}$$

where we used $\sin(\frac{\bar{\nu}_n}{2}-\frac{\pi l}{2}) = (-1)^n\cos(\frac{\pi l}{2})$ and $\cos(\frac{\bar{\nu}_n}{2}-\frac{\pi l}{2}) = (-1)^n\sin(\frac{\pi l}{2})$. Now for even values of l, we have $\sin(\frac{\pi l}{2}) = 0$, $\cos(\frac{\pi l}{2}) = (-1)^{\frac{l}{2}}$ and $i^l = (-1)^{\frac{l}{2}}$. Thus,

$$\begin{aligned} T_{nl_{even}} &= -2\sqrt{2l+1}\sum_{k=0}^{\lfloor\frac{l}{2}\rfloor}\frac{(l+2k)!}{(2k)!(l-2k)!}\frac{1}{(i\bar{\nu}_n)^{2k+1}} \\ &= -2\sqrt{2l+1}\sum_{p=1}^{l+1}\frac{(l+p-1)!}{(p-1)!(l-p+1)!}\frac{1}{(i\bar{\nu}_n)^p}\delta_{l+p,odd}, \end{aligned} \tag{E.10}$$

in which $p = 2k+1$; therefore, $l+p$ is odd. In this relation, $\delta_{l+p,odd}$ shows that l has only even values in the expansion. Similarly for odd values of l, $\cos(\frac{\pi l}{2})$ is zero, $\sin(\frac{\pi l}{2}) = (-1)^{\frac{l-1}{2}}$ and $i^l = i(-1)^{\frac{l-1}{2}}$. Therefore, we obtain the following relation for $T_{nl_{odd}}$.

$$\begin{aligned} T_{nl_{odd}} &= 2\sqrt{2l+1}\sum_{k=0}^{\lfloor\frac{l-1}{2}\rfloor}\frac{(l+2k+1)!}{(2k+1)!(l-2k-1)!}\frac{1}{(i\bar{\nu}_n)^{2k+2}} \\ &= 2\sqrt{2l+1}\sum_{p=2}^{l+1}\frac{(l+p-1)!}{(p-1)!(l-p+1)!}\frac{1}{(i\bar{\nu}_n)^p}\delta_{l+p,odd}, \end{aligned} \tag{E.11}$$

where $p = 2k+2$ and obviously $l+p$ is odd. Here we use delta function $\delta_{l+p,odd}$ to guarantee that l will choose odd values. It is possible to derive a more compact relation for T_{nl} with arbitrary values of l using Eqs. (E.10) and (E.11).

$$T_{nl} = 2\sqrt{2l+1}\sum_{p=1}^{l+1}\frac{(l+p-1)!}{(p-1)!(l-p+1)!}\frac{(-1)^p}{(i\bar{\nu}_n)^p}\delta_{l+p,odd}. \tag{E.12}$$

The other advantage of using Legendre expansion is that the Legendre representation of $\mathcal{G}(\tau)$ is much more compact than the standard Matsubara representation. It means that the coefficients $\mathcal{G}_l$ in the expansion of Green's function $\mathcal{G}(\tau)$ in Legendre representation decay faster than the standard Fourier expansions coefficients in Matsubara representation. Coefficients in Fourier expansion decay as power law determined by discontinuities of the function and its

derivatives, while the coefficients $\mathcal{G}_l$ decay as $\mathcal{O}\left(1/l^k\right)$ if $\mathcal{G}_l$ is k times differentiable. For this reason the information about Green's function can be saved in a smaller storage volume in Legendre representation.

For the Fourier expansion of Green's function in asymptotic limit (high frequency), it can be seen that $\mathcal{G}$ decays as $\mathcal{O}\left(1/\nu_n\right)$ because of the discontinuities in the anti-periodic Green's function in $\tau \in [0, \beta]$.

$$\begin{aligned}
\mathcal{G}(i\nu_n) &= \int_0^\beta d\tau\ e^{i\nu_n\tau}\mathcal{G}(\tau) \\
&= \frac{\mathcal{G}(\tau)e^{i\nu_n\tau}|_0^\beta}{i\nu_n} - \int_0^\beta d\tau\ \mathcal{G}'(\tau)\frac{e^{i\nu_\tau}}{i\nu_n} \\
&= -\frac{\mathcal{G}(\beta^-)+\mathcal{G}(0^+)}{i\nu_n} + \mathcal{O}\left(\frac{1}{\nu_n^2}\right). \qquad \text{(E.13)}
\end{aligned}$$

This causes a slow decay $\mathcal{O}\left(1/\nu_n\right)$ at large frequencies. For Legendre expansion of $\mathcal{G}(\tau)$ which is a smooth function[1] in $\tau \in [0, \beta]$, we can proceed in a similar way by using Legendre polynomials.

$$\begin{aligned}
\mathcal{G}_l &= \sqrt{2l+1}\int_0^\beta d\tau\ \mathcal{G}(\tau)P_l(x(\tau)) \\
&= \frac{1}{\sqrt{2l+1}}\int_0^\beta d\tau\ \mathcal{G}(\tau)\left[P'_{l+1}(x(\tau)) - P'_{l-1}(x(\tau))\right] \\
&= \frac{1}{\sqrt{2l+1}}\left\{\mathcal{G}(\tau)\Big[P_{l+1}(x(\tau)) - P_{l-1}(x(\tau))\Big]\Big|_0^\beta - \int_0^\beta d\tau\ \mathcal{G}'(\tau)\Big[P_{l+1}(x(\tau)) - P_{l-1}(x(\tau))\Big]\right\} \\
&= \frac{-1}{\sqrt{2l+1}}\int_0^\beta d\tau\ \mathcal{G}'(\tau)\Big[P_{l+1}(x(\tau)) - P_{l-1}(x(\tau))\Big] \\
&= \frac{-1}{\sqrt{2l+1}}\int_0^\beta d\tau\ \mathcal{G}'(\tau)\left\{\frac{1}{2l+3}\Big[P'_{l+2}(x(\tau)) - P'_l(x(\tau))\Big] - \frac{1}{2l-1}\Big[P'_l(x(\tau)) - P'_{l-2}(x(\tau))\Big]\right\} \\
&= \frac{1}{\sqrt{2l+1}}\left\{\frac{1}{2l+3}\int_0^\beta d\tau\ \mathcal{G}''(\tau)P_{l+2}(x(\tau)) - (\frac{1}{2l-1}+\frac{1}{2l+3})\int_0^\beta d\tau\ \mathcal{G}''(\tau)P_l(x(\tau)) + \right. \\
&\quad \left. + \frac{1}{2l-1}\int_0^\beta d\tau\ \mathcal{G}''(\tau)P_{l-2}(x(\tau))\right\} \\
&\leq \frac{1}{\sqrt{2l+1}(2l-1)}\left\{\int_0^\beta d\tau\ \mathcal{G}''(\tau)P_{l+2}(x(\tau)) + 2\int_0^\beta d\tau\ \mathcal{G}''(\tau)P_l(x(\tau))\right. \\
&\quad \left. + \int_0^\beta d\tau\ \mathcal{G}''(\tau)P_{l-2}(x(\tau))\right\}, \qquad \text{(E.14)}
\end{aligned}$$

where we applied the Legendre function properties (3). Here, we use a mathematical theorem to continue calculations.

[1] A smooth function is a function that has continuous derivatives up to some desired orders over some domains. A function can therefore be said to be smooth over a restricted interval such as (a, b) or $[a, b]$. The number of continuous derivatives necessary for a function to be considered smooth depends on the problem at hand and may vary from two to infinity.(http://mathworld.wolfram.com/SmoothFunction.html)

Theorem: Let f(x) and g(x) be piecewise continuous for $a \leq x \leq b$. Then $|(f,g)| \leq ||f||.||g||$. The equality holds precisely when f and g are linearly dependent. Furthermore $||f+g|| \leq ||f|| + ||g||$ where $(f,g) \equiv \int_a^b dx\ f(x)g(x)$ and $||f|| = \sqrt{(f,f)} = \left\{\int_a^b dx\ f(x)^2\right\}^2$ [85].

$$\begin{aligned}
\mathcal{G}_l &\leq \frac{1}{\sqrt{2l+1}(2l-1)} \left\{||\mathcal{G}''||.||P_{l+2}|| + 2||\mathcal{G}''||.||P_l|| + ||\mathcal{G}''||.||P_{l-2}||\right\} \\
&\leq \frac{||\mathcal{G}''(\tau)||}{\sqrt{2l+1}(2l-1)} \left\{\sqrt{\frac{\beta}{2l+5}} + 2\sqrt{\frac{\beta}{2l+1}} + \sqrt{\frac{\beta}{2l-3}}\right\} \\
&\leq \frac{4\ ||\mathcal{G}''(\tau)||}{\sqrt{2l+1}(2l-1)} \times \sqrt{\frac{\beta}{2l-3}} \\
&\sim const. \left(\frac{1}{l}\right)^2. \qquad \text{(E.15)}
\end{aligned}$$

Aa a result, it is clear that if Legendre coefficient $\mathcal{G}_l$ is k times differentiable, it decays as $\mathcal{O}(1/l)^k$. So $\mathcal{G}(\tau)$ (and other physical quantities such as χ) has a very weak dependence on $\mathcal{G}_l$ (or $\chi_{ll'}$) for large values of l (or ll'). As we saw in these calculations, in Legendre expansion for $l \geq 1$, the boundary terms always are canceled ($\mathcal{G}(\tau)\left\{P_{l+1}(x(\tau)) - P_{l-1}(x(\tau))\right\}\ |_0^\beta = 0$), while in Fourier expansion are not ($\mathcal{G}(\tau)e^{i\nu_n\tau}/i\nu_n|_0^\beta = -[\mathcal{G}(\beta^-)+\mathcal{G}(0^+)]/i\nu_n$). Actually this is a crucial difference between standard Fourier and Legendre expansion.

The problem in Legendre representation is statistical noise for large values of l or higher order of Legendre functions. If we consider higher and higher order of Legendre functions, then the coefficients $\mathcal{G}_l$ with large error bar are included in numerical computations. Thus the result will be polluted. To overcome this problem we need to truncate the expansion in Legendre polynomials at an order l_{max} and set $\mathcal{G}_l = 0$ for $l \geq l_{max}$.

E.1.1 Matsubara Green's function in terms of Legendre coefficient $\mathcal{G}_l$ and high frequencies expansion

In terms of $\mathcal{G}_l$, Matsubara Green's function $\mathcal{G}(\nu_n)$ can be obtained by the following relation:

$$\begin{aligned}
\mathcal{G}(\nu_n) &= \sum_{l\geq 0} \mathcal{G}_l\ \frac{\sqrt{2l+1}}{\beta} \int_0^\beta d\tau\ e^{i\nu_n\tau} P_l(x(\tau)) \\
&= \sum_{l\geq 0} T_{nl}\ \mathcal{G}_l. \qquad \text{(E.16)}
\end{aligned}$$

Where T_{nl} is a β independent unitary matrix (Eq. E.8). Thus the knowledge of the Legendre coefficients $\mathcal{G}_l$ would help us to obtain Matsubara Green's function more accurately especially in high expansion frequencies if we choose an appropriate cut-off l_{max}. Actually appropriate choice of l_{max} filters statistical noises in high frequency expansion. It is possible to obtain coefficients of the Fourier expansion in terms of Legendre coefficients at high frequencies expansion, accurately. Through studying the relation between high frequencies expansion of Matsubara Green's function $\mathcal{G}(\nu_n)$

$$\mathcal{G}(\nu_n) = \frac{c_1}{i\nu_n} + \frac{c_2}{(i\nu_n)^2} + \frac{c_3}{(i\nu_n)^3} + \dots\ , \qquad \text{(E.17)}$$

and unitary matrix T_{nl} (Eq. E.12)

$$T_{nl} = \frac{t_l^{(1)}}{i\nu\beta} + \frac{t_l^{(2)}}{(i\nu\beta)^2} + \frac{t_l^{(3)}}{(i\nu\beta)^3} + \dots , \tag{E.18}$$

we can obtain the relation between Fourier expansion coefficients c_p and Legendre ones $\mathcal{G}_l$.

$$c_p = \frac{1}{\beta^p} \sum_{l\geq 0} t_l^{(p)} \mathcal{G}_l \tag{E.19}$$

Here $t_l^{(p)}$ is

$$t_l^{(p)} = (-1)^p 2\sqrt{2l+1} \frac{(l+p-1)!}{(p-1)!(l-p+1)!} \delta_{p+l,odd}. \tag{E.20}$$

It is easy to calculate the first moments c_p. For instance for c_1 we have

$$\begin{aligned} c_1 &= \frac{1}{\beta} \sum_{l\geq 0} t_l^{(1)} \mathcal{G}_l = \frac{1}{\beta} \sum_{l_{even}\geq 0} t_l^{(1)} \mathcal{G}_l \\ &= \frac{1}{\beta} \sum_{l\geq 0} (-1)\sqrt{2l+1}\, \mathcal{G}_l. \end{aligned} \tag{E.21}$$

Similarly, for the other moments:

$$c_2 = \sum_{l_{odd}>0} \frac{2\sqrt{2l+1}}{\beta^2}\, \mathcal{G}_l (l+1)l \tag{E.22}$$

$$c_3 = \sum_{l_{even}\geq 0} (-1) \frac{2\sqrt{2l+1}}{\beta^3} \frac{1}{2!}\, \mathcal{G}_l (l+2)(l+1)l(l-1) \tag{E.23}$$

$$c_4 = \sum_{l_{odd}>0} \frac{2\sqrt{2l+1}}{\beta^4} \frac{1}{3!}\, \mathcal{G}_l (l+3)(l+2)(l+1)l(l-1)(l-2). \tag{E.24}$$

Some points about c_p:

1. It is clear that for a proper cut-off l_{max}, c_p has an stable value since $t_l^{(p)} \sim l^{2p-3/2}$ and $G_{l_{max}} = 0$.
2. If we want to calculate higher moments, we need more Legendre coefficients.

Note that equation (E.16) also would be useful to compute self energy via Dyson equation.

E.2 Legendre representation of the susceptibility

According to Eq. (4.94), we consider that[2]

$$\chi(\tau_{14} - \tau_{24}, \tau_{34}, \tau_{14}) = \Big\langle \mathcal{T} c^\dagger(\tau_{14}) c(\tau_{24}) c^\dagger(\tau_{34}) c(0) \Big\rangle - \Big\langle \mathcal{T} c^\dagger(\tau_{14}) c(\tau_{24}) \Big\rangle \Big\langle \mathcal{T} c^\dagger(\tau_{34}) c(0) \Big\rangle. \tag{E.25}$$

[2] There is a possibility to consider $\chi(\tau_{14}, \tau_{24}, \tau_{34})$ for (local) imaginary time susceptibility which is anti-periodic in τ_{14}, τ_{24} and τ_{34}. In mathematical point of view, this choice of time dependency for χ is not proper for Legendre-Fourier transformation.

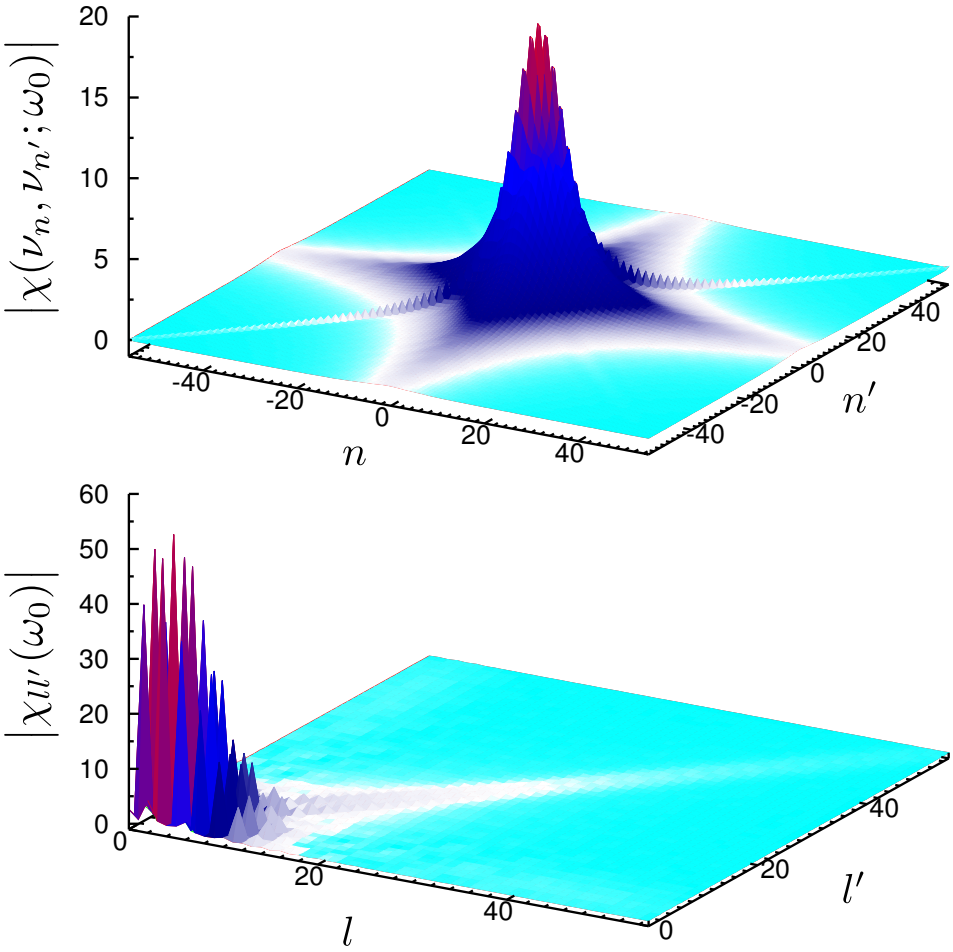

Figure E.1: Top: Absolute value of the local magnetic susceptibility at $\omega_m = 0$ calculated in Matsubara frequencies space for $VOMoO_4$, $U = 5$ and $\beta = 30$. Bottom: The coefficients $|\chi_{ll'}(\omega_m = 0)|$ calculated in the mixed Legendre-Fourier representation for the same material.

Since the $\chi(\tau_{12}, \tau_{34}, \tau_{14})$ is β-antiperiodic in τ_{12} and τ_{34} and β-periodic in τ_{14}, the Fourier transformed susceptibility χ is a function of two fermionic (ν_n and $\nu_{n'}$) and one bosonic (ω_m) Matsubara frequencies. Also $\chi(\tau_{12}, \tau_{34}, \tau_{14})$ has discontinuities at $\tau_{14} = 0$ and $\tau_{14} = \tau_{12} + \tau_{34}$ as well as kinks at $\tau_{12} = 0$. These discontinuities and kinks cause a slow decay in the Fourier transformation of susceptibility. But in the Legendre representation, as we see in the following, the kinks at $\tau_{12} = 0$ are in the border of the imaginary-time region (See Eq. E.34) and do not have any effect on decaying of Legendre coefficients.

In the following, we look for a unitary matrix T_{nl} which transforms the Matsubara susceptibility $\chi(\nu_n, \nu_{n'}; \omega_m)$ from the standard Fourier space to Fourier-Legendre space, $\chi_{ll'}(i\omega_m)$.

$$\chi(\nu_n, \nu_{n'}; \omega_m) \quad = \quad \sum_{ll' \geq 0} T_{nl}\, \chi_{ll'}(i\omega_m)\, T^*_{n'l'}, \tag{E.26}$$

where the unitary condition implies that $\sum_{n \in \mathbb{Z}} T_{nl} T^*_{nl'} = \delta_{ll'}$. By considering the

$$\chi(\nu_n, \nu_{n'}; \omega_m) = \int_0^\beta d\tau_{12} \int_0^\beta d\tau_{34} \int_0^\beta d\tau_{14}\, e^{-i\nu_n \tau_{12}} e^{-i\nu_{n'} \tau_{34}} e^{-i\omega_m \tau_{14}}\, \chi(\tau_{12}, \tau_{34}, \tau_{14}), \tag{E.27}$$

and its inverse Fourier transform, we have

$$\begin{aligned}
\chi(\tau_{12},\tau_{34},\tau_{14}) &= \frac{1}{\beta^3}\sum_{nn'm} e^{i\nu_n\tau_{12}}e^{i\nu_{n'}\tau_{34}}e^{i\omega_m\tau_{14}}\ \chi(\nu_n,\nu_{n'};\omega_m) \\
&= \sum_{ll'\geq 0}\left\{\left(\frac{1}{\beta}\sum_n e^{i\nu_n\tau_{12}}T_{nl}\right)\left(\frac{1}{\beta}\sum_m e^{i\omega_m\tau_{14}}\chi_{ll'}(\omega_m)\right)\left(\frac{1}{\beta}\sum_n e^{i\nu_{n'}\tau_{34}}T^*_{n'l'}\right)\right\} \\
&\equiv \sum_{ll'\geq 0}\left\{C_l(\tau_{12})\left(\frac{1}{\beta}\sum_m e^{i\omega_m\tau_{14}}\ \chi_{ll'}(\omega_m)\right)C^\star_{l'}(\tau_{34})\right\}, \qquad \text{(E.28)}
\end{aligned}$$

Where $C_l(\tau)$ and $C^\star_{l'}(\tau)$ are

$$C_l(\tau) = \frac{1}{\beta}\sum_n e^{i\nu_n\tau}T_{nl}, \qquad \text{(E.29)}$$

$$C^\star_{l'}(\tau) = \frac{1}{\beta}\sum_n e^{i\nu_n\tau}T^*_{nl'}. \qquad \text{(E.30)}$$

Now, If we define that the T_{nl} equals to Fourier transformation of $P_l(x(\tau))$

$$T_{nl} = \frac{\sqrt{2l+1}}{\beta}\int_0^\beta d\tau\ e^{i\nu_n\tau}P_l(x(\tau)), \qquad \text{(E.31)}$$

we easily derive

$$\begin{aligned}
C_l(\tau) &= \frac{1}{\beta}\sum_n e^{i\nu_n\tau}T_{nl} \\
&= \frac{1}{\beta}\sum_n e^{i\nu_n\tau}\frac{\sqrt{2l+1}}{\beta}\int_0^\beta d\tau'\ e^{i\nu_n\tau'}P_l(x(\tau')) \\
&= \frac{\sqrt{2l+1}}{\beta}\int_0^\beta d\tau' P_l(x(\tau'))\ \left(\frac{1}{\beta}\sum_n e^{i\nu_n(\tau+\tau'-\beta)}e^{i\nu_n\beta}\right) \\
&= -\frac{\sqrt{2l+1}}{\beta}\int_0^\beta d\tau' P_l(x(\tau'))\delta(\tau'-\beta+\tau) \\
&= -\frac{\sqrt{2l+1}}{\beta}P_l(x(-\tau+\beta)) \\
&= \frac{\sqrt{2l+1}}{\beta}(-1)^{l+1}P_l(x(\tau)) \\
&= C^*_l(\tau), \qquad \text{(E.32)}
\end{aligned}$$

and in a similar way

$$\begin{aligned} C^{\star}_{l'}(\tau) &= \frac{1}{\beta}\sum_{n} e^{i\nu_n\tau} T^{*}_{nl} \\ &= \frac{1}{\beta}\sum_{n} e^{i\nu_n\tau}\frac{\sqrt{2l+1}}{\beta}\int_0^\beta d\tau\; e^{-i\nu_n\tau'} P_l(x(\tau')) \\ &= \frac{\sqrt{2l+1}}{\beta}\int_0^\beta d\tau' P_l(x(\tau'))\left(\frac{1}{\beta}\sum_n e^{i\nu_n(\tau-\tau')}\right) \\ &= \frac{\sqrt{2l'+1}}{\beta}P_{l'}(x(\tau)) \\ &= [C^{\star}_{l'}(\tau)]^{*}. \end{aligned} \tag{E.33}$$

Now, we can find the $\bar{\chi}^{\sigma\sigma'}_{ll'}(i\omega_m)$ by inverting the Eq. (E.26).

$$\begin{aligned} \chi_{ll'}(i\omega_m) &= \sum_{nn'} T^{*}_{nl}\,\chi(\nu_n,\nu_{n'};\omega_m)\,T_{n'l'} \\ &= \int_0^\beta d\tau_{12}\int_0^\beta d\tau_{34}\int_0^\beta d\tau_{14}\; C^{*}_{l}(\tau_{12})\; e^{-i\omega_m\tau_{14}}\chi(\tau_{12},\tau_{34},\tau_{14})\;\; [C^{\star}_{l'}(\tau_{34})]^{*} \\ &= \int_0^\beta d\tau_{12}\int_0^\beta d\tau_{34}\int_0^\beta d\tau_{14}\; C_{l}(\tau_{12})\; e^{-i\omega_m\tau_{14}}\;\chi(\tau_1,\tau_2,\tau_3,\tau_4)\; C^{\star}_{l'}(\tau_{34}) \\ &= \int_0^\beta d\tau_{12}\int_0^\beta d\tau_{34}\int_0^\beta d\tau_{14}\;\sqrt{2l+1}\sqrt{2l'+1}(-1)^{l+1}P_l(x(\tau_{12}))P_{l'}(x(\tau_{34})) \\ &\quad\times e^{-i\omega_m\tau_{14}}\;\bar{\chi}^{\sigma\sigma'}(\tau_{12},\tau_{34},\tau_{14}). \end{aligned} \tag{E.34}$$

Thus, the explicit relation for $\chi(\tau_{12},\tau_{34},\tau_{14})$ is

$$\begin{aligned} \chi(\tau_{12},\tau_{34},\tau_{14}) &= \frac{1}{\beta}\sum_{m\in\mathbb{Z}}\sum_{ll'\geq 0} C_l(\tau_{12})\; e^{i\omega_m\tau_{14}}\;\chi_{ll'}(\omega_m)\; C^{\star}_{l'}(\tau_{34}) \\ &= \frac{1}{\beta}\sum_{m\in\mathbb{Z}}\sum_{ll'\geq 0}\frac{\sqrt{2l+1}\sqrt{2l'+1}}{\beta^2}(-1)^{l+1} \\ &\quad\times P_l(x(\tau_{12}))P_{l'}(x(\tau_{34}))\; e^{i\omega_m\tau_{14}}\;\chi_{ll'}(\omega_m), \end{aligned} \tag{E.35}$$

where the $\chi(\tau_{12},\tau_{34},\tau_{14})$ was expanded in term of a mixture of Fourier and Legendre coefficients.

In DMFT framework, lattice susceptibility $\chi(\mathbf{q},\omega_m)$ is obtained from the Bethe-Salpeter equation (4.36). In the Fourier-Legendre representation, the matrices in the Bethe-Salpeter equation is changed so that the bare susceptibilities matrices $\left[\chi^{\mathbf{0}}(\mathbf{q},\omega_m)\right]$ and $\left[\chi_{\mathbf{loc}}(\omega_m)\right]$ are given by

$$\begin{aligned} \chi^{\mathbf{0}}_{ll'}(\mathbf{q},\omega_m) &= \sum_{n,n'\in\mathbb{Z}} T^{*}_{nl}\left\{-\sum_{\mathbf{kk'}}\mathcal{G}(\mathbf{k}+\mathbf{q},\nu_n+\omega_m)\mathcal{G}(\mathbf{k'},\nu_n)\delta_{nn'}\delta_{\mathbf{kk'}}\right\}T_{n'l'} \\ &= -\sum_{n\in\mathbb{Z}} T^{*}_{nl}\left\{\sum_{\mathbf{k}\sigma}\frac{1}{i(\nu_n+\omega_m)+\mu-H(\mathbf{k}+\mathbf{q})-\Sigma_{\mathbf{loc}}(\nu_n+\omega_m)}\right. \\ &\quad\left.\times\frac{1}{i\nu_n+\mu-H(\mathbf{k})-\Sigma_{\mathbf{loc}}(\nu_n)}\right\}T_{nl'}, \end{aligned} \tag{E.36}$$

and

$$\chi^{\mathbf{0}}_{\mathbf{loc},ll'}(\omega_m) = -\sum_{n,n'\in\mathbb{Z}} T^*_{nl}\, \mathcal{G}_{\mathbf{loc}}(\nu_n+\omega_m)\mathcal{G}_{\mathbf{loc}}(\nu_n)\delta_{nn'}\, T_{n'l'}. \tag{E.37}$$

Finally the lattice susceptibility $\chi(\mathbf{q};\omega_m)$ which equals summation over spins and Matsubara frequencies can be calculated in mixed Fourier-Legendre representation:

$$\begin{aligned}
\chi(\mathbf{q};\omega_m) &= \frac{1}{\beta^2}\sum_{nn'\in\mathbb{Z}} \chi(\nu_n,\nu_{n'};\mathbf{q},\omega_m) \\
&= \frac{1}{\beta^2}\sum_{nn'\in\mathbb{Z}}\int_0^\beta d\tau_{12}\int_0^\beta d\tau_{34}\, e^{-i\nu_n\tau_{12}}e^{-i\nu_{n'}\tau_{34}}\sum_{ll'}\frac{\sqrt{2l+1}\sqrt{2l'+1}}{\beta^2} \\
&\quad \times P_l(x(\tau_{12}))P_{l'}(x(\tau_{34}))\ \chi_{ll'}(\mathbf{q},\omega_m) \\
&= \sum_{\sigma\sigma'}\sum_{ll'}\frac{\sqrt{2l+1}\sqrt{2l'+1}}{\beta^2}\, P_l(x(\tau_{12}))P_{l'}(x(\tau_{34}))\delta(\tau_{12})\delta(\tau_{34})\ \chi_{ll'}(\mathbf{q},\omega_m) \\
&= \frac{1}{\beta^2}\sum_{ll'}(-1)^{l+l'}\sqrt{2l+1}\sqrt{2l'+1}\ \chi_{ll'}(\mathbf{q},\omega_m).
\end{aligned} \tag{E.38}$$

Thus it is possible to compute susceptibility in Fourier-Legendre representation which has (at least) 2 benefits:

1. convergence of susceptibility (or Green's function) as a function of the truncation,
2. storage size of susceptibility (or Green's function) matrix.

E.3 Legendre representation method in time discretized quantum Monte Carlo

In numerical point of view, the Legendre representation of the imaginary time Green's function is a powerful method in different continuous time quantum Monte Carlo (CTQMC) methods [59] due to continuously behavior of time in these algorithms.

In the other types of the quantum Monte Carlo methods wherein the time interval is discretized such as Hirsch-Fye QMC, this method is not applicable. The reason can be found in the behavior of the Legendre function $P_l(x)$ in the small interval $x \approx \Delta\tau$ where the Legendre function for large l is a highly oscillating function[3](See Fig. E.2). Therefore, these oscillations can not be captured when we are calculating the $\mathcal{G}_l$ coefficients by

$$\begin{aligned}
\mathcal{G}_l &= \sqrt{2l+1}\int_0^\beta d\tau\, P_l(x(\tau))\, \mathcal{G}(\tau) \\
&\approx \sqrt{2l+1}\,\frac{\beta}{N_\tau}\sum_{i=0}^{N_\tau-1} P_l(2\tau_i/N_\tau+1)\mathcal{G}(\tau_i),
\end{aligned} \tag{E.39}$$

where N_τ is the number of time interval $\Delta\tau = \beta/N_\tau$ and $\tau_i = i\Delta\tau$. For this reason, the coefficients $\mathcal{G}_l$ has very large numerical error for $\Delta\tau \sim \mathcal{O}(1/10)$ (which we usually consider it as time interval in Hirsch-Fye QMC) even for small l (See Fig. E.3). However, as it is shown in Fig. E.3, it is possible to obtain accurate $\mathcal{G}_l$ if $\Delta\tau \to 0$ which is very time consuming in time discretized QMC algorithms.

[3]Usually the time interval in Hirsch-Fye QMC is around $\Delta\tau = \beta/L \approx 0.33$.

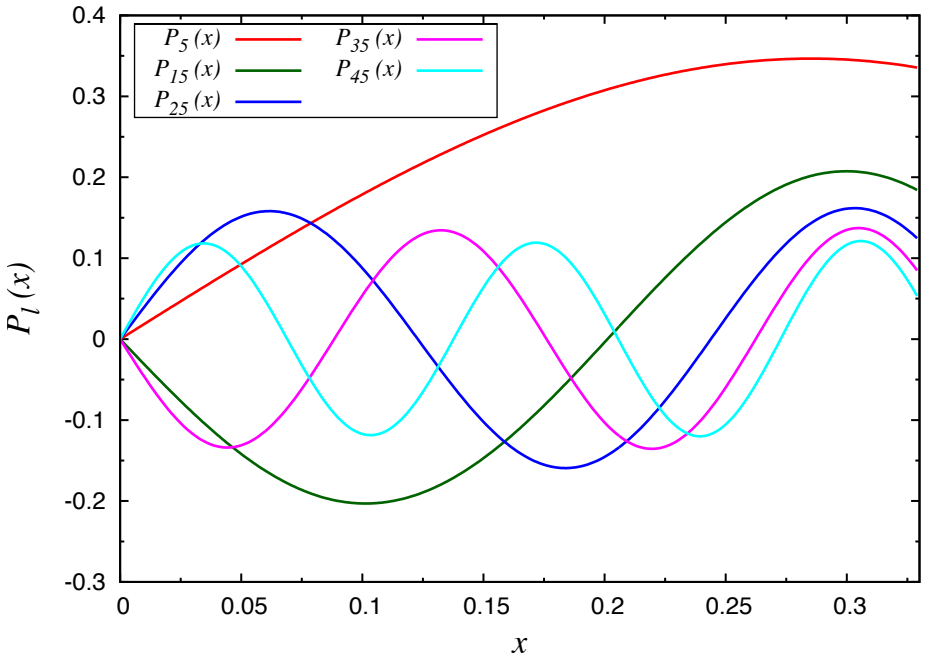

Figure E.2: The Legendre function $P_l(x)$ for $l = 5, 15, 25, 35, 45$ and $x \in [0 : 0.33]$.

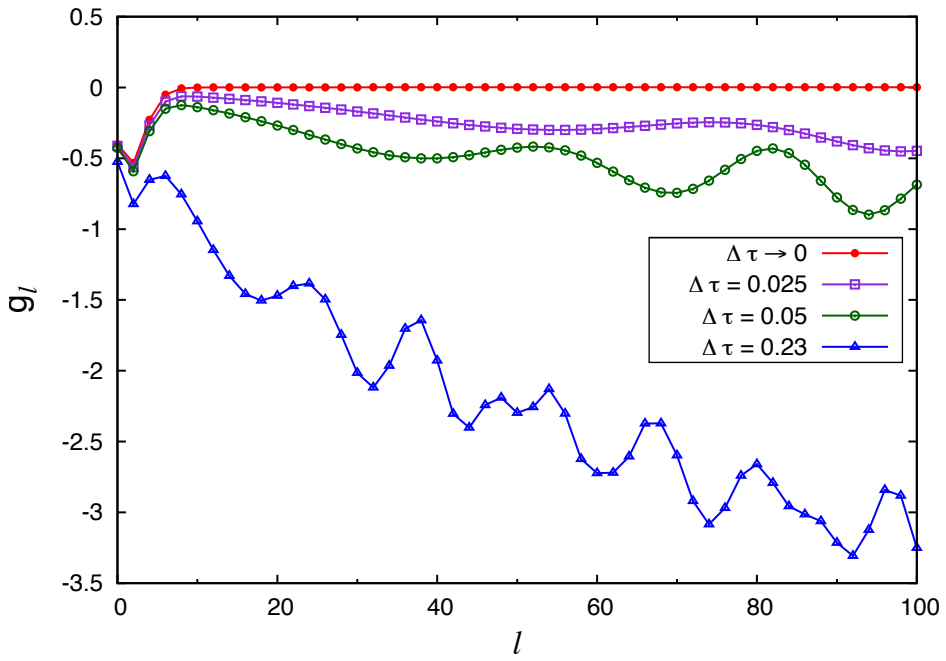

Figure E.3: $\mathcal{G}_l$ coefficients calculated for a one-band system Li_2VOSiO_4 at $U = 5$ and $\beta = 5$ for different $\Delta\tau$. The fast decay of the coefficients $\mathcal{G}_l$ is obtained for a very small $\Delta\tau$.

APPENDIX F

Appendix

F.1 2D trapezoidal Fourier transform of $\mathcal{G}(\tau, \tau')$

$$\begin{aligned}\mathcal{G}_{\alpha_i\alpha_j}(\nu_n, \nu_{n'}) &= \int_0^\beta d\tau \int_0^\beta d\tau' e^{i[\nu_n\tau - \nu_{n'}\tau']}\, \mathcal{G}_{\alpha_i\alpha_j}(\tau, \tau') \\ &\approx \left(\frac{\beta}{L}\right)^2 \sum_{l=1}^{L+1}\sum_{l'=1}^{L+1} e^{i\nu_n\tau_l} e^{-i\nu_{n'}\tau_{l'}}\, \mathcal{G}_{\alpha_i\alpha_j}(\tau_l, \tau_{l'}) \end{aligned} \tag{F.1}$$

In order to simplify this relation, we split $\sum_{l=1}^{L+1}\sum_{l'=1}^{L+1}$ as follows.

$$\begin{aligned}\mathcal{G}_{\alpha_i\alpha_j}(\nu_n, \nu_{n'}) &\approx \sum_{l=1}^{L+1}\Bigg(w_{l1}\, \mathcal{G}_{\alpha_i\alpha_j}(\tau_l, \tau_1 = 0)\, e^{i\nu_n\tau_l} + \sum_{l'=2}^{L} w_{ll'}\, \mathcal{G}_{\alpha_i\alpha_j}(\tau_l, \tau_{l'}) e^{i\nu_n\tau_l} e^{-i\nu_{n'}\tau_{l'}} \\ &\quad + w_{l,L+1}\mathcal{G}_{\alpha_i\alpha_j}(\tau_l, \tau_{L+1} = \beta) e^{i\nu_n\tau_l} e^{-i\nu_{n'}\beta}\Bigg) \\ &\approx w_{11}\mathcal{G}_{\alpha_i\alpha_j}(0,0) + w_{L+1,1}\mathcal{G}_{\alpha_i\alpha_j}(\beta, 0)\, e^{i\nu_n\beta} + \sum_{l=2}^{L} w_{l,1}\mathcal{G}_{\alpha_i\alpha_j}(\tau_l, 0)\, e^{i\nu_n\tau_l} \\ &\quad - w_{1,L+1}\mathcal{G}_{\alpha_i\alpha_j}(0, \beta) - w_{L+1,L+1}\mathcal{G}_{\alpha_i\alpha_j}(\beta, \beta)\, e^{i\nu_n\beta} - \sum_{l=2}^{L} w_{l,L+1}\mathcal{G}_{\alpha_i\alpha_j}(\tau_l, \beta)\, e^{i\nu_n\tau_l} \\ &\quad + \sum_{l=2}^{L} w_{1,l}\mathcal{G}_{\alpha_i\alpha_j}(0, \tau'_l)\, e^{-i\nu_{n'}\tau'_l} - \sum_{l=2}^{L} w_{L+1,l}\mathcal{G}_{\alpha_i\alpha_j}(\beta, \tau'_l) e^{-i\nu_{n'}\tau_l} \\ &\quad + \sum_{l=2}^{L}\sum_{l'=2}^{L} w_{ll'} e^{i\nu_n\tau_l} e^{-i\nu_{n'}\tau'_{l'}} \mathcal{G}_{\alpha_i\alpha_j}(\tau_l, \tau'_{l'}). \end{aligned} \tag{F.2}$$

Based on the weight matrix element w_{ij} given by Eq. (5.36) and properties of the Green's function (see Sec. 5.2.2), we have

$$\begin{aligned}\mathcal{G}_{\alpha_i\alpha_j}(\nu_n, \nu_{n'}) &\approx \frac{\Delta\tau^2}{4}\Big(\mathcal{G}_{\alpha_i\alpha_j}(0,0) - \mathcal{G}_{\alpha_i\alpha_j}(\beta, 0) - \mathcal{G}_{\alpha_i\alpha_j}(0, \beta) + \mathcal{G}_{\alpha_i\alpha_j}(\beta, \beta)\Big) \\ &\quad + \frac{\Delta\tau^2}{2}\sum_{l=2}^{L}\Big(\mathcal{G}_{\alpha_i\alpha_j}(\tau_l, 0)\, e^{i\nu_n\tau_l} - \mathcal{G}_{\alpha_i\alpha_j}(\tau_l, \beta)\, e^{i\nu_n\tau_l} + \mathcal{G}_{\alpha_i\alpha_j}(0, \tau'_l)\, e^{-i\nu_{n'}\tau'_l} \\ &\quad - \mathcal{G}_{\alpha_i\alpha_j}(\beta, \tau'_l)\, e^{-i\nu_{n'}\tau'_l}\Big) + \Delta\tau^2 \sum_{l=2}^{L}\sum_{l'=2}^{L} e^{i\nu_n\tau_l} e^{-i\nu_{n'}\tau'_{l'}} \mathcal{G}_{\alpha_i\alpha_j}(\tau_l, \tau'_{l'}). \end{aligned} \tag{F.3}$$

From this relation we can directly derive Eq. (5.38).

F.2 2D Filon-trapezoidal Fourier transform

Considering Eqs. (5.48) and (5.50), we have

$$\begin{aligned}
I[f] &= h^2(\alpha_x-\eta_x)(\alpha_y-\eta_y)\sum_{i=0}^{N-1}\sum_{j=0}^{N-1} e^{i\omega x_i}e^{i\nu y_j}f_{ij} + h^2\eta_x(\alpha_y-\eta_y)\sum_{i=0}^{N-1}\sum_{j=0}^{N-1} e^{i\omega x_i}e^{i\nu y_j}f_{i+1,j} \\
&\quad + h^2\eta_y(\alpha_x-\eta_x)\sum_{i=0}^{N-1}\sum_{j=0}^{N-1} e^{i\omega x_i}e^{i\nu y_j}f_{i,j+1} + h^2\eta_x\eta_y\sum_{i=0}^{N-1}\sum_{j=0}^{N-1} e^{i\omega x_i}e^{i\nu y_j}f_{i+1,j+1} \\
&\approx h^2(\alpha_x-\eta_x)(\alpha_y-\eta_y)\sum_{i=0}^{N-1}\sum_{j=0}^{N-1} e^{i\omega x_i}e^{i\nu y_j}f_{ij} + h^2\eta_x(\alpha_y-\eta_y)\sum_{i=1}^{N}\sum_{j=0}^{N-1} e^{i\omega (x_i-h)}e^{i\nu y_j}f_{ij} \\
&\quad + h^2\eta_y(\alpha_x-\eta_x)\sum_{i=0}^{N-1}\sum_{j=1}^{N} e^{i\omega x_i}e^{i\nu (y_j-h)}f_{ij} + h^2\eta_x\eta_y\sum_{i=1}^{N}\sum_{j=1}^{N} e^{i\omega x_i}e^{i\nu y_j}f_{ij},
\end{aligned} \tag{F.4}$$

where $h=\dfrac{b-a}{N}$, $f_{ij}\equiv f(x_i,y_j)$ and

$$\alpha_p=\frac{e^{i\theta_p}-1}{i\theta_p};\qquad \eta_p=\frac{e^{i\theta_p}}{i\theta_p}+\frac{1}{\theta_p^2}\left(e^{i\theta_p}-1\right), \tag{F.5}$$

which $p=x,y$ and $\theta_x=\omega h$, $\theta_y=\nu h$. In order to simplify Eq. (F.4), we rewrite it so that all summations are started from $i,j=0$ till $N-1$, i.e.,

$$\begin{aligned}
I[f] &\approx h^2\Big[(\alpha_x-\eta_x)(\alpha_y-\eta_y)+\eta_x e^{-i\theta_x}(\alpha_y-\eta_y)+\eta_y e^{-i\theta_y}(\alpha_x-\eta_x) \\
&\quad +(e^{-i\theta_x}\eta_x)(e^{-i\theta_y}\eta_y)\Big]\sum_{i=0}^{N-1}\sum_{j=0}^{N-1} e^{i\omega x_i}e^{i\nu y_j}f_{ij} \\
&\quad + h^2\Big[\eta_x(\alpha_y-\eta_y)e^{-i\theta_x}+\eta_x\eta_y e^{-i\theta_x}e^{-i\theta_y}\Big]\sum_{j=0}^{N-1} e^{i\nu y_j}\left(e^{i\omega x_N}f_{Nj}-e^{i\omega x_0}f_{0j}\right) \\
&\quad + h^2\Big[\eta_y(\alpha_x-\eta_x)e^{-i\theta_y}+\eta_x\eta_y e^{-i\theta_x}e^{-i\theta_y}\Big]\sum_{i=0}^{N-1} e^{i\omega x_i}\left(e^{i\nu y_N}f_{iN}-e^{i\nu y_0}f_{i0}\right) \\
&\quad + h^2\eta_x\eta_y e^{-i\theta_x}e^{-i\theta_y}\Big\{e^{i\omega x_N}\left(e^{i\nu y_N}f_{NN}-e^{i\nu y_0}f_{N0}\right)-e^{i\omega x_0}\left(e^{i\nu_N}f_{0N}-e^{i\nu y_0}f_{00}\right)\Big\}
\end{aligned} \tag{F.6}$$

With simple mathematics, we can derive Eq. (5.50) for the Fourier transform of $f(x,y)$.

F.3 2D Filon-trapezoidal relations for Fourier transform of $\mathcal{G}(\tau',\tau'')$

To derive the approximate relation for 2D Fourier transform of the $\mathcal{G}(\tau+\tau'',\tau'')$ (see Eq. (5.72)), we can either use Eq. (5.50) and the properties of the Green's function $\mathcal{G}(\tau+\tau'',\tau'')$ at boundaries or alternatively perform the Filon-trapezoidal's rule for first τ'' and then for τ. We follow the latter way to derive Eq. (5.72).

proof:

$$\begin{aligned}
\mathcal{G}_{\alpha_i\alpha_j}(\nu_n, \nu_{n'}) &= \int_0^\beta d\tau' \int_0^\beta d\tau''\ e^{i\nu_n\tau'} e^{-i\nu_{n'}\tau''}\ \mathcal{G}_{\alpha_i\alpha_j}(\tau', \tau'') \\
&= \int_0^\beta d\tau \int_0^\beta d\tau''\ e^{i\nu_n\tau} e^{i(\nu_n-\nu_{n'})\tau''}\ \mathcal{G}_{\alpha_i\alpha_j}(\tau+\tau'', \tau'') \\
&= \int_0^\beta d\tau\ e^{i\nu_n\tau}\ \mathcal{F}_{\alpha_i\alpha_j}(\tau), \qquad \text{(F.7)}
\end{aligned}$$

where

$$\begin{aligned}
\mathcal{F}_{ij}(\tau) &= \int_0^\beta d\tau''\ e^{i(\nu_n-\nu_{n'})\tau''}\ \mathcal{G}_{\alpha_i\alpha_j}(\tau+\tau'', \tau'') \\
&\approx \tilde{w}(\theta_B) \sum_{l_2=1}^{L} e^{i(\nu_n-\nu_{n'})\tau_{l_2}}\ \mathcal{G}_{\alpha_i\alpha_j}(\tau+\tau_{l_2}, \tau_{l_2}) \\
&\quad +\tilde{w}_{L+1}(\theta_B)\left[e^{i(\nu_n-\nu_{n'})\beta}\mathcal{G}_{\alpha_i\alpha_j}(\tau+\beta, \beta) - \mathcal{G}_{\alpha_i\alpha_j}(\tau+0, 0)\right] \\
&\approx \tilde{w}(\theta_B) \sum_{l_2=1}^{L} e^{i(\nu_n-\nu_{n'})\tau_{l_2}}\ \mathcal{G}_{\alpha_i\alpha_j}(\tau+\tau_{l_2}, \tau_{l_2}). \qquad \text{(F.8)}
\end{aligned}$$

By using this relation, we can derive the $\mathcal{G}_{\alpha_i\alpha_j}(\nu_n, \nu_{n'})$ as follows.

$$\begin{aligned}
\mathcal{G}_{\alpha_i\alpha_j}(\nu_n, \nu_{n'}) &\approx \tilde{w}(\theta_B) \sum_{l_2=1}^{L} e^{i(\nu_n-\nu_{n'})\tau_{l_2}} \int_0^\beta d\tau\ e^{i\nu_n\tau}\mathcal{G}_{\alpha_i\alpha_j}(\tau+\tau_{l_2}, \tau_{l_2}) \\
&\approx \tilde{w}(\theta_B) \sum_{l_2=1}^{L} e^{i(\nu_n-\nu_{n'})\tau_{l_2}} \Bigg\{ \tilde{w}(\theta_F) \sum_{l_1=1}^{L} e^{i\nu_n\tau_{l_1}}\mathcal{G}_{\alpha_i\alpha_j}(\tau_{l_1}+\tau_{l_2}, \tau_{l_2}) \\
&\quad +\tilde{w}_{L+1}(\theta_F)\Big[e^{i\nu_n\beta}\mathcal{G}_{\alpha_i\alpha_j}(\beta+\tau_{l_2}, \tau_{l_2}) - \mathcal{G}_{\alpha_i\alpha_j}(0+\tau_{l_2}, \tau_{l_2})\Big]\Bigg\} \\
&\approx \tilde{w}(\theta_F)\tilde{w}(\theta_B) \sum_{l_1=1}^{L}\sum_{l_2=0}^{L} e^{i(\nu_n-\nu_{n'})\tau_{l_2}} e^{i\nu_n\tau_{l_1}}\mathcal{G}_{\alpha_i\alpha_j}(\tau_{l_1}+\tau_{l_2}, \tau_{l_2}) \\
&\quad +\tilde{w}(\theta_B)\tilde{w}_{L+1}(\theta_F) \sum_{l_2=1}^{L} e^{i(\nu_n-\nu_{n'})\tau_{l_2}}\delta_{\alpha_i\alpha_j} \\
&\approx \tilde{w}(\theta_F)\tilde{w}(\theta_B) \sum_{l_1=1}^{L}\sum_{l_2=0}^{L} e^{i(\nu_n-\nu_{n'})\tau_{l_2}} e^{i\nu_n\tau_{l_1}}\mathcal{G}_{\alpha_i\alpha_j}(\tau_{l_1}+\tau_{l_2}, \tau_{l_2}) \\
&\quad -\tilde{w}_{L+1}(\theta_F)\beta\delta_{nn'}\delta_{\alpha_i\alpha_j}. \qquad \text{(F.9)}
\end{aligned}$$

To obtain this relation, we used the Filon-trapezoid approximation of δ-function,

$$\begin{aligned}
\beta\delta_{nn'} &= \int_0^\beta d\tau\ e^{i(\nu_n-\nu_{n'})\tau} \\
&\approx \tilde{w}(\theta_B) \sum_{l=1}^{L} e^{i(\nu_n-\nu_{n'})\tau_l}. \qquad \text{(F.10)}
\end{aligned}$$

F.4 Derivation: Two-particle correlation function inside the QMC

With the knowledge of the QMC Green's functions $\widetilde{G}$, we are able to compute the two-particle correlation function for a fixed QMC configuration in Matsubara frequency space by Eq. (5.80) if the local Hamiltonian is real. To prove this equation, we start with the most general form of the Matsubara Fourier integral

$$\begin{aligned}\widetilde{\chi}_{\alpha_i\alpha_j\alpha_k\alpha_l}(\nu_n,\nu_{n'},\omega_m) &= \frac{1}{16}\int_{-\beta}^{\beta}d\tau_1\int_{-\beta}^{\beta}d\tau_2\int_{-\beta}^{\beta}d\tau_3\int_{-\beta}^{\beta}d\tau_4\; e^{-i\nu_n\tau_1+i(\nu_n+\omega_m)\tau_2}\\ &\quad\times e^{-i(\nu_{n'}+\omega_m)\tau_3+i\nu_{n'}\tau_4}\,\widetilde{\mathcal{C}}_{\alpha_i\alpha_j\alpha_k\alpha_l}(\tau_1,\tau_2,\tau_3,\tau_4),\end{aligned} \tag{F.11}$$

with

$$\widetilde{\mathcal{C}}_{\alpha_i\alpha_j\alpha_k\alpha_l}(\tau_1,\tau_2,\tau_3,\tau_4) = c^\dagger_{\alpha_i}(\tau_1)c_{\alpha_j}(\tau_2)c^\dagger_{\alpha_k}(\tau_3)c_{\alpha_l}(\tau_4). \tag{F.12}$$

To calculate this integral, we break it into minor integral from $-\beta$ to 0 and major one from 0 to β.

$$\int_{-\beta}^{\beta} = \int_{-\beta}^{0} + \int_{0}^{\beta}. \tag{F.13}$$

In this case, we can rewrite Eq. (F.11) as follows

$$\begin{aligned}\widetilde{\chi}_{\alpha_i\alpha_j\alpha_k\alpha_l}(\nu_n,\nu_{n'},\omega_m) &= \frac{1}{16}\Big\{\mathcal{I}^{>>>>}+\mathcal{I}^{>>><}+\mathcal{I}^{>><>}+\mathcal{I}^{>><<}+\mathcal{I}^{><>>}+\mathcal{I}^{><><}\\ &\quad+\mathcal{I}^{><<>}+\mathcal{I}^{><<<}+\mathcal{I}^{<>>>}+\mathcal{I}^{<>><}+\mathcal{I}^{<><>}+\mathcal{I}^{<><<}\\ &\quad+\mathcal{I}^{<<>>}+\mathcal{I}^{<<><}+\mathcal{I}^{<<<>}+\mathcal{I}^{<<<<}\Big\},\end{aligned} \tag{F.14}$$

where, e.g.,

$$\begin{aligned}\mathcal{I}^{>>><} &= \int_{0}^{\beta}d\tau_1\int_{0}^{\beta}d\tau_2\int_{0}^{\beta}d\tau_3\int_{-\beta}^{0}d\tau_4\; e^{-i\nu_n\tau_1+i(\nu_n+\omega_m)\tau_2-i(\nu_{n'}+\omega_m)\tau_3+i\nu_{n'}\tau_4}\\ &\quad\times c^\dagger_{\alpha_i}(\tau_1)c_{\alpha_j}(\tau_2)c^\dagger_{\alpha_k}(\tau_3)c_{\alpha_l}(\tau_4).\end{aligned} \tag{F.15}$$

If we define

$$\begin{aligned}\widetilde{\mathcal{C}}_{\alpha_i\alpha_j\alpha_k\alpha_l}(\nu_n,\nu_{n'},\omega_m) &\equiv \int_{0}^{\beta}d\tau_1\int_{0}^{\beta}d\tau_2\int_{0}^{\beta}d\tau_3\int_{0}^{\beta}d\tau_4\; e^{-i\nu_n\tau_1+i(\nu_n+\omega_m)\tau_2-i(\nu_{n'}+\omega_m)\tau_3+i\nu_{n'}\tau_4}\\ &\quad\times\widetilde{\mathcal{C}}_{\alpha_i\alpha_j\alpha_k\alpha_l}(\tau_1,\tau_2,\tau_3,\tau_4),\end{aligned} \tag{F.16}$$

we can prove that each the same colored couple integrals are equal to

$$\begin{aligned}\mathcal{I}^{>>>>}+\mathcal{I}^{<<<<} &= \left(\widetilde{\mathcal{C}}_{\alpha_i\alpha_j\alpha_k\alpha_l}(\nu_n,\nu_{n'},\omega_m)+\widetilde{\mathcal{C}}_{\alpha_l\alpha_k\alpha_j\alpha_i}(\nu_{n'},\nu_n,\omega_m)\right),\\ \mathcal{I}^{>>><}+\mathcal{I}^{<<<>} &= \left(\widetilde{\mathcal{C}}_{\alpha_i\alpha_j\alpha_k\alpha_l}(\nu_n,\nu_{n'},\omega_m)+\widetilde{\mathcal{C}}_{\alpha_l\alpha_k\alpha_j\alpha_i}(\nu_{n'},\nu_n,\omega_m)\right)\\ \vdots &= \vdots\\ \mathcal{I}^{<>>>}+\mathcal{I}^{><<<} &= \left(\widetilde{\mathcal{C}}_{\alpha_i\alpha_j\alpha_k\alpha_l}(\nu_n,\nu_{n'},\omega_m)+\widetilde{\mathcal{C}}_{\alpha_l\alpha_k\alpha_j\alpha_i}(\nu_{n'},\nu_n,\omega_m)\right).\end{aligned} \tag{F.17}$$

Therefore,

$$\widetilde{\chi}_{\alpha_i\alpha_j\alpha_k\alpha_l}(\nu_n,\nu_{n'},\omega_m)=\frac{1}{2}\left(\widetilde{\mathcal{C}}_{\alpha_i\alpha_j\alpha_k\alpha_l}(\nu_n,\nu_{n'};\omega_m)+\widetilde{\mathcal{C}}_{\alpha_l\alpha_k\alpha_j\alpha_i}(\nu_{n'},\nu_n;\omega_m)\right). \tag{F.18}$$

In the following, we present the proof for some coupled terms. The rest can be done similarly.

1. proof of $\mathcal{I}^{>>>>}+\mathcal{I}^{<<<<}=\widetilde{\mathcal{C}}_{\alpha_i\alpha_j\alpha_k\alpha_l}(\nu_n,\nu_{n'},\omega_m)+\widetilde{\mathcal{C}}_{\alpha_l\alpha_k\alpha_j\alpha_i}(\nu_{n'},\nu_n,\omega_m)$

   Form the definition (F.16), we know that $\mathcal{I}^{>>>>}=\widetilde{\mathcal{C}}_{\alpha_i\alpha_j\alpha_k\alpha_l}(\nu_n,\nu_{n'},\omega_m)$. For $\mathcal{I}^{<<<<}$, we have

$$\begin{aligned}
\mathcal{I}^{<<<<} &= \int_{-\beta}^{0}d\tau_1\int_{-\beta}^{0}d\tau_2\int_{-\beta}^{0}d\tau_3\int_{-\beta}^{0}d\tau_4\, e^{-i\nu_n\tau_1+i(\nu_n+\omega_m)\tau_2-i(\nu_{n'}+\omega_m)\tau_3+i\nu_{n'}\tau_4}\\
&\quad\times c^{\dagger}_{\alpha_i}(\tau_1)c_{\alpha_j}(\tau_2)c^{\dagger}_{\alpha_k}(\tau_3)c_{\alpha_l}(\tau_4)\\
&= \int_{0}^{\beta}d\tau_1\int_{0}^{\beta}d\tau_2\int_{0}^{\beta}d\tau_3\int_{0}^{\beta}d\tau_4\, e^{i\nu_n\tau_1-i(\nu_n+\omega_m)\tau_2+i(\nu_{n'}+\omega_m)\tau_3-i\nu_{n'}\tau_4}\\
&\quad\times c^{\dagger}_{\alpha_i}(-\tau_1)c_{\alpha_j}(-\tau_2)c^{\dagger}_{\alpha_k}(-\tau_3)c_{\alpha_l}(-\tau_4)\\
&= \int_{0}^{\beta}d\tau_1\int_{0}^{\beta}d\tau_2\int_{0}^{\beta}d\tau_3\int_{0}^{\beta}d\tau_4\, e^{i\nu_n\tau_1-i(\nu_n+\omega_m)\tau_2+i(\nu_{n'}+\omega_m)\tau_3-i\nu_{n'}\tau_4}\\
&\quad\times \left(c^{\dagger}_{\alpha_l}(\tau_4)c_{\alpha_k}(\tau_3)c^{\dagger}_{\alpha_j}(\tau_2)c_{\alpha_i}(\tau_1)\right)^{*}\\
&= c^{\dagger}_{\alpha_l}(\nu_{n'})c_{\alpha_k}(\nu_{n'}+\omega_m)c^{\dagger}_{\alpha_j}(\nu_n+\omega_m)c_{\alpha_i}(\nu_n)\\
&= \widetilde{\mathcal{C}}_{\alpha_l\alpha_k\alpha_j\alpha_i}(\nu_{n'},\nu_n,\omega_m),
\end{aligned} \tag{F.19}$$

   where we used the fact that the complex conjugate of $c^{\dagger}_{\alpha_i}(\tau_1)c_{\alpha_j}(\tau_2)c^{\dagger}_{\alpha_k}(\tau_3)c_{\alpha_l}(\tau_4)$ is equal to $c^{\dagger}_{\alpha_l}(-\tau_4)c_{\alpha_k}(-\tau_3)c^{\dagger}_{\alpha_j}(-\tau_2)c_{\alpha_i}(-\tau_1)$ because the local Hamiltonian is real. Also, we know that

$$c(i\nu_n) = \int_0^{\beta}d\tau\, e^{i\nu_n\tau}c(\tau). \tag{F.20}$$

2. proof of $\mathcal{I}^{>>><}+\mathcal{I}^{<<<>}=\widetilde{\mathcal{C}}_{\alpha_i\alpha_j\alpha_k\alpha_l}(\nu_n,\nu_{n'},\omega_m)+\widetilde{\mathcal{C}}_{\alpha_l\alpha_k\alpha_j\alpha_i}(\nu_{n'},\nu_n,\omega_m)$

$$\begin{aligned}
\mathcal{I}^{>>><} &= \int_{0}^{\beta}d\tau_1\int_{0}^{\beta}d\tau_2\int_{0}^{\beta}d\tau_3\int_{-\beta}^{0}d\tau_4\, e^{-i\nu_n\tau_1+i(\nu_n+\omega_m)\tau_2-i(\nu_{n'}+\omega_m)\tau_3+i\nu_{n'}\tau_4}\\
&\quad\times c^{\dagger}_{\alpha_i}(\tau_1)c_{\alpha_j}(\tau_2)c^{\dagger}_{\alpha_k}(\tau_3)c_{\alpha_l}(\tau_4)\\
&= \int_{0}^{\beta}d\tau_1\int_{0}^{\beta}d\tau_2\int_{0}^{\beta}d\tau_3\int_{0}^{\beta}d\tau_4\, e^{-i\nu_n\tau_1+i(\nu_n+\omega_m)\tau_2-i(\nu_{n'}+\omega_m)\tau_3-i\nu_{n'}\tau_4}\\
&\quad\times c^{\dagger}_{\alpha_i}(\tau_1)c_{\alpha_j}(\tau_2)c^{\dagger}_{\alpha_k}(\tau_3)c_{\alpha_l}(-\tau_4)\\
&= c^{\dagger}_{\alpha_i}(\nu_n)c_{\alpha_j}(\nu_n+\omega_m)c^{\dagger}_{\alpha_k}(\nu_{n'}+\omega_m)c_{\alpha_l}(\nu_{n'})\\
&= \widetilde{\mathcal{C}}_{\alpha_i\alpha_j\alpha_k\alpha_l}(\nu_n,\nu_{n'},\omega_m).
\end{aligned} \tag{F.21}$$

To prove this relation, we use

$$\begin{aligned} I &= \int_0^\beta d\tau\ e^{-i\nu_n\tau} c(-\tau) \\ &= \int_0^\beta d\tau\ e^{-i\nu_n\tau} \left(c^\dagger(\tau)\right)^\dagger \\ &= \left(\int_0^\beta d\tau\ e^{-i(-\nu_n)\tau} c^\dagger(\tau)\right)^\dagger \\ &= \left(c^\dagger(-i\nu_n)\right)^\dagger \\ &= c(i\nu_n). \end{aligned} \tag{F.22}$$

For the other term $\mathcal{I}^{<<<>}$, we have

$$\begin{aligned} \mathcal{I}^{<<<>} &= \int_{-\beta}^0 d\tau_1 \int_{-\beta}^0 d\tau_2 \int_{-\beta}^0 d\tau_3 \int_0^\beta d\tau_4\ e^{-i\nu_n\tau_1 + i(\nu_n+\omega_m)\tau_2 - i(\nu_{n'}+\omega_m)\tau_3 + i\nu_{n'}\tau_4} \\ &\quad \times c^\dagger_{\alpha_i}(\tau_1) c_{\alpha_j}(\tau_2) c^\dagger_{\alpha_k}(\tau_3) c_{\alpha_l}(\tau_4) \\ &= \int_0^\beta d\tau_1 \int_0^\beta d\tau_2 \int_0^\beta d\tau_3 \int_0^\beta d\tau_4\ e^{i\nu_n\tau_1 - i(\nu_n+\omega_m)\tau_2 + i(\nu_{n'}+\omega_m)\tau_3 - i\nu_{n'}\tau_4} \\ &\quad \times c^\dagger_{\alpha_i}(-\tau_1) c_{\alpha_j}(-\tau_2) c^\dagger_{\alpha_k}(-\tau_3) c_{\alpha_l}(\tau_4) \\ &= \int_0^\beta d\tau_1 \int_0^\beta d\tau_2 \int_0^\beta d\tau_3 \int_0^\beta d\tau_4\ e^{i\nu_n\tau_1 - i(\nu_n+\omega_m)\tau_2 + i(\nu_{n'}+\omega_m)\tau_3 - i\nu_{n'}\tau_4} \\ &\quad \times\ c^\dagger_{\alpha_l}(-\tau_4) c_{\alpha_k}(\tau_3) c^\dagger_{\alpha_j}(\tau_2) c_{\alpha_i}(\tau_1) \\ &= c^\dagger_{\alpha_l}(\nu_{n'}) c_{\alpha_k}(\nu_{n'}+\omega_m) c^\dagger_{\alpha_j}(\nu_n+\omega_m) c_{\alpha_i}(\nu_n) \\ &= \widetilde{\mathcal{C}}_{\alpha_l\alpha_k\alpha_j\alpha_i}(\nu_{n'}, \nu_n, \omega_m). \end{aligned} \tag{F.23}$$

3. proof of $\mathcal{I}^{>><<} + \mathcal{I}^{<<>>} = \widetilde{\mathcal{C}}_{\alpha_i\alpha_j\alpha_k\alpha_l}(\nu_n, \nu_{n'}, \omega_m) + \widetilde{\mathcal{C}}_{\alpha_l\alpha_k\alpha_j\alpha_i}(\nu_{n'}, \nu_n, \omega_m)$

$$\begin{aligned} \mathcal{I}^{>><<} &= \int_0^\beta d\tau_1 \int_0^\beta d\tau_2 \int_{-\beta}^0 d\tau_3 \int_{-\beta}^0 d\tau_4\ e^{-i\nu_n\tau_1 + i(\nu_n+\omega_m)\tau_2 - i(\nu_{n'}+\omega_m)\tau_3 + i\nu_{n'}\tau_4} \\ &\quad \times\ c^\dagger_{\alpha_i}(\tau_1) c_{\alpha_j}(\tau_2) c^\dagger_{\alpha_k}(\tau_3) c_{\alpha_l}(\tau_4) \\ &= \int_0^\beta d\tau_1 \int_0^\beta d\tau_2 \int_0^\beta d\tau_3 \int_0^\beta d\tau_4\ e^{-i\nu_n\tau_1 + i(\nu_n+\omega_m)\tau_2 + i(\nu_{n'}+\omega_m)\tau_3 - i\nu_{n'}\tau_4} \\ &\quad \times\ c^\dagger_{\alpha_i}(\tau_1) c_{\alpha_j}(\tau_2) c^\dagger_{\alpha_k}(-\tau_3) c_{\alpha_l}(-\tau_4) \\ &= c^\dagger_{\alpha_i}(\nu_n) c_{\alpha_j}(\nu_n+\omega_m) c^\dagger_{\alpha_k}(\nu_{n'}+\omega_m) c_{\alpha_l}(\nu_{n'}) \\ &= \widetilde{\mathcal{C}}_{\alpha_i\alpha_j\alpha_k\alpha_l}(\nu_n, \nu_{n'}, \omega_m). \end{aligned} \tag{F.24}$$

For the other term we have

$$\begin{aligned}
\mathcal{I}^{<<>>} &= \int_{-\beta}^{0} d\tau_1 \int_{-\beta}^{0} d\tau_2 \int_{0}^{\beta} d\tau_3 \int_{0}^{\beta} d\tau_4 \; e^{-i\nu_n\tau_1 + i(\nu_n+\omega_m)\tau_2 - i(\nu_{n'}+\omega_m)\tau_3 + i\nu_{n'}\tau_4} \\
&\quad \times c^{\dagger}_{\alpha_i}(\tau_1) c_{\alpha_j}(\tau_2) c^{\dagger}_{\alpha_k}(\tau_3) c_{\alpha_l}(\tau_4) \\
&= \int_{0}^{\beta} d\tau_1 \int_{0}^{\beta} d\tau_2 \int_{0}^{\beta} d\tau_3 \int_{0}^{\beta} d\tau_4 \; e^{i\nu_n\tau_1 - i(\nu_n+\omega_m)\tau_2 - i(\nu_{n'}+\omega_m)\tau_3 + i\nu_{n'}\tau_4} \\
&\quad \times c^{\dagger}_{\alpha_i}(-\tau_1) c_{\alpha_j}(-\tau_2) c^{\dagger}_{\alpha_k}(\tau_3) c_{\alpha_l}(\tau_4) \\
&= \int_{0}^{\beta} d\tau_1 \int_{0}^{\beta} d\tau_2 \int_{0}^{\beta} d\tau_3 \int_{0}^{\beta} d\tau_4 \; e^{i\nu_n\tau_1 - i(\nu_n+\omega_m)\tau_2 - i(\nu_{n'}+\omega_m)\tau_3 + i\nu_{n'}\tau_4} \\
&\quad \times c^{\dagger}_{\alpha_l}(-\tau_4) c_{\alpha_k}(-\tau_3) c^{\dagger}_{\alpha_j}(\tau_2) c_{\alpha_i}(\tau_1) \\
&= c^{\dagger}_{\alpha_l}(\nu_{n'}) c_{\alpha_k}(\nu_{n'}+\omega_m) c^{\dagger}_{\alpha_j}(\nu_n+\omega_m) c_{\alpha_i}(\nu_n) \\
&= \widetilde{\mathcal{C}}_{\alpha_l\alpha_k\alpha_j\alpha_i}(\nu_{n'}, \nu_n, \omega_m). \qquad \text{(F.25)}
\end{aligned}$$

The rest of the terms can be shown identically.

APPENDIX G

Appendix

G.1 Least squares method

Least square method is a mathematical approach to find the best regression line to a given set of points. This procedure is performed by minimizing the sum of the squares of vertical distances among points and the line. The power of the least square method is based on the fact that this method leads to a system of linear equations which can be solved simply by linear algebra methods. In this mathematical method, one can find the best approximation of an over-determined system where there are more observed values than unknown adjustable parameters [86]. Given a data set of n independent variables, x_{ij}, and corresponding observed variables, Y_i, and a model $f(x_{ij}, \{a_j\})$ depending on $m+1 < n$ adjustable parameters, a_j, the method works by minimizing the sum of the squares of the residuals, r_i of the model approximation and the observed points, χ^2

$$\chi^2 = \sum_i r_i^2. \tag{G.1}$$

The residual is defined by the difference between an observed value and the fitted value provided by a model so that

$$r_i = Y_i - f(x_{ij}, \{a_j\}). \tag{G.2}$$

For polynomial regression, the model is

$$\begin{aligned} f(x_i, \{a_j\}) &= \sum_{j=1}^{m+1} x_{ij} a_j \\ &= x_{i1}a_1 + x_{i2}a_2 + x_{i3}a_3 + ... + x_{im+1}a_{m+1} \\ &= a_1 + a_2 x_i + a_3 x_i^2 + ... + a_{m+1} x_i^m. \end{aligned} \tag{G.3}$$

For finding the optimal parameters, one needs to determine the values of $a_1, a_2, ..., a_{m+1}$ that minimize

$$\sum_{i=1}^{n} \left(Y_i - \sum_{j=1}^{m+1} x_{ij} a_j \right)^2.$$

This can be done by taking partial derivatives with respect to $a_1, a_2, ..., a_{m+1}$ equal to zero. In this way, $l = 1, 2, ..., m+1$ equations are produced so that

$$0 = \frac{\partial}{\partial a_l} \sum_{i=1}^{n} \left(Y_i - \sum_{j=1}^{m+1} x_{ij} a_j \right)^2 = (-2) \sum_{i=1}^{n} \left(Y_i - \sum_{j=1}^{m+1} x_{ij} a_j \right) x_{il}. \tag{G.4}$$

This leads to a system of $m+1$ linear equations in $m+1$ unknown $a_1, a_2, ..., a_{m+1}$ which can be rewritten as

$$\sum_{i=1}^{n} x_{il} Y_i = \sum_{i=1}^{n} \sum_{j=1}^{m+1} x_{il} x_{ij} a_j. \tag{G.5}$$

Using matrix algebra, this system can be written in matrix notation as

$$\mathbf{X^T Y} = (\mathbf{X^T X})\mathbf{a}, \tag{G.6}$$

wherein

$$\mathbf{X} = \begin{pmatrix} 1 & x_1 & x_1^2 & ... & x_1^m \\ 1 & x_2 & x_2^2 & ... & x_2^m \\ \vdots & \vdots & \vdots & \ddots & \vdots \\ 1 & x_n & x_n^2 & \dots & x_n^m \end{pmatrix}, \mathbf{Y} = \begin{pmatrix} y_1 \\ y_2 \\ \vdots \\ y_n \end{pmatrix}, \mathbf{a} = \begin{pmatrix} a_1 \\ a_2 \\ \vdots \\ a_{m+1} \end{pmatrix}, \tag{G.7}$$

If the matrix $\mathbf{X^T X}$ is invertible, the explicit relation for $\mathbf{a}$ coefficients is

$$\mathbf{a} = (\mathbf{X^T X})^{-1} \mathbf{X^T Y}. \tag{G.8}$$

In this case, the matrices $\mathbf{X^T X}$ and $\mathbf{X^T Y}$ are

$$\mathbf{X^T X} = \begin{pmatrix} \sum_{i=1}^n 1 & \sum_{i=1}^n x_i & \sum_{i=1}^n x_i^2 & ... & \sum_{i=1}^n x_i^m \\ \sum_{i=1}^n x_i & \sum_{i=1}^n x_i^2 & \sum_{i=1}^n x_i^3 & ... & \sum_{i=1}^n x_i^{m+1} \\ \vdots & \vdots & \vdots & \ddots & \vdots \\ \sum_{i=1}^n x_i^m & \sum_{i=1}^n x_i^{m+1} & \sum_{i=1}^n x_i^{m+2} & \dots & \sum_{i=1}^n x_i^{2m} \end{pmatrix}, \tag{G.9}$$

$$\mathbf{X^T Y} = \begin{pmatrix} \sum_{i=1}^n y_i \\ \sum_{i=1}^n x_i y_i \\ \vdots \\ \sum_{i=1}^n x_i^m y_i \end{pmatrix}. \tag{G.10}$$

Bibliography

[1] W. Kohn. Nobel lecture: Electronic structure of matter—wave functions and density functionals. *Rev. Mod. Phys.*, 71:1253–1266, Oct 1999.

[2] U von Barth. Basic Density-Functional Theory-an overview. *Physica Scripta*, 2004(T109):9, 2004.

[3] K. Terakura, T. Oguchi, A. R. Williams, and J. Kübler. Band theory of insulating transition-metal monoxides: Band-structure calculations. *Phys. Rev. B*, 30:4734–4747, Oct 1984.

[4] C. S. Wang, B. M. Klein, and H. Krakauer. Theory of magnetic and structural ordering in iron. *Phys. Rev. Lett.*, 54:1852–1855, Apr 1985.

[5] John Hubbard. Electron correlations in narrow energy bands. *Proceedings of the Royal Society of London. Series A. Mathematical and Physical Sciences*, 276(1365):238–257, 1963.

[6] John Hubbard. Electron correlations in narrow energy bands. iii. an improved solution. *Proceedings of the Royal Society of London. Series A. Mathematical and Physical Sciences*, 281(1386):401–419, 1964.

[7] P. W. Anderson. Localized magnetic states in metals. *Phys. Rev.*, 124:41–53, Oct 1961.

[8] J. E. Hirsch. Two-dimensional hubbard model: Numerical simulation study. *Phys. Rev. B*, 31:4403–4419, Apr 1985.

[9] S. Akbar Jafari. Introduction to hubbard model and exact diagonalization. *Iranian Journal of Physics Research*, 8, 2008.

[10] Raimundo R. dos Santos. Introduction to quantum monte carlo simulations for fermionic systems. *Brazilian Journal of Physics*, 33:1, March 2003.

[11] Gabriel Kotliar and Dieter Vollhardt. Strongly correlated materials: Insights from dynamical mean-field theory. *Physicstoday*, 57(3):53–59, 2004.

[12] Antoine Georges, Gabriel Kotliar, Werner Krauth, and Marcelo J. Rozenberg. Dynamical mean-field theory of strongly correlated fermion systems and the limit of infinite dimensions. *Rev. Mod. Phys.*, 68:13–125, Jan 1996.

[13] J. E. Hirsch and R. M. Fye. Monte carlo method for magnetic impurities in metals. *Phys. Rev. Lett.*, 56:2521–2524, Jun 1986.

[14] Emanuel Gull, Andrew J. Millis, Alexander I. Lichtenstein, Alexey N. Rubtsov, Matthias Troyer, and Philipp Werner. Continuous-time monte carlo methods for quantum impurity models. *Rev. Mod. Phys.*, 83:349–404, May 2011.

[15] V.I. Anisimov. Electron structure of compounds with strong electron correlations in the theory of dynamic mean field. *The Physics of Metals and Metallography*, 112(7):682–710, 2011.

[16] R. Melzi, P. Carretta, A. Lascialfari, M. Mambrini, M. Troyer, P. Millet, and F. Mila. $Li_2VO(Si,Ge)O_4$, a prototype of a two-dimensional frustrated quantum Heisenberg antiferromagnet. *Phys. Rev. Lett.*, 85:1318–1321, Aug 2000.

[17] R. Melzi, S. Aldrovandi, F. Tedoldi, P. Carretta, P. Millet, and F. Mila. Magnetic and thermodynamic properties of Li_2VOSiO_4: A two-dimensional S=1/2 frustrated antiferromagnet on a square lattice. *Phys. Rev. B*, 64:024409, Jun 2001.

[18] P. Carretta, N. Papinutto, C. B. Azzoni, M. C. Mozzati, E. Pavarini, S. Gonthier, and P. Millet. Frustration-driven structural distortion in $VOMoO_4$. *Phys. Rev. B*, 66:094420, Sep 2002.

[19] E. Pavarini, E. Koch and U. Schollwöck (Eds.). *Emergent Phenomena in Correlated Matter*, volume 3 of *Schriften des Forschungszentrums Jülich / Reihe Modeling and Simulation: Reihe Modeling and Simulation*. Forschungszentrum Jülich, Inst. for Advanced Simulation, 2013.

[20] G. Kotliar, S. Y. Savrasov, K. Haule, V. S. Oudovenko, O. Parcollet, and C. A. Marianetti. Electronic structure calculations with dynamical mean-field theory. *Rev. Mod. Phys.*, 78:865–951, Aug 2006.

[21] V. Anisimov and Y. Izyumov. *Electronic Structure of Strongly Correlated Materials*. Springer Series in Solid-State Sciences. Springer, 2010.

[22] E. Pavarini, E. Koch, D. Vollhardt, and A. Lichtenstein (Eds.). *The LDA+DMFT approach to strongly correlated materials*, volume 1 of *Schriften des Forschungszentrums Jülich / Reihe Modeling and Simulation: Reihe Modeling and Simulation*. Forschungszentrum Jülich, Zentralbibliothek, Verlag, 2011.

[23] P. Hohenberg and W. Kohn. Inhomogeneous electron gas. *Phys. Rev.*, 136:B864–B871, Nov 1964.

[24] W. Kohn and L. J. Sham. Self-consistent equations including exchange and correlation effects. *Phys. Rev.*, 140:A1133–A1138, Nov 1965.

[25] R.G. Parr and W. Yang. *Density-Functional Theory of Atoms and Molecules*. International Series of Monographs on Chemistry. Oxford University Press, USA, 1989.

[26] D. M. Ceperley and B. J. Alder. Ground state of the electron gas by a stochastic method. *Phys. Rev. Lett.*, 45:566–569, Aug 1980.

[27] E. Pavarini, E. Koch, and A. I. Lichtenstein. Mechanism for orbital ordering in $KCuF_3$. *Phys. Rev. Lett.*, 101:266405, Dec 2008.

[28] E. Pavarini, E. Koch, F. Anders, and M. Jarrell (Eds.). *Correlated Electrons: From Models to Materials*, volume 2 of *Schriften des Forschungszentrums Jülich / Reihe Modeling and Simulation: Reihe Modeling and Simulation*. Forschungszentrum Jülich, Zentralbibliothek, Verlag, 2012.

[29] Elliott H. Lieb and F. Y. Wu. Absence of mott transition in an exact solution of the short-range, one-band model in one dimension. *Phys. Rev. Lett.*, 20:1445–1448, Jun 1968.

[30] S. Kehrein. *The Flow Equation Approach to Many-Particle Systems*. Number no. 217 in Springer Tracts in Modern Physics. Springer, 2006.

[31] Walter Metzner and Dieter Vollhardt. Correlated lattice fermions in $d = \infty$ dimensions. *Phys. Rev. Lett.*, 62:324–327, Jan 1989.

[32] Antoine Georges and Gabriel Kotliar. Hubbard model in infinite dimensions. *Phys. Rev. B*, 45:6479–6483, Mar 1992.

[33] D. Vollhardt. Dynamical mean-field theory for correlated electrons. *Annalen der Physik*, 524(1):1–19, 2012.

[34] Philipp Werner, Armin Comanac, Luca de' Medici, Matthias Troyer, and Andrew J. Millis. Continuous-time solver for quantum impurity models. *Phys. Rev. Lett.*, 97:076405, Aug 2006.

[35] Kristjan Haule. Quantum monte carlo impurity solver for cluster dynamical mean-field theory and electronic structure calculations with adjustable cluster base. *Phys. Rev. B*, 75:155113, Apr 2007.

[36] Andreas Robert Flesch. *Electronic structure of strongly correlated materials*. PhD thesis, Universitätsbibliothek, 2013.

[37] A. N. Rubtsov, V. V. Savkin, and A. I. Lichtenstein. Continuous-time quantum monte carlo method for fermions. *Phys. Rev. B*, 72:035122, Jul 2005.

[38] O. Parcollet E. Gull, P. Werner and M. Troyer. Continuous-time auxiliary-field monte carlo for quantum impurity models. *EuroPhys. Lett*, 82:57003, May 2008.

[39] Michel Caffarel and Werner Krauth. Exact diagonalization approach to correlated fermions in infinite dimensions: Mott transition and superconductivity. *Phys. Rev. Lett.*, 72:1545–1548, Mar 1994.

[40] Andreas Dolfen. *Strong electronic correlations in low-dimensional systems*. PhD thesis, Aachen, Techn. Hochsch., Diss., 2010, 2010.

[41] R. Bulla, T. A. Costi, and D. Vollhardt. Finite-temperature numerical renormalization group study of the mott transition. *Phys. Rev. B*, 64:045103, Jun 2001.

[42] Henrik Kajueter and Gabriel Kotliar. New iterative perturbation scheme for lattice models with arbitrary filling. *Phys. Rev. Lett.*, 77:131–134, Jul 1996.

[43] E. Pavarini, A. Yamasaki, J. Nuss and O. K. Andersen. How chemistry controls electron localization in $3d^1$ perovskites: a wannier-function study. *New J. Phys.*, 7:188, Mar 2005.

[44] K. Held. Electronic structure calculations using dynamical mean field theory. *Advances in Physics*, 56(6):829–926, 2007.

[45] V. I. Anisimov and O. Gunnarsson. Density-functional calculation of effective coulomb interactions in metals. *Phys. Rev. B*, 43:7570–7574, Apr 1991.

[46] T. Pang. *An Introduction to Computational Physics*. Cambridge University Press, 2006.

[47] W. Krauth. *Statistical Mechanics: Algorithms and Computations*. Oxford Master Series in Physics. Oxford University Press, UK, 2006.

[48] Masuo Suzuki. Quantum statistical monte carlo methods and applications to spin systems. *Journal of Statistical Physics*, 43(5-6):883–909, 1986.

[49] J. Yoo, S. Chandrasekharan, R. K. Kaul, D. Ullmo and H. U. Baranger. On the sign problem in the hirschÐfye algorithm for impurity problems. *J. Phys. A: Math. Gen.*, 38:10307, November 2005.

[50] Raimundo R. dos Santos. Introduction to quantum Monte Carlo simulations for fermionic systems. *Brazilian Journal of Physics*, 33:36 – 54, 03 2003.

[51] A. Altland and B.D. Simons. *Condensed Matter Field Theory*. Cambridge books online. Cambridge University Press, 2010.

[52] G. Grosso and G.P. Parravicini. *Solid State Physics*. Elsevier Science, 2013.

[53] P. Coleman. *Introduction to Many Body Physics*. http://www.physics.rutgers.edu/ coleman/mbody/pdf/bk.pdf, 2011.

[54] S. Blundell. *Magnetism in Condensed Matter*. Oxford Master Series in Condensed Matter Physics 4. OUP Oxford, 2001.

[55] P. Atkins and J. de Paula. *Physical Chemistry*. W. H. Freeman, 2007.

[56] H. Bruus and K. Flensberg. *Many-Body Quantum Theory in Condensed Matter Physics: An Introduction*. Oxford Graduate Texts. OUP Oxford, 2004.

[57] SudhanshuS Jha. Nonlinear response theory. *Pramana*, 22(3-4):173–182, 1984.

[58] E. E. Salpeter and H. A. Bethe. A relativistic equation for bound-state problems. *Phys. Rev.*, 84:1232–1242, Dec 1951.

[59] Lewin Boehnke, Hartmut Hafermann, Michel Ferrero, Frank Lechermann, and Olivier Parcollet. Orthogonal polynomial representation of imaginary-time green's functions. *Phys. Rev. B*, 84:075145, Aug 2011.

[60] G. Giuliani and G. Vignale. *Quantum Theory of the Electron Liquid*. Cambridge University Press, 2005.

[61] P. Nozieres. *Theory Of Interacting Fermi Systems*. Advanced Books Classics. Westview Press, 1997.

[62] G. Dahlquist and Å. Björck. *Numerical Methods in Scientific Computing: Vol. 1*. Number v. 1 in SIAM e-books. Society for Industrial and Applied Mathematics, 2008.

[63] P. J. Davis and I. Polonsky. *Handbook of Mathematical Functions*. Dover, New York, 1970.

[64] O. Gunnarsson, G. Sangiovanni, A. Valli, and M. W. Haverkort. Fourier transformation and response functions. *Phys. Rev. B*, 82:233104, Dec 2010.

[65] M. Jarrell, Th. Maier, C. Huscroft, and S. Moukouri. Quantum monte carlo algorithm for nonlocal corrections to the dynamical mean field approximation. *Phys. Rev. B*, 64:195130, Oct 2001.

[66] S. V. Streltsov, E. Gull, A. O. Shorikov, M. Troyer, V. I. Anisimov, and P. Werner. Magnetic susceptibility of cerium: An lda+dmft study. *Phys. Rev. B*, 85:195109, May 2012.

[67] S. L. Skornyakov, A. A. Katanin, and V. I. Anisimov. Linear-temperature dependence of static magnetic susceptibility in lafeaso from dynamical mean-field theory. *Phys. Rev. Lett.*, 106:047007, Jan 2011.

[68] KI Kugel and DI Khomskii. Crystal structure and magnetic properties of substances with orbital degeneracy. *Zh. Eksp. Teor. Fiz*, 64:1429–1439, 1973.

[69] C. Lacroix, P. Mendels, and F. Mila. *Introduction to Frustrated Magnetism: Materials, Experiments, Theory*. Springer Series in Solid-State Sciences. Springer, 2011.

[70] Leon Balents. Spin liquids in frustrated magnets. *Nature*, 464:199–208, March 2010.

[71] Roderich Moessner and Arthur P. Ramirez. Geometrical frustration. *Physicstoday*, 59(2):24–29, 2006.

[72] AP Ramirez. Strongly geometrically frustrated magnets. *Annual Review of Materials Science*, 24(1):453–480, 1994.

[73] H.T. Diep. *Frustrated Spin Systems*. World Scientific, 2004.

[74] D. Feng and G. Jin. *Introduction to Condensed Matter Physics*. Number v. 1 in Introduction to Condensed Matter Physics. World Scientific, 2005.

[75] Alexander A. Tsirlin and Helge Rosner. Extension of the spin-$\frac{1}{2}$ frustrated square lattice model: The case of layered vanadium phosphates. *Phys. Rev. B*, 79:214417, Jun 2009.

[76] A. Bombardi, L. C. Chapon, I. Margiolaki, C. Mazzoli, S. Gonthier, F. Duc, and P. G. Radaelli. Magnetic order and lattice anomalies in the J_1-J_2 model system $\mathrm{VOMoO_4}$. *Phys. Rev. B*, 71:220406, Jun 2005.

[77] A. Bombardi, J. Rodriguez-Carvajal, S. Di Matteo, F. de Bergevin, L. Paolasini, P. Carretta, P. Millet, and R. Caciuffo. Direct determination of the magnetic ground state in the square lattice $S = 1/2$ antiferromagnet $\mathrm{Li_2VOSiO_4}$. *Phys. Rev. Lett.*, 93:027202, Jul 2004.

[78] H. Rosner, R. R. P. Singh, W. H. Zheng, J. Oitmaa, S.-L. Drechsler, and W. E. Pickett. Realization of a large J_2 quasi-2d spin-half heisenberg system: $\mathrm{Li_2VOSiO_4}$. *Phys. Rev. Lett.*, 88:186405, Apr 2002.

[79] H. A. Eick and L. Kihlborg. The crystal structure of $\mathrm{VOMoO_4}$. *Acta Chem. Scand.*, 20:722, 1966.

[80] K. K. Rangan, Y. Piffard, O. Joubert, and M. Tournoux. Li_2VOSiO_4: a Natisite-Type Structure. *Acta Crystallographica Section C*, 54(2):176–177, Feb 1998.

[81] H. Rosner, R. R. P. Singh, W. E. Pickett, W. H. Zheng, and J. Oitmaa. Electronic structure and exchange in Li_2VOSiO_4. *International Journal of Modern Physics B*, 16(11n12):1649–1653, 2002.

[82] E Pavarini, A Yamasaki, J Nuss, and OK Andersen. How chemistry controls electron localization in 3d1 perovskites: a wannier-function study. *New Journal of Physics*, 7(1):188, 2005.

[83] E. Pavarini, S. Biermann, A. Poteryaev, A. I. Lichtenstein, A. Georges, and O. K. Andersen. Mott transition and suppression of orbital fluctuations in orthorhombic $3d^1$ perovskites. *Phys. Rev. Lett.*, 92:176403, Apr 2004.

[84] A. Jeffrey and H.H. Dai. *Handbook of Mathematical Formulas and Integrals*. Handbook of Mathematical Formulas and Integrals Series. Elsevier Science, 2008.

[85] Wilfred Kaplan. *Advanced Calculus*. Advanced Book Program, Addison-Wesley Publishing Company, 1991.

[86] Herold Dehling. *Lecture notes of Numerical Methods and Stochastics*. Rhur-Universität Bochum, 2013.

Acknowledgements

This work would not have been possible without the encouragement, assistance and help of several people. I would therefore like to express my sincere appreciations to all of them.

Prof. Dr. Eva Pavarini, my cordial thanks for giving me an opportunity to continue my educations as Ph.D. student in RWTH Aachen university, for giving me a chance to experience working in an international atmosphere in Jülich research center, for introducing me to the field of strongly correlated materials, for your all encouragements and supports, for many guidances and comments, and for correction of my thesis.
I want to express my deep thanks to **Prof. Dr. Erik Koch,** for the trust, for useful discussions and for a second review of this thesis.
I am very thankful to **Prof. Dr. Matthias Wuttig,** for heading my Ph.D. committee and to **Prof. Dr. Stefan Wessel** for being member of my committee.
I would like to thank my former office mate **Dr. Andreas Flesch** for discussions, for his friendly advices, especially for his help with the paperwork and translation of many German letters.
I thank my former and current colleagues, **Dr. Evgeny Gorelov** and **Dr. Guoren Zhang**, for several discussions. My special thanks go to **Esmaeel Sarvestani,** not only for his friendship but also for many discussions.
I greatly appreciate **Dr. Mohammad Rahimi,** for his help and comments regarding to Fortran and bash scripting.
I particularly thank **Luise Snyders** for her help in all administrative issues and for assisting me in handling paperworks.
I am grateful to my former and current colleagues **Dr. Carmine Autieri, Dr. Fabio Baruffa, Dr. Joaquin Miranda, Michael Baumgärtel, Monica Bugeanu, Khaldoon Ghanem, Dr. Hunter Sims, Dr. German Ulm,** and **Julian Musshoff** for providing nice and friendly atmosphere in the research group.
I appreciate **Vahid Ebrahimzade** and especially **Forough Kiani** for proof-reading of this thesis, often on quite short notice.
I would like to thank **Prof. Dr. David P. Divincenzo** and Institute for Advanced Simulations (IAS-3) where this Ph.D. project was performed. All the calculations were done on the JARA RWTH cluster. I gratefully acknowledge financial support from the Deutsche Forschungsgemeinschaft through research unit FOR 1346.
I am very thankful to **Assoc. Prof. Dr. Keivan Aghababaei Samani** who indeed encouraged me in physics in the first year of my Bachelor degree in Isfahan University of Technology. I gratefully acknowledge my M.Sc supervisor **Prof. Dr. Farhad Shahbazi** who changed my scientific life in both Bachelor and Master degrees. **Assoc. Prof. Dr. Seyed Akbar Jafari,** thank you too for your encouragements in computational physics course.
Sima Farazi, Ehsan Rezaei and **Davoud Baratian**, I would like to thank you all. I never forget our pleasant times in our hiking, backpacking and adventure trips not only in Europe but also in Iran. **Sima,** my heartily appreciations go to you for your assistance, support, encouragement, and for being a wonderful friend to me.
This dissertation is dedicated to my beloved parents, **Touran Aghili** and **Gholamreza Kiani**, and to my dearest sisters and brother **Forough Kiani, Atefeh Kiani** and **Ali Kiani**.